# Oxidation Processes: Experimental Study and Theoretical Investigations

By

**Nada Mohammed Al-Ananzeh**

**A Dissertation**

Submitted to the Faculty

of the

**WORCESTER POLYTECHNIC INSTITUTE**

in partial fulfillment of the requirements for the

**Degree of Doctor of Philosophy**

in

**Chemical Engineering**

April 2004

Approved by:

--------------------------------------------------------------------------------
Robert Thompson, Ph.D., Advisor
Professor of Chemical Engineering
Worcester Polytechnic

--------------------------------------------------------------------------------
John Bergendahl, Ph.D.
Assistant Professor of Civil and Environmental Engineering
Worcester Polytechnic Institute

--------------------------------------------------------------------------------
Fabio H. Ribeiro, Ph.D.
Professor of Chemical Engineering
Purdue University

# Abstract

Oxidation reactions are of prime importance at an industrial level and correspond to a huge market. Oxidation reactions are widely practiced in industry and are thoroughly studied in academic and industrial laboratories. Achievements in oxidation process resulted in the development of many new selective oxidation processes. Environmental protection also relies mainly on oxidation reactions. Remarkable results obtained in this field contributed to promote the social image of chemistry which gradually changes from being the enemy of nature to becoming its friend and savior. This study dealt with two aspects regarding oxidation process. The first aspect represented an experimental study for the catalytic partial oxidation of benzene to phenol using Pd membrane in the gaseous phase. The second part was a theoretical study for some of the advanced oxidation process (AOPs) which are applied for contaminant destructions in polluted waters.

Niwa and coworkers[*] reported a one step catalytic process to convert benzene to phenol using Pd membrane. According to their work, this technique will produce a higher yield than current cumene and nitrous oxide based industrial routes to phenol. A similar system to produce phenol from benzene in one step was studied in this work. Results at low conversion of benzene to phenol were obtained with a different selectivity from the reported work. High conversion to phenol was not obtained using the same arrangement as the reported one. High conversion to phenol was obtained using a scheme different from the one reported by Niwa $et$ $al$[1]. It was found that producing phenol from benzene is not related to Pd-membrane since phenol was produced by passing all reactants over a Pd catalyst. Within the studied experimental conditions, formation of phenol was related to Pd catalyst since Pt catalyst was not capable of activating benzene to produce phenol. Other evidence was the result of a blank experiment, where no catalyst was used. From this experiment no phenol was produced.

A kinetic model for the advanced oxidation process using ultraviolet light and hydrogen peroxide ($UV/H_2O_2$) in a completely mixed batch reactor has been tested for the destruction of humic acid in aqueous solutions. Known elementary chemical reactions with the corresponding rate constants were taken from the literature and used in this model. Photochemical reaction parameters of hydrogen peroxide and humic acid were also taken from the literature. Humic acid was assumed to be mainly destroyed by direct photolysis and $^\bullet OH$ radicals. The rate constant for the HA-$^\bullet OH$ reaction was optimized from range of values in the literature. Other fitted parameters were the rate constant of direct photolysis of hydrogen peroxide and humic acid. A series of reactions were proposed for formation of organic byproducts of humic acid destruction by direct photolysis and $^\bullet OH$ radicals. The corresponding rate constants were optimized based on the best fit within the range of available published data. This model doesn't assume the net formation of free radicals species is zero. The model was verified by predicting the degradation of HA and $H_2O_2$ for experimental data taken from the literature. The kinetic model predicted the effect of initial HA and $H_2O_2$ concentration on the process performance regarding the residual fraction of hydrogen peroxide and nonpurgeable dissolved organic carbon (NPDOC). The kinetic model was used to study the effect of the presence of carbonate/bicarbonate on the rate of degradation of NPDOC using hydrogen peroxide and UV ($H_2O_2/UV$) oxidation. Experimental data taken from literature were used to test the kinetic model in the presence of carbonate/bicarbonate at different concentrations. The kinetic model was able to describe the trend of the experimental data. The kinetic model simulations, along with the experimental data for the conditions in this work, showed a retardation effect on the rate of degradation of NPDOC due to the presence of bicarbonate and carbonate. This effect was attributed to the scavenging of the hydroxyl radicals by carbonate and bicarbonate.

A kinetic model for the degradation of methyl tert-butyl ether (MTBE) in a batch reactor applying Fenton's reagent ($Fe^{II}/H_2O_2$) and Fenton-like reagent ($Fe^o/H_2O_2$) in aqueous solutions was proposed. All of the rate and equilibrium constants for hydrogen peroxide chemistry in aqueous solutions were taken from the literature. Rate and equilibrium constants for ferric and ferrous ions reactions in this model were taken from the reported values in the literature, except for the rate constant for the reaction of ferric ions with hydrogen peroxide where it was fitted within the range that was reported in the literature. Rate constant for iron dissolution was also a fitted parameter. The mechanism of MTBE degradation by the

---

[*] Niwa, S. $et$ $al$., $Science$ **295** (2002) 105

hydroxyl radicals was proposed based on literature studies. The kinetic model was tested on available experimental data from the literature which involved the use of Fenton's reagent and Fenton-like reagent for MTBE degradation. The degradation of MTBE in Fenton's reagent work was characterized to proceed by two stages, a fast one which involved the reaction of ferrous ions with hydrogen peroxide ($Fe^{II}/H_2O_2$ stage) and another, relatively, slower stage which involved the reaction of ferric ions with hydrogen peroxide ($Fe^{III}/H_2O_2$ stage). The experimental data of MTBE degradation in the $Fe^{II}/H_2O_2$ stage were not sufficient to validate the model, however the model predictions of MTBE degradation in the $Fe^{III}/H_2O_2$ stage was good. Also, the model was able to predict the byproducts formation from MTBE degradation and their degradation especially methyl acetate, and tert-butyl alcohol. The effect of each proposed reaction on MTBE degradation and the byproducts formation and degradation was elucidated based on a sensitivity analysis. The kinetic model predicted the degradation of MTBE for Fenton-like reagent for the tested experimental data. Matlab (R13) was used to solve the set of ordinary nonlinear stiff differential equations that described rate of species concentrations in each advanced oxidation kinetic model.

# Extended Abstract

Oxidation reactions are of prime importance at an industrial level and correspond to a huge market, for example in the US in 1994, about 31% of the catalytic production of major organic chemicals corresponded to oxidation catalytic processes. Oxidation reactions are widely practiced in industry and are thoroughly studied in academic and industrial laboratories. Catalyzed oxidation reactions are today one of the most dynamic and fruitful field in catalysis. Major achievements were attained in oxidation catalysis. They resulted in the development of many new selective oxidation processes; for example, oxidation of ethylene to acetaldehyde, oxidation of butylenes to maleic anhydride, oxidation of methanol to formaldehyde, etc. These processes have deeply affected the structure of the global chemical industry. Environmental protection also relies mainly on oxidation reactions. Remarkable results obtained in this field contribute to promote the social image of chemistry which gradually changes from being the enemy of nature to becoming its friend and savior.

This study dealt with two major aspects regarding oxidation processes. The first aspect represented an experimental study of the partial oxidation of benzene to phenol in the gaseous phase using Pd membrane. The second part was a theoretical study for some of the advanced oxidation process (AOPs) which are applied for contaminant destructions in polluted waters. In both parts the main oxidant was the hydroxyl radical ($^{\bullet}OH$) which was produced insitu from the system reagents. The first chapter of this thesis addresses the experimental study and the remaining chapters address the theoretical study. In Chapter 2, a kinetic model for the destruction of humic acids (HA) using $UV/H_2O_2$ was tested on experimental data from the literature. The study conducted in Chapter 2 was investigated further in Chapter 3 by including the effect of bicarbonate/carbonate on the rate of HA degradation. This was performed by testing the kinetic model on reported experimental data. In Chapter 4 another type of AOPs, which relies on the use of Fenton's reagent and Fenton-like reagent, was studied. Experimental data, taken from the literature, for methyl tert-butyl ether (MTBE) degradation in such systems, was used to test a kinetic model for such systems.

Phenol is an important intermediate for the synthesis of petrochemicals, agrochemicals, and plastics. An example of using phenol as an intermediate in the synthetic fibers is Nylon 66 and Nylon 6. In quantity produced, phenol ranks near the top of the list of synthetic aromatic compounds. Global production of phenol was nearly 6.4 million metric tons in 2001, valued at approximately $4 billion. Currently, phenol is produced from benzene by the cumene process, which is a three-step process. The most important drivers for technology innovation are competitiveness and environmental concern. Thus, the high amount of acetone produced in cumene process is one of the major driving forces to search for new catalytic processes, which enable a one-step synthesis of phenol without byproducts. Thus, direct introduction of a hydroxyl group into benzene is one of the most challenging tasks in oxidation catalysis.

Niwa[1] and coworkers reported a one step catalytic process to convert benzene to phenol using Pd membranes. According to their work, this technique is higher yielding than current Cumene and nitrous oxide based industrial routes to phenol. If the reported data in their work is correct, then this will be an important chemistry from industrial and research points of view. A similar system, to produce phenol from benzene in one step, to

the one reported one was designed in order to reproduce the results. Results at low conversion of benzene to phenol were obtained with a different selectivity from the reported work. High conversion to phenol was not obtained using the same arrangement as the reported one. High conversion to phenol was obtained using a scheme different from that of Niwa *et al*. From the present work, it was found that producing phenol from benzene was not a Pd-membrane technology since phenol was produced using either Pd in the form of a supported catalyst or pure metal. Within the studied experimental conditions, formation of phenol was related to Pd catalyst since Pt catalyst wasn't capable of activating benzene to produce phenol. Other evidence was the result of a blank experiment, where no catalyst was used. From this experiment no phenol was produced. The produced amount of water (secondary product) was at least 23 times greater than the produced amount of phenol (primary product). The reaction between hydrogen and oxygen at the studied conditions produced water in the primary reaction and active intermediates especially $^\bullet OH$ radical based on analysis from literature. It is established that the reaction of $^\bullet OH$ radical with benzene proceeds by addition to the aromatic ring and after subsequent reactions phenol is produced. Formation of other detected products was proposed based on the available literature. Observed chain products were proposed to be produced as a consequence of aromatic ring opening.

A kinetic model for the advanced oxidation process using ultraviolet light and hydrogen peroxide (UV/$H_2O_2$) in a completely mixed batch reactor has been tested for the destruction of humic acid in aqueous solutions. The experimental data for this model were taken from the literature. Known elementary chemical reactions with the corresponding rate constants were taken from the literature and used in this model. Photochemical reaction parameters of hydrogen peroxide and humic acid were taken from the literature. Humic acid was assumed to be mainly destroyed by direct photolysis and $^\bullet OH$ radicals. The rate constant for the HA-$^\bullet OH$ reaction was optimized from a range of values in the literature. Other fitted parameters were the rate constant of direct photolysis of hydrogen peroxide and humic acid. A series of reactions were proposed for formation of organic byproducts of humic acid destruction by direct photolysis and $^\bullet OH$ radicals. The corresponding rate constants were optimized based on the best fit within the range of available published data. This model doesn't assume the net formation of free radicals species is zero. The model was verified by predicting the degradation of HA and $H_2O_2$. The results of model simulation showed good prediction of the residual hydrogen peroxide ($H_2O_2$) and non purgeable dissolved organic carbon (NPDOC) for the set of experimental data taken from Wang[2]. A correction was applied to the experimental data of hydrogen peroxide in a second Wang[3] work. The model simulated the experimental data of Wang[2] after applying this correction. From the kinetic model the concentration of radicals, produced in the system, was predicted within the studied experimental conditions and time. Such kind of information gave a more thorough look to this system and provided an understanding of the effect of initial HA and $H_2O_2$ concentration on the process performance regarding the residual fraction of hydrogen peroxide and nonpuregable dissolved organic carbon (NPDOC).

The kinetic model which was developed earlier using UV/$H_2O_2$ oxidation was used to study the effect of the presence of carbonate/bicarbonate on the rate of degradation of NPDOC using hydrogen peroxide and UV ($H_2O_2$/UV) oxidation. Experimental data taken from Wang[2] was used to test the kinetic model in the presence of

carbonate/bicarbonate. The kinetic model was able to describe the trend of the experimental data. The kinetic model simulations, along with the experimental data for the conditions in this work, showed a retardation effect on the rate of degradation of NPDOC due to the presence of bicarbonate and carbonate. This effect was attributed to the scavenging of the hydroxyl radicals by carbonate and bicarbonate. Also at these conditions, it was hypothesized that carbonate radicals produced from the reaction of carbonate and bicarbonate ions with hydrogen peroxide, were contributing to the rate of NPDOC degradation. However, the reaction of carbonate radicals was considerable for the degradation of hydrogen peroxide also. Based on the previous analysis it was found that at the studied conditions of hydrogen peroxide concentration, HA concentration, carbonate/bicarbonate concentration, and pH value that the system was sensitive to the presence of bicarbonate/carbonate in the system. The kinetic model simulation for the data reported by another work of Wang[3] showed that carbonate and bicarbonate concentration had a negligible effect at the high concentration of hydrogen peroxide concentration. However, the experimental results showed a significant retardation effect on the degradation of NPDOC. The simulation described the system behavior well for the case where no carbonate/bicarbonate was present.

A kinetic model for the degradation of methyl tert-butyl ether (MTBE) in a batch reactor applying Fenton's reagent ($Fe^{II}/ H_2O_2$) and Fenton's like reagent ($Fe^{o}/ H_2O_2$) in aqueous solutions was proposed. This kinetic model consisted of three major parts, hydrogen peroxide chemistry in aqueous solutions, iron chemistry, and MTBE chemistry. Hydrogen peroxide chemistry in aqueous solutions is well documented, and, therefore, all of the rate and equilibrium constants for this chemistry were taken from the literature. The iron chemistry consisted of many of the possible reactions of ferrous and ferric ions in aqueous systems containing hydrogen peroxide beside iron dissolution by hydrogen peroxide. Rate and equilibrium constants for ferric and ferrous ions reactions in this model were taken from the reported values in the literature except for the rate constant for the reaction of ferric ions with hydrogen peroxide where it was fitted within the range that was reported in the literature. The rate constant for iron dissolution was also a fitted parameter and it was a function of the solution acidity. The mechanism of MTBE degradation by the hydroxyl radicals, which were formed from ferrous ions and hydrogen peroxide reaction, the pathways for the formation of the byproducts that follow MTBE by these radicals, and the degradation of these byproducts was proposed based on  studies performed by Stefan[4], Wu[5], and Cooper[6]. Most of the rate constants regarding MTBE mechanism were taken from the literature and when a rate constant for a certain reaction was not available, analogy between this reaction and another reaction that proceed in a similar  way was made.  Proportions of one reaction that proceeds in different routes, other than hydrogen abstraction from MTBE which was taken from the literature, was optimized based on the best fitting of the model to the experimental data.

The proposed model was tested on available experimental data from the literature which involved the use of Fenton's reagent and Fenton's like reagent for MTBE degradation. The set of ordinary nonlinear stiff differential equations that described rate of species concentrations in this system was solved using Matlab (R13) software.  The degradation of MTBE in Fenton's reagent work was characterized to proceed by two stages, a fast one which involved the reaction of ferrous ions with hydrogen peroxide ($Fe^{II}/H_2O_2$ stage) and another, relatively, slower stage which involved the reaction of

ferric ions with hydrogen peroxide ($Fe^{III}/H_2O_2$ stage). The experimental data of MTBE degradation in the (first) $Fe^{II}/H_2O_2$ stage were not enough to validate the model; however the model predictions of MTBE degradation in the $Fe^{III}/H_2O_2$ stage were good. Also, the model was able to predict the byproducts formation from MTBE degradation and their degradation especially methyl acetate (MA), and tert-butyl alcohol (TBA). A sensitivity analysis, which was based on calculating the sum of the squares of the residual (SSR) after making a perturbation in one rate constant at a time, was applied for MTBE degradation by Fenton's reagent at one set of conditions. The effect of each proposed reaction on MTBE degradation and the byproducts formation and degradation was elucidated based on this analysis. The kinetic model was able to predict the experimental degradation of MTBE for the case where Fenton's like reagent was applied. However, for the only reported byproduct in this study, acetone, the model predictions were different from the experimental results.

References:
1. Niwa, S. *et al.*, *Science* **295** (2002) 105
2. Wang, G.-S.; Hsieh, S.-T.; Hong, C. S. *Wat. Res.*, **34**(15), 3882-3887 (2000)
3. Wang, Gen-Shuh; Liao, Chih-Hsiang; Wu, Fang-Jui. *Chemosphere* **42**(4), 379-387 (2001)
4. Stefan, M.; Mack, J.; Bolton, J. R. *Environ. Sci. Technol*. **34**, 650-658 (2000)
5. Cooper, W. J.; Christopher Cramer, C;Ned H. Martin, N. H.; Mezyk, S. P.; O'Shea., K. E.; Von Sonntag, C. (2004) In press
6. Wu, T.; Cruz, V.; Mezyk, S.; Cooper, W. J.; O'Shea, K. E. *Radiat. Phys. Chem.* 65(4-5), 335-341 (2002)

# Index of Contents

**Chapter 2**     **167**
*(A Kinetic Model for Humic Acid Oxidation using Hydrogen Peroxide in Presence of UV light)*

# Index of Figures

## Chapter 1:

xiv

xvi

xvii

## Chapter 3:

## **Chapter 4**:

# Index of Tables

## Chapter 2:

## Chapter 3:

## Chapter 4:

# Acknowledgments

I would like to thank Chemical Engineering Department at Worcester Polytechnic Institute (WPI) for funding me through the three years of my Ph. D. work. This work was made possible by its funding either through teaching assistantship or research assistantship.

I would like to thank my advisors and my committee members, Prof. Robert Thompson, Prof. Fabio Ribeiro, and Prof. John Bergendahl. My work in Ph. D was unique since it allowed me to work with the previous professors and gain different experiences from each one. Each one of these professors contributed greatly to my Ph. D work. I would like to thank Prof. Thompson for giving me the freedom to do the research I want, for giving me valuable advices in my project, for being such an open mind person, for his very fast reviewing of my work, and for partially funding me in this work. Thanks also to Prof. Bergendahl; he was always there to answer all of my questions and giving direction where to go next in my theoretical study. From Prof. Ribeiro I gained my experimental experience. He was always available, and helped me in fixing my experimental setup. I would like to thank all the previous professors for reviewing this thesis.

Additionally, I want to thank the faculty members and staff members of the Department of Chemical Engineering at WPI. The staff members were always there when you want some help. Thanks also to Giacomo Ferraro and Douglas White for their help with the experimental part of this thesis. I also want to thank graduate students in the Chemical Engineering Department; they have been helpful during the time I have been here. I would like to thank my current and previous lab partners, Jingyi Han, Dr. Natalia A. Koryabkina, Dr. Guanghui Zhu, Dr. Nan Chen, Vinay Medhekar, Abhijit Phatak, Dr. Zvinevich, Dr. Joseph Gnanaraj for their help and for useful discussions.

Finally, I especially want to dedicate my dissertation to my family members. My parents, Mohammed Al-Ananzeh and Mufidah Katab, have continued to give me help and encouragement unconditionally. Their love and understanding has allowed me to be the person I am today, and for that I will be eternally grateful. I also want to thank my lovely husband, Mamoun Khdair. His love, caring, help, and support allowed me to carry on through both the good and difficult days of the last three years. I am blessed to have him. Also, my thanks go to my daughters, Aseel Khdair and deema Khdair. They are too young, but this experience made them mature and independent people. My daughters were so helpful; they took care of their young brother, Adam, to whom I also give my thanks. He was a unique baby by being quite and laughing all of the time. My thanks also go to my brothers and lovely sister, Mamoun, Barham, Hazem, and Noor for their love and support. Also, I want to thank my parents and sisters in law for their love and caring.

# Chapter 1

## Catalytic Oxidation of Benzene to Phenol Using Pd Membrane

## Abstract

Phenol is an important intermediate for the synthesis of petrochemicals, agrochemicals, and plastics. An example of using phenol as an intermediate in the synthetic fibers is Nylon 66 and Nylon 6. In quantity produced, phenol ranks near the top of the list of synthetic aromatic compounds. Global production of phenol was nearly 6.4 million metric tons in 2001, valued at approximately \$4 billion. Currently, phenol is produced from benzene by the cumene process, which is a three-step process. The first step is the alkylation of benzene with propylene to cumene in presence of silica-supported phosphoric acid. This reaction can also be performed with Friedel-Crafts catalysts such as aluminum trichloride ($AlCl_3$) at 100 or $200^o$ C. Then cumene is converted to cumene hydroperoxide in a non-catalytic auto-oxidation reaction. The final step is the acidic cleavage of cumene hydroperoxide into phenol and acetone (which are one to one in stoichiometric ratio) that is catalyzed by free sulfuric acid at $60-100^o$ C.

The most important drivers for technology innovation are competitiveness and environmental concern. The high amounts of produced acetone in cumene process are one of the major driving forces to search for new catalytic process, which enable a one-step synthesis of phenol without byproducts. Thus, direct introduction of a hydroxyl group into benzene is one of the most challenging tasks in oxidation catalysis.

Niwa and coworkers reported a one step catalytic process to convert benzene to phenol using Pd membrane. According to their work, this technique is higher yielding than current cumene and nitrous oxide based industrial routes to phenol. If the reported

data in their work is correct, then this will be an important chemistry from industrial and research points of view.

A similar system, to produce phenol from benzene in one step, to the one reported one was designed in order to reproduce the results. Results at low conversion of benzene to phenol were obtained with a different selectivity from the reported work. High conversion to phenol was not obtained using the same arrangement as the reported one. High conversion to phenol was obtained using a scheme different from Niwa *e. al* one.

From the present work, it was found that producing phenol from benzene was not a Pd-membrane technology since phenol was produced using either Pd in the form of a supported catalyst or pure metal. Within the studied experimental conditioned, formation of phenol was related to Pd catalyst since Pt catalyst wasn't capable of activating benzene to produce phenol. Another evident was the result of a blank experiment, where no catalyst was used. From this experiment no phenol was produced.

## 1. Introduction

Phenol is a valuable intermediate for the synthesis of petrochemicals, agrochemicals (phenoxyacetic acids as a herbicide), and plastics [1,2,3]. An example of using phenol as an intermediate in the synthetic fibers is Nylon 66 and Nylon 6 synthesis (The difference between Nylon 66 and Nylon 6 is that the first one is made out of two monomers while the second one is synthesized from a single bifunctional monomer). Nylon 6 and 66 account for more than 95 % of the overall world production of polyamides [2]. Phenol is also a disinfectant effective against vegetative Gram-positive and Gram-negative bacteria and certain viruses [3]. In quantity produced, phenol ranks

near the top of the list of synthetic aromatic compounds [4]. Global production of phenol was nearly 6.4 million metric tons in 2001, valued at approximately $4 billion [5, 6, 7, 8].

Currently, phenol is produced from benzene by the Cumene process. This process consists of three steps as can be seen in Figure 1.1
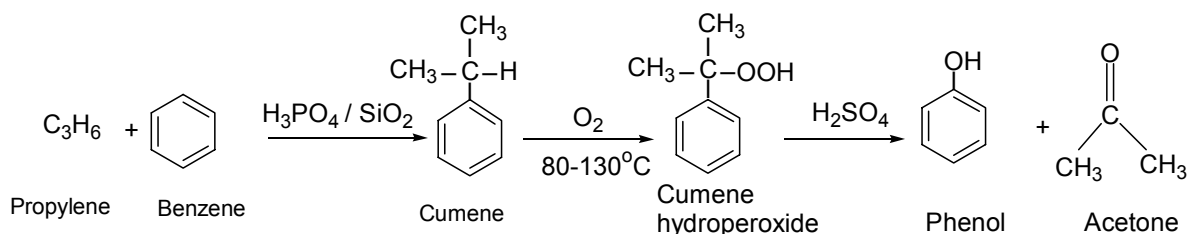


Fig. 1.1: Reactions for Cumene process

The first step is the alkylation of benzene with propylene to Cumene in presence of silica-supported phosphoric acid. This reaction can also be performed with Friedel-Crafts catalysts such as aluminum trichloride ($AlCl_3$) at 100 or 200 $^{o}$C. Then Cumene is converted to Cumene hydroperoxide in a non-catalytic auto-oxidation reaction. The final step is the acidic cleavage of hydroperoxide into phenol and acetone that is catalyzed by free sulfuric acid AT 60-100$^{o}$ C [2, 5, 7, 8]. Cumene can be produced using either supported phosphoric acid (UOP process) or $AlCl_3$ (Monsanto process) as alkylation process.

The most important drivers for technology innovation are competitiveness and environmental concern. The high amounts of produced acetone in Cumene process are one of the major driving forces to search for new catalytic process, which enable a one-step synthesis of phenol without byproducts. Thus, direct introduction of a hydroxyl group into benzene is one of the most challenging tasks in oxidation catalysis.

## 1.1. Background and historical Overview of Phenol Industrial Process

Phenol was firstly known as carbolic acid. It received this name because it was isolated from coal tar when it was discovered for the first time in 1834 [8]. The demand for phenol has increased enormously which led to synthetic preparation of phenol. The following is a summary in the progress of phenol process industry.

### 1.1.1. The Sulfonation Process

This process was the first process applied on industrial scale by BASF in 1899. This process was applied for about 80 years. This process requires the use of aggressive reagents and produces large amounts of waste sodium sulfate. Equations 1 and 2 summarize the main reactions in this process [8].

$$\text{C}_6\text{H}_6 + H_2SO_4 \longrightarrow \text{C}_6\text{H}_5SO_3H + H_2O \tag{1}$$

$$\text{C}_6\text{H}_5SO_3H + 2NaOH \longrightarrow \text{C}_6\text{H}_5OH + Na_2SO_3 \tag{2}$$
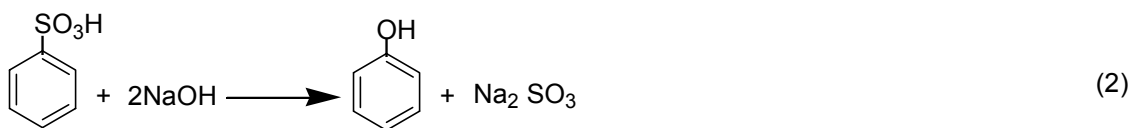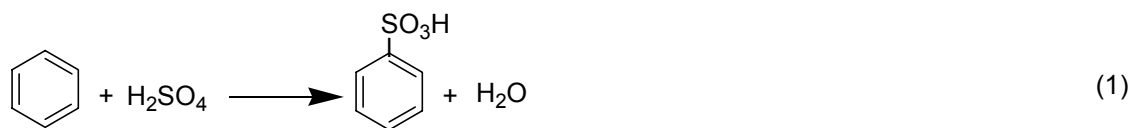
### 1.1.2. Chlorination Process

This process appeared in 1924 in the USA and was used by DOW Chemical. Independently, a similar technology was developed in Germany. Reactions 3 and 4 explain this process [8, 10]

$$\text{C}_6\text{H}_6 + 1/2Cl_2 \xrightarrow[\text{FeCl}_3]{25\text{-}50^oC} \text{C}_6\text{H}_5Cl \tag{3}$$

$$\text{C}_6\text{H}_5Cl + NaOH \xrightarrow[300 \text{ atm}]{300\text{-}390^oC} \text{C}_6\text{H}_5OH + NaCl \tag{4}$$

4
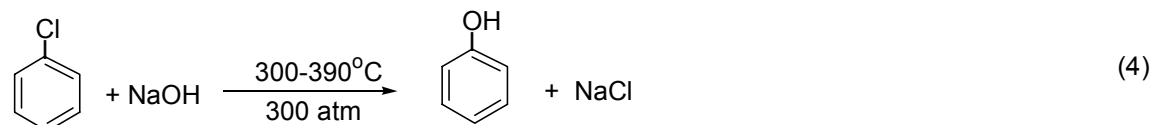
### 1.1.3. Cyclohexanone Process

Another process known as cyclohexanone process has appeared. In this process cyclohexane is oxidized to a mixture of cyclohexanol and cyclohexanone and then dehydrogenated to phenol. This process appeared in the sixties and was used by Monsanto in Australia for few years before converting to another process [8]. Reactions 5-7, describe this process.



$$(5)$$



$$(6)$$



$$(7)$$
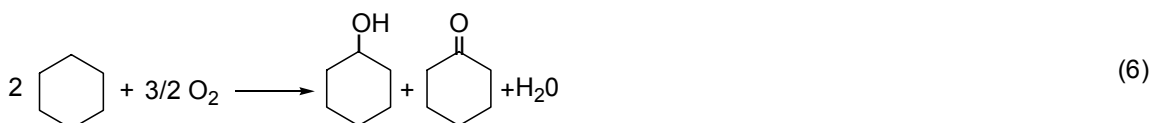
### 1.1.4. Benzoic Acid Process

Dow Chemical of Canada commercialized another process, based on a non-benzene raw material, in 1961. It was known as the benzoic acid process. Reactions 8 and 9 describe this process. Reaction 8, was practiced in Germany since the early forties. This reaction has high selectivity under mild conditions oppose to reaction 9, which has a low selectivity. This process accounts for 5 % of world production of phenol [8, 11].



$$(8)$$



$$(9)$$

**1.1.5. Cumene process**

Currently most of the phenol is produced via the cumene process which accounts for more than 90 % of the world output of phenol [11]. This process consists of three steps as was shown in Figure 1.1 earlier. This route was first discovered in 1942 in Russia. The first industrial plant was put to operation in 1949 in Dzerzhinsk city. This process started to work in the USA in early 50's [8]. The advantage of the "Cumene Process" is that it takes two inexpensive starting materials, benzene and propylene, and converts them into two expensive useful products, phenol and acetone, just using air [11]. In spit of its great success, Cumene process has some disadvantages such as explosive intermediate (cumene hydroperoxide), high environmental impact, corrosive catalysts, and the formation of agliomers and other impurities. It is a multi-step process, which makes it difficult to achieve high phenol yields with respect to benzene and needs a high capital investment due to its characteristic multi-step process. It requires the use of aggressive media ($H_2SO_4$) and has a high acetone production as a coproduct resulting in an oversupply of the market. This problem is serious since the acetone market demand is much smaller than that of phenol. Therefore the economics of this process significantly depends on the marketability of the acetone by-product [1, 2, 8, 9, 11]. For these reasons, a process is desired whereby phenol can be formed in one step.

Many approaches for this objective have been reported in the literature. For example, there were many attempts to replace the corrosive catalyst in the Cumene process with a zeolite-based catalyst. In 1996 EniChem developed an industrial alkylation technology, which is based on beta-zeolite catalyst [2].

6

Most of the studies which were performed to study the possibility of converting benzene to phenol represented a system that either has a low phenol yield or a quite complex one. A study was carried to produce phenol in a one step using Cu ion-exchanged HZSM-5 (Cu-HZSM-5) and Cu-Na HZSM-5 zeolite using molecular oxygen as an oxidant for this gas phase reaction. Phenol was produced in a very low yield using this system. Also, it was found that for a C- HZSM-5 with a larger Si/Al atomic ratio inhibits the formation of carbon dioxide and increases the selectivity of phenol formation [7].

Another study reported the pathways of phenol and benzene photooxidation using $TiO_2$ supported on a zeolite. For benzene photooxidation, phenol yield was very low [13]. Heteropolyacids were used as the reoxidant for palladium in the direct oxidation of benzene to phenol using molecular oxygen which represents one of the complicated methods for producing phenol [14]. Direct catalytic hydroxylation of benzene with hydrogen peroxide using titanium- silicate zeolites was reported. This was a liquid phase reaction, in the presence of the catalyst, using hydrogen peroxide, which is an expensive oxidant [15].

Liptakova [16] studied the direct synthesis of phenol from benzene over hydroxapatite catalysts in the gas phase. He was able to achieve 97% selectivity for phenol with 3.5% conversion of phenol. However, the system, which he worked with, was complex regarding the catalyst and the operating conditions beside the formation of aniline [16]. Hydroxylation of benzene over vanadium-containing molecular sieves and using $H_2O_2$ as an oxidant gave low benzene conversions [17]. Direct hydroxylation of aromatic nuclei with oxygen and hydrogen has been done by simultaneously mixing an

aromatic compound, oxygen, and hydrogen in liquid phase [18-22]. The system in these studies was complicated containing a mutilcomponent catalyst, a solvent and some additives. Also, the aromatic alcohol yields were very low.

Other routes included direct liquid phase-hydroxylation of benzene with $H_2O_2$ in the presence of titanium silicate or supported vanadium oxide catalysts, but the costs for the $H_2O_2$ are higher than for $N_2O$ [6, 7, 1]. A recent study was performed for the direct oxidation of benzene to phenol applying an $O_2/H_2$ mixture on silica supported Pt-$VO_x$ and Pd-$VO_x$ catalysts. Using the first catalyst benzene conversion was 1 % with phenol selectivity of 86%. For the other catalyst the benzene conversion was 0.2 % [1].

There is currently a considerable interest in the gas-phase catalytic oxidation process for phenol manufacture because the gas-phase reaction process has a potential advantage over the corresponding liquid-phase process from an economic point of view. A new route for producing phenol directly from benzene was based on using $N_2O$ as an oxidizing agent in the gas phase and the iron –containing Zeolites (FeZSM-5) as the catalyst. Solutia Inc. and the Boreskov Institute of Catalysis (BIC) are currently developing this new process jointly [2, 8]. Producing phenol from $N_2O$, is presently used only if the expensive $N_2O$ is supplied as a valuable industrial waste product since $N_2O$ is expensive for the use as an oxidant on a large scale [1, 2, 9, 12].

In a summary, we may conclude that the oxidation of benzene to phenol is most probably a champion catalytic reaction as for the variety of approaches, number of tested catalysts, and amount of effort which has been dedicated to its realization. It probably can be compared only with the oxidation of methane to methanol which also appears to be

very simple but is very difficult to achieve. This elegant chemical transformation will continue to challenge catalytic researchers.

**I.2. Importance of oxidation process**

Oxygen, which is an inseparable participant of oxidation reactions, is the most available chemical element on the earth. The amount of oxygen represents more than 50 % among the more than 1000 known elements in the atmosphere, hydrosphere and lithosphere. This would explain the outstanding role of oxygen reaction in our life [8]. Molecular oxygen is economically favorable as an oxidant because it is easy to handle and readily available [12].

Oxidation catalytic reactions are of prime importance at an industrial level and correspond to a huge market, For example in the US in 1994, about 31 % of the catalytic production of major organic chemicals corresponded to oxidation catalytic processes. The market corresponds to 20 billions US $ in the USA and world wide such numbers have roughly to be multiplied by a factor of 2.5 [23, 24]. Majority of the oxidation catalysts corresponds to metallic oxides, some noble metals like Pd, and Pt , and cations of variable oxidation states such as $F^{3+}/Fe^{2+}$, $V^{5+}/V^{3+}$, $Cu^{2+}/Cu^+$, etc.

Oxidation reactions are widely practiced in industry and are thoroughly studied in academic and industrial laboratories. Catalyzed oxidation reactions are today one of the most dynamic and fruitful field in catalysis. Major achievements were attained in oxidation catalysis during the last four decades. They resulted in the development of many new selective oxidation processes; for example, oxidation of ethylene to acetaldehyde, oxidation of butylenes to maleic anhydride, oxidation of methanol to

formaldehyde, etc [8, 25-28]. These processes have deeply affected the structure of the global chemical industry.

Environmental protection also relies mainly on oxidation reactions. Remarkable results obtained in this field contribute to promote the social image of chemistry which gradually changes from being the enemy of nature to becoming its friend and savior.

Thus the achievements of oxidation catalysis are diverse and evident but there is an area, where the achievements of oxidation catalysis are still modest regardless of many efforts, such as the oxidative hydroxylation of paraffin and aromatic hydrocarbons [8]. There is a need for such processes, especially for the preparation of various alcohols and phenols and we have presented earlier that there are many attempts to replace the exciting cumene process for phenol production by a single step process which should avoid the use of a corrosive media or explosive intermediates

## 1.3. Newa *et al* work

Newa at the National Institute of Advanced Industrial Science & Technology, Tuskuba, Japan, and coworkers reported a one step catalytic process to convert benzene to phenol using Pd membrane [9]. According to their work, this technique was higher yielding than the current Cumene and nitrous-oxide based industrial routes to phenol [9].

Their work was an attempt to produce phenol from benzene in a one step using palladium membrane. In this system hydrogen and oxygen were separately supplied. Hydrogen was fed into a mixed gas stream of a substrate and oxygen through a metallic thin layer. The membrane was prepared by coating a porous $\alpha$-alumina tube with a thin layer of palladium by means of metallic chemical vapor deposition technique. At 300 $^{\circ}$C, the hydrogen and nitrogen permeation rates of their membranes were 1.0 to $3.0 \times 10^{-3}$ mol

m$^{-2}$ s$^{-1}$ Pa$^{-0.5}$ (10.5 to 3.5 m$^3$ m$^{-2}$ h-1) and 0.1 to 1.0 X 10$^{-10}$ mol m$^{-2}$ s$^{-1}$ Pa$^{-0.5}$ respectively

[9]. Figure 3.1.1 and Table 3.1.1 summarizes the main results obtained by this group [9].

This chemistry would be commercial from industrial point of view with such conversions

to phenol in one step.

**Table 1.3.1:** Direct hydroxylation of benzene to phenol with oxygen and hydrogen catalyzed by a palladium membrane. "Inner" and "Outer" mean that a gaseous mixture containing a hydrocarbon was flowed inside or outside of the palladium membrane tube, respectively. Selectivity was based on the amount of benzene consumed

| Catalyst | Reaction temp. (°C) | Reaction system (volume ratio) | | Results | |
| | | Aromatic/O$_2$/He (28 ml/min) | H$_2$/He (14 ml/min) | Reactant conversion (%) | Product selectivity (%) |
| --- | --- | --- | --- | --- | --- |
| | | *Benzene* | | | |
| Pd membrane (inner) | 150 | 0.40/1.29/24.6 | 2.43/20.0 | 13.25 | 85.3 |
| Pd membrane (inner) | 160 | 0.45/4.70/29.8 | 6.72/28.2 | 1.60 | 96.3 |
| Pd membrane (inner) | 250 | 1.80/8.51/24.6 | 10.06/24.9 | 2.05 | 92.7 |
| Pd membrane (outer) | 150 | 2.00/1.29/24.6 | 2.43/20.0 | 2.11 | 94.8 |
| Pd membrane (outer) | 200 | 2.00/1.29/24.6 | 2.43/20.0 | 3.00 | 93.3 |
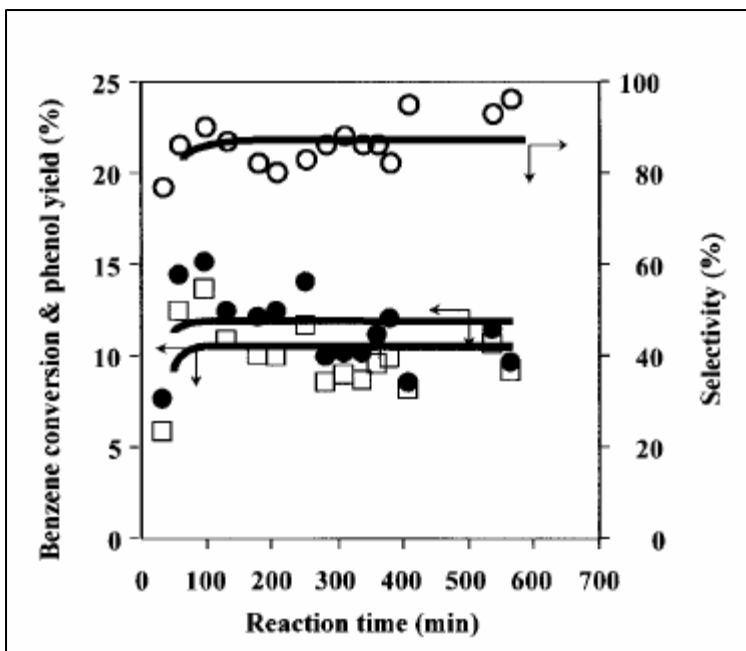
**Fig. 1.3.1**: Oxidation of benzene with oxygen and hydrogen catalyzed by a palladium membrane at $200^o$ C. Flow rates: shell, 25 ml/min ($H_2$/He = 5.6/20, volume ratio); tube, 25 ml/min (benzene/$O_2$/He = 0.4/3.8/25, volume ratio). Solid circles, squares, and open circles denote benzene conversions, phenol yields, and phenol selectivities, respectively

## 1.4. Objectives

This current work was initially based on reproducing the data of Niwa *et al* [9]. As said earlier, their work was an attempt to produce phenol from benzene in a one step using palladium membrane. This chemistry would be commercial from industrial point of view with the obtained conversion of benzene to phenol in one step. Also, their work was regarded as one of the chemistry highlights of the year 2002 [22]. Therefore, it seems that producing phenol using the setup described by Niwa *et al* [9] is an interesting and important work.

Hence, we wanted to make a fundamental study for such a system. In order to do that we have built a system similar to Niwa *et al* work [9] as will be seen later in Section 2 in the experimental setup.

The objectives of the work presented in this chapter were:

1. To reproduce the data from Niwa *et al*.

2. To try to understand the theory behind the formation of phenol in such a system. In order to understand the theory, different design schemes were tried like:

- Using Pd supported on Carbon (Pd/C)

- Using a ¼ in stainless steel tubing coated with Pd/ZrO$_2$.

- Using pure Pd metal welded in different shapes to a non porous stainless steel ¼ tubes in the shell and tube reactor setup.

- Running experiment with a different catalyst like Pt, to investigate whether the formation of phenol is related to catalyst type or not.

- Running blank experiment to figure out whether phenol formation is related to the presence of the catalyst or not.

## 2. Experimental Methods

### 2.1. Chemicals

Hydrogen was purchased from MG Industries. Argon was purchased from SpecAir Specialty Gases. He and Oxygen were purchased from BOC GASES. Benzene (99.9 %), 1,4-Cyclohexanedione (98 %), Cyclohexanone (99 %), and Phenol (99 %) were purchased from Aldrich.

### 2.2. Experimental Setup

The reaction of benzene to produce phenol has been studied using different experimental schemes in order to reproduce the work of Niwa *et al* [9] and to understand the chemistry behind the formation of phenol from benzene.

### 2.2.1. Membrane system

The system consisted of a ¾ in shell and ¼ in tube reactor. The shell has a total length of 10 in. The ¼ in tube has two parts welded to each other. The central part was a porous part that was welded from both ends to a nonporous stainless steel tube. The unit's support was porous 316L seamless stainless steel tube having an outside diameter (OD)= O.25 " (6.35mm),  inside diameter (Id)= 0.125" (3.175mm) and nominal retention size of 0.2 μm. The tube was cut into 42.5 mm long segment welded to a dense stainless steel tubes with the same OD as porous one. Porous part of this unit has 8.5 cm$^2$ permeable surface area. Palladium membrane 39.5 μm was formed on the outer side of the porous tube by electrolysis plating technique [30]. He and $H_2$ fluxes through the Pd membrane were measured by pressurizing one side of the shell and tube reactor with the gas under study at the required temperature. Then the gas will permeate through the Pd membrane from the shell side to the tube side if the shell side was pressurized and vice versa at a certain flow rate. This flow was a function of the pressure difference through the shell and tube sides of the reactor, operating temperature, and properties of the membrane system [30]. The flow rate of the gas permeating through the membrane was measured by a glass bubble flow meter (BFM) connected to the exit of the reactor. The BFM gives measured volume of the gas bubble traveling through the solution inside of it for a certain time. Therefore, this measured volume was divided by the measured time to obtain flow rate. Finally, the flux was obtained by dividing the flow rate over the permeable surface area of the Pd membrane.

Hydrogen and nitrogen permeation rates, for the membranes prepared according to Ma *et al* [30] method, were 2-4 $m^3 m^{-2} h^{-1}$ and 0.0005-0.001$m^3$ $m^{-2}$ $h^{-1}$, respectively at

atmospheric pressure difference and 350 $^o$C [30]. A stainless steel shell of ¾ in OD surrounded this tube. Figure 2.2.1 show the whole experimental setup for this scheme. In this setup, $H_2$ was fed to the shell side of the shell and tube reactor and the remaining gases (Ar, $O_2$, He, Benzene) were entered to the tube side. The experimental setup was built in a way to allow reversing the flow directions where $H_2$ can flow to the tube side and the other gases enter to the shell side. A mass flow controller (MFC) (Porter type) was used for each gas to set the flow at the required value. These mass flow controllers were precise up to $\pm 0.2$ ml/min. A heating tape (dual element, cloth insulated heat tape, 4ft x 1/2in, 312 watts, 120 VAC, purchased from Cole-Parmer) was wrapped around the exterior shell to provide the system with the required heating. A temperature controller (TC) ($\pm 0.1^o$C precision of reading) (Eurotherm 2408) was used to control the temperature inside the tube at the set point. Thermocouples of K-type (1/16 in diameter from Omega) were inserted inside the tube for control of temperature and were used for temperature measurements within the system. The exit line from the tube was connected to the gas chromatograph electron ionization detector (GCD) system (G1800 A Hewlett Packard). This line was also wrapped with heating tape and connected with a powerstat (Warner Electric). The purpose of heating was to prevent condensation of the possible products and hence prevent plugging of the lines to the GCD. An OMEGA DP462 digital panel thermometer for thermocouples was used to take the temperature readings ($\pm 0.1^o$C precision of reading). A thermowell was extending from the inlet nut of the ¾ in shell, which allowed measuring temperature profile very close to the ¼ in tube external surface using a K-type thermocouple. The pressure at the $H_2$ side was controlled using a manual needle valve installed at the exit part of the $H_2$ line (316 stainless steel, Whiley) with a

15

pressure gauge (Ashcroft, 0-100 psig) installed at the exit side of $H_2$ flow. A pressure Gauge (Ashcroft, 0-15 psig) at the inlet side of the reaction mixture was installed to measure the pressure in the reactant side. The benzene mixture was fed at atmospheric pressure with the other gases. All fittings for this system were bought from Swagelok. The reaction mixture consisted from Benzene, $O_2$, $H_2$, He, and Ar. All of these reactants were fed into the shell in the gas phase.
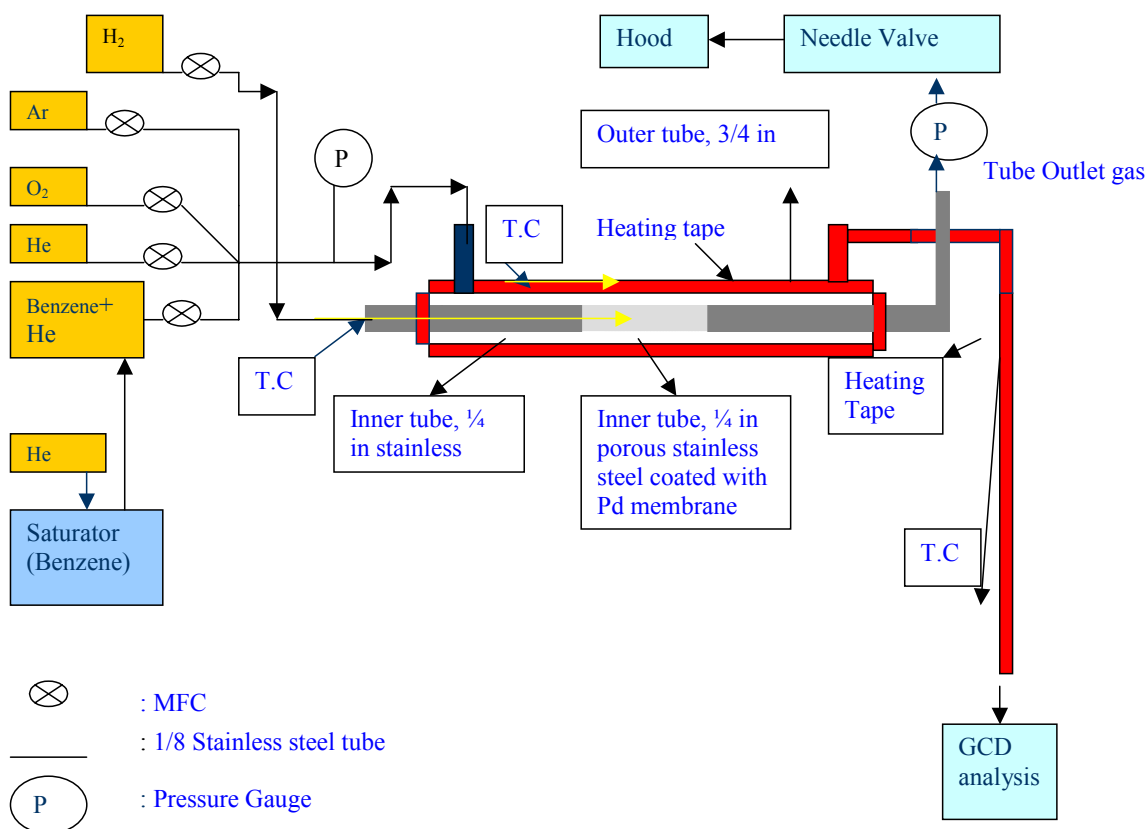


**Fig. 2.2.1**: Experimental setup for the Pd-membrane system

A glass bubbler, which was immersed in water bath, was used to obtain benzene vapor at room temperature by passing He through the liquid benzene. Ar was used as an

internal standard for the GCD. He was also used as a balance gas. The outlet gases after being analyzed by the GCD were sent to the hood with the non-reacted $H_2$.

### 2.2.2. Pd/ZrO$_2$ system

This scheme was a non-porous ¼ in stainless steel tube coated at the center for 3 in, on the exterior side, with Pd/ZrO$_2$ (10% Pd by weight). The weight of this catalyst was 0.183 g (8.2 m$^2$). This tube was inserted inside the ¾ in OD stainless steel shell. The gaseous reaction mixture (benzene, He, Ar, $H_2$, and $O_2$) was flowing into the shell side of the system where it would come in contact with the catalyst over the ¼ in tube. This system was heated in the same manner as the membrane system for the exterior shell and all the lines within the system.

### 3.2.3. Pd/Carbon system

The reaction of benzene to phenol took place in a three-inch length of a ¼ in stainless steel tube loaded with Pd/Carbon (Pd/C) catalyst. The tube was packed with 0.12 g of the catalyst. The composition of the catalyst was 5 % Pd (weight ratio). The total surface area was 2.7 m$^2$. The outer side of the tube was wrapped with heating tape and connected with the same temperature controller as the membrane system, to set the reaction temperature at the required value. The catalyst was reduced with $H_2$ at 200 $^o$C for three hours before starting the reaction. The gases mixture to this system consisted of; $H_2$, $O_2$, He, Benzene, and Ar. The exit from this tube was sent to the GCD for analysis. All experiments were run under atmospheric pressure

**2.2.4.1. Pd foils obtained from Ma. Et al (23)**

The experimental setup for this part consisted of a shell and tube reactor. The shell had a ¾ in OD and 10 in lengths and the inner tube was made of stainless steel 316 and has a ¼ in OD. The exit nut of the ¾ in shell was connected with the ¼ in tubing using a graphite Ferrule (Altech Associates Inc) that withstand high temperature during heating.

A Pd foil [30] was cut into three different shapes and welded to the outer surface of the ¼ in tube. The first shape was a cone shape (0.9 cm$^2$) that was welded at 1.5 in from the center of the ¼ in tube toward the inlet of the reactant. A rectangle Pd piece (1.2 x 0.6 cm$^2$) was welded at the center of the non-porous ¼ tube. Another rectangle Pd piece (0.7 x 0.5 cm$^2$) was welded at 1.5 in from the center of the non-porous ¼ tube toward the exit of the reactor. The reported areas of the Pd pieces were based on the external dimensions of each piece. The whole assembly was inserted into ¾ in OD stainless steel shell. The reaction mixture (benzene, He, Ar, O$_2$, and H$_2$) was allowed to enter to the shell and pass over the ¼ in tube, and hence come into contact with the Pd catalyst. After that, it would exit from the other end of the shell to the GCD for analysis. The system was heated in the same manner as the Pd-membrane system with the K-type thermocouple inserted inside the ¼ in tube close to the Pd cone for control purposes.

**2.2.4.2. Pd foil obtained from Ma. Et al (23)**

In this arrangement instead of welding three Pd pieces only one piece was welded at a distance 1.5 in from the center of the ¼ in tube. The shape of this piece was conical

with a 1.5 cm$^2$ surface area (area of the outside surface). The system was assembled and heated in the same manner as the previous one.

### 2.2.4.3. Pd foil obtained from Alfa Aesar

A Pd foil (bought from Alfa Aesar, 0.025 mm thickness) was welded at 1.5 in from the center of the non-porous ¼ tube. The final shape of the welded Pd was conical with a 1.8cm$^2$ surface area (area of the outside surface). The whole assembly was inserted into ¾ in OD stainless steel shell. The reaction mixture was allowed to enter to the shell and pass over the ¼ in tube, and hence come into contact with the Pd catalyst. After that, it would exit from the other end of the shell to the GCD for analysis. The system was heated in the same manner as before.

### 2.2.4.4. (7) Pieces of Pd on Nonporous Stainless Steel Tube

The ¼ in tube has 7 holes with 0.10 cm diameter. Hole number 4 was allocated at the center of the ¼ in with the three holes allocated on both sides from this hole were 0.5 in apart from each other. Spot welding was used to fix the seven Pd pieces in a tilted way close to the 0.1 cm diameter hole. Figure 2.2.4.4.1 gives a sketch of the ¼ in tube with Pd pieces welded to it. The Pd pieces were prepared according to the method of Ma *et al* [30] and each one has a rectangular shape. Different modes were applied to flow the reactant to the reactor. First, H$_2$ was flowed inside the ¼ in tube and hence emerge through the 0.1 cm holes and come in contact with the Pd catalyst. At the same time the remaining reaction mixture (Benzene, O$_2$, He, and Ar) was fed through the ¾ shell and then will come into contact with the Pd catalyst. After that, the whole mixture would exit from the other end of the shell to the GCD for analysis. The exit part of the ¼ in tube

was closed to assure that all the flow inside the tube would emerge from the 0.1 cm holes. Another mode of flow consisted of flowing all of the reactants into the ¼ in tube, emerging from the 0.1 cm hole and then exiting to the GCD for analysis.
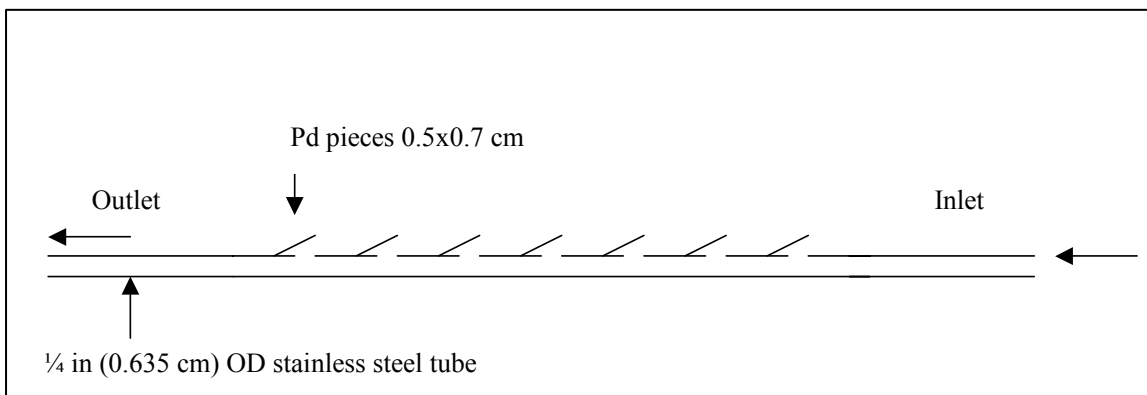


**Fig. 2.2.4.4.1**: The ¼ in stainless steel tube  with seven pieces of Pd welded to its exterior surface close to the 0.1 cm  hloes

This setup was tested at different flow rate of gases in to the shell and no flow was observed from the shell side to the ¼ in tube through the 0.1 cm holes.

### 2.2.5. Blank Experiment

To confirm that the produced phenol in the earlier experiments, was due to the presence of the catalyst the previously a blank experiment was designed. The experimental setup for this part consisted of a shell and tube reactor. The shell has a ¾ OD and 10 in length, and the inner tube has a ¼ in OD with no catalyst welded to its surface.

### 2.2.6. Pt Cone

A Pt foil (bought from Alfa Aesar, 0.05 mm thickness) was welded at 1.5 in from the center of the non-porous ¼ tube. The final shape of the welded Pt was conical with a 1.5cm$^2$ surface area (of the exterior side). The whole assembly was inserted into ¾ in OD

stainless steel shell. The reaction mixture was allowed to enter to the shell and pass over

the ¼ in tube, and hence come into contact with the Pt catalyst. After that, it would exit

from the other end of the shell to the GCD for analysis. A thermocouple for control was

held inside the ¼ in tube at a distance of 1 in from the Pt cone.

## 2.3. Calibration of Mass flow Controllers (MFCs)

In order to set the flow rate of the gases at the required flow rate, a mass flow

controller (MFC) of Porter type was used to control the inlet flow rate of each gas line to

the reactor. The allocation of these MFCs is shown in Figure 2.2.1 which gives the

experimental setup for the Pd-membrane system. These MFCs gives a reading in

percentage opening which indicates how much of the valve inside these controllers is

opened and hence how much gas is flowing through this opening. The percentage

opening is going from 0 to 100 % which indicates a closed and fully opening

respectively. In order to convert the percentage opening to a reading of flow rate, for

example in ml/min, calibration of each MFC with working gas was carried.  Each gas

was allowed to enter to the specified MFC from its source (usually the gas cylinder). The

MFC opening was set at a certain percentage and the exit line from the MFC was

connected with a glass bubble flow meter. The glass bubble flow meter (BFM) was filled

with a Swagelok snoop solution. Once the gas exits the MFC it will pass through the

liquid solution in the BFM in a form of a bubble. This bubble will travel a certain volume

in the BFM with a certain time. Therefore in order to obtain the gas flow rate in ml min$^{-1}$

for example, the MFC was opened at different percentage opening. Then the time

required by the gas bubble to pass through a specified volume was measured. The time

measurements were repeated three times at each percentage opening of the MFC. The

volumetric flow rate was obtained by dividing the measured volume over the measured time. The average volumetric flow rate was plotted vs. percentage opening of the MFC. The resultant plot was fitted to a linear fit and the obtained equation was used to calculate the volumetric flow rate for each gas through each MFC. The results of the calibration for each used gas are shown in Figure 2.3.1 to Figure 2.3.6.
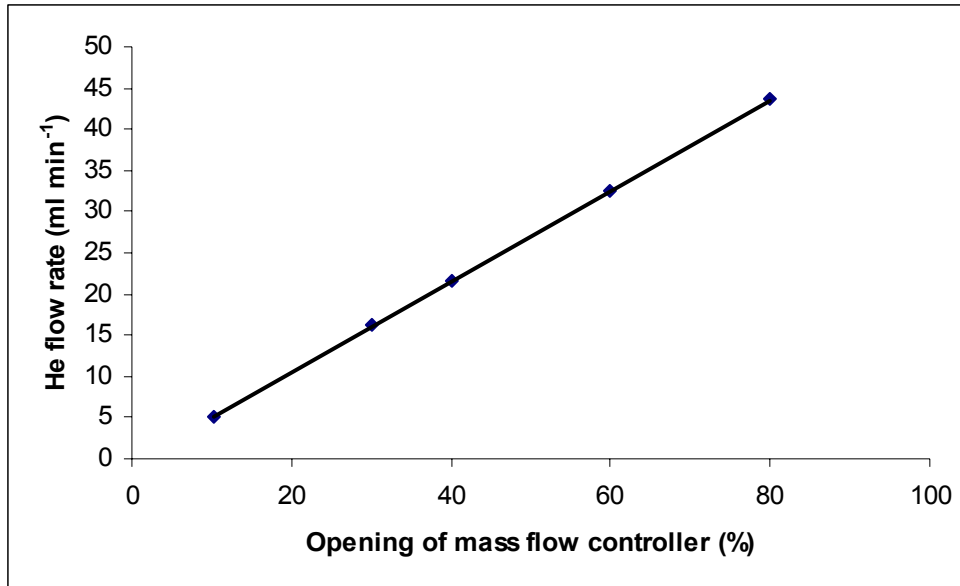


**Fig. 2.3.1**: Calibration of He mass flow controller, channel 2 on the MFM unit, saturator line
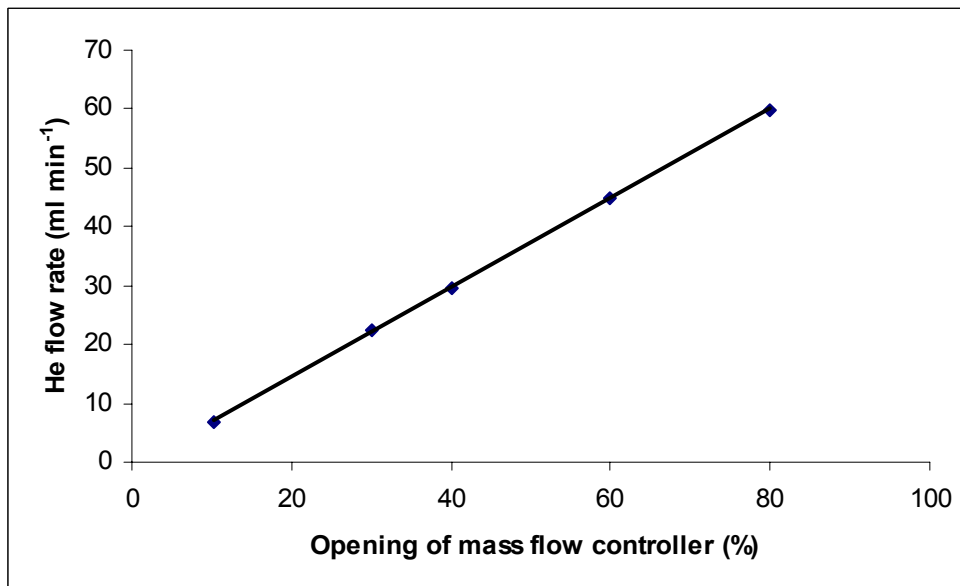


**Fig. 2.3.2**: Calibration of He mass flow controller, channel 3 on the MFM unit, tube line
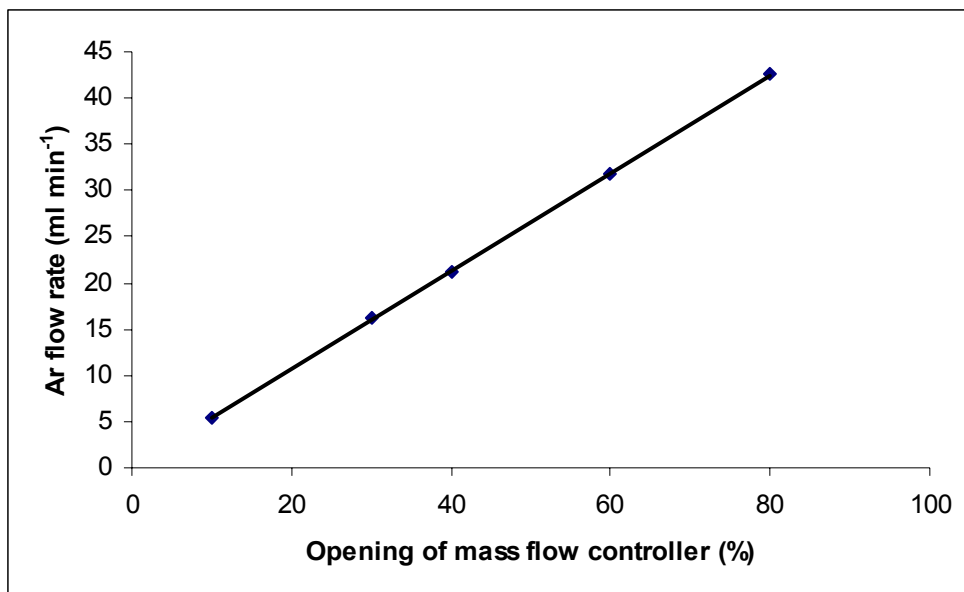
**Fig. 2.3.3**: Calibration of Ar mass flow controller
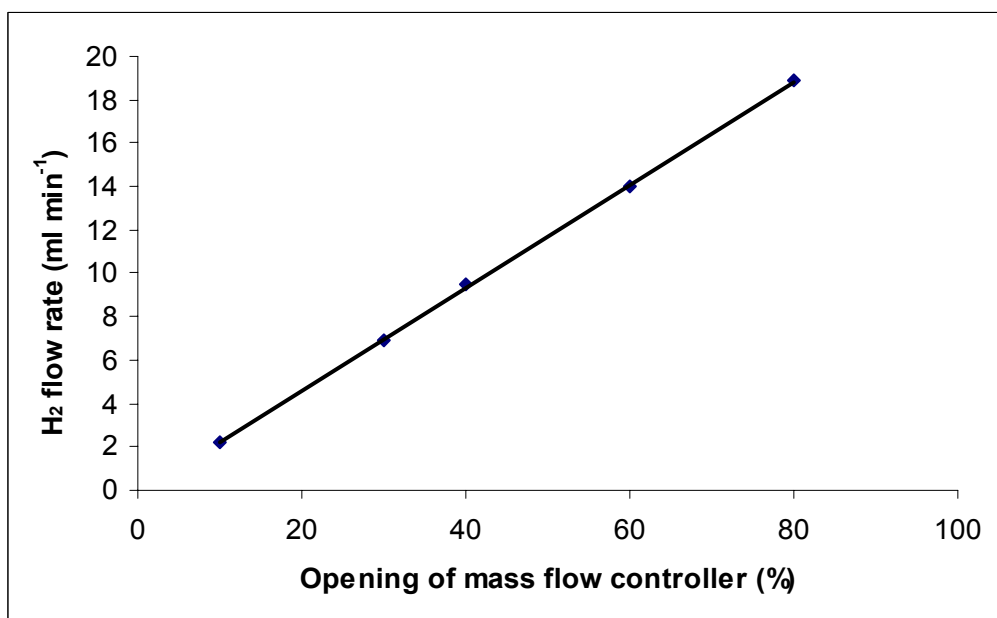


**Fig. 2.3.4**: Calibration of $H_2$ mass flow controller, channel1 unit 2
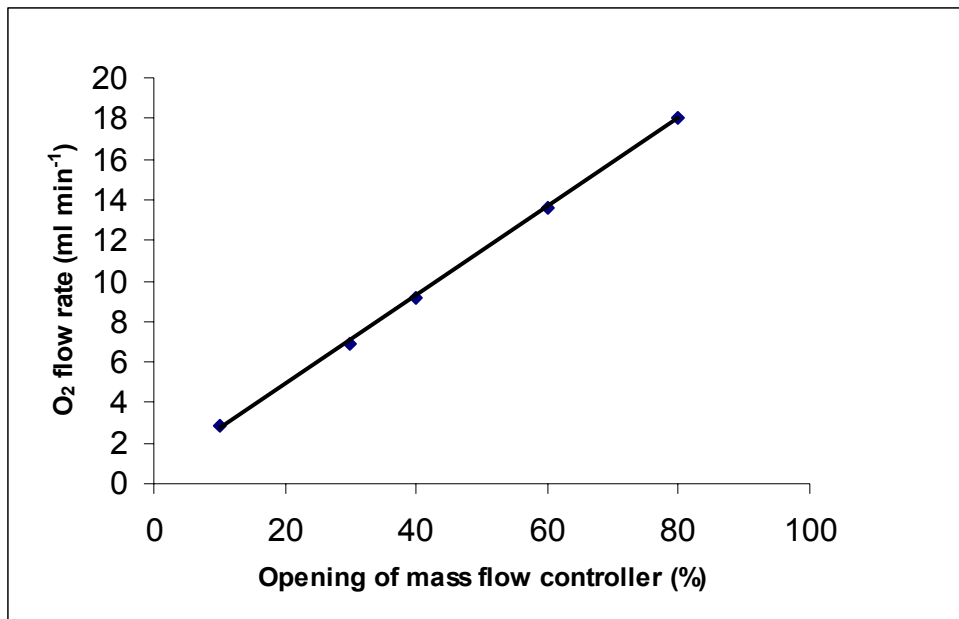
**Fig. 2.3.5**: Calibration of $O_2$ mass flow controller, channel 4 unit 2
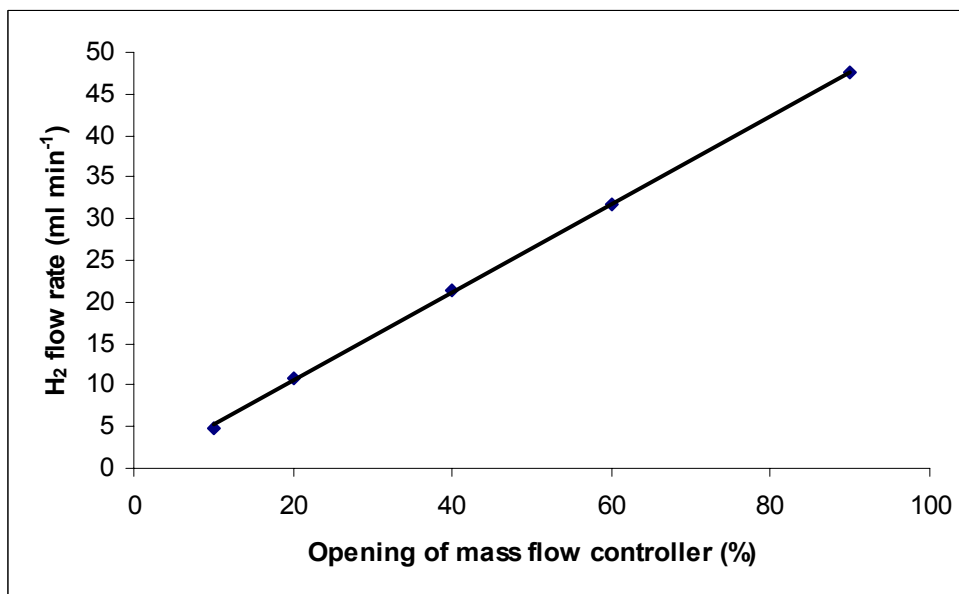


**Fig. 2.3.6**: Calibration of $H_2$ mass flow controller, channel 3 unit 2
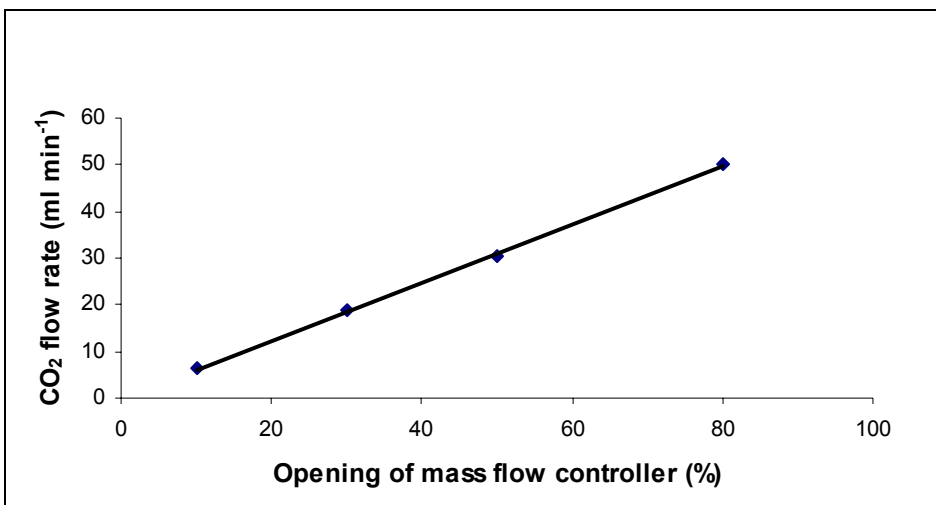
**Fig. 2.3.7**: Calibration of $CO_2$ mass flow controller

## 2.4. Calibration of the gas chromatograph detector (GCD)

### 2.4.1. Water Calibration

The calibration for water was performed to obtain moles of $H_2O$ produced from the reaction at a certain time and at a certain experimental conditions. This was done, by introducing a mixture of Ar, He, $H_2$ and $O_2$ with known flow rates and hence known molar flow rate to the Pd membrane reactor. The reactor was fixed at a certain temperature for example $150^o$ C. Once this mixture enters the reactor, a fast reaction between $H_2$ and $O_2$ was observed and the product of this reaction is $H_2O$. He was introduced as a diluent's while Ar was used as a standard for the calibration. The system was operated so that $H_2$ is always in excess and all $O_2$ is consumed and $5 < H_2/O_2$ (molar ratio) $< 20$ which is greater than the stoichiometric ratio of 2 according to the following reaction:

$$H_2 + 0.5O_2 \rightarrow H_2O$$

Based on the above reaction, at complete conversion of $O_2$, produced moles of $H_2O$ were found. The GCD analysis of the exit stream confirmed the total consumption of $O_2$ since no $O_2$ was detected in the exit stream other than the one already present in the

background of the GCD analysis. The inlet volumetric flow rate for each gas was obtained from the calibration of each mass flow controller. The inlet volumetric flow rate was converted to molar flow rate assuming ideal gas low where:

n = PV/RT

where P= 1atm, T = 298.15 K, R = 0.082 l atm mol$^{-1}$ K$^{-1}$, n = molar flow rate (mol min$^{-1}$), and V= inlet flow rate (ml min$^{-1}$). By plotting produced moles of $H_2O$ vs. $H_2O$/Ar (GCD area ratio), as can be seen in Figure 2.4.1.1, an equation was obtained, by linear fitting of the plot, which gives the produced moles of $H_2O$ as a function of the GCD area readings of $H_2O$ and Ar. This equation is:

$$H_2O\,(mol\ \ min^{-1}) = 0.0002 * \frac{H_2O\ \ GCD\ \ area}{Ar\ \ GCD\ \ area} + 2.0E - 5$$
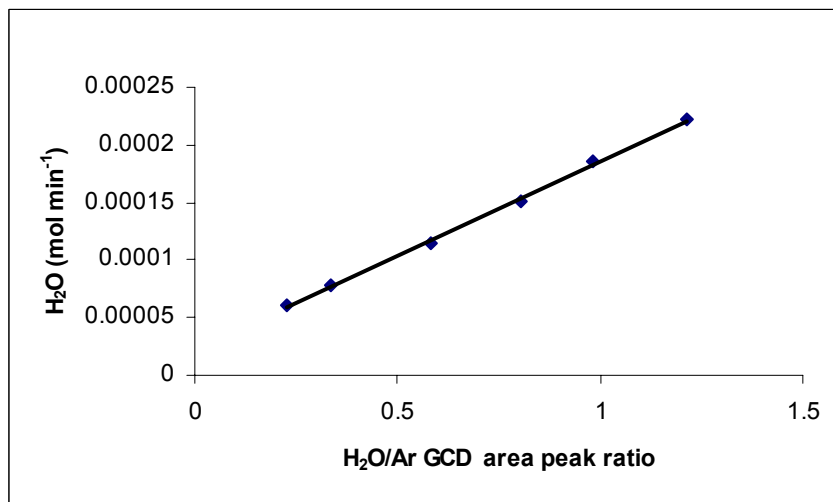


**Fig. 2.4.1.1**: Produced moles of $H_2O$ vs. $H_2O$/Ar area peak ratio from GCD

### 2.4.2.2. Benzene Calibration

Benzene was available in the form of a liquid. In order to obtain vapor benzene, He gas was bubbled into a saturator (bubbler) which contain liquid benzene. At the exit of the saturator, the gas stream will consist of He gas and vapor benzene. The fraction of

benzene in this stream is a function of temperature and He flow rate. Vapor pressure data are available in the literature [Perry]. A plot of benzene vapor pressure vs. temperature was constructed (Figure 2.4.2.1) and fitted to a polynomial fitting. This fitting equation was used to calculate benzene vapor pressure at the recorded room temperature which was usually in the range 19-25 $^{\circ}$C.

For benzene calibration a mixture of inlet flow rates of He, Ar, and benzene was injected to the GCD to obtain the area peak for each gas. The total flow rate of this mixture was kept constant while varying the inlet benzene and He. The inlet flow rate of benzene is plotted vs. the ratio of the area peak of benzene to Ar as is shown in Figure 2.4.2.2. The GCD area of benzene during experiments lies within the range of Benzene GCD area in Figure 2.4.2.2.
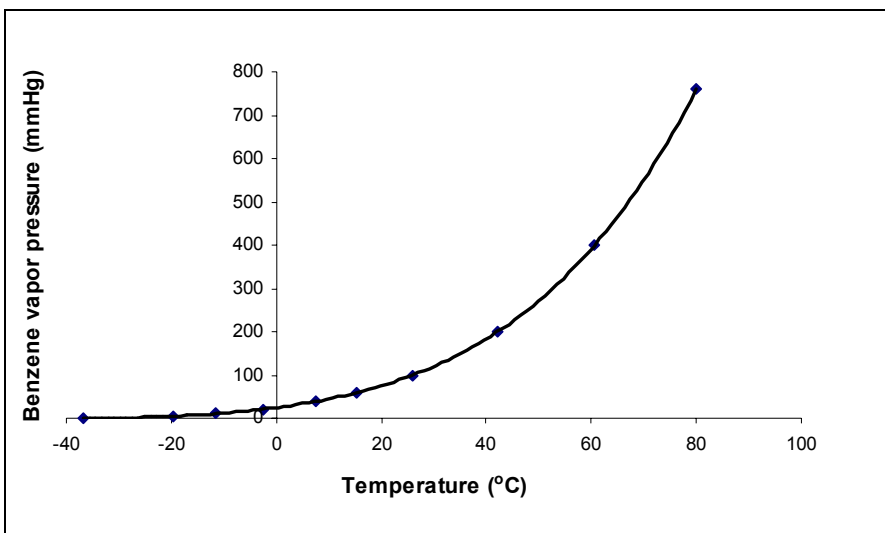


**Fig. 2.4.2.1**: Vapor pressure of benzene vs. temperature. Points are literature data, and curve is polynomial fitting of the data

27
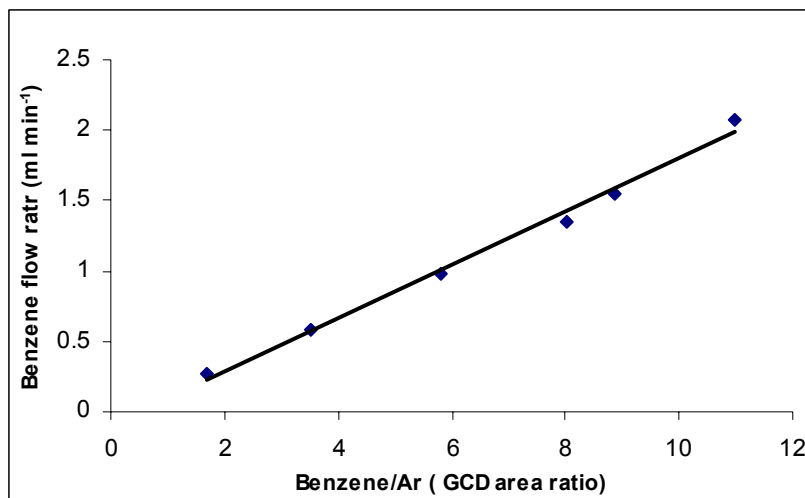
**Fig. 2.4.2.2**: Calibration of benzene, benzene flow rate vs. Benzene/Ar GCD area ratio

## 2.4.3. CO$_2$ respond factor with respect to benzene

The respond factor of CO$_2$ with respect to benzene was found experimentally to be 4.0. This value compares with the reported values by Lampe and compares well with the calculated values based on Fitch work based.

**Table 2.4.3.1:** CO$_2$ to Benzene respond factor

| CO$_2$:Benzene respond factor | Reference |
|---|---|
| 4.0 | Experimental measurement |
| 3.92 | Table I, column III, Lampe |
| 3.51 | Equation 2, Fitch |

## 2.4.4. O$_2$ calibration

Different mixtures of O$_2$, Ar, and He with know composition, were entered into the GCD system to obtain the GCD signal at these compositions. Figure 2.4.4.1 shows O$_2$ molar flow rate vs. the ratio of O$_2$/Ar GCD signal. The obtained molar flow rate was calculated based on ideal gas law at atmospherics pressure and room temperature.
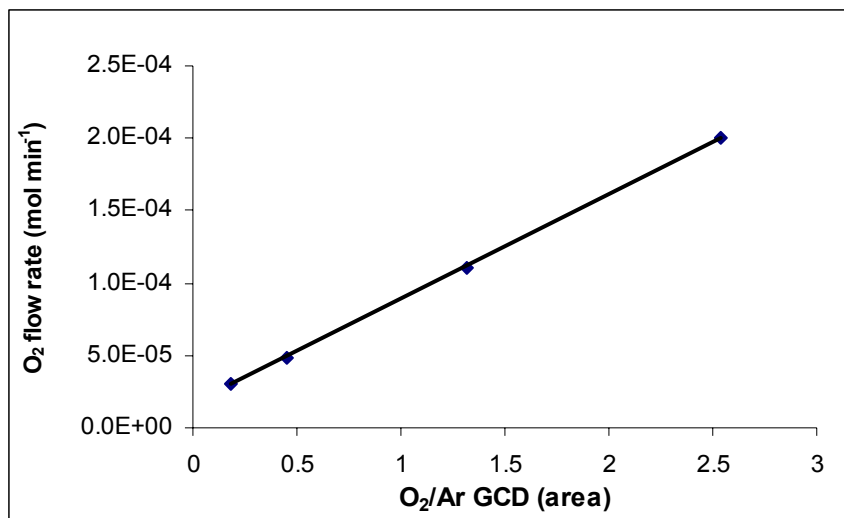
**Fig. 2.4.4.1**: $O_2$ molar flow rate vs. the ratio of $O_2/Ar$ GCD area at room temperature and atmospheric pressure

**2.4.5. Respond factor of the produced organic compounds with respect to benzene**

Respond factor of phenol, 1,4-cyclohexanedione, and catechol and cyclohexanone with respect to benzene were measured experimentally. The measured values of the respond factors for the previous compounds were close to unity. This was consistent with theoretical calculations of the respond factor and the reproted ones in Lampe [31] and Fitch [32] works. Respond factors of the other organic compounds that were produced from benzene reaction (hydroquinone, resorcinol, cyclohexanol, cyclohexanone, 2-hydroxy, cyclohexanone, 4-hydroxy, pentanoic acid, 4-oxo, and pentanoic acid) with respect to benzene were approximately one based on the calculations according to Lampe [31] and Fitch [32].

# 3. Results

## 3.1. Pd-membrane system:

### 3.1.1. Properties of the Pd –membrane before running reaction

A similar system to the system reported by Niwa *et al* was built to reproduce the reported data by this group. In Niwa *et al* work (2002) phenol was reported to be

produced from benzene in a one step using palladium membrane. Hydrogen was fed into a mixed gas stream of a substrate and oxygen through a metallic thin layer. Their membrane was prepared by coating a porous $\alpha$-alumina tube with a thin layer of palladium by means of metallic chemical vapor deposition technique. At $300^o$ C, the hydrogen and nitrogen permeation rates of their membranes were 1.0 to $3.0\times10^{-3}$ mol $m^{-2}$ $s^{-1}$ $Pa^{-0.5}$ (10.5 to 3.5 $m^3$ $m^{-2}$ h-1) and 0.1 to 1.0 X $10^{-10}$ mol $m^{-2}$ $s^{-1}$ $Pa^{-0.5}$ respectively [Niwa, 2002].

In our system, the unit's support was porous 316 L seamless stainless steel tube having an OD= O.25 " (6.35 mm), ID= 0.125" (3.175 mm) and nominal retention size 0.2 μm. The tube was cut into 42.5 mm long segment and welded to a dense stainless steel tubes with the same OD as the porous one. Porous part of this unit has 8.5 $cm^2$ permeable surface area. Palladium membrane 39.5 μm was formed on the outer side of the porous tube by electrolysis plating technique [30].

Hydrogen and nitrogen permeation rates of these membranes were 2-4 $m^3$ $m^{-2}$ $h^{-1}$ and 0.0005-0.001 $m^3$ $m^{-2}$ $h^{-1}$ respectively at atmospheric pressure difference and 350 $^o$C [30]. From experimental measurements, hydrogen permeation rate was 0.72 $m^3$ $m^{-2}$ $h^{-1}$ (1.22 ml $cm^{-2}$ $min^{-1}$) at $150^o$ C and 5 Psig pressure difference between the shell side and the tube side. Figure 3.1.1.1 shows the measured $H_2$ flux over time at 150 $^o$C and 5 Psig pressure difference.
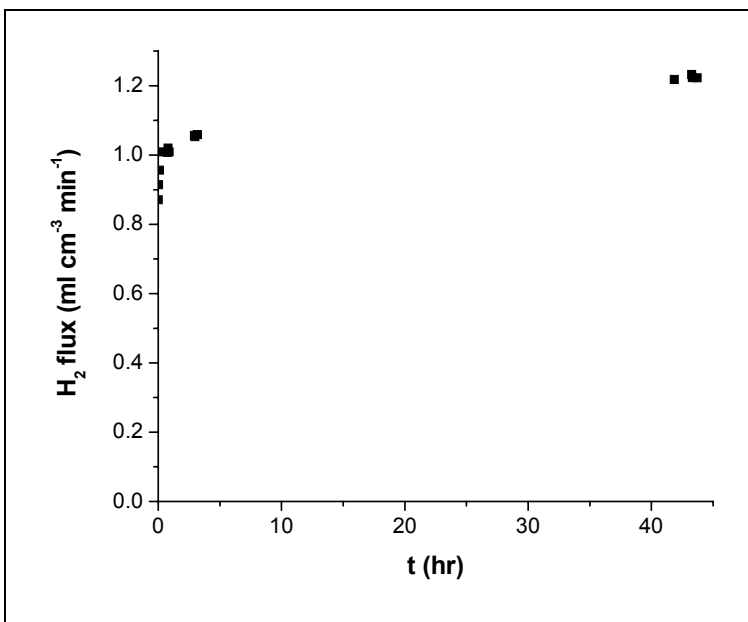
**Fig. 3.1.1.A**: $H_2$ flux vs. time at 150 °C and $\Delta P = 5$ psig before running reaction for Pd membrane

According to figure 3.1.1.1, $H_2$ flux was 1.22 ml cm$^{-2}$min$^{-1}$. He flux was 0.02 ml cm$^{-2}$ min$^{-1}$ before flowing $H_2$ and 0.12 after pressurizing the shell with $H_2$ at the same conditions of temperature and pressure (150 °C, Delta P =5 Psig). Therefore, the separation factor (defined as the ratio of $H_2$ flux to He flux) based on these fluxes was 61 and 12 before and after pressurizing the shell with $H_2$, respectively.

**3.1.2. Properties of the Pd –membrane after running all experiments**

Fluxes of He and $H_2$ from shell side to tube side were measured at 150 °C, the results are shown in Figures 3.1.2.1, 3.1.2.2, and 3.1.2.3. Figure 3.1.2.1 gives He flux vs. pressure difference before measuring $H_2$ flux. Figure 3.1.2.2 shows He flux after flowing $H_2$ to the reactor. Based on Figures 3.1.2.1 and 3.1.2.2, the separation factor (slope of Figure 3.1.2.2/slpoe of Figure 3.1.2.1) was 10.0, based on Figure 3.1.2.4 it was 9.0.
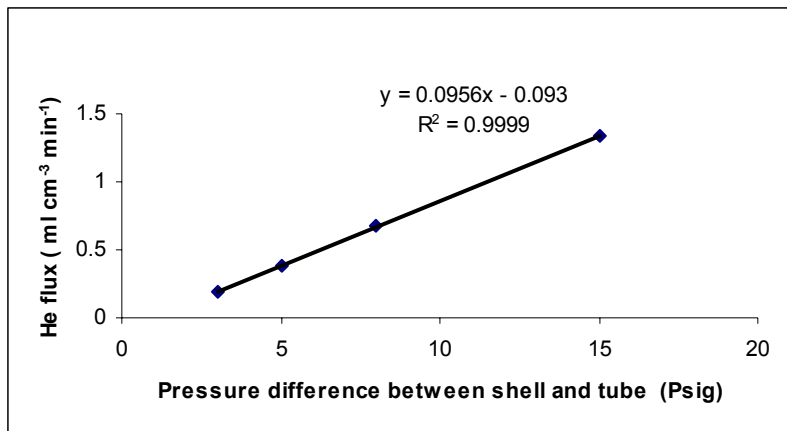
**Fig. 3.1.2.A**: He flux at $150^o$ C vs. pressure difference between shell and tube in the reactor before flowing $H_2$
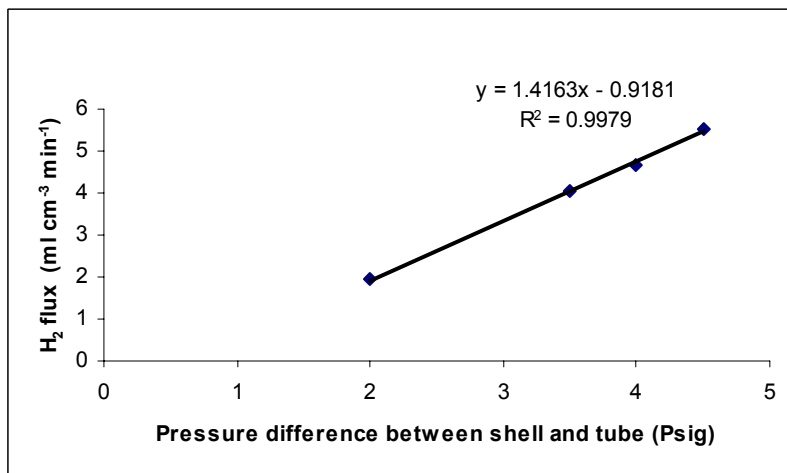


**Fig. 3.1.2.B**: $H_2$ flux at $150^o$ C vs. pressure difference between shell and tube in the reactor
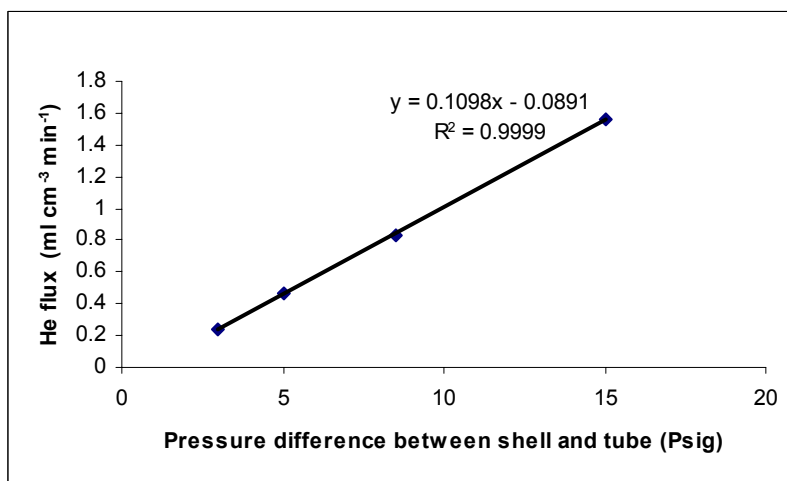


**Fig. 3.1.2.C**: He flux at $150^o$ C vs. pressure difference between shell and tube in the reactor after flowing $H_2$

He and $H_2$ fluxes were measured at 200 $^o$C. The results are shown in Figures 3.1.2.4 and 3.1.2.5. Based on these figure the separation factor was 10.2. The calculated value of the separation factor at 200$^o$ C was close to the calculated one at 150$^o$ C.
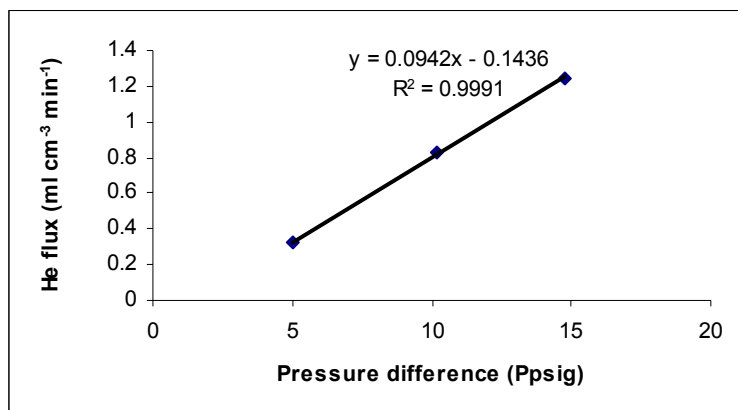


**Fig. 3.1.2.D**: He flux at 200$^o$ C vs. pressure difference between shell and tube in the reactor
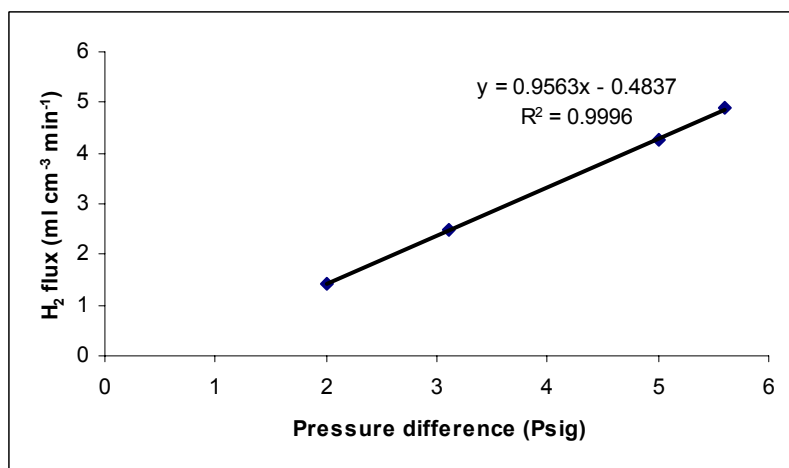


**Fig. 3.1.2.E**: $H_2$ flux at 200$^o$ C vs. pressure difference between shell and tube in the reactor

### 3.1.3. Results with Pd membrane (mixed and non-mixed gases)

### 3.1.3.1. Non-mixed gases

### 3.1.3.1.1. $H_2$ in the shell side

In order to reproduce the data presented in Figure 1.3.1 and Table 1.3.1, similar flow conditions were applied but they ended with low benzene to phenol conversion and selectivity. An example of a reaction mixture is given in Table 3.1.3.1.1.1.

**Table 3.1.3.1.1.1:** Conversion of Benzene, selectivity and produced moles of products at 150$^{\circ}$ C. Flow rates: shell; 14.1 ml min$^{-1}$ H$_2$, tube; 37.5 ml min$^{-1}$ (Benzene/O$_2$/He/Ar= 1.1/10.1/85.5/3.3 % of total flow rate) after 3 hours of starting reaction

| Product | Conversion % | Selectivity % | Produced moles/min |
|---|---|---|---|
| Phenol | 0.09 | 5.9 | 1.6E-8 |
| Cyclohexanone | 0.58 | 36.3 | 1.0E-7 |
| CO$_2$ | 0.93 | 57.8 | 9.6E-7 |
| 1,4-Cyclohexanedione | 0.0 | 0.0 | 0 |

**Table 3.1.3.1.1.2:** O$_2$ conversion and produced water at 150$^{\circ}$ C. Flow rates: shell, H$_2$, tube, 37.5 ml min$^{-1}$ (Benzene/O$_2$/He/Ar= 1.1/10.1/85.5/3.55 % of total flow rate). After 3 hr of starting reaction

| | |
|---|---|
| O$_2$ total conversion % | 79.0 |
| O$_2$ conversion to water % | 77.0 |
| H$_2$O produced, mole/min | 2.4E-4 |

He flux was 0.18 mlcm$^{-2}$min$^{-1}$ before reaction and 0.22 mlcm$^{-2}$min$^{-1}$ after reaction. H$_2$ flux was 1.22 mlcm$^{-2}$min$^{-1}$ before reaction and 1.7 mlcm$^{-2}$min$^{-1}$ after reaction (for 4 psig, couldn't pressurize more than that). A new mixture has been tested with the flow conditions and results shown in Tables 3.1.3.1.1.3 and 3.1.3.1.1.4.

**Table 3.1.3.1.1.3**: Conversion of Benzene, selectivity and produced moles of products at 150$^{\circ}$ C. Flow rates: shell, 14.1 ml min$^{-1}$ H$_2$, tube, 37 ml min$^{-1}$ (Benzene/O$_2$/He/Ar= 4.5/21.0/71.2/3.3 % of total flow rate) after 7 hours of reaction. New gas mixture

| Product | Conversion % | Selectivity % | Produced moles/min |
|---|---|---|---|
| Phenol | 1.3 | 35.6 | 7.3E-7 |
| Cyclohexanone | 0.3 | 10.5 | 2.1E-7 |
| CO$_2$ | 1.5 | 53.9 | 6.5E-6 |

**Table 3.1.3.1.1.4**: O$_2$ conversion and produced water at 150$^{\circ}$ C, 37.5 ml min$^{-1}$. Flow rates: shell, 14.1 ml min$^{-1}$ H$_2$, tube, 37 ml min$^{-1}$ (Benzene/O$_2$/He/Ar= 4.5/21.0/71.2/3.3 % of total flow rate)

| | |
|---|---|
| O$_2$ total conversion % | 65.0 |
| O$_2$ conversion to water % | 61.0 |
| H$_2$O produced, mole/min | 3.9 E-4 |

As O$_2$ was entered into the system, the pressure in H$_2$ side dropped and T increased from 150$^{\circ}$ C to 177$^{\circ}$ C. He flux was 0.25 ml cm$^{-2}$ min$^{-1}$ after reaction and 0.22 mlcm$^{-2}$min$^{-1}$ before reaction so the membrane is still good.

### 3.1.3.1.2. $H_2$ in the tube side

The directions of flow were reversed with $H_2$ being in the tube side and the remaining reaction mixture (benzene, He, Ar, and $O_2$) being flowed to the shell side. The results for one set of flow conditions are shown in Tables 3.1.3.1.2.1 and 3.1.3.1.2.2

**Table 3.1.3.1.2.1**: Conversion of Benzene, selectivity and produced moles of products at 150$^o$ C. Flow rates: tube; 14.1 ml min$^{-1}$ $H_2$, shell; 37 ml min$^{-1}$ (Benzene/$O_2$/He/Ar= 4.5/21.0/71.2/3.3 % of total flow rate). Up to 1.7 hr of reaction

| Product | Conversion % | Selectivity % | Produced moles/min |
|---|---|---|---|
| Phenol | 1.35 | 60.8 | 9.6E-7 |
| Cyclohexanone | 0.58 | 26.1 | 4.1E-7 |
| $CO_2$ | 0.16 | 7.2 | 6.8E-7 |
| Cyclohexanone,2-hydroxy | 0.08 | 3.6 | 5.9E-8 |
| 1,4-Cyclohexanedione | 0.05 | 2.1 | 3.4E-8 |

**Table 3.1.3.1.2.2**: $O_2$ conversion and produced water at 150$^o$ C. Flow rates: tube; 14.1 ml min$^{-1}$ $H_2$, shell; 37 ml min$^{-1}$ (Benzene/$O_2$/He/Ar= 4.5/21.0/71.2/3.3 % of total flow rate)

| | |
|---|---|
| $O_2$ total conversion % | 43.3 |
| $O_2$ conversion to water % | 43.0 |
| $H_2O$ produced, mole/min | 2.8E-4 |

The results after seven hours are shown in   Tables 3.1.3.2.3 and 3.1.3.1.2.4.

**Table 3.1.3.1.2.3**: Conversion of Benzene, selectivity and produced moles of products at 150$^o$ C. Flow rates: tube; 14.1 ml min$^{-1}$ $H_2$, shell; 37 ml min$^{-1}$ (Benzene/$O_2$/He/Ar= 4.5/21.0/71.2/3.3 % of total flow rate). Up to 7.3 hr of reaction

| Product | Conversion % | Selectivity % | Produced moles/min |
|---|---|---|---|
| Phenol | 1.6 | 57.3 | 1.1E-6 |
| Cyclohexanone | 0.58 | 22.8 | 4.5E-7 |
| $CO_2$ | 0.16 | 6.3 | 7.4E-7 |
| Cyclohexanone,2-hydroxy | 0.24 | 9.4 | 1.9E-7 |
| 1,4-Cyclohexanedione | 0.09 | 3.5 | 6.9E-8 |
| Catechol | 0.02 | 0.8 | 1.6E-8 |

**Table 3.1.3.1.2.4**: $O_2$ conversion and produced water at 150$^o$ C. Flow rates: tube; 14.1 ml min$^{-1}$ $H_2$, shell; 37 ml min$^{-1}$ (Benzene/$O_2$/He/Ar= 4.5/21.0/71.2/3.3 % of total flow rate).After 7.3 hr

| | |
|---|---|
| $O_2$ total conversion % | 44.0 |
| $O_2$ conversion to water % | 43.6 |
| $H_2O$ produced, mole/min | 2.8E-4 |

A similar reaction mixture to the one in Table 3.1.3.1.2.1 was used and the results are shown in Figures 3.1.3.1.2.1, 3.1.3.1.2.2, and 3.1.3.1.2.3. Tables 3.1.3.1.2.5, .6, and .7 summarize the final results in Figures 3.1.3.1.2.1, 3.1.3.1.2.2, and 3.1.3.1.2.3, respectively.
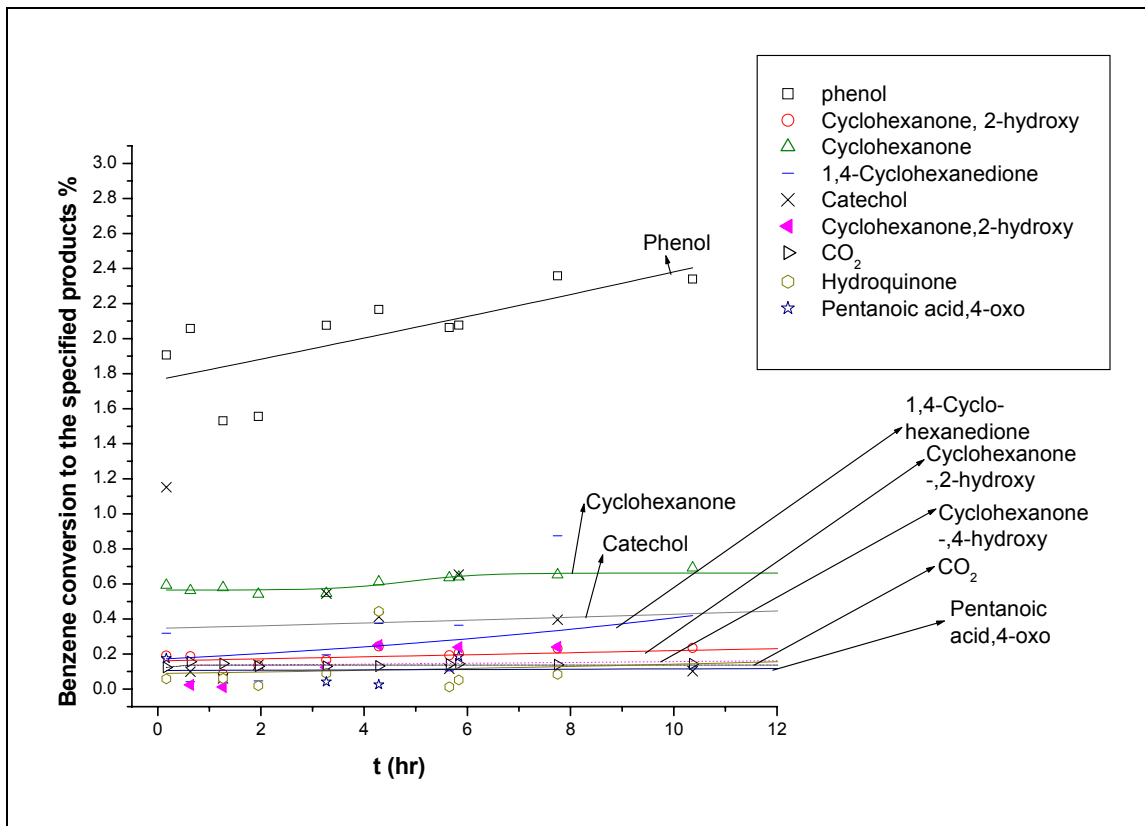


**Fig. 3.1.3.1.2.1**: Conversion of Benzene to the individual products vs. time of reaction at 150 $^o$C. Flow rates: tube; 14.1 ml min$^{-1}$ H$_2$, shell; 37.0 ml min$^{-1}$ (Benzene/O$_2$/He/A r= 5.0/21.0/71.0/3.3 % of total flow rate)
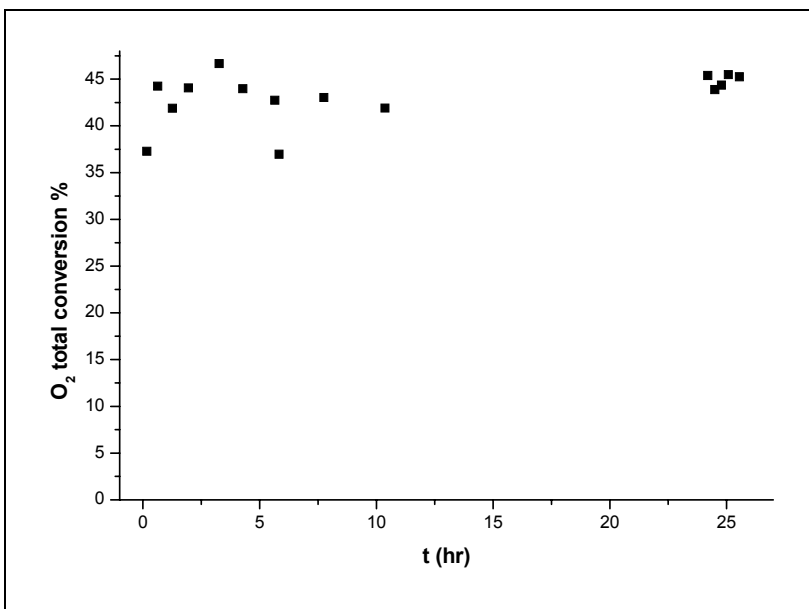
**Fig. 3.1.3.1.2.2**: Total conversion of benzene vs. time of reaction at $150^o$ C. Flow rates: tube; 14.1 ml min$^{-1}$ H$_2$, shell; 37.0 ml min$^{-1}$ (Benzene/O$_2$/He/Ar= 5.0/21.0/71.0/3.3 % of total flow rate)
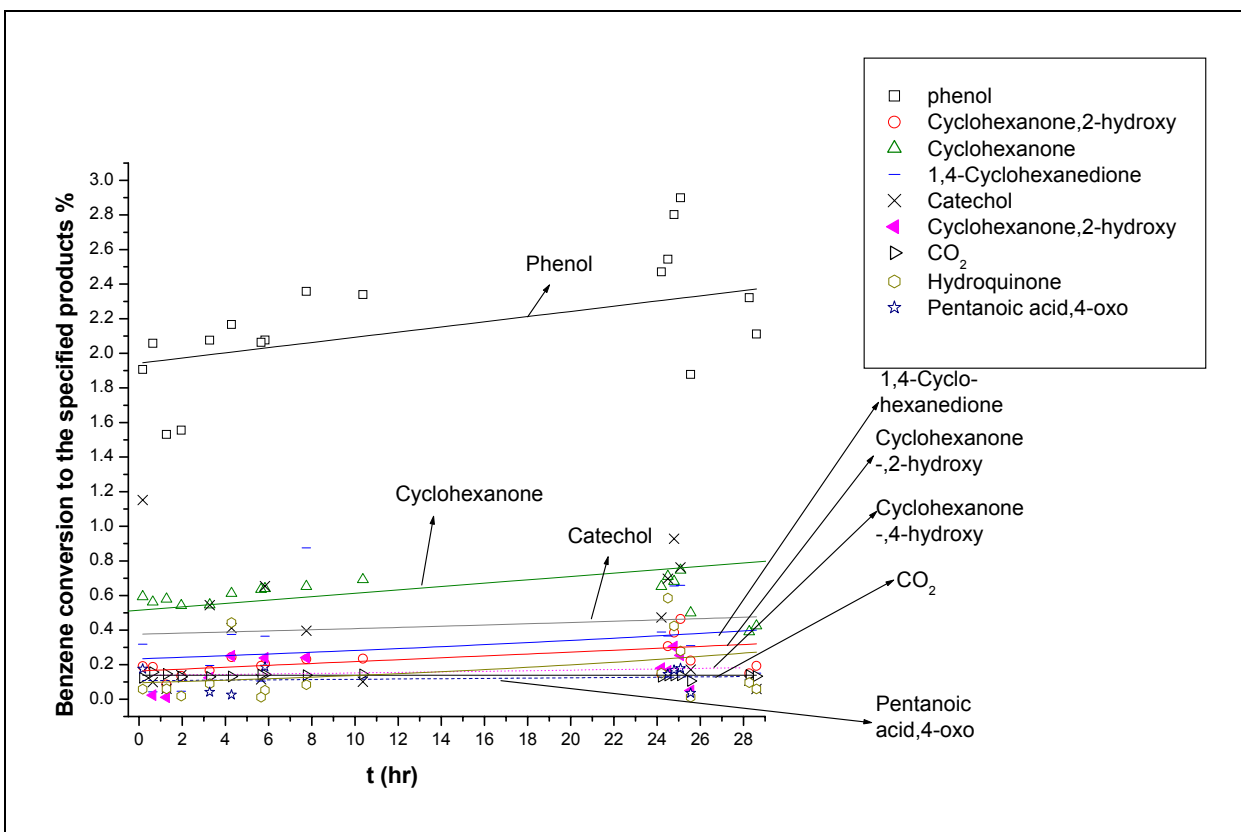


**Fig. 3.1.3.1.2.3**: Conversion of Benzene to the individual products vs. time of reaction at 150 $^o$C. Flow rates: tube; 14.1 ml min$^{-1}$ H$_2$, shell; 37.0 ml min$^{-1}$ (Benzene/O$_2$/He/Ar= 5.0/21.0/71.0/3.3 % of total flow rate). Same flow conditions as in figure 1, but for longer reaction time

**Table 3.1.3.1.2.5**: A Summary of the results in Figure 3.1.3.1.2.1. Conversion of Benzene to the individual products at 150 $^o$C. Flow rates: tube; 14.1 ml min$^{-1}$ H$_2$, shell; 37.0 ml min$^{-1}$ (Benzene/O$_2$/He/Ar= 5.0/21.0/71.0/3.3 % of total flow rate)

| Product | Conversion % | Selectivity % | Produced moles/min |
|---|---|---|---|
| Phenol | 2.3 | 64.3 | 2.0E-6 |
| Cyclohexanone | 0.69 | 19.0 | 5.9E-7 |
| CO$_2$ | 0.14 | 3.9 | 7.3E-7 |
| Cyclohexanone,2-hydroxy | 0.23 | 6.5 | 2.0E-7 |
| 1,4-Cyclohexanedione | 0.13 | 3.5 | 1.1E-7 |
| Cyclohexanone, 4-hydroxy | 0 | | |
| Catechol | 0.1 | 2.8 | 8.6E-8 |
| Hydroquinone | 0.0 | 0 | 0 |
| Resorcinol | 0.0 | | |
| Pentanoic acid, 4-oxo | 0.0 | | |

**Table 3.1.3.1.2.6**: A Summary of the results in Figure 4.1.3.1.2.2. O$_2$ conversion and produced water at 150 $^o$C. Flow rates: tube; 14.1 ml min$^{-1}$ H$_2$, shell; 37.0 ml min$^{-1}$ (Benzene/O$_2$/He/Ar= 5.0/21.0/71.0/3.3 % of total flow rate)

| | |
|---|---|
| O$_2$  total conversion % | 42.0 |
| O$_2$  conversion to water % | 41.5 |
| H$_2$O produced, mole/min | 2.6E-4 |

**Table 3.1.3.1.2.7:** A Summary of the results in Figure 3.1.3.1.2.3. Conversion of Benzene to the individual products at 150 $^o$C: tube; 14.1 ml min$^{-1}$ H$_2$, shell; 37.0 ml min$^{-1}$ (Benzene/O$_2$/He/Ar= 5.0/21.0/71.0/3.3 % of total flow rate)

| Product | Conversion % | Selectivity % | Produced moles/min |
|---|---|---|---|
| Phenol | 2.1 | 67.4 | 1.7E-6 |
| Cyclohexanone | 0.42 | 13.6 | 3.5E-7 |
| CO$_2$ | 0.13 | 4.3 | 6.6E-7 |
| Cyclohexanone,2-hydroxy | 0.20 | 6.2 | 1.6E-7 |
| 1,4-Cyclohexanedione | 0.15 | 4.8 | 1.2E-7 |
| Cyclohexanone, 4-hydroxy | 0 | | |
| Catechol | 0.06 | 1.9 | 4.9E-8 |
| Hydroquinone | 0.06 | 1.9 | 4.9E-8 |
| Resorcinol | 0.0 | | |
| Pentanoic acid, 4-oxo | 0.0 | | |

**Table 3.1.3.1.2.8**: A Summary of the results in Figure 3.1.3.1.2.2 after 28 hrs of reaction. $O_2$ conversion and produced water at 150 °C. Flow rates: tube; 14.1 ml min$^{-1}$ $H_2$, shell; 37.0 ml min$^{-1}$ (Benzene/$O_2$/He/Ar= 5.0/21.0/71.0/3.3 % of total flow rate)

| | |
|---|---|
| $O_2$ total conversion % | 41.0 |
| $O_2$ conversion to water % | 40.0 |
| $H_2O$ produced, mole/min | 2.5E-4 |

### 3.1.3.1.2.1. Varying $H_2$ flow to the tube

Other flow conditions were applied in order to explore the effects of changing $O_2$, benzene. And hydrogen flow rates on the produced amounts of phenol. Also the temperature was increased to 200 °C. Tables 3.1.3.1.2.1.1 and 3.1.3.1.2.1.2 summarize the results for increasing $H_2$ flow rate in the tube side. Then $H_2$ flow rate to the tube was reduced and the results are given in Tables 3.1.3.1.2.1.3 and 3.1.3.1.2.1.4.

**Table 3.1.3.1.2.1.1:** Conversion of Benzene to the individual products at 150 °C. Flow rates: tube; 21.2 ml min$^{-1}$ $H_2$, shell; 37.0 ml min$^{-1}$ (Benzene/$O_2$/He/Ar= 5.1/21.0/71.1/3.3 % of total flow rate)

| Product | Conversion % | Selectivity % | Produced moles/min |
|---|---|---|---|
| Phenol | 1.9 | 57.1 | 1.5E-6 |
| Cyclohexanone | 0.5 | 15.2 | 3.9E-7 |
| $CO_2$ | 0.11 | 3.2 | 5.0E-7 |
| Cyclohexanone,2-hydroxy | 0.22 | 6.8 | 2.4E-7 |
| 1,4-Cyclohexanedione | 0.31 | 9.4 | 2.4E-7 |
| Cyclohexanone, 4-hydroxy | 0.05 | 1.5 | 4.0E-8 |
| Catechol | 0.17 | 5.1 | 1.3E-7 |
| Hydroquinone | 0.01 | 0.4 | 9.5E-9 |
| Resorcinol | 0.0 | | |
| Pentanoic acid, 4-oxo | 0.04 | 1.0 | 2.8E-8 |

**Table 3.1.3.1.2.1.2**: $O_2$ conversion and produced water at 150 °C. Flow rates: tube; 21.2 ml min$^{-1}$ $H_2$, shell; 37.0 ml min$^{-1}$ (Benzene/$O_2$/He/Ar= 5.1/21.0/71.1/3.3 % of total flow rate)

| | |
|---|---|
| $O_2$ total conversion % | 45.3 |
| $O_2$ conversion to water % | 44.8 |
| $H_2O$ produced, mole/min | 2.5E-4 |

**Table 3.1.3.1.2.1.3**: Conversion of Benzene to the individual products at 150 $^{\circ}$C. Flow rates: tube; 11.7 ml min$^{-1}$ H$_2$, shell; 37.0 ml min$^{-1}$ (Benzene/O$_2$/He/Ar= 5.3/21.0/71.0/3.3 % of total flow rate)

| Product | Conversion % | Selectivity % | Produced moles/min |
|---|---|---|---|
| Phenol | 2.1 | 67.4 | 1.7E-6 |
| Cyclohexanone | 0.42 | 13.6 | 3.5E-7 |
| CO$_2$ | 0.13 | 4.3 | 6.6E-7 |
| Cyclohexanone,2-hydroxy | 0.20 | 6.2 | 1.6E-7 |
| 1,4-Cyclohexanedione | 0.15 | 4.8 | 1.2E-7 |
| Cyclohexanone, 4-hydroxy | 0.0 | 0.0 | 0.0 |
| Catechol | 0.06 | 1.9 | 4.9E-8 |
| Hydroquinone | 0.06 | 1.9 | 4.9E-8 |
| Resorcinol | 0.0 | 0.0 | 0.0 |
| Pentanoic acid, 4-oxo | 0.0 | 0.0 | 0.0 |

**Table 3.1.3.1.2.1.4**: O$_2$ conversion and produced water at 150$^{\circ}$ C. Flow rates: tube; 11.7 ml min$^{-1}$ H$_2$, shell; 37.0 ml min$^{-1}$ (Benzene/O$_2$/He/Ar= 5.1/21.0/71.1/3.3 % of total flow rate)

| | |
|---|---|
| O$_2$ total conversion % | 41.0 |
| O$_2$ conversion to water % | 40.0 |
| H$_2$O produced, mole/min | 2.5E-4 |

### 3.1.3.1.2.2. Varying O$_2$ flow to the shell

O$_2$ flow rate to the shell side of the reactor was varied and the results are shown in Figure 3.1.3.1.2.2.1.
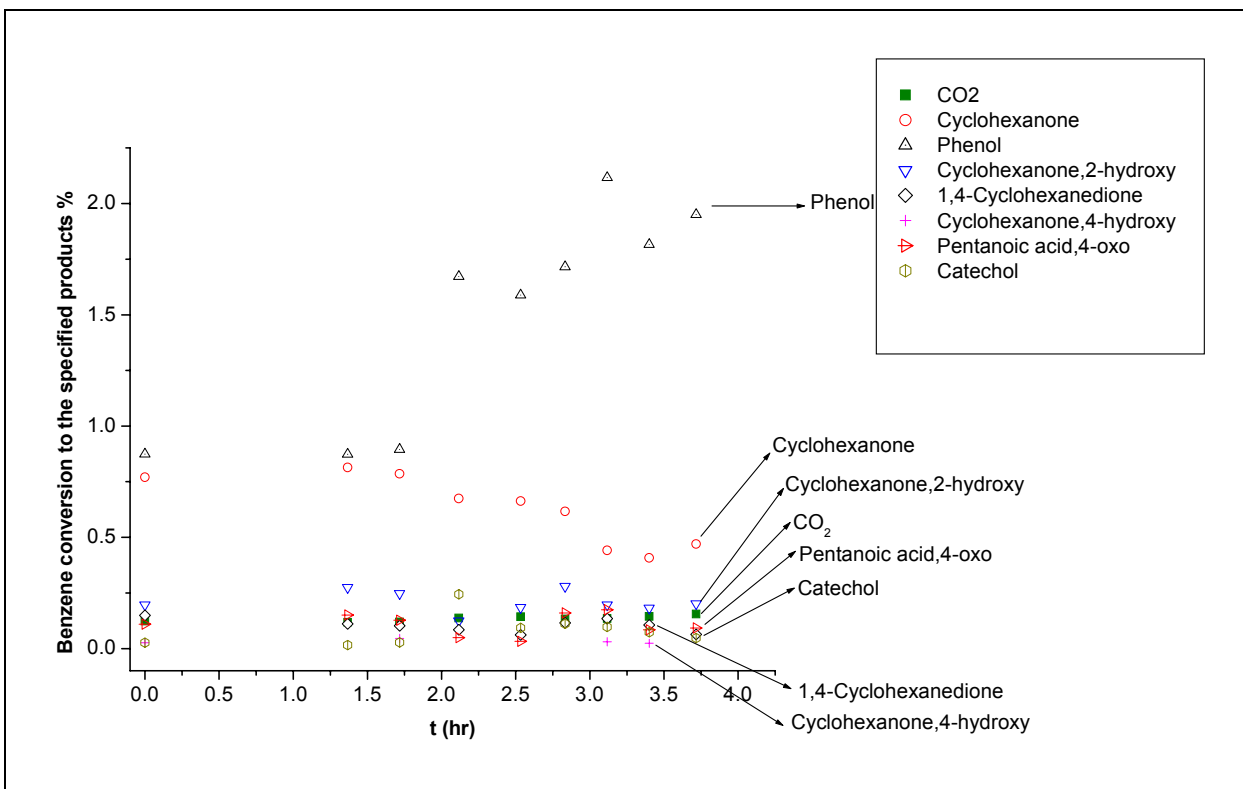
**Fig. 3.1.3.1.2.2.1**: Conversion of Benzene to the individual products vs. time of reaction at 150 $^{\circ}$C using different $O_2$ flow rates to the shell. 1) 0-1.8 hr: Flow rates: tube; 14.1 ml min$^{-1}$ $H_2$, shell; 36.5 ml min$^{-1}$ (Benzene/$O_2$/He/Ar= 5.5/10.5/81.0/3.0 % of total flow rate). 2) 2-3 hr: Flow rates: tube; 14.1 ml min$^{-1}$ $H_2$, shell; 37.0 ml min$^{-1}$ (Benzene/$O_2$/He/Ar= 5.3/20.0/72.0/3.3 % of total flow rate).   3): 3-4 hr: Flow rates: tube; 14.1 ml min$^{-1}$ $H_2$, shell; 37.5 ml min$^{-1}$ (Benzene/$O_2$/He/Ar= 5.1/30.5/61.0/3.4 % of total flow rate)

## 3.1.3.2. Mixed gases (all gases flow to the shell side)

A new method for introducing the reactants to the shell was applied where all the reactants including $H_2$ were fed directly to the shell side. The results for one flow conditions after 8 hours of reaction, with no flow to the tube side, are presented in Figure 3.1.3.2.1, 4.1.3.2.2, and 3.1.3.2.3. Figure 3.1.3.1 shows the conversion of benzene to each specified product, Figure 3.1.3.2.2 shows the produced moles of the detected products, and Figure 3.1.3.2.3 shows the selectivity of each product defined as the moles produced from the specified products divided by the moles of all other products from benzene reaction. Conversion of benzene to each specified product means how many moles of benzene have been converted to each specified product. Therefore, total conversion of

41

benzene will be the sum of conversions for all the specified products. A summary of benzene conversion, product selectivity, and produced moles of each product by the end of reaction time, based on the results shown in Figures 3.1.3.2.1, 3.1.3.2.2, and 3.1.3.2.3, is given in Table 3.1.3.2.1. Table 3.1.3.2.2 gives total conversion of benzene for the flow conditions given in Figure 3.1.3.2.1 along with the produced moles of water. Conversion of oxygen was calculated based on the produced moles of water and carbon dioxide along with the existing amount of oxygen from the reactor. Oxygen converted to the organic products was neglected since their amounts were smaller than the amount of produced water, beside the stoichiometry of oxygen in these reactions is not available.
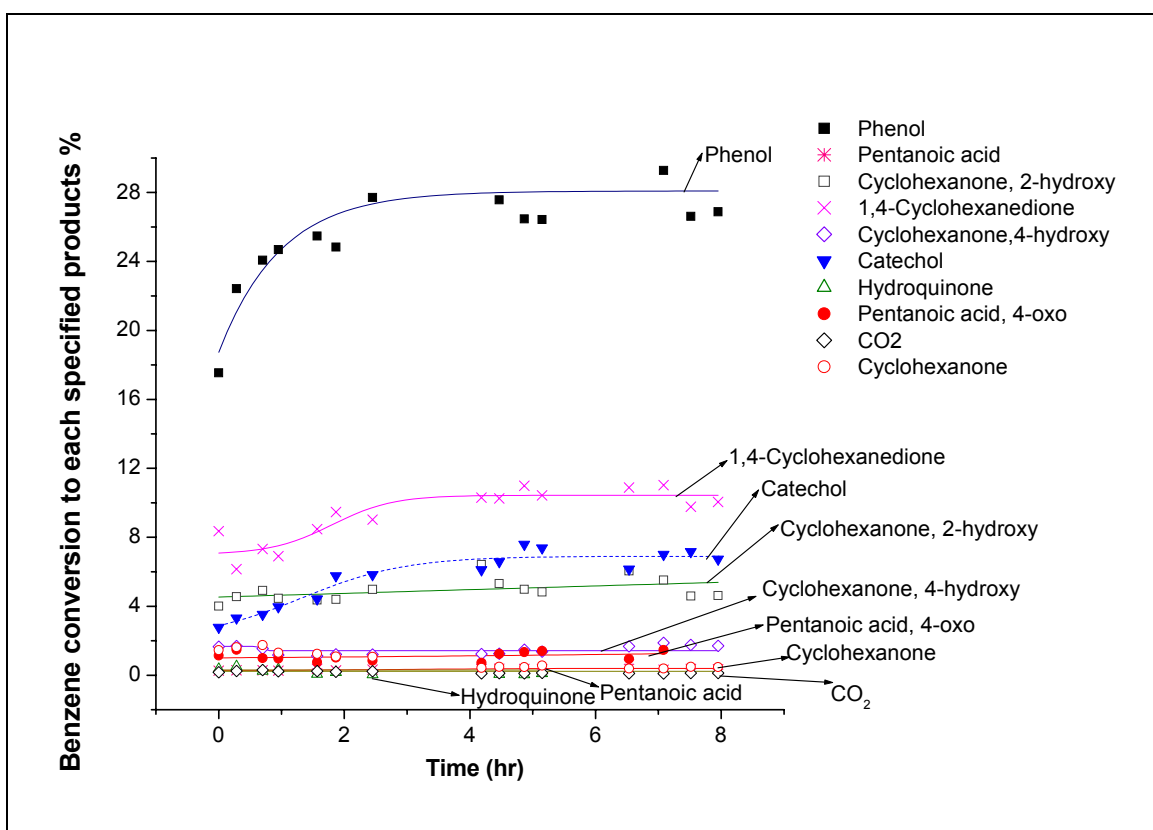


**Fig. 3.1.3.2.1**: Conversion of Benzene to the individual products at 150 °C. Flow rate to the shell: 43.3 ml min⁻¹ ($H_2$/Benzene/$O_2$/He/Ar = 34.0/4.1/17.9/41.0/3.18 % of total flow rate). ($O_2$/($O_2$+$H_2$)) = 34.4% (molar ratio)

42
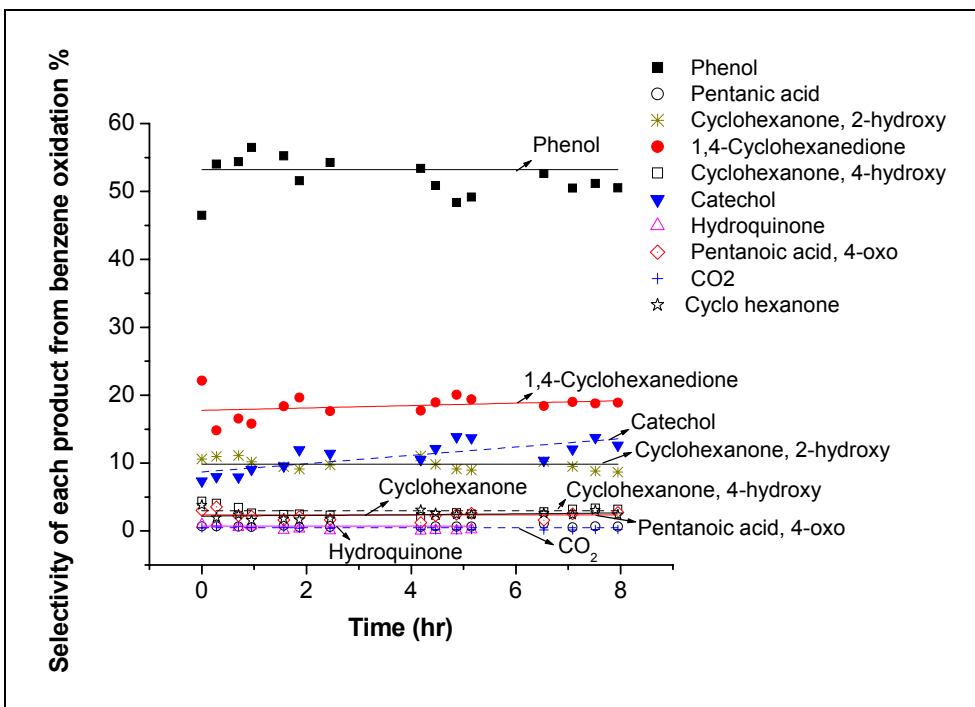
**Fig. 3.1.3.2.2**: Selectivity of Benzene to the individual products at 150 $^{\circ}$C. Flow rate to the shell: 43.3 ml min$^{-1}$ (H$_2$/Benzene/O$_2$/He/Ar = 34.0/4.1/17.9/41.0/3.18 % of total flow rate). (O$_2$/(O$_2$+H$_2$)) = 34.4% (molar ratio)
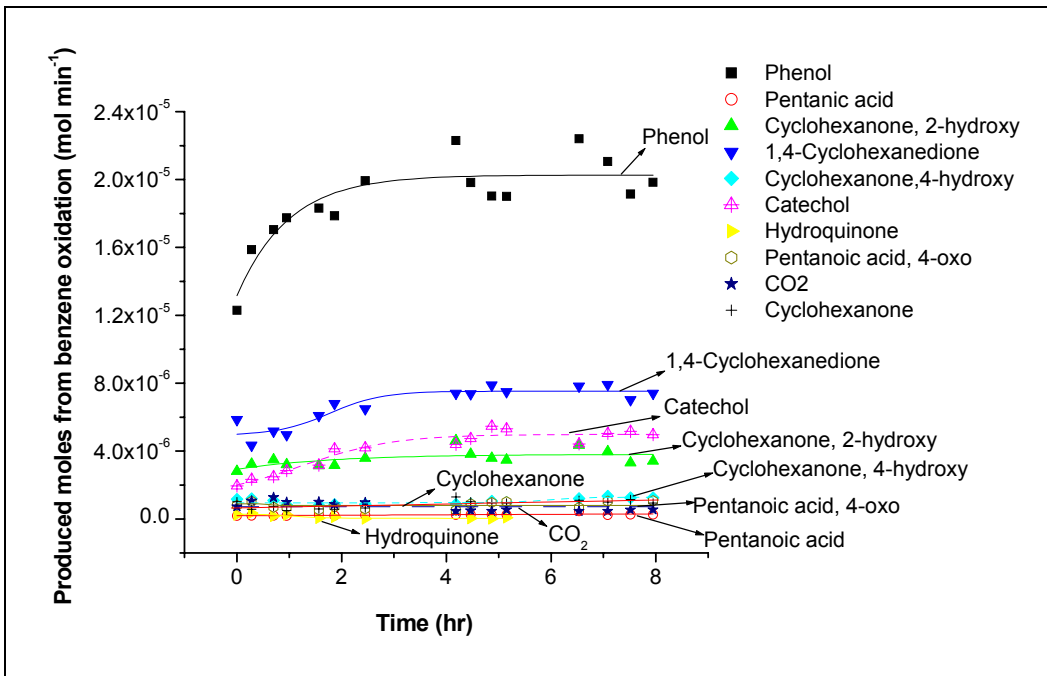


**Fig. 3.1.3.2.3**: Produced moles for products from benzene oxidation at 150 $^{\circ}$C. Flow rate to the shell: 43.3 ml min$^{-1}$ (H$_2$/Benzene/O$_2$/He/Ar = 34.0/4.1/17.9/41.0/3.18 % of total flow rate). (O$_2$/(O$_2$+H$_2$)) = 34.4% (molar ratio)

**Table 3.1.3.2.1**: Summary of the final results in Figures 3.1.3.2.1, 3.1.3.2.2, and 3.1.3.3. Flow rate to the shell: 43.3 ml min$^{-1}$ ($H_2$/Benzene/$O_2$/He/Ar= 34.0/4.1/17.9/41.0/3.18 % of total flow rate). ($O_2$/($O_2$+$H_2$))= 34.4% (molar ratio) after 8 hours of reaction

| Product | Conversion % | Selectivity % | Produced moles/min |
|---|---|---|---|
| Phenol | 27.0 | 50.5 | 2.0E-5 |
| Cyclohexanone | 1.3 | 2.4 | 9.4E-7 |
| $CO_2$ | 0.123 | 0.23 | 5.4E-7 |
| Cyclohexanone,2-hydroxy | 4.6 | 8.7 | 3.4E-6 |
| 1,4-Cyclohexanedione | 10.1 | 19.0 | 7.4E-6 |
| Cyclohexanone, 4-hydroxy | 1.7 | 3.2 | 1.3E-6 |
| Catechol | 6.8 | 12.7 | 5.0E-6 |
| Hydroquinone | 0 | | |
| Resorcinol | 0 | | |
| Pentanoic acid | 0.35 | 0.7 | 2.6E-7 |
| Pentanoic acid, 4-oxo | 1.5 | 2.7 | 1.1E-6 |

**Table 3.1.3.2.2:** $O_2$ conversion and produced water at 150$^{\circ}$ C. Flow rate to the shell: 43.3 ml min$^{-1}$ ($H_2$/Benzene/$O_2$/He/Ar= 34.0/4.1/17.9/41.0/3.18 % of total flow rate). ($O_2$/($O_2$+$H_2$))= 34.4% (molar ratio) after 8 hours of reaction

| $O_2$ total conversion % | 83.0 |
|---|---|
| $O_2$ conversion to water % | 82.0 |
| $H_2O$ produced, mole/min | 4.6E-4 |

The experiment, with the flow condition given by Figure 3.1.3.2.1, was run for 18 hours to investigate the oxidation of benzene after such a long time and compare the results with the ones given in Figure 3.1.3.2.1. Figure 3.1.3.2.4 shows benzene conversion to each specified product over 18 hours of reaction time. The summary of benzene conversion to each product, selectivity of each product and produced moles of each product is given in Table 31.3.2.3. Oxygen conversion was similar to the one in Table 3.1.3.2.2.
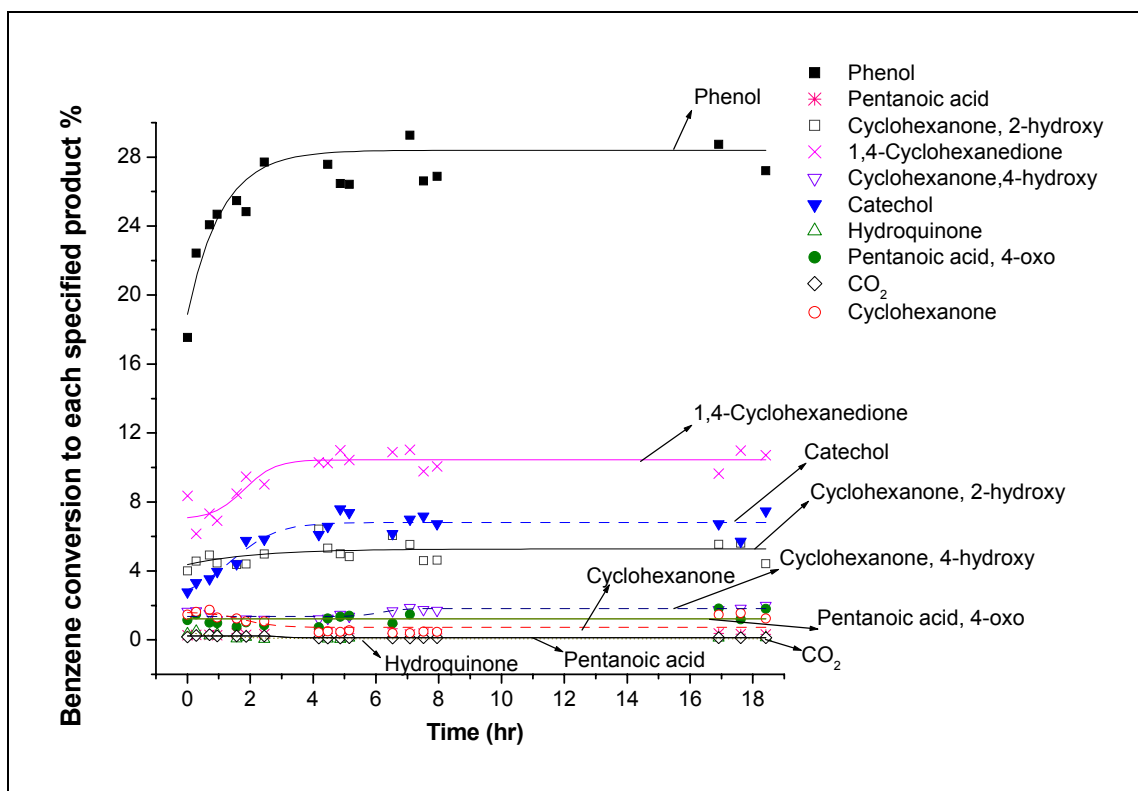
**Fig. 3.1.3.2.4**: Conversion of Benzene to the individual products at 150 $^o$C. Flow rate to the shell: 43.3 ml min$^{-1}$ (H$_2$/Benzene/O$_2$/He/Ar = 34.0/4.1/17.9/41.0/3.18 % of total flow rate). (O$_2$/(O$_2$+H$_2$)) = 34.4% (molar ratio) after 18 hours of reaction

**Table 3.1.3.2.3**: Summary of the final results in Figure 4.1.3.2.2. Flow rate to the shell: 43.3 ml min$^{-1}$ (H$_2$/Benzene/O$_2$/He/Ar= 34.0/4.1/17.9/41.0/3.18 % of total flow rate). (O$_2$/(O$_2$+H$_2$))= 34.4% (molar ratio) after 18 hours of reaction

| Product | Conversion % | Selectivity % | Produced moles/min |
|---|---|---|---|
| Phenol | 27.0 | 49.1 | 2.0E-5 |
| Cyclohexanone | 1.2 | 2.2 | 9.2E-7 |
| CO$_2$ | 0.129 | 0.23 | 5.8E-7 |
| Cyclohexanone,2-hydroxy | 4.4 | 8.0 | 3.3E-6 |
| 1,4-Cyclohexanedione | 10.7 | 19.3 | 8.0E-6 |
| Cyclohexanone, 4-hydroxy | 2.0 | 3.6 | 1.5E-6 |
| Catechol | 7.5 | 13.5 | 5.6E-6 |
| Hydroquinone | 0.1 | 0.22 | 9.2E-8 |
| Resorcinol | 0 | | |
| Pentanoic acid | 0.31 | 0.56 | 2.3E-7 |
| Pentanoic acid, 4-oxo | 1.8 | 2.7 | 1.3E-6 |

### 3.1.3.2.1. Mixed gases effect of total flow rate

With the same composition of the feed as the one given in Table 3.1.3.2.3, the flow rate was changed to investigate the effect of residence time on product distribution. The temperature was set at 150 $^{o}$C Results are given in Figures 3.1.3.2.1.1, 3.1.3.2.1.2, and 3.1.3.2.1.1. Figure 3.1.3.2.1.1 shows the variation of benzene conversion to each specified product as a function of changes in the total flow rate keeping the composition of the reaction mixture the same. On the other hand, the changes in selectivity for each product due to the changes in benzene conversion for the different flow rates are shown in Figure 3.1.3.2.1.2. Figure 3.1.3.2.1.2 shows the produce moles of each product from benzene reaction in this system at the different flow rate. Temperature was kept the same at all different flow rates.
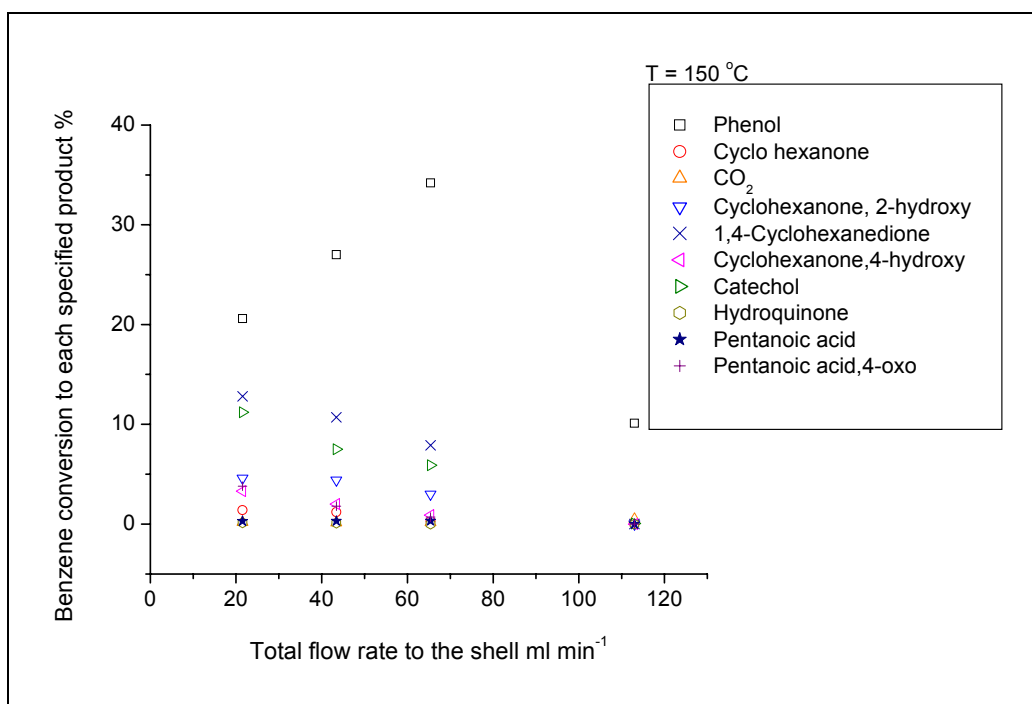


**Fig. 3.1.3.2.1.1**: Benzene conversion to each product from the reaction of benzene over Pd using different flow rates at 150 $^{o}$C. Reaction mixture composition: Benzene/$O_2$/He/Ar/ $H_2$ = 4.1/17.9/41.0/3.18/34 (% of total flow rate)

46
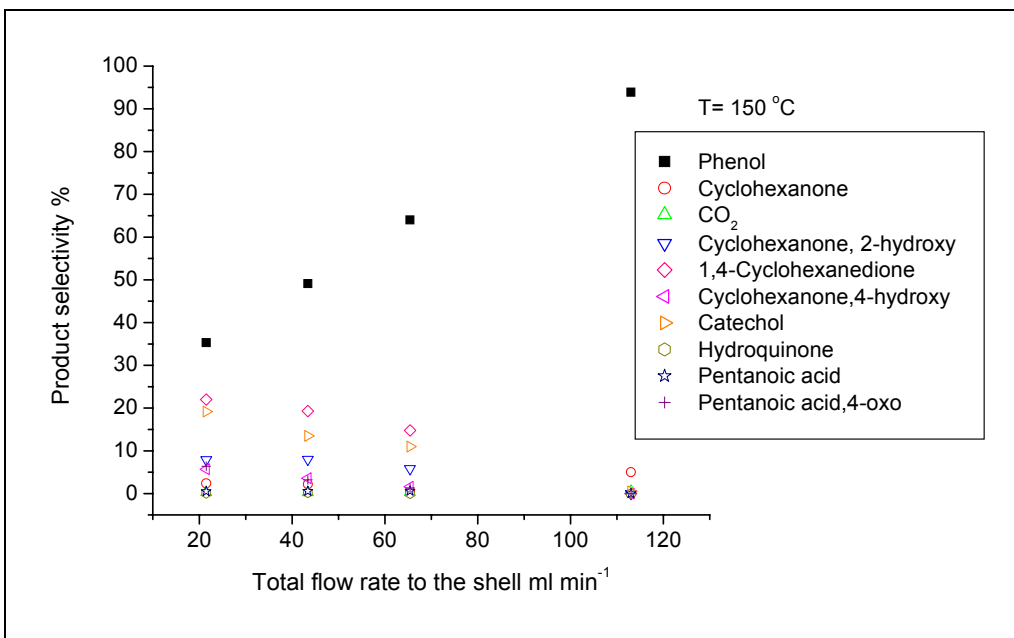
**Fig. 3.1.3.2.1.2**: Product selectivity from the reaction of benzene over Pd using different flow rates at 150 $^{o}$C vs. total flow rate. Reaction mixture composition: Benzene/$O_2$/He/Ar/ $H_2$ = 4.1/17.9/41.0/3.18/34 (% of total flow rate)
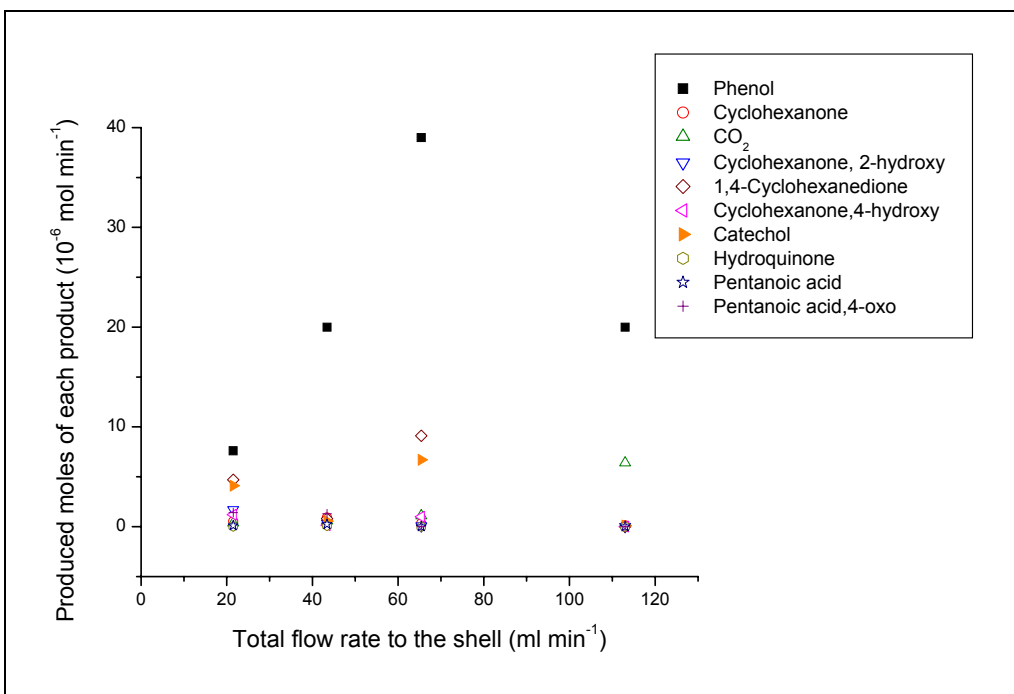


**Fig. 3.1.3.2.1.3:** Produced moles of each product from the reaction of benzene over Pd at 150 $^{o}$C vs. total flow rate. Reaction mixture composition: Benzene/$O_2$/He/Ar/ $H_2$ = 4.1/17.9/41.0/3.18/34 (% of total flow rate)
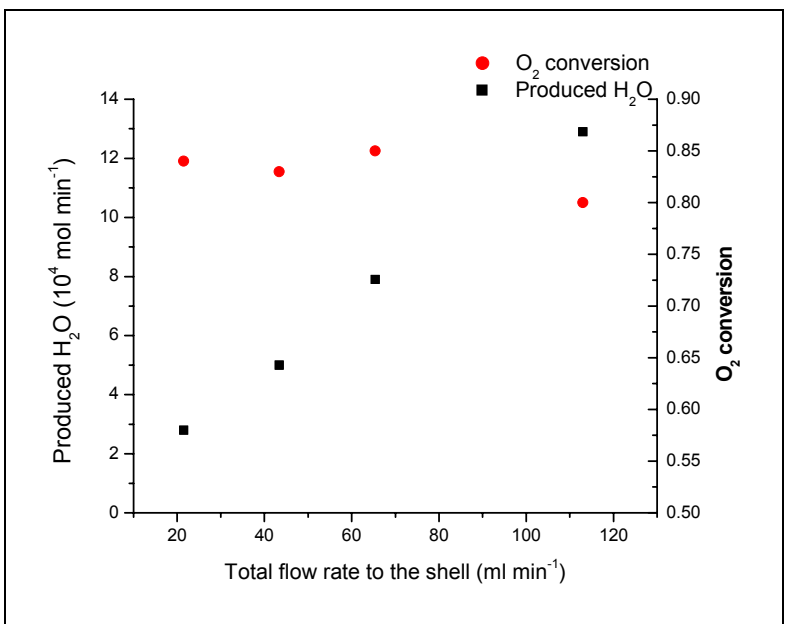
**Fig. 3.1.3.2.1.4**: Produced moles of $H_2O$ and conversion of $O_2$ at 150 $^oC$ vs. total flow rate. Reaction mixture composition: Benzene/$O_2$/He/Ar/$H_2$= 4.1/17.9/41.0/3.18/34 (% of total flow rate)

### 3.1.3.2.2. Effect of varying $O_2/(O_2+H_2)$ % in the reaction mixture at 150 $^oC$

The reaction mixture consisted of $O_2$, He, $H_2$, Ar, and Benzene which was entered to the shell side of the reactor. The temperature was set at 150 $^oC$. The flow rates $H_2$, Ar, and Benzene were 38.5, 3.6, and 4.7 ml min$^{-1}$, respectively. Flow rate of $O_2$ was varied from 2 to 21.5 ml min$^{-1}$, the balance was obtained from the flow of He gas to get on total flow rate of 113 ml min$^{-1}$. Therefore the ratio of $O_2/(O_2+H_2)$ will be varied due to the variation of oxygen flow rate. Benzene conversion to each product is given in Table 3.1.3.2.2.1. The calculated molar flow rate of each product is shown in Table 3.1.3.2.2.2. By increasing the flow rate of oxygen in the reaction mixture, production of $H_2O$ increased. The produced amount of $H_2O$ was 0.71, 0.97, 1.6, 2.9, and 6.1 x 10$^{-4}$ mol min$^{-1}$ at 4, 6.8, 12.6, 23, and 36.5 % of $O_2/(O_2+H_2)$, respectively.

48

**Table 3.1.3.2.2.1**: Benzene conversion to each specified product (%) at different $O_2/(O_2+H_2)$ % and 150 $^o$C. Total flow rate = 113 ml min$^{-1}$

| | $O_2/(O_2+H_2)$ | $O_2/(O_2+H_2)$ | $O_2/(O_2+H_2)$ | $O_2/(O_2+H_2)$ | $O_2/(O_2+H_2)$ |
|---|---|---|---|---|---|
| | 4 % | 6.8 % | 12.6 % | 23 % | 36.5 % |
| Product | Conversion (%) | Conversion (%) | Conversion (%) | Conversion (%) | Conversion (%) |
| Phenol | 0 | 0 | 0 | 0.3 | 10.6 |
| Cyclohexanone | 0.03 | 0.01 | 0.05 | 0.19 | 0.15 |
| $CO_2$ | 0.02 | 0.02 | 0.025 | 0.05 | 1.1 |
| Cyclohexanone, 2-hydroxy | 0.02 | 0 | 0 | 0.1 | 0 |
| 1,4-Cyclohexan-edione | 0 | 0 | 0 | 0.16 | 1.4 |
| Cyclohexanone, 4-hydroxy | 0 | 0 | 0 | 0.05 | 0 |
| Catechol | 0.6 | 0.3 | 0.6 | 2.1 | 12.6 |
| Hydroquinone | 3.3 | 3.3 | 5.1 | 7.7 | 7.1 |
| Resorcinol | 1.0 | 0.7 | 0.8 | 2.7 | 0 |
| Pentanoic acid | 0.1 | 0 | 0 | 0 | 0.47 |
| Pentanoic acid, 4-oxo | 0.1 | 0 | 0 | 0.8 | 1.9 |
| Benzoic acid | 0.03 | 0.0 | 0 | 0.05 | 0.0 |

## 3.1.3.2.3. Effect of varying $O_2/(O_2+H_2)$ % in the reaction mixture at 300 $^o$C

The ratio of $O_2/(O_2+H_2)$ was varied in the feed to the shell of the reactor by varying the flow rate of $O_2$. The temperature of the reactor for this set of data was kept at 300 $^o$C. The flow rate of benzene, Ar, and $H_2$ were 23, 1.5, and 2 ml min$^{-1}$, respectively, to give the same compositions of the total flow rate as these ones at 150 $^o$C. Oxygen flow rate was changed in order to obtain 4%, 14% and 23 % of $O_2/(O_2+H_2)$ with the balance being He flow rate. The total flow rate was 50 ml min$^{-1}$. The produced water was 0.75, 2.4, 4.3 x 10$^{-4}$ mol min$^{-1}$ at 5, 14, and 23 % of $O_2/(O_2+H_2)$, respectively. Results at these flow conditions are presented in Tables 3.1.3.2.3.1 and 3.1.3.2.3.2.

**Table 3.1.3.2.3.1**: Benzene conversion to each specified product (%) at different $O_2/(O_2+H_2)$ % and 300 $^o$C

| $O_2/(O_2+H_2)$ (%) | Phenol (%) | Catechol (%) | 1,4-Cyclohexanedione (%) | Hydro-quinone (%) | $CO_2$ (%) | Cycloh-exanone (%) |
|---|---|---|---|---|---|---|
| 5 | 0.00 | 0.0 | 0.0 | 0.0 | 0.03 | 0 |
| 14 | 0.15 | 0.0 | 0.05 | 0.3 | 0.05 | 0.05 |
| 23 | 0.53 | 0.18 | 0.06 | 2.8 | 0.11 | 0.06 |

**Table 3.1.3.2.3.2**: Produced moles of each product (mol min$^{-1}$) at different $O_2/(O_2+H_2)$ % (volume ratio) in the feed at 300 $^o$C

| Product | $O_2/(O_2+H_2)$ 5 % | $O_2/(O_2+H_2)$ 14.0 % | $O_2/(O_2+H_2)$ 23 % |
|---|---|---|---|
| Phenol | 0 | 1.2E-7 | 4.4E-7 |
| Catechol | 0 | 0 | 1.5E-7 |
| 1,4-Cyclohexanedione | 0 | 4.3E-8 | 5.0E-8 |
| Hydroquinone | 0 | 2.4E-7 | 2.3E-6 |
| $CO_2$ | 2.1E-8 | 4.0E-8 | 8.8E-8 |
| Cyclohexanone | 0 | 4.3E-8 | 5.0E-8 |

### 3.1.3.2.4. Reproducing the experimental results in Figure 3.1.3.2.4

A new set of experiment was performed in order to reproduce the experimental results that were obtained in Figure 3.1.3.2.4. This was done by setting the experimental conditions of gases flow rates and reaction temperature similar to these ones that were used to obtain the results in Figure 3.1.3.2.4. Figure 3.1.3.2.4.1 gives the conversion of benzene to each specified product.
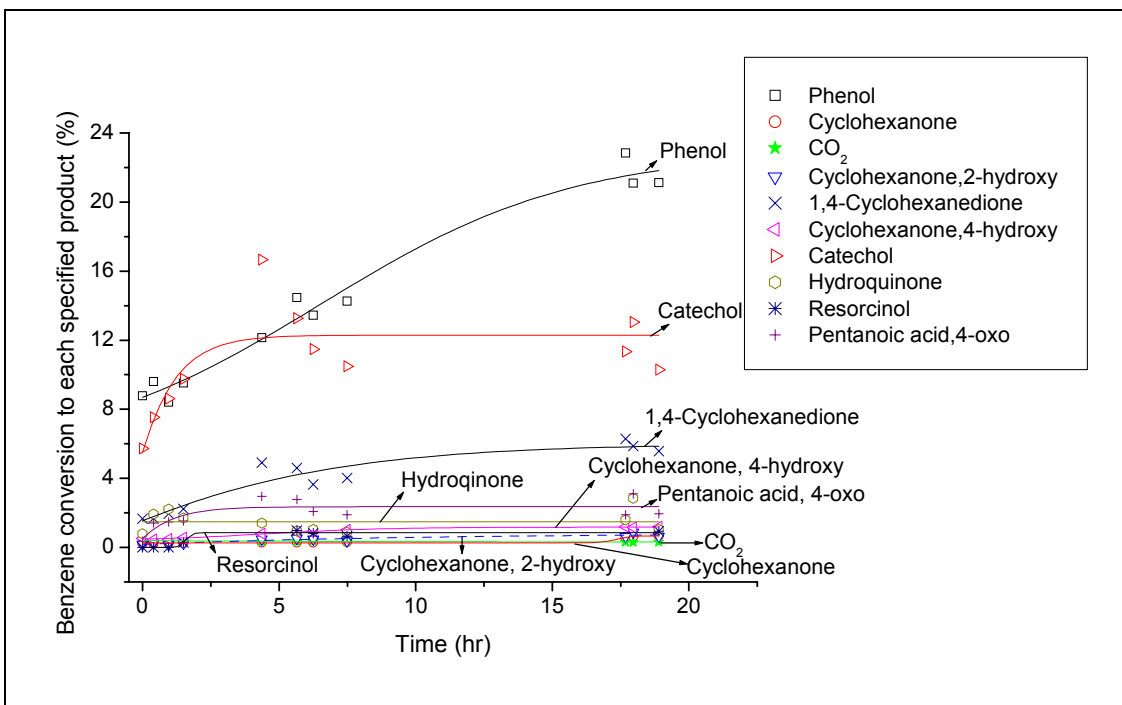
**Fig. 3.1.3.2.4.1**: Conversion of benzene to the specified products 150$^{\rm o}$ C. Flow rate: shell, 43.3 ml min$^{-1}$ (Benzene/O$_2$/He/Ar/ H$_2$ = 4.0/17.9/41.0/3.18/34.0 % of total flow rate)

### 3.1.3.2.5. Experimental results at 180 $^{\rm o}$C:

Reaction mixture was introduced to the shell side of the reactor with flow composition similar to the one in Figure 3.1.3.2.5. The temperature of the reactor was set to 180 $^{\rm o}$C. Different flow rates of the total reaction mixture have been tested at this temperature while keeping the composition of the reaction mixture the same in the different mixtures.
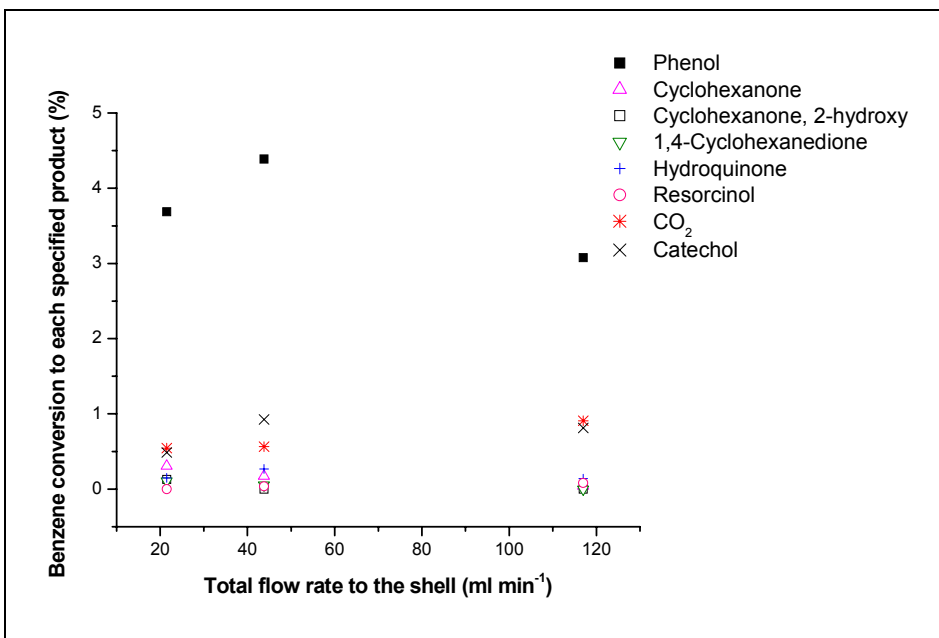
**Fig. 3.1.3.2.5.1**: Conversion of benzene to the specified products vs. flow rate at 180 °C. Flow rate composition: (Benzene/$O_2$/He/Ar/ $H_2$ = 4.0/17.7/41.0/3.15/34.0 % of total flow rate)
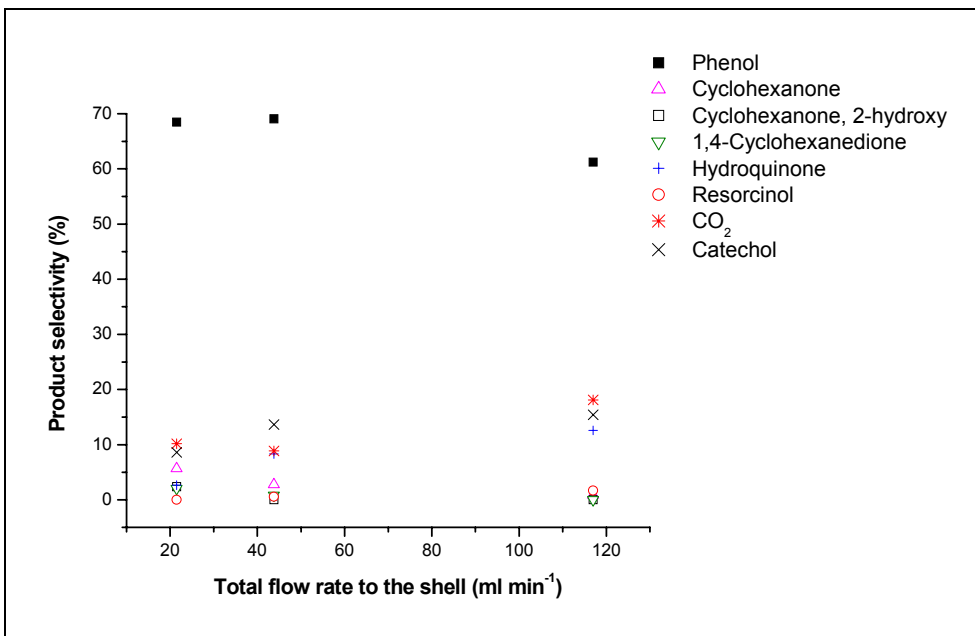


**Fig. 3.1.3.2.5.2**: Product selectivity from benzene reaction using Pd membrane vs. flow rate at 180 °C. Flow rate composition: (Benzene/$O_2$/He/Ar/ $H_2$ = 4.0/17.7/41.0/3.15/34.0 % of total flow rate)
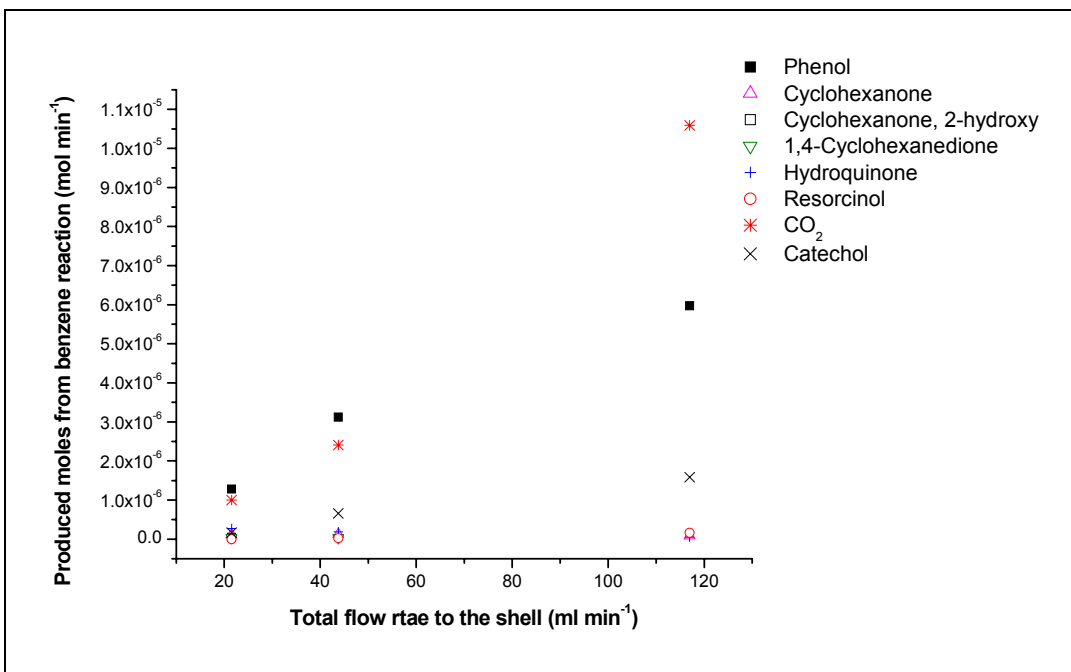
**Fig. 3.1.3.2.5.3**:  Produced moles of the products from benzene reaction using Pd membrane vs. flow rate at 180 $^{o}$C. Flow rate composition: (Benzene/$O_2$/He/Ar/ $H_2$ = 4.0/17.7/41.0/3.15/34.0 % of total flow rate)
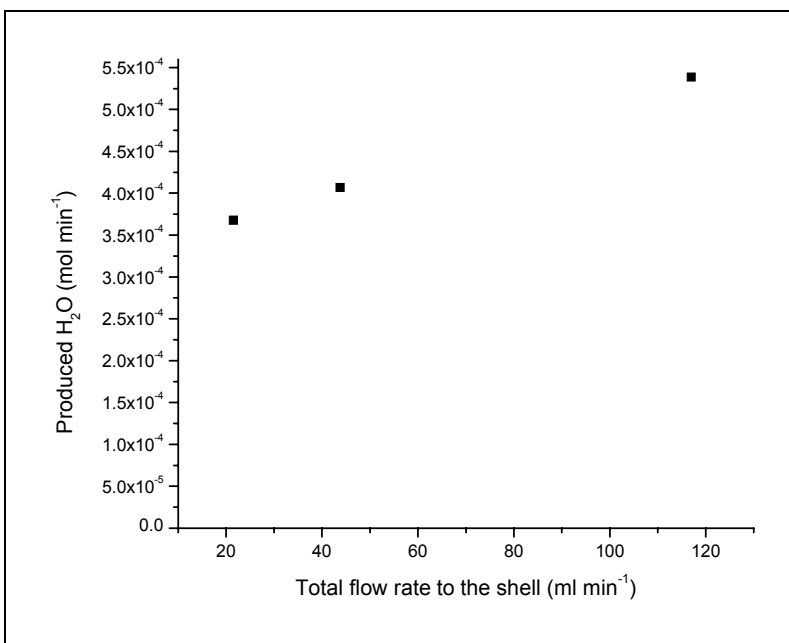


**Fig. 3.1.3.2.5.4:** Produced moles of water from benzene reaction using Pd membrane vs. flow rate at 180 $^{o}$C. Flow rate composition: (Benzene/$O_2$/He/Ar/ $H_2$ = 4.0/17.7/41.0/3.15/34.0 % of total flow rate)

### 3.1.3.2.6. Experimental results at 200 $^o$C

The Pd membrane reactor was used again at 150 $^o$C in order to partially oxidize benzene to phenol. With the same flow conditions to the reactor the temperature of the reactor was raised up to 200 $^o$C. Figure 3.1.3.2.6.1 shows the conversion of benzene to each detected product at 150 $^o$C and 200 $^o$C using a total flow rate of 42.3 ml min$^{-1}$. Figure 3.1.3.2.6.2 shows the product selectivity at these conditions.
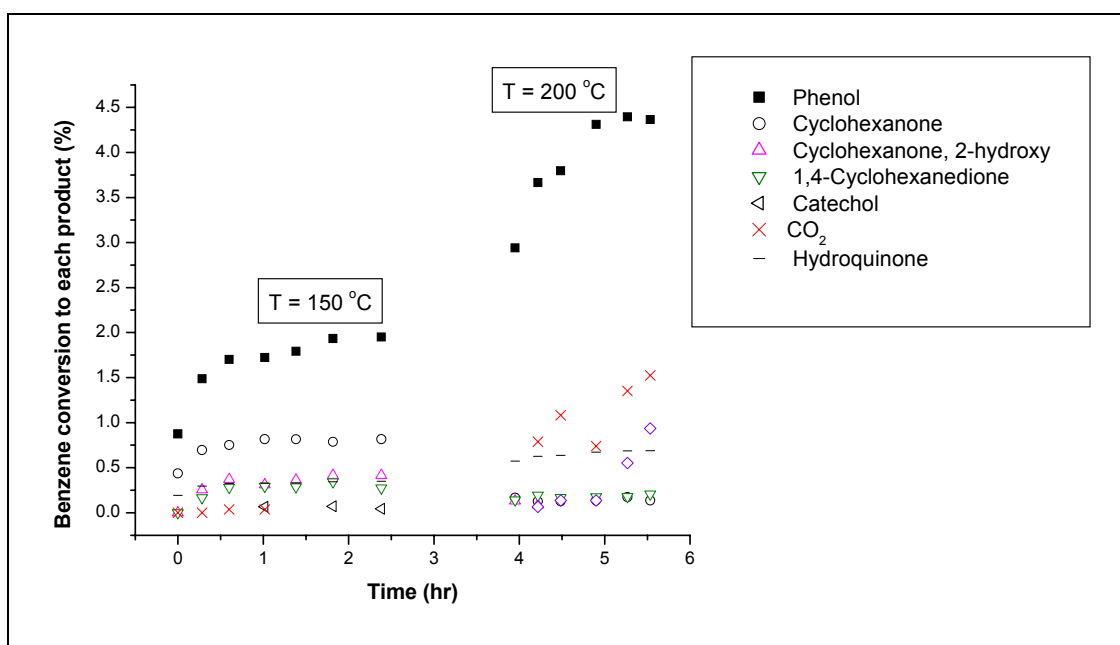


**Fig. 3.1.3.2.6.1**: Benzene conversion to the detected products at 150 $^o$C and 200 $^o$C vs. time. Flow rate to the shell = 42.3 ml min$^{-1}$, flow composition: Benzene/Ar/He/O$_2$/H$_2$ = 4.2/3.13/39.3/18.2/35.0 (% of total flow rate)

The data at 200 $^o$C were repeated again in order to investigate if higher conversion of benzene can be obtained and to investigate the reproducibility of the results. The results are shown in Figures 3.1.3.2.6.4.
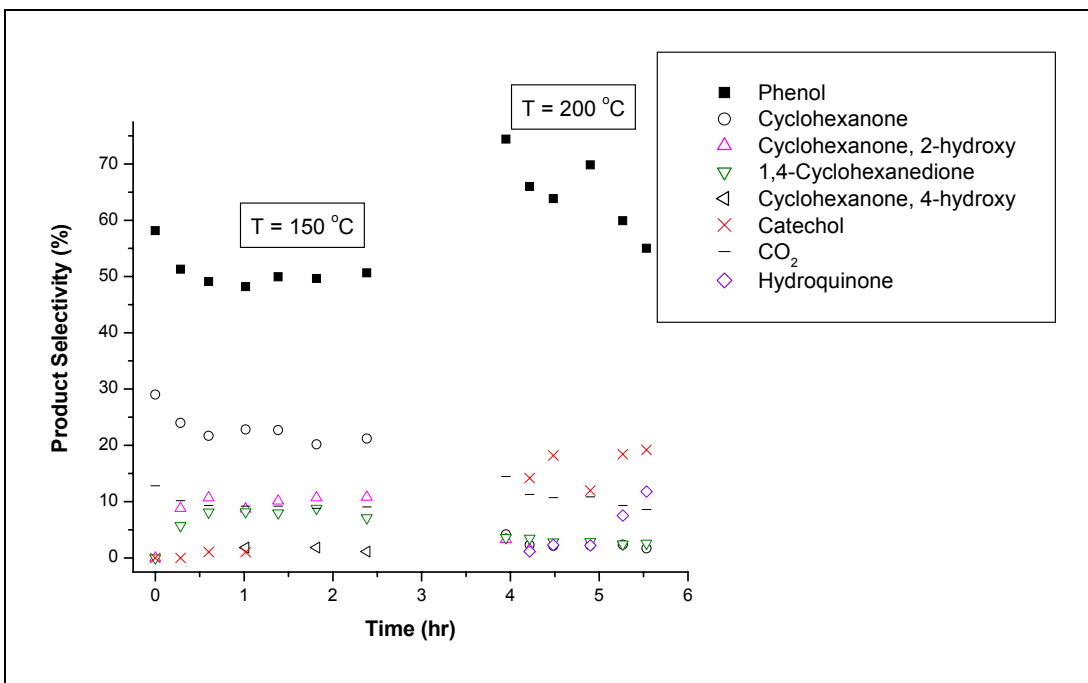
**Fig. 3.1.3.2.6.2**: Selectivity of products from benzene reaction over Pd membrane at 150 $^o$C and 200 $^o$C vs. time. Flow rate to the shell = 42.3 ml min$^{-1}$, flow composition: Benzene/Ar/He/O$_2$/H$_2$ = 4.2/3.13/39.3/18.2/35.0 (% of total flow rate)
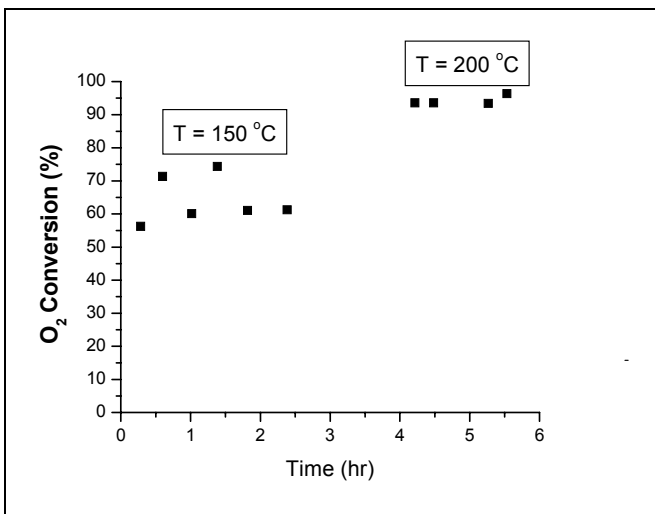


**Fig. 3.1.3.2.6.3**: Oxygen conversion at 150 $^o$C and 200 $^o$C vs. time. Flow rate to the shell = 42.3 ml min$^{-1}$, flow composition: Benzene/Ar/He/O$_2$/H$_2$ = 4.2/3.13/39.3/18.2/35.0 (% of total flow rate)
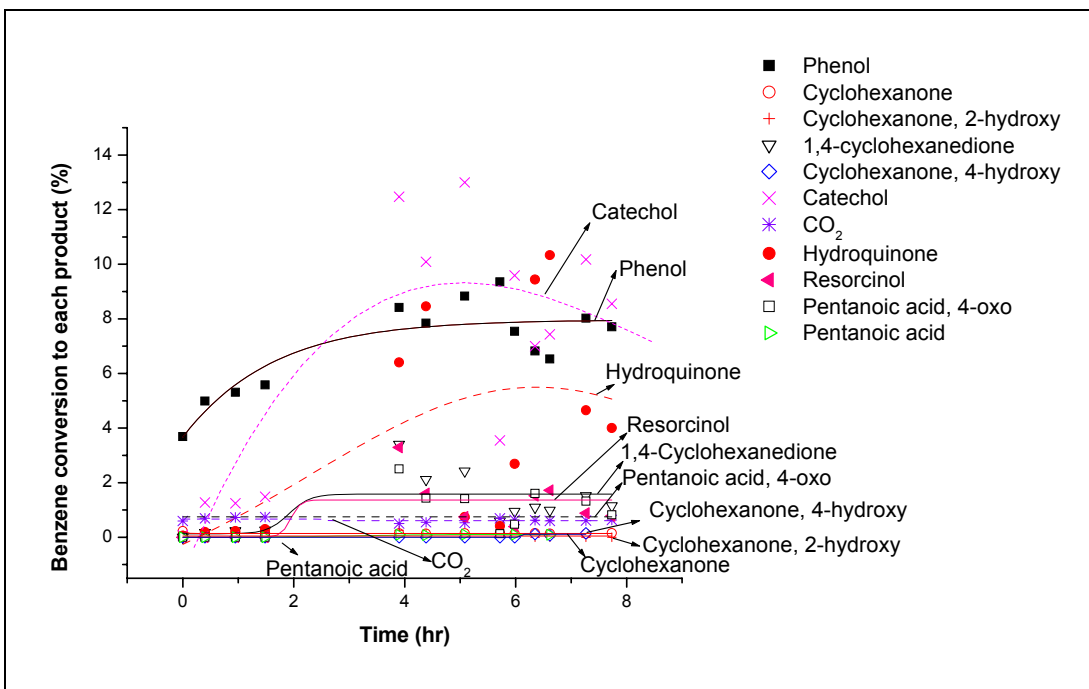
**Fig. 3.1.3.2.6.4**: Benzene conversion to the detected products at 200 °C vs. time. Flow rate to the shell= 43.3 ml min⁻¹, flow composition: Benzene/Ar/He/O₂/H₂ = 4.0/3.18/40.9/17.9/34.0 (% of total flow rate)

The experiment in Figure 3.1.3.2.6.4 was extended for a longer time at the same flow conditions and reaction temperature. Figure 3.1.3.2.6.5 shows the experimental results after running the experiment for a longer time. Oxygen conversion to water and carbon dioxide at these conditions is shown in Figure 3.1.3.2.6.6.

Then the same flow conditions were applied again at 200 °C and the results after two hours of running the reaction are shown in Figure 3.1.3.2.6.7. The temperature distribution within the reactor was measured at different locations from the reactor inlet in order to see if there is any hot spot(s). This is shown in Figure 3.1.3.2.6.8

56
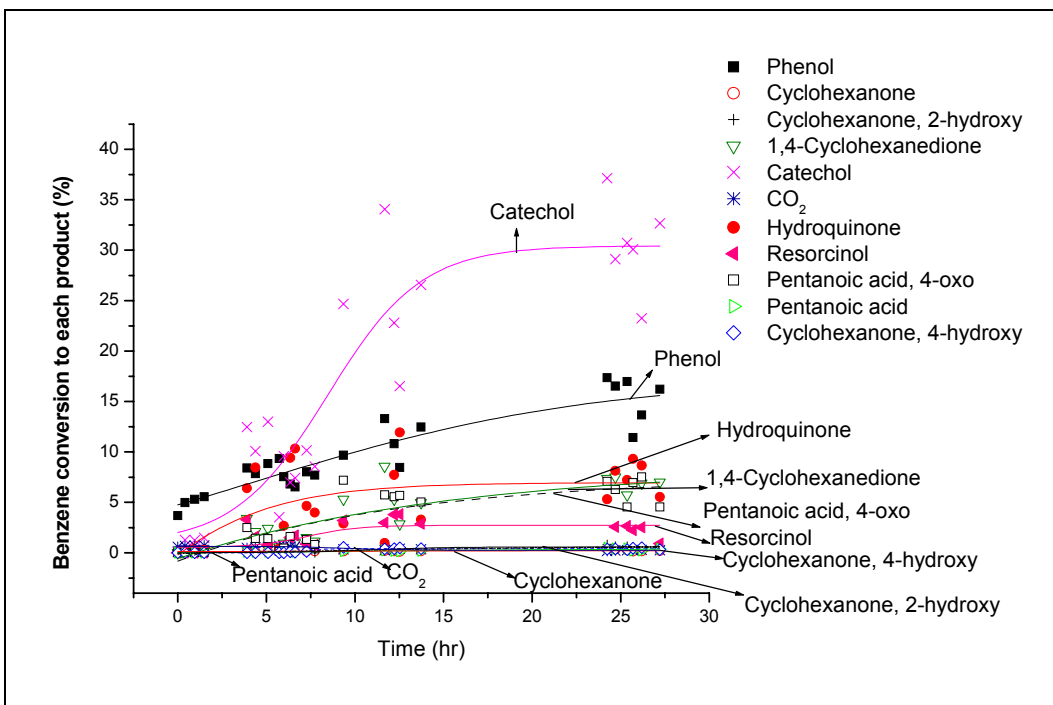
**Fig. 3.1.3.2.6.5**: Benzene conversion to the detected products at 200 °C vs. time. Flow rate to the shell = 43.3 ml min⁻¹, flow composition: Benzene/Ar/He/$O_2$/$H_2$ = 4.0/3.18/40.9/17.9/34.0 (% of total flow rate)
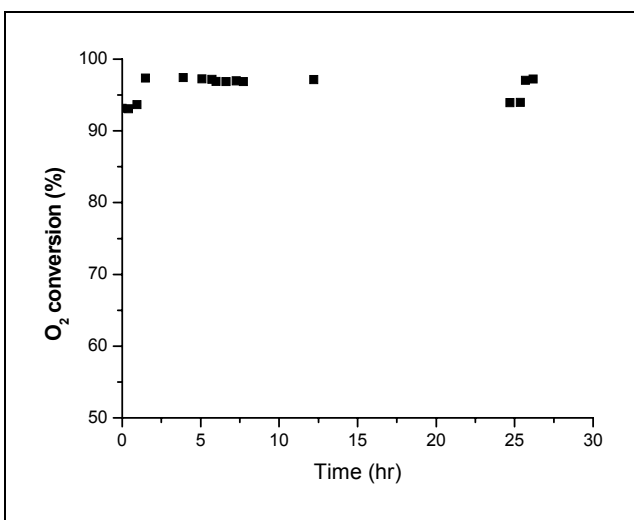


**Fig. 3.1.3.2.6.6**: Conversion of $O_2$ to $H_2O$ and $CO_2$ at 200 °C vs. time. Flow rate to the shell = 43.3 ml min⁻¹, flow composition: Benzene/Ar/He/$O_2$/$H_2$ = 4.0/3.18/40.9/17.9/34.0 (% of total flow rate)
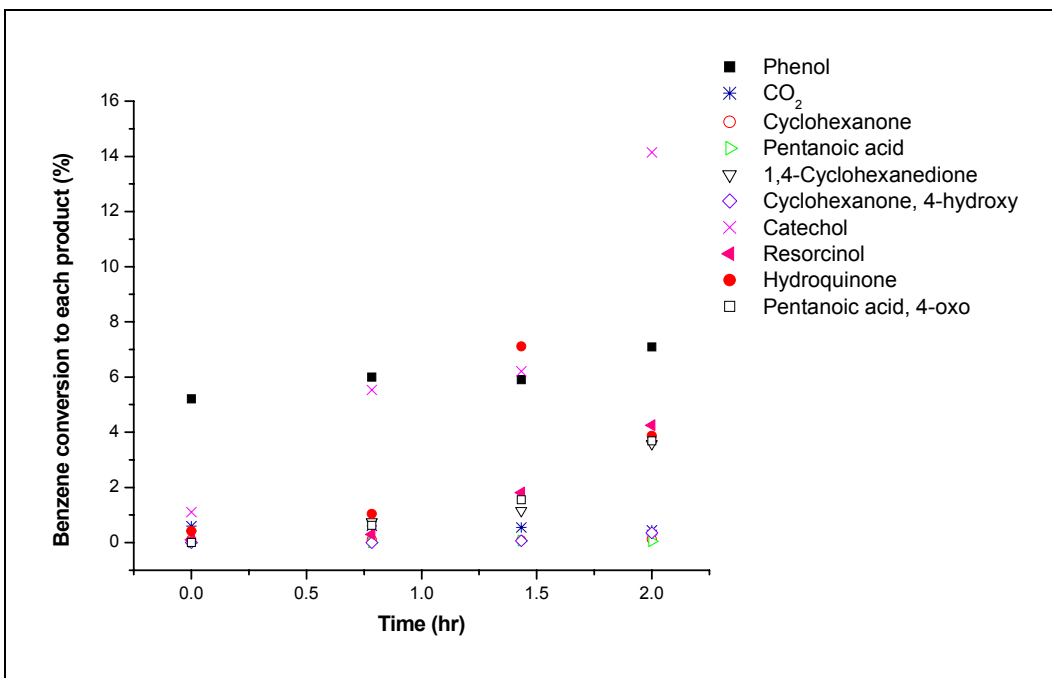
**Fig. 3.1.3.2.6.7**: Benzene conversion to the detected products at 200 $^o$C vs. time. Flow rate to the shell = 43.3 ml min$^{-1}$, flow composition: Benzene/Ar/He/O$_2$/H$_2$ = 4.0/3.18/40.9/17.9/34.0 (% of total flow rate)
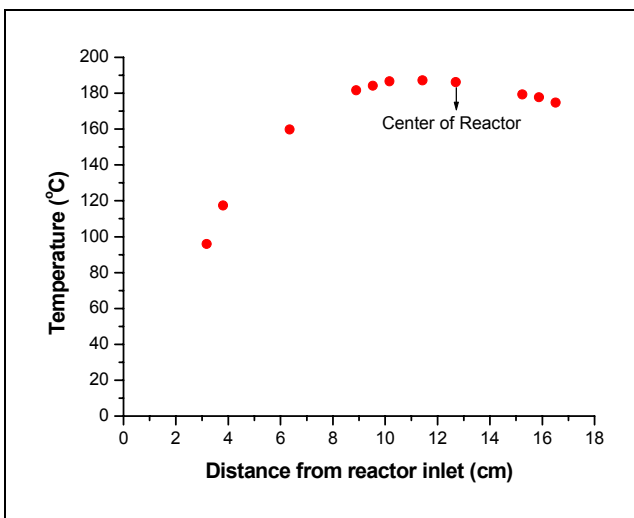


**Fig. 3.1.3.2.6.8**: Temperature distribution inside the reactor for the reaction of benzene at 200 $^o$C . Flow rate to the shell = 43.3 ml min$^{-1}$, flow composition: Benzene/Ar/He/O$_2$/H$_2$ = 4.0/3.18/40.9/17.9/34.0 (% of total flow rate)

The same flow conditions were used to carry the reaction of benzene at 300 $^o$C to study the effect of increasing reactor temperature. The results at this temperature are

shown in Figure 3.1.3.2.6.8. As can be seen from this figure reaction was carried only for

a short time since benzene conversion was lower than the one at 200 $^{o}$C.
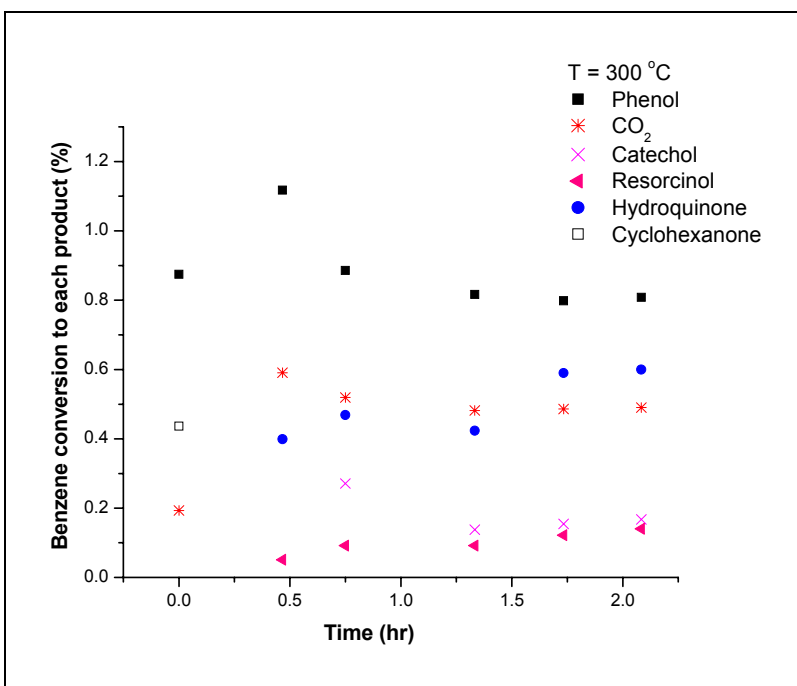


**Fig. 3.1.3.2.6.9**: Benzene conversion to the detected products at 300 $^{o}$C vs. time. Flow rate to the shell = 42.3 ml min$^{-1}$, flow composition: Benzene/Ar/He/O$_2$/H$_2$ = 4.0/3.14/40.9/18/35.0 (% of total flow rate)

The reaction with the flow conditions given in Figures 3.1.3.2.6.7 and 3.1.3.2.6.5 was repeated after few days at the same flow conditions and temperature. Figure 3.1.3.2.6.10 shows benzene conversion to each product at the previous flow conditions and at 200 $^{o}$C. Oxygen conversion was similar to the one in Figure 3.1.3.2.6.6.
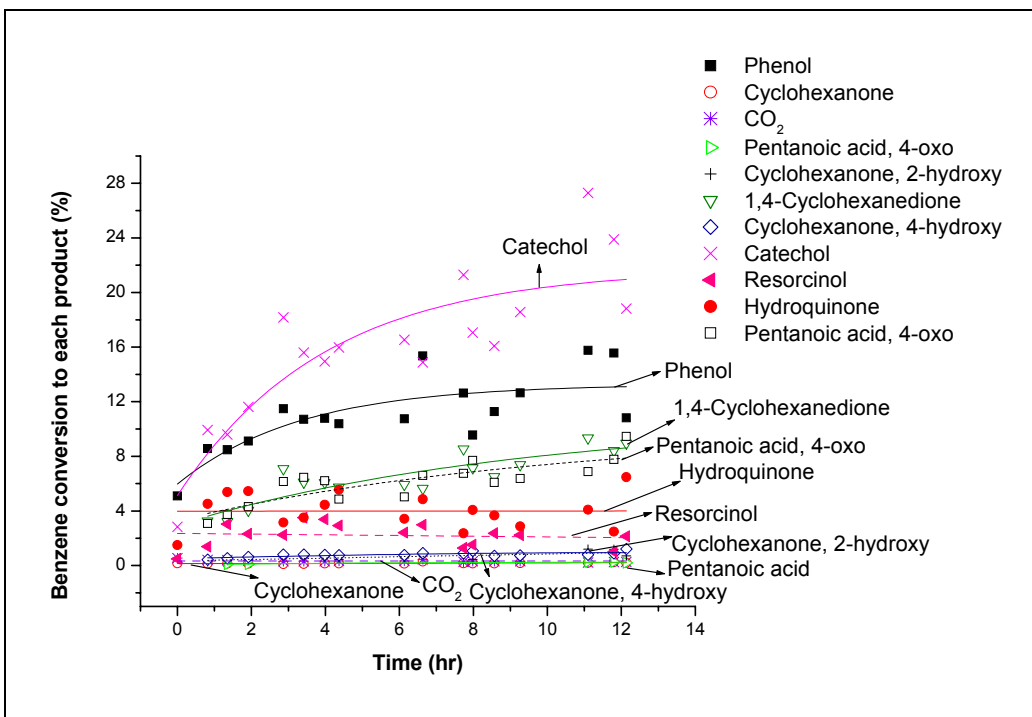
**Fig. 3.1.3.2.6.10**: Benzene conversion to the detected products at 200 $^{\circ}$C vs. time. Flow rate to the shell = 43.0 ml min$^{-1}$, flow composition: Benzene/Ar/He/O$_2$/H$_2$ = 4.0/3.18/40.0/17.9/34.5 (% of total flow rate)

The flow rate effect on benzene conversion was studied at 200 $^{\circ}$C and results are shown in Figure 3.1.3.2.6.11. The system was stared with as flow rate of 21 ml min$^{-1}$ then flow rate was increased to 119 ml min$^{-1}$ and then flow rate was decreased for 43 ml min$^{-1}$. These results were obtained by running the reaction at least 8 hours at each flow rate.
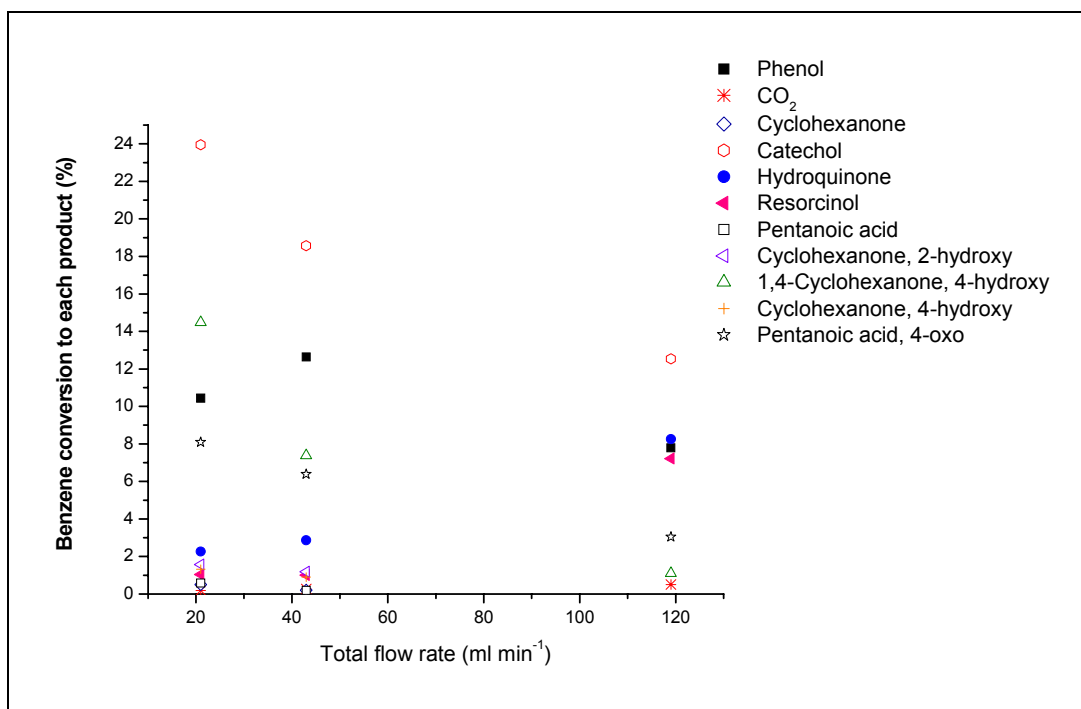
**Fig. 3.1.3.2.6.11**: Conversion of benzene to the specified products vs. flow rate at 200 $^{\circ}$C. Flow rate composition: (Benzene/$O_2$/He/Ar/ $H_2$ = 4.0/17.7/41.0/3.15/34.0 % of total flow rate)

### 3.1.4. Pd/ZrO$_2$ system

New design for the shell and tube reactor with a new catalyst has been tested for the possibility of converting benzene to phenol. As said earlier, the reactor assembly consisted of a shell and tube reactor. A certain length of the outer surface of the inner tube was coated with a thin layer of Pd supported on ZrO$_2$. In this system the whole gaseous reaction mixture (benzene, He, Ar, $O_2$, and $H_2$) was entered to the shell and passed over the ¼ in tube, which was coated with Pd/ZrO$_2$ catalyst. One set of flow conditions for the above gases, which is similar to one of the flow conditions used in Pd-membrane reactor, was entered to the shell at 150 $^{\circ}$C. Benzene conversion to each detected product at these flow conditions is shown in Figure 3.1.4.1.
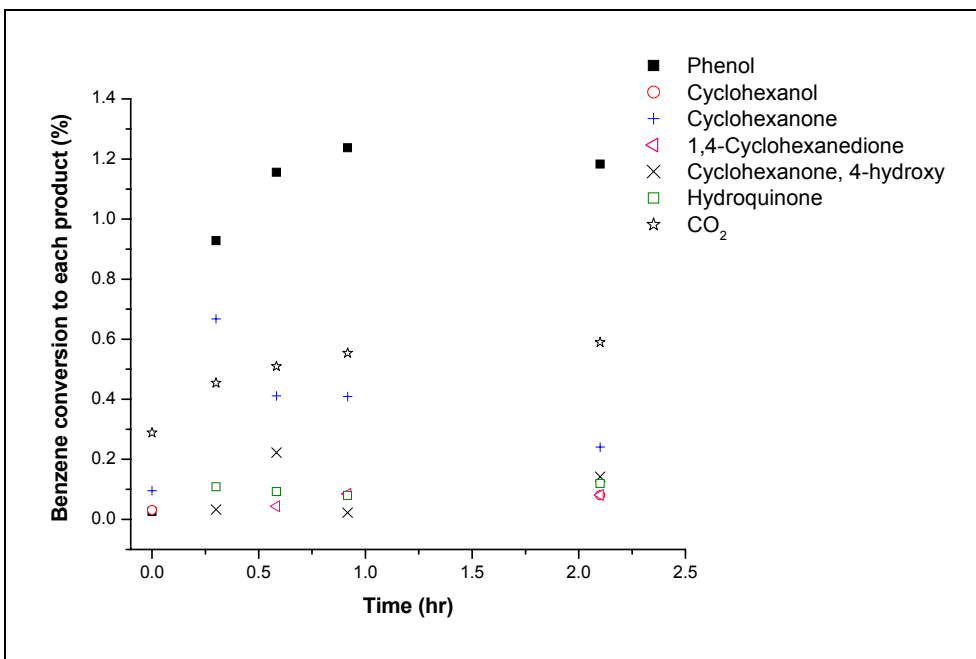
**Fig. 3.1.4.1**: Benzene conversion to the detected products at 150 $^{o}$C vs. time. Flow rate to the shell = 45.0 ml min$^{-1}$, flow composition: Benzene/Ar/He/O$_2$/H$_2$ = 4.0/3.17/43.0/17.2/33.0 (% of total flow rate)
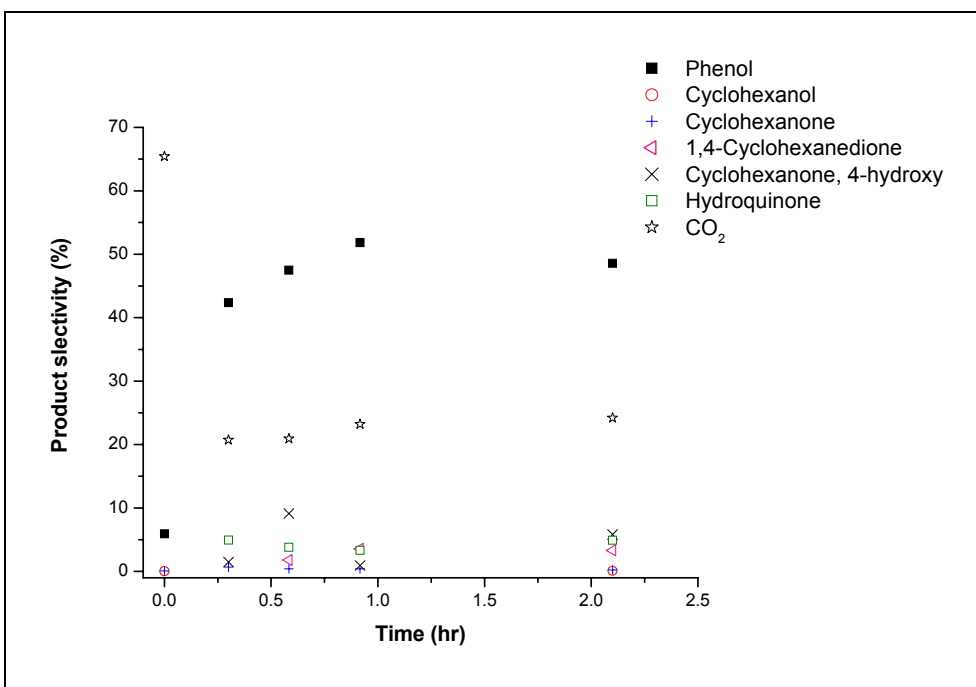


**Fig. 3.1.4.2**: Selectivity of each product from benzene reaction using Pd/ZrO$_2$ at 150 $^{o}$C vs. time. Flow rate to the shell = 45.0 ml min$^{-1}$, flow composition: Benzene/Ar/He/O$_2$/H$_2$ = 4.0/3.17/43.0/17.2/33.0 (% of total flow rate)

On the other hand, Figure 3.1.4.2 shows the selectivity for each product from the reaction of benzene using $Pd/ZrO_2$. Total conversion of oxygen at the same flow conditions is shown in Figure 3.1.4.3.
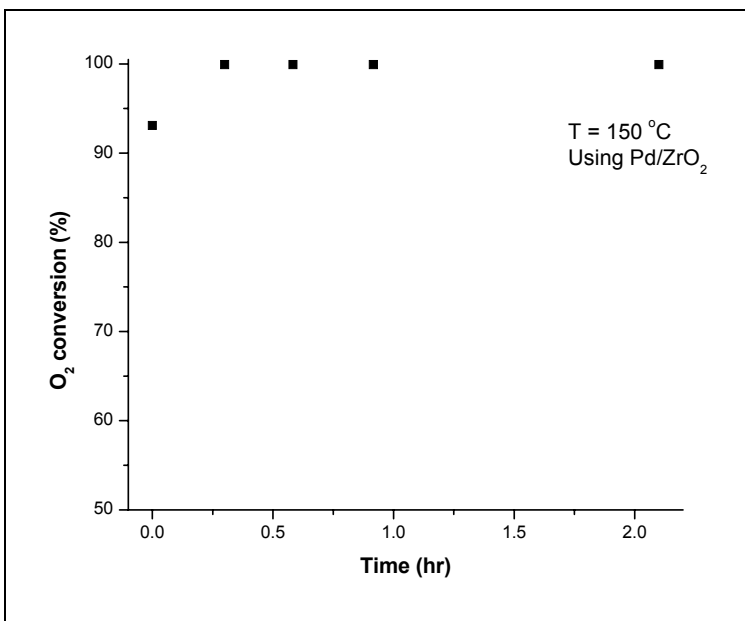


**Fig. 3.1.4.3**: Conversion of $O_2$ at 150 $^o$C using $Pd/ZrO_2$ vs. time. Flow rate to the shell = 43.3 ml min$^{-1}$, flow composition: Benzene/Ar/He/$O_2$/$H_2$ = 4.0/3.18/40.9/17.9/34.0 (% of total flow rate)

A reaction with similar flow composition to the ones given in Figure 3.1.4.1 and with flow rate of 45 ml min$^{-1}$ was run at 150 $^o$C. Benzene conversion to each product is given in Figure 3.1.4.4. Selectivity of each product is shown in Figure 3.1.4.5. The selectivity of each product is shown in Figure 3.1.4.5 at the previous flow conditions. On the other hand, total conversion of oxygen at these flow conditions is shown in Figure 3.4.4.6. The experiment at 71 ml min$^{-1}$ total flow rate was repeated and gave the same results.
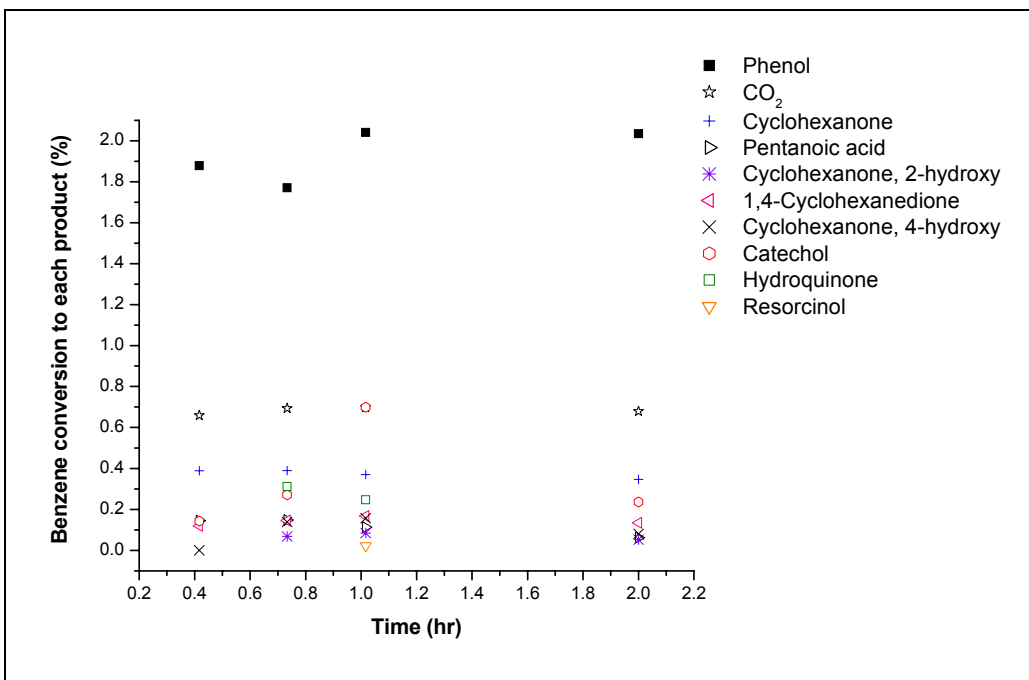
**Fig. 3.1.4.4:** Benzene conversion to the detected products at 150 $^o$C vs. time. Flow rate to the shell = 45.0 ml min$^{-1}$, flow composition: Benzene/Ar/He/O$_2$/H$_2$ = 4.0/3.17/43.0/17.2/33.0 (% of total flow rate)
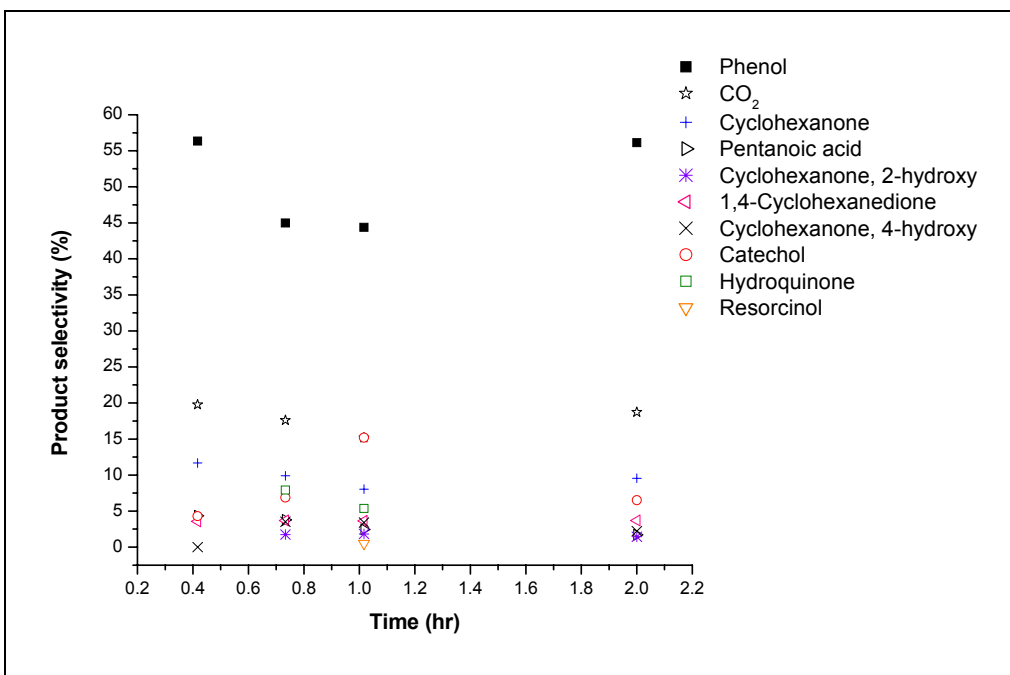


**Fig. 3.1.4.5**: Selectivity of each product from benzene reaction using Pd/ZrO$_2$ at 150 $^o$C vs. time. Flow rate to the shell = 45.0 ml min$^{-1}$, flow composition: Benzene/Ar/He/O$_2$/H$_2$ = 4.0/3.17/43.0/17.2/33.0 (% of total flow rate)
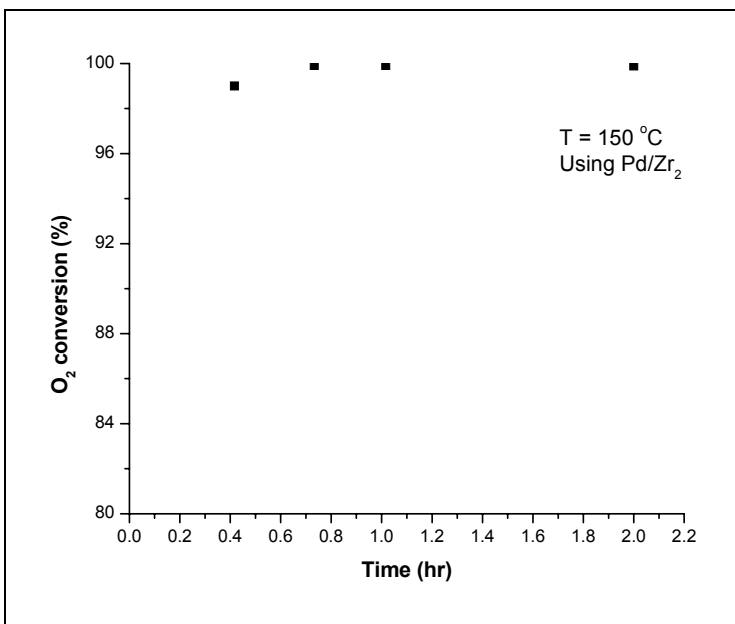
**Fig. 3.1.4.6:** Conversion of $O_2$ at 150 $^o$C using Pd/ZrO$_2$ vs. time. Flow rate to the shell = 43.3 ml min$^{-1}$, flow composition: Benzene/Ar/He/O$_2$/H$_2$ = 4.0/3.18/40.9/17.9/34.0 (% of total flow rate)

### 3.1.4.1. Effect of total flow rate using Pd/ZrO$_2$ system:

The total flow rate of the gaseous mixture into the shell side of Pd/ZrO$_2$ system was varied, keeping the same feed composition and temperature, in order to investigate the effect on benzene conversion to phenol in this reactor configuration. Three different flow rates were investigated, 45 ml min$^{-1}$, 71 ml min$^{-1}$, and 112 ml min$^{-1}$. Figure 3.1.4.1.1 shows benzene conversion to each product at the different flow rates. The selectivity of each detected product at the different flow rates is shown in Figure 3.1.4.1.2. The produced moles of each product at the different flow rates are shown in Figure 3.1.4.1.3

65
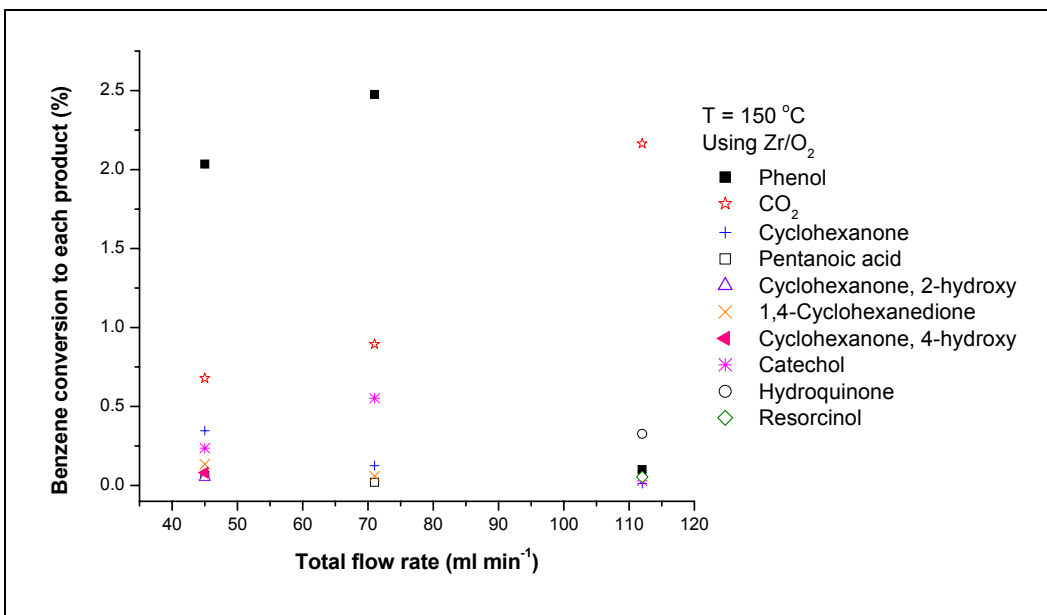
**Fig. 3.1.4.1.1:** Benzene conversion to the detected products at 150 °C vs. total flow rate to the shell. Flow composition: Benzene/Ar/He/$O_2$/$H_2$ = 4.0/3.17/43.0/17.2/33.0 (% of total flow rate)
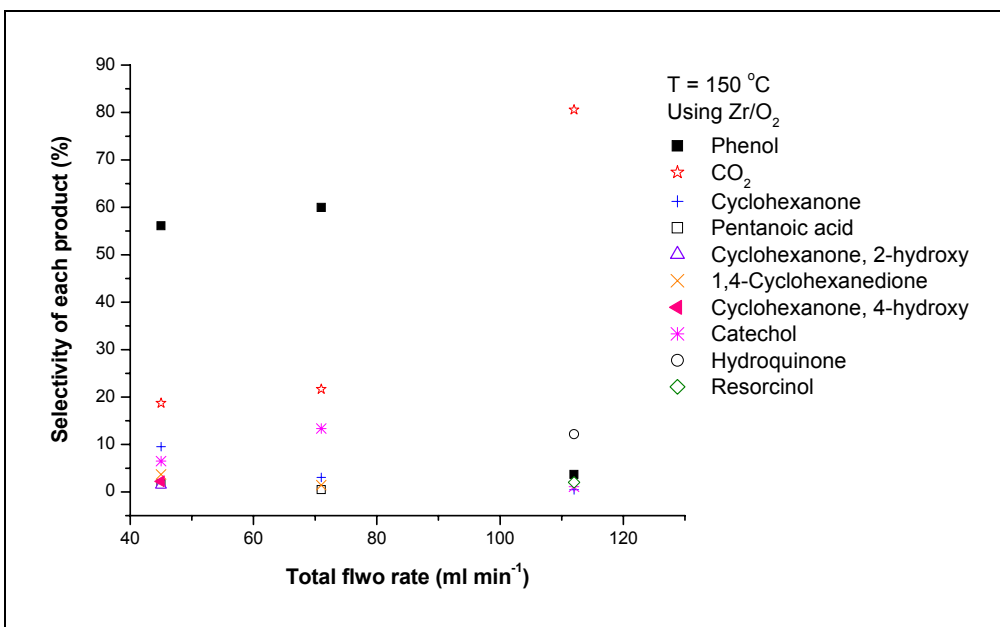


**Fig. 3.1.4.1.2:** Selectivity of each product from benzene reaction using Pd/$ZrO_2$ at 150 °C vs. total flow rate. Flow composition: Benzene/Ar/He/$O_2$/$H_2$ = 4.0/3.17/43.0/17.2/33.0 (% of total flow rate)

66
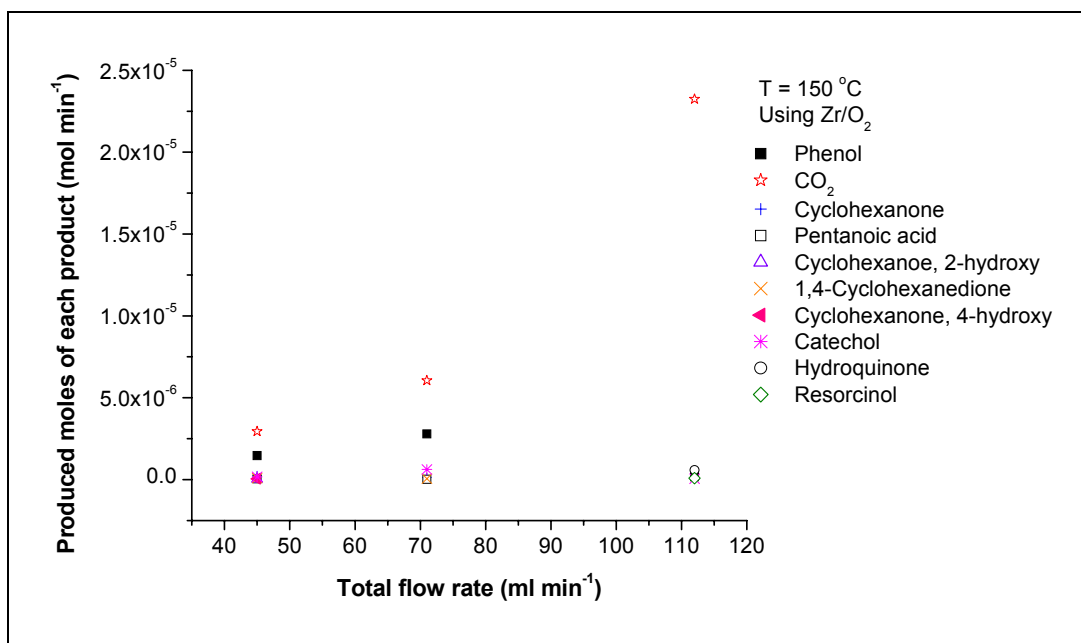
**Fig. 3.1.4.1.3:** Produced moles of each product from benzene reaction using $Pd/ZrO_2$ at 150 $^{\circ}$C vs. total flow rate. Flow composition: Benzene/Ar/He/$O_2$/$H_2$ = 4.0/3.17/43.0/17.2/33.0 (% of total flow rate)

### 3.1.4.2. Effect of temperature using Pd/ZrO$_2$ system:

The reactor temperature was varied in order to investigate the effect of temperature on benzene conversion to phenol using $Pd/ZrO_2$ catalyst. The reaction mixture was kept at the same total flow rate and composition for the different reaction temperature. Figurer 3.1.4.2.1 shows benzene conversion to each specified product at the different reaction temperature. Selectivity of each product from benzene reaction at the different reaction temperature is shown in Figure 3.1.4.2.2.

67
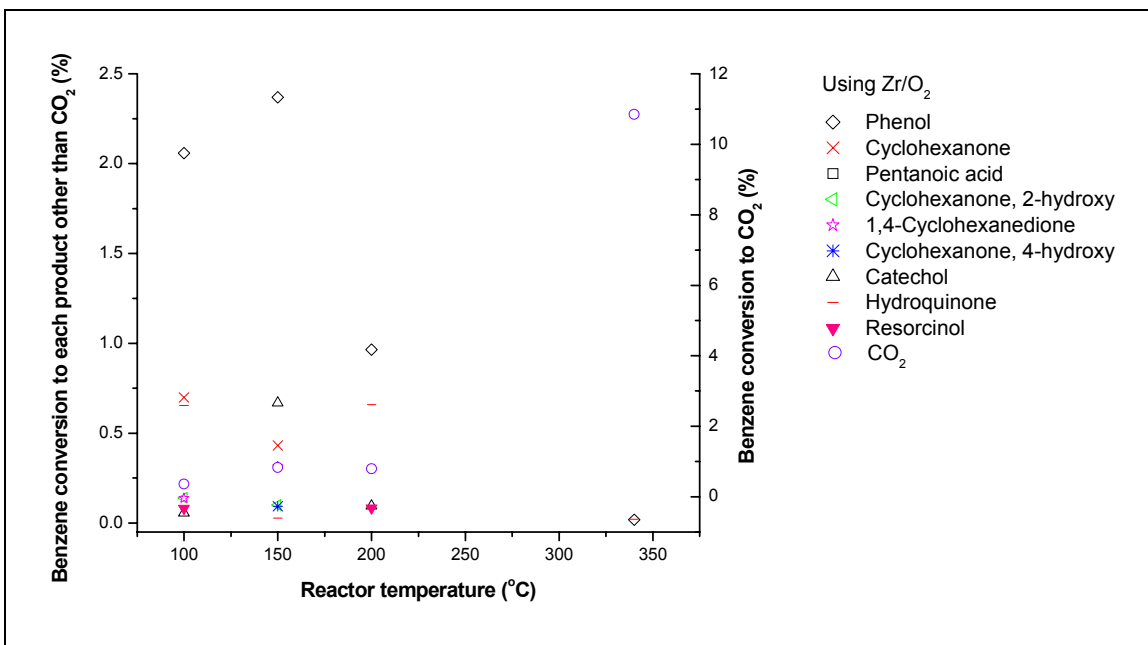
**Fig. 3.1.4.2.1:** Benzene conversion to the each detected product vs. temperature. Total flow rate to the shell = 45 ml min$^{-1}$. Flow composition: Benzene/Ar/He/O$_2$/H$_2$ = 4.0/3.17/43.0/17.2/33.0 (% of total flow rate)
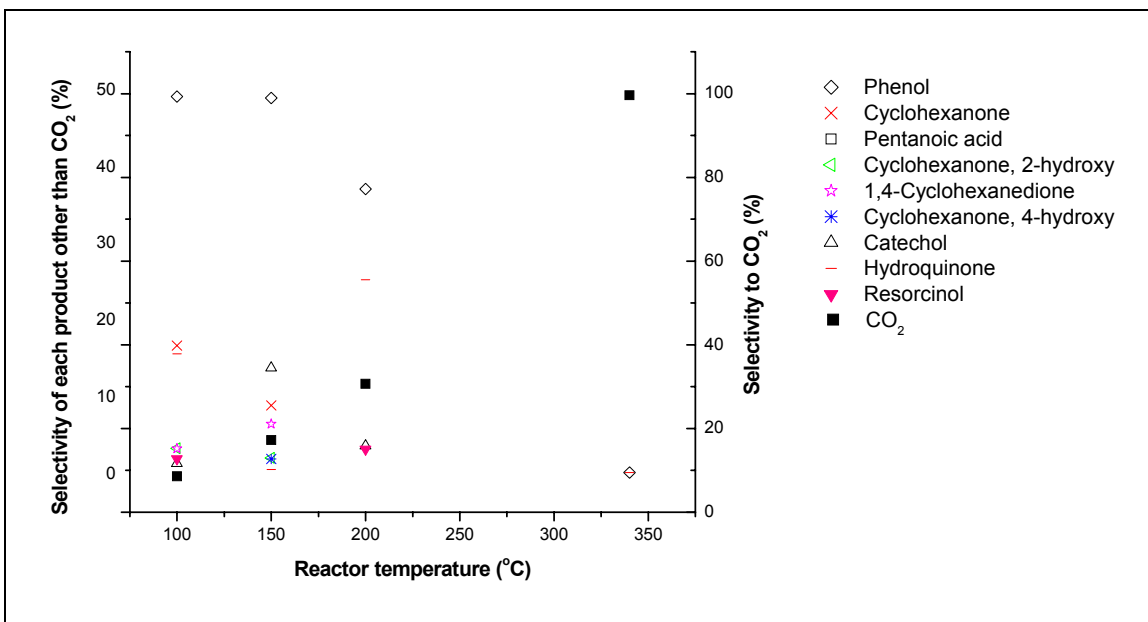


**Fig. 3.1.4.2.2:** Selectivity of each product from benzene reaction using Pd/ZrO$_2$ vs. reaction temperature. Total flow rate to the shell = 45 ml min$^{-1}$. Flow composition: Benzene/Ar/He/O$_2$/H$_2$ = 4.0/3.17/43.0/17.2/33.0 (% of total flow rate)

### 3.1.5. Pd/Carbon (Pd/C):

The reaction mixture (benzene, $H_2$, $O_2$, He, and Ar) was introduced to a the packed bed reactor which contained Pd catalyst supported on carbon (Pd/C) . The results for one set of flow conditions is shown in Figure 3.1.5.1
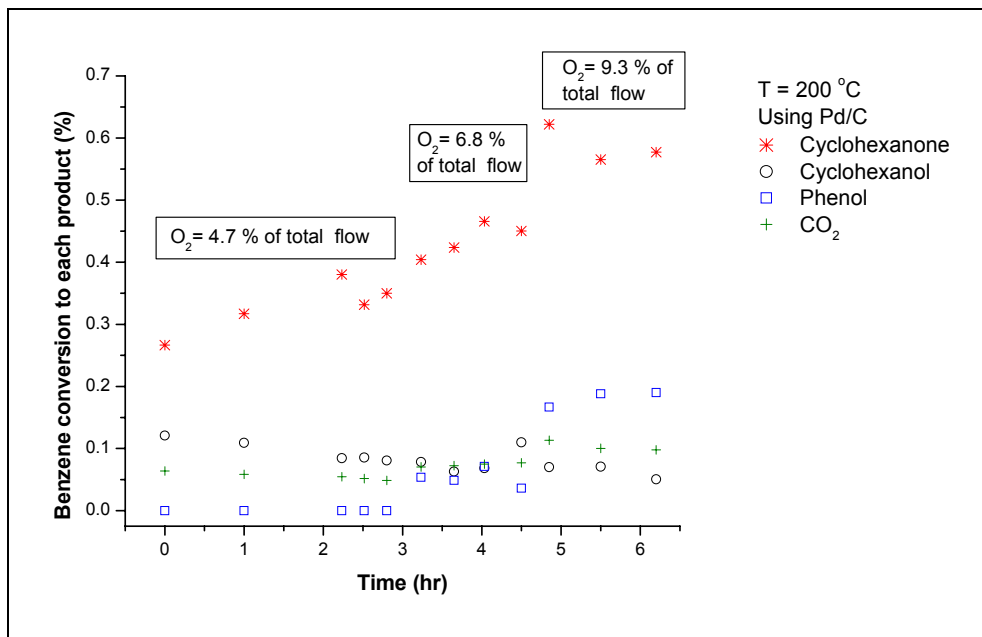


**Fig. 3.1.5.1**: Benzene conversion to the detected products at 200 $^o$C vs. time. Total flow rate = 40 ml min$^{-1}$, flow composition: Benzene/Ar/$H_2$ = 1.15/3.1/36.0, $O_2$ flow rate was increased and the balance was He

Other feed compositions were tested using the Pd/C catalyst in order to investigate the possibility of converting benzene to phenol. One set of flow conditions was tested and the results are shown in Figure 3.1.5.2. Another reaction mixture was tested. This reaction mixture has similar flow rates of $O_2$, $H_2$, and Ar as these ones in Figure 3.1.5.2 except that more He was used. The results at these new conditions are shown in Figure 3.1.5.3. Other reaction mixtures were tested and the results are shown in Figures 3.1.5.4 and 3.1.5.5. The aim of the changes in reaction mixtures was to find the conditions at which benzene can be converted to phenol at good conversion.

69
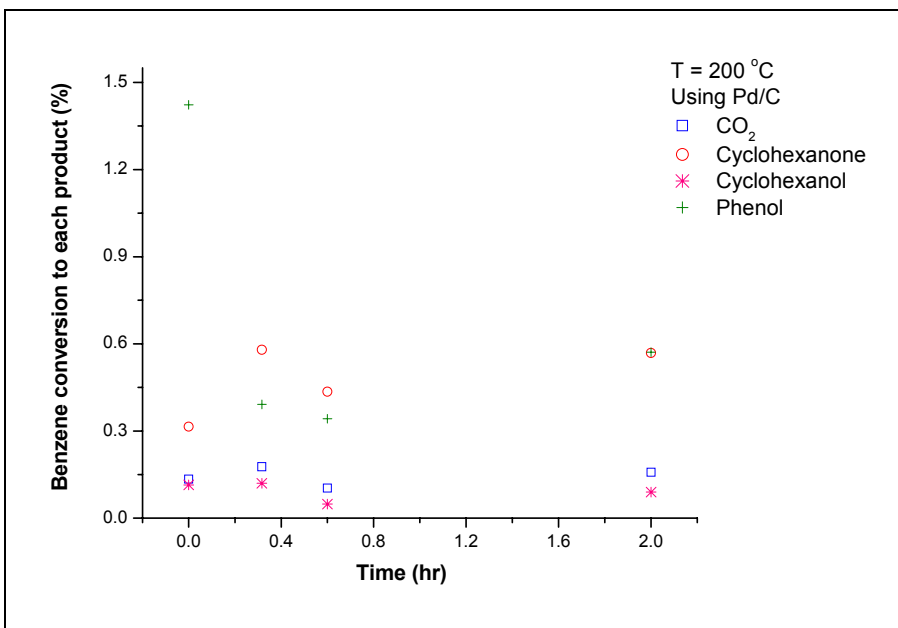
**Fig. 3.1.5.2:** Benzene conversion to the detected products at 200 °C vs. time. Total flow rate = 11.6 ml min$^{-1}$, flow composition: Benzene/Ar/O$_2$/He/H$_2$ = 4/5/19.6/30/41.8 (O$_2$/(O$_2$+H$_2$) = 32 %)
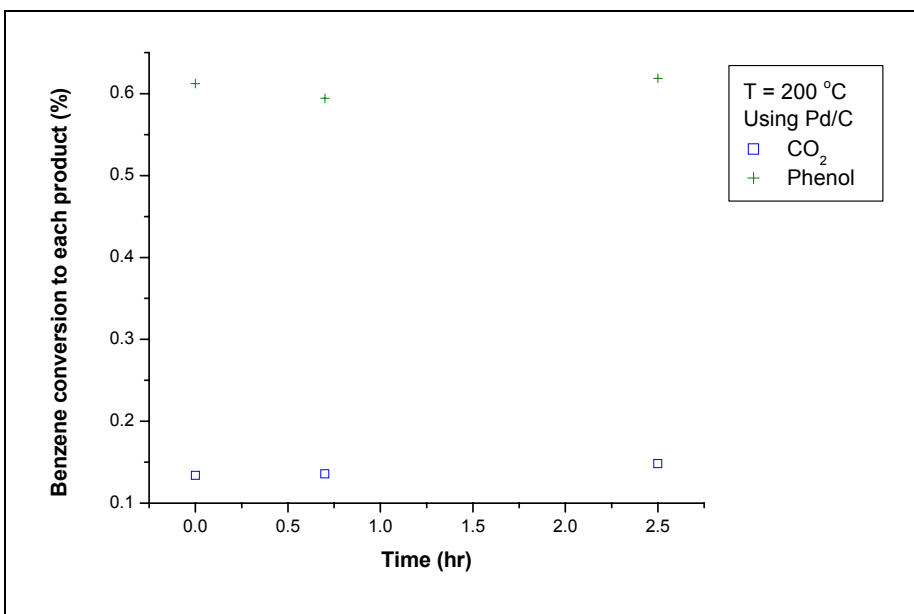


**Fig. 3.1.5.3:** Benzene conversion to the detected products at 200 °C vs. time. Total flow rate = 11.6 ml min$^{-1}$, flow composition: Benzene/Ar/O$_2$/He/H$_2$ = 1.2/3.2/6/76.9/41.8 (O$_2$/(O$_2$+H$_2$) = 32 %)
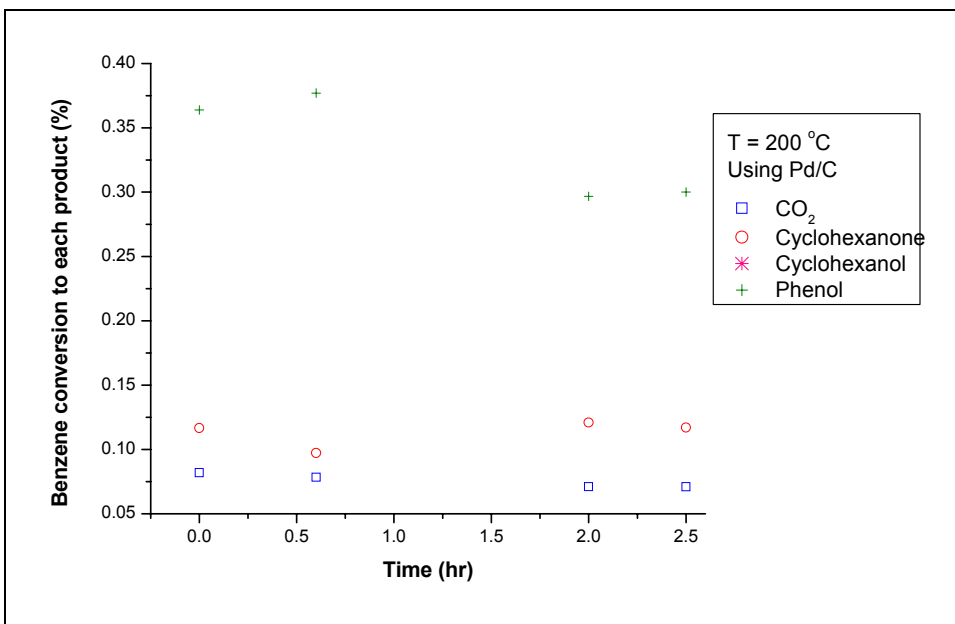
**Fig. 3.1.5.4:** Benzene conversion to the detected products at 200 $^o$C vs. time. Total flow rate = 35 ml min$^{-1}$, flow composition: Benzene/Ar/O$_2$/He/H$_2$ = 1.2/3.2/5/77.7/12.9 (O$_2$/(O$_2$+H$_2$)  = 32 %)
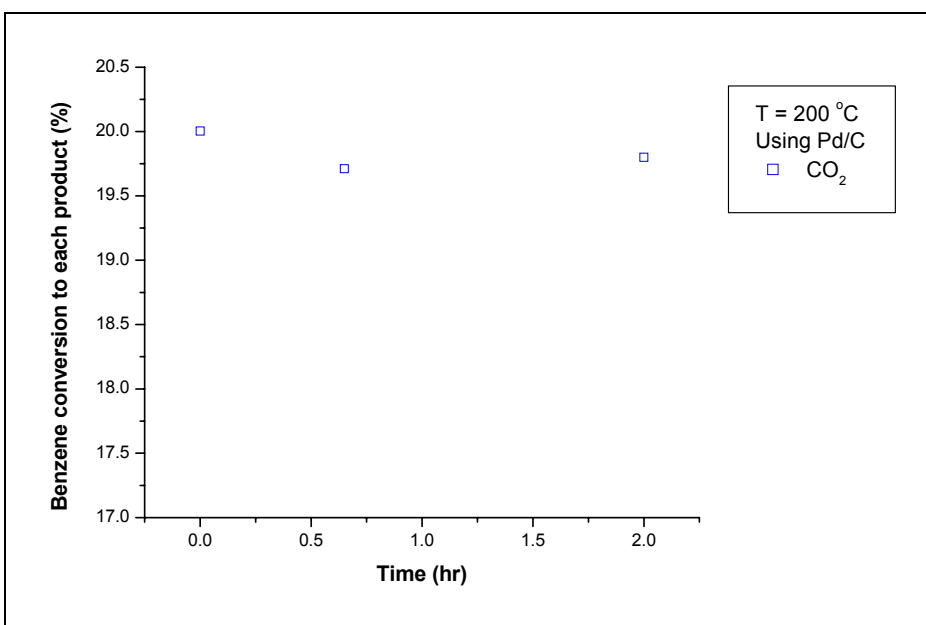


**Fig. 3.1.5.5:** Benzene conversion to the detected products at 200 $^o$C vs. time. Total flow rate = 35.5 ml min$^{-1}$, flow composition: Benzene/Ar/O$_2$/He/H$_2$ = 1.3/3.4/6.3/82.5/6.4 (O$_2$/(O$_2$+H$_2$)  = 50 %)

After finishing the above experiments the catalyst was tested to see if deactivation took place or not. This was performed by repeating the experiment with the flow

conditions in Figure 3.1.5.2. The results after repeating the experiments are shown in Table 3.1.5.1.

**Table 3.1.5.1:** Benzene conversion to each product (%) at 200 $^{\circ}$C . Total flow rate = 11.6 ml min$^{-1}$, flow composition: Benzene/Ar/$O_2$/He/$H_2$ = 4/5/19.6/30/41.8 ($O_2$/($O_2$+$H_2$) = 32 %)  after 2 hours of reaction.

| Phenol | Cyclohexanone | Cyclohexanol | $CO_2$ |
|---|---|---|---|
| 0.5 | 0.59 | 0.05 | 0.10 |

### 3.1.6. Pd foils obtained from Ma *et al* [30]

The design for this system consisted of the same ¾ in shell with the ¼ in tube inserted inside it. Now the catalyst is a Pd foil prepared according to Ma *et al* method [30]. The catalyst consisted of three different pieces cut into three different shapes that were welded to the exterior surface of the ¼ in tube.

A gaseous reaction mixture (benzene, He, Ar, $O_2$, and $H_2$) with a total flow rate of 22 ml min$^{-1}$ was entered to the reactor. The reaction temperature was 200 $^{\circ}$C. The benzene flow rate (or percentage) in the feed was varied in order to investigate its effect on benzene conversion to the detected products. Flow of He was varied in order to keep the total flow rate constant by changing feed inlet flow rate of benzene. Figure 4.1.6 shows benzene conversion to each product as a function of the feed inlet flow rate of benzene. Figure 3.1.6.2 shows the selectivity of the products from benzene reaction as a function of the variation in benzene inlet flow rate in the feed. The produced moles of these products at the previous conditions are shown in Figure 3.1.6.3. The conversion of $O_2$ (to $H_2O$ and $CO_2$) was 82 % and it was similar at all benzene inlet flow rates in the feed. Conversion of $O_2$ to $H_2O$ was 80 % and hence produced water was 2.5 x 10$^{-4}$ mol min$^{-1}$.The experiments at 3.4 % and 1.5 %   of benzene in the feed were repeated and gave the same results.
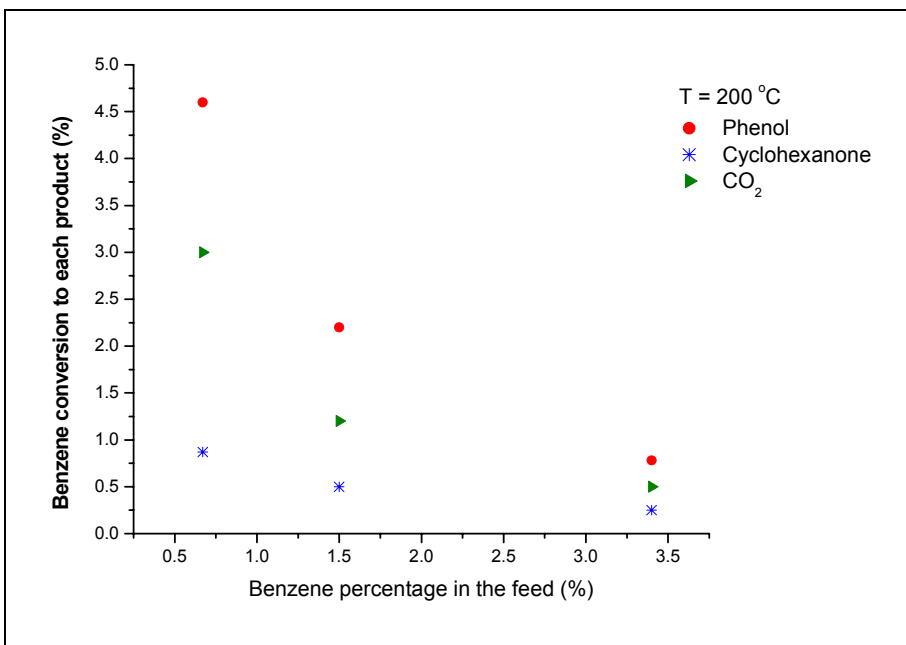
**Fig. 3.1.6.1**: Benzene conversion to the detected products at 200 $^{o}$C vs. benzene inlet flow rate in the feed (%). Total flow rate = 22 ml min$^{-1}$, flow composition: Ar/O$_2$/H$_2$ = 3.16/17.7/34.1 (O$_2$/ (O$_2$+H$_2$) = 34 %)
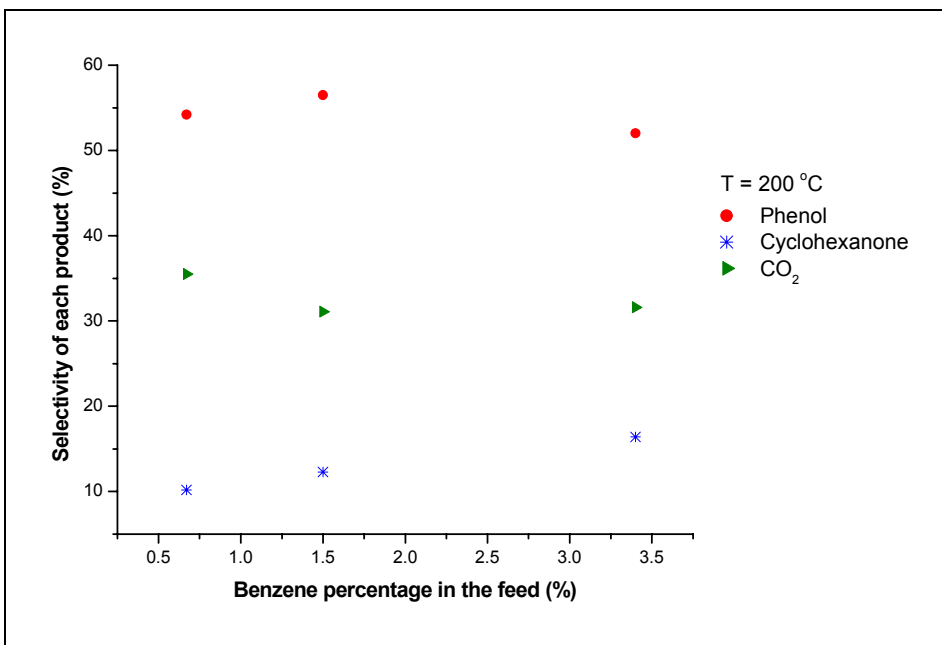


**Fig. 3.1.6.2:** Selectivity of each product from benzene reaction at 200 $^{o}$C vs. benzene inlet flow rate in the feed (%). Total flow rate = 22 ml min$^{-1}$, flow composition: Ar/O$_2$/H$_2$ = 3.16/17.7/34.1 (O$_2$/ (O$_2$+H$_2$) = 34 %)
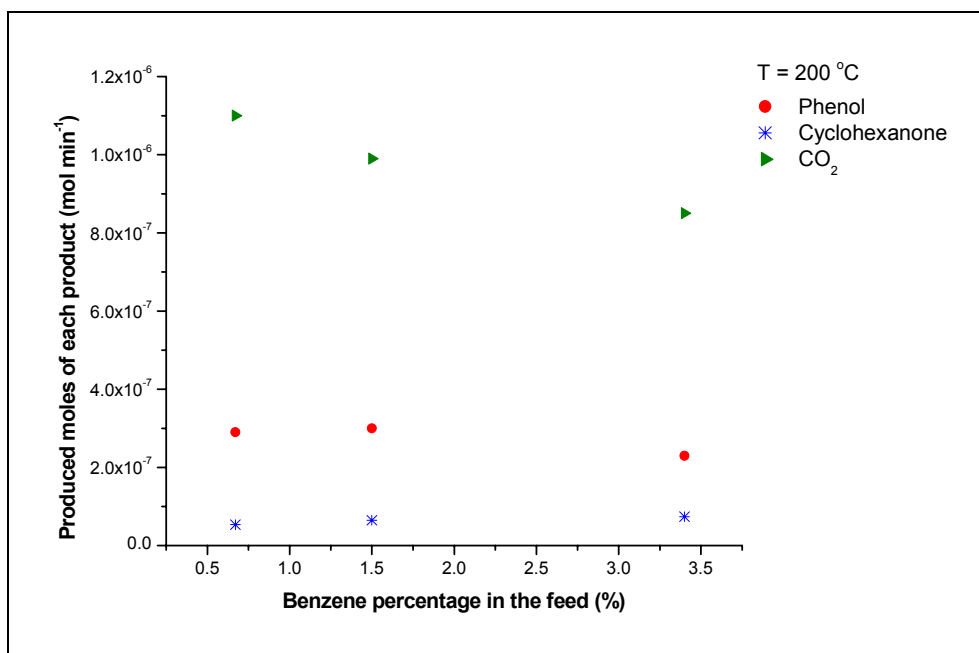
**Fig. 3.1.6.3:** Produced moles of each product from benzene reaction at 200 $^o$C vs. benzene inlet flow rate in the feed (%). Total flow rate = 22 ml min$^{-1}$, flow composition: Ar/O$_2$/H$_2$ = 3.16/17.7/34.1 (O$_2$/ (O$_2$+H$_2$) = 34 %)

The temperature distribution in the system was followed. This was performed by a thermocouple that extends inside the ¼ in tube and another thermocouple that extends inside a well that was very close to the exterior surface of the ¼ in tube. Both thermocouples were moved in order to be at a distance that reveals the location of each Pd piece on the ¼ in tube. The readings from both thermocouples for one flow conditions are summarized in Table 3.1.6.1.

**Table 3.1.6.1:** Temperature reading close to the three Pd pieces, 0.67 % Benzene in feed, total flow rate = 22 cc/min, 200$^o$ C

| Pd piece order | Thermocouple outside ¼ in tube Temperature $^o$ C | Thermocouple inside ¼ in tube Temperature $^o$ C |
|---|---|---|
| 1 (cone) | 193.8 | 200.0 |
| 2 (rectangular) | 200.0 | 202.0 |
| 3 (rectangular) | 197.7 | 194.7 |

A reaction mixture with flow rates of O$_2$, H$_2$, and benzene similar to the flow rates with the previous reaction mixture at 0.67 % of benzene in feed, and a higher He flow

rate was introduced into the reactor at 200 °C. Benzene conversion to each product, selectivity of the products, and produced moles of each product at these conditions are shown in Table 3.1.6.2 Oxygen conversion was 72 % (0.7 to $H_2O$) and produced water was 2.2 x $10^{-4}$ mol $min^{-1}$ at these flow rates of gases.

Table **3.1.6.2**: Reaction mixture at 200 °C. Total flow rate = 40 ml $min^{-1}$, flow composition: $Ar/O_2/H_2/Benzene/He$ = 3.16/9.5/18.4/0.36/68.5 ($O_2/ (O_2+H_2)$ = 34 %)

| Product | Conversion % | Selectivity % | Moles Produced |
|---------|-------------|---------------|----------------|
| Phenol | 4.6 | 59.3 | 2.8E-7 |
| Cyclohexanone | 0.0 | 0.0 | |
| $CO_2$ | 3.2 | 40.7 | 1.1E-6 |

A new reaction mixture was introduced into the reactor with lower $H_2$ and $O_2$ flow rates compared to the reaction mixture at 0.67 % benzene in Figure 3.1.6.1. Benzene conversion to each product, selectivity of the products, and produced moles of each product at these conditions are shown in Table 3.1.6.3. Oxygen conversion was 86 % (0.84 to $H_2O$) and produced water was 1.4 x $10^{-4}$ mol $min^{-1}$ at these flow rates of gases.

Table **3.1.6.3:** Reaction mixture at 200 °C. Total flow rate = 22 ml $min^{-1}$, flow composition: $Ar/O_2/H_2/Benzene/He$ = 3.16/9.2/17.6/0.67/69 ($O_2/ (O_2+H_2)$ = 34 %)

| Product | Conversion % | Selectivity % | Moles Produced |
|---------|-------------|---------------|----------------|
| Phenol | 1.6 | 55.3 | 1.0E-7 |
| Cyclohexanone | 0.0 | 0.0 | |
| $CO_2$ | 1.3 | 44.7 | 4.8E-7 |

A reaction mixture similar in total flow rate and composition to the conditions for the Pd-membrane system in section 3.1.3 (Figure 3.1.3.2.6.4) was introduced into the reactor at 200 °C. Benzene conversion to each detected product is shown in Figure 3.1.6.4. Selectivity of each product at these conditions is shown in Figure 3.1.6.5. Oxygen conversion was 70 % (0.68 to $H_2O$ producing 4 x $10^{-4}$ ml $min^{-1}$ of $H_2O$). The reaction was carried over night and gave the same results as after 2.5 hours. The previous

reaction mixture was introduced to the reactor at a higher reaction temperature. $O_2$ conversion was 0.87 (0.85 to $H_2O$ producing $5.4 \times 10^{-4}$ ml min$^{-1}$ of $H_2O$). Results at 250 $^o$C are shown in Figure 3.1.6.6.
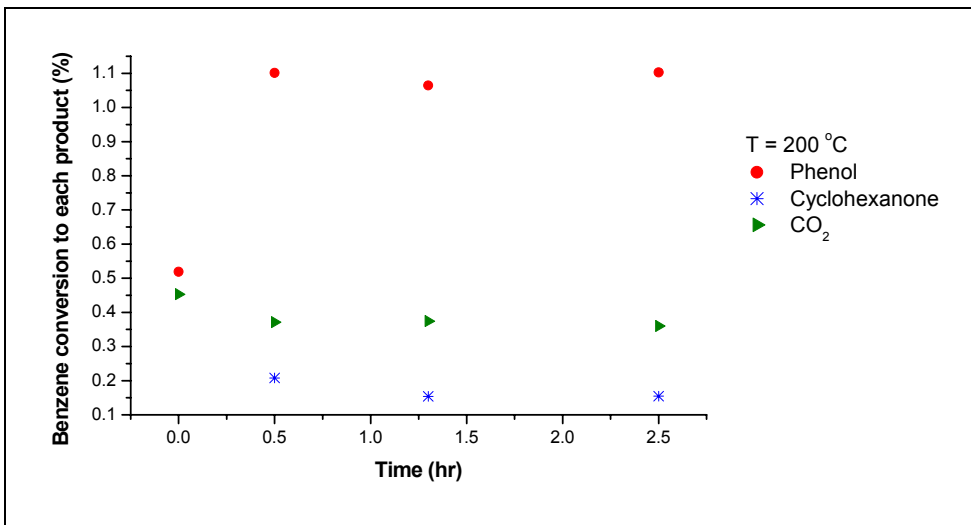


**Fig. 3.1.6.4:** Benzene conversion to the detected products at 200 $^o$C vs. time. Total flow rate = 43.1 ml min$^{-1}$, flow composition: Ar/$O_2$/$H_2$/benzene/He = 3.2/17.9/34.3/3.4/41 ($O_2$/ ($O_2$+$H_2$) = 34 %)
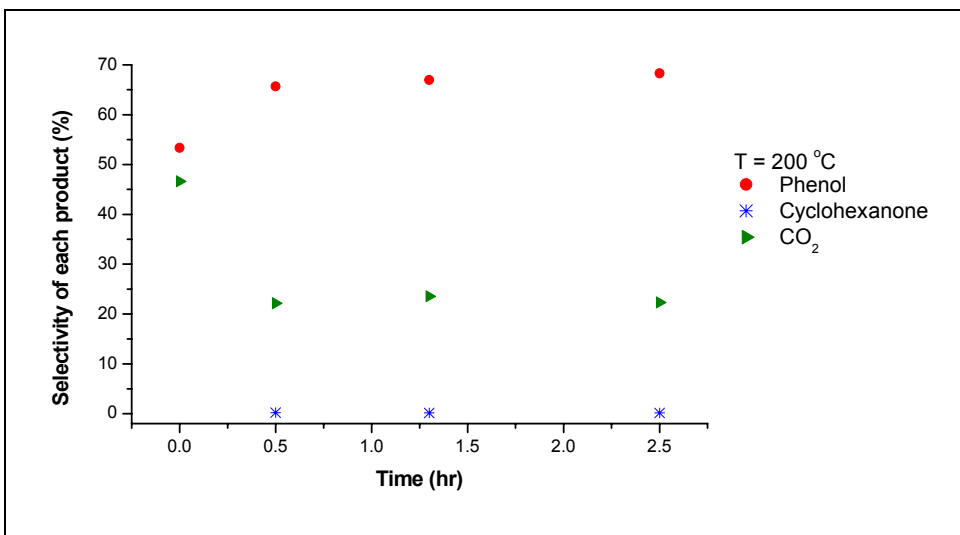


**Fig. 3.1.6.5:** Selectivity of each product from benzene reaction at 200 $^o$C vs. time. Total flow rate = 43.1 ml min$^{-1}$, flow composition: Ar/$O_2$/$H_2$/benzene/He = 3.2/17.9/34.3/3.4/41 ($O_2$/ ($O_2$+$H_2$) = 34 %)
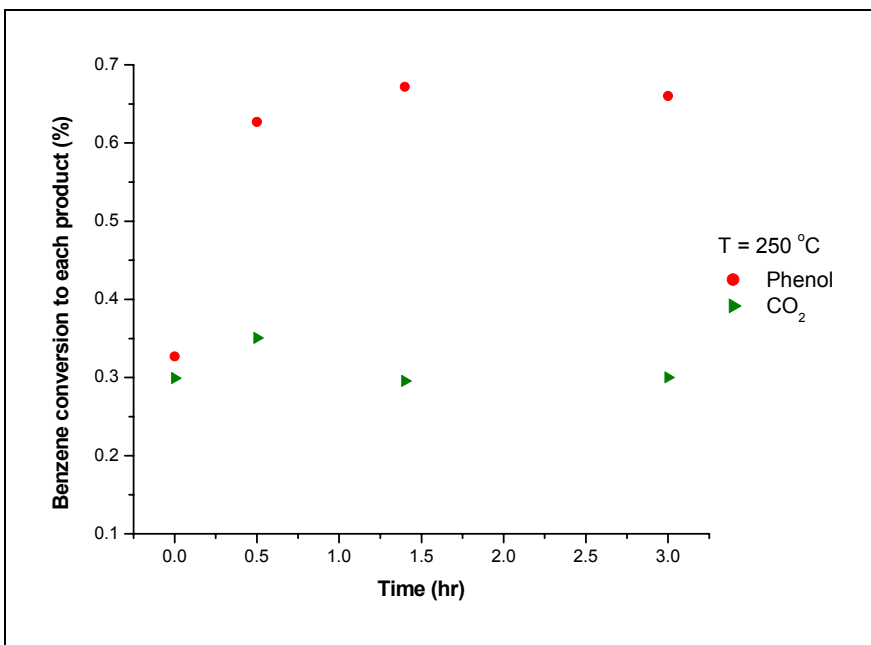
**Fig. 3.1.6.6:** Benzene conversion to the detected products at 250 $^o$C vs. time. Total flow rate = 43.1 ml min$^{-1}$, flow composition: Ar/O$_2$/H$_2$/benzene/He = 3.2/17.9/34.3/3.4/41 (O$_2$/ (O$_2$+H$_2$)  = 34 %)

The temperature distributions over the three Pd pieces were measured for the reaction conditions shown in Figure 3.1.6.4 and 3.1. 6.6 are shown in Figures 3.1.6.7 and 3.1.6.8, respectively.
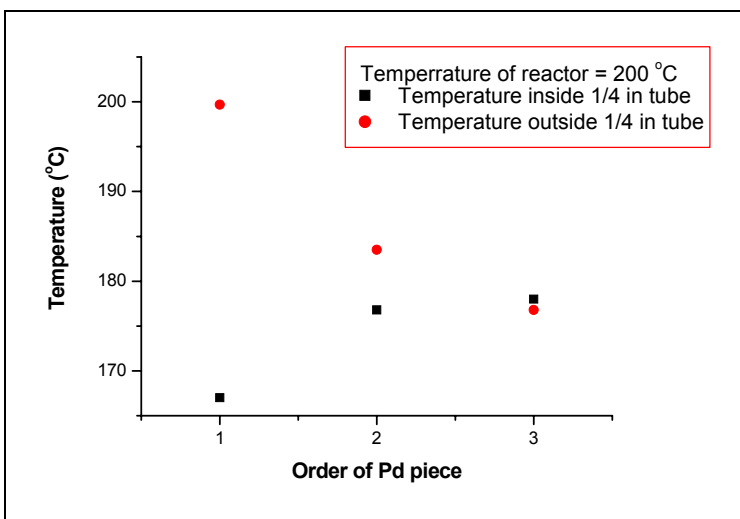


**Fig. 3.1.6.7:** Temperature distribution over the three Pd pieces for benzene reaction at 200 $^o$C vs. time. Total flow rate = 43.1 ml min$^{-1}$, flow composition: Ar/O$_2$/H$_2$/benzene/He = 3.2/17.9/34.3/3.4/41 (O$_2$/ (O$_2$+H$_2$)  = 34 %)

**Fig. 3.1.6.8:** Temperature distribution over the three Pd pieces for benzene reaction at 250 $^{o}$C vs. time. Total flow rate = 43.1 ml min$^{-1}$, flow composition: Ar/$O_2$/$H_2$/benzene/He = 3.2/17.9/34.3/3.4/41 ($O_2$/ ($O_2$+$H_2$) = 34 %)

The reaction mixture which was used in Figure 3.1.6.4 was carried at 200 $^{o}$C with lower benzene inlet flow rate in the feed and the results are shown in Figures 3.1.6.9, 3.1.6.10. Table 3.1.6.4 gibes the produced moles of each product for the flow conditions in Figures 3.1.6.4 and 3.1.6.9. $O_2$ conversion and produced $H_2O$ were similar to the ones at the conditions in Figure 3.1.6.4.

**Table 3.1.6.4:** Produced moles of each product from benzene reaction at 200 $^{o}$C vs. time. Total flow rate = 43.1 ml min$^{-1}$, flow composition: Ar/$O_2$/$H_2$/benzene/He = 3.2/17.9/34.3/1.5/43 ($O_2$/ ($O_2$+$H_2$) = 34 %)

| Products | Flow conditions in Figure 3.1.6.4 (mol min$^{-1}$) | Flow conditions in Figure 3.1.6.9 (mol min$^{-1}$) |
|---|---|---|
| Phenol | 6.74 E-07 | 6.83 E-07 |
| Cyclohexanone | 9.29 E-08 | 9.11 E-08 |
| $CO_2$ | 1.32 E-06 | 1.42 E-06 |
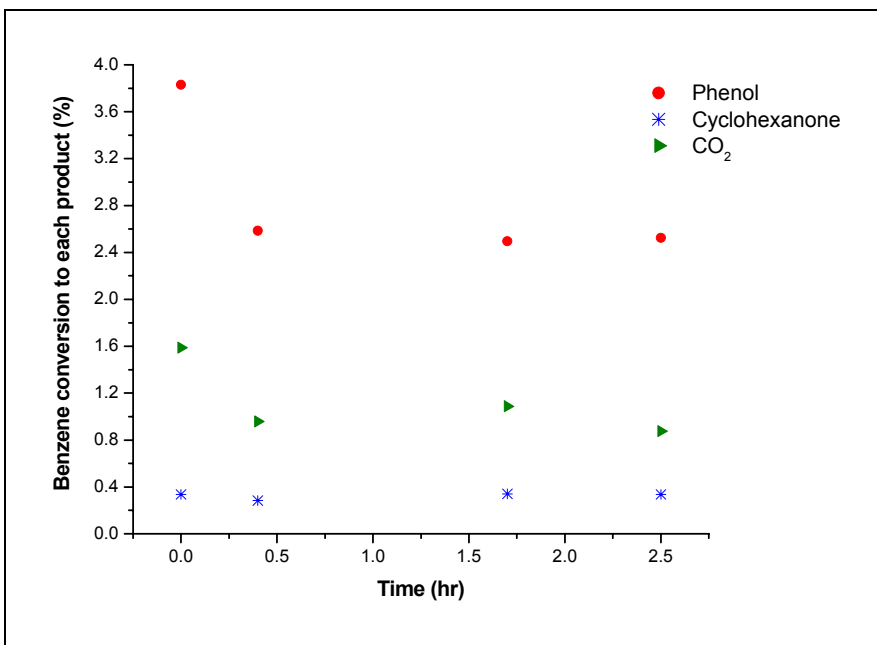
**Fig. 3.1.6.9:** Benzene conversion to the detected products at 200 $^{\circ}$C vs. Total flow rate= 43.1 ml min$^{-1}$. Flow composition: Ar/O$_2$/H$_2$/benzene/He = 3.2/17.9/34.3/1.5/43 (O$_2$/ (O$_2$+H$_2$) = 34 %)
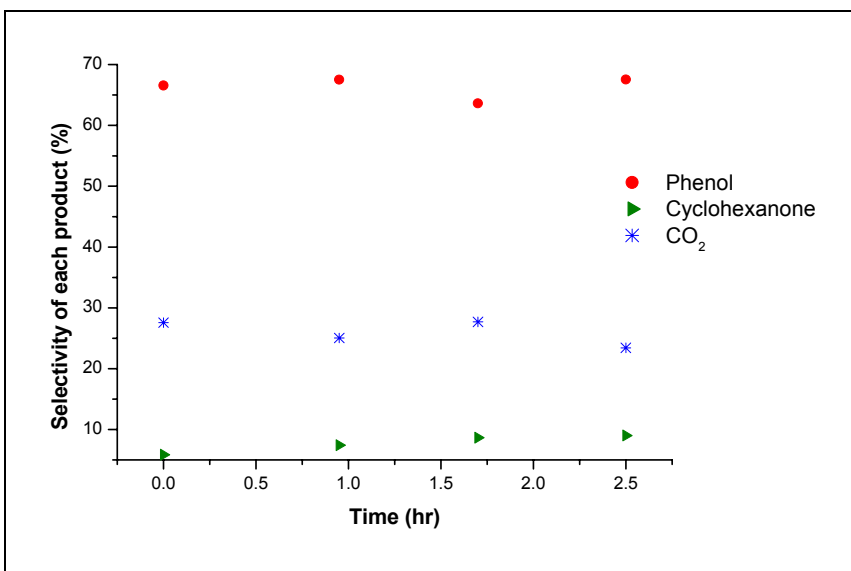


**Fig. 3.1.6.10:** Selectivity of each product from benzene reaction at 200 $^{\circ}$C vs. time. Total flow rate = 43.1 ml min$^{-1}$, flow composition: Ar/O$_2$/H$_2$/benzene/He = 3.2/17.9/34.3/1.5/43 (O$_2$/ (O$_2$+H$_2$) = 34 %)

### 3.1.7. Pd cone prepared according to the method of Ma *et al* [30]

The catalyst for this setup was Pd. As said earlier, Pd was cut in the form of a cone and welded to the exterior surface of the ¼ in tube. Gaseous reaction mixture was fed into the shell side and hence will come into contact with the Pd. With the same feed composition, the total flow rate was changed from 22 to 108 ml min$^{-1}$. Conversion of benzene to each product, selectivity of each product, and produced moles of each products are shown in Figures 3.1.7.1, 3.1.7.2, and 3.1.7.3, respectively. These experiments were repeated and gave the same results. Oxygen total conversion, oxygen conversion to $H_2O$, and produced water at the different flow rates are given in Table 3.1.7.1
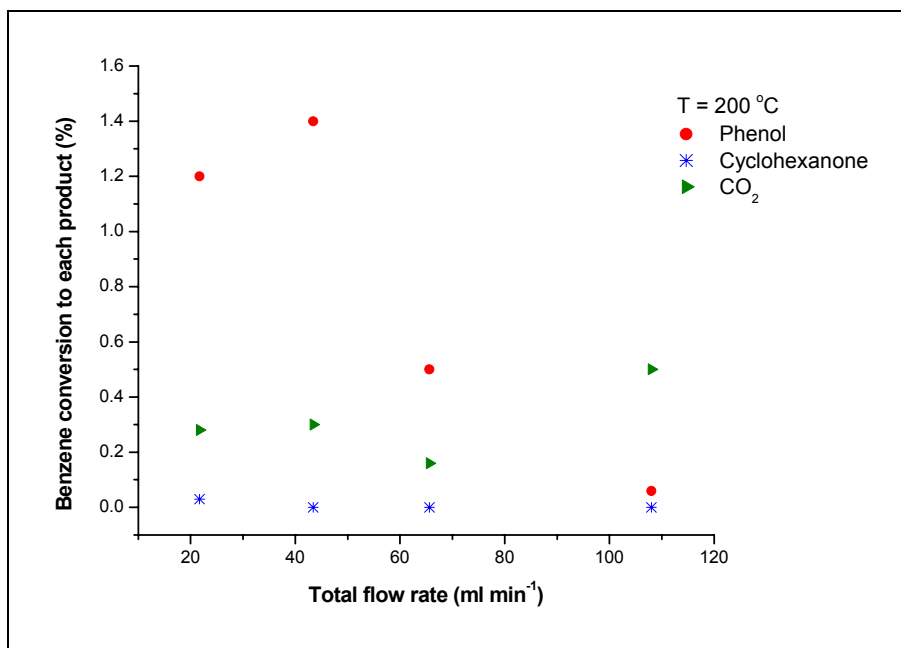


**Fig. 3.1.7.1:** Benzene conversion at 200 $^o$C vs. total flow rate. Flow composition: Benzene/Ar/He/$O_2$/$H_2$ = 3.6/3.17/41.0/17.8/34.0 (% of total flow rate) ($O_2$/ ($O_2$+$H_2$) = 34 %)
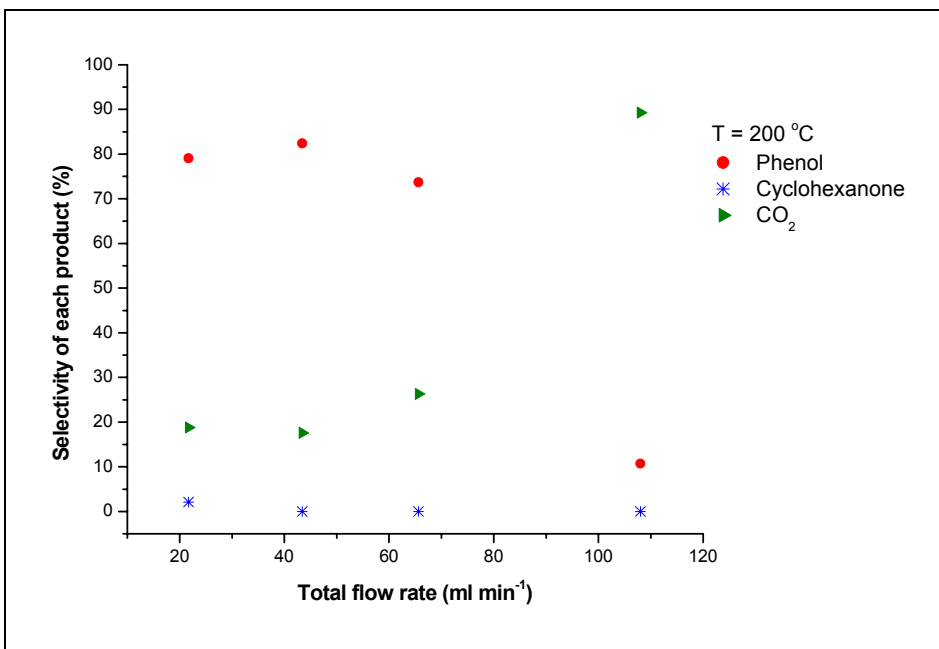
**Fig. 3.1.7.2:** Selectivity of each product from benzene reaction at 200 $^o$C vs. total flow rate. Flow composition: Benzene/Ar/He/$O_2$/$H_2$ = 3.6/3.17/41.0/17.8/34.0 (% of total flow rate) ($O_2$/ ($O_2$+$H_2$) = 34 %)



**Fig. 3.1.7.3**: Produced moles of each product from benzene reaction at 200 $^o$C vs. total flow rate. Flow composition: Benzene/Ar/He/$O_2$/$H_2$ = 3.6/3.17/41.0/17.8/34.0 (% of total flow rate) ($O_2$/ ($O_2$+$H_2$) = 34 %)

**Table 3.1.7.1:** Oxygen total conversion, oxygen conversion to $H_2O$, and produced water at 200 $^o$C for the different flow rates

| Total flow rate (ml min$^{-1}$) | $O_2$ conversion (%) | $O_2$ conversion to $H_2O$ (%) | Produced $H_2O$ ($10^{-4}$ mol min$^{-1}$) |
|---|---|---|---|
| 22 | 76 | 74 | 2.4 |
| 43 | 72 | 70 | 4.1 |
| 65.5 | 74 | 72 | 6.9 |
| 108 | 84 | 82 | 12.8 |

Temperature distribution outside the ¼ in tube, for the different flow rates, was measured using a thermocouple inside the thermowell that extends very close to the exterior surface of the ¼ in tube and the results are shown in Figure 3.1.7.4.

The reaction mixture at a total flow rate of 43 ml min$^{-1}$ was carried at different temperatures. Benzene conversion to each product vs. reaction temperature is shown in Figure 3.1.7.5. Total conversion of $O_2$ is shown in Figure 3.1.7.6.
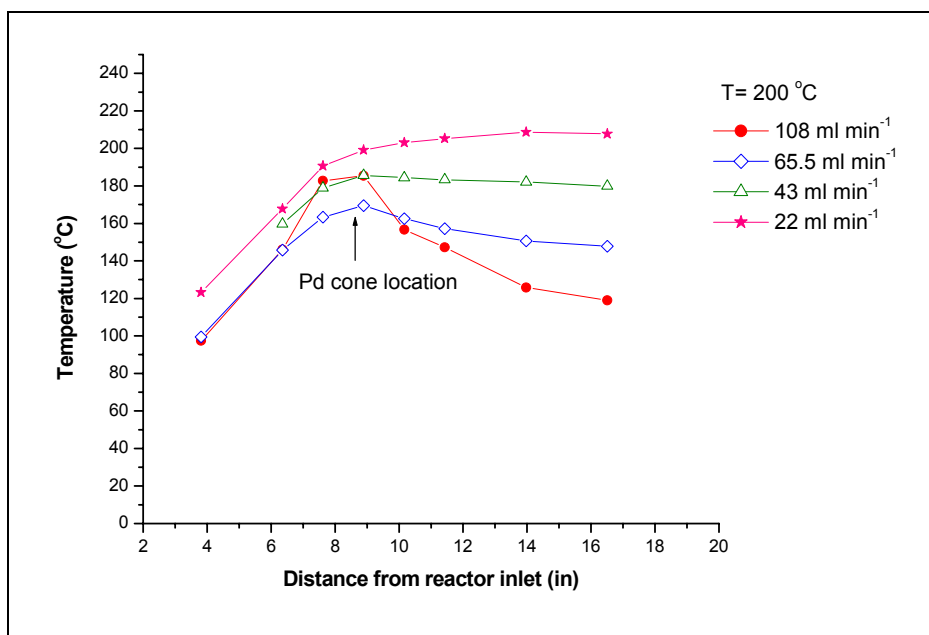


**Fig. 3.1.7.4:** Temperature inside the reactor vs. distance from reactor inlet at different total flow rates. Reaction temperature= 200 $^o$C. Flow composition: Benzene/Ar/He/$O_2$/$H_2$ = 3.6/3.17/41.0/17.8/34.0 (% of total flow rate) ($O_2$/ ($O_2$+$H_2$) = 34 %)
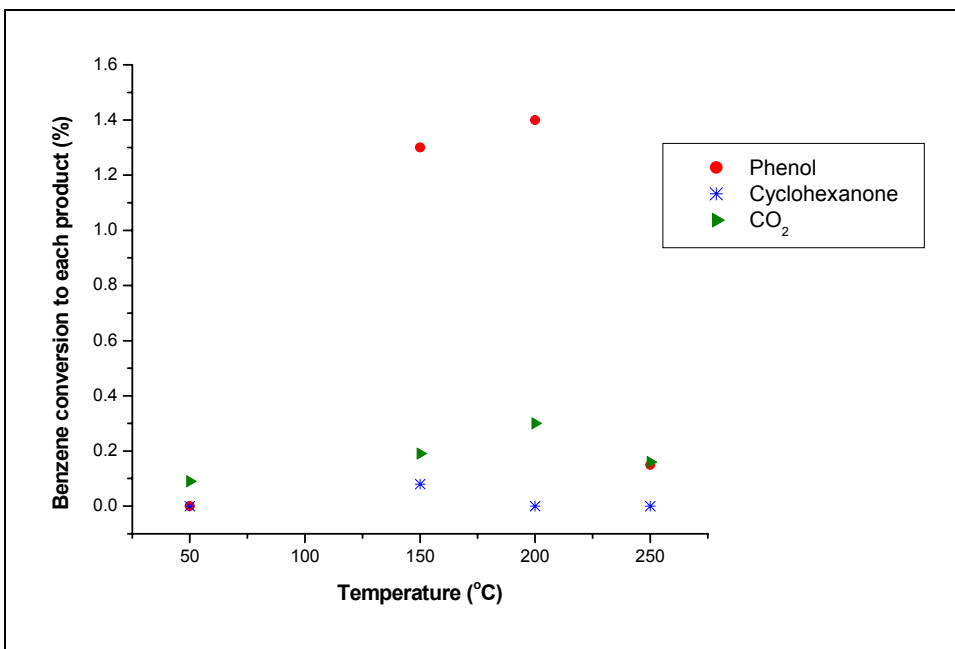
**Fig. 3.1.7.5:** Benzene conversion to each product vs. reaction temperature. Total flow rate= 43 ml min$^{-1}$. Flow composition: Benzene/Ar/He/$O_2$/$H_2$ = 3.6/3.17/41.0/17.8/34.0 (% of total flow rate) ($O_2$/ ($O_2$+$H_2$) = 34 %)
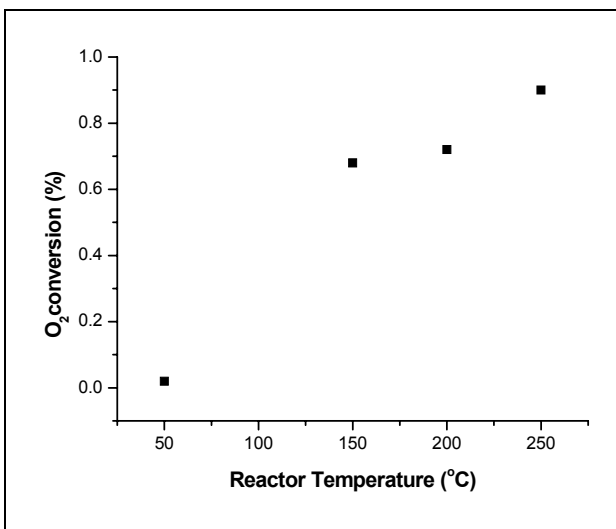


**Fig. 3.1.7.6**: Oxygen total conversion vs. reaction temperature. Total flow rate= 43 ml min$^{-1}$. Flow composition: Benzene/Ar/He/$O_2$/$H_2$ = 3.6/3.17/41.0/17.8/34.0 (% of total flow rate) ($O_2$/ ($O_2$+$H_2$) = 34 %)

Produced amount of water at the different reaction temperatures is shown in Table 3.1.7.2.

**Table 3.1.7.2:** Produced water at the different reaction temperature. Total flow rate= 43 ml min$^{-1}$. Flow composition: Benzene/Ar/He/$O_2$/$H_2$ = 3.6/3.17/41.0/17.8/34.0 (% of total flow rate) ($O_2$/($O_2$+$H_2$) = 34 %)

| Total flow rate (ml min$^{-1}$) | Produced $H_2O$ ($10^{-4}$ mol min$^{-1}$) |
|---|---|
| 50 | 0.083 |
| 150 | 2.7 |
| 200 | 4.1 |
| 250 | 5.8 |

The flow rate of oxygen in the feed, for the reaction mixture with total flow rate of 43 ml min$^{-1}$, was varied keeping hydrogen, benzene, and Ar flow rates constants with the balance gas being He. This was performed in order to investigate the effect of this variation on benzene conversion. The temperature of reaction at these conditions was 200 $^o$C. Benzene conversion to each product at the different $O_2$ percentages in the feed is shown in Figure 3.1.7.7. Selectivity of each product from benzene reaction is shown in Figure 3.1.7.8. For the three studied $O_2$ inlet flow rates in the feed 9 %, 17.8 %, and 22 % the ratio $O_2$/($O_2$+$H_2$) was 20 %, 34 %, and 39 %, respectively.
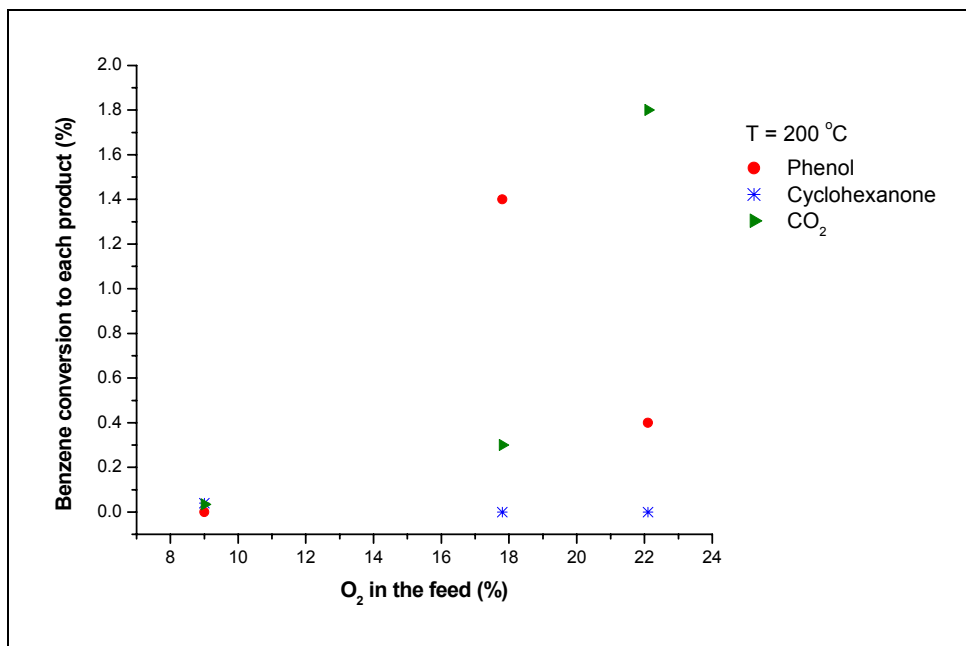


**Fig. 3.1.7.7:** Benzene conversion to each product vs. $O_2$ inlet flow rate in the feed at 200 $^o$C. Total flow rate= 43 ml min$^{-1}$. Flow composition: Benzene/Ar/$H_2$ = 3.6/3.17/34.0 (% of total flow rate)
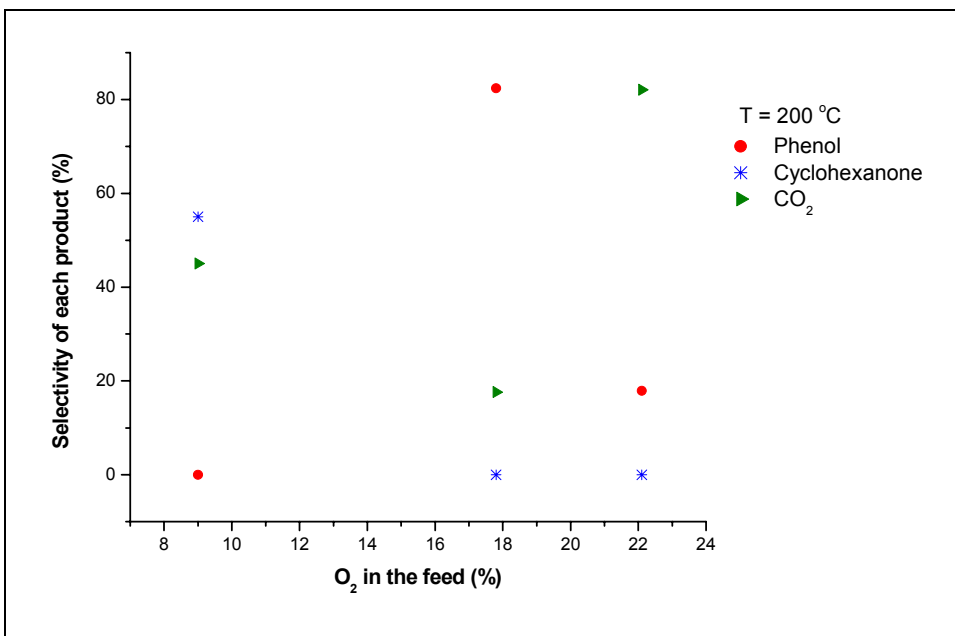
**Fig. 3.1.7.8:** Selectivity of each product from benzene reaction vs. $O_2$ inlet flow rate in the feed at 200 °C. Total flow rate= 43 ml min⁻¹. Flow composition: Benzene/Ar/$H_2$ = 3.6/3.17/34.0 (% of total flow rate)

Figure 3.1.7.9 shows $O_2$ conversion and the corresponding produced water at the different percentages of $O_2$ in the feed.
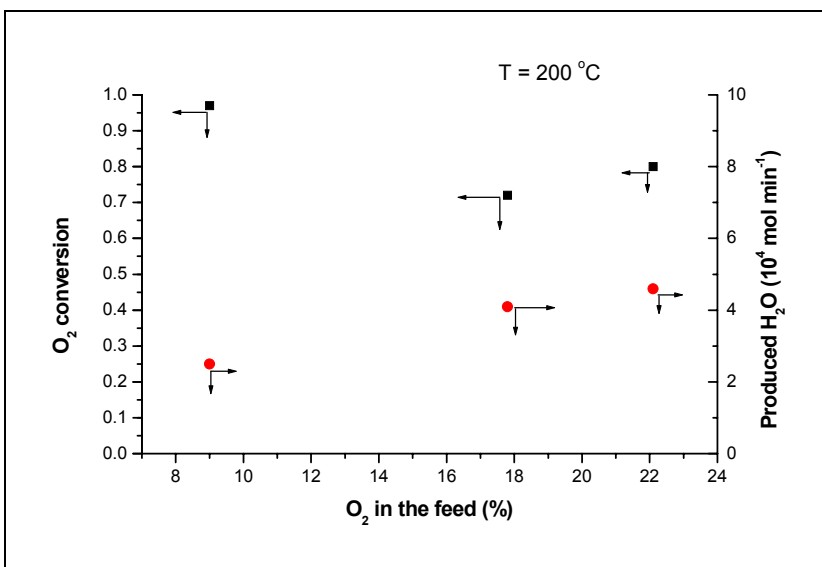


**Fig. 3.1.7.9:** Conversion of $O_2$ and produced $H_2O$ vs. $O_2$ inlet flow rate in the feed at 200 °C. Total flow rate= 43 ml min⁻¹. Flow composition: Benzene/Ar/$H_2$ = 3.6/3.17/34.0 (% of total flow rate)

Temperature distribution in the reactor at the different $O_2$ inlet flow rates in the feed, for the conditions given in Figure 3.1.7.9, is shown in Figure 3.1.7.10.

85
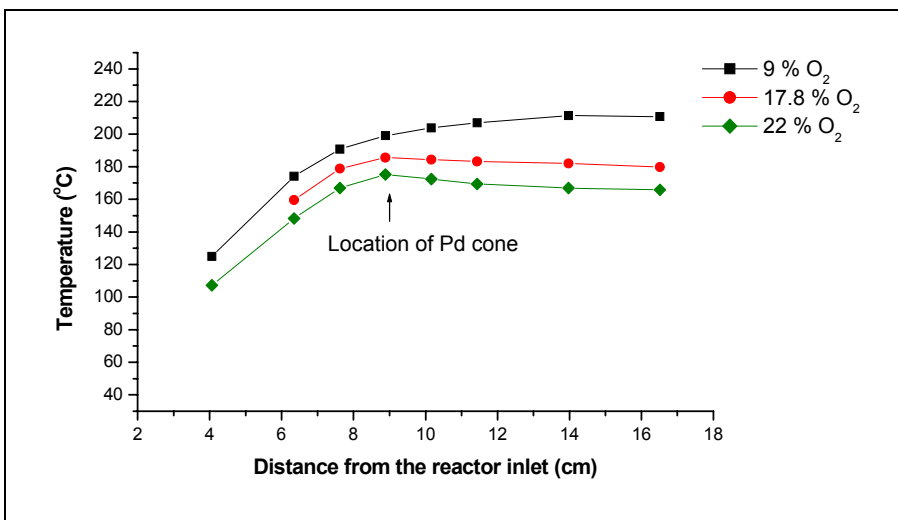
**Fig. 3.1.7.10:** Temperature vs. distance from reactor inlet at the different $O_2$ inlet flow rates in the feed. Total flow rate= 43 ml min$^{-1}$. Flow composition: Benzene/Ar/$H_2$ = 3.6/3.17/34.0 (% of total flow rate)

The flow rate of hydrogen in the feed to reactor was varied at constant total flow rate of the feed, constant temperature, constant flow rate of benzene, constant flow rate of oxygen, constant flow rate of Ar, and varying the flow rate of He (the balance gas). Benzene conversion as a function of variations of $H_2$ IS shown in Figure 3.1.7.11. Selectivity of each product at these conditions is shown in Figure 3.1.7.12. Conversion of $O_2$ and produced amount of water at the different percentages of $H_2$ in the feed are shown in Figure 3.1.7.13. At least 0.9 of $O_2$ conversion was used for water based on the calculated conversion of $O_2$ to $CO_2$ and $H_2O$. The measured temperature distributions, at the different flow rates of hydrogen in the feed to the reactor, inside the reactor is shown in Figure 3.1.7.14.
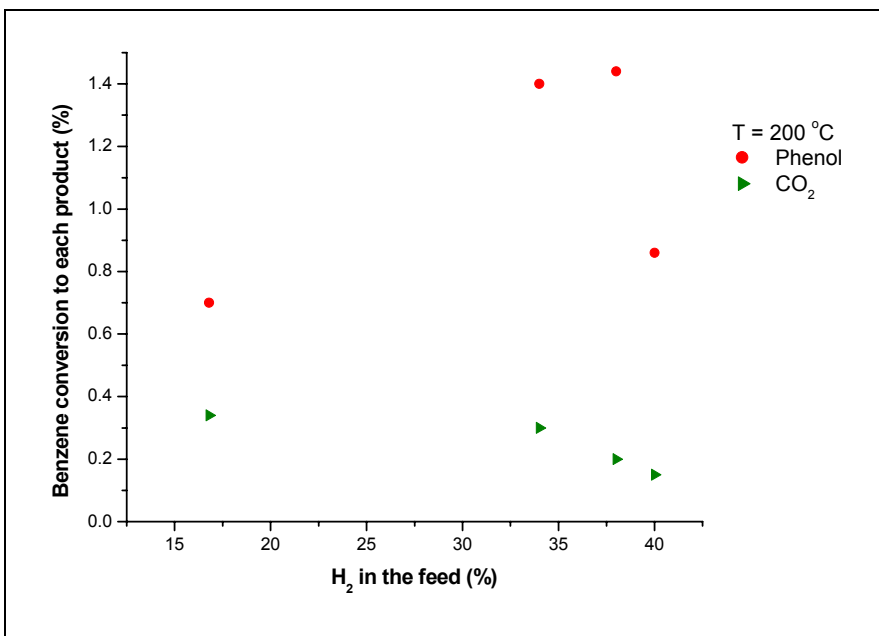
**Fig. 3.1.7.11:** Benzene conversion to each product vs. $H_2$ percentage of the total flow rate in the feed at 200 $^{\circ}C$. Total flow rate= 43 ml min$^{-1}$. Flow composition: Benzene/Ar/$O_2$ = 3.6/3.17/17.8 (% of total flow rate)
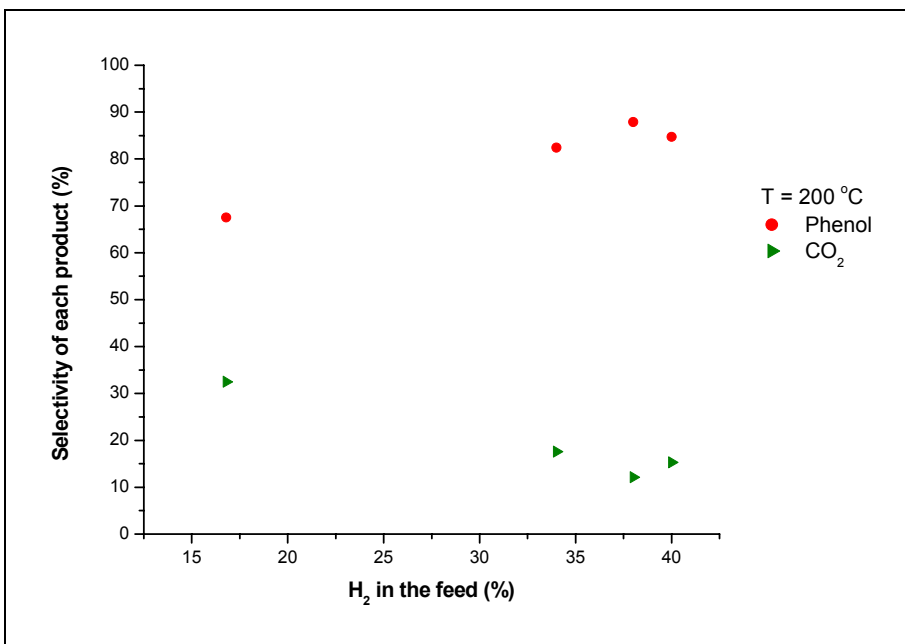


**Fig. 3.1.7.12:** Selectivity of each product from benzene conversion at 200 $^{\circ}C$ vs. $H_2$ percentage of the total flow rate in the feed. Total flow rate= 43 ml min$^{-1}$. Flow composition: Benzene/Ar/$O_2$ = 3.6/3.17/17.8 (% of total flow rate)
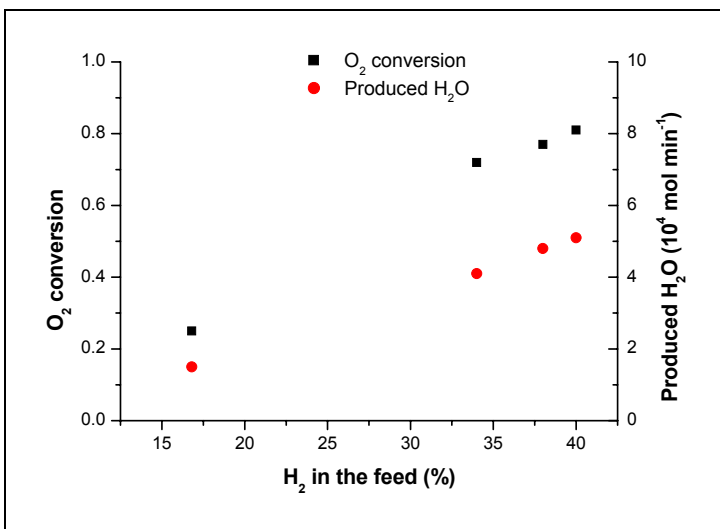
**Fig. 3.1.7.13:** Conversion of $O_2$ and produced $H_2O_2$ at 200 $^o$C vs. $H_2$ percentage of the total flow rate in the feed. Total flow rate= 43 ml min$^{-1}$. Flow composition: Benzene/Ar/$O_2$ = 3.6/3.17/17.8 (% of total flow rate)
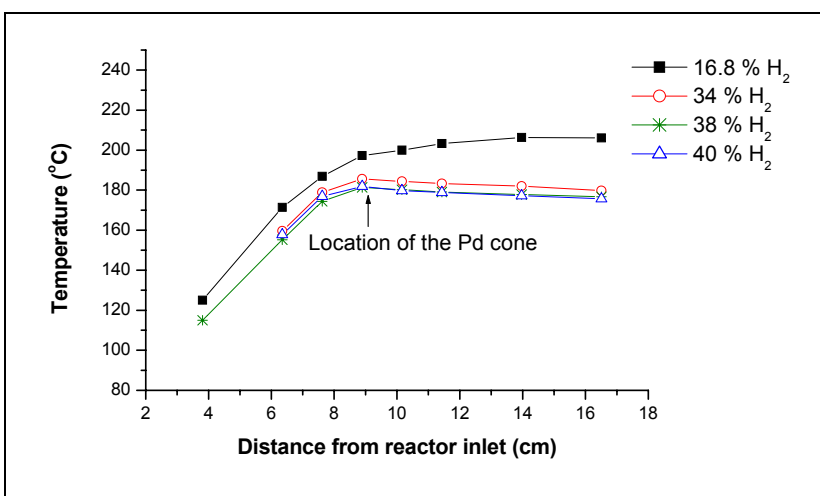


**Fig. 3.1.7.14:** Temperature vs. distance from reactor inlet at the different $H_2$ inlet flow rates in the feed. Total flow rate= 43 ml min$^{-1}$. Flow composition: Benzene/Ar/$O_2$ = 3.6/3.17/17.8 (% of total flow rate)

### 3.1.8. Pd cone from Alfa Aesar:

For this part the catalyst was Pd foil, purchased from Alfa Aesar, and this foil was cut and welded to the exterior surface of the ¼ in tube to form a cone. Basically this is a similar design to the one Pd cone that was described in section 3.1.7.

Gaseous mixture of benzene, He, Ar, $O_2$, and $H_2$ was entered into the shell side of the reactor and hence was allowed to come into contact with the Pd catalyst. For one set of flow conditions, similar to one of the flow conditions in section 3.1.7, benzene

conversion to each product, produced moles of each product and products selectivity are shown in Tables 3.1.8.1 and 3.1.8.2 for two different total flow rates. Conversion of $O_2$ was 0.71 (0.69 to $H_2O$) at 43 ml min$^{-1}$ producing 4.3 x10$^{-4}$ mol min$^{-1}$ of $H_2O$. At the higher flow rate, Conversion of $O_2$ was 0.83 at 76 ml min$^{-1}$ and produced 8 x10$^{-4}$ mol min$^{-1}$ of $H_2O$. Experiment at 43 ml min$^{-1}$ was repeated and gave the same results.

**Table 3.1.8.1:** Benzene conversion to each product, selectivity of each product, and produced moles of each product at 200 $^o$C vs. time. Total flow rate= 43.2 ml min$^{-1}$. Flow composition: Benzene/Ar/He/$O_2$/$H_2$ = 3.5/3.19/41.0/17.9/34.0 (% of total flow rate) ($O_2$/ ($O_2$+$H_2$) = 34 %)

| Product | Conversion (%) | Selectivity (%) | Produced moles (mol min$^{-1}$) |
|---|---|---|---|
| Phenol | 1.2 | 79.0 | 7.7E-7 |
| Cyclohexanone | 0.0 | 0.0 | 0.0 |
| $CO_2$ | 0.32 | 21.0 | 1.2E-6 |

**Table 3.1.8.2:** Benzene conversion to each product, selectivity of each product, and produced moles of each product at 200 $^o$C vs. time. Total flow rate= 76 ml min$^{-1}$. Flow composition: Benzene/Ar/He/$O_2$/$H_2$ = 3.5/3.13/41.3/17.9/34.0 (% of total flow rate) ($O_2$/ ($O_2$+$H_2$) = 34 %)

| Product | Conversion (%) | Selectivity (%) | Produced moles (mol min$^{-1}$) |
|---|---|---|---|
| Phenol | 0.12 | 36.8 | 1.4E-7 |
| Cyclohexanone | 0.0 | 0.0 | 0.0 |
| $CO_2$ | 0.21 | 63.2 | 1.4E-6 |

### 3.1.9. (7) Pieces of Pd On Nonporous Stainless Steel Tube

The design of this system was described earlier in the experimental setup. As a reminder, the ¼ in tube now has 7 holes above each a rectangular foil of Pd was welded. The reactants can be fed directly to the shell and come in contact with Pd, or they may be fed in to the ¼ in tube and emerge from the holes and come in contact with PD. Another possibility is that some of the reactants might be fed to the ¼ in tube and the remaining reactants can be fed into the shell.

### 3.1.9.1. Using $H_2$ in tube side and the other gases in the shell side

When using this system first $H_2$ was being flowed to the tube side and hence would emerge from the holes and come into contact with the other gases (benzene, He, Ar, $O_2$ that were fed into the shell side. The tube exit was closed so that all the flow will emerge from the ¼ in tube through the holes to the shell.

Results for one set of experiment, where flow conditions similar to the flow conditions in Pd system using either membrane or welded foils, are shown in table 3.1.9.1.1. Conversion of $O_2$ was 0.88 (0.81 to $H_2O$) and produced $H_2O$ was 5.1 x $10^{-4}$ mol $min^{-1}$.

**Table 3.1.9.1:** Conversion of benzene to each product, selectivity of the products, and produced moles of each product at 200 $^o$C. Total flow rate= 43.4 ml $min^{-1}$. Flow composition: Benzene/Ar/He/$O_2$/$H_2$ = 3.3/3.1/41.6/17.8/34.0 (% of total flow rate) ($O_2$/ ($O_2$+$H_2$)  = 34 %)

| Product | Conversion % | Selectivity % | Produced moles (mol $min^{-1}$) |
|---|---|---|---|
| Phenol | 0.0 | 0.0 | 0.0 |
| Cyclohexanone | 0.0 | 0.0 | 0.0 |
| $CO_2$ | 2.0 | 100.0 | 6.2E-7 |

Another reaction mixture was tested to explore the possibility of getting higher conversions of benzene to phenol. The results are shown in Table 4.1.9.1.2. Conversion of $O_2$ was 0.91 (0.89 to $H_2O$) and produced $H_2O$ was 5.7 x $10^{-4}$ mol $min^{-1}$.

**Table 3.1.9.2:** Conversion of benzene to each product, selectivity of the products, and produced moles of each product at 200 $^o$C. Total flow rate= 56 ml $min^{-1}$. Flow composition: Benzene/Ar/He/$O_2$/$H_2$ = 2.4/3.0/24/13.8/57.0 (% of total flow rate) ($O_2$/ ($O_2$+$H_2$)  = 20 %)

| Product | Conversion % | Selectivity % | Produced moles (mol $min^{-1}$) |
|---|---|---|---|
| Phenol | 0.52 | 51.8 | 2.9E-7 |
| Cyclohexanone | 0.15 | 15.4 | 8.7E-8 |
| $CO_2$ | 0.33 | 32.8 | 1.1E-6 |

A third mixture of the gaseous reactants was tested. This mixture has higher flow rate of $O_2$ than the other mixtures beside a higher total flow rate. The results are shown in

Table 3.1.9.1.3. Conversion of $O_2$ was 0.91 (0.89 to $H_2O$) and produced $H_2O$ was 8.7 x $10^{-4}$ mol min$^{-1}$.

**Table 3.1.9.3:** Conversion of benzene to each product, selectivity of the products, and produced moles of each product at 200 $^o$C. Total flow rate= 58 ml min$^{-1}$. Flow composition: Benzene/Ar/He/$O_2$/$H_2$ = 2.3/3.1/22/19.7/52.7 (% of total flow rate) ($O_2$/ ($O_2$+$H_2$) = 27 %)

| Product | Conversion % | Selectivity % | Produced moles (mol min$^{-1}$) |
|---|---|---|---|
| Phenol | 0.71 | 61.3 | 4.0E-7 |
| Cyclohexanone | 0.0 | 0.0 | 0.0 |
| $CO_2$ | 0.45 | 38.7 | 1.6E-6 |

The reaction mixture in Table 3.1.9.1.2 was carried at different total flow rates (from shell and tube sides) keeping both the compositions of the reaction mixtures and the temperature constants for the different flow rates. Benzene conversion to each product at the different flow rates is shown in Figure 3.1.9.1.1. Selectivity of each product from this reaction is shown in Figure 3.1.9.1.2. Total conversion of $O_2$ and produced $H_2O$ are shown in Figure 3.1.9.3.
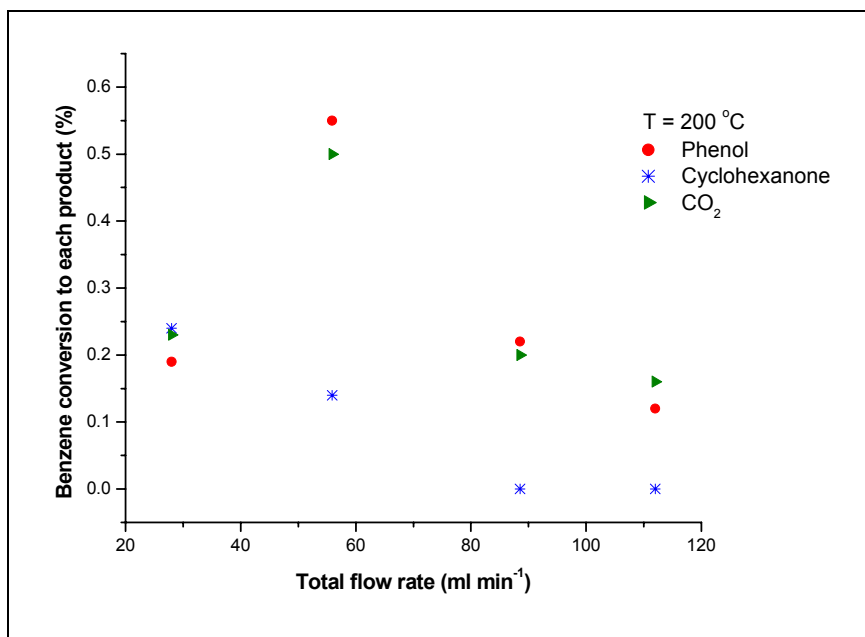


**Fig. 3.1.9.1.1:** Conversion of benzene to each product vs. total flow rate at 200 $^o$C. Flow composition: Benzene/Ar/He/$O_2$/$H_2$= 2.4/3.0/24/13.8/56.8 (% of total flow),($O_2$/($O_2$+$H_2$) = 20 %)

91
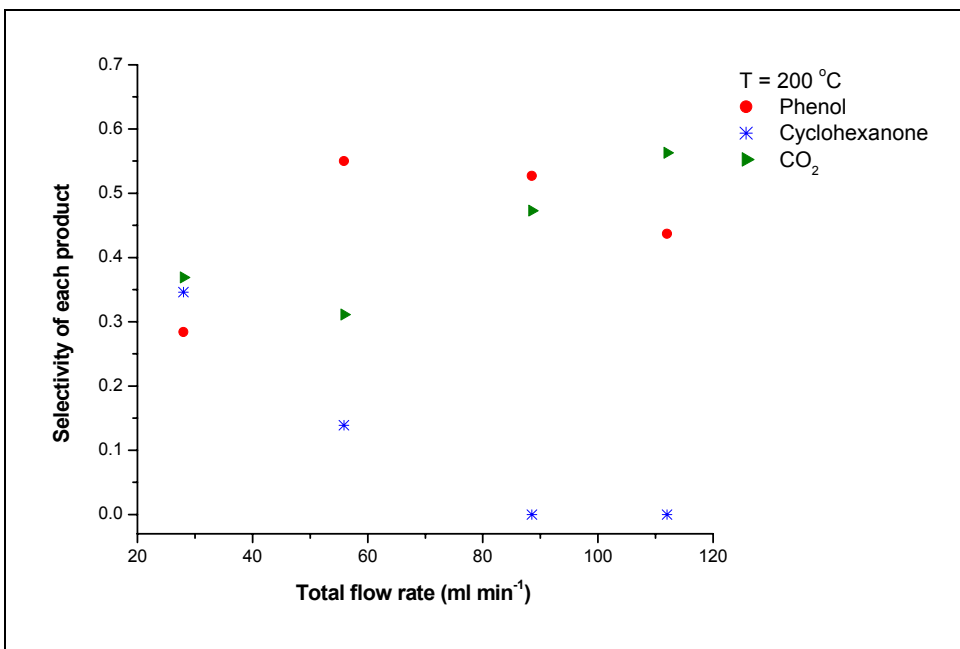
**Fig. 3.1.9.1.2:** Selectivity of each product from benzene reaction vs. total flow rate at 200 $^o$C. Flow composition: Benzene/Ar/He/$O_2$/$H_2$= 2.4/3.0/24/13.8/56.8 (% of total flow), ($O_2$/($O_2$+$H_2$) = 20 %)
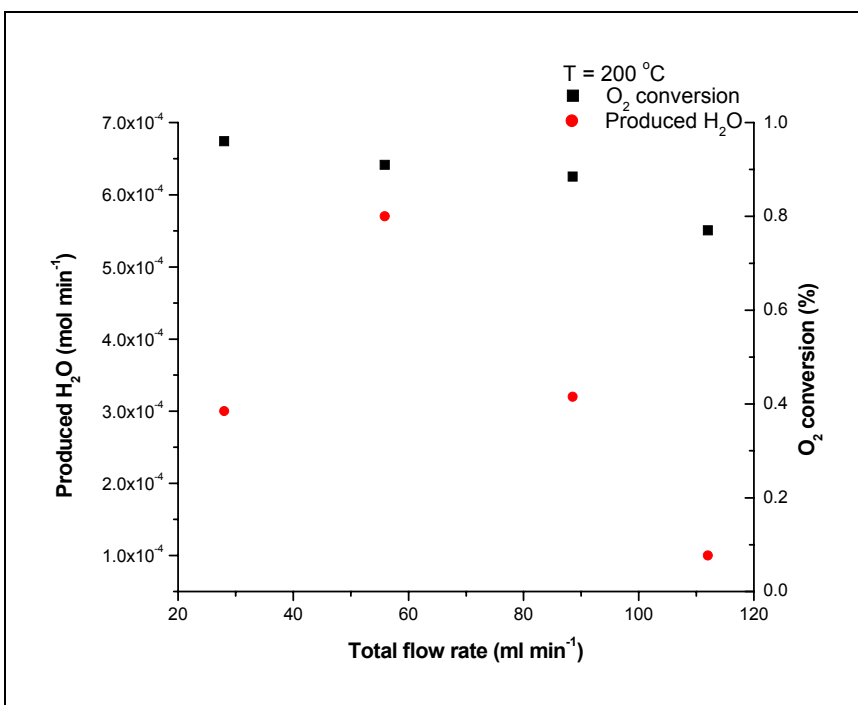


**Fig. 3.1.9.1.3:** Produced $H_2O$ and conversion of $O_2$ vs. total flow rate at 200 $^o$C. Flow composition: Benzene/Ar/He/$O_2$/$H_2$= 2.4/3.0/24/13.8/56.8 (% of total flow), ($O_2$/($O_2$+$H_2$) = 20 %)

Temperature distribution inside the reactor for the different flow rates is shown in Figure 3.1.9.1.4.
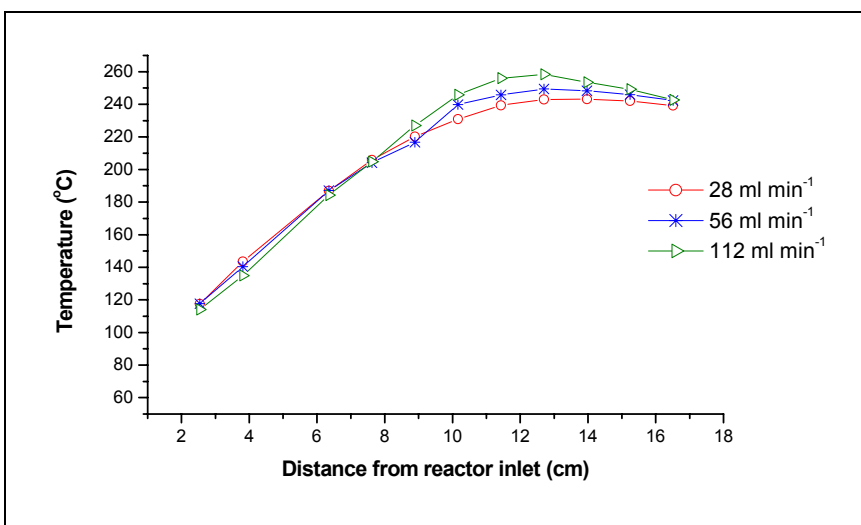
**Fig. 3.1.9.1.4:** Temperature distribution vs. distance from reactor inlet for the different flow rates at 200 $^o$C. Flow composition: Benzene/Ar/He/$O_2$/$H_2$= 2.4/3.0/24/13.8/56.8 (% of total flow), ($O_2$/($O_2$+$H_2$) = 20 %)

### 3.1.9.2. $H_2$ was entered to tube and shell sides and the other gases into the shell side

For this part, part of $H_2$ flow rate was entered with other gases (He, Ar, benzene, and $O_2$) to the shell at the same time where a separate feed of $H_2$ was being fed into the ¼ in tube keeping the total $H_2$ % (from shell and tube feeds) in the reaction mixture constant. This reaction was carried at 200 $^o$C with a total flow rate of 55.8 ml min$^{-1}$. The results are shown in Figures 3.1.9.2.1 and 3.1.9.2.1. Figure 3.1.9.2.1 shows benzene conversion to each product for the different arrangements of $H_2$ flow rate in the reactor. Conversion of oxygen at the conditions of Figure 3.1.9.2.1 is shown in Figure 3.1.9.2.2. Produced water was at an average vale of 5.7 x 10$^{-4}$ mol min$^{-1}$ for these conditions.
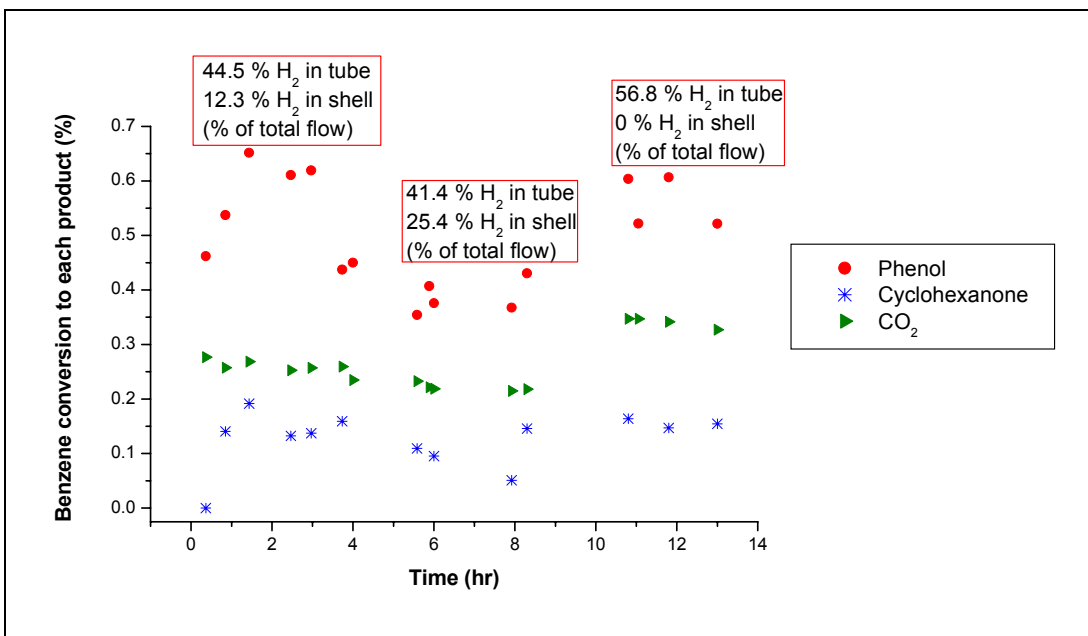
**Fig. 3.1.9.2.1:** Conversion of benzene to each product vs. time at 200 $^o$C. Total flow rate= 55.8 ml min$^{-1}$. Flow composition: Benzene/Ar/He/O$_2$= 2.4/3.0/24/13.8 (% of total flow)
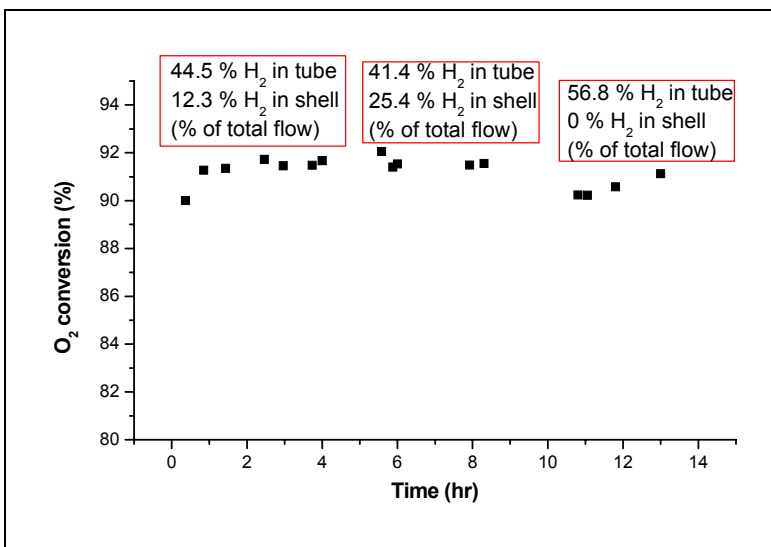


**Fig. 3.1.9.2.2:** Conversion of O$_2$ at 200 $^o$C. Total flow rate= 55.8 ml min$^{-1}$. Flow composition: Benzene/Ar/He/O$_2$= 2.4/3.0/24/13.8 (% of total flow)

### 3.1.9.3. H$_2$ and the other gases (He, Ar, benzene, and O$_2$) were fed into the tube side

The flow conditions were changed so that all the reaction mixture will enter to the ¼ in tube and emerge from the 0.05 cm holes and come in contact with the catalyst. Results for one set of slow conditions and are shown in Table 3.1.9.3.1. Conversion of O$_2$ was 0.88 (0.86 to H$_2$O) and produced H$_2$O was 5.4 x 10$^{-4}$ mol min$^{-1}$.

94

**Table 3.1.9.3.1**: Conversion of benzene to each product, selectivity of the products, and produced moles of each product at 200 $^oC$. Total flow rate= 43.4 ml min$^{-1}$. Flow composition: Benzene/Ar/He/O$_2$/H$_2$ = 4.1/3.1/41/17.8/34.0 (% of total flow rate) (O$_2$/(O$_2$+H$_2$) = 34 %)

| Product | Conversion % | Selectivity % | Moles Produced (mol min$^{-1}$) |
|---|---|---|---|
| Phenol | 1.0 | 75.3 | 7.0E-7 |
| Cyclohexanone | 0.0 | 0.0 | 0.0 |
| CO$_2$ | 0.31 | 24.7 | 1.4E-6 |

Another reaction mixture with different benzene flow rate has been tested. The same mixture was tested at different flow rates keeping mixture compositions and temperature constant. Benzene conversion at these flow conditions is shown in Figure 3.1.9.3.1. Selectivity of each product is shown in Figure 3.1.9.3.2. Produced water and conversion of oxygen are shown in Figure 3.1.9.3.3 for the different flow rates.
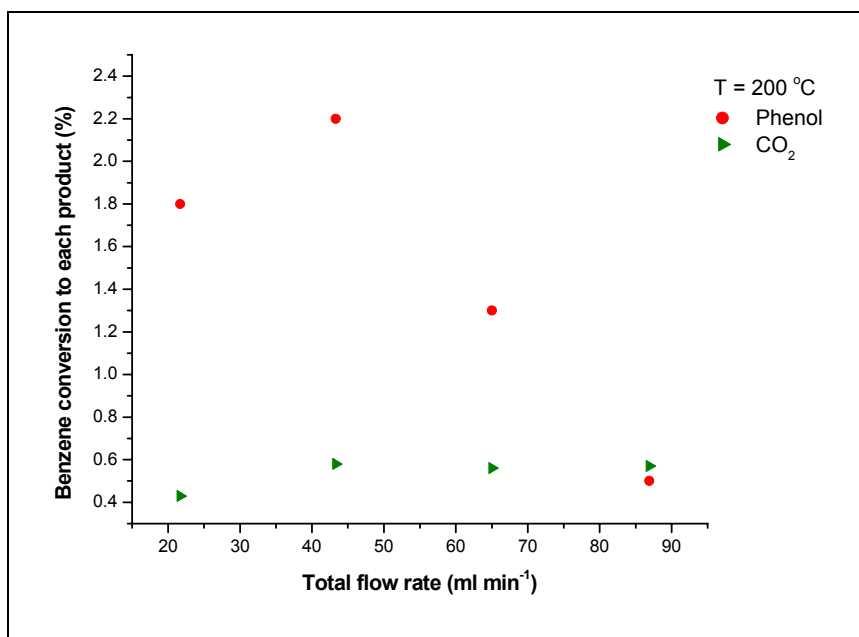


**Fig. 3.1.9.3.1:** Conversion of benzene to each product vs. total flow rate at 200 $^oC$. Flow composition: Benzene/Ar/He/O$_2$/H$_2$= 2.5/3.1/42/17.8/34 (% of total flow), (O$_2$/(O$_2$+H$_2$) = 34 %)
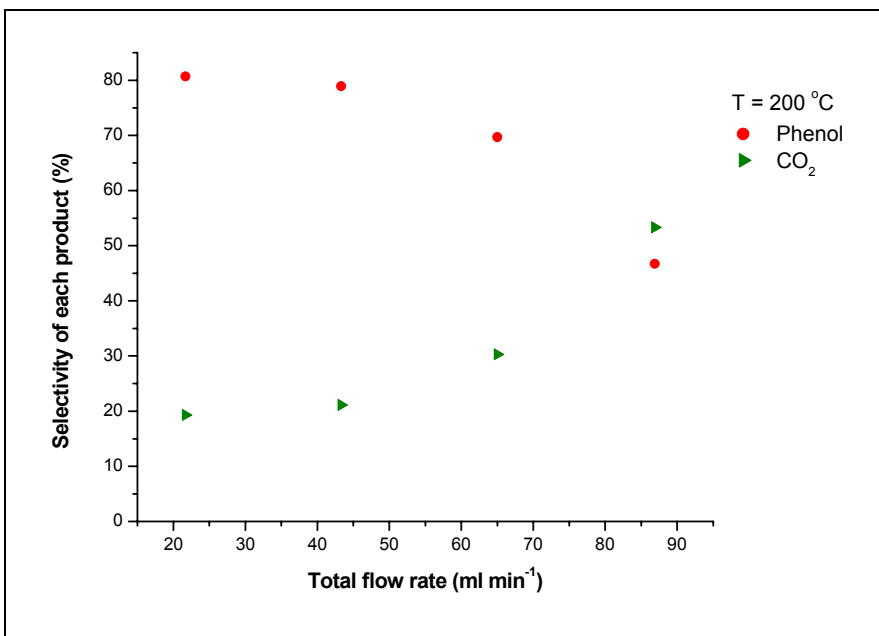
**Fig. 3.1.9.3.2:** Selectivity of each product from benzene reaction vs. total flow rate at 200 °C. Flow composition: Benzene/Ar/He/$O_2$/$H_2$= 2.5/3.1/42/17.8/34 (% of total flow), ($O_2$/($O_2$+$H_2$) = 34 %)
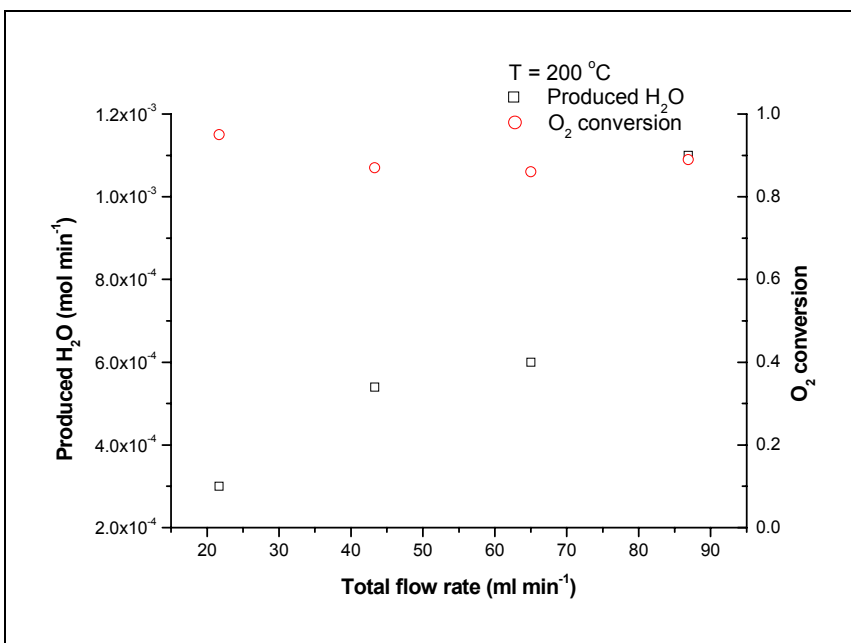


**Fig. 3.1.9.3.3:** Produced $H_2O$ and conversion of $O_2$ vs. total flow rate at 200 °C. Flow composition: Benzene/Ar/He/$O_2$/$H_2$= 2.5/3.1/42/17.8/34 (% of total flow), ($O_2$/($O_2$+$H_2$) = 34 %)

Temperature measured at a distance from the reactor inlet, using a thermocouple close to the exterior surface of ¼ in tube, for the different total flow rates is shown in Figure 3.1.9.3.4.
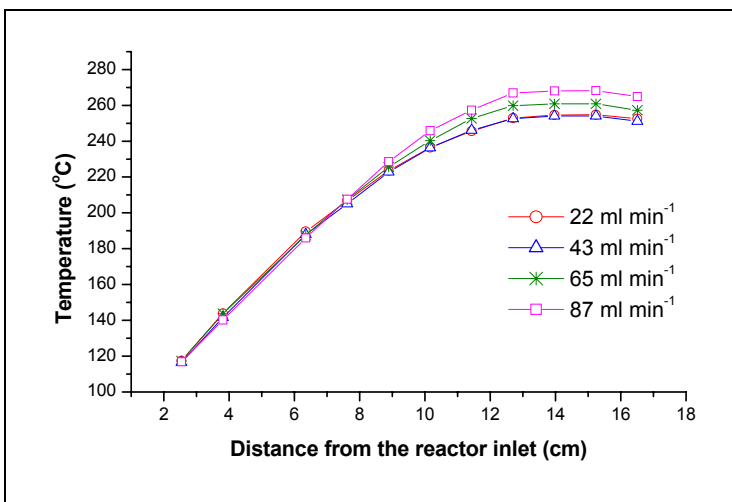


**Fig. 3.1.9.3.4:** Temperature distribution vs. distance from reactor inlet at 200 $^\circ$C. Flow composition: Benzene/Ar/He/$O_2$/$H_2$= 2.5/3.1/42/17.8/34 (% of total flow), ($O_2$/($O_2$+$H_2$) = 34 %)

### 3.1.9.3.1. Effect of ($H_2$+$O_2$) flow rates

The flow rate of both hydrogen and oxygen was varied keeping the ratio of oxygen to hydrogen constant in order to investigate the effect of this variation on benzene conversion when the all the gases were fed to the ¼ in . Therefore the percentage of the sum of oxygen and hydrogen ($H_2$+$O_2$) of the total flow rate was varied. Also, He flow rate was varied in order to keep total flow rate constant. On the other hand flow rate of benzene and Ar were constant. Figure 3.1.9.3.1.1 shows benzene conversion to each product at the different ($H_2$+$O_2$) percentages of the total flow rate. The selectivity of each product from benzene reaction is shown in Figure 3.1.9.3.1.2. The produced amounts of water along with oxygen conversion ($CO_2$ and $H_2O$) are shown in Figure 3.1.9.3.1.3.

97
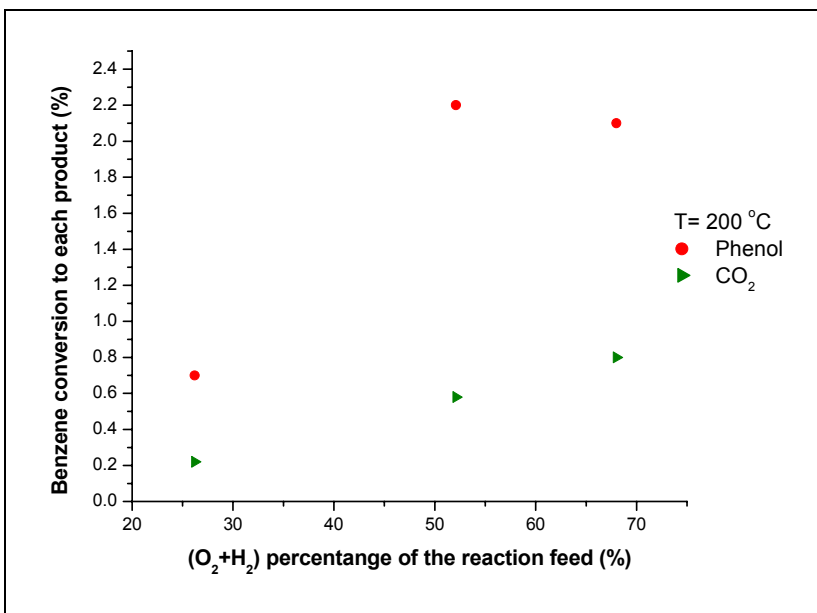
**Fig. 3.1.9.3.1.1:** Benzene conversion to each product vs. $(H_2+O_2)$ % in the feed at 200 $^o$C. Total flow rate= 43 ml min$^{-1}$. Flow composition: Benzene/Ar= 2.5/3.1(% of total flow), $(O_2/(O_2+H_2) = 34$ %)
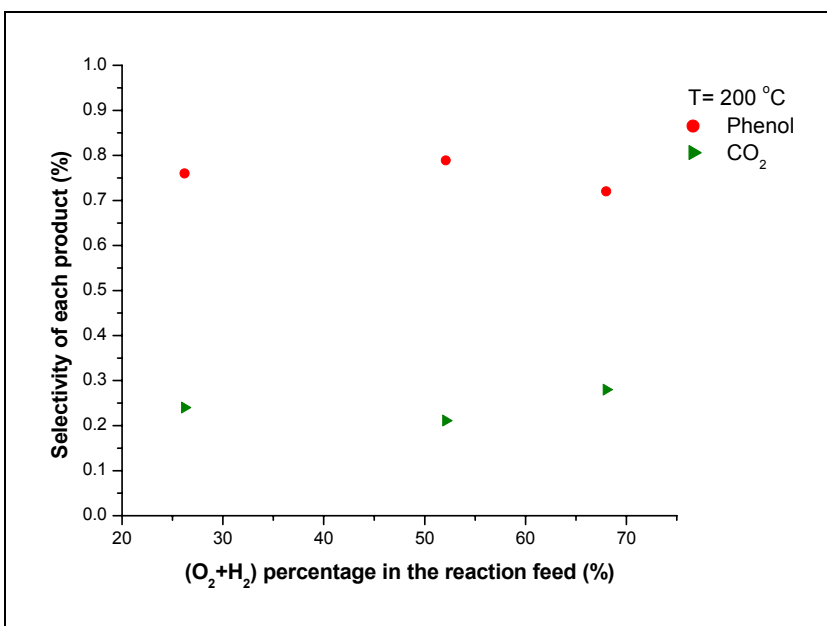


**Fig. 3.1.9.3.1.2:** Selectivity of each product from benzene reaction vs. $(H_2+O_2)$ % in the feed at 200 $^o$C. Total flwo rate= 43 ml min$^{-1}$. Flow composition: Benzene/Ar= 2.5/3.1(% of total flow), $(O_2/(O_2+H_2) = 34$ %)
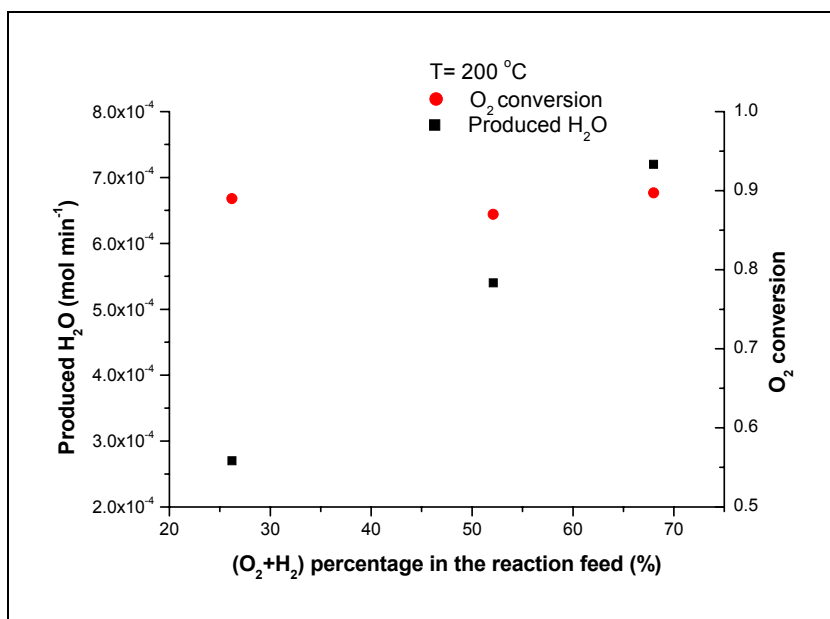
**Fig. 3.1.9.3.1.3:** Produced $H_2O$ and conversion of $O_2$ vs. $(H_2+O_2)$ % in the feed at 200 $^o$C. Total flow rate= 43 ml min$^{-1}$. Flow composition: Benzene/Ar= 2.5/3.1(% of total flow), $(O_2/(O_2+H_2) = 34$ %)

### 3.1.9.3.2. Effect of benzene concentration in the feed

Benzene flow rate in the feed was changed in order to investigate the effect of this change on benzene conversion. The flow rate of benzene was varied by varying the flow rate of He to the saturator (gas bubbler) where gaseous benzene was obtained. The total flow rate was fixed while varying benzene flow rate in the feed. Also the flow rate of the other gases, $H_2$, $O_2$, and Ar, were the same for the different flow rates (percentage of benzene in the feed) of benzene. Another line of He was used as the balance gas to keep total flow rate constant. The temperature of reaction was 200 $^o$C. Conversion of benzene to each product at the different percentages of benzene in the feed is shown in Figure 3.1.9.3.2.1. The selectivity and produced moles of each product are shown in Figures 3.1.9.3.2.2 and 3.1.9.3.2.3, respectively. Oxygen conversion was 0.87 for the different benzene percentages in the feed. Also produced water was 5.4 x 10$^{-4}$ mol min$^{-1}$ for all the cases.
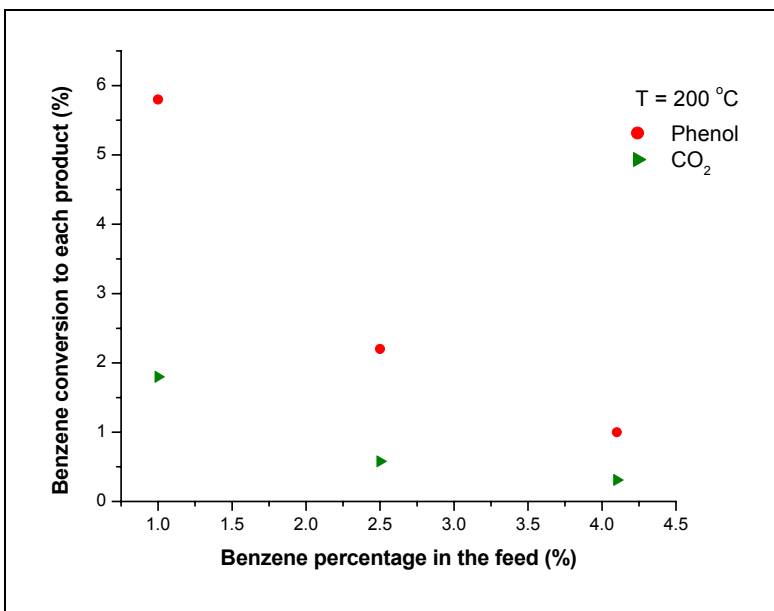
**Fig. 3.1.9.3.2.1:** Benzene conversion to each product vs. benzene % in the feed at 200 $^o$C. Total flow rate= 43 ml min$^{-1}$. Ar/O$_2$/H$_2$= 3.1/17.8/34 (% of total flow), (O$_2$/(O$_2$+H$_2$) = 34 %)
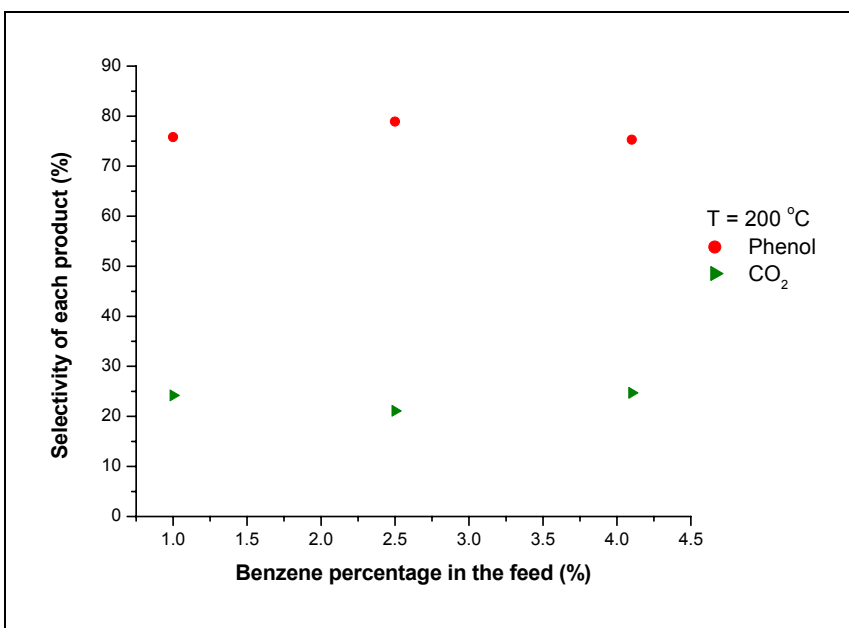


**Fig. 3.1.9.3.2.2:** Selectivity of each product from benzene reaction vs. benzene % in the feed at 200 $^o$C. Total flow rate= 43 ml min$^{-1}$. Ar/O$_2$/H$_2$= 3.1/17.8/34(% of total flow), (O$_2$/(O$_2$+H$_2$) = 34 %)
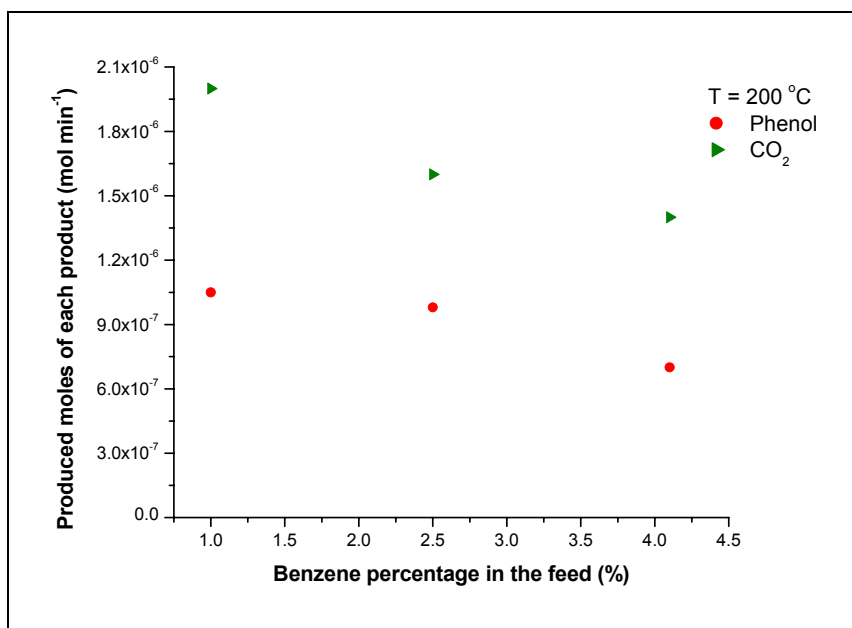
**Fig. 3.1.9.3.2.3:** Produced moles of each product from benzene reaction vs. benzene % in the feed at 200 $^{o}$C. Total flow rate= 43 ml min$^{-1}$. Ar/O$_2$/H$_2$= 3.1/17.8/34(% of total flow), (O$_2$/(O$_2$+H$_2$) = 34 %)

### 3.1.10. Blank Experiment

Using the experimental setup, which was described earlier, different experiments were performed applying different flow conditions. Results for one set of flow conditions are shown in Table 4.1.10.1. The same reaction was carried over night and gave the same results. Other flow conditions gave the same results as these ones in Table 3.1.10.1.

**Table 3.1.1.10.1:** Conversion of benzene to each product, selectivity of the products, and produced moles of each product at 200 $^{o}$C. Total flow rate= 43.0 ml min$^{-1}$. Flow composition: Benzene/Ar/He/O$_2$/H$_2$ = 2.7/3.1/42/17.8/34.0 (% of total flow rate) (O$_2$/(O$_2$+H$_2$) = 34 %)

| Product | Conversion % | Selectivity % | Moles Produced (mol min$^{-1}$) |
|---|---|---|---|
| Phenol | 0.0 | 0.0 | 0.0 |
| Cyclohexanone | 0.0 | 0.0 | 0.0 |
| CO$_2$ | 0.0 | 0.0 | 0.0 |

### 3.1.11. Pt Cone

In this setup, Pt foil was cut into conical shape and welded to the exterior surface of the ¼ in tube. The reaction mixture was fed through the shell and come into contact

with the catalyst. Different flow conditions were tested using Pt as a catalyst. Results for one set of flow conditions are given in Table 3.1.11.1. In this table, benzene percentage in the feed was varied at constant total flow rate, temperature, and flow rates of $H_2$, $O_2$, and Ar. Oxygen conversion was 0.64 and the produced water was $4 \times 10^{-4}$ mol min$^{-1}$ at both benzene percentages in the feed.

Flow rate of oxygen in the feed was varied in order to investigate the possibility of converting benzene to phenol. This was performed by keeping the total flow rate constant. He flow rate was varied to balance the total flow rate. Flow rate of other gases in the reaction mixture was fixed. Temperature of reaction was 200 $^o$C. At the different tested flow rates of $O_2$ only $CO_2$ and $H_2O$ were detected.

**Table 3.1.11.1:** Conversion of benzene to each product, selectivity of the products, and produced moles of each product at 200 $^o$C at different benzene percentages in the feed. Total flow rate= 43.0 ml min$^{-1}$. Flow composition: Ar/$O_2$/$H_2$= 3.1/17.8/34.0 (% of total flow rate) ($O_2$/($O_2$+$H_2$) = 34 %)

| Product | Conversion % | | Selectivity % | | Moles Produced (mol min$^{-1}$) | |
|---|---|---|---|---|---|---|
| | 2.6 % benzene | 3.6 % benzene | 2.6 % benzene | 3.6 % benzene | 2.6 % benzene | 3.6 % benzene |
| Phenol | 0.0 | 0.0 | 0.0 | 0.0 | 0.0 | 0.0 |
| Cyclohexanone | 0.0 | 0.0 | 0.0 | 0.0 | 0.0 | 0.0 |
| $CO_2$ | 0.16 | 0.22 | 100 | 100 | 0.0 | |

$O_2$ percentage in the feed was varied and the results of benzene reaction are shown in Figure 3.1.11.1. Produced water was $2 \times 10^{-4}$, $4 \times 10^{-4}$, and $5 \times 10^{-4}$ mol min$^{-1}$ for 9 %, 17.8 %, and 27 % $O_2$ in the feed, respectively. Conversion of $O_2$ was 0.68, 0.63, and 0.53 for 9 %, 17.8 %, and 27 % $O_2$ in the feed, respectively.
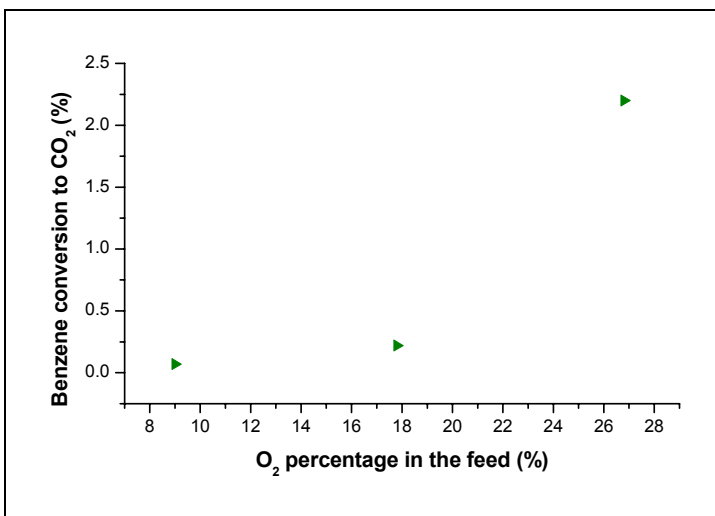
**Fig. 3.1.11.1:** Conversion of benzene to $CO_2$ vs. $O_2$ percentage in the feed at 200 $^o$C Total flow rate= 43.0 ml min$^{-1}$. Flow composition: Ar/Benzene/$H_2$= 3.1/2.6/34.0 (% of total flow rate)

After that percentage of $H_2$ was varied by changing its inlet flow rate keeping the total flow rate constant and results are shown in Figure 3.1.11.2. Only $CO_2$ and $H_2O$ were detected as products. Produced water was 2 x10$^{-4}$, 4 x10$^{-4}$, and 5 x10$^{-4}$ mol min$^{-1}$ and conversion of $O_2$ was 0.35, 0.63, and 0.77 for 17 %, 34 %, and 48 % $H_2$ in the feed, respectively.
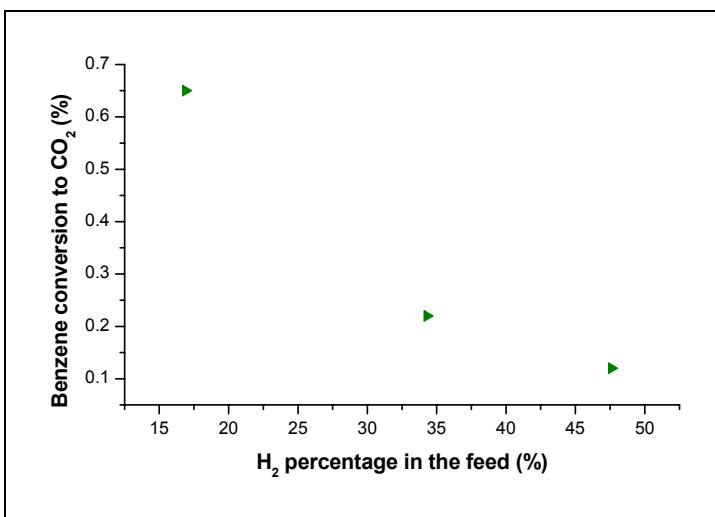


**Fig. 3.1.11.2:** Conversion of benzene to $CO_2$ vs. $H_2$ percentage in the feed at 200 $^o$C Total flow rate= 43.0 ml min$^{-1}$. Flow composition: Ar/Benzene/$O_2$= 3.1/2.6/17.8 (% of total flow rate)

# 4. Discussion:

The discussion section will consist of two parts. The first part of the discussion will be devoted toward understanding the mechanism for the formation of the several detected products from benzene reaction using a mixture of hydrogen and oxygen in presence of Pd. The second part will discuss the experimental results that were obtained in Section 4 of this chapter.

## 4.1. Products formed from benzene reaction using $H_2$ and $O_2$ in presence of Pd.

In the results section of this chapter it was observed that under certain reaction conditions and reactor setup benzene was converted to several organic compounds beside the target product (phenol). A summary of the physical properties of these compounds is shown in Table 4.1.

**Table 4.1:** Physical properties of the obtained organic compounds from benzene reaction [33]

| Compound | Chemical Structure | Chemical formula Synonyms | MW | m.p °C | b.p[a] °C | Solubility[b] | | | | |
|---|---|---|---|---|---|---|---|---|---|---|
| | | | | | | w | al | eth | ace | bz |
| Phenol | OH | $C_6H_6O$ <br><br> Carbolic acid | 94.1 | 43 | 181.7 5[760] | s | s | v | ∞ | ∞ |
| Cyclohexanol | OH | | 100.2 | 25.15 | 161.1 | s | s | s | | ∞ |
| Catechol | OH OH | $C_6H_6O_2$ Benzene,1,2-dihydroxy | 110.1 | 105 | 245[750] | s | s | s | v | s[h] $\delta$ |
| Hydroquinone | OH HO | $C_6H_6O_2$ Benzene,1,4-dihydroxy | 110.1 | 173-4 | 285[730] | s v[h] | v | s | v | i |

| | | | | | | | | | | |
|---|---|---|---|---|---|---|---|---|---|---|
| Resorcinol |  HO—⟨⟩—OH | $C_6H_6O_2$ Benzene,1,3-dihydroxy | 110.1 | 111 | $178^{16}$ | s | s | s | | $\delta$ |
| 1,2-cyclohexane-dione |  | Dihydropyro-catechol | 112.1 | 38-40 | $193$-$5^{760}$ | s | s | s | | s |
| 1,4-cyclohexane-dione |  | Tetrahydroq-uinone | 112.1 | | Sub 100 | s | s | s | s | s |
| Cyclohexanone |  | $C_6H_{10}O$ Pimelic ketone | 98.15 | -16.4 | $155.6$ $5^{760}$ | s | s | s | s | s |
| Cyclohexanone, 4-hydroxy |  | $C_6H_{10}O_2$ | 114.1 | | | | | | | |
| Cyclohexanone, 2-hydroxy |  | $C_6H_{10}O_2$ Adipoin | 114.1 | 113 | $92^{20}$ | $v^h$ | $v^h$ | i | | i |
| Pentanoic acid, 4-oxo |  | $CH_3COCH_2CH_2$-$CO_2H$ Levulinic acid | 116.1 | 37.2 | $139$-$40^8$ | v | v | v | | |
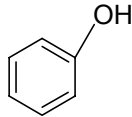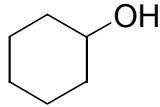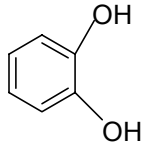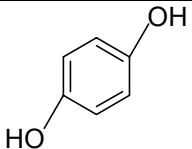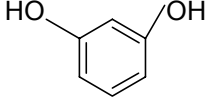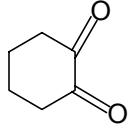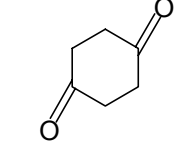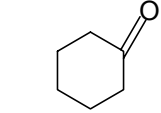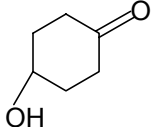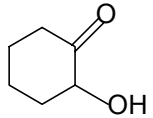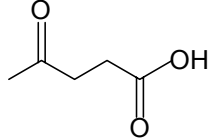
a: b.p.= boiling point , the pressure (in mm Hg )at which this physical property was determined appears as a superscript, if no superscripts pressure is about 1 atm.

b: Solubility: insoluble (i), slightly soluble($\delta$), soluble (s), very soluble (v), miscible ($\infty$). If no special remark is made about the temperature, the reference is to room temperature; otherwise, a superscript appears. ace: acetone, al: alcohol (usually ethyl alcohol), bz: benzene, eth: ether, w: water, h: hot, sub: sublimes.

### 4.1.1. Formation of phenol, pentanoic acid, 4-oxo, and pentanoic acid

Many of the methods to produce phenol would suggest the addition of hydrogen peroxide ($H_2O_2$) as a monoxygen donor to convert benzene to phenol; Figure 4.1.1.1 illustrates one example [8]. This reaction is limited by the low $H_2O_2$ selectivity.
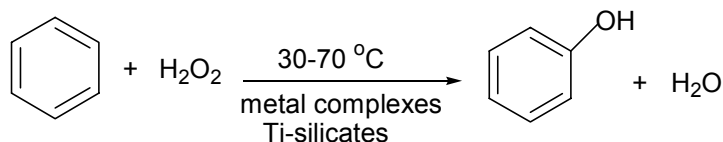


**Fig. 4.1.1.1:** Production of phenol by the addition of $H_2O_2$ to benzene

Instead of adding $H_2O_2$ externally as was shown by Figure 4.1.1.1 it can also be produced in situ and immediately used for oxidation as shown in Figure 4.1.1.2. In this case, reaction selectivity as referred to $H_2O_2$ is higher and this method is considered as one of the most promising ways for performing demanding oxidation reactions. This coupling mechanism lead to the formation of a common intermediate (water) in the primary reaction and benzene oxidation to phenol is the secondary reaction [8, 34].
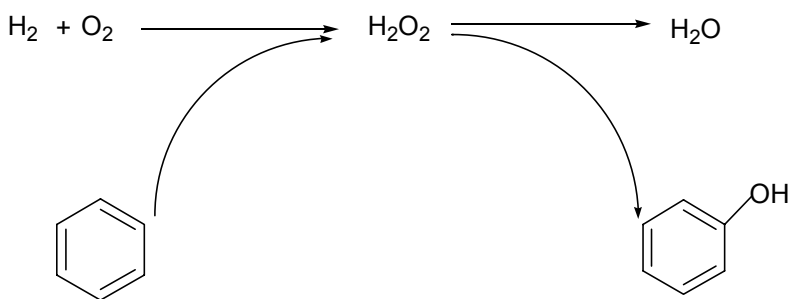


**Fig. 4.1.1.2:** Converting benzene to phenol through in situ production of $H_2O_2$

Other researchers found that hydrogen peroxide can be synthesized in situ starting with $H_2$ and $O_2$ and an appropriate catalyst [28, 35, 36]. Most of the time direct synthesis of hydrogen peroxide is pursued through the catalytic hydrogenation of oxygen carried out on Pd-based heterogeneous catalysts [10].

For example, hydrogen peroxide was synthesized starting from hydrogen and oxygen using a system consisted of a catalyst (containing at least one metal of the platinum group as active component), a polyolefin, and a carrier [37]. The catalyst contained 0.05-2 wt.% of Pd, 0.005-0.5 wt.% of Pt with an atomic ratio of Pt/Pd of (1-30)/(70-99), and optionally Ru, Rh, Ir, and Au. The carrier was silica, alumina, silica-alumina, zeolite, and preferably activated carbon or activated carbon. The reaction solvent contained a halogenated promoter and an acid promoter. The solvent consisted of at least one alcohol or a mixture of alcohol- water optionally containing aliphatic ether and/or one or more

$C_{5-32}$ hydrocarbons. The hydrocarbon could be benzene. The reaction was carried out at 20-40° C, 30-100 bars, and in the presence of an inert gas such as Ar [37].

Another study [38] reported the hydroxylation of alkanes performed with $O_2$ and $H_2$ and a catalyst. The catalyst was a 5 $\overset{\circ}{A}$ small pore zeolite loaded with Pd(0)/Fe(II). According to this study hydrogen peroxide was likely formed on Pd(0) and consumed in the Fe(II) promoted hydroxylation of the alkane. More than 95 % of $H_2/O_2$ ended into water with low yield of the hydroxylation of the alkane. These studies, support the in situ formation of $H_2O_2$ staring with oxygen and hydrogen and an appropriate catalyst.

Based on the previous studies for the in situ formation of hydrogen peroxide, it is possible that hydrogen peroxide was formed in situ in our system and led to the formation of hydroxyl radicals that would add to benzene as will be seen later. In the reaction mixture that was used in this chapter both oxygen and hydrogen were present along with the Pd catalyst. Hydrogen could be dissociated in permeating through the palladium membrane to form $^\bullet H$ [38]. Then $^\bullet H$ radical appears on the surface of the opposite side of the membrane and reacts immediately with oxygen to give $H_2O_2$ and $HOO^\bullet$. $H_2O_2$ then decomposes to $^\bullet OH$, water and atomic oxygen [9]. The following reactions summarize the dissociation of $H_2$:

$$H_2 \xrightarrow{\quad Pd \quad} 2^\bullet H$$
$$2^\bullet H + O_2 \rightarrow H_2O_2 \rightarrow {^\bullet OH} + \frac{1}{2}H_2O + \frac{1}{2}{^\bullet O}$$
$$^\bullet H + O_2 \rightarrow HOO^\bullet$$
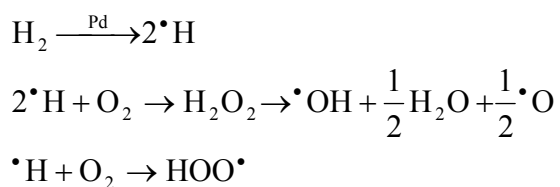
Xiao [24], by characterization of the catalytic phenol hydroxylation over $Cu_2(OH)PO_4$ catalyst using hydrogen peroxide by electron spin resonance (ESR), found

that hydroxyl radicals were important intermediates in this reaction. Therefore, $^\bullet OH$

radicals are expected to play a significant rule in the oxidation of benzene and phenol.

The simplest aromatic hydrocarbon, benzene, reacts exclusively with $^\bullet OH$

radicals under troposphere conditions. This reaction is rather slow when compared to

those of alkylbenzenes, the rate constant $k_{OH+benzene} = 1.2 \times 10^{-12}$ $cm^3$ $molecule^{-1}$ $s^{-1}$ is a

factor of five to fifty lower than $k_{OH}$ of toluene and trimethylbenzenes, respectively[40].

Benzene oxidation proceeds, in contrast to alkylated aromatic hydrocarbons, exclusively

through the addition pathway of the $^\bullet OH$ radical to the aromatic ring [36, 40, 41].

It is well established that the reaction of the $^\bullet OH$ radical with benzene proceeds

by addition to the aromatic ring giving  a hydroxycyclohexadienyl, radical 1 reaction 1 in

Figure 4.1.1.3, which will reversibly add $O_2$ to give a hydroxycyclohexadienyl peroxyl,

radical 3 Figure 4.1.1.3. This equilibrium adjusts rapidly and a multitude of subsequent

reaction channels have been proposed and reaction 4 in Figure 4.1.1.3 is one of these

possible reactions that give phenol. A method to distinguish pathways on the basis of

temperature dependent considerations confirmed that the majority of phenol is probably

formed *via* channel (5) (Figure 4.1.1.3). Channel (5) forms $HO_2^\bullet$ radical through a

hydrogen abstraction reaction of Radical 2 with molecular oxygen. The experimental

evidence for Channel (3) has been disputed and it is unlikely that this pathway is actually

operative. Channel (4) in principal yields those same products through the direct

elimination of $HO_2$ from Radical 3. The formation of phenol without involvement of $O_2$

has been proposed by elimination of a ring bound $^\bullet H$ atom from Radical 2, Reaction 3 in

Figure 4.1.1.3, and this pathway has been the topic of intensive discussion in the

literature.
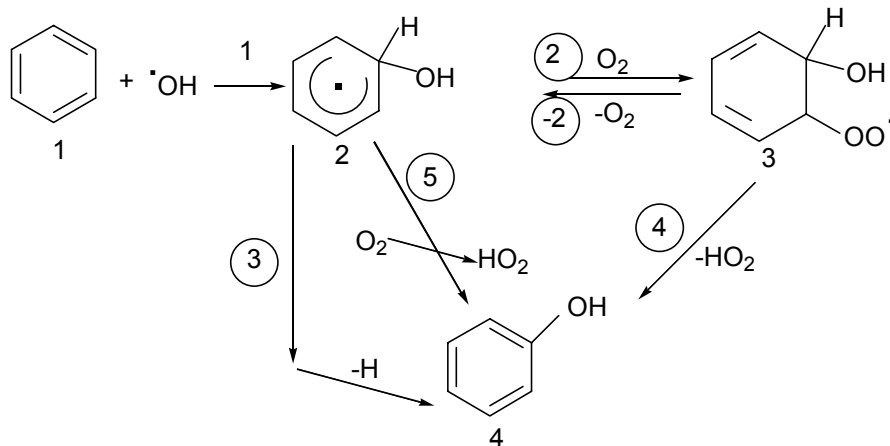
**Fig. 4.1.1.3:** Proposed pathways for the initial steps in the $^\bullet OH$ -radical initiated degradation of benzene in the gas-phase

Radical 3 in Figure 4.1.1.3 was proposed to go through other reactions depending on the reaction conditions. A mechanism for catechol formation in presence of oxygen and nitrous oxide from Radical 3 in Figure 4.1.1.3 was proposed by Klatz [1997, 40] and Volkamer [41]. The same proposed mechanism was applied to the reaction system that was studied in this chapter but with the replacement of nitrous oxide with hydrogen. The mechanism, starting from Radical 3 in Figure 4.1.1.3, is shown in Figure 4.1.1.4.

It can be seen from Figure 4.1.1.4 that radical 3, which was produced from reaction 2 in Figure 4.1.1.3, may react with hydrogen and especially if only dissociated hydrogen ($^\bullet H$) is available on this reaction side to form radical 6. Then this radical will react with oxygen and this can be through route 7 or 8. Route 8, will lead to the opening of the aromatic ring after the reaction with oxygen and forms molecule 9a. Upon further heating, and in presence of $^\bullet OH$ radicals, molecule 9a will finally give pentanoic acid, 4-oxo. Another possible product from the last reaction is pentanoic acid.

Another possible route for the formation of pentanoic acid, 4-oxo and pentanoic acid is based on the work of Alzueta [43] and Brezinsky [44]. It was found that phenol at

high temperature (900-1100 $^o$K) may dissociate through CO elimination forming cyclopentadiene [43, 44], Figure 4.1.1.5. Also phenol might react with $^\bullet$OH radical and form cyclopentadienone ($C_6H_5O$) [43, 44], this later compound under high temperature might react with radical pool and leads to ring opening [43], and a possible reaction products are pentanoic acid, 4-oxo and pentanoic acid as can be seen From Figure 4.1.1.5.

It can be seen that for the formation of pentanoic acid, 4-oxo high temperature is needed to lead to the ring opening and form a chain product. The reaction temperature was set at either 200 $^o$C or 150 $^o$C in the reaction systems that were studied in this chapter. Therefore, it might be possible that there was a hot spot in the reaction system that would allow for ring opening. Also, it might be possible that under the reaction conditions (concentration of reactants and presence of Pd catalyst) that ring opening might take place at a lower temperature than what Alzueta and Brezinsky have suggested.
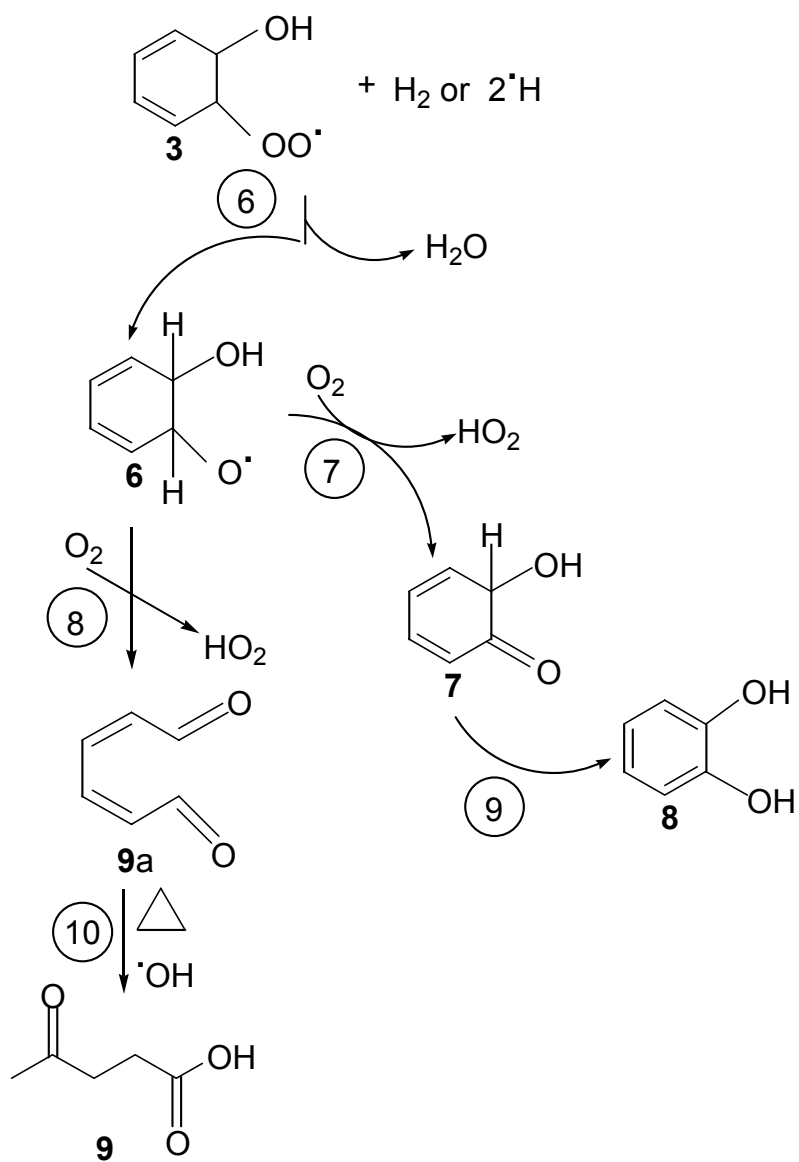
**Fig. 4.1.1.4:** Proposed mechanisms for the reaction of the hydroxycyclohexadienyl peroxyl (radical 3) with hydrogen. The formation pathways of catechol (8) and pentanoic acid, 4-oxo (9) are shown

$$\text{C}_6\text{H}_5\text{OH} \rightleftharpoons \text{C}_5\text{H}_6 + \text{CO}$$

$$\text{C}_6\text{H}_5\text{OH} + {}^\bullet\text{OH} \rightleftharpoons \text{C}_5\text{H}_6\text{O} + \text{CO}$$

$$\text{C}_5\text{H}_6\text{O} \xrightarrow[\text{High Temp.}]{{}^\bullet\text{OH}} \text{ring opening} \longrightarrow \text{CH}_3\text{COCH}_2\text{CH}_2\text{CO}_2\text{H}$$
(pentanoic acid, 4-oxo)
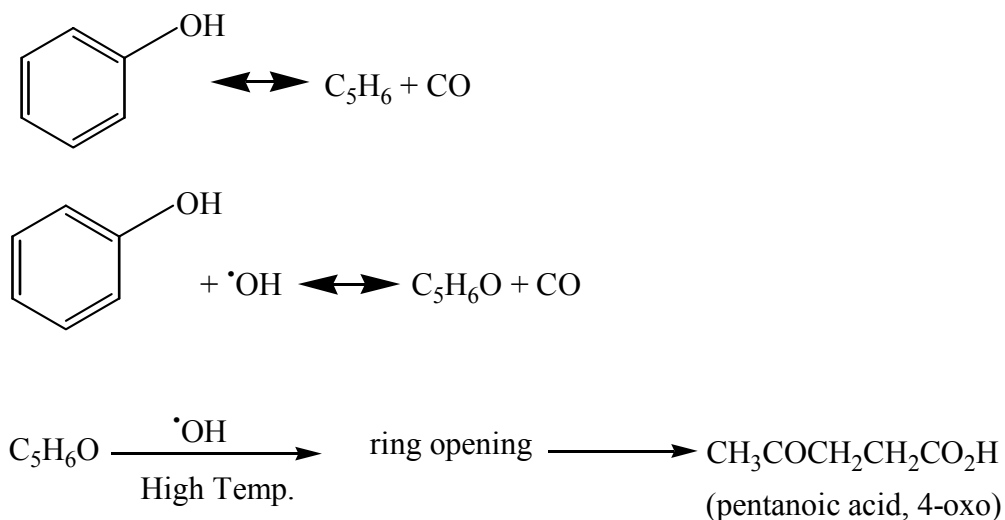
**Fig. 4.1.1.5:** A possible path way for pentanoic acid, 4-oxo production starting with phenol

## 4.1.2. Production of hydroquinone and Catechol from phenol

Hydroquinone, catechol and resorcinol are some of the most important products of phenol oxidation. The dihydroxybenzenes, such as catechol, and hydroquinone, are high value chemicals. They are widely used as photography chemicals, antioxidants and polymerization inhibitors, pharmaceuticals, flavors and aromas and also used in pesticides [45, 46]. Resorcinol is also used as an intermediate for dyes and for ultraviolet stabilizers of polyolefins and pharmaceutical products [46].

The most desirable method for producing dihydroxybenzenes is the direct hydroxylation of phenol with hydrogen peroxide in presence of a catalyst. This can be achieved through homogeneous catalyst or heterogeneous catalyst. Homogeneous catalysts such as mineral acids, metal ions and metal complexes are difficult to be separated and recovered from the reaction mixture, which prevents their practical utilization. Therefore, numerous heterogeneous catalysts such as metal oxides, supported metal complexes, metallosilicalites, hydrotalcite-like compounds, metal-bearing

112

mesoporous materials, metal hydroxylphosphates, and heteropoly compounds have been attracting research interest recently [45, 46, 47, 48].

Once benzene is oxidized to phenol, phenol is easily converted to other products, unlike benzene ring which is very stable. Phenol has extremely high reactivity of its ring toward electrophilic substitution. Phenol undergoes not only those electrophilic substitution reactions that are typical of most aromatic compounds, but also many others that are possible only because of the unusual reactivity of the ring. In ring substitution, acidity plays an important part; ionization of a phenol yields the $-O^-$ group, which of its full-fledged negative charge, is even more strongly electron releasing than the $-{}^{\bullet}OH$ group [5]. From Figure 4.1.1.4, in the previous section, it can be seen that route 7 will lead through atoms arrangements within the same molecule to the formation of catechol (compound number 8 in Figure 4.1.4) [40, 41, 42].

Franco *et al* [49] reported the oxidation reaction of phenol in aqueous acetonitrile media employing Cu-modified MCM-41 mesoporous catalyst and using $H_2O_2$ as oxidant. In their work ${}^{\bullet}OH$ radical and hydroperoxyl radical ($HO_2^{\bullet}$) were assumed to be produced through the interaction of $H_2O_2$ with the catalyst. Hydroquinone and catechol were subsequently obtained in parallel processes, involving the attack of ${}^{\bullet}OH$ radicals to phenol, Figure 4.1.2.1. Oxygen and water were formed in side reactions by the decomposition of the hydroperoxy radical and hydrogen peroxide, respectively. Further oxidation of hydroquinone and catechol can lead to other compounds like benzoquinone in their case. In our system further oxidation followed by reaction with dissociated hydrogen can lead to cyclohexanone, 2-hydroxy, cyclohexanone 4- hydroxy , 1,4-cyclohexanedione, and 1,2-cyclohexanedione as  shown in Figure 4.1.2.2. It was found,

from Franco's study, that for maximum utilization of hydrogen peroxide in the conversion of phenol into catechol and hydroquinone, the phenol/hydrogen peroxide ratio must be kept as high as possible, whereas the catechol/hydroquinone ratio decreases at high concentrations of hydrogen peroxide.
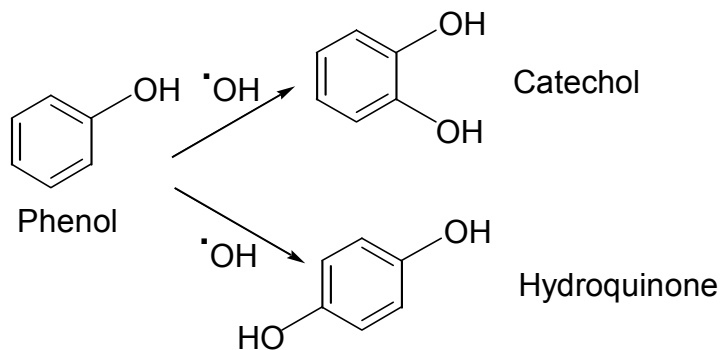


**Fig. 4.1.2.1:** Reaction paths for the hydroxylation of phenol
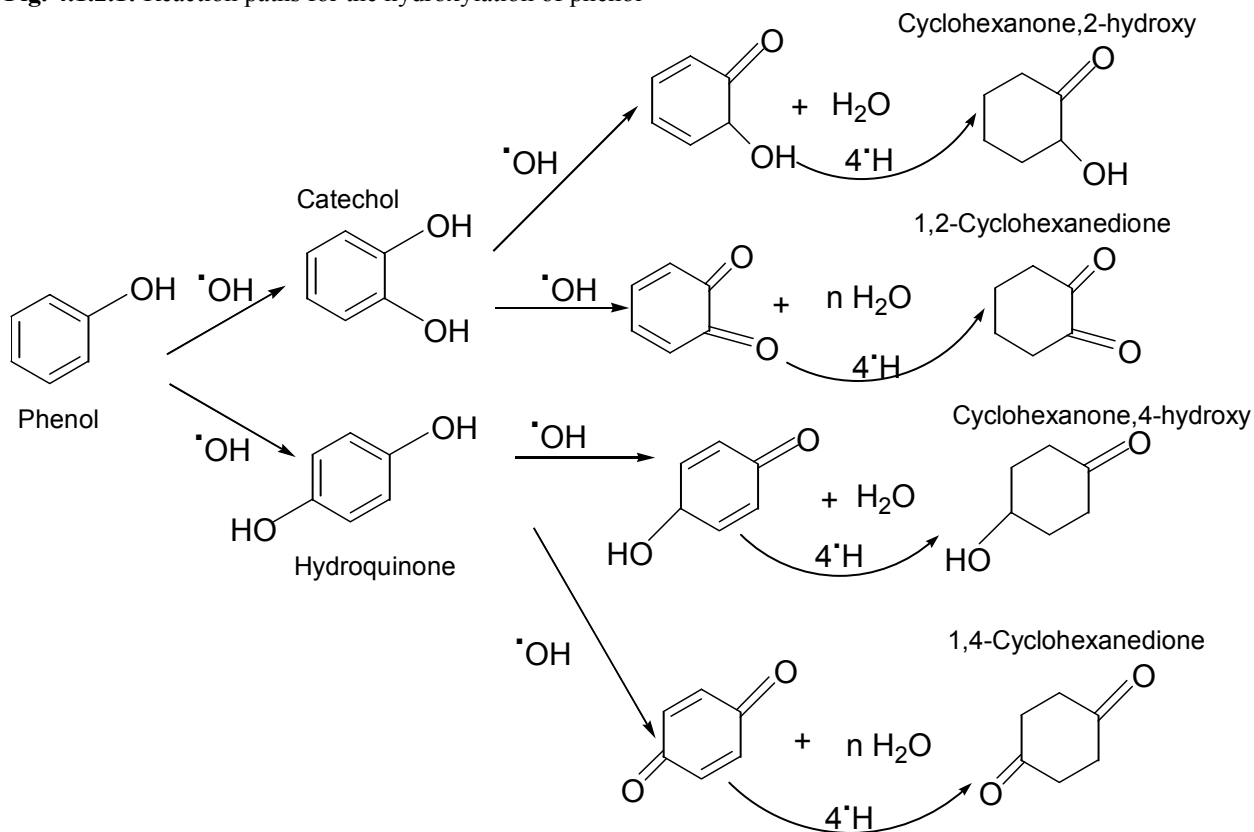


**Fig. 4.1.2.2:** Reaction paths for the hydroxylation of catechol and hydroquinone

Alan [50] reported that they could oxidize phenol by aqueous $H_2O_2$ in the presence of a transition-metal replaced strong acid-type action exchange polymer to catechol, hydroquinone, and resorcinol. The catalyst was prepared by incorporating vanadium ion into Nafion perfluorosulfonate polymer and used for the oxidation of phenol with 70 % $H_2O_2$. This reaction is shown in Figure 4.1.2.3.
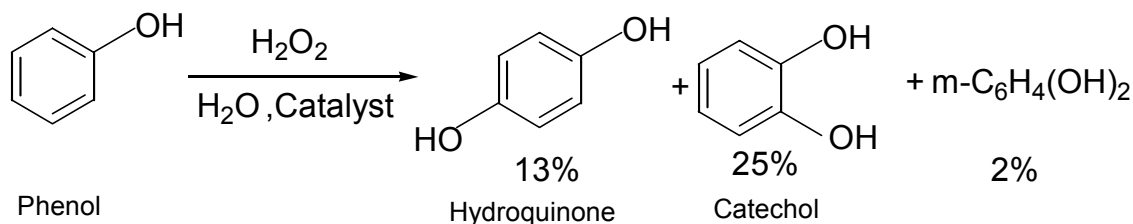


**Fig. 4.1.2.3:** Production of hydroquinone and catechol from phenol

Catechol and hydroquinone were the expected products of phenol oxidation by $H_2O_2$ as shown by Figure 4.1.2.4 as $^{\bullet}OH$ group of phenol is ortho and para directing [46, 47]. Catechol formation was always higher than hydroquinone formation in [47].
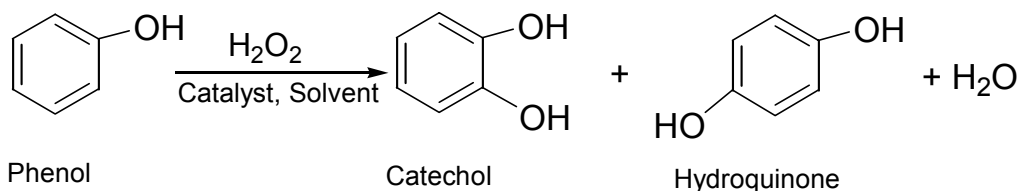


**Fig. 4.1.2.4**: Oxidation of phenol to catechol and hydroquinone

Oxovanadium arsenate has been used as a catalyst for phenol hydroxylation using hydrogen peroxide as the oxidant. Catechol, hydroquinone, and benzoquinone were the main products when the reaction was performed in water at 60 $^{\circ}$C for 6hours [48].

In summary we can see the involvement of $H_2O_2$ as an oxidant for phenol conversion to catechol, resorcinol, and hydroquinone. This involvement is understood from the production of $^{\bullet}OH$ radical which is responsible for this kind of transformation as was evident from the previous examples. As was seen in Section 4.1 $^{\bullet}OH$ radical can

be produced from the direct reaction between oxygen and hydrogen using Pd catalyst. Therefore, the formation of hydroquinone and its isomers (catechol and resorcinol) should be expected under the reaction conditions. In this chapter the feed consisted of $H_2$, $O_2$, and benzene and passed over the Pd catalyst under heating therefore, the conditions were appropriate to convert benzene to phenol and then phenol will go through further reaction that will lead to the formation of hydroquinone, catechol, and resorcinol as was shown from the studies in the literature.

### 4.1.3. Cyclohexanol and cyclohexanone:

Cyclohexanol and cyclohexanone are important intermediates for the production of carpolactom, a monomer used in the synthesis of nylon-6. Industrially cyclohexanol is produced by the oxidation of cyclohexane or by the hydrogenation of phenol. The first route requires high temperatures and pressures and generates undesirable by-products that lower the product yield and complicate the recovery/separation steps. In the latter route, phenol is hydrogenated to cyclohexanone either in a single step or in a two-step process via cyclohexanol [51].

Cyclohexanone can be obtained from phenol in two-step process; in the first step phenol is hydrogenated to cyclohexanol over a nickel catalyst and then cyclohexanol is dehydrogenated to cyclohexanone. The one-step process for selective hydrogenation, which can avoid the endothermic step of dehydrogenation, is advantageous for investment and energy savings [52]. Palladium supported catalysts have shown their possibility for use in the one step process. In industrial plants, the selective hydrogenation is carried over palladium supported on $Al_2O_3$ pellets. Pure palladium membranes showed the best performance with a phenol conversion of 90 % and a high cyclohexanone

116

selectivity of 75 % in the gas phase [52, 53]. The activity and selectivity of the catalysts depends strongly on the support of the catalyst. Basic and neutral supports seemed to favor the formation of cyclohexanone [53]. Pd supported on calcined Mg/Al hydrotalcites (CHTs) was investigated for the hydrogenation of phenol to cyclohexanone in the gas phase and compared with Pd performance using other supports [53].

Using Palladium (Pd) 1-10 wt %, loaded on the mesoporous support (MS) $CeO_2$ and $ZrO_2$, vapor phase hydrogenation of phenol was achieved in the temperature range 160 and 230 $^o$C at atmospheric pressure. At 180 $^o$C, reaction over 3 % Pd/ $CeO_2$-MS offered cyclohexanone as the major product (50 %) along with some amounts of cyclohexanol (35 %) and cyclohexane (15 %) [51]. The Pd adsorbs $H_2$ molecules and supplies hydrogen atoms to the aromatic ring, while the support adsorb phenol molecule near the Pd particles. Depending on acid-base properties of the support, the mode of adsorption varies and this mode directs the product selectivity to cyclohexanol or cyclohexanone. It was found that phenol hydrogenation over Pd/$CeO_2$-MS is structure sensitive. Conversion decreased with temperature. This is due to a decrease in the fraction of the surface covered by reactants. Selectivity of cyclohexanone increased with temperature while that of cyclohexanol decreased with temperature. Conversion of phenol increased, cyclohexanone selectivity decreased and, cyclohexanol was insensitive with increasing partial pressure of $H_2$. At low phenol, conversions cyclohexanone is the predominant product, as the conversion increases its selectivity declines at the expense of the selectivity of cyclohexanol. These results suggest that cyclohexanone is the predominant and primary product in the phenol hydrogenation and that cyclohexanol is formed by the subsequent hydrogenation of cyclohexanone.

The ease of hydrogenation activity over the studied catalyst in Velu study decreased in the order phenol> cyclohexanone> cyclohexanol. The higher catalytic activity of mesoporous support can be attributed to a higher Pd surface area, higher dispersion and smaller crystalline size.

Based on the above it was found that cyclohexanone is the major product of the hydrogenation reaction and cyclohexanol and cyclohexane were formed from subsequent hydrogenation [51]. Figure 4.1.3.1 shows the proposed reaction. It was found that the standard free energy $(\Delta G)$ for each step is negative which indicates that these steps are thermodynamically favorable.
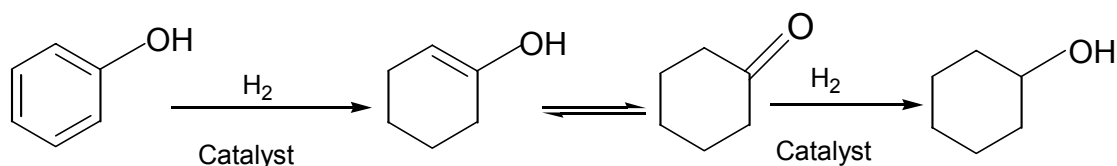


**Fig. 4.1.3.1: Oxidation of phenol to cyclohexanone and cyclohexanol**

Phenol was converted to $C_6H_5OH$ by reaction with the radical pool mainly, $^\bullet OH$ according to the reaction in Figure 4.1.3.2 [43]. If molecule 2 followed a hydrogenation reaction in presence of Pd as a catalyst and heating then this will lead to cyclohexanone production as can be seen from Figure 4.1.3.3 [43]. The rate constant for the reaction in Figure 4.1.3.3 is fairly well established.
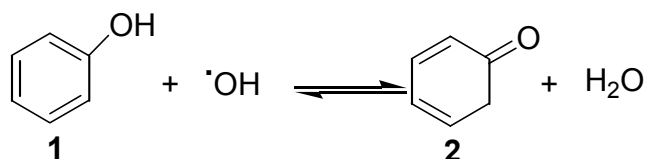


**Fig. 4.1.3.2:** Reaction of phenol with $^\bullet OH$ radical
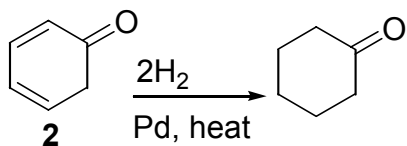
**Fig. 4.1.3. 3:** Production of cyclohexanone

Hydrogenation of phenol was carried over $Rh/SiO_2$ and $Rh/Al_2O_3$ at 323-353 $^{\circ}K$ and at atmospheric pressure and phenol was converted into cyclohexanol [54]. Phenol was supplied to one side of a metal membrane layered on a porous support, selectively transmitting hydrogen, while hydrogen was allowed to flow on the other side of the metal membrane. Phenol was hydrogenated to cyclohexanone by activated hydrogen transmitted through the metal membrane consisting of Pd. 0.32 % of gaseous phenol in Ar was fed to one side of the Pd membrane placed in a hydrogenation chamber heated at 200 $^{\circ}C$ and on the other side of the membrane a stream of hydrogen was supplied at 1 atm [55].

Membrane (100 $\mu$m) catalysts consisting of binary Pd alloys with Ru were evaluated in the hydrogenation of phenol in the gas phase. The selectivity for cyclohexanone was temperature independent. Complete conversion of phenol was obtained with $H_2$ applied to the opposite face of the membrane as phenol [56].

Selective hydrogenation of phenol to cyclohexanone was accomplished in the gas phase at 373-473 $^{\circ}K$ in the presence of a modified $Pd-Al_2O_3$ catalyst [57]. The hydrogenation was conducted in tubular reactor containing the catalyst. After activation at 453 $^{\circ}K$, the reactor was fed 840 L/h of a hydrogen gas mixture containing 80 ppm CO and 540 g vaporized phenol. After 10 h of operation the product stream contained cyclohexanone 97.4 %, cyclohexanol 2.4 %, phenol 0.2 %, and light- or high-boiling side products 0.1% [57].

Itoh (52) studied the possibility of hydrogenating phenol to cyclohexanone using Pd –based membranes as catalysts at atmospheric pressure and temperatures ranging from 150 to 300 $^o$C. The catalytic membranes were either pure Pd or an alloy of Pd with another metal. According to this study, pure Pd membrane showed the highest activity for the production of cyclohexanone.

It can be seen from the above literature studies that phenol can be converted to cyclohexanone or cyclohexanol by hydrogenation reaction in presence of hydrogen, a catalyst, and heat. In our system both hydrogen and the catalyst were presents along with the heating and this would explain the appearance of cyclohexanone and cyclohexanol in the product stream.

## 4.2. Discussion of the experimental results

### 4.2.1. Pd-membrane system

### 4.2.1.1. Properties of the Pd –membrane before running reaction

The Pd membrane which used in this study was formed on the outer side of the porous ¼ tube by electrolysis plating technique. In the original work of Niwa *et al* [9], the Pd membrane was prepared by coating a porous $\alpha$-alumina tube with a thin layer of palladium by means of metallic chemical vapor deposition technique. Therefore the major difference between the two systems lies in using different support materials. It was not clear from the results whether this process is a pure catalytic process or a catalytic process (heterogeneous reaction) combined with gas phase reaction (homogenous reaction). If the reaction of benzene is only a catalytic process, then the support might affect the reactivity of benzene. Therefore, the difference in the obtained results from this work compared to Niwa work cannot be attributed to the difference in the support.

At 300° C, the reported hydrogen and nitrogen permeation rates of by Niwa were 1.0-3.0 x$10^{-3}$ mol m$^{-2}$ s$^{-1}$ Pa$^{-0.5}$ (10.5 to 3.5 m$^3$ m$^{-2}$ h$^{-1}$) and 0.1- 1.0 x$10^{-10}$ mol m$^{-2}$ s$^{-1}$ Pa$^{-0.5}$, respectively [Niwa, 2002]. Hydrogen and nitrogen permeation rates of the Pd membranes were 2-4 m$^3$ m$^{-2}$ h$^{-1}$ and 0.0005-0.001 m$^3$ m$^{-2}$ h$^{-1}$ respectively at atmospheric pressure difference and 350° C based on the work of Ma *et. al.* [23]. From experimental measurements, hydrogen permeation rate was 0.72 m$^3$ m$^{-2}$ h$^{-1}$ (1.22 ml cm$^{-2}$ min$^{-1}$) at 150° C and 5 Psig pressure difference between the shell side and the tube side. The measured values were close to the calculated ones based on the work of Ma et. al. [23]. Therefore, the calculation of permeability at 350°C seems to be reasonable. This allows comparing the permeability of Pd membrane in this study to the ones reported by Niwa *et. al.* []. Based on this comparison it can be seen that the permeation rate for H$_2$ in this study is within the range reported by Niwa *e  al.*

Hydrogen flux through the Pd membrane was measured at 150 ° C and a pressure difference of 5 psig overnight as was shown in Figure 3.1.1.1 It can be seen that H$_2$ flux was relatively stable at 0.72 m$^3$ m$^{-2}$ h$^{-1}$. He flux was 0.02 ml cm$^{-2}$ min$^{-1}$ before flowing H$_2$ and 0.122 after pressurizing the shell with H$_2$ at the same conditions of temperature and pressure. At these conditions was 61 and 11 before and after flowing hydrogen, respectively.  Such low separation factors are due to the pressure difference was low. The change in He flux after pressurizing with hydrogen is expected since the Pd membrane was operated below the thermal stability region. The change in the separation factor of the Pd membrane is due to the Pd embrittlement. This phenomenon accrues when the operating temperature for H$_2$-Pd system is below 300° C. It appears as a results of $\beta$ palladium hydride nucleation from $\alpha$ phase. This causes loss in density in the Pd layer

and the selectivity of the membrane as a result of alternative Pd lattice expansion and reduction [23,24].

### 4.2.1.2. Properties of the Pd –membrane after running all experiments

The calculated separation factor after running all the experiments using this membrane was 10 at 150 $^o$C and 9 at 200 $^o$C. Hence the properties of the Pd membrane seem not to have changed after running all the reactions compared to its properties before running the reactions based on the calculated values of the separation factors in this section and the previous section. However, be comparing the absolute values of $H_2$ flux at 5 psig ( by extrapolating the data) to its flux at the same temperature before running the reactions (Figure 4.1.1) it can be seen that $H_2$ flux is at least 4 times its value before running the reaction. The same findings apply to He flux too. The increment in the fluxes of both He and $H_2$ after running the reactions is due to the appearance of more cracks in the Pd membrane. This is due to the repeated cycling of hydrogen flow at a lower temperature than 300 $^o$C which will lead to the appearance of membrane embrittlement phenomenon as was explained earlier.

### 4.2.1.3. Results with Pd membrane (mixed and non-mixed gases)

### 4.2.1.3.1. Non-mixed gases

### 4.2.1.3.1.1. $H_2$ in the shell side

The attempt to reproduce the results of Niwa *et al* that were presented in Figure 1.3.1 and Table 1.3.1, when $H_2$ was entered to the shell side was presented by the results in Tables 3.1.3.1.1.1, 3.1.3.1.1.2, 3.1.3.1.1.3 and 3.1.3.1.1.4. For the flow conditions in Tables 3.1.3.1.1.1, the flow composition is close to the second mixture in Table 1.3.1 with a higher total flow rate. From this experiment benzene conversion to phenol was

0.09 % while the reported value in Table 1.3.1 was 1.6 %. Also the selectivity toward phenol was 5.9 % compared to 96.3 % in Table 1.3.1. The data in Table 3.1.3.1.1.2 are the results for a flow composition close to the third set of experiment in Table 1.3.1 at 150 $^o$C (lower temperature). The obtained phenol conversion was 1 % compared to 2.05 % in Table 1.3.1. The selectivity was 35.6 % while the reported one in Table 1.3.1 was 92.7 %. It seems that the conversions of benzene from this work were close to the reported ones when the conversions of benzene were low. Using this arrangement didn't allow to obtain the reported conversion of 13.25 % even when other experiments were conducted at similar conditions. Even in the reported data it self it can be seen that the flow compositions in Figure 1.3.1 seem to be close to the ones in the second raw of Table 1.3.1 with a 40 degree  increment in Temperature and yet conversion was much higher.

### 4.2.1.3.1.2. H$_2$ in the tube side

The flow of hydrogen was reversed and it was fed to the tube side while the other reactants and gases were fed to the shell side. In Figure 3.1.3.1.2.3, feed composition was similar to the third set of experiment in Table 3.1.1. Regarding benzene to phenol conversion, the obtained value is close to the reported one. However, the selectivity is 64.3 % compared to 92.7 %.

The experimental conditions in Figure 3.1.3.1.2.3 were the same as these ones in Table 3.1.3.1.2.3. The data in Figure 3.1.3.1.2.3 were reproduction of the experimental results for the data in Table 3.1.3.1.2.3. Comparing the final results of Figure 3.1.3.1.2.3, that were given in Table 3.1.3.1.2.7, to the results at the same flow conditions in Table 3.1.3.1.2.3 it can be seen that benzene conversion to each product and the selectivity of the products were close. This means that these experiments were reproducible.

The experimental data in Figure 3.1.3.1.2.3 were taken over a long period of time. The data were obtained first up to 10 hours (Figure 3.1.3.1.2.3) then the reaction was allowed to proceed over night as can be seen from Figure 3.1.3.1.2.3. From running the reaction for such a long time it can be seen that the system was quite stable since the conversion of benzene to each product didn't vary considerably. This can be seen also from oxygen conversion in Figure 3.1.3.1.2.2. Also, by comparing the data in Tables 3.1.3.1.2.6 and 3.1.3.1.2.8, it can be seen that conversion of oxygen and produced water are similar for the 10 hours and 27 hours of reaction time. In this section, and in the previous one, other organic compounds were formed beside phenol. These compounds were cyclohexanone, cyclohexanone, 2-hydroxy, catechol, hydroquinone, and 1,4-Cyclohexanedione. The mechanism for the formation of these compounds was explained in Section 4.1. At the experimental conditions that were presented in section 3.1.3.1.2 produced amount of water was at least 120 times the amount of produced phenol. Niwa *et al* [9] reported that the ratio of water to phenol was 5/9.

### 4.2.1.3.1.2.1. Varying $H_2$ flow rate to the tube

$H_2$ flow rate to the tube side was varried compared to its flow rate in section 3.1.3.1.2. The flow rates of the other gases to the shell side were the same. Comparing the results in Tables 3.1.3.1.2.1.1 and Table 3.1.3.1.2.1.3, which were obtained by increasing and decreasing $H_2$ flow rate, respectively, to the results in Table 3.1.3.1.2.7, it can be seen that conversion of benzene to the detected organic compounds was almost insensitive to these changes. The same true for $O_2$ conversion and produced water. This should be expected since the amount of hydrogen available for the reaction depends on its flux through the Pd membrane which is a function of temperature and pressure

difference. Since both temperature and pressure difference was constant in all cases. Then theoretically same flux of $H_2$ was obtained. Regardless of these changes benzene conversion to phenol didn't exceed 2 % and produced water was always at least 140 times higher than the amount of the target product phenol.

### 4.2.1.3.1.2.2. Varying $O_2$ flow rate to the shell

The flow rate of oxygen to the shell side of the reactor was varied and the results were shown in Figure 3.1.3.1.2.2.1. It can be seen from this figure that there is a little improvement in benzene conversion to phenol as more oxygen was used. This improvement was on the expense of producing less carbon dioxide. Other products from benzene reaction didn't changes greatly.

### 4.2.1.3.2. Mixed gases (all gases flow to the shell side)

From previous discussions, it can be seen that using the Pd-membrane to permeate $H_2$ to the benzene mixture didn't yield the high conversion to phenol as the reported value in Figure 1.3.1. In the reported work of Niwa *et al* [9], they said that the membrane was deteriorating after a while and was pealing of the support. This might be the reason for getting up to 13 % of benzene conversion in their system. In other words all the reactants might be mixed together through the leaks due to membrane deterioration. This was the motivation behind mixing all the reactants and introducing them through the shell side.

A reaction mixture with a total flow rate of 43.3 ml min$^{-1}$ ($H_2$/Benzene/$O_2$/He/Ar = 34.0/4.1/17.9/41.0/3.18 % of total flow rate) at 150 $^o$C was introduced to the shell side. Also in this reaction mixture the ratio of $O_2$/($O_2$+$H_2$) was 34.4 % which means that 2

moles of $H_2$ was available per mole of $O_2$. This ratio is close to the stoichiometric ratio for the reaction between $H_2$ and $O_2$ to produce water. Also this ratio was within the flammability limit for a mixture of $H_2$ and $O_2$.

The results for these flow conditions were presented in Figures 3.1.3.2.1, 3.1.3.2.2, and 3.1.3.2.3 for 8 hours of reaction time. The reaction was allowed to run for a longer time (18 hours) and the results were presented in Figures 3.1.3.2.4, 3.1.3.2.5, and 3.1.3.2.6. From the results presented in the previous figures, it can be seen that the reaction of benzene was stable over time. This is clear from the summary of the results after 8 and 18 hours of reaction in Tables 3.1.3.2.1 and 3.1.3.2.3, respectively. From these tables, it can be seen that benzene conversion was the same after 8 and 18 hours of reaction.

Also, it can be seen that high conversions of benzene were obtained. According to the summary of these results given in Table 3.1.3.2.3, conversion of benzene to phenol was 27 % with selectivity of 49 %. The other compounds which were present in a relatively large amounts were 1,4-cyclohexanedioe and catechol. Benzene conversion to 1,4-cyclohexanedione and catechol were 10.7 % and 7.5 %, respectively. In section 4.2, in the suggested mechanism for the formation of 1,4-cyclohexanedione as was given in Figure 4.1.2.2 for the reaction paths for the hydroxylation of catechol and hydroquinone, it was suggested that further oxidation of catechol and reactions with hydrogen atom will lead to the appearance of 1,4-cyclohexanedione. Also it seems that part of catechol has been converted to cyclohexanone, 4-hydroxy where benzene conversion to it was 2%. At the same time lower conversions were obtained for hydroquinone. Cyclohexanone, 2-hydroxy, according to the suggested mechanism in Figure 4.1.2.2 has appeared as a result

of further oxidation and hydrogenation of hydroquinone. In the GCD analysis the peaks of cyclohexanone, 2-hydroxy and 1,2-cyclohexanedioe appeared at a very close retention time therefore the measured conversion to cyclohexanone, 2-hydroxy is actually for both cyclohexanone. Benzene conversion to cyclohexanone, 2-hydroxy was 4.4 % compared to 0.1 % conversion to hydroquinone. Conversion of benzene to pentanoic acid, 4-oxo was 4 %  and as said earlier the appearance of this compound might due to the ring opening of phenol under the experimental conditions. Cyclohexanone was obtained in low amounts compared to phenol in this system. This would mean that direct hydrogenation of benzene to cyclohexanone might be slow at these conditions.

The selectivity of each product from benzene reaction at the mentioned conditions was shown in Figure 3.1.3.2.2. The results in this figure were consistent with the obtained benzene conversions in the previous figures. The highest selectivity was for phenol since benzene has the highest conversion toward this compound. Then 1,4-cycloheaxneione comes next in selectivity.

The total conversion of oxygen was stable over time and its value was 0.83 for the 8 and 18 hours reaction time. The produced amount of water (Table 3.1.3.2.2) was 4.6 x $10^{-4}$ mol min$^{-1}$. The ratio of produced moles of water to the produced moles of phenol (Table 3.1.3.2.2) was 23/1. Produced water is still higher than produced phenol but this ratio is much lower than the one in section 4.1.3.1.2.

### 4.2.1.3.2.1. Mixed gases effect of total flow rate

The reaction mixture which was described in section 4.1.3.2 was varied in total flow rate. The flow rate of each gas was fixed at each total flow rate. Also, the reaction temperature was fixed at each flow rate. This was performed in order to study the effect

of residence time on benzene conversion. It can be seen from Figure 3.1.3.2.1.1 that conversion of benzene increased with increasing total feed flow rate from 22 ml min^{-1} to 65 ml min^{-1}. At the same time benzene conversions to catechol and 1,4-cyclohexanedione decreased as the total flow rate of the feed was increased from 22 ml min^{-1} to 65 ml min^{-1}. Benzene conversions to the other products decreased also but this decrease was not so apparent since benzene conversions to the other product were small compared to its conversion to phenol. At the highest total flow rate in this study, which was 113 ml min^{-1}, benzene conversions to all products have decreased. The data in Figure 3.1.3.2.1.1 at the low conversions were not clear, therefore Figure 4.1.3.2.1.1 below was obtained to show the portion of Figure 3.1.3.2.1.1 at the low conversion of benzene.
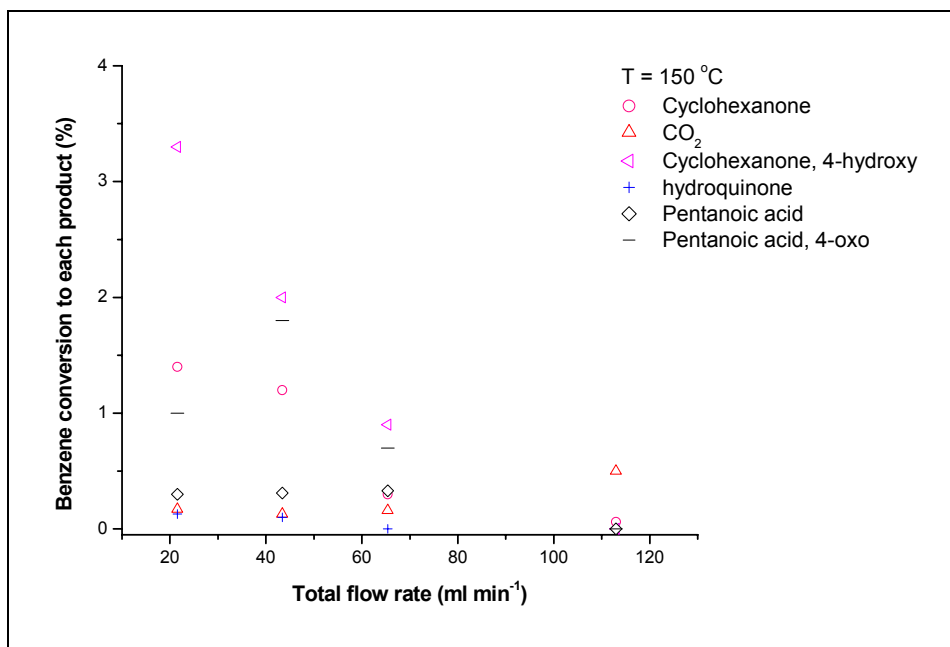


**Fig. 4.1.3.2.1.1:** Benzene conversion to each product from the reaction of benzene over Pd using different flow rates at 150 $^oC$. Reaction mixture composition: Benzene/$O_2$/He/Ar/ $H_2$ = 4.1/17.9/41.0/3.18/34 (% of total flow rate)

It is clear from Figure 4.1.3.2.1.1 that conversion of benzene to each product was decreasing with increasing total flow rate except for $CO_2$ where it seems that more

benzene has converted to $CO_2$ at the highest total flow rate. At the highest total flow rate benzene conversion to phenol, $CO_2$, cyclohexanone, catechol, and pentanoic acid, 4-oxo were 10.2 %, 0.55 %, 0.07 %, 0.06 %, and 0.7 %, respectively. The other products mentioned in Figure 3.1.3.2.1.1 were not detected at the highest total flow rate. By taking the sum of benzene conversion to each product then the total conversion of benzene at 22 ml $min^{-1}$, 43 ml $min^{-1}$, 65 ml $min^{-1}$, and 113 ml $min^{-1}$ will be 55 %, 55.5 %, 53 % and 10.7 %, respectively. Hence total benzene conversion was decreasing with increasing total flow rate for total flow rate greater than 43 ml $min^{-1}$. This might due to the reduction in contact time which will give less chance for benzene to react in the system. However, at a lower total flow rate than 43 ml $min^{-1}$, which was 22 ml $min^{-1}$, total conversion was similar to the one at 43 ml $min^{-1}$. This might indicate also that there is gas chemistry beside the surface chemistry.

The selectivity of each product from benzene reaction by varying the total flow rate was shown in Figure 3.1.3.2.1.2. It cab be seen that the selectivity of phenol increase with flow rate up to 65 ml $min^{-1}$. This is due to the increase in benzene conversion to phenol, and decrease of benzene conversion to the other products within this range of total flow rate. The selectivity to phenol continues to increase at the highest total flow rate of 113 ml $min^{-1}$. Conversion to benzene has decreased at 113 ml $min^{-1}$ as was seen in Figure 3.1.3.2.1.1. Conversion to the other products has decreased also, as said earlier, at 113 ml $min^{-1}$ and some products were not detected. This combined effect of decreasing conversion to all the products and disappearance of some of them allow the selectivity of phenol to be high at the highest total flow rate.

The results in Figure 3.1.3.2.1.3 show the produced moles of each product at each total flow rate. It can be seen that the amount of phenol produced increased by increasing the total flow rate from 22 to 65 ml min$^{-1}$. This was expected since both benzene conversion to phenol and molar flow rate of benzene have increased in this period. At 113 ml min$^{-1}$ the decrease in benzene conversion to phenol had overcome the increase in inlet benzene flow rate; therefore, produced amount of phenol at this flow rate was lower than the ones at the other flow rates. The same analysis applies for the other products. It can be seen that if the decrease in benzene conversion to a specific product overcomes the increase in the inlet amount of benzene then the net effect will be a decrease in the produced amount of that product and vice versa.

From studying the effect of total flow rate on benzene conversion to each product it can be seen that there is an optimum value for the total flow rate with regard to benzene conversion to phenol. However, at enough high flow rate conversion of benzene to phenol might be lower than the one at the optimum flow rate but yet selectivity will be higher. At the same time if conversion to benzene was low enough to overcome the increase of benzene inlet flow rate then the net effect will be a decrease in the amount produced of phenol. Selection of the total flow rate then would depend on the overall economy of the process.

Conversion of oxygen has slightly decreased as total flow rate was increased as can be seen from Figure 3.1.3.2.1.4. This small change in oxygen conversion accompanied by a higher inlet flow rate of oxygen led to increment of produced water as total flow rate was increased.

**4.2.1.3.2.2. Effect of varying $O_2/(O_2+H_2)$ % in the reaction mixture at 150 $^oC$**

The previous results that were discussed all of them were obtained by running the reaction at 34 % of $O_2/(O_2+H_2)$. This number would mean that two moles of hydrogen were fed per mole of oxygen. Such a mixture will be explosive. Therefore, the ratio of $O_2/(O_2+H_2)$ was varied in the reaction mixture, by varying $O_2$ inlet amount, to find other values that will give good conversion of benzene to phenol and at the same time be out of the flammability limit for hydrogen and oxygen. Results for different values of the ratio of $O_2/(O_2+H_2)$ were presented in Table 3.1.2.2.2.1 for a reaction that was carried at 150 $^oC$ and a total flow rate of 43.3 ml min $^{-1}$. It can be seen from the results in Table 3.1.2.2.2.1 that for a ratio of $O_2/(O_2+H_2)$ lower than 23 % no phenol was detected at these conditions. Very small conversions of benzene to cyclohexanone, cyclohexanone, 2-hydroxy, resorcinol, and catechol were observed at a ratio of $O_2/(O_2+H_2)$ less than 23 %. Hydroquinone was present in a relatively high amounts compared to the other compound at a ratio of $O_2/(O_2+H_2)$ of less than 23 %. It could be possible that at low ratios of $O_2/(O_2+H_2)$ that all the produced phenol has converted to the detected products or these products were trapped somewhere in the reactor and once the reaction was started they got dissolved in water which was produced from the reaction since most of these compounds are soluble in water (Table 4.1.1). In this work, Ar was flowed into the reactor before any experiment and analysis was made by the GCD to check for the presence of any compound in the reactor. Also, the reactor, most of the time, was flushed before the start of any experiments by introducing a mixture of hydrogen and oxygen that will produce water and dissolve anything that might got trapped in the system. Therefore

131

it could be that traces of the organic compounds was left in the system after the flushing and appeared in the analysis later

The conversions of benzene to the different products at a ratio of $O_2/(O_2+H_2)$ less or equal 23 % were very small and negligible except for hydroquinone and its isomers (resorcinol and catechol). Considerable conversion of benzene to phenol was obtained once the ratio of $O_2/(O_2+H_2)$ was 36.5 %. Conversion of benzene to phenol at 36.5 % of $O_2/(O_2+H_2)$ were close to the ones obtained at the same total flow rate in Figure 3.1.3.2.1.1. However, more hydroquinone and catechol were produced at 36.5 % of $O_2/(O_2+H_2)$.

### 4.2.1.3.2.3. Effect of varying $O_2/(O_2+H_2)$ % in the reaction mixture at 300 $^o$C

The reaction at 300 $^o$C was carried at different flow rates of oxygen in the feed keeping the flow rates of other gases, except for He which was the balance gas, and the total flow rate constants. The system was heated at 300 $^o$C and flushed for 48 hours before the start of the reaction to be sure that nothing was trapped in the system. It can be seen from the results in Table 3.1.3.2.3.1 that at 5 % of $O_2/(O_2+H_2)$ only a small conversion of benzene to $CO_2$ was observed. Even at the highest tested ratio of $O_2/(O_2+H_2)$ conversion of benzene to phenol was 0.53 %. At 23 % of $O_2/(O_2+H_2)$ benzene conversion to catechol, 1,4-cyclohexanedione, hydroquinone, cyclohexanone, and $CO_2$ were 0.18 %, 0.06 %, 2.8 %, 0.11 %, and 0.06%, respectively. Therefore benzene conversions to the detected products was small except, relatively, for hydroquinone.

It can be seen that using 23 % of $O_2/(O_2+H_2)$ at the high temperature (300 $^o$C) the benzene reactivity was low. Therefore it seems that the system at 150 $^o$C might have

produced, internally, an amount of energy that will provide a higher temperature than the studied one at 300 $^{o}$C and this might be the reason to obtain high conversions at 150 $^{o}$C.

**4.2.1.3.2.4. Reproducing the experimental results in Figure 3.1.3.2.4**

The results shown in Figure 3.1.3.2.4.1 were obtained in an attempt to reproduce the results that were shown in Figure 3.1.3.2.4. Comparing the results in both figures it can be seen that conversion of benzene to phenol was high in both cases. However, the obtained conversions in Figure 3.1.3.2.4 were different than these ones in Figure 3.1.3.2.4.1. Benzene conversion was lower after reproducing the data. Catechol conversion was higher after the reproduction of the data. 1,4-cyclohexanedione was lower after reproducing the data. It seems like that when conversion of benzene to catechol has reduced at the same time conversion to 1,4-cyclohexanedione has increased. This might due to that 1,4-cyclohexanedione is derived from catechol as was shown in Section 4.1.Also by comparing the results in Figure 3.1.3.2.6.1 to the ones in Figure 3.1.3.2.4, it can be seen that benzene conversions in Figure 3.1.3.2.6.1 was lower than the obtained ones in Figure 3.1.3.2.4 at the same temperature and flow conditions. Therefore, it can be seen that the reproducibility was weak for this setup at the studied conditions of temperature and flow conditions.

This behavior of not being able to reproduce the same results might due to that what was happening in the system was not only heterogeneous reaction but there might be also gas phase chemistry. It might be that the surface chemistry was necessary to provide the required energy for the initiation of the gas phase chemistry. Similar phenomenon was observed by other workers [58, 57] where there was a gas phase reaction assisted by the presence of surface chemistry. If this was the case, then the

reactions between $H_2$ and $O_2$ and the oxidation of benzene to carbon dioxide, which are the heterogeneous reactions, will provide the required energy for the initiation of the gas phase reaction and produce free radicals from benzene oxidation. Some of these free radicals might not be stable but it is believed that, due to the presence of surface chemistry, there might be a hot spot within the system where the temperature will be high enough to produce these free radicals and then there will be a fast quenching that will keep these radical in the system [26, 27]. The distribution of these organic radicals, and hence the produced organic compounds, will depend on the energy available within this hot spot. This energy might not be constant. This might explain the weak reducibility of the results since the production of phenol and the other organic compounds was not the same at the same conditions when the experiment was repeated.

For the used ratio of $O_2/(O_2+H_2)$, it was within the flammability limits (5% to 75%). Several experiments where tried to explore the reaction at different $O_2/(O_2+H_2)$% but the one, which gave high conversion of benzene where 34-37%. This might be associated with the amount of energy that should be available within the system to initiate the homogeneous chemistry.

### 4.2.1.3.2.5. Experimental results at 180 °C

The reaction with the same flow conditions as these ones in Figure 3.1.3.2.4 but at a higher temperature (180 °C). It can be seen from Figure 3.1.3.2.5.1 that benzene conversion to phenol was much lower than the obtained ones at 150 °C in Figure 3.1.3.2.4 (from the results in Table 3.1.3.2.3). Conversions of benzene to the other products listed in Figure 3.1.3.2.5.1 were also lower than the ones in Figure 3.1.3.2.4. However, selectivity of phenol at the lower conversions at 180 °C, as can be seen from

Figure 3.1.3.2.5.1, was higher that its selectivity at the same flow conditions at 150 $^{o}$C ( from the results in Table 3.1.3.2.3). This higher selectivity at the lower conversion is due to lower benzene conversions to the other products, other than phenol, at the lower benzene conversion to phenol were obtained. Therefore, produced amount of phenol was much higher than the other products in the system.

The reaction at 180 $^{o}$C was carried at different flow rates, keeping the flow composition the same at the different flow rates. It can be seen from Figure 3.1.3.2.5.1, for the studied flow rates, that a total flow rate of 43 ml min-1 gave the highest conversion of benzene to phenol. At the same total flow rate conversion of benzene to catechol was higher than the other studied flow rates, especially compared to 22 ml min$^{-1}$. Other compounds were obtained in small amounts therefore changes in benzene conversion to these compounds were not considerable compared to changes in benzene conversion to phenol. Total conversion of benzene which is the sum of benzene conversion to each product was 5.4 %, 6.4 %, and 5 % at 22 ml min$^{-1}$, 43 ml min$^{-1}$, and 117 ml min$^{-1}$, respectively. It seems that total conversion of benzene was highest at 43 ml min$^{-1}$.

From Figure 3.1.3.2.5.2, it can be seen that selectivity of phenol was the same at 22 ml min$^{-1}$ and 43 ml min$^{-1}$ although; conversion to phenol was higher at the later flow rate. This is due to higher conversion to catechol at the 43 ml min$^{-1}$. Selectivity of phenol at 118 ml min$^{-1}$ was lower than the ones at the other flow rates. This due to the reduction in benzene conversion to phenol at the same time there was increment in conversion to $CO_2$ and conversion to catechol was slightly reduced. Therefore, the net effect will be a reduction in selectivity of phenol. Produced amount of water increased as total flow rate

was increased as can be seen from Figure 3.1.3.2.5.3. The same behavior was observed for the results at 150 $^{\circ}$C. Conversion of oxygen to water didn't changes significantly but the amount of oxygen in feed has increased as total flow rate was increased therefore the calculated amount of water based on the inlet feed of oxygen will increase.

### 4.2.1.3.2.6. Experimental results at 200 $^{\circ}$C

The reaction mixture with a total flow rate of 43 ml min$^{-1}$ and feed composition that was used to obtain the results in Figure 3.1.3.2.4 at 150 $^{\circ}$C was studied at a higher temperature (200 $^{\circ}$C). Benzene conversion to each product at 200 $^{\circ}$C was shown in Figure 3.1.3.2.6.1. Selectivity of the products at these conditions was shown in Figure 3.1.3.2.6.2. It can be seen from the previous figures that benzene conversions to phenol and the other products were lower than the obtained ones at 150 $^{\circ}$C in Figure 3.1.3.2.4. Selectivity of phenol was high since other compounds were produced with low amounts. High conversion of oxygen ( mainly to water) were observed at 200 $^{\circ}$C as can be seen in Figure 3.1.3.2.6.3.

The experiment at 200 $^{\circ}$C was repeated and the results were shown in Figure 3.1.3.2.6.4. Comparing the results in Figures 3.1.3.2.6.1 and 3.1.3.2.6.4 for the same time range (up to 2 hours), it can be seen that conversion of benzene to phenol were comparable in both figures. Conversion of benzene to hydroquinone in Figure 3.1.3.2.6.1 was comparable to benzene conversion to catechol in Figure 3.1.3.2.6.4. Both hydroquinone and catechol are isomers and they appear at a very close retention tine in the GCD, therefore it might be expected that equilibrium might shift from catechol to hydroquinone. Overall conversions of benzene in Figures 3.1.3.2.6.1 and 3.1.3.2.6.4 were comparable for the same time scale hence these results were reproducible.

136

Upon allowing the reaction in Figure 3.1.3.2.6.4 to run to 8 hours it can be seen that conversion of benzene to phenol has increased to 7.7 %. Also, conversion of benzene to catechol has increased to 8.6 % and benzene conversion to 4 %. The previous compounds were present in the largest amounts in the product stream. The reaction was allowed to proceed for a longer time up to 27 hours as can be seen in Figure 3.1.3.2.6.5. From the results in the previous figure it can be seen that benzene conversions to most of the observed products were stable for reaction time above 10 hours. A slight increment was observed in benzene conversions to phenol, 1,4-cyclohexanone, and pentanoic acid, 4-oxo from time 10 hours until the end of the reaction. Total conversion of oxygen was also stable over the reaction period as can be seen in Figure 3.1.3.2.6.6. Fig. 3.1.3.2.6.7

The results in Figure 3.1.3.2.6.4 were repeated again by running the experiment for 2 hours as can be seen in Figure 3.1.3.2.6.7. Benzene conversion in the previous figure was at the same value as in Figures 3.1.3.2.6.4 and 3.1.3.2.6.1. Other than catechol, benzene conversions to the remaining organic compounds were similar to the values obtained earlier at the same reaction conditions. Benzene conversion to catechol was higher than the obtained values earlier for the same time scale.

Temperature profile very close to the Pd membrane was measured as can be seen in Figure 3.1.3.2.6.8 for the reaction conditions at $200^{\circ}C$ and 43 ml $min^{-1}$. The profile was normal and no high temperature was observed.

The reaction mixture of 43 ml $min^{-1}$ total flow rate and flow compositions as the one given in Figure 3.1.3.2.6.4 was entered to the shell side of the Pd membrane reactor at 300 $^{\circ}C$. From the results in Figure 3.1.3.2.6.8, it can be seen that benzene conversions to phenol and the other organic compounds were lower than these ones at 200 $^{\circ}C$ (Figure

3.1.3.2.6.4). Conversion of benzene to $CO_2$ was 0.45 at 300 $^o$C and 0.75 at 200 $^o$C (Figure 3.1.3.2.6.4).

The results shown in Figure 3.1.3.2.6.10 were obtained by repeating the experiments with the flow conditions shown in Figure 3.1.3.2.6.4. The following table summarizes benzene conversion after 12 hours of reaction in both Figures 3.1.3.2.6.10 and 3.1.3.2.6.4.

**Table 4.1.3.2.6.1:** Benzene conversion to each product after 12 hours of reaction in Figures 3.1.3.2.6.10 and 3.1.3.2.6.4

| Product | Conversion from Figure 3.1.3.2.6.10 (%) | Conversion from Figure 3.1.3.2.6.4 (%) |
|---|---|---|
| Phenol | 10.8 | 10.81 |
| Cyclohexanone | 0.21 | 0.17 |
| $CO_2$ | 0.27 | 0.32 |
| Pentanoic acid | 0.19 | 0.19 |
| Cyclohexanone, 2-hydroxy | 0.71 | 0.40 |
| 1,4-Cyclohexanedione | 8.95 | 5.31 |
| Cyclohexanone, 4-hydroxy | 1.21 | 0.40 |
| Catechol | 18.82 | 22.8 |
| Resorcinol | 2.14 | 3.80 |
| Hydroquinone | 6.47 | 7.72 |

From the data given in Table 4.1.3.2.6.1 for the 12 hours of reaction time, it can be seen that benzene conversions to the obtained products are quite similar in both figures. Although, the shape of the results vs. time, from the start of the reaction up to the 12 hours of reaction, does not look the same in Figures 3.1.3.2.6.10 and Figure 3.1.3.2.6.4.

Figure 3.1.3.2.6.11 shows benzene conversion for flow compositions similar to the ones in Figures 3.1.3.2.6.11 and 3.1.3.2.6.4 at different total flow rate and constant reaction temperature (200 $^o$C). From this figure it can be seen benzene conversion to the obtained products, except for phenol, hydroquinone, and resorcinol, decreased as total flow rate was increased. For phenol, benzene conversion increased by increasing total

138

flow rate from 22 ml min$^{-1}$ to 43 ml min$^{-1}$ and then decreased at 119 ml min$^{-1}$. Conversions of benzene to hydroquinone and resorcinol were quite similar at 22 ml min$^{-1}$ to 43 ml min$^{-1}$ and then decreased at 119 ml min$^{-1}$ which is different from the results behavior at 150 $^{o}$C. This might be due to that benzene conversion to catechol is higher than benzene conversion to phenol at 200 $^{o}$C as was seen from the results at 200 $^{o}$C. Total conversion of benzene which is defined as the sum of benzene conversion to each product was 0.72, 0.64, and 0.58 at 22 ml min$^{-1}$, 43 ml min$^{-1}$, and 119 ml min$^{-1}$, respectively. It can be seen that total conversion slightly decreased with total flow. The change in total flow rate might not be enough to see a considerable change in benzene conversion at the previous conditions. The total flow rate of the reaction mixture was limited by the range of flow rates provided by the used mass flow controllers hence higher flow rate was not possible to obtain using the available mass flow controllers.

The results obtained from mixing all the reactants to the shell side of the Pd membrane were not easy to understand especially regarding the reproducibility of the data where at for the same reaction conditions the same results might not be reproduced. Also, it was not obvious whether this was a surface chemistry or a combination of surface chemistry and gas phase chemistry.

In order to understand the chemistry of benzene reaction in the presence of a mixture of hydrogen and oxygen and a catalyst like Pd other configuration of the Pd catalysts were used. The other reactor setups were intended only to understand this chemistry and not to make kinetic study. In order to perform kinetic study at least good mixing should be provided in the setup which might not be achieved in the different

reactor setups that were used in this chapter. In the first group of these setups supported Pd was used as the catalyst.

Also, after removing the membrane from the system there were some parts pealing out of it. It was thought that these parts might serve as pockets that would allow the gas to have low velocity that would serve to generate the different observed products from benzene reaction. That was the motivation behind the design of different systems. In these systems Pd foil, with as mall dimensions compared to the Pd membrane, was cut to form a certain shape and welded to the exterior surface of the ¼ in tube.

### 4.2.1.4. Pd/ZrO₂ system

In section 3.1.3, the exterior surface of the ¼ tube was covered with a thin layer of Pd supported on Zr/O₂ for a length of the ¼ in tube similar to the length of ¼ tube that has the Pd membrane.

From the results in Figure 3.1.4.1 it can be seen that benzene was converted to phenol and other products using this setup. The reaction mixture flow rate, composition and reaction temperature were similar to the ones in Figure 3.1.3.2.4 for the Pd membrane system. It can be seen that lower conversion of benzene were obtained using this setup. Also, some of the compounds that were produced at the high conversions of benzene in Figure 3.1.3.2.4 were not detected in the Pd/ZrO₂ as can be seen in Figure 3.1.4.1. This is due to the low conversion of benzene to phenol which means that small amount of phenol were produced and hence the available amount of phenol that would react further and produce other product in the system was low. It is not really clear why this system gave low conversion to phenol. It might be possible due to nature of the catalyst that it was a supported one then the available active sites to initiate the reactions

140

in the system might be lower than the active sites on the Pd membrane surface. Also, for supported catalyst they could deactivate quickly and hence some of the active sites will be blocked. From Figure 3.1.4.2 it can be seen that phenol has the highest selectivity, about 50 %, and $CO_2$ was the second selective compound even at the start of the reaction it was more selective than phenol. This might be due to the in sufficient mixing at the start of the reaction.

Total conversion of oxygen, as can be seen from Figure 3.1.4.3, was stable cover time and it was also high. Almost, all of the entered oxygen was consumed and this was mainly toward the production of water.

Another reaction mixture, similar in composition to the one in Figure 3.1.4.2, was used with a higher total flow rate (45 ml min$^{-1}$). Benzene conversion to phenol and the other products was stable over time as can be seen from Figure 3.1.4.4. It can be seen from Figure 3.1.4.4 that higher conversion of benzene to phenol and benzene conversion to the other products didn't change considerably compared to the results in Figure 3.1.4.2 (at 43 ml min$^{-1}$). Selectivity of the products, overall, was quite stable as can be seen in Figure 3.1.4.5, although selectivity to phenol has dropped at the send and third data points in this figure. This drop was due to the decrease of benzene conversion to phenol in the second data point and to the increase in catechol for the third data point. Conversion of oxygen was also high these flow conditions as can be seen from Figure 3.1.4.6.

### 4.2.1.4.1. Effect of total flow rate using Pd/ZrO$_2$ system

The reaction mixture that was used in Figure 3.1.4.4 was studied again by changing the total flow and keeping the flow composition and reaction temperature the

same. It can be seen from Figure 3.1.4.1.1 that conversion of benzene to phenol, catechol, and $CO_2$ slightly increased when the total flow rate was increased from 45 ml min$^{-1}$, 71 ml min$^{-1}$. Conversions of benzene to the other products decreased. At the highest studied flow rate, 112 ml min$^{-1}$, Conversion of benzene to phenol dropped remarkably. At the same time conversion to $CO_2$ has increased. Conversion to catechol has decreased at the high flow rate. It seems that the high flow rate allows for more conversion of benzene to $CO_2$ while it gives lower conversion to phenol. Total conversion of benzene was 3.6 %, 4.2 %, and 2.3 % at 45 ml min$^{-1}$, 71 ml min$^{-1}$, and 112 ml min$^{-1}$, respectively. It can be seen slight increment in benzene conversion was obtained in going from 45 ml min$^{-1}$ to 71 ml min$^{-1}$ with a decrease for 112 ml min$^{-1}$.

The changes in conversion as a function of total flow rate were reflected on the products selectivity and produced amounts of the products as can be seen from Figures 3.1.4.1.2 and 3.1.4.1.3. It can be seen that selectivity of the products at 45 ml min$^{-1}$ and 71 ml min$^{-1}$ was similar since conversions of benzene were similar. At 112 ml min$^{-1}$, the system became more selective to $CO_2$, and hence more $CO_2$ was produced, since more conversion of benzene to $CO_2$ was obtained.

### 4.2.1.4.2. Effect of temperature using Pd/ZrO$_2$ system

It can be seen from Figure 3.1.4.2.1 that benzene conversions to phenol, catechol, and $CO_2$ have increased, slightly, by increasing the reaction temperature from 100 $^{\circ}$C to 150 $^{\circ}$C. Conversions of benzene to the other products have decreased for the same temperature increase which means that the produced amounts of these products have reduced. Conversion of benzene to phenol has decreased by increasing the temperature from 150 $^{\circ}$C to 325 $^{\circ}$C. At 325 $^{\circ}$C only phenol, hydroquinone, and $CO_2$ were detected.

Also, at this temperature the sharp decrease in produced phenol was accompanied by high increase in produced $CO_2$. Therefore its seems at this flow rate and feed composition high temperature using the $Pd/ZrO_2$ favors less production of phenol and more production of $CO_2$. This might be due to catalyst poising at the high temperature by carbon dioxide. The results at 150 $^o$C were repeated, after the regeneration of the catalyst, and gave the same results.

### 4.2.1.5. Pd/Carbon (Pd/C)

Another form of Pd supported catalyst was used. This time Pd supported on carbon was used to pack a tubular reaction to which the reaction mixture was fed. It can be seen from Figure 3.1.5.1 that increasing $O_2$ percentage in the feed led to higher conversion to cyclohexanone. Also higher conversion to phenol was obtained at 9.3 % $O_2$ in the feed. Overall, benzene conversion phenol is slower than Pd membrane system. Other flow conditions were tested as can be seen but none of the tested conditions gave high conversion of benzene to phenol as can be seen from the results in Figure 3.1.5.1 through Figure 3.1.5.4. When the ratio of $O_2/(O_2+H_2)$ was 50 % no phenol was produced and only benzene was oxidized to $CO_2$ as can be seen in Figure 3.1.5.5. It seems that high concentration of oxygen will provide excess $O_2$ in the system that will go for the benefit of oxidizing benzene to $CO_2$. This excess amount of oxygen might have led to poisoning of the catalyst by the production of excessive amounts of carbon dioxide.

In this system with low conversion of benzene, it was observed that only phenol, cyclohexanone, cyclohexanol, and $CO_2$ were produced unlike the Pd membrane where other products were produced.

At all the reaction conditions, except for 50 % of $O_2/(O_2+H_2)$ , all of the entered oxygen was consumed and was mainly converted to water. For 50 % of $O_2/(O_2+H_2)$, 50 % of oxygen was converted to water production and the remaining 50 % converted to $CO_2$. The results which were obtained using this setup were reproducible as can be seen by comparing the results in Table 3.1.1.5 and Figure 3.1.1.2. The results in Table 3.1.1.5 were stable by carrying the reaction for 10 hours.

### 4.2.1.6. Pd foils obtained from Ma *et al* (23)

Pd foils were welded to the exterior surface of the ¼ in tube as was explained in the experimental setup for this part. This design was made in order to investigate if benzene conversion to phenol was related to some irregularities in the flow since, as said earlier, parts of the Pd membrane were pealed off the ¼ in tube and it was thought these parts might provide lower flow rate that might affect benzene conversion to phenol.

Benzene conversion to each product is shown in Figure 3.1.6.1 for different concentrations of benzene in the feed. The total flow rate was 22 ml min$^{-1}$ and reaction temperature was 200 $^o$C. It can be seen from this figure that as more benzene was fed to the reactor less conversion was obtained. Also, it can be seen that only phenol, cyclohexanone, and $CO_2$ were produced unlike the Pd membrane where other products were produced. This might be due to the small produced amount of phenol. Therefore, the chance that phenol might react further in the system and produce other compounds has been decreased.

The selectivity of each product from benzene reaction seems to be sensitive to changes in benzene concentration in the feed as can be seen from Figure 3.1.6.2. This due to that produced amounts of all products were reduced as was seen in Figure 3.1.6.1.

144

It can be seen from Figure 3.1.6.3 that the reduction in benzene conversion to phenol and cyclohexanone was balanced by the increase in benzene concentration in the feed, therefore, produced moles of phenol and cyclohexanone were the same at the different concentrations of benzene. This balance was not reached for $CO_2$, therefore, less $CO_2$ was produced at higher concentrations of benzene in the feed.

The temperature close to the three Pd pieces was measured. This was performed by a thermocouple inserted in side the ¼ in tune and another thermocouple that was inserted inside a well that extends close the exterior surface of the ¼ in tune without touching the Pd foils. From Table 3.1.6.1 it can be seen that the measured temperature was close to the reaction temperature and no unusual reading was observed.

The results in Table 3.1.6.2 were obtained by using a reaction mixture with flow rates of $O_2$, $H_2$, and benzene similar to the flow rates with the reaction mixture at 0.67 % benzene in Figure 3.1.6.1 but with a higher He flow than Figure 3.1.6.1. It can be seen from this table that diluting the mixture with He did not affect benzene conversion to phenol however cyclohexanone was not produced. Also $2.2 \times 10^{-4}$ mol min$^{-1}$ water was produced compared to $2.5 \times 10^{-4}$ mol min$^{-1}$ at the conditions of figure

The reaction mixture with 0.67 % benzene in the feed in Figure 3.1.6.1 was used again but with a lower flow rates of hydrogen and oxygen , while keeping the ratio of $O_2$/ $(O_2+H_2)$ at 34 % as in Figure 3.1.6.1. From the results in Table 3.1.6.3, for the new conditions, it can be seen that less phenol and $CO_2$ were produced since less benzene was converted to these products compared to the results in Figure 3.1.6.1. Also, cyclohexanone was not produced at these conditions. It seems that reducing the flow rates

of both hydrogen and oxygen will lower the available energy in the system that is required for benzene reactions.

A new reaction mixture with flow conditions similar to the ones in Figure 3.1.3.2.6.4 (Pd membrane) was introduced to the shell side of the reactor in this setup at 200 $^o$C. It can be seen from the results in Figure 3.1.6.4, and by running g the reaction over night that low conversions of benzene to phenol were obtained compared to the ones obtained in Figure 3.1.3.2.6.4. Also, in this system only cyclohexanone and $CO_2$ were produced along with phenol. From Figure 3.1.6.5, it can be seen that the system has high selectivity for phenol and phenol is the second selective product from this reaction. Cyclohexanone was produced in small amounts therefore; its selectivity was much lower than phenol selectivity. The same reaction mixture was carried at a higher temperature (250 $^o$C) and from the results in Figure 3.1.6.6 it can be seen that benzene conversion to phenol was reduced, conversion of benzene to phenol was almost the same, and cyclohexanone was not produced. Also, at the higher temperature more water was produced.

The temperature close to the three Pd pieces was measured for the flow conditions in Figure 3.1.6.4. The results were shown in Figure 3.1.6.7. It can be seen that the temperature measured by the thermocouple outside the ¼ in rube and close to the Pd foils was highest at the first Pd foil. This might be expected since the reaction mixture will come in contact with the first Pd piece (foil) and the hence most of the reaction might have taken place at this foil. The temperature measured inside the ¼ in was lowest at the 1$^{st}$ Pd pieces. This is also related to that most of the reaction was taking place at the first Pd piece, therefore the temperature controller will try to decrease the heating input in

146

order to keep the temperature at the set point. The thermocouple for the temperature controller was inside the ¼ in tube as explained earlier. The similar observations were noticed when the reaction temperature was 250 $^{o}$C as can be seen from Figure 3.1.6.8. The measured temperatures in Figures 3.1.6.7 and 3.1.6.8 did not show unusual readings.

By decreasing the concentration of benzene in the feed for the flow conditions in Figure 3.1.6.4, it can be seen from the results in Figure 3.1.6.9 that conversion of benzene to phenol, $CO_2$, and cyclohexanone has increased compared to the results in Figure 3.1.6.4. Benzene conversions to phenol, $CO_2$, and cyclohexanone were 2.5 %, 0.34 %, and 0.9 %, respectively, for the results in Figure 3.1.6.9 compared to 1.1 %, 0.15 % and 0.4 %, respectively, for the results in Figure 3.1.6.4. The selectivity of each product was similar at both concentrations of benzene as can be seen from Figures 3.1.6.10 and 3.1.6.6. The produced moles of each product at 3.4 % benzene (flow conditions of Figure 3.1.6.4) and 1.5 % (flow conditions of Figure 3.1.6.4) as can be seen from Table 3.1.6.10 were similar. This is due to that the higher conversion of benzene   was accompanied by lower feed of benzene at the same time where lower conversion of benzene was accompanied by a higher feed of benzene. Therefore, at these conditions, the reduction in benzene conversion was balanced by the increase in its concentration.   Since the produced products were based on the converted amount of the fed benzene, then the net results were similar amounts of the products at the different concentrations of benzene.

Regardless of the changes in the flow conditions the high conversion of benzene to phenol that was obtained in Figure 3.1.3.2.6.4 for the Pd membrane reactor, when all of the gases were mixed, was not obtained using the reactor setup in this section.

**4.2.1.7. Pd cone prepared according to the method of Ma *et al* [23]**

In this design the three Pd pieces that were used in Section 3.1.6 were replaced by one conical piece of Pd that was welded to the exterior surface of the ¼ in tube. A feed with a composition similar to the one given in Figure 3.1.3.2.6.5 (Pd membrane system with mixed gases), at different total flow rates, was fed to the reactor and the results were shown in Figures 3.1.7.1, 3.1.7.2, and 3.1.7.3. It can be seen from the results in Figure 3.1.7.1 that the obtained conversion of benzene to phenol at a total flow rate of 43 ml min$^{-1}$ was 1.4 % which is lower than the obtained one in Figure 3.1.3.2.6.5 (15 %) at the same flow conditions. Also, phenol, $CO_2$, and cyclohexanone were observed at this flow rate. Interestingly is that benzene conversions to the obtained products, at 43 ml min$^{-1}$, in Figure 3.1.7.1 were close to the ones obtained at the same conditions when three pieces of Pd was used as can be seen by comparing the results in Figure 3.1.7.1 and Figure 3.1.6.4 at the end of the reaction. This would mean that for the system with the three Pd prices it might be possible that most of the reaction was taking place at the first Pd piece which has the conical shape.

It can be seen from Figure 3.1.7.1 that benzene conversion to phenol increased from 1.2 % to 1.4 % when total flow rate was increased from 22 ml min$^{-1}$ to 43 ml min$^{-1}$. Benzene conversion to cyclohexanone and $CO_2$ was similar at 22 ml min$^{-1}$ to 43 ml min$^{-1}$. At a total flow rate of 66 ml min$^{-1}$ conversion of benzene to phenol dropped to 0.5 % and at the same time conversion of benzene to $CO_2$ slightly dropped from 0.3 % at 43 ml min$^{-1}$ to 0.16 % at 66 ml min$^{-1}$. Increasing the total flow rate to 108 ml min$^{-1}$ caused more reduction in conversion of benzene to phenol (0.06 %). Conversion of benzene to phenol has increased to 0.5 % at the highest total flow rate. Changes in benzene conversion to

cyclohexanone were insignificant as a function of total flow rate since it was produced in small amounts. Total conversion of benzene was 1.5 %, 1.7 %, 0.7 %, and 0.6 % at 22 ml min$^{-1}$, 43 ml min$^{-1}$, 66 ml min$^{-1}$, and 108 ml min$^{-1}$, respectively. It can be seen that total conversion of benzene decussated for total flow rate greater or less than 43 ml min$^{-1}$.

It can be seen from Figure 3.1.7.2 that phenol has the highest selectivity up to a total flow rate of 66 ml min$^{-1}$. Phenol electivity was 82 % at 43 ml min$^{-1}$. At 108 ml min$^{-1}$ phenol selectivity was 11 % since benzene has higher conversion to $CO_2$ than its conversion to phenol as was seen in Figure 3.1.7.1.

The produced moles of each product at the above conditions wee shown in Figure 3.1.7.3. It can be seen that at the highest total flow rate that was fed to the reactor that $CO_2$ has the highest produced moles since benzene conversion to it was the heist compared to phenol and cyclohexanone.

Oxygen in this system at the different flow rates was mainly being converted to water as can be seen from Table 3.1.7.1 which was similar to the other reactor setup. Variations of $O_2$ conversion with total flow rate were small except at 108 ml min$^{-1}$ where it has a higher conversion (0.84) compared to the other flow rates. Also, it can be seen that the produced water was at least 260 times more than the highest produced amount of phenol in this system.

By following the temperature distribution inside the reactor at the different flow rates it can be seen from Figure 3.1.4 that no hot spot was observed within the reactor since the temperature readings were always close to the reaction temperature (200 $^{\circ}$C) especially close to the location of the Pd cone.

By carrying the reaction at different temperature and using a total flow rate of 43 ml min$^{-1}$ it can be seen from Figure 3.1.7.5 that the highest conversion of benzene to phenol was obtained at 200 $^{o}$C and then at 150 $^{o}$C. At 50 $^{o}$C no phenol or cyclohexanone were observed and only a small portion (0.02 %) of benzene was converted to $CO_2$. Cyclohexanone was only produced at 150 $^{o}$C. At 250 $^{o}$C conversion of benzene to phenol was lower (0.15 %) compared to 200 $^{o}$C (1.4 %). Reduction of benzene conversion 250 $^{o}$C was also observed using three Pd pieces. On the other hand, oxygen conversion and produced water increased by increasing temperature as can be seen from Figure 1.3.7.6 and Table 1.3.7.2.

The concentration of $O_2$ in the feed was varied to give 9 %, 17.8 % and 22 % in the reaction mixture of total flow rate of 43 ml nin$^{-1}$ at 200 $^{o}$C. It can be seen from Figure 3.1.7.8 that at 9 % $O_2$ a small conversion of benzene to $CO_2$ was observed (0.034 %) , benzene converted to cyclohexanone was 0.04 %, and no phenol was produced. At the same $O_2$ concentration it can be seen that almost all of the fed oxygen was converted to water producing 2.5 x 10$^{-4}$ mol min$^{-1}$ of $H_2O$ as can be seen from Figure 3.1.7.9. At 22 % $O_2$ in the feed, conversion of benzene to $CO_2$ was higher than its conversion to phenol. At this condition conversion of benzene to phenol was 0.4 % which was lower than the conversion at 17.8 % $O_2$ in the feed. The patterns in the benzene conversions at the different $O_2$ percentages in the feed was reflected on the product selectivity as can be seen from Figures 3.1.7.8 where phenol was more selective than the other products at 17.8 % $O_2$ since it was produced in the highest amount as was shown in Figure 3.1.7.7.

The temperature profile in the reactor with respect to the reactor inlet shows that temperature was higher at the lower $O_2$ % in the feed as can be seen from Figure 3.1.7.10.

This is due to that at the lower concentration of $O_2$ less energy will be produced in the system from the oxidation reactions hence the temperature controller will feed more heat to the reactor to keep the reaction temperature at the set point. On the contrary, when more oxygen was in the feed more energy was produced and hence less heat will be provided by the temperature controller to keep the temperature at 200 $^o$C.

By increasing $H_2$ concentration in the feed from 17 % to 38 % conversion of benzene to phenol increased from 0.7 % to 1.44 %. At the same time conversion of benzene to $CO_2$ slightly decreased from 0.34 to 0.2 % as can be seen from Figure 3.1.7.11. Increasing $H_2$ concentration more to 40 % led to a decrease in benzene conversion to both phenol and $CO_2$. Selectivity of phenol was higher than $CO_2$ at all $H_2$ concentrations as can be seen from Figure 3.1.7.12. Total conversion of $O_2$ increased as more $H_2$ was fed as can be seen from Figure 3.1.7.13. Consequently, produced water has increased as more $H_2$ was fed.

The temperature profile at the different concentration of $H_2$ in the feed showed that temperature was higher as less $H_2$ was fed as can be seen in Figure 3.1.7.14. This is similar to the finding for less $O_2$ in the feed that was discussed earlier. The temperature was lower at the higher $H_2$ concentration since more energy was produced within the system as more hydrogen was fed and hence the controller will feed less energy to the reactor to keep the temperature at the set point.

From the studied variations in $H_2$ and $O_2$ concentration in the feed it seems that there is an optimum concentration of both reactants that will provide the system with the required energy to convert benzene which was 17.8 % $O_2$ and 34 % o $H_2$ in the feed.

**4.2.1.8. Pd cone from Alfa Aesar**

This setup was similar to the one used in section 3.1.6 except that the source of Pd foil was different. From the results in Table 3.1.8.1 it can be seen that benzene conversion to phenol was 1.2 % and to $CO_2$ was 0.32 %. These results were similar to the ones obtained with the other Pd cone in section 3.1.7. Therefore, the source of Pd foil didn't affect benzene reactivity. Also, produced oxygen conversion and produced water in this section were similar to the ones in section 3.1.7 at the same flow conditions.

A higher total flow rate using this Pd cone gave lower benzene conversion to phenol and $CO_2$ as can be seen from comparing the results in Tables 3.1.8.1 and 3.1.8.2. Total benzene conversion to phenol was 1.5 % at 43 ml min$^{-1}$ compared to 0.33 % 76 ml min$^{-1}$. This behavior of having lower conversion of benzene for total flow rate greater than 43 ml min$^{-1}$ was observed with other reactor setups that were studied earlier in this chapter. Also, $O_2$ conversion was 0.83 at 76 ml min$^{-1}$ compared to 0.71 % at ml min$^{-1}$. Hence increasing flow rate went to the benefit of increasing oxygen conversion to water.

**4.2.1.9. (7) Pieces of Pd on Nonporous Stainless Steel Tube**

**4.2.1.9.1. Using $H_2$ in tube side and the other gases in the shell side**

Hydrogen was fed to the ¼ in tube while the other gases (benzene, He, and Ar) were fed to the shell side. Therefore these gases will come in contact with $H_2$ when it emerges from the holes in the ¼ in tube. The flow conditions were given in terms of the gases percentages of the total flow rate although $H_2$ was fed into the tube side and the other gases to the shell side. This was done since the entire feed of $H_2$ to the tube side will be mixed in the shell side gases once it emerged from the holes in the ¼ in tube.

For the flow conditions given in Table 3.1.9.1 it can be seen no phenol was produced and only 2 % of benzene was converted to $CO_2$. Also 0.88 of $O_2$ has reacted with 0.81 of $O_2$ produced $H_2O$ at the previous reaction conditions.

Other reaction mixtures were tested to find the conditions that will provide the highest conversion of benzene to phenol. For the reaction conditions in Table 3.1.9.2 it can be seen that 0.51 % of benzene was converted to phenol producing $2.9 \times 10^{-7}$ mol $min^{-1}$ of phenol at the same time where $5.7 \times 10^{-4}$ mol $min^{-1}$ of $H_2O$ was produced. Hence, produced water was much more than produced phenol at these conditions. Another reaction mixture, as shown in Table 3.1.9.3, with more $O_2$ in the feed gave a slightly higher conversion of benzene to phenol with 61.3 % selectivity of phenol.

The reaction mixture with the gases compositions shown in Table 3.1.9.3 was investigated further by changing the total flow rate and keeping its compositions constant at 200 $^o$C. It can be seen from Figure 3.1.9.1.1 that increasing total flow rate from 58 ml $min^{-1}$ to 112 ml $min^{-1}$ led to a decrease in benzene conversion to phenol, $CO_2$. Cyclohexanone was not produced at flow rates higher than 58 ml $min^{-1}$. Total conversion of benzene was 0.66 %, 1.2 %, 0.4 %, and 0.28 % at 22 ml $min^{-1}$, 58 ml $min^{-1}$, 89 ml $min^{-1}$, and 112 ml $min^{-1}$, respectively. It can be seen that 58 ml $min^{-1}$ gave the highest conversion of benzene.

It seems that for studied flow rates that increasing total flow rate will decrease the contact time between the different reactants and the catalyst surface therefore fewer products were produced. However, at a total flow rate lower than 58 ml $min^{-1}$ which was 22 ml $min^{-1}$, conversion of benzene to phenol and total conversion were lower than these ones at 58 ml $min^{-1}$. Therefore if we would follow the same analysis which was done at

the high flow rates that by increasing flow rate contact time will decrease then produced phenol should be higher at 22 ml min$^{-1}$ than the one at 58 ml min$^{-1}$. Therefore it is not clear that more phenol was produced at the lower flow rate, because if this was true then this will be reflected on producing more cyclohexanone considering that cyclohexanone is derived from produced phenol. Therefore it is not only the contact time that control benzene conversion but also something else which might be related as said earlier to the presence of gas chemistry beside the surface chemistry.

The selectivity of each product shown in Figure 3.1.9.1.2 changed according to the changes in benzene conversion to each product in 3.1.9.1.1. Therefore phenol has the highest selectivity when it was produced in the biggest amount in the system. Total oxygen conversion slightly decreased by increasing total flow rate as was shown in Figure 3.1.9.1.3. Produced amount of water was calculated based on the amount of oxygen in the feed that was converted to water; therefore it will depend on both conversion and concentration of oxygen.

The temperature distribution close to the exterior surface of the ¼ in tube was similar for the different flow rates of the reaction mixture as can be seen from Figure 3.1.9.1.4. Regardless of the changes that was made when H$_2$ was in the tube side and the other reactants in the shell side conversion of benzene was low and the high conversion that was obtained with the Pd membrane set up could not be reached.

**4.2.1.9.2 H$_2$ was entered to tube and shell sides and the other gases into the shell side**

In this scheme part of the feed of hydrogen was mixed with the reaction mixture and fed to the shell and the remaining part was fed separately into the shell side. It can be seen from Figure 3.1.9.2.1 that for the studied conditions no significant changes were

154

observed in benzene conversion to phenol, cyclohexanone, and $CO_2$. Also conversion of oxygen at the same conditions was not affected by these changes as can be seen from Figure 3.1.9.2.2.

**4.2.1.9.3 $H_2$ and the other gases (He, Ar, benzene, and $O_2$) were fed into the tube side**

The final flow mode that was tested using the 7 Pd pieces setup was by flowing all of the gases in the reaction mixture in to the tube side and then they would emerge from the 0.1 cm holes and come in contact with Pd.

A reaction mixture similar in total flow rate, feed composition, and reaction temperature to the ones in Figure 3.1.3.2.6.5 (Pd membrane system with mixed gases) was fed to the ¼ in tube. It can be seen from Table 3.1.9.3.1 that a small conversion of benzene to phenol was obtained (1 %) accompanied by with a small conversion to $CO_2$ (0.31 %). These conversions were much lower than the ones in Figure 3.1.3.2.6.5.

Other flow rates were tested with a lower concentration of benzene in the feed compared to the reaction mixture in Table 3.1.9.3.1. It can be seen from Figure 3.1.9.3.1 that conversion of benzene to phenol slightly increased from 1.8 % at 22 ml min$^{-1}$ to 2.2 % at 43 ml min$^{-1}$ then it decreased to 0.5 % at 87 ml min$^{-1}$. Changes in benzene conversion to $CO_2$ slightly increased from 0.43 % at 22 ml min$^{-1}$ to 0.6 % at 43 ml min$^{-1}$ and remained at the later value for the higher total flow rate. For the studied flow rates in this system it can be seen that as the selectivity of phenol has decreased then the selectivity of $CO_2$ has increased as can be seen in Figure 3.1.9.3.2. This is due to that at the same times were amount of produced phenol was decreased produced $CO_2$ was the same as was seen in Figure 3.1.9.3.1.

Conversion of oxygen decreased from 0.95 at 22 ml min$^{-1}$ to 0.87 at 43 ml min$^{-1}$ and was stable around 0.87 for the higher total flow rates as can be seen from Figure 3.1.9.3.3. The produced water increased with increasing flow rate as a result of increasing oxygen amount in the feed.

**4.2.1.9.3.1. Effect of ($H_2$+$O_2$) flow rates**

From the previous results when all the gases were fed to the tube side it was found that benzene conversion to phenol was low. Therefore, the flow rate of ($H_2$+$O_2$) was changed in order to find if this would allow for higher conversion of benzene to phenol. The flow rate of hydrogen and oxygen was varied in a way to keep $O_2/(O_2+H_2)$ fixed at 34 %, since this ratio was found to give high conversion of benzene in the studied reactor setups. It can be seen from Figure 3.1.9.3.1.1 that increasing ($H_2$+$O_2$) % in the feed from 26 % to 52 % led to an increase in benzene conversion to phenol from 0.7 % to 2.2 %. Also, benzene conversion to $CO_2$ increased from 0.2 % to 0.6 %. Increasing ($H_2$+$O_2$) % further to 68 % didn't affect benzene conversion to phenol at the same time conversion of benzene to phenol increased to 0.8 %. Total conversion of benzene was 0.94 %, 2.4 % and 2.4 % at 26 %, 52 %, and 68 % of ($H_2$+$O_2$) %, respectively.

Selectivity to phenol was always higher than selectivity of $CO_2$ at these conditions as can be seen from Figure 3.1.9.3.1.2. Selectivity of phenol and $CO_2$ didn't vary significantly at 26 % to 52 % of ($H_2$+$O_2$) %, since produced amounts of phenol and $CO_2$ increased at 52 % of ($H_2$+$O_2$) % as was seen in Figure 3.1.9.3.1.1. At 68 % of ($H_2$+$O_2$) %, selectivity of phenol decreased and selectivity of $CO_2$ since at this condition produced phenol has decreased at the same time where produced $CO_2$ has increased as was shown in Figure 3.1.9.3.1.1.

O$_2$ conversion was similar at the different (H$_2$+O$_2$) percentages in the feed as can be seen from Figure 3.1.9.3.1.3. This is due to that the ratio of O$_2$/(O$_2$+H$_2$) was fixed at the different conditions. Consequently, produced water has increased since the amount of oxygen has increased as (H$_2$+O$_2$) % in the feed was increasing.

It seems that increasing (H$_2$+O$_2$) % in the reaction mixture will increase the amount of energy produced that will be utilized for benzene reactions. However, it seems that increasing the produced energy more will lead to oxidation of benzene to phenol.

### 4.2.1.9.3.2. Effect of benzene concentration in the feed

By decreasing benzene concentration in the feed more benzene was converted to phenol and CO$_2$ as can be seen from Figure 3.1.9.3.2.1 which is similar to what was observed earlier for the three Pd foils in Figure 3.1.6.1. Selectivity of phenol and CO$_2$ were similar at the different concentrations of benzene, as can be seen from Figure 3.1.9.3.2.2, since concentrations of both products were decreasing by increasing benzene. Produced moles of phenol and CO$_2$ deceased as more benzene was fed (Figure 3.1.9.3.2.3) since conversion of benzene to these products decreased.

### 4.2.1.10. Blank Experiment

In this design the shell and tube reactor was used without the addition of any catalyst to investigate if the benzene reactivity was related to the catalyst or not. By using one set of flow conditions that was used in most of the studied reactor setups with Pd catalyst, it can be seen from Table 3.1.10 that no reactivity of benzene was observed at all even when the reaction was carried over night. Other flow conditions similar to the ones that were studied all over in the Pd reactors were tested and the same results were

157

obtained. Therefore, it can be said that benzene reactivity in these systems was related to the presence of Pd.

### 4.2.1.11. Pt Cone

In this setup Pt foil was cut and welded to the exterior surface of the ¼ in tube to form a conical shape as was done for Pd foil earlier. It can be from Table 3.1.11.1, in which the flow conditions were similar to the ones used with Pd cone system, on reactivity of benzene toward producing phenol was observed and that only a small conversion of benzene to $CO_2$ was observed at the different concentrations of benzene in the feed.

Other concentrations of oxygen in the feed were tested as was shown in Figure 3.1.11.1 but phenol was not produced at any of the used $O_2$ concentrations and only $CO_2$ was found in the product stream. The main product from the reaction mixtures with different oxygen concentrations in the feed was water. Oxygen conversion was 0.63 t 17.8 % in the feed for the conditions in Figure 3.1.11.1. At the same flow conditions using Pd cone $O_2$ conversion was 0.71. It can be seen changes in amount of oxygen that was reacted was not significant for Pt and Pd catalyst.

Then concentration of hydrogen in the feed was varied in order to find if benzene can be converted to phenol. Non of the studied concentration of $H_2$ , as can be seen from Figure 3.1.11.2 , showed any production of phenol from benzene and only $CO_2$ and $H_2O$ were found in the product stream.

It can be seen that regardless of the changes of hydrogen and oxygen flow rates at the studied condition using Pt as a catalyst didn't initiate benzene reactions toward the

production of phenol. Parvulescu () through experimental investigation found that catalyst activity and selectivity is a function of the metal type incorporated in the catalyst.

# 5. Conclusions

From the experimental results that were obtained in this chapter which were described earlier, we can summarize the conclusions in the following lines:

❖ Regarding reproducing the data of Niwa *et al* [9]:

- It was possible to obtain the low benzene to phenol conversion (1-3 %) using the same experimental arrangement but with a lower selectivity than the reported one.

- For the results reported in Figure 1.3.1 [9], where benzene to phenol conversion was 13 % using the Pd membrane system in New et al work [9], it was not possible to obtain such a high conversion of benzene to phenol using the Pd membrane system that was described by this work.

- Once all the gases in reaction mixture were fed together into the shell side of the Pd-membrane reactor, a high conversion of benzene to phenol at 27 % was obtained

- The reproducibility of the data was weak for the high benzene to phenol conversion that was obtained and this might due to the presence of gas chemistry beside the surface chemistry. Therefore, any change inside the system and in flow conditions will change the results.

❖ Producing phenol was not a Pd-membrane technology since phenol was produced using other designs where Pd was in the form of a supported catalyst or a pure metal (the different designs in which Pd foil was used).

❖ The obtained phenol using a small surface area (0.5 cm$^2$) (for the Pd foils) was comparable to the one obtained using Pd/ZrO$_2$ with 8.2 m$^2$, suggests that this is surface and gas phase chemistry.

❖ The produced phenol within the studied conditions was related to the presence of the catalyst as was evident by the blank experiment where no reactivity of benzene was observed.

❖ Pt catalyst, within the studied conditions, was not able to initiate the reaction to produce phenol from benzene using O$_2$ as the oxidizing agent.

❖ The results obtained using systems other than Pd-membrane system, where benzene to phenol conversion is low, were reproducible.

❖ When the reaction mixture was fed to the shell side of the Pd membrane reactor it was found, for the studied conditions that the total benzene conversion was decreasing with increasing total flow rate for total flow rate greater than 43 ml min$^{-1}$. This might due to the reduction in contact time which will give less chance for benzene to react in the system. However, at a lower total flow rate than 43 ml min$^{-1}$, which was 22 ml min$^{-1}$, total conversion was similar to the one at 43 ml min$^{-1}$. This might indicate also that there is gas chemistry beside the surface chemistry. Also, benzene conversion to phenol was highest at 43 ml min$^{-1}$.

❖ In the studied reactor setups water was produced and was at least 23 times the amount of produced phenol when high conversion of benzene to phenol was obtained (27%). A higher ratio of produced water to produced phenol was obtained (at least 120) at low conversions of benzene to phenol ( $\leq$ 2 %).

❖ Regarding the observed products:

The reaction between hydrogen and oxygen at the studied conditions produced water in the primary reaction and active intermediates especially $^{\bullet}OH$ radical. It is established that the reaction of $^{\bullet}OH$ radical with benzene proceeds by addition to the aromatic ring and after subsequent reactions phenol is produced. Formation of other detected products was proposed based on the available literature. Observed chain products were proposed to be produced as a consequence of aromatic ring opening.

# 6. References

**1**. Ehrich, H.; Berndt, H.; Pohl, M.; Janhnisch, K.; Baerns, M., *Appl. Catal. A: Gen*. **230** (2002) 271.

**2.** Bellussi, G. and Perego, C., *CATTECH* **4** (2000) 4

**3**. http://www.baa.org.uk/content/knowledgebase/

**4.** http://www.speclab.com/compound/

**5.** Morrison, R. and Boyd, R.T., Organic Chemistry, Sixth edition, Prentice Hall, Englewood Cliffs, New Jersey, 1992

**6**. http://ceh.sric.sri.com/Enframe/Report.html

**7**. Yamanaka, H.; Hamada, R.; Nibuta, H.; Nishiyama, S.; Tsuruya, S., *J. Mol. Catal. A: Chem*. **178** (2002) 89-95

**8**.  Panov, G. I., *CATTECH* **4** (2000) 18

**9**. S. Niwa, S.; Eswaramoorthy, M.; Nair, J.; Raj, A.; Itoh, N.; Shoji, H.; Namba, Y.; Mizukami, F., *Science*  **295** (2002) 105.

**10**. Kirk-Othmer, Encyclopedia of Chemical Technology, 3$^{rd}$ edition, v.17, p.373

**11**. Brownstain, A. M., *CHEMTECH*, September (1994) 58

**12**. Hamada, R.; Shibata, Y.; Nishiyama, S.; Tsuruya, S., *Phys. Chem. Chem. Phys*.  **5**(5) (2003) 956-965

**13**. Chen, J.;  Eberlein, L.; Langford, C. H., *J. Photochem. Photobio. A,* **148**, (2002) 183-189

**14**. Passoni, L.; Cruz, A.; Buffon, R.; Schuchardt, U.; *J. Mol. Catal. A: Chem*. **120** (1997) 117-123

**15**. Thangaraji, A.; Kumar, R.; Ratnasamy, P., *Appl. Catal*. **57** (1990) L1-L3

**16**. Liptakova, B.; Hronce, M.; Cvengrosova, Z., *Catal. Today* **61** (2000) 143-148

**17**. Lee, C.; Lee, W.; Park, Y.; S. Park, S., *Catal. Today* **61** (2000) 137-141

**18**. Clerici, M. G. and Ingallina, P., *Catal. Today* **41** (1998) 351

**19**. Moro-oka, Y. and Akita, M., *Catal. Today* **41** (1998) 327

**20**. Miyake, T.; Hamada, M.; Sasaki, Y.; Oguri, M., *Appl. Catal. A Gen.* **131** (1995) 33

**21**. Yamanaka, I.; Nakagaki, K.; Akimoto, T.; Otsuka, K., *J. Chem. Soc. Perkin Trans.* **2** (1996) 2511

**22**. Otsuka, K.  and Yamanaka, I., *Catal. Today* **57** (2000) 71

**23.** Vedrine, J. C. Coudurier, G., Millet, J.M, *Catal. Today*, **33** (1997) 3-13

**24**. Xiao, F.; Sun. J.; Meng, X.; Yu, Ranbo, Yuan, H.; Jiang, D.; Qiu, S.; Xu, R., *Appl. Catal. A*, **201** (2001)   267-271

**25**. Maulijn, J. A.; Van Leeuwen, P.W; Van Santen, R. A. *Stud. Surf. Sci. Catal*. **79** (1993) 3

**26**. Sheldon, R.A. and Dakka, J. , *Catal. Today* **19** (1994) 215

**27**. Cavany, F., and Trifiro, F., *Catal. Today* **34** (1997) 269

**28**. Clerici, M. and Ingallina, P., *Catal. Today* **41** (1998) 352-364

**29.** Borman, S., *Chemical & Engineering News*, December 16, (2002) 35-48

**30.** P. Mardilovich, Y. She, and Y. Ma, *Separations*, February **44**, 1998

**31**. Lampe, F.W.; Frankli, J. L.; Field, F. H., " Cross Section for Ionization by Electrons."

**32**. Fitch, W.L and Sauter, A.D., "Calculation of Relative Impact total Inonization Cross Sections for Organic Molecules."

**33**. CRC, Handbook of Chemistry and Physics, 55th edition, 1974-1975, CRC Press

**34**. Centi, G. and Misono, M.,  *Catal. Today*, **41** (1998) 287

**35**. Tatsumi, T.; Yuasa, K.; Tmoinaga, *J. Chem. Soc. Chem. Commun.*, (1992) 1446

**36**. Kitano, T.; Kuroda, Y.; Itoh, A.; Li-Fen, J.; Kunai, A.; Sasaki, K., *Chem. Soc. Perkin. Trans.* **2** (1990) 1991-1995

**37**. Giuseppe, P.; Giordano; D. A.; Rino, D.; Roberto, B., *PCT Int. Appl.* **31** (2003)

**38**. Herron, N and Tolman, C.A., J. *Am. Chem. Soc.* **109** (1987) 2837

**39**. Gryaznov, V. M. and Slin'ko, M. G., *Farda. Discuss. Chem. Soc.* **72** (1981) 73

**40**. Klotz, B.; Volkamer, R.; Hurley, M. D.; Andersen, M. P. S.; Nielsen, O. J.;  Barnes, I; Imamura, T.; Wirtz, K.;  Becker, K-H.; Platt, U.; Wallington, T. J.; N.  Washida. N., *Phys. Chem. Chem. Phys.* 4(18) (2002) 4399-4411.

**41**. Volkamer, R.; Klotz, B.; Barnes, I.; Imamura, T.; Wirtz, K.; Washida, N.; Becker, K. H.; Platt,U.,  *Phys. Chem. Chem. Phys.* **4** (9) (2002) 1598 – 1610.

**42**. Klotz, B.; I. Barnes, I.; Becker, K. H.; Golding, B. T., *J. Chem. Soc. Farady. Trans.*, **93**(8) (1997) 1507-1516

**43**. Alzueta, M.U.; Glarborg, P.; Dam-Johansen, K., *International Journal of Chemical Kinetics* **32**(8) (2000) 498-522

**44**. Brezinsky, K.; Pecullan, M.; Glassman, I., *J. Phys. Chem. A* **102** (1998) 8614-8619

**45**. Wang, J.; Park, J.; Weiac, X.; Lee, C. W., *CHEM. COMMUN.*, (2003) 628–629.

**46**. Rocha, G.M.; Joohnstone, R. A. W.; Neves. M. G., *J. Mol. Catal. A: Chem.* **187** (2002) 95-104

**47**. Maurya, M. R.; Titinchi, S. Chand, S., *Journal of Molecular Catalysis A: Chemical* **193** (2003) 165–176

**48**. Zhao, Y.; Y. Li, Y.; Liu, Q.; Chen, X.; Wang, Y., *Journal of Solid State Chemistry* **169**, (2002),160–167

**50**. Alan, B. R.,  *Eur. Pat. Appl.* (1985)

**51**. Velu, S.; Kapoor, M. P.; Inagaki, S.; Suzuki, K., *Appl. Catal. A* **245** (2003) 317-331

**52**. Itoh, N. and Xu W.C., *Appl.  Catal.  A* **107**(1993) 83-100

**53**. Chen, Y. Z.; Liaw, C.W.; Lee, L. I., *Appl. Catal. A* **177** (1999) 1-8

**54.** Konuspaev, S. R.; Nurrbaeva, R. K.; Zhanbekov, K. N.; Imankulov, T. S., *Seriya Khimicheskaya* **2** (1999) 49-52

**55**. Naoji, I. and Ishun. K., Kokai *Tokkyo Koho* (1994) 3

**56**. Basov, N.L.; Gryaznov, V. M.; Ermilova, M. M., *Zhurnal Fizicheskoi Khimii* **67**(12) (1993) 2413-15

**57.** Schaefer, H.; Grasshoff, E., Leine, D.; Naumann, H. J.; Schoedel, R.; Schubert, R.; Strecker, P.; Veit, J., (1987) 8.

**58**. O'Connor, R.P., Kelvin, E. J.; Henning, D.;  Schmid L. D.; , *Applied Catalysis A: General,* **238** (2003) 29-40

**59.** O'Connor, R. P., Schmidt L. D., *Studies in Surface Science and Catalysis*, **133** (2001) 289

# Chapter 2

**A Kinetic Model for Humic Acid Oxidation using Hydrogen Peroxide in Presence of UV light**

## Abstract

A kinetic model for the advanced oxidation process using hydrogen peroxide and ultraviolet light in a completely mixed batch reactor has been tested for the destruction of humic acid in aqueous solutions. The experimental data for this model were taken from the literature [Wang, 2000, 2001). Known elementary chemical reactions with the corresponding rate constants were taken from the literature and used in this model. Photochemical reaction parameters of hydrogen peroxide and humic acid were taken from the literature. Humic acid was assumed to be mainly destroyed by direct photolysis and $^\bullet OH$ radicals. The rate constant for the HA-$^\bullet OH$ reaction was optimized from range of values in the literature. Other fitted parameters were the rate constant of direct photolysis of hydrogen peroxide and humic acid. A series of reactions were proposed for formation of organic byproducts of humic acid destruction by direct photolysis and $^\bullet OH$ radicals. The corresponding rate constants were optimized based on the best fit within the range of available published data. This model doesn't assume the net formation of free radicals species is zero. The model was verified by predicting the degradation of HA and $H_2O_2$. The results of model simulation showed good prediction of the residual hydrogen peroxide ($H_2O_2$) and non purgeable dissolved organic carbon (NPDOC) for the set of experimental data taken from Wang (2000). A correction was applied to the experimental data of hydrogen peroxide in a second Wang work (2001). The model was able to predict the experimental data of Wang (2001) after applying this correction. From the kinetic model the concentration of radicals, produced in the system, was predicted within the

studied experimental conditions and time. Such kind of information gave a more thorough look to this system and provided an understanding of the effect of initial HA and $H_2O_2$ concentration on the process performance regarding the residual fraction of hydrogen peroxide and NPDOC.

## 1. Introduction

The ideal process of destruction of hazardous organic wastes would consist of oxidation with oxygen ($O_2$) at ambient temperature and pressure with the end products being water and carbon dioxide. However till now catalysts have not been developed that will allow oxidation process to occur at room temperature and pressure for the oxidation of a broad array of organics in waste water in a cost-effective manner [Glaze, 1989a].

An alternative for the direct oxidation with $O_2$ is to find more reactive oxidants for waste treatment. Chlorine and ozone are examples of such conventional oxidation process. Advanced oxidation processes (AOPs) may overcome the rate and cost limitations in conventional oxidation processes.

AOPs are those processes which involve the production of reactive free radicals in the reaction mixture, especially the most important $^\bullet$OH radical, and utilize them for the destruction of organic compounds. AOPs are particularly attractive when waste destruction is important in that they can mineralize hazardous organic contaminants, not simply transfer them to another phase.

AOPs have been commercially applied for more than two decades; however major growth in the interest and use of AOPs has taken place only in the last few years primary because increasing stringent environmental regulations has made attractive the prospect of organic compound destruction rather than transferring to another phase.

Therefore, AOPs have become attractive for the control of organic compounds in waste water treatment [Kang, 1997; Stepnowshki, 2002; Hou, 2001].

The hydroxyl radical is an extremely reactive and nonselective oxidant and, thus, when produced in sufficient quantities, can lead to complete oxidation of organic compounds to carbon dioxide, water, and inorganic ions [Acero, 2000; Liao, 1995]. The $^\bullet OH$ radical may oxidize substrate, but because of its high reactivity it also may react with a variety of other substances commonly found in natural water. Hydroxyl radicals attack organic compounds with rate constants ranging from $10^7$ to $10^{10}$ $M^{-1}$ $s^{-1}$ oxidizing them by hydrogen atom abstraction or by addition to double bonds [Buxton, 1988]. These high rate constants values mean AOP treatment of typical organic substrates will be practical, even if the steady state concentration of $^\bullet OH$ radical is only $10^{-8}$-$10^{-12}$ M. For example for a rate constant of 2.3 $x10^9$ $M^{-1}$ $s^{-1}$, the first order rate constant will be 0.023 $s^{-1}$. This means that the half life of organic substrate is approximately 30 second which is practical for treatment [Glaze, 1989a].

In AOPs, $^\bullet OH$ radicals can be produced by

- Ionizing radiation on water

- Hydrogen peroxide with ozone ($H_2O_2/O_3$)

- Fenton reagent ($H_2O_2$ and Fe(II)),  ($H_2O_2$ and Fe(III))

- Fenton-like reagent ($H_2O_2$ and $Fe^o$ or Fe(III))

- Direct photolysis of $H_2O_2$ by UV light ($H_2O_2/UV$)

- Titanium dioxide ($TiO_2$) and ozone

- Ozone with ultraviolet radiation ($UV/O_3$)

- $UV/H_2O_2/O_3$

The UV/$H_2O_2$ process is an example of a homogeneous AOP. The effectiveness of this process is associated with very reactive species such as hydroxyl radicals which are generated in the reaction mixture. This is based on the fundamental law of photochemistry which states that only light which is absorbed by a molecule can be effective in producing photochemical change in the molecule. The amount of change depends on the energy available in this light and the nature of the absorbing molecules. [Taylor, 1928; Calvert, 1966; Blazka, 1983].

The differences between photochemical and thermal reactions come solely from the following facts. First, thermal reactions commonly involve molecules in their ground electronic states whose vibrational, rotational, and translation energies are in the upper range of the distribution described by the Maxwell-Boltzman law; reaction can occur, with a certain probability, between any of the molecules which have energies above some minimum amount necessary for the reaction (activation energy). Monoenergetic thermal reactants have only been realized in special systems through the use of molecular beams and in these cases only a few extremely simple reactions have been studied. However, in photochemical systems it is possible to control closely and relatively simply the degree of excitation of the reactant molecules through the use of monochromatic radiation of any desired wavelength or energy. The reactions of electronically excited molecules in photochemical processes may occur from an entirely different array of potential energy surfaces from those encountered in thermal systems. Therefore, the products of photochemical reactions may differ drastically from those found in thermal process carried out at a temperature equivalent to the energy introduced by absorption of light photons. A given molecular and electronic configuration of an electrically excited

molecule may never be reached thermally because in the later case a variety of reaction paths of much lower energy is available and these paths will be utilized before the molecule can reach the desired state. An important consequence of this is that, thermodynamically highly unstable, structurally strained compounds may be normal photolysis products formed in good yields but completely inaccessible to dark chemistry. In theory specific bond cleavage and other forms of chemical change can be affected photochemically with the reactant molecule at any desired initial temperature. Therefore photochemical techniques are ideally suited to the generation of free radicals and the study of their reactions. On the contrary, free radicals formed from thermally excited molecules will be very reactive as a result of the high temperatures used so that they are very short lived and occur at such low concentrations that the studies of their reactions are most difficult [Calvert, 1966].

Since the late 1960s, many studies have indicated that the UV/$H_2O_2$ process is able to oxidize a wide variety of organic pollutants in aqueous solutions [Stephan, 1996]. A patent was awarded to Koubeck for oxidation of refractory organics in aqueous waste streams by hydrogen peroxide and UV light [Koubeck, 1977]. The UV- based advanced oxidation processes are well-established industrially and have been installed at over 200 sites (primarily in North America) [Stephan, 1996]. Now, this technology is being utilized by several companies for the oxidation of organic contaminants in water and many researches have been, and still are, performing in this area to examine the possibility of applying this technology for different organic contaminants [Glaze, 1995; Stephan, 1996; Chu, 2002; De Laat, 1994, 1995; Liao, 1995; Sharpless, 2001; Chen, 1997].

The chemistry of hydrogen peroxide in aqueous systems has been studied extensively. Therefore, many of the reaction steps with the corresponding rate constants are well documented in the literature to represent the mechanism of hydrogen peroxide photolysis with the corresponding chemical reactions. [Bielski, 1977, 1985; Baxendale, 1988; Hunt, 1952; Behar, 1970; Christensen, 1982, 1989; Sehested, 1968; Weeks, 1955; Daniton, 1955, 1953; Pagsberg, 1969; Thomas, 1965; Vollman, 1959; Brezonik, 1998; Guittonneau, 1990; Weinstein, 1979].

There is great interest in AOPs for water treatment which imposes the need to understand this chemistry in more detail, with regard to both the primary processes and the evolution of organic byproducts. Process models for AOPs are needed to determine if an AOP is potentially useful for treatment of specific water for specific objectives without resorting to expensive experimental studies, especially with regard to its cost effectiveness compared to conventional process [Glaze, 1995]. These models will help to determine the important design and operational variables for AOPs such as; effect of oxidant dose, light intensity for UV process, etc.

The usual trend in modeling the kinetics of the destruction of organic compounds by $UV/H_2O_2$ or other AOPs is to assume a first order kinetic model for the rate of contaminant destruction [Behnajady, 2004; Fung, 2001; Chu, 2001; Cater, 2000; Benitez, 2000; Beltran, 1997; Sorensen, 1997; Selcuk, 2003]

Recently a number of researchers started to apply a non $1^{st}$ order kinetic modeling for the advanced oxidation process [Gallard, 1998; Stephan, 1996; Liao, 1995]. However most of these models assume the pseudo-steady state approximation for the free radicals in the system [De Latt, 1994, 1997; Glaze, 1995; Weir, 1993].

Glaze (1995) studied the destruction of 1,2-dibromo-3-chloropropanein aqueous solution using $UV/H_2O_2$ technology in a batch reactor. Glaze in his work proposed a reaction mechanism for $H_2O_2$ chemistry in water using UV light which is consistent with the mechanism which we used in our kinetic model with the exception that he didn't incorporate reactions number 9, 10, 20, and 22 in his scheme. Also in his work he assumed steady state conditions for all the radicals which were produced in the system. There was discrepancy between his model predictions and experiment at low peroxide concentrations. For example, by comparing the predicted pseudo-first order rate constant measured directly from experimental data to the one calculated based on his simulation, the percentage error between the two values increased from 16 to 575 when initial hydrogen peroxide was decreased from 6.6 to 0.054 mM in presence of 4 mM carbonate/bicarbonate. This poor agreement between experimental data and model simulation was attributed to the occurrence of another mechanism for degradation of the organic compound at these conditions such as reaction of the organic with carbonate ion radical. A similar finding was observed by Glaze (1989a) using hydrogen peroxide ozone technology ($H_2O_2/O_3$) where the agreement between model predictions and experimental data was low when ($H_2O_2/O_3$) ratios are below stoichiometric level. He also attributed this to some inaccuracies in some of the assumed rate constants or failure of the model to accurately account for the fate of carbonate.

Glaze (1995) assumed that the rate of photolysis of the target contaminant is negligible compared to its reaction with $^\bullet OH$ radicals. As a consequence he neglected this term from his model and assumed that the fraction of UV light absorbed by $H_2O_2$ is equal to unity and the total change of light intensity as it passes through the solution is

due only to $H_2O_2$. Glaze (1995) didn't incorporate the possibility of UV absorbance by humic acids that were present in the treatment of actual waste waters and hence he didn't include $^\bullet OH$ radical scavenging by humic acid. Steady-sate concentrations were assumed for all of the radicals in his work.

Stephan (1996) tried to simulate the kinetics of acetone degradation by UV/$H_2O_2$ process. In his model he assumed steady state concentration for $^\bullet OH$ radicals and neglected the photolysis of acetone. Also he did not incorporate all of the reactions for the $H_2O_2$ reaction mechanism which were proposed by Glaze (1995). He assumed that $H_2O_2$ concentration and hence the corresponding rate constant were not functions of pH.

Liao (1995) proposed a kinetic model for the destruction of the organic contaminant in a completely mixed flow reactor. The assumption of steady-state concentration free radicals was used. For such kind of reactors this assumption can be invoked for steady state operating conditions.

Crittenden (1999) modified the proposed model by Glaze (1995). His model didn't utilize the pseudo-steady state assumption of Glaze. Also he added more reactions into the model. He assumed pH is varying and he found that the maximum pH change that occurs from degradation of the pollutant change in water doesn't affect the model significantly. He also incorporated the UV photolysis term of the target contaminant. Also, he considered the humic substance as an absorber of UV light, but he neglected the degradation of humic substance by photolysis. His model didn't consider the influence of byproducts from $^\bullet OH$-HA reactions. He incorporated HA reaction with $^\bullet OH$ and its absorbance of light as completeness for the model, but the data which he used didn't have initial concentration of HA. Liao (1995) corrected for the effect of humic acid on the total

absorbance of light by the reaction mixture without taking into account the degradation of HA by light which is similar to what Crittenden did.

In Crittenden's work (1999), he compared the experimental data and model predictions obtained with pseudo-first order kinetic. He did this by plotting the natural logarithm of the predicted and experimental residual fraction of the target compound vs. time. The slope of each plot represented the pseudo first order rate constant. Only in one of his figures, a model to experimental data was shown for the concentration of the destructed contaminant and hydrogen peroxide. Based on a comparison between the pseudo first order rate constant calculated from experimental data, his model predictions, and Glaze model predictions (1995) Crittenden proposed model was able to predict the experimental data more accurately than Glaze's did. Based on his model a slight difference in the predicted first order rate constant was observed between assuming a constant and a variable pH.

Most of the prior simulation models neglected the degradation of humic material by UV light. In our kinetic model this degradation term was incorporated. This was based on the experimental evidence that humic acid can be destructed by UV light alone and based on the absorbance band of HA [Wang, 2000, 2001]. Also many studies were conducted on the humic acid that show the possibility of the production of hydrated electrons from  photolysis of humic material [Power, 1987; Fisher ;1985, 1987; Zepp; 1985, 1987a, 1987b; Aguer, 1999, 2002; Cooper,1989; Thomas-Smith, 2001].

Humic substances are a relatively stable organic carbon ubiquitous in the biosphere. About 60-90 % [Aguer, 2002] of dissolved organic carbon in natural waters consists of humic substances. Humic substances constitute refractory products of

chemical and biological degradation and condensation reactions of plant and animal residue and play a crucial role in many biogeochemical processes. Aquatic humic substances are a class of heterogeneous, moderate molecular weight, yellow-colored organic acids of biological origin present in all natural waters. This ubiquitous organic is a result of the diverse sources and pathways of formation of humic substances and their slow degradation by geochemical or microbial process. Aquatic dissolved organic matter is in part composed of light-absorbing polymers that are resistant to microbial assimilation and breakdown. Humic substances are probably the most variable substance to have a generic chemical name. They have been characterized to vary from 500 to 200,000 in molecular weight and contain conjugate olefinic and aromatic functional groups, as well as carboxyl and hydroxyl and sometimes a small percentage of nitrogenous functional groups [Aguer, 2001, 2002; Fischer, 1987; McKnight, 1989; Lyderson, 1989; Kim, 2003; Goldstone, 2002; Chu, 2003].

Humic materials consists mainly of humic acid (HA) and fulvic acids (FA) [Aguer, 2002; Fisher, 1987]. Humic acid are heterogeneous molecules which are yellow to brown or black in color, high to moderate molecular weight ranging from several hundred thousands to several hundreds [Aguer, 2002], and biologically recalcitrant. Humic acids are soluble above pH = 2 [McKnight, 1989]. Humic acid is present in the sediments and dissolved in water in all aquatic ecosystems [McKnight, 1989].

The concentration of dissolved organic matter (DOM) in lakes derived from terrestrial and aquatic primary production typically has values between 2 and 12 mg $L^{-1}$ [Curtis, 1989]. Our kinetic model was applied to experimental data that has concentrations of humic acid within the typical range of DOM in natural waters.

Based on the above discussion of humic material origin and their existence in all natural waters it may be expected that the presence of HA will affect AOPs either by direct photolysis or $^{\bullet}OH$ radical scavenging. Such behavior was verified experimentally by Liao (1995). He found that the oxidation efficiency of chlorobutane using $H_2O_2/UV$ treatment was hindered with increasing humic acid concentration in the solution. Also, Glaze (1995) found that the rate of the contaminant degradation in natural waters was slower than in distilled water. He attributed this to the presence of some compound(s) that could absorb UV light and scavenge $^{\bullet}OH$ radicals.

The presence of organic matter affects the desalination process by using reverse osmoses in several ways; it causes a gradual decline of the membrane flux and a decrease in the permeation, high pumping pressure, deterioration in the membrane [Lin, 1999; Selcuk, 2003]. Also humic substances increase the chlorine demand of waters, cause corrosion in pipelines, and form complex species with metals and pesticides [Selcuk, 2003]. Natural organic matter (NOM) in drinking water supplies poses significant concerns during water treatment during to its reactivity with oxidants and disinfectants [Westerhoff, 1999]. These effects of humic substances make their removal a necessity for the success of treatment process.

The mentioned studies and others in the literature [Rodriguez, 1996; Goldstone, 2002; Brezoink, 1998; De Laat, 1994; Al-Rasheed, 2003; AWWA, 1998] imply that the presence of humic acid will have an impact on the efficiency. Therefore, it is necessary to understand the chemistry of humic acid degradation in such kinds of treatment in order to design the process at optimal conditions and test whether a certain type of AOPs would be beneficial for the contaminant treatment. This understanding could be accomplished

through kinetic modeling for humic acid in AOPs. This chapter will help understanding advanced oxidation of humic acids.

## 1.1 . Solvated (hydrated) electrons

Researchers reported, through independent studies, the photolysis of humic material was found to produce active transients. These transients were identified as hydrated (solvated) electrons, hydroxyl radicals, singlet oxygen and the triplet state of the humic material. Hydroxyl radicals and singlet oxygen appear in the system due to the interaction of solvated electron with water as given by the solvated electron reactions in Table 2.1. Therefore, the direct intermediates of photolysis of humic acids are solvated electrons and triplet state. Most of the chemically stable organic molecules contain even number of electrons which are paired, and their ground states are singlet. Photoexcitation raises one electron to a higher quantum state in which its spin can remain parallel to its partner, so that the multiplicity is still singlet, or it may become antiparallel to its partner, so that the multiplicity is three, and a set of triplet energy level is formed (triplet state) [Calvert, 1966]. The solvated electron was firmly identified [Power, 1987; Fisher, 1985, 1987; Zepp, 1987a, 1978b, 1985; Aguer; 1999, 2002; Cooper, 1989, Thomas-Smith, 2001]. The following reaction was suggested to explain the production of solvated electron [Fischer, 1987; Aguer, 1999]:

$$HS \xrightarrow{\lambda=254nm} HS^{\bullet+} + \overline{e}_{(aq)}$$
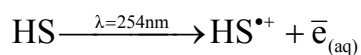
where $\overline{e}_{(aq)}$ is the hydrated electron and $HS^{\bullet+}$ is the triplet state of HA [Fischer, 1987; Aguer, 1999] .

Most of the above studies were performed using Laser flash spectroscopy for photolysis. For example, Fisher (1987) used Laser flash kinetic spectroscopy to study the photolysis of dissolved organic carbon (DOC). Two transients common to most samples were detected. One transient with a maximum around 720 nm (obtained after irradiation with 266 nm laser light) was quenched by decreasing pH and nitrous oxide. It was present in all waters with DOC and has a spectrum which resembled that of a solvated electron. Samples with higher ground state absorbance yielded a transient with a maximum at 475 nm (after the 355 nm laser pulse) that was quenched by oxygen. This transient seemed to be a photophysical hybrid with triplet and radical cation character.

$$HA + h\nu \leftrightarrow HS^{+\bullet} + \overline{e}_{(aq)}$$
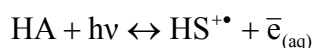
Also Zepp (1987a, 1987b) used Laser flash photolysis to investigate the transients formed on absorption of 355-nm light by dissolved organic matter (DOM) from natural water bodies and from soil. Absorption spectra and quenching studies of the transients provided confirming evidence that hydrated electrons were formed in these experiments. Despite the high variability in absorption coefficients, the primary quantum yields for electron ejection from the Greifensee and Suwannee dissolved organic matter (DOM) fell in a narrow range (0.005-0.008).

Aguer (1999) found that humic substances absorb photons in the UV and the visible region of the solar spectrum up to 500 nm. The energy absorbed in this way lies within the range 58-98 KJ mol$^{-1}$ making a number of photochemical processes possible. In particular, reactive species capable of transforming a great variety of organic compounds can be produced. Irradiation of samples was performed at 253.7, 365, and

300-450 nm. Humic acids solution irradiated at 253.7 nm using dichloromethane as substrate led to the release of chloride ions.

$$HS \xrightarrow{\lambda=254nm} HS^{\bullet+} + \bar{e}_{(aq)}$$

$$\bar{e}_{(aq)} + CH_2Cl_2 \rightarrow Cl^- + \text{dechlorinated organic compounds}$$
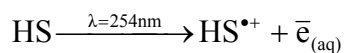
The quantum yield of chloride formation which is defined as the ratio between the numbers of molecules formed over the number of photons absorbed during the same time was evaluated as 0.0047 [Aguer, 1999]. Various humic substances were found to photogenerate the solvated electrons at 253.7 nm and at longer wavelength (300-450 nm).

Liao (1995) from experimental work revealed the production of active transients from direct photolysis of humic materials, but he didn't incorporate this effect into the kinetic model for his system.

## 1.2. Objectives

The present study attempts to add to the existing literature through the development of a kinetic model that was evaluated with published data for the removal of humic acid (HA) utilizing UV/$H_2O_2$ process. Known elementary chemical reactions with corresponding rate constants were taken from the literature and used in this model. The reactions for $H_2O_2$ photochemistry were extracted from different sources. Some or all of these elementary reactions which were utilized to describe the $H_2O_2$/UV reactions for the destruction of other contaminants were incorporated in the other models by Crittenden (1999) Glaze, (1995) and Mak (1997).

A systematic investigation of the effect of the process parameters such as, the initial concentration of HA and $H_2O_2$ on the performance in terms of the rate of $H_2O_2$

photolysis and the oxidation rate of the organic contaminant of interest will be made by applying the model to experimental data available in the literature. The experimental data were taken from the work published by Wang [2000, 2001].

Also, in this model humic acid will be destroyed by two routes; oxidation by $^\bullet$OH radicals and direct photolysis of UV light. The importance of each route on the degradation of humic acid will be evaluated from model simulation.

The direct photolysis of humic acid was assumed to produce solvated electron. The production of solvated electron will bring a series of new reactions that will be added to the kinetic model. The corresponding chemical reactions with the rate constants of hydrated electrons were taken from the literature as shown in Table 2.1. The effect of solvated electron will be tested by running the model in the presence and absence of the related reaction steps.

Intermediates from the other route of humic acid degradation, oxidation by $^\bullet$OH radicals produced from direct photolysis of hydrogen peroxide, with their possible reactions were suggested and incorporated into the kinetic model. The other product of the photolysis of humic acid, the triplet state, was assumed to be degraded by self combination.

The work documented in this chapter attempts to relate the proposed reaction byproducts in the proposed scheme to the byproducts observed in the literature.

# 2. Kinetic model

## 2.1. Reactions mechanism

### 2.1.1. Reaction Mechanism in Pure Water

The chemistry of hydrogen peroxide in aqueous systems has been studied extensively by many [Belski, 1977, 1985; Baxendale, 1988; Hunt, 1952; Behar, 1970; Christensen, 1989; Sehested, 1968; Weeks, 1955; Daniton, 1955, 1953; Pagsberg, 1969, Thomas, 1965; Vollman, 1959; Guittonneau, 1990]. Many of the $H_2O_2$ reactions are presented in Table 2.1.1. Degradation of $H_2O_2$ by UV light arises essentially from the absorption of incident radiation at 254 nm and leads to the production of two hydroxyl radicals per molecule of $H_2O_2$ decomposed, reaction 1 Table 2.1. Then these radicals initiate chain reactions as shown in Table 2.1. The propagation reaction includes the reaction of $H_2O_2$ and its conjugate with hydroxyl radicals and hydroperoxyls radical and its conjugate, reactions 3, 19, 20, and 21 in Table 2.1. The termination reactions include radical-radical reactions which are reactions 4, 5, 6, 7, and 8 in Table 2.1.

**Table 2.1:** Reactions and rate constants in the kinetic model for the degradation of humic acid degradation using hydrogen peroxide and UV light[*]

| # | Reaction | Rate Constant | Reference(s) |
|---|----------|---------------|--------------|
| 1 | $H_2O_2 + h\nu \rightarrow 2\,^{\bullet}OH$ | $k_1 = \Phi_{H_2O_2} f_{H_2O_2} I_o$ | Glaze (1995) Crittenden (1999) |
| 2 | $HA + h\nu \rightarrow$ | $k_2 = \Phi_{HA} f_{HA} I_o$ | Glaze (1995) |
| 3 | $^{\bullet}OH + H_2O_2 \rightarrow H_2O + O_2^{\bullet -} + H^+$ $^{\bullet}OH + H_2O_2 \rightarrow H_2O + HO_2^{\bullet}$ | $k_3$=2.7 x10$^7$ M$^{-1}$ s$^{-1}$ $k_3$=2.7 x10$^7$ M$^{-1}$ s$^{-1}$ (used) | Glaze (1995) Buxton (1988) Gallard (2000) Crittenden (1999) Christensen (1982) |
| 4 | $HO_2^{\bullet} + O_2^{\bullet -} + H_2O \rightarrow H_2O_2 + O_2 + OH^-$ | $k_4$=9.7 x 10$^7$ M$^{-1}$ s$^{-1}$ (used) $k_4$=1.02x 10$^8$ M$^{-1}$ s$^{-1}$ | Gallard (2000) Weinstein (1979) |
|   | $HO_2^{\bullet} + O_2^{\bullet -} + H_2O \rightarrow H_2O_2 + O_2 +^{\bullet}OH$ $HO_2^{\bullet} + O_2^{\bullet -} \rightarrow HO_2^- + O_2$ $HO_2^{\bullet} + O_2^{\bullet -} \xrightarrow{H^+} H_2O_2 + O_2$ | $k_4$=9.7 x 10$^7$ M$^{-1}$ s$^{-1}$ $k_4$=9.7 x 10$^7$ M$^{-1}$ s$^{-1}$ $k_4$=9.7 x 10$^7$ M$^{-1}$ s$^{-1}$ | Glaze (1995) Gallard (1998) Chen(1997) |

| 5 | $HO_2^\bullet + {}^\bullet OH \rightarrow H_2O + O_2$ | $k_5 = 0.71 \times 10^{10}$ M$^{-1}$ s$^{-1}$ (used)<br>$k_5 = 6.6 \times 10^9$ M$^{-1}$ s$^{-1}$ | Buxton (1988)<br>Sehested (1968) |
|---|---|---|---|
| 6 | ${}^\bullet OH + O_2^{\bullet -} \rightarrow O_2 + OH^-$ | $k_6 = 1.01 \times 10^{10}$ M$^{-1}$ s$^{-1}$ (used)<br><br>$k_6 = 1.0 \times 10^{10}$ M$^{-1}$ s$^{-1}$<br>$k_6 = 9.4 \times 10^9$ M$^{-1}$ s$^{-1}$ | Gallard, 1999,<br>Buxton, 1988<br>Christensen (1989)<br>Sehested (1968) |
| 7 | ${}^\bullet OH + {}^\bullet OH \rightarrow H_2O_2$ | $k_7 = 5.2 \times 10^9$ M$^{-1}$ s$^{-1}$ (used)<br>$k_7 = 5.2 \times 10^9$ M$^{-1}$ s$^{-1}$<br>$k_7 = 4.2 \times 10^9$ M$^{-1}$ s$^{-1}$ | Pasberg (1969)<br>Thomas (1965)<br>Buxton (1988) |
| 8 | $HO_2^\bullet + HO_2^\bullet \rightarrow H_2O_2 + O_2$ | $k_8 = 8.3 \times 10^5$ M$^{-1}$ s$^{-1}$ | Bielski (1985) |
| 9 | $O_2^{\bullet -} + H^+ \rightarrow HO_2^\bullet$ | $k_9 = 1 \times 10^{10}$ M$^{-1}$ s$^{-1}$ (used)<br>$k_9 = 5 \times 10^{10}$ M$^{-1}$ s$^{-1}$ | De Laat (1999)<br>Bielski (1985) |
| 10 | $HO_2^\bullet \rightarrow O_2^{\bullet -} + H^+$ | $k_{10} = 1.58 \times 10^5$ s$^{-1}$<br>$k_{10} = k_9$ K<br>pK$_a$=4.8 | De Laat (1999),<br>Chen (1997),<br>Sehested (1968),<br>Bielski (1977) |
| 11 | ${}^\bullet OH + HCO_3^- \rightarrow H_2O + {}^\bullet CO_3^-$ | $k_{11} = 8.5 \times 10^6$ M$^{-1}$ s$^{-1}$<br><br>$k_{11} = 8.5 \times 10^6$ M$^{-1}$ s$^{-1}$<br>$k_{11} = 1.5 \times 10^7$ M$^{-1}$ s$^{-1}$ (used) | Glaze (1995),<br>Buxton (1988)<br>Crittenden (1999)<br>Brezonik (1998),<br>Hogine (1982),<br>Weeks (1966) |
| 12 | $O_2^{\bullet -} + {}^\bullet CO_3^- \rightarrow CO_3^{-2} + O_2$ | $k_{12} = 6.5 \times 10^8$ M$^{-1}$ s$^{-1}$ (used)<br>$k_{12} = 6.0 \times 10^8$ M$^{-1}$ s$^{-1}$<br>$k_{12} = 4.0 \times 10^8$ M$^{-1}$ s$^{-1}$ | Glaze (1995)<br>Crittenden (1999)<br>Behar (1970) |
| 13 | ${}^\bullet CO_3^- + H_2O_2 \rightarrow HCO_3^- + O_2^{\bullet -} + H^+$<br>${}^\bullet CO_3^- + H_2O_2 \rightarrow products$<br>==${}^\bullet CO_3^- + H_2O_2 \rightarrow HCO_3^- + HO_2^\bullet$== | $k_{13} = 8.0 \times 10^5$ M$^{-1}$ s$^{-1}$ (used)<br><br>$k_{13} = 8.0 \times 10^5$ M$^{-1}$ s$^{-1}$<br><br>$k_{13} = 4.3 \times 10^5$ M$^{-1}$ s$^{-1}$ | Glaze (1995)<br><br>Behar (1970)<br><br>Crittenden (1999), |
| 14 | ${}^\bullet OH + CO_3^{2-} \rightarrow OH^- + {}^\bullet CO_3^-$ | $k_{14} = 3.9 \times 10^8$ M$^{-1}$ s$^{-1}$ (used)<br><br>$k_{14} = 4.2 \times 10^8$ M$^{-1}$ s$^{-1}$ | Glaze (1995),<br>Buxton (1988)<br>Brezonik (1998),<br>Weeks (1966) |
| 15 | ${}^\bullet CO_3^- + {}^\bullet CO_3^- \rightarrow ?$ | $k_{15} = 3.0 \times 10^7$ M$^{-1}$ s$^{-1}$ (used)<br><br>$k_{15} = 2.2 \times 10^6$ M$^{-1}$ s$^{-1}$<br>$2k_{15} = 2.2 \times 10^6$ M$^{-1}$ s$^{-1}$<br>$k_{15} = 3.0 \times 10^7$ M$^{-1}$ s$^{-1}$ | Glaze (1995),<br>Crittenden (1999)<br>Huie (1990)<br>Weeks (1966)<br>Dragnice (1991) |
| 16 | $CO_{2(g)} \leftrightarrow CO_{2(aq)}$ | $K_5 = 10^{-1.468}$ | Stumm & Morgan (1996)<br>Snoeyink (1980) |

| | | | |
|---|---|---|---|
| 17 | $CO_{2(aq)} + H_2O \leftrightarrow HCO_3^- + H^+$ | $K_6 = 10^{-6.352}$ $(k_{f1}/k_{b1})$ | Stumm & Morgan (1996), Huie (1990) |
| | | $K_6 = 10^{-6.3}$ | Snoeyink (1980) |
| | | $(4.46 \times 10^5 / 3 \times 10^{12})$ pKa=6.352 | Hug (2003) |
| 18 | $HCO_3^- \leftrightarrow CO_3^{2-} + H^+$ | $K_7 = 10^{-10.33}$ $(k_{f2}/k_{b2})$ | Stumm & Morgan (1996), Huie (1990) |
| | | $K_7 = 10^{-10.3}$ | Snoeyink (1980) |
| | | $(4.67 \times 10^1 / 1 \times 10^{12})$ pKa=10.33 | Hug (2003) |
| 19 | $O_2^{\bullet -} + H_2O_2 \rightarrow {}^{\bullet}OH + OH^- + O_2$ | $k_{16} = 0.13$ M$^{-1}$ s$^{-1}$ | Crittenden (1999), Weinstein (1979) |
| 20 | $H_2O_2 + HO_2^{\bullet} \rightarrow HO^{\bullet} + O_2 + H_2O$ | $k_{17} = 3$ M$^{-1}$ s$^{-1}$ | Weinstein (1979), Koppenel (1978) |
| 21 | $HO^{\bullet} + HO_2^- \rightarrow HO_2^{\bullet} + OH^-$ | $k_{18} = 7.5 \times 10^9$ M$^{-1}$ s$^{-1}$ | Glaze (1995), Crittenden (1999), Christensen (1982) |
| 22 | $H_2O_2 \leftrightarrow H^+ + HO_2^-$ | pK$_a$=11.6, $K_8$<br>pK$_a$=11.65 (used)<br>pK$_a$=11.65 | Crittenden (1999)<br>Buxton (1988)<br>Dean (1979) |
| 23 | ${}^{\bullet}CO_3^- + HO_2^- \rightarrow CO_3^{2-} + HO_2^{\bullet}$ | $k_{19} = 3 \times 10^7$ M$^{-1}$ s$^{-1}$ | Crittenden (1999) |
| | ${}^{\bullet}CO_3^- + HO_2^- \rightarrow HCO_3^- + O_2^{\bullet -}$ | $k_{19} = 3 \times 10^7$ M$^{-1}$ s$^{-1}$ (used) | Glaze (1995), Dragnice (1991) |
| | ${}^{\bullet}CO_3^- + HO_2^- \rightarrow products$ | $k_{19} = 3 \times 10^7$ M$^{-1}$ s$^{-1}$ | Behar (1970) |
| 24 | $HO^{\bullet} + NOM \rightarrow$ | $k_{20} = 2 \times 10^8$ M$^{-1}$ s$^{-1}$ ( fitted from a rage of $10^8$ -$10^9$) | Westerhoff (1997), (1999) |
| | | $k_{20} = 2.3 \times 10^4$ (mg of C/L)$^{-1}$ s$^{-1}$ $(2.3 \times 10^4$l/mg*(1000mg/g*12g/ mole))=2.8 \times 10^8$ M$^{-1}$ s$^{-1}$ | Brezonik (1998) |
| | | 0.1-1 x $10^4$ (mg of C/L)$^{-1}$ s$^{-1}$<br>1.7x $10^4$ (mg of C/L)$^{-1}$ s$^{-1}$<br>1 x$10^8$ M$^{-1}$ s$^{-1}$<br>(8.3 x1 x$10^3$ (mg of C/L)$^{-1}$ s$^{-1}$ | Liao (1995)<br>Nowell (1992)<br>Mak (1997) |
| | $HO^{\bullet} + HA \rightarrow$ | 1 x$10^8$ M$^{-1}$ s$^{-1}$ ( used at pH =7)<br>7 x$10^8$ M$^{-1}$ s$^{-1}$ ( used at pH =10) | |
| 25 | $CO_3^{\bullet -} + NOM \rightarrow$ | $k_{21} = 50$ (mg of C/L)$^{-1}$ s$^{-1}$ $(50 \times 10^4$ l/mg*(1000 mg/g*12g/ mole))=4.2 x$10^3$ M$^{-1}$ s$^{-1}$<br>$k_{21} = 5 \times 10^5$ M$^{-1}$ s$^{-1}$ (used value) | AWWA (1989) |
| 27 | ${}^{\bullet}CO_3^- + {}^{\bullet}OH \rightarrow ?$ | $k_{22} = 3.0 \times 10^9$ M$^{-1}$ s$^{-1}$ | Buxton (1988) |

Solvated (hydrated) electron chemistry

| # | Reaction | Rate Constant | pH, Wave length (nm) | Ref. |
|---|---|---|---|---|
| 28 | $\bar{e}_{aq} + H_2O \rightarrow H^\bullet + OH^-$ | k=19.0 M$^{-1}$ s$^{-1}$ (used) (average) | | Buxton (1988) |
| | | k=1000 s$^{-1}$ | 9.15,670 | Schwarz (1992) |
| | | k=1200 s$^{-1}$ | 11 | Swallow (1968) |
| | | k=890 s$^{-1}$ | 8.3-9.0 | Hart (1966) |
| 29 | $\bar{e}_{aq} + \bar{e}_{aq} \rightarrow H_2 + OH^-$ solvent H$_2$O | $2k_{23}$=1.1x 10$^{10}$ M$^{-1}$ s$^{-1}$ (used) | | Buxton (1988) |
| | | k=0.6 x 10$^{10}$ M$^{-1}$ s$^{-1}$ | 10, 720 | Schmidt (1995) |
| | | k=0.50x 10$^{10}$ M$^{-1}$ s$^{-1}$ | 11-13 | Christensen (1986) |
| | | k=0.5x 10$^{10}$ M$^{-1}$ s$^{-1}$ | 12.8, 700 | Telser (1986) |
| | | k=0.7x 10$^{10}$ M$^{-1}$ s$^{-1}$ | 12, 600 | Hickel (1985) |
| | | k=0.55x 10$^{10}$ M$^{-1}$ s$^{-1}$ | 11 | Christensen (1980) |
| | | k=0.62x 10$^{10}$ M$^{-1}$ s$^{-1}$ | 10.5, 575 | Meisel (1975), Boyle (1969) |
| 30 | $\bar{e}_{aq} + H^\bullet \rightarrow H_2 + OH^-$ | $K_{24}$=2.5 x 10$^{10}$ M$^{-1}$ s$^{-1}$ (used) | | Buxton (1988) |
| | | k=2.4x 10$^{10}$ M$^{-1}$ s$^{-1}$ | 6-7 | Christensen (1994) |
| | | k=2.4x 10$^{10}$ M$^{-1}$ s$^{-1}$ | 8.27, 670 | Scharz (1992) |
| | | k=2.5 x 10$^{10}$ M$^{-1}$ s$^{-1}$ | 10, 578 | Matheson (1965) |
| | | k=2.0 x 10$^{10}$ M$^{-1}$ s$^{-1}$ | | Dragnice (1991) |
| 31 | $\bar{e}_{aq} + {}^\bullet OH \rightarrow OH^- + H_2O$ | $k_{25}$=3.0 x 10$^{10}$ M$^{-1}$ s$^{-1}$ (used) | | Buxton (1988) |
| | | $k_{25}$=3.1 x 10$^{10}$ M$^{-1}$ s$^{-1}$ | 10-10.6 | Christensen (1994) |
| | | $k_{25}$=3.0 x 10$^{10}$ M$^{-1}$ s$^{-1}$ | 10.5, 578 | Matheson (1965) |
| | | $k_{25}$=2.5 x 10$^{10}$ M$^{-1}$ s$^{-1}$ | | Dragnice (1991) |
| 32 | $\bar{e}_{aq} + H^+ \rightarrow H^\bullet$ | $k_{26}$=2.3 x 10$^{10}$ M$^{-1}$ s$^{-1}$ (used) | 0 ionic strength | Buxton (1988) |
| | | $k_{26}$=2.3 x 10$^{10}$ M$^{-1}$ s$^{-1}$ | 2, 0 ionic strength | Jonah (1977) |
| | | $k_{26}$=2.8 x 10$^{10}$ M$^{-1}$ s$^{-1}$ | 4-5, 578 | Gordon (1963) |
| 33 | $\bar{e}_{aq} + H_2O_2 \rightarrow {}^\bullet OH + OH^-$ | $k_{27}$=1.1 x 10$^{10}$ M$^{-1}$ s$^{-1}$ (used) | | Buxton (1988) |
| | | $k_{27}$=1.2 x 10$^{10}$ M$^{-1}$ s$^{-1}$ | | Christensen (1994) |
| | | $k_{27}$=1.2 x 10$^{10}$ M$^{-1}$ s$^{-1}$ | 9.8, 650 | Gordon (1963) |
| | | $k_{27}$=1.6 x 10$^{10}$ M$^{-1}$ s$^{-1}$ | 7, 578 | Dragnice (1991) |
| 34 | $\bar{e}_{aq} + HO_2^- \rightarrow {}^\bullet OH + 2OH^-$ | $k_{28}$=0.35 x 10$^{10}$ M$^{-1}$ s$^{-1}$ (used) | | Buxton (1988) |
| | | $k_{28}$=1.2 x 10$^{10}$ M$^{-1}$ s$^{-1}$ | 13, 720 | Felix (1967) |
| 35 | $\bar{e}_{aq} + O_2^{\bullet-} \rightarrow O_2^{2-}$ | $k_{29}$=1.3 x 10$^{10}$ M$^{-1}$ s$^{-1}$ | | Buxton (1988) |
| 36 | $H^\bullet + H_2O \rightarrow H_2 + OH^-$ | $k_{30}$=10 M$^{-1}$ s$^{-1}$ (used) | | Buxton (1988) |
| | | $k_{30}$=550 s$^{-1}$ | 10-13, | Hartig (1982) |
| 37 | $H^\bullet + H^\bullet \rightarrow H_2$ | $2k_{31}$=1.55 x 10$^{10}$ M$^{-1}$ s$^{-1}$ (used) | | Buxton (1988) |
| | | $k_{31}$=0.5 x 10$^{10}$ M$^{-1}$ s$^{-1}$ | 2, 200-210 | Sehested (1990) |
| | | $k_{31}$=0.59 x 10$^{10}$ M$^{-1}$ s$^{-1}$ | 1, | Beckert (1983) |
| | | $k_{31}$=0.78 x 10$^{10}$ M$^{-1}$ s$^{-1}$ | 3, 200 | Pasberg (1969) |
| 38 | $H^\bullet + {}^\bullet OH \rightarrow H_2O$ | $k_{32}$=0.7 x 10$^{10}$ M$^{-1}$ s$^{-1}$ (used) | | Buxton (1988) |

| | | | | |
|---|---|---|---|---|
| | | $k_{32}$=0.7 x $10^{10}$ $M^{-1}$ $s^{-1}$ | 3, 260 | Thomas (1965) |

39   $H^\bullet + OH^- \xrightarrow{H_2O} \bar{e}_{aq}$     $k_{33}$=2.2 x $10^7$ $M^{-1}$ $s^{-1}$ (used)      Buxton (1988)

40   $H^\bullet + H_2O_2 \rightarrow^\bullet OH + H_2O$    $k_{34}$=9 x $10^7$ $M^{-1}$ $s^{-1}$      Buxton (1988)
(used)

                          $k_{34}$=3.6x $10^7$ $M^{-1}$ $s^{-1}$    1-2,720      Mezyk (1995)

  $H^\bullet + HO_2^- \rightarrow^\bullet OH + H_2O$    $k_{35}$=1.2x $10^9$ $M^{-1}$ $s^{-1}$      Mezyk (1995)

41   $H^\bullet + HO_2^\bullet \rightarrow H_2O_2$      $k_{36}$=1 x $10^{10}$ $M^{-1}$ $s^{-1}$ (used)      Buxton (1988)

  $H_2 +^\bullet OH \xrightarrow{H_2O} H^\bullet$      $k_{37}$=4.2x $10^7$ $M^{-1}$ $s^{-1}$      Buxton (1988)

**Reactions that are not included in the model**

42   $HA(DOC) + \bar{e}_{aq} \rightarrow products$    Selected value      Mak (1997)
                          $k = 1x 10^7 M^{-1} s^{-1}$

43   $HA(DOC) + H^\bullet \rightarrow products$    Selected va;ue      Mak (1997)
                          $k = 1x 10^7$ $M^{-1}$ $s^{-1}$

44   $HCO_3^- + \bar{e}_{aq} \rightarrow products$    $k < 1x 10^6$ $M^{-1}$ $s^{-1}$      Thomas (1965)
                          No reaction      Weeks (1966)

45   $HCO_3^- + H^\bullet \rightarrow products$    $k = 4.4x 10^4$ $M^{-1}$ $s^{-1}$    8      Mak (1997)

46   $CO_3^{2-} + \bar{e}_{aq} \rightarrow products$    $k = 3.9x 10^5$ $M^{-1}$ $s^{-1}$    11.4      Mak (1997)

47   $CO_3^{2-} + H^\bullet \rightarrow products$    No available data

**Reactions with $O_2$ are neglected**

48   $\bar{e}_{aq} + O_2 \rightarrow O_2^{\bullet-}$      $k = 1.9 x 10^{10}$ $M^{-1}$ $s^{-1}$      Buxton (1988)
                          $k = 2.2 x 10^{10}$ $M^{-1}$ $s^{-1}$    6.4, 650   Hentz (1972)
                          $k = 1.9 x 10^{10}$ $M^{-1}$ $s^{-1}$    7, 578   Gordon (1963)

49   $H^\bullet + O_2 \rightarrow HO_2^\bullet$      $k = 2.1 x 10^{10}$ $M^{-1}$ $s^{-1}$      Buxton(1988)
                          $k = 1.0 x 10^{10}$ $M^{-1}$ $s^{-1}$    2, 650   Elliot (1989)
                          $k = 2.1 x 10^{10}$ $M^{-1}$ $s^{-1}$    1.2, 240   Gordon (1964)

The following reactions are neglected because they were measured at alkaline conditions, and their occurrence depend on the production of hydrated electron from the photolysis of humic acid which will results in very low concentrations of electrons opposite to the treatment methods where electron beam is used to destroy contaminants [Mak, 1997] and in that case electrons are available at a much higher concentrations and these reaction can't be neglected.

50   $OH^- +^\bullet OH \rightarrow O^{\bullet-} + H_2O$    $k$=1.2 x $10^{10}$ $M^{-1}$ $s^{-1}$    11      Buxton (1988)

  $O^{\bullet-} + H_2O \rightarrow^\bullet OH + OH^-$    $k = 1.8 x 10^6$ $M^{-1}$ $s^{-1}$    11
                          $k = 9.3 \times 10^7 (s^{-1})$      Buxton (1988)
                          pKa=11.9

| # | Reaction | k | | Reference |
|---|----------|---|---|-----------|
| 51 | $O^{\bullet-} + O_2 \rightarrow O_3^{\bullet-}$ | $k = 3.6 \times 10^9$ $M^{-1}s^{-1}$ | 11,13, alkaline | Buxton (1988) |
| 52 | $O^{\bullet-} + HO_2^- \rightarrow O_2^{\bullet-} + OH^-$ | $k = 4 \times 10^8$ $M^{-1}s^{-1}$ | 13 | Buxton (1988) |
| 53 | $O^{\bullet-} + OH^- \rightarrow HO_2^-$ | $k \leq 1 \times 10^{10}$ $M^{-1}s^{-1}$ | | Buxton (1988) |
| 54 | $O^{\bullet-} + {}^{\bullet}OH \rightarrow HO_2^-$ | $k \leq 2 \times 10^{10}$ $M^{-1}s^{-1}$ | >12 | Buxton (1988) |
| 55 | $O^{\bullet-} + H_2 \rightarrow H^{\bullet} + OH^-$ | $k = 8 \times 10^7$ $M^{-1}s^{-1}$ | 13.3 | Buxton (1988) |
| 56 | $O^{\bullet-} + H_2O_2 \rightarrow O_2^{\bullet-} + H_2O$ | $k \leq 5 \times 10^8$ $M^{-1}s^{-1}$ | | Buxton (1988) |
| 57 | $O^{\bullet-} + HO_2^- \rightarrow O_2^{\bullet-} + OH^-$ | $k = 4 \times 10^8$ $M^{-1}s^{-1}$ | 13 | Buxton (1988) |
| 58 | $O^{\bullet-} + O_2^{\bullet-} \rightarrow O_2 + 2OH^-$ | $k = 6 \times 10^8$ $M^{-1}s^{-1}$ | | |
| 59 | $\bar{e}_{aq} + O^{\bullet-} \rightarrow OH^-$ | $k = 2.2 \times 10^{10}$ $M^{-1}s^{-1}$ | 13, 578 | Matheson (1965) |

[*] Shaded equations are not used in the kinetic model

According to the definition of quantum yield and the Beer-Lambert Law, the overall decomposition rate of $H_2O_2$ in pure water by direct photolysis can be described as follows:

$$r_{H_2O_2} = -\frac{dH_2O_2}{dt} = \Phi_{H_2O_2} I_{ab} \quad \text{[Liao, 1995; Glaze, 1995]}$$

Where:

$\Phi_{H_2O_2}$ = the primary quantum yield of $H_2O_2$ photolysis

$I_{ab}$ = the light intensity absorbed by $H_2O_2$ (Einstein $L^{-1}s^{-1}$) and is defined as

$$I_{ab} = I_o(1 - e^{-A_t}) \quad \text{[Liao, 1995; Glaze ,1995]}$$

Where:

$I_o$ = the incident light intensity (Einstein $L^{-1}s^{-1}$)

$A_t$ = the total absorbance of UV light by species that absorb light. For an aqueous solution containing hydrogen peroxide this will be $H_2O_2$.

For example if the following reaction is taking place due to UV light

$$A \xrightarrow{\quad h\nu \quad} B$$
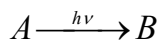
then $\Phi$ for A reacted or B produced is defined as molecules of A reacted/moles of B produced per unit volume per unit time divided by the quanta of light absorbed by A per unit volume per unit time. Photon is usually used to define 1 mole of light or quanta. The moles of A reacted or B produced is found by conventional chemical analysis. The quanta of light absorbed is calculated from the measured total energy of the absorbed light of wavelength $\lambda$ and the assumption that each quantum has an energy equal to

$\dfrac{hc}{\lambda}$ where h is blank's constant ($6.6256 \times 10^{-27}$ erg-sec/quantum) and c is the velocity of radiation. The size of $\Phi$ varies greatly with different reaction systems (e.g., from 0.0 to $10^6$) [Calvert, 1966].

### 2.1.2. Reaction Mechanism in the presence of Humic Acid

The presence of humic acids (HA) may affect $UV/H_2O_2$ oxidation process through two mechanisms. The process might be inhibited due to absorption of UV light by HA (reaction 2 Table 2.1). HA is also known as effective $^\bullet OH$ scavenger (Reaction 24, Table 2.1) [Liao, 1995; Westerhoff, 1997, 1999; Brezonik, 1998; Mak, 1997, Nowell, 1992]. The rate constant for the reaction of HA with $^\bullet OH$ radicals is usually expressed in terms of dissolved organic carbon (DOC). The reactions of HA with ($HO_2^\bullet / O_2^{\bullet -}$) was found to be negligible from model simulation of Liao (1995). Hence in this model reactions between ($HO_2^\bullet / O_2^{\bullet -}$) and HA were neglected. Also, it was assumed that there is no interaction between oxidation byproducts with UV light. The rate of hydrogen peroxide destruction by UV light in the presence of HA will be given by [Glaze, 1995]:

$$-\frac{dH_2O_2}{dt} = \Phi_{H_2O_2} f_{H_2O_2} I_{ab}$$

$$I_{ab} = I_o(1 - e^{-A_t})$$

For HA the rate of disappearance of HA will be given by

$$\frac{dHA}{dt} = -k_{20}[HA][{}^\bullet OH] - \Phi_{HA} f_{HA} I_o(1 - e^{-A_t})$$

where $I_{ab}$ is light intensity in the reaction mixture (Einstein $L^{-1}$ $s^{-1}$), $I_o$ is the incident light intensity (Einstein $L^{-1}$ $s^{-1}$), $A_t$ is the total absorbance of the solution ($cm^{-1}$), $f_{H_2O_2}$, and $f_{HA}$ is the fraction of radiation absorbed by $H_2O_2$ and HA, respectively, and $\Phi_i$ is the quantum yield and it is the number of moles of species i decomposed per mole of light photon absorbed [Baxendale, 1988; Hunt, 1952; Liao,1995].

The total absorbance of the solution is given by:

$$A_t = 2.303b(\varepsilon_{H_2O_2}[H_2O_2] + \varepsilon_{HA}[HA]) \quad [Glaze, 1995; Crittenden, 1999]$$

where $\varepsilon_i$ is the molar absorptivity of specie i ($M^{-1}$ $cm^{-1}$) , and b is effective optical path length of the reactor [Baxendale, 1988; Glaze, 1995] , and is equal to the radius of the reactor [Glaze, 1995; Crittenden, 1999; Liao, 1995]

The fraction of absorbed radiation absorbed by species i in a mixture is given by:

$$f_i = \frac{2.303b\varepsilon_i[M_i]}{A_t} = \frac{2.303b\varepsilon_i[M_i]}{2.303b\sum_i \varepsilon_i[M_i]}$$

$H_2O_2$ is a weak acid with $pk_a$ value of 11.65 [Buxton, 1988; Dean, 1979] and its dissociation is given by:

$$H_2O_2 \leftrightarrow H^+ + HO_2^-$$

The total hydrogen peroxide concentration is:

$$[H_2O_2]_T = [H_2O_2] + [HO_2^-] = [H_2O_2] + \frac{K_8}{[H^+]}[H_2O_2] = [H_2O_2](1 + \frac{K_8}{[H^+]})$$

$$HO_2^- = \frac{K_8[H_2O_2]}{[H^+]}$$

where $K_8$ is the equilibrium constant for $H_2O_2$ dissociation.

If $H_2O_2$ and HA are the only UV light absorbers the fraction of UV light absorbed by $H_2O_2$ and HA is given by:

$$f_{H_2O_2} = \frac{\varepsilon_{H_2O_2}[H_2O_2] + \varepsilon_{HO_2^-}[HO_2^-]}{\varepsilon_{HA}[HA] + \varepsilon_{H_2O_2}[H_2O_2] + \varepsilon_{HO_2^-}[HO_2^-]}$$

$$f_{HA} = \frac{\varepsilon_{HA}[HA]}{\varepsilon_{HA}[HA] + \varepsilon_{H_2O_2}[H_2O_2] + \varepsilon_{HO_2^-}[HO_2^-]}$$

## 2.1.2.1. Solvated (hydrated) electrons

As said earlier, the photolysis of humic material was found to produce active transients. The direct intermediates of photolysis of humic acids are solvated electrons and triplet state. The solvated electron was firmly identified [Power, 1987; Fisher, 1985, 1987; Zepp, 1985, 1987a, 1987b; Aguer; 1999, 2002; Cooper, 1989, Thomas-Smith, 2001]. The production of solvated electron by direct photolysis of humic acids was included in the kinetic model. The presence of this intermediate led to a series of other reactions, as shown in Table 2.1, that were incorporated in the kinetic model. The other product of the photolysis of humic acid, the triplet state, was assumed to be degraded by self combination. The corresponding chemical reactions with the rate constants of hydrated electrons were taken from the literature as shown in Table 2.1.

**2.1.2.2. Proposed mechanism for HA acid byproducts**

The products of UV photolysis of HA were assumed to be the solvated electron and an intermediate, $I_1$ which was defined earlier as $HS^{\bullet+}$. Researchers found that this intermediate could be the triplet state of HA [Zepp, 1987, 1985; Aguer; 1999; Aguer, 2002; Cooper, 1989]. $I_1$ could be degraded through self recombination [Calvert, 1966]. The end product of this reaction and other fast reactions would be a smaller compound $I_2$ and x moles of $CO_2$ and y moles of $H_2O$ [Fukushima, 2001]. $I_2$ has been assumed to be volatile compound so it doesn't interfere with the measurement of non purgeable dissolved organic carbon (NPDOC) [Miller, 1987]. These reactions are summarized by:

$$HA \xrightarrow{\;h\upsilon\;} I_1 + \overline{e}$$

$$I_1 + I_1 \rightarrow I_2 + xCO_2 + yH_2O, k_{I1}$$
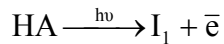
On the other hand, the product of HA reaction with $^{\bullet}OH$ is assumed to be $I_3$. There is no reason to assume that direct photolysis of humic acid proceeds in the same mechanism as that for reactions of humic acid with $^{\bullet}OH$ radicals [Goldstone, 2002]. $I_3$ was assumed to react with $^{\bullet}OH$ and form a new compound $I_4$. Also it was assumed that $I_3$ will react with $H_2O_2$ to form $CO_2$ and water [Weeks, 1955]. These reactions are:

$$HA + {^{\bullet}OH} \rightarrow I_3$$

$$HA + {^{\bullet}OH} \rightarrow I$$

$$I_3 + H_2O_2 \rightarrow xCO_2 + yH_2O, k_{I3'}$$

$$I_3 + {^*OH} \rightarrow I_4 + xCO_2 + yH_2O, k_{I3}$$
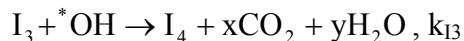
In the above scheme it was assumed that 0.5 of $^{\bullet}OH$ and HA reaction forms $I_3$ which goes through other reactions, and the remaining fraction of $^{\bullet}OH$ and HA reaction

forms I which could be water and carbon dioxide. The reason that we have two different products from the reaction of HA with $^\bullet$OH radicals is that HA consists of heterogeneous mixture of organic compounds and based upon Brezonik's work (1998) $^\bullet$OH could be added to aromatic sites of the HA and the abstraction of hydrogen from the hydrocarbons part of HA. $I_4$ in turn will react with $^\bullet$OH to form a new compound or intermediate $I_5$, water and carbon dioxide. $I_5$ again will react with $^\bullet$OH forming $I_6$, $CO_2$, and water. $I_6$ was assumed to be a small molecule compared to the other products and hence was assumed to be volatile. A summary of these reactions is given by:

$$2I_4 + {}^\bullet OH \rightarrow I_5 + xCO_2 + yH_2O, \ k_{I4}$$

$$I_5 + {}^\bullet OH \rightarrow I_6 + xCO_2 + yH_2O \ , \ k_{I5}$$
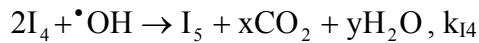
Therefore, at the time of TOC measurement the NPDOC is:

NPDOC=HA+$I_1$+$I_3$+$I_4$+$I_5$

Fukushima (2001) found from a study on degradation characteristics of humic acid during photo-Fenton process that the molecular size of HA decreased as result of the irradiation. After irradiation, he could identify ether and epoxide functional groups. He suggested that these products could be formed via radical coupling and/or via hydroxyl radical addition to the unsaturated group in the HA such as vinyl and aromatics group.

Goldstone (2002), found that $^\bullet$OH reactions with humic substances produced dissolved inorganic carbon with a high efficiency of 0.3 mol of $CO_2$/mol of $^\bullet$OH radical. Also, he measured production rates of low molecular weight acids including acetic acid, formic, malonic, and oxalic acids by reaction of Suwannee River fulvic and humic acids with $^\bullet$OH radicals. The calculated concentrations of these compounds were within 1-3

μM starting with 5 mg L$^{-1}$ dissolved organic matter. Low molecular weight organic compounds including carboxylic acid and carbonyl compounds were identified as photoproducts of dissolved organic matter [Goldstone, 2002]. $^\bullet$OH reactions with compounds is processed either by addition (hydroxylation), generally to aromatic ring, or hydrogen atom ($H^\bullet$) abstraction, both of which may lead to formation of low molecular weight (LMW) compounds [Goldstone, 2002]. Goldstone suggested that ring opening after the $^\bullet$OH addition to the aromatics could lead to mono- and diacids. The humic acid which he used contained significant concentrations of carboxylic acid and phenolic residues. Substituted phenolic residue in particular might contribute to the production of LMW acids.

The work documented in this chapter attempts to relate the proposed reaction byproducts in the proposed scheme to the byproducts observed in the literature, but it is obvious that due to the heterogeneities of humic acids and the dependence of their structure on their origin this is not an easy task. The identification of these byproducts should be done directly on the humic acid which were studied in Wang work and used in our simulation. The rate constants for some of the proposed reaction intermediates $k_{I3}$, $k_{I4,}$ $k_{I5}$, are 3 x 10$^8$, 1 x 10$^7$, and 10 M$^{-1}$ s$^{-1}$ respectively. The rate constants for the reactions of formic acid, acetic acid, malonic acid, and oxalic acid, which were detected in Goldstone's work, with $^\bullet$OH radicals are 1.3 x 10$^8$, 1.6 x 10$^7$, 1.6 x 10$^7$, and 1.4 x10$^6$ M$^{-1}$ s$^{-1}$, respectively [Buxton, 1988]. Therefore, the assumed values for the rate constants for the reactions of the proposed byproducts in this kinetic model with $^\bullet$OH radicals, and obtained from best fitting, is close to these reported values. Although neither our mechanism nor Goldstone's products might represent the actual oxidation process of HA.

### 2.1.3. Model parameters

The quantum yield for the photolysis of hydrogen peroxide ($\Phi_{H_2O_2}$) in pure water has been estimated as 1 for the overall reactions of $H_2O_2$ including the initiation, propagation and termination step [Glaze, 1995; Baxendale, 1957; Guittonneau, 1990; Crittenden, 1999]. The primary quantum yield is estimated as 0.5 (reaction 1 in Table 2.1), i.e, for the initiation reaction, for relatively high light intensity, and low peroxide concentrations [Baxendale, 1957; Volman, 1959; Liao, 1995]. Molar absorptivity of hydrogen peroxide ($\varepsilon_{H_2O_2}$) is available in the literature within the range 17.8 - 19.7 M$^{-1}$ cm$^{-1}$ at 254 nm [Baxendale, 1956; Bielski, 1977; Guittonneau, 1990; Morgan, 1988]. The value for $\varepsilon_{H_2O_2}$ used in this kinetic model is 17.8 M$^{-1}$ cm$^{-1}$. The molar absorptivity of the conjugate base of hydrogen peroxide ($HO_2^-$) ($\varepsilon_{HO_2^-}$) is 228 M$^{-1}$cm$^{-1}$ at 254 nm [Baxendale, 1957; Morgan, 1988].

$I_o$ which is the light intensity (Einstein L$^{-1}$ s$^{-1}$) was not measured for this system. Therefore it was lumped in the fitting parameters $k_1$ and $k_2$ where:

$$k_1 = \Phi_{H_2O_2} I_o$$

$$k_2 = \Phi_{HA} I_o$$

where $\Phi_{H_2O_2}$ and $\Phi_{HA}$ are the quantum yield for $H_2O_2$ and HA photolysis, respectively.

The parameter b represents the effective path length of the UV light inside the reactor (cm). The value of this parameter has been taken as the radius of the reactor which contains the reaction solution. The reactor used by Wang (2001) has a diameter of 20 cm, with a hollow UV quartz tube of 5.5 cm outside diameter, therefore the effective radius for this set up was 7.25 cm (reactor diameter less hollow UV quartz tube

194

diameter). The radius of the reactor was used as the effective path length by Glaze (1995) and Crittenden (1999). Liao (1995) used the diameter as the effective path length since his reactor was surrounded by the equally spaced UV sources.

The molar absorptivity of humic acid $\varepsilon_{HA}$ is 0.066 (mg/L of DOC)$^{-1}$ cm$^{-1}$ at 254 nm [Wang, 2001]. This value is consistent with the value reported by Liao (1995) which is $\varepsilon_{HA}$ = 0.0867 cm$^{-1}$ (mg/L of DOC)$^{-1}$. Also, Westerhoff (1999) found an average value for $\varepsilon_{HA}$ of 0.037 cm$^{-1}$ (mg/L of DOC)$^{-1}$ at 254 nm for different isolates of natural organic matter (NOM). Since all of the measurement are based on dissolved carbon (which has 12 gm per mole), then $\varepsilon_{HA} = 840$ M$^{-1}$cm$^{-1}$ after converting from mass to mole unit.

We assumed that contributions of wave lengths other than 254 nm are negligible and therefore molar absorptivity was taken at a wave length of 254 nm. Baxendale (1957) made a similar assumption although the output of the light source which he used was concentrated into three regions, 254, 313 and 365 nm and visible.

Also, we considered pH to remain constant. This is based on the experimental observation of Wang (2001, 2000) who didn't notice a significant change in pH during the experiment. Also, in Crittenden model (1999) he made a comparison in his model prediction between assuming a constant and a variable pH and he didn't find a significant difference.

Also, we assumed that the only absorbers for UV light in this system are hydrogen peroxide with its conjugate base and humic acid.

### 2.1.4. Model equations

Some or all of the proposed elementary reaction (reaction 1-30) in Table 2.1 have been included by others to describe the destruction of organic compounds by $H_2O_2$/UV process or other AOP which involve the production of $^\bullet OH$ radicals from $H_2O_2$ [Glaze, 1995; Crittenden , 1999; Chen, 1997; Gallard, 2000]. However, in the previous work although humic acid was present its rate of destruction by photolysis was neglected [Crittenden, 1999; Glaze, 1995]. This could be applicable when $H_2O_2$ is relatively high compared to HA. When the concentration of $H_2O_2$ is comparable to humic acid, then this term may not be neglected. To our knowledge, this is the first time any one has tried to describe the kinetics of humic acid destruction by $H_2O_2$/UV process for the available experimental data in the literature.

A completely mixed batch reactor was used in running the experimental work of Wang (2000, 2001). The mass balance of species i at any time will be given by the following ordinary differential equation:

$\dfrac{dC_i}{dt} = r_i$ which describes the change of species i concentration as a function of time starting with initial concentration $C_{io}$ in a completely mixed batch reactor in a liquid solution.

Substituting each species in Table 2.1 into this equation, we get a set of ordinary nonlinear differential equation that describes the rate of changes in the concentration of each species with respect to time.

Humic acid:

$$\frac{d[HA]}{dt} = -k_{20}[HA][{}^\bullet OH] - \Phi_{HA}f_{HA}I_o(1-e^{-At}) - k_{21}[CO_3^{\bullet-}][HA]$$

$$= -k_{20}[HA][{}^\bullet OH] - k_2 f_{HA}(1-e^{-At}) - k_{21}[CO_3^{\bullet-}][HA]$$

where $k_2 = \Phi_{HA}I_o$

Hydrogen peroxide:

$$\frac{d[H_2O_{2T}]}{dt} = -\Phi_{H2O2}f_{H2O2}I_o(1-e^{-At}) - k_3[H_2O_2][{}^\bullet OH] - k_{13}[H_2O_2][{}^\bullet CO_3^-] + k_8[HO_2^\bullet][HO_2^\bullet]$$
$$+ k_4[HO_2^\bullet][O_2^{\bullet-}] + k_7[{}^\bullet OH][{}^\bullet OH] - k_{16}[H_2O_2]_T[O_2^{\bullet-}] - k_{17}[H_2O_2]_T[HO_2^\bullet] -$$
$$k_{18}[HO_2^-][{}^\bullet OH] - k_{19}[HO_2^-][CO_3^{\bullet-}] - k_{27}[\bar{e}_{aq}][H_2O_2] - k_{28}[\bar{e}_{aq}][HO_2^-] -$$
$$k_{34}[H_2O_2][H^\bullet] - k_{35}[HO_2^-][H^\bullet] - k_{I3'}[H_2O_2]_T[I_3] + k_{36}[H^\bullet][HO_2^\bullet]$$

with $k_1 = \Phi_{H2O2}I_o$ and taking $\Phi_{H2O2} = \Phi_{HO_2^-}$ then:

$$\frac{d[H_2O_{2T}]}{dt} = -k_1 f_{H2O2}(1-e^{-At}) - k_3[H_2O_2][{}^\bullet OH] - k_{13}[H_2O_2][{}^\bullet CO_3^-] + k_8[HO_2^\bullet][HO_2^\bullet]$$
$$+ k_4[HO_2^\bullet][O_2^{\bullet-}] + k_7[{}^\bullet OH][{}^\bullet OH] - k_{16}[H_2O_2]_T[O_2^{\bullet-}] - k_{17}[H_2O_2]_T[HO_2^\bullet] -$$
$$k_{18}[HO_2^-][{}^\bullet OH] - k_{19}[HO_2^-][CO_3^{\bullet-}] - k_{27}[\bar{e}_{aq}][H_2O_2] - k_{28}[\bar{e}_{aq}][HO_2^-] -$$
$$k_{34}[H_2O_2][H^\bullet] - k_{35}[HO_2^-][H^\bullet] - k_{I3'}[H_2O_2]_T[I_3] + k_{36}[H^\bullet][HO_2^\bullet]$$

where the total hydrogen peroxide concentration is given by:

$$[H_2O_2]_T = [H_2O_2] + [HO_2^-] = [H_2O_2] + \frac{K_8}{[H^+]}[H_2O_2] = [H_2O_2](1+\frac{K_8}{[H^+]})$$

$$HO_2^- = \frac{K_8[H_2O_2]}{[H^+]}$$

Hydroxyl radical:

$$\frac{d[^{\bullet}OH]}{dt} = 2\Phi_{H_2O_2}f_{H_2O_2}I_o(1-e^{-At}) - k_3[H_2O_2][^{\bullet}OH] - k_5[^{\bullet}OH][HO_2^*] - k_6[^{\bullet}OH][O_2^{\bullet-}]$$
$$- 2k_7[^{\bullet}OH][^{\bullet}OH] - k_{11}[^{\bullet}OH][HCO_3^-] - k_{14}[^{\bullet}OH][CO_3^{2-}] - k_{20}[^{\bullet}OH][HA]$$
$$- k_{18}[^{\bullet}OH][HO_2^-] - k_{16}[H_2O_2]_T[O_2^{\bullet-}] + k_{17}[H_2O_2]_T[HO_2^{\bullet}] - k_{22}[^{\bullet}OH][CO_3^{\bullet-}]$$
$$- k_{25}[^{\bullet}OH][\bar{e}_{aq}] + k_{27}[H_2O_2][\bar{e}_{aq}] + k_{28}[HO_2^-][\bar{e}_{aq}] - k_{32}[^{\bullet}OH][H^{\bullet}]$$
$$+ k_{34}[H_2O_2][H^{\bullet}] + k_{35}[HO_2^-][H^{\bullet}] - k_{37}[H_{2aq}][^{\bullet}OH] + k_{30}[H^{\bullet}][H_2O]$$
$$- k_{I3}[I_3][^{\bullet}OH] - k_{I4}[I_4][^{\bullet}OH] - k_{I5}[I_5][^{\bullet}OH]$$

$$\frac{d[^{\bullet}OH]}{dt} = 2k_1f_{H_2O_2}(1-e^{-At}) - k_3[H_2O_2][^{\bullet}OH] - k_5[^{\bullet}OH][HO_2^*] - k_6[^{\bullet}OH][O_2^{\bullet-}]$$
$$- 2k_7[^{\bullet}OH][^{\bullet}OH] - k_{11}[^{\bullet}OH][HCO_3^-] - k_{14}[^{\bullet}OH][CO_3^{2-}] - k_{20}[^{\bullet}OH][HA]$$
$$- k_{18}[^{\bullet}OH][HO_2^-] - k_{16}[H_2O_2]_T[O_2^{\bullet-}] + k_{17}[H_2O_2]_T[HO_2^{\bullet}] - k_{22}[^{\bullet}OH][CO_3^{\bullet-}]$$
$$- k_{25}[^{\bullet}OH][\bar{e}_{aq}] + k_{27}[H_2O_2][\bar{e}_{aq}] + k_{28}[HO_2^-][\bar{e}_{aq}] - k_{32}[^{\bullet}OH][H^{\bullet}]$$
$$+ k_{34}[H_2O_2][H^{\bullet}] + k_{35}[HO_2^-][H^{\bullet}] - k_{37}[H_{2aq}][^{\bullet}OH] + k_{30}[H^{\bullet}][H_2O]$$
$$- k_{I3}[I_3][^{\bullet}OH] - k_{I4}[I_4][^{\bullet}OH] - k_{I5}[I_5][^{\bullet}OH]$$

Hydrperoxyl radical:

$$\frac{d[HO_2^{\bullet}]}{dt} = k_3[H_2O_2][^{\bullet}OH] - k_4[HO_2^{\bullet}][O_2^{\bullet-}] - k_5[^{\bullet}OH][HO_2^{\bullet}] - 2k_8[HO_2^{\bullet}][HO_2^{\bullet}]$$
$$- k_{10}[HO_2^{\bullet}] + k_9[O_2^{\bullet-}][H^+] - k_{17}[H_2O_2]_T[HO_2^{\bullet}] + k_{18}[^{\bullet}OH][HO_2^-] - k_{36}[H^{\bullet}][HO_2^{\bullet}]$$

Superoxide radical anion:

$$\frac{d[O_2^{\bullet-}]}{dt} = k_{10}[HO_2^{\bullet}] + k_{13}[CO_3^{\bullet-}][H_2O_2]_T - k_9[O_2^{\bullet-}][H^+] - k_4[HO_2^{\bullet}][O_2^{\bullet-}]$$
$$- k_6[^{\bullet}OH][O_2^{\bullet-}] - k_{12}[O_2^{\bullet-}][CO_3^{\bullet-}] - k_{16}[H_2O_2]_T[O_2^{\bullet-}] + k_{19}[CO_3^{\bullet-}][HO_2^-] - k_{29}[O_2^{\bullet-}][\bar{e}_{aq}]$$

Carbonate radical ion:

$$\frac{d[CO_3^{\bullet-}]}{dt} = k_{11}[HCO_3^-][^{\bullet}OH] - k_{12}[O_2^{\bullet-}][CO_3^{\bullet-}] - k_{13}[CO_3^{\bullet-}][H_2O_2]$$
$$- 2k_{15}[CO_3^{\bullet-}][CO_3^{\bullet-}] + k_{14}[CO_3^{2-}][^{\bullet}OH] - k_{19}[CO_3^{\bullet-}][HO_2^-]$$
$$- k_{22}[^{\bullet}OH][CO_3^{\bullet-}] - k_{21}[CO_3^{\bullet-}][HA]$$

Bicarbonate ion:

$$\frac{d[HCO_3^-]}{dt} = -k_{11}[HCO_3^-][^{\bullet}OH] + k_{13}[H_2O_2][CO_3^{\bullet-}] + k_{19}[HO_2^-][CO_3^{\bullet-}]$$

$$- k_{b1}[HCO_3^-][H^+] + k_{f1}[CO_{2(aq)}] - k_{f2}[HCO_3^-] + k_{b2}[CO_3^{2-}][H^+]$$

Carbonate ion:

$$\frac{d[CO_3^{2-}]}{dt} = k_{12}[CO_3^{\bullet-}][O_2^{\bullet-}] - k_{14}[^{\bullet}OH][CO_3^{2-}] + k_{f2}[HCO_3^-] - k_{b2}[CO_3^{2-}][H^+]$$

Aqueous carbon dioxide:

$$\frac{d[CO_{2(aq)}]}{dt} = -k_{b1}[HCO_3^-][H^+] + k_{f1}[CO_{2(aq)}]$$

Solvated or hydrated electron:

$$\frac{d[\bar{e}_{aq}]}{dt} = k_2 f_{HA}(1 - e^{-At}) - k\ [\bar{e}_{aq}][H_2O] - 2k_{23}[\bar{e}_{aq}][\bar{e}_{aq}] - k_{24}[\bar{e}_{aq}][H^{\bullet}] - k_{25}[\bar{e}_{aq}][^{\bullet}OH]$$

$$- k_{26}[\bar{e}_{aq}][H^+] - k_{27}[\bar{e}_{aq}][H_2O_2] - k_{28}[\bar{e}_{aq}][HO_2^-] - k_{29}[\bar{e}_{aq}][O_2^{\bullet-}] + k_{33}[H^{\bullet}][OH^-]$$

Singlet hydrogen atom:

$$\frac{d[H^{\bullet}]}{dt} = k\ [\bar{e}_{aq}][H_2O] - k_{24}[\bar{e}_{aq}][H^{\bullet}] + k_{26}[\bar{e}_{aq}][H^+] - k_{30}[H^{\bullet}][H_2O] - 2k_{31}[H^{\bullet}][H^{\bullet}] - k_{32}[H^{\bullet}][^{\bullet}OH]$$

$$- k_{33}[H^{\bullet}][OH^-] - k_{34}[H^{\bullet}][H_2O_2] - k_{35}[H^{\bullet}][HO_2^-] - k_{36}[H^{\bullet}][HO_2^{\bullet}] + k_{37}[H_2][^{\bullet}OH]$$

Aqueous Hydrogen:

$$\frac{d[H_{2aq}]}{dt} = k_{23}[\bar{e}_{aq}][\bar{e}_{aq}] + k_{24}[\bar{e}_{aq}][H^{\bullet}] + k_{30}[H^{\bullet}][H_2O] + k_{31}[H^{\bullet}][H^{\bullet}] - k_{37}[H_2][^{\bullet}OH]$$

Intermediates from humic acid destruction:

$$\frac{d[I_3]}{dt} = 0.5k_{20}[HA][^{\bullet}OH] - k_{I3}[I_3][^{\bullet}OH] - k_{I3'}[I_3][H_2O_2]_T$$

$$\frac{d[I_4]}{dt} = k_{I3}[I_3][^{\bullet}OH] - k_{I4}[I_4][^{\bullet}OH]$$

$$\frac{d[I_5]}{dt} = k_{14}[I_4][{}^{\bullet}OH] - k_{15}[I_5][{}^{\bullet}OH]$$

The above system of stiff nonlinear ordinary differential equations was solved numerically using Matlab (R13) program developed by Math Works Inc. For this, the process parameters t, pH, initial concentration of $H_2O_2$ ($[H_2O_2]_o$) and HA ($[HA]_o$), b, and molar absorptivity of $H_2O_2$ ($H_2O_2/HO_2^-$) and HA were specified as inputs to the program. Initial concentration of all radicals was taken as zero. The reaction rate constants along with the equilibrium constants presented in Table 2.1.1 were also used as input to the program. The rate constant for the reaction between humic acid and ${}^{\bullet}OH$ radicals is reported in the literature in terms of dissolved organic carbon. Westerhoff (1996) used a value of $2 \times 10^8$ $M^{-1}$ $s^{-1}$ which was fitted from a rage of $1\text{-}10^8$ $M^{-1}$ $s^{-1}$. Westerhoff (1999) reported a measured average value, from experimental data, of the rate constant for the reaction of ${}^{\bullet}OH$ with dissolved organic carbon of $3.6 \times 10^8$ $M^{-1}$ $s^{-1}$ ($3.0 \times 10^4$ (mg of C/L)$^{-1}$ $s^{-1}$). He converted from M to mg L$^{-1}$ unit by did dividing $3.6 \times 10^8$ $M^{-1}$ $s^{-1}$ by 12 (molecular weight of carbon) and 1000 to go from mg to g.

On the other hand, Brezoink (1998) found that the rate constant for ${}^{\bullet}OH$ radicals scavenging by dissolved organic matter (DOM) is $2.3 \times 10^4$ (mg of C/L)$^{-1}$ $s^{-1}$ and if it is divided by the molecular weight of carbon (12), similar to what Westerhoff (1999) did, this will give a value of $2.8 \times 10^8$ $M^{-1}$ $s^{-1}$. Also, he found that rate constants for ${}^{\bullet}OH$ radicals scavenging by the five different DOM sources were in a narrow range suggesting that the importance of DOM as ${}^{\bullet}OH$ sink can be estimated simply from the dissolved organic carbon (DOC) concentration in water. This value lies within the range of Westerhoff's rang (1996, 1999). A value of $2.6 \times 10^4$ (mg of C/L)$^{-1}$ $s^{-1}$ was reported by

Zepp and Hogine (1987 b). Goldstone, 2002 measured a value of 1.9 x $10^4$ (mg of C/L)$^{-1}$ s$^{-1}$ for the reaction of $^\bullet$OH radicals with humic acid. Cooper (1999) based on experimental data found a value of 1.0 x $10^8$ M$^{-1}$ s$^{-1}$. Liao (1995), from model fitting, obtained a value of 0.12-1.2 x $10^8$ M$^{-1}$ s$^{-1}$ (0.1-1 x $10^4$ (mg of C/L)$^{-1}$ s$^{-1}$) with the best fitting at a value of 1.9 x $10^8$ M$^{-1}$ s$^{-1}$ (1.6 x $10^4$ (mg of C/L)$^{-1}$ s$^{-1}$). Another value for this rate constant was reported by Nowell (1992) and it was 2.0 x $10^8$ M$^{-1}$ s$^{-1}$ (1.7 x $10^4$ (mg of C/L)$^{-1}$ s$^{-1}$). For our model a value of 1.0 x $10^8$ M$^{-1}$ s$^{-1}$ gave the best fit to the experimental data. The other fitted parameters were $k_1$ and $k_2$. Also the rate constants for the by products of HA photolysis and $^\bullet$OH reactions were found from fitting to the data. The best fit was found using least square error analysis.

Based on our simulation, the value of the rate constant for the reaction of $I_3$ with $^\bullet$OH radicals is 3 x $10^8$ M$^{-1}$ s$^{-1}$. This value is close to the rate constant of formic acid (one of the identified products of Goldstone's work (2002)) reaction with $^\bullet$OH radical which is 1.3 x $10^8$ M$^{-1}$ s$^{-1}$ [Buxton, 1988].

# 3. Results

## 3.1. Part 1: Simulation of the experimental data of Wang (2000)

To test the proposed reaction mechanism, the kinetic model was used to simulate the experimental data which were taken from the work of Wang (2000) unless mentioned otherwise. In their work humic acid (HA) was destroyed in the presence of hydrogen peroxide ($H_2O_2$) and UV light. The experimental work of Wang (2000) included different kinetic experiments. In some of Wang's experiments the concentration of HA was varied while keeping the concentration of $H_2O_2$ and pH value at a constant value. This procedure was repeated for different $H_2O_2$ concentrations to investigate the effect of changing initial concentration of both HA and $H_2O_2$.

Figure 3.1.1 shows the experimental data and model prediction for the direct UV photolysis of a solution contains $H_2O_2$ at 0.0249 M with no HA acid at pH 7. This figure was used to obtain the value of $k_1$ in equation (1) for the photolysis of $H_2O_2$ by UV light. On the other hand, Figure 3.1.2-A is giving the model predictions vs. experimental data of the residual fraction of nonpurgeable dissolved organic carbon (NPDOC) [Wang, 2001] for a solution containing initially 6 mg $L^{-1}$ NPDOC (HA) at pH 7 with no $H_2O_2$. From this figure, the value of $k_2$ in the kinetic model was obtained. Figure 3.1.2-B, is giving the model predictions for the remaining fraction of HA at the above experimental conditions.

The definition of $k_1$ was given by the following equation in the kinetic model:

$$k_1 = \Phi_{H_2O_2} I_o \quad (1)$$

The quantum yield of $H_2O_2$ ($\Phi_{H_2O_2}$) is available in the literature [Baxendale, 1988; Guittonneau, 1990; Glaze, 1995; Crittenden, 1999; Hunt, 1952] and the value of it has been either 0.5 or 1. Therefore light intensity ($I_o$) (Einstein $L^{-1}$ $s^{-1}$) is needed to calculate $k_1$. This value was not measured (personal communication with the author). $I_o$ need to be measured for the used UV source for each set of experimental data. Its value depends on the UV source and life time of the source. Therefore, since $I_o$ was not available, $k_1$ was a fitting parameter instead of being a calculated quantity. The value of $k_1$ was in the order of 2.5-5.8 x $10^{-6}$ M $s^{-1}$ and if it is divided by $\Phi_{H_2O_2}$, then the value of $I_o$ from relation 1 above will be in the range 2.5-5.8 x $10^{-6}$ Einstein $L^{-1}$ $s^{-1}$. This value of $I_o$ lies within the range that other workers measured for their UV sources [Daniton, 1953; Baxendale, 1957; Liao, 1995; Glaze, 1995; Hunt, 1952]. For example Glaze (1995) used low pressure mercury UV lamp with light intensity in the order of magnitude of $10^{-6}$ Einstein $L^{-1}$ $s^{-1}$ and Baxendale (1957) used UV intensity of 0.08-8 x $10^{-6}$ Einstein $L^{-1}$ $s^{-1}$. Therefore the obtained value of $k_1$ is realistic.

The rate of HA photolysis in solutions containing only HA is given by:

$$-\frac{dHA}{dt} = \Phi_{HA} I_o (1 - e^{-At}) = k_2(1 - e^{-At}) \text{ with } k_2 = \Phi_{HA} I_o$$

Using the results of simulation for pure HA by UV in Figures 3.1.2-A and 3.1.2-B $k_2$ was found to be 2.5 x $10^{-8}$ M $sec^{-1}$ from best fitting. Assuming that the light intensity was the same in both cases, i.e for the photolysis of pure $H_2O_2$ and pure HA in water, since it is the same UV source, then the only reason that $k_1$ and $k_2$ are different is the quantum yield value.

To calculate the quantum yield ($\Phi_{HA}$) for humic acid, $k_1$ (obtained Figure 3.1.1) was divided by $\Phi_{H_2O_2}$ which is 0.5 to obtain the used value of light intensity ($I_o$). This gave a value of 5.0 x$10^{-6}$ Einstein $L^{-1}$ $s^{-1}$ for $I_o$. Dividing $k_2$ by this value the result is 0.005 which is the quantum yield for HA destruction by UV or products formation from HA destruction by UV photolysis. A summary of the results of this is given in Table 3.1.1.

**Table 3.1. 1:** Comparison between $\Phi_{HA}$ calculated based on the kinetic model results and from literature

| Compound | Rate constant in this work M $s^{-1}$ | $\Phi$ | Source of $\Phi$ |
|---|---|---|---|
| $H_2O_2$ | $k_1$= 2.3x$10^{-6}$ | 0.5 | Crittenden 1998, Glaze, 1995, Baxendale, 1957 |
| HA | $k_2$= 2.5x$10^{-8}$ - | 0.005 0.00012 | This work Thomas-smith, 2001 |
| Natural Organic Matter including HA | - | 0.002-0.008 | Zepp, 1987 |
| Humic substances | - | 0.0047 | Aguer, 1999 |

It can be seen from Table 3.1.1 that the calculated $\Phi_{HA}$ is within the reported range of Zepp (1987), for different sources of natural organic solutes and humic acids, and Aguer (1999). Since $\Phi_{HA}$ calculated from this work is close to the values in the literature this make the value of the fitting parameter $k_2$ realistic.

Figure 3.1.3-A illustrates the residual fraction of the nonpurgable dissolved organic carbon (NPDOC) with reaction time starting with 0.0294 M $H_2O_2$ and increasing initial NPDOC (HA) concentration from 3, 5, to 6 mg $L^{-1}$ in the reaction mixture. The working pH value was 7. The model which we developed was applied to Wang's experimental data (2000) under the different initial concentrations of HA. Residual fraction of $H_2O_2$ at the same experimental conditions is shown in Figure 3.1.3-B.
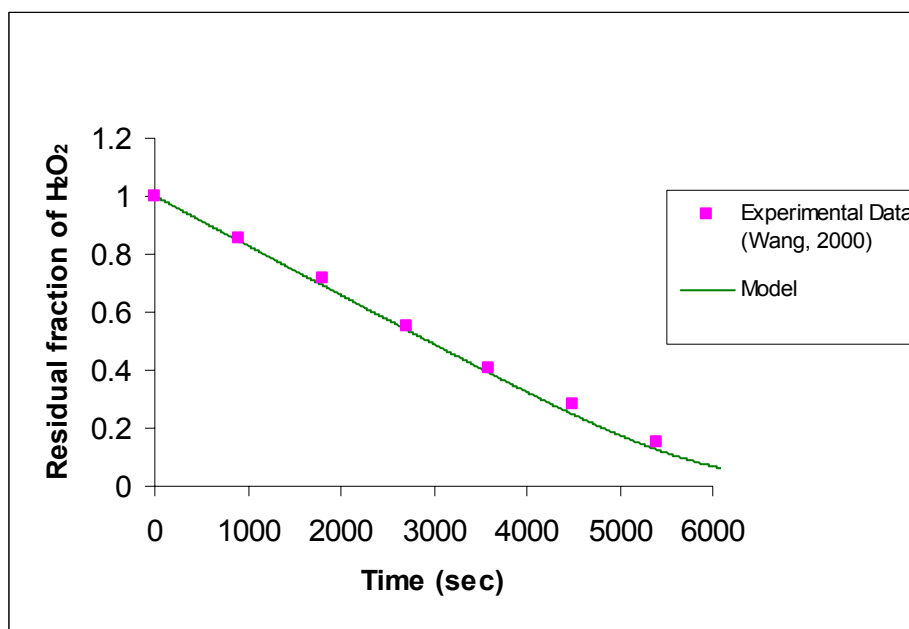
**Fig. 3.1.1:** Residual fraction of $H_2O_2$ vs. time. Initial concentration: $[H_2O_2]_o = 0.0294$ M, $[NPDOC]_o = 0$ mg $L^{-1}$, pH = 7
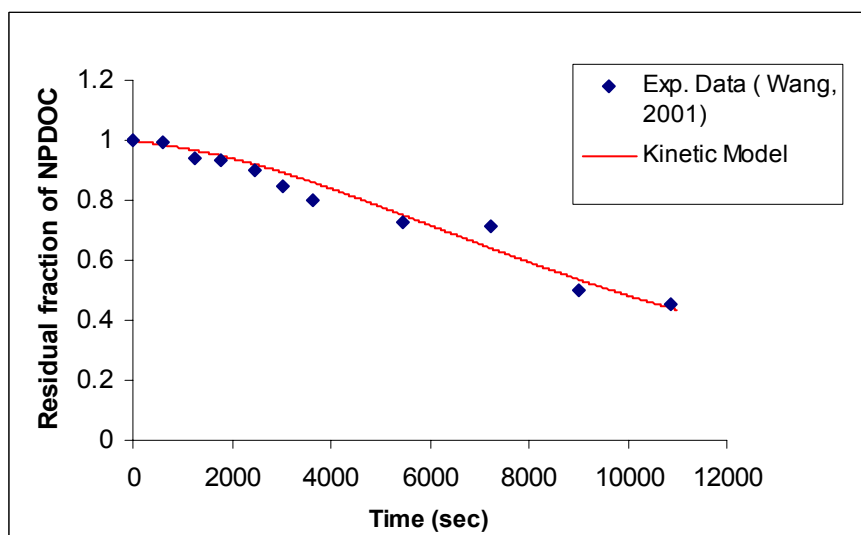


**Fig. 3.1.2-A:** Residual fraction of NPDOC vs. time. Initial concentration: $[H_2O_2]_o = 0.0$ M, $[NPDOC]_o = 6$ mg $L^{-1}$, pH = 7
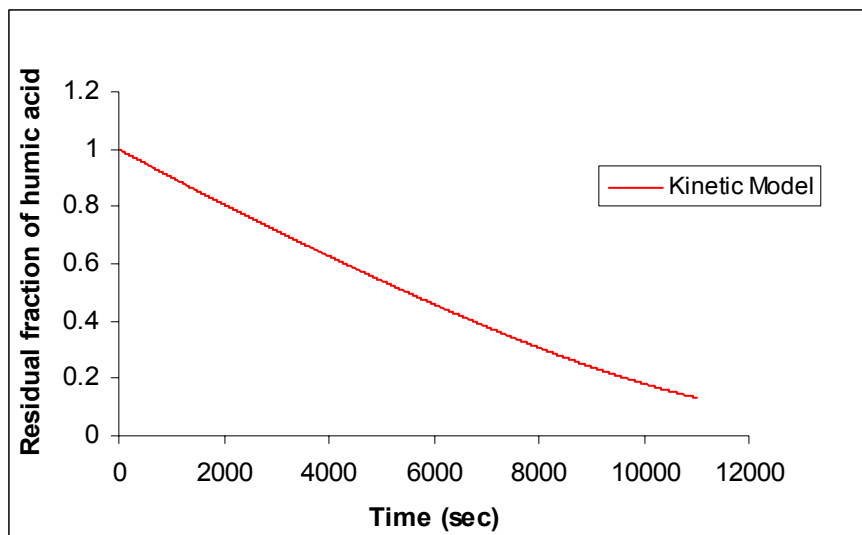
**Fig. 3.1.2-B:** Residual fraction of HA vs. time. Initial concentration: $[H_2O_2]_o = 0.0$ M, $[NPDOC]_o = 6$ mg $L^{-1}$, pH = 7

The reported NPDOC carbon was obtained from TOC analysis [Wang, 2000], and therefore it reflects the total amount of organic carbon remaining in the system. This would include remaining HA and the other intermediates from HA destruction by direct photolysis and through oxidation by $^\bullet OH$. Therefore, the reported residual NPDOC is a sum of all these compounds. HA concentration hence is reported in Figure 3.1.3-C.

The experimental [Wang, 2000] and predicted residual fraction of NPDOC with reaction time starting with 0.0882 M $H_2O_2$ and increasing initial NPDOC (HA) concentration from 3, 5, to 6 mg $L^{-1}$ is given in Figure 3.1.4-A. Residual fraction of $H_2O_2$ at the same experimental conditions is shown in Figure 3.1.4-B. On the other hand, predicted residual fraction of HA at the same conditions is reported in Figure 3.1.4-C.

Figures 3.1.5-A illustrates the residual fraction of NPDOC from experimental data [Wang, 2000] and model simulations by increasing initial NPDOC concentration from 3, 5, to 8 mg $L^{-1}$ starting with 0.147 M $H_2O_2$ for all NPDOC at pH value of 7. At the same initial conditions, the model predictions along with the experimental data are given in

206

Figure 3.1.5-B for residual fraction of $H_2O_2$. Predicted residual fraction of HA is given in Figure 3.1.5-C.
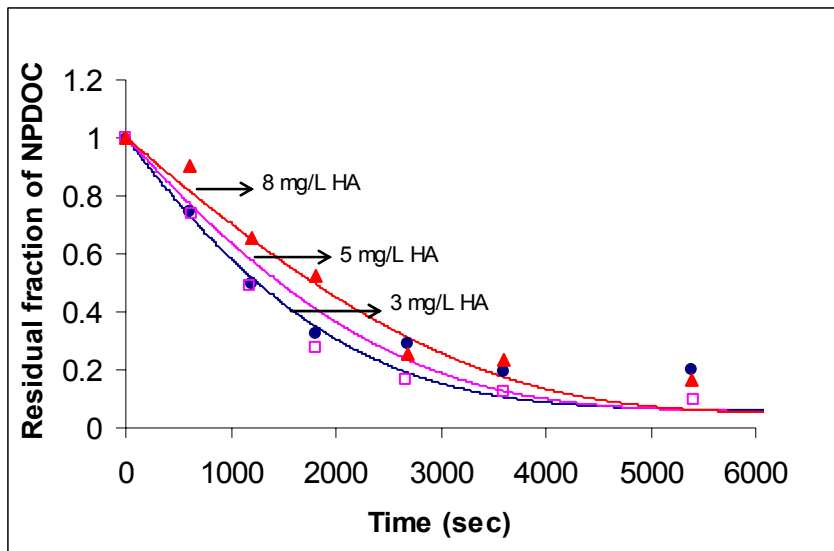


**Fig. 3.1.3-A:** Residual fraction of NPDOC vs. time at constant initial $H_2O_2$ concentration . Experimental Conditions [Wang, 2000]; ●: $[NPDOC]_o = 3$ mg $L^{-1}$, □: $[NPDOC]_o = 5$ mg $L^{-1}$, ▲: $[NPDOC]_o = 8$ mg $L^{-1}$, $[H_2O_2]_o = 0.0294$ M, pH = 7. Solid lines: Model prediction
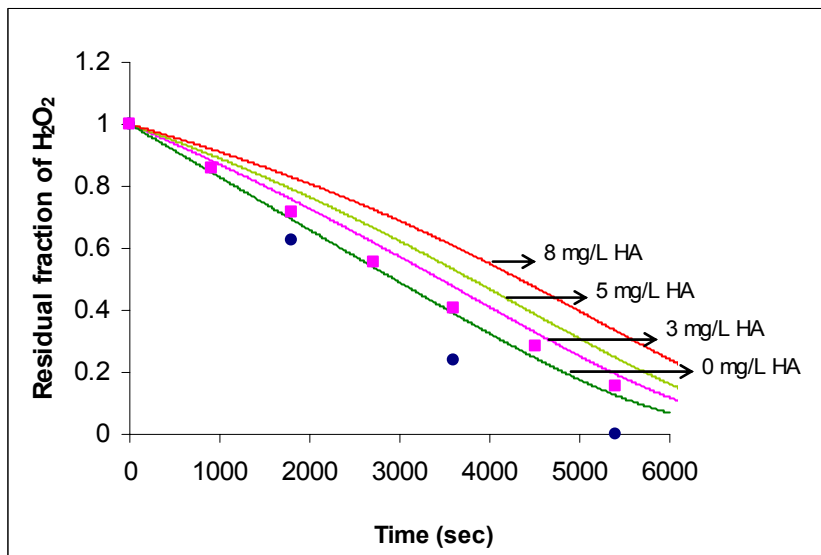


**Fig. 3.1.3-B:** Residual fraction of $H_2O_2$ vs. time at constant initial $H_2O_2$ concentration. Experimental Conditions [Wang, 2000]; ●: $[NPDOC]_o = 3$ mg $L^{-1}$, ■: $[NPDOC]_o = 0$ mg $L^{-1}$. $[H_2O_2]_o = 0.0294$ M, pH = 7. Solid lines: Model prediction
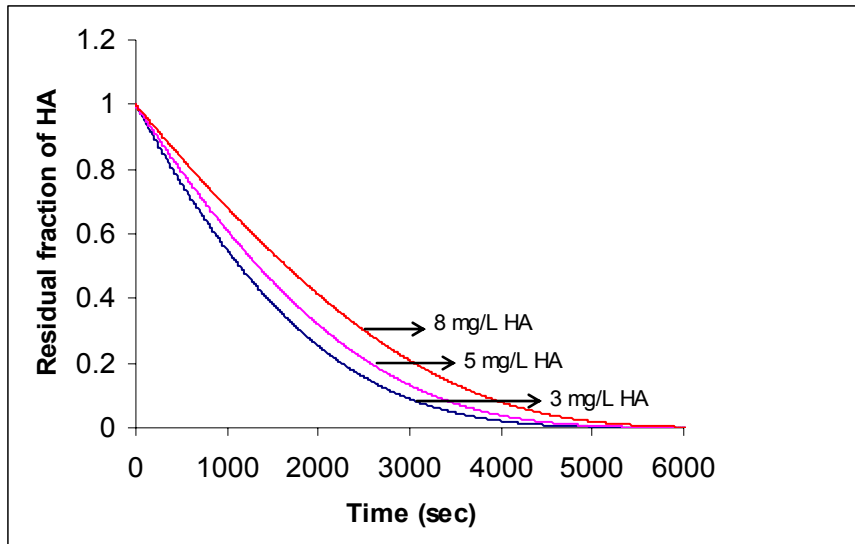
**Fig. 3.1.3-C:** Predicted residual fraction of HA vs. time at constant initial $H_2O_2$ concentration. Initial conditions; ▬: $[NPDOC]_o$ = 3 mg $L^{-1}$, ▬: $[NPDOC]_o$ = 5 mg $L^{-1}$, ▬: $[NPDOC]_o$ = 8 mg $L^{-1}$, $[H_2O_2]_o$ = 0.0294 M, pH = 7
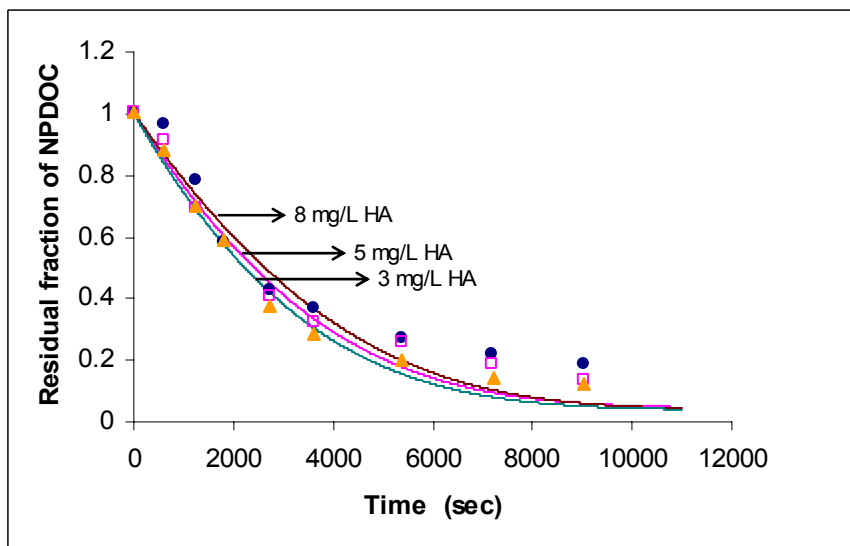


**Fig. 3.1.4-A:** Residual fraction of NPDOC vs. time at constant initial $H_2O_2$ concentration. Experimental conditions [Wang, 2000]; ●: $[NPDOC]_o$ = 3 mg $L^{-1}$, □: $[NPDOC]_o$ = 5 mg $L^{-1}$, ▲: $[NPDOC]_o$ = 8 mg $L^{-1}$, $[H_2O_2]_o$ = 0.0882 M, pH = 7. Solid lines: Model prediction
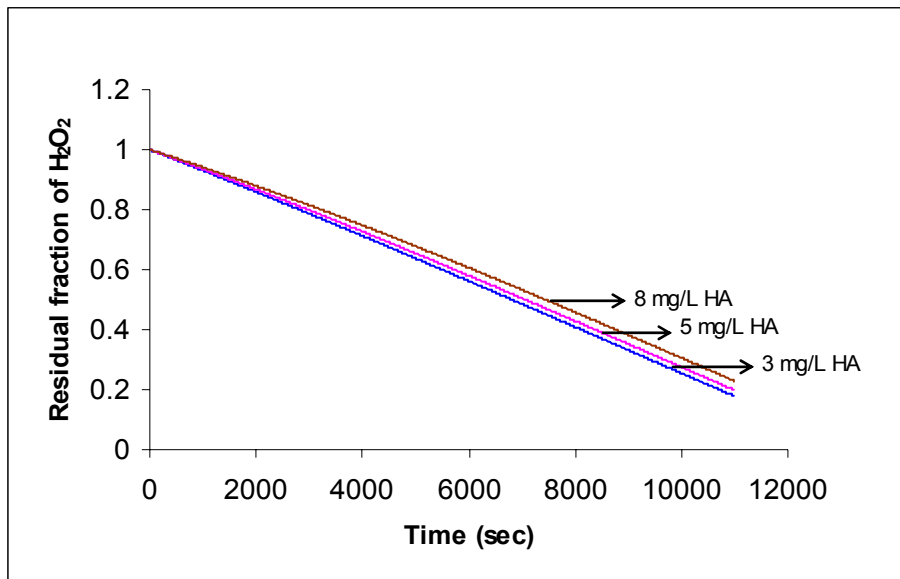
**Fig. 3.1.4-B:** Predicted residual fraction of $H_2O_2$ vs. time at constant initial $H_2O_2$ concentration. Initial concentration; —: $[NPDOC]_o = 3$ mg $L^{-1}$, —: $[NPDOC]_o = 5$ mg $L^{-1}$, —: $[NPDOC]_o = 8$ mg $L^{-1}$. $[H_2O_2]_o = 0.0882$ M, pH = 7
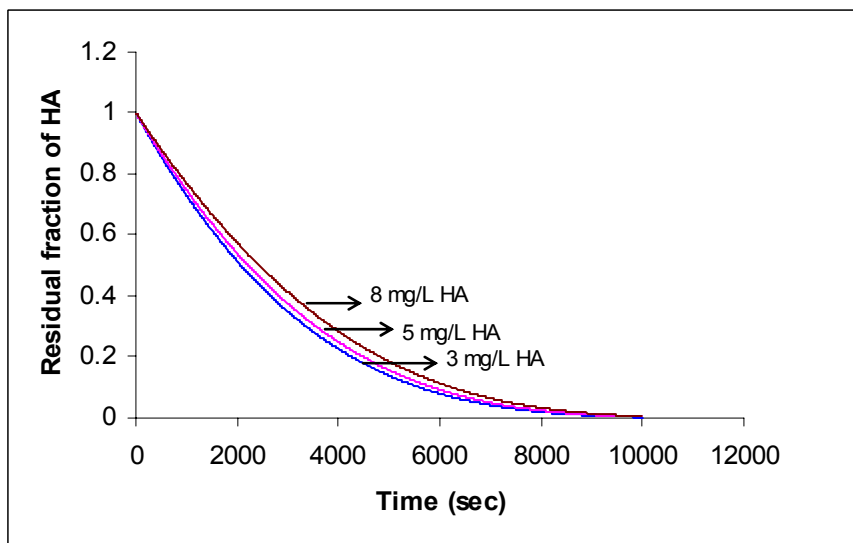


**Fig. 3.1.4-C:** Predicted residual fraction of HA vs. time at constant initial $H_2O_2$ concentration. Initial concentration; —: $[NPDOC]_o = 3$ mg $L^{-1}$, —: $[NPDOC]_o = 5$ mg $L^{-1}$, —: $[NPDOC]_o = 8$ mg $L^{-1}$, $[H_2O_2]_o = 0.0882$ M, pH = 7
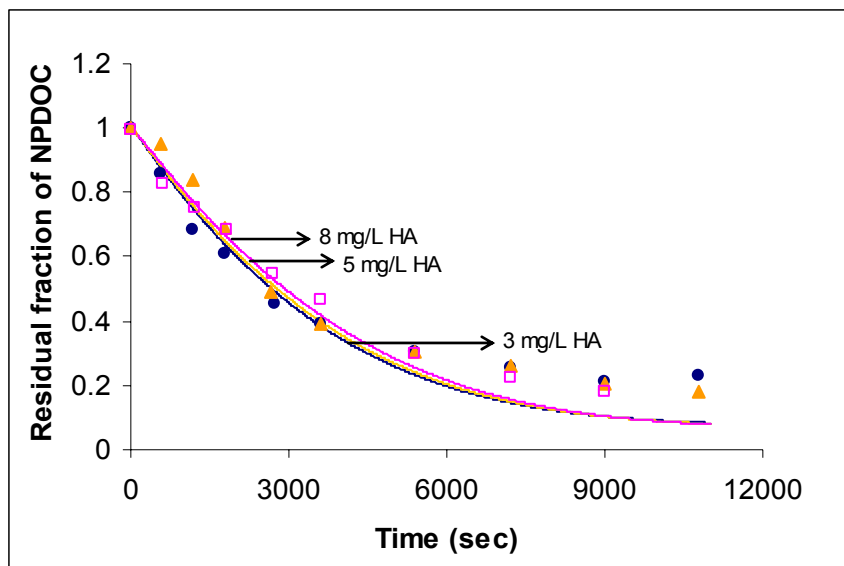
**Fig. 3.1.5-A:** Residual fraction of NPDOC vs. time at constant initial $H_2O_2$ concentration. Experimental conditions [Wang, 2000]; $\bullet$: $[NPDOC]_o = 3$ mg $L^{-1}$, $\blacktriangle$: $[NPDOC]_o = 5$ mg $L^{-1}$, $\square$: $[NPDOC]_o = 8$ mg $L^{-1}$, $[H_2O_2]_o = 0.147$ M, pH = 7. Solid lines: Model prediction
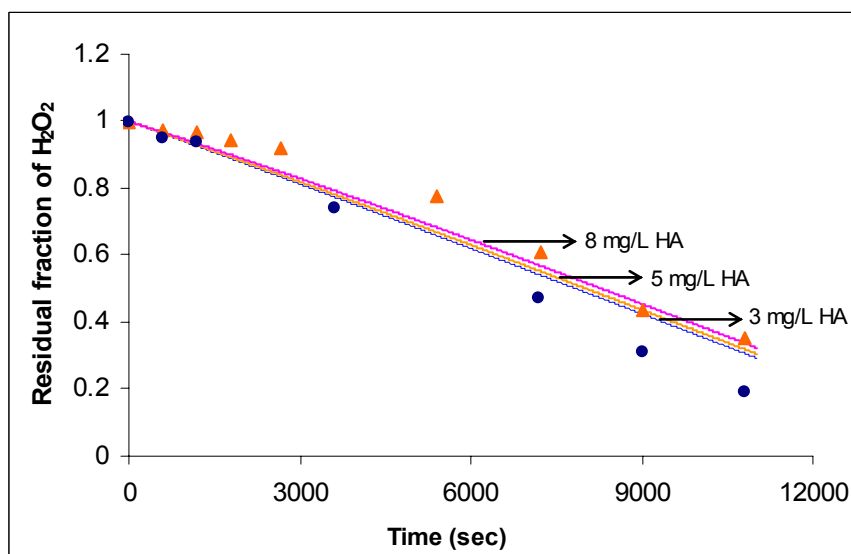


**Fig. 3.1.5-B:** Residual fraction of $H_2O_2$ vs. time at constant initial $H_2O_2$ concentration. Experimental conditions [Wang, 2000, 2001]; $\bullet$: $[NPDOC]_o = 3$ mg $L^{-1}$, $\blacktriangle$: $[NPDOC]_o = 5$ mg $L^{-1}$, $[H_2O_2]_o = 0.147$ M, pH = 7. Solid lines: Model prediction
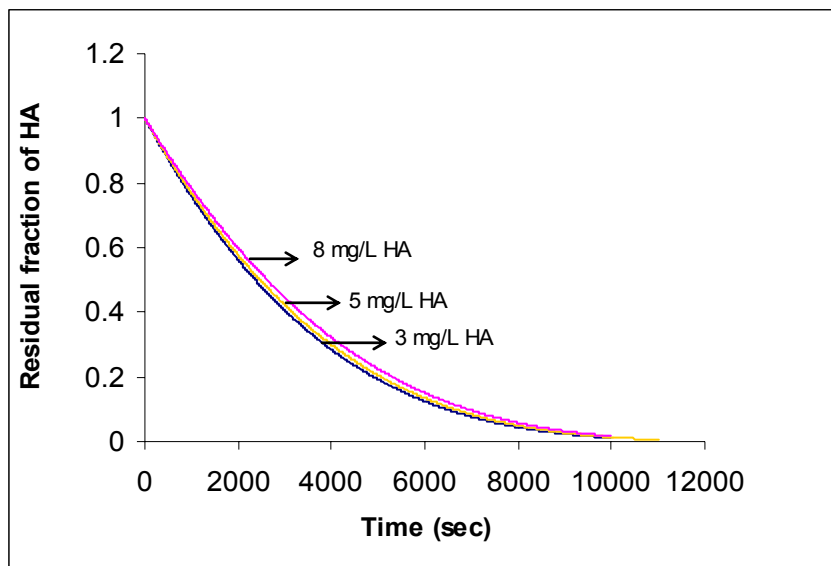
**Fig. 3.1.5-C:** Predicted residual fraction of HA vs. time at constant initial $H_2O_2$ concentration. Initial concentration; —: $[NPDOC]_o = 3$ mg $L^{-1}$, —: $[NPDOC]_o = 5$ mg $L^{-1}$, —: $[NPDOC]_o = 8$ mg $L^{-1}$, $[H_2O_2]_o = 0.147$ M, pH = 7

## 3.1.1. Effect of $H_2O_2$ concentration

The residual fraction of NPDOC from experimental data presented in Figures 3.1.3, 3.1.4, and 3.1.5 along with the model simulation is plotted again in figure 3.1.6-A, B, and C, to show the effect of initial $H_2O_2$ on residual fraction of NPDOC.
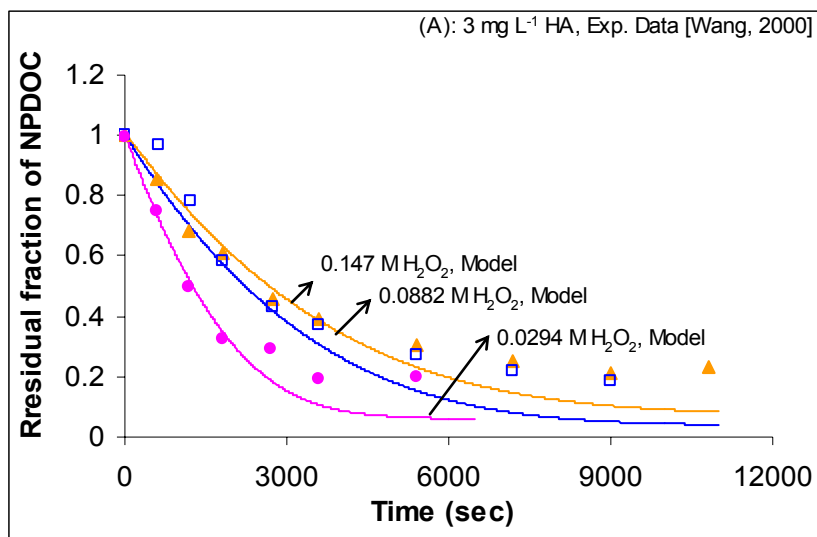


**Fig. 3.1.6-A:** Residual fraction of NPDOC from experiment vs. time at constant initial NPDOC concentration. Initial conditions; ●: $[H_2O_2]_o = 0.0294$ M, □: $[H_2O_2]_o = 0.0882$ M, ▲: $[H_2O_2]_o = 0.147$ M,. $[NPDOC]_o = 3$ mg L$^{-1}$, pH $= 7$
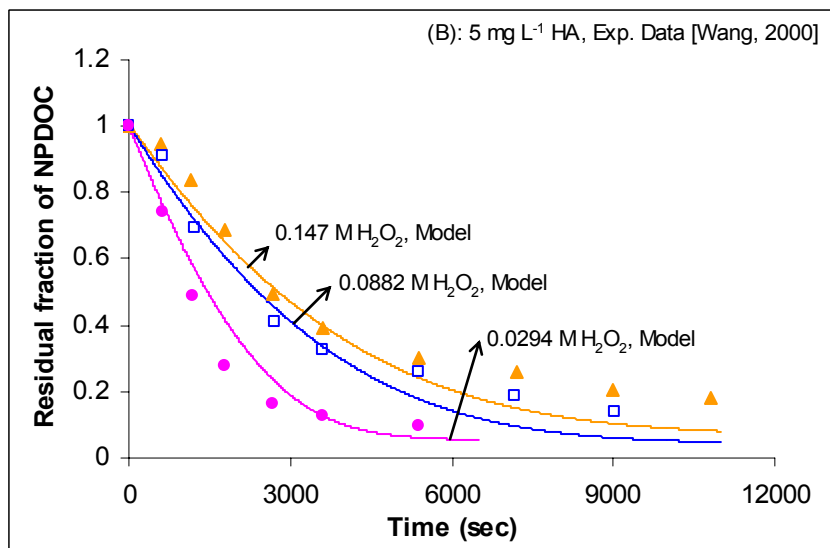


**Fig. 3.1.6-B:** Residual fraction of NPDOC from experiment vs. time at constant initial NPDOC concentration. Initial concentration; ●: $[H_2O_2]_o = 0.0294$ M, □: $[H_2O_2]_o = 0.0882$ M, ▲: $[H_2O_2]_o = 0.147$ M, $[NPDOC]_o = 5$ mg L$^{-1}$, pH $= 7$
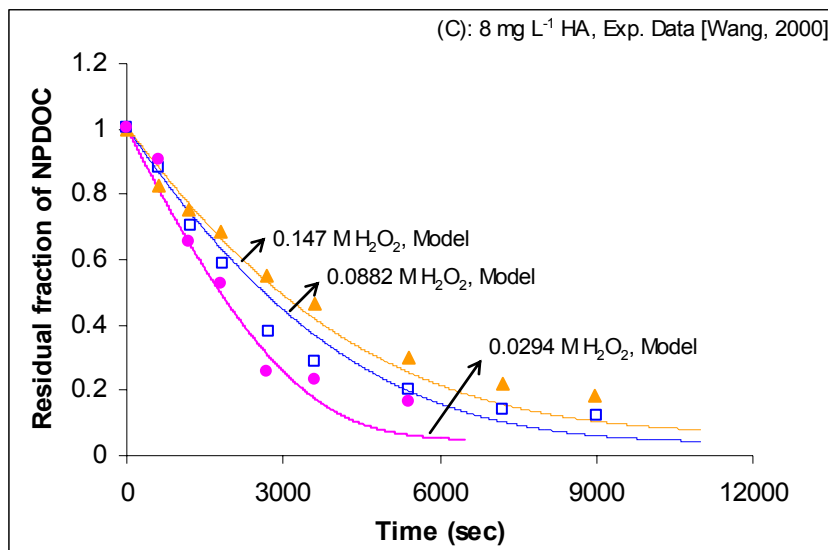
**Fig. 3.1.6-C:** Residual fraction of NPDOC from experiment vs. time at constant initial NPDOC concentration. Initial concentration; ●: $[H_2O_2]_o = 0.0294$ M, □: $[H_2O_2]_o = 0.0882$ M, ▲: $[H_2O_2]_o = 0.147$ M, $[NPDOC]_o = 8$ mg L$^{-1}$, pH = 7

Figure 3.1.7-A, B, C shows the residual $H_2O_2$ from model simulation. Each figure is at constant initial NPDOC and different initial $H_2O_2$ concentration. Finally, predicted residual fraction of humic acid the same conditions is presented in Figures 3.1.8-A, B, and C.
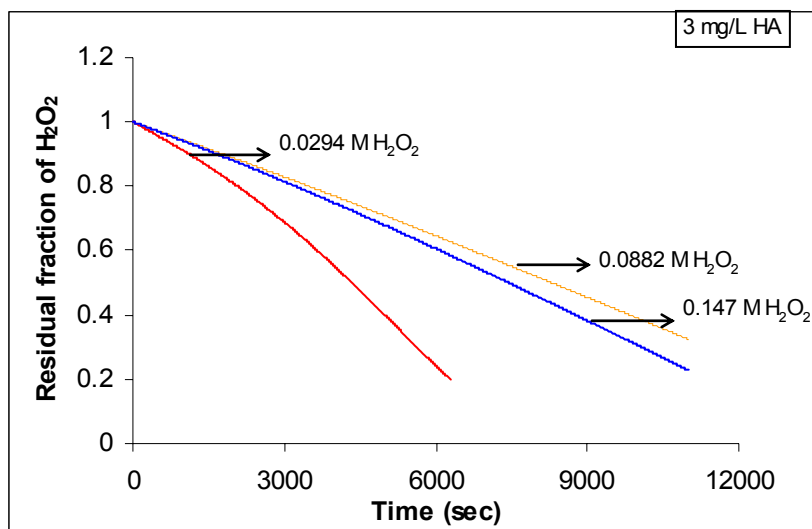
**Fig. 3.1.7-A:** Predicted residual fraction of $H_2O_2$ vs. time at constant initial concentration of NPDOC. Initial conditions; ▬: $[H_2O_2]_o = 0.147$ M, ▬: $[H_2O_2]_o = 0.0882$ M, ▬: $[H_2O_2]_o = 0.0294$ M, $[NPDOC]_o = 3$ mg $L^{-1}$, pH = 7
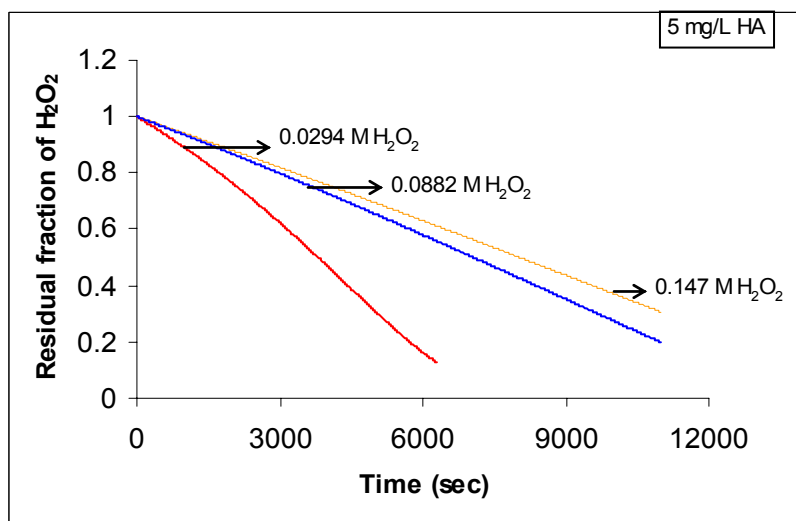


**Fig. 3.1.7-B:** Predicted residual fraction of $H_2O_2$ vs. time at constant initial concentration of NPDOC. Initial conditions; ▬: $[H_2O_2]_o = 0.147$ M, ▬: $[H_2O_2]_o = 0.0882$ M, ▬: $[H_2O_2]_o = 0.0294$ M, $[NPDOC]_o = 5$ mg $L^{-1}$, pH = 7
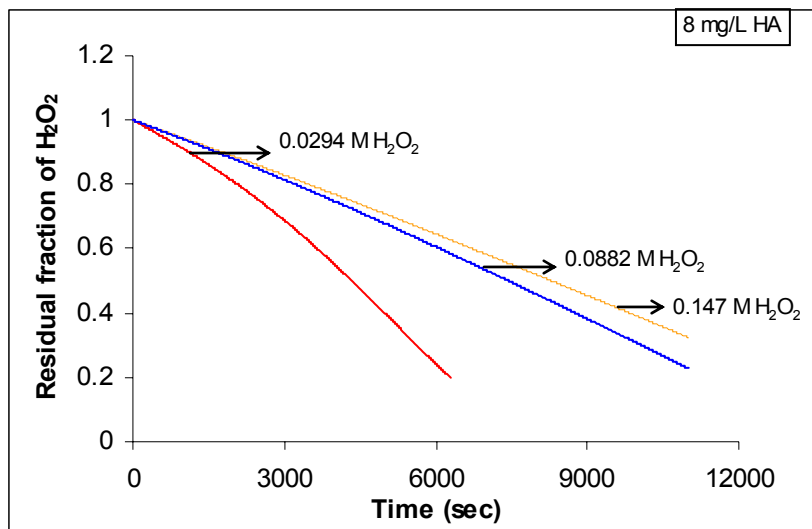
**Fig. 3.1.7-C:** Predicted residual fraction of $H_2O_2$ vs. time at constant initial concentration of HA. Initial conditions; ▬: $[H_2O_2]_o = 0.147$ M, ▬: $[H_2O_2]_o = 0.0882$ M, ▬: $[H_2O_2]_o = 0.0294$ M. $[NPDOC]_o = 8$ mg L$^{-1}$, pH = 7
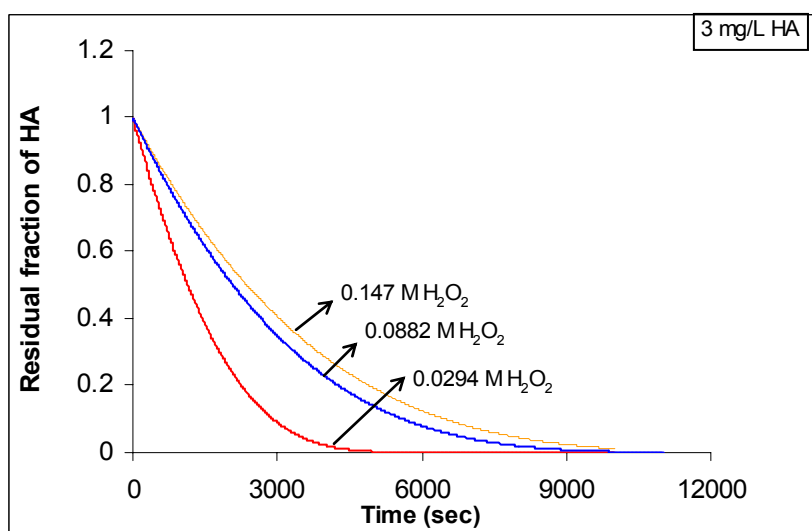


**Fig. 3.1.8-A:** Predicted residual fraction of HA vs. time at constant initial concentration of NPDOC. Initial conditions; ▬: $[H_2O_2]_o = 0.147$ M, ▬: $[H_2O_2]_o = 0.0882$ M, ▬: $[H_2O_2]_o = 0.0294$ M, $[NPDOC]_o = 3$ mg L$^{-1}$, pH = 7
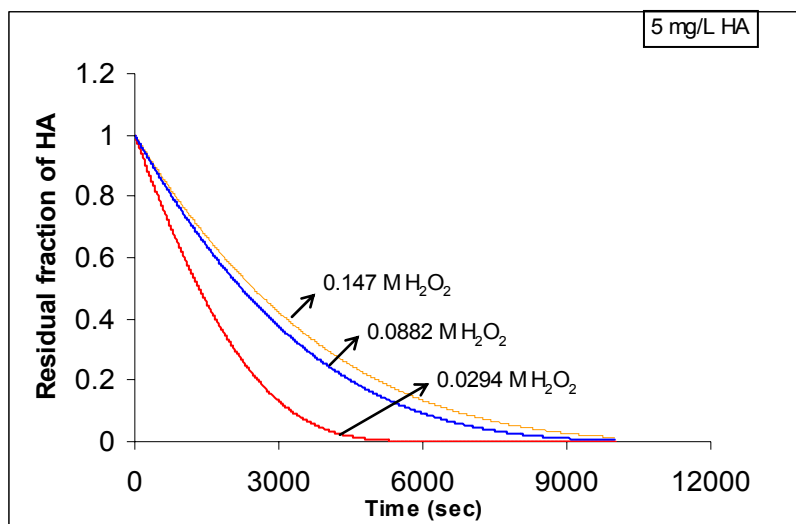
**Fig. 3.1.8-B:** Predicted residual fraction of HA vs. time at constant initial concentration of NPDOC. Initial concentration; ▬: $[H_2O_2]_o = 0.147$ M, ▬: $[H_2O_2]_o = 0.0882$ M, ▬: $[H_2O_2]_o = 0.0294$ M. $[NPDOC]_o = 5$ mg $L^{-1}$, pH = 7
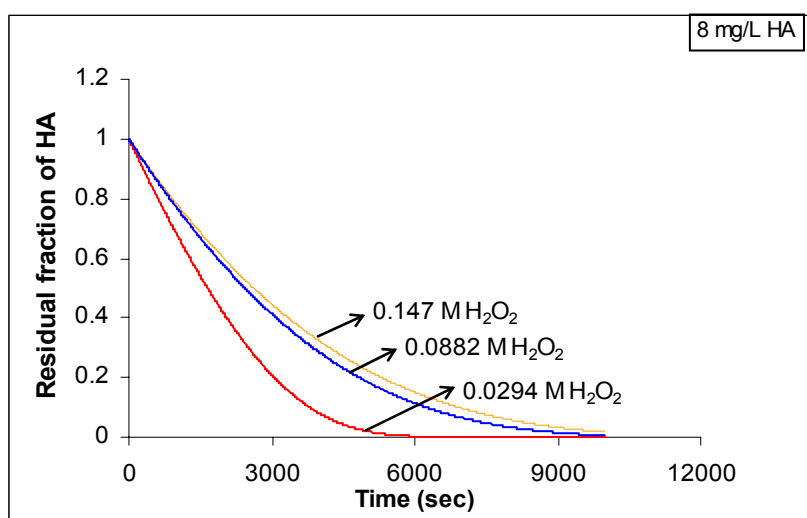


**Fig. 3.1.8-C:** Predicted residual fraction of HA vs. time at constant initial concentration of NPDOC. Initial concentration; ▬: $[H_2O_2]_o = 0.147$ M, ▬: $[H_2O_2]_o = 0.0882$ M, ▬: $[H_2O_2]_o = 0.0294$ M. $[NPDOC]_o = 8$ mg $L^{-1}$, pH = 7

## 3.2. Part II:  Simulation of the experimental data of Wang (2001)

This is the second part of the simulations that are done in this chapter. The kinetic

model developed in this chapter was used to simulate the experimental data given in

Figure 6 of Wang work (2001). Figure 6 [Wang, 2001] shows the effect of increasing

$H_2O_2$ concentration under constant concentration of nonpurgeable dissolved organic carbon (NPDOC) on the residual fraction of NPDOC and $H_2O_2$. Table 3.2.1 gives a brief summary of the experimental conditions and the corresponding fitted kinetic values in Part 1 of this chapter. $k_1$ is the rate constant of direct photolysis of hydrogen peroxide, $k_2$ is the rate constant for direct photolysis of humic acid, and $k_{20}$ is the rate constant for humic acid oxidation by $^{\bullet}OH$ radicals.

**Table 3.2.1:** Summary of the parameters used in simulating the work of Wang [Fig 6, 2000] in Part 1 of this chapter

| [H$_2$O$_2$] (M) | [HA] (mg/l) [M] | $k_1$ $10^{-6}$ (M s$^{-1}$) | $k_2$ $10^{-8}$ (M s$^{-1}$) | $k_{20}$ $10^{8}$ (M$^{-1}$ s$^{-1}$) | $k_{13'}$ (M$^{-1}$ s$^{-1}$) |
|---|---|---|---|---|---|
| 0 | (3,5,8) [0.0025, 0.004167,0.000557 | 2.5 | 2.5 | 1.0 | 2 |
| 0.0294(0.1%) | (3,5,8) [0.0025, 0.004167,0.000557 | 2.5 | 2.5 | 1.0 | 2 |
| 0.0882(0.3%) | (3,5,8) [0.0025, 0.004167,0.000557 | 3.4 | 2.5 | 1.0 | 0.3 |
| 0.147(0.5%) | (3,5,8) [0.0025, 0.004167,0.000557 | 4.8 | 2.5 | 1.0 | 0.06 |

As a first attempt for modeling the set of experimental data [Wang, 2001] the values of the fitting parameters which were obtained during simulating the data of Part 1 at 0.147 M $H_2O_2$ were used to reproduce the experimental data at 0.147 M $H_2O_2$ and 6 mg L$^{-1}$ NPDOC. Experimental conditions which were presented in Figure 6 [Wang, 2001] are summarized in Table 3.2.2. Also, this table gives the value of the fitting parameters that were used in the simulation. The experimental conditions in Table 3.2.2 are the ones which will be simulated in this part.

**Table 3.2.2:** Initial conditions in Figure 6 [Wang, 2001] and fitting parameters in the kinetic model

| [H$_2$O$_2$] (M) | [HA] (mg l$^{-1}$), [$10^{-3}$ M] | $k_1$ $10^{-6}$ (M s$^{-1}$) | $k_2$ $10^{-8}$ (M s$^{-1}$) | $k_{20}$ $10^{8}$ (M$^{-1}$ s$^{-1}$) | $k_{13'}$ (M$^{-1}$ s$^{-1}$) |
|---|---|---|---|---|---|
| 0 | 6, 5 | 2.5 | 2.5 | 1.0 | |
| 0.147 | 6, 5 | 4.8 | 2.5 | 1.0 | 0.06 |
| 0.178 | 6, 5 | 4.8 | 2.5 | 1.0 | 0.05 |
| 0.356 | 6, 5 | 4.8 | 2.5 | 1.0 | 0.02 |

The simulation results are given in the following figures. The model simulation for the case where no $H_2O_2$ was present with the solution of 6 mg $L^{-1}$ HA was presented in Part 1 of this chapter in Figure 3.1.2.

On the other hand, Figures 3.2.1-A and -B are showing the simulation results vs. experimental data for the residual fraction of NPDOC and hydrogen peroxide for the case where initial concentration of hydrogen peroxide is 0.147 M and that one of NPDOC is 6 mg $L^{-1}$.
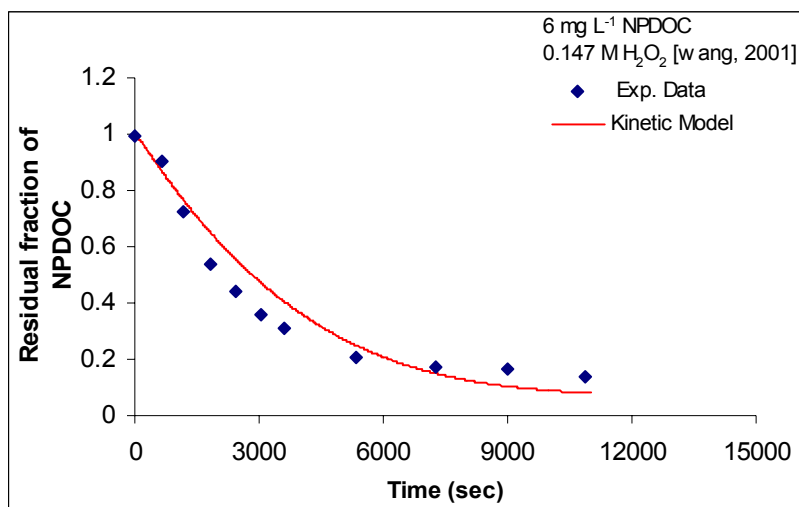


**Fig. 3.2.1-A:** Residual fraction of NPDOC vs. time. Initial concentration: $[H_2O_2]_o = 0.147$ M, $[NPDOC]_o = 6$ mg $L^{-1}$, pH = 7
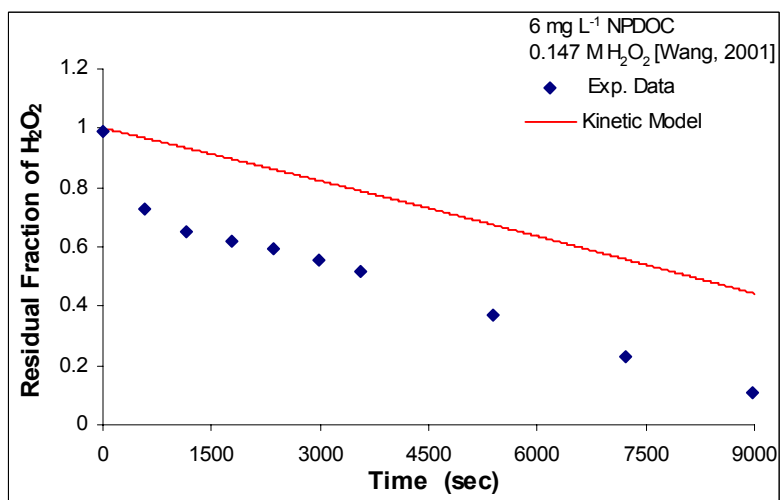


**Fig. 3.2.1-B:** Residual fraction of $H_2O_2$ vs. time. Initial conditions: $[H_2O_2]_o = 0.147$ M, $[NPDOC]_o = 6$ mg $L^{-1}$, pH = 7

218

The hydrogen peroxide concentration was increased to 0.178 M keeping NPDOC and pH at the same values as those for 0.147 M hydrogen peroxide. The results of simulation are shown in Figures 3.2.2-A, and B.
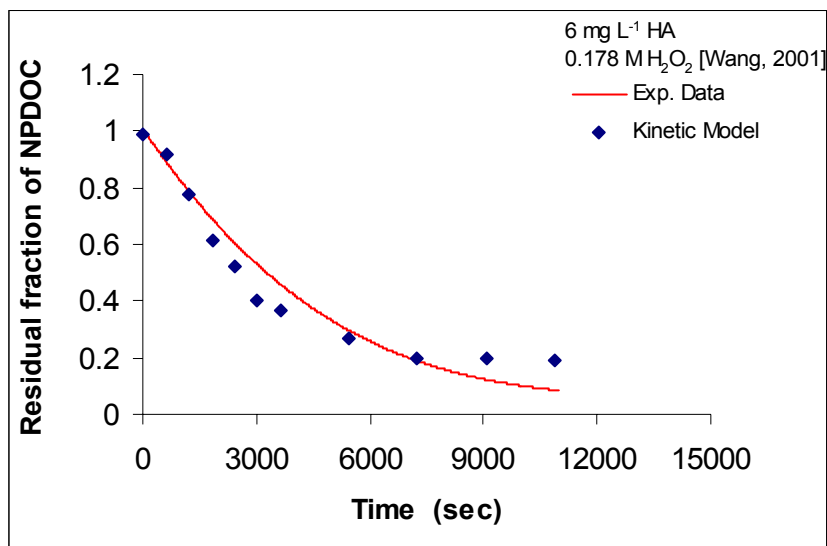


**Fig. 3.2.2-A:** Residual fraction of NPDOC vs. time. Initial conditions: $[H_2O_2]_o = 0.178$ M, $[NPDOC]_o = 6$ mg $L^{-1}$, pH = 7
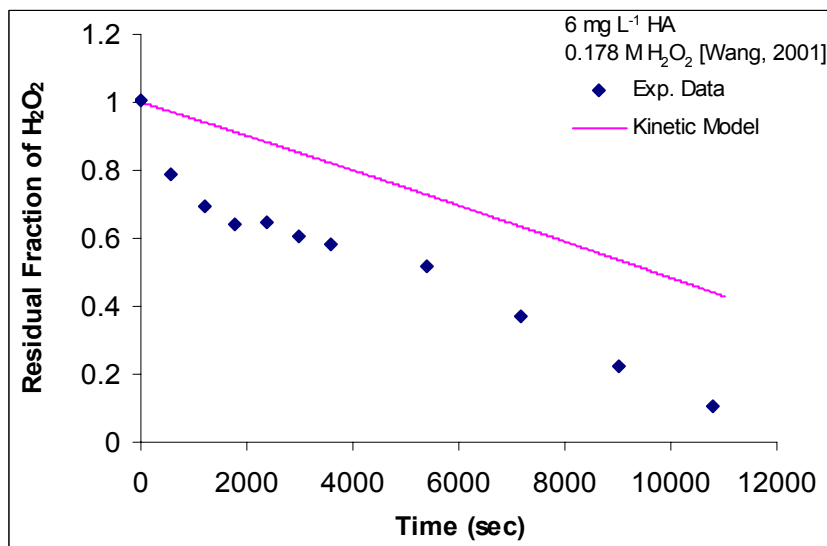


**Fig. 3.2.2-B:** Residual fraction of $H_2O_2$ vs. time. Initial conditions: $[H_2O_2]_o = 0.178$ M, $[NPDOC]_o = 6$ mg $L^{-1}$, pH = 7

After this the hydrogen peroxide concentration was increased to 0.356 M keeping NPDOC and pH at the same values as those for 0.147 M hydrogen peroxide. The results of simulation are shown in Figures 3.2.3-A, and B.
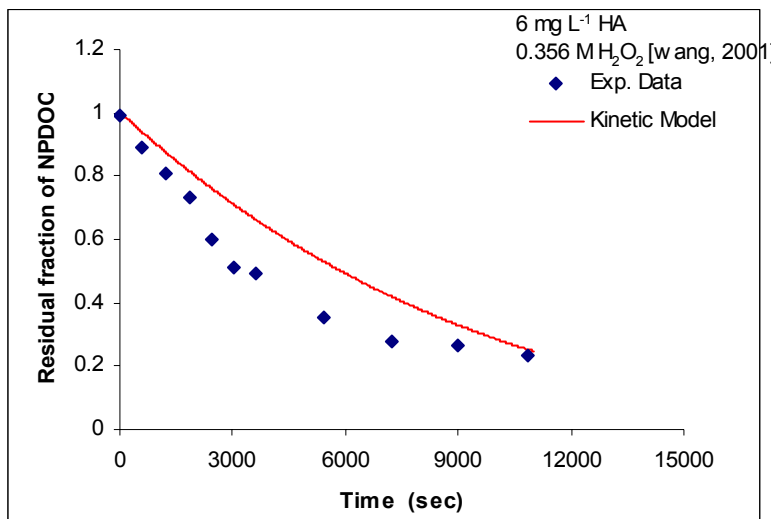


**Fig. 3.2.3-A:** Residual fraction of NPDOC vs. time. Initial conditions: $[H_2O_2]_o$= 0.356 M, $[NPDOC]_o$= 6 mg $L^{-1}$, pH= 7
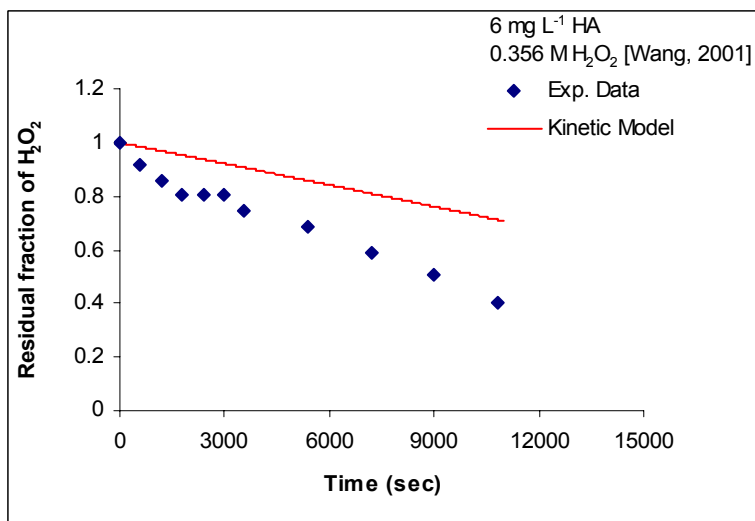


**Fig. 3.2.3-B:** Residual fraction of $H_2O_2$ vs. time. Initial conditions: $[H_2O_2]_o$ = 0.356 M, $[NPDOC]_o$ = 6 mg $L^{-1}$, pH = 7

The predicted residual fraction of NPDOC at the different initial concentrations of hydrogen peroxide is given in Figure 3.2.4-A. The corresponding predicted residual fraction of hydrogen peroxide at the same condition is given in Figure 3.2.4-C.

220
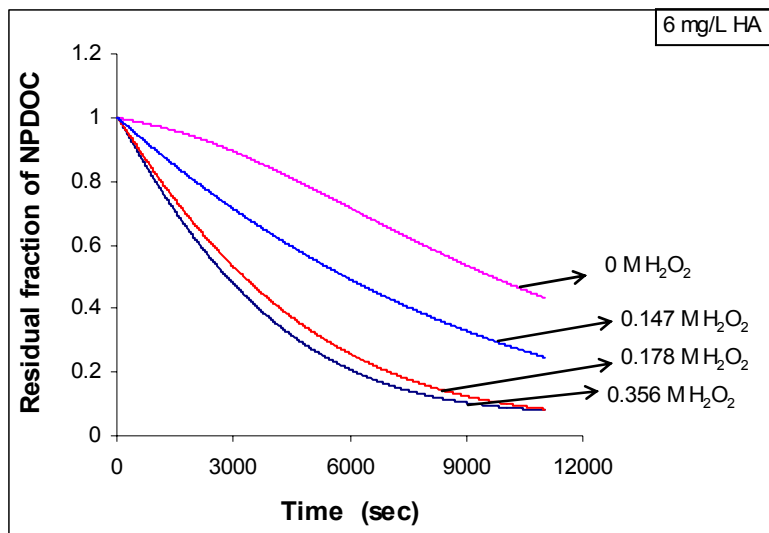
**Fig. 3.2.4-A:** Model prediction of residual fraction of NPDOC vs. time at different initial concentrations of $H_2O_2$ and constant initial NPDOC concentration. $[NPDOC]_o = 6$ mg $L^{-1}$, pH = 7
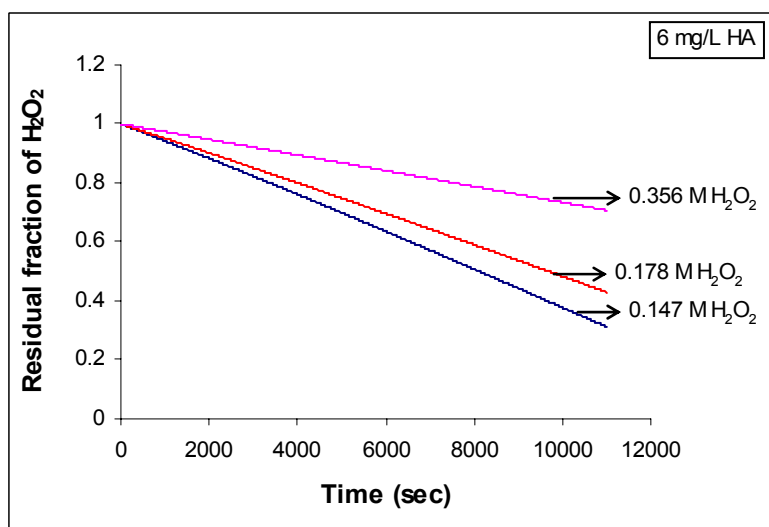


**Fig. 3.2.4-B:** Model prediction of residual fraction of NPDOC vs. time at different initial concentrations of $H_2O_2$ and constant initial NPDOC concentration. NPDOC = 6 mg $L^{-1}$, pH = 7

From the results presented in Figures 3.2.1 through 3.2.3 it can be seen that the fitted parameters in Table 3.2.2 were able to describe residual fraction of NPDOC while they overestimate the residual fraction of $H_2O_2$ for the cases where $[H_2O_2]$ initially is 0.147 and 0.178 M. When the concentration of $H_2O_2$ is 0.356 M, the residual fraction of NPDOC vs. time is also overestimated. However, the general trend which was observed earlier in part 1 of this chapter of retarding the degradation of NPDOC and hydrogen

peroxide as more hydrogen peroxide is used is also observed here as can be seen from Figures 3.2.4.-A and –B.

In simulating the data given by Wang (2000), part 1 of this chapter, when different initial concentrations of $H_2O_2$ were used we varied the value of the rate constant of $k_1$ in order to give a better fit of the model to the experimental data. For example, for 0.356 M $H_2O_2$, $k_1$ has been increased from 4.8 to 7.0 x$10^{-6}$ M sec$^{-1}$. The results are given in Figure 3.2.5. Although $k_1$ has been increased, the model was able to describe HA behavior in a better way than $H_2O_2$ behavior as the $H_2O_2$ residual is still overestimated as can be seen in Figures 3.2.5-A and –B.
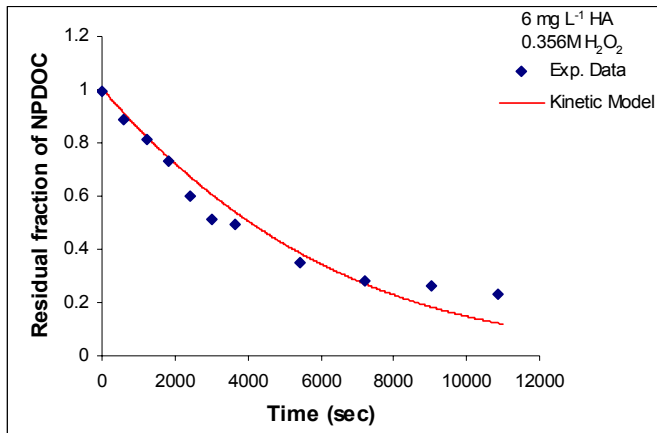


**Fig. 3.2.5-A:** Residual fraction of NPDOC vs. time. Initial concentration: $H_2O_2$ = 0.356 M, NPDOC = 6 mg L$^{-1}$, pH= 7
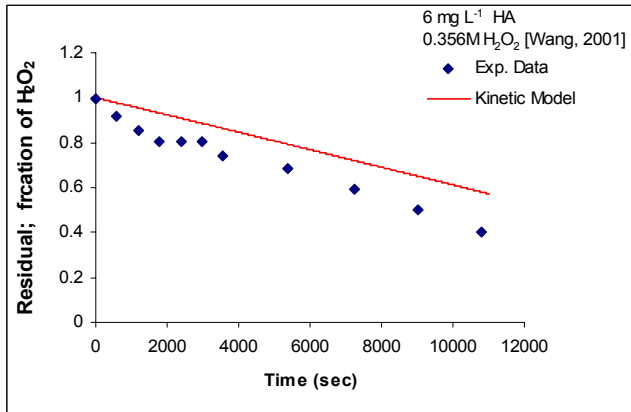


**Fig. 3.2.5-B:** Residual fraction of $H_2O_2$ vs. time. Initial concentration: $[H_2O_2]_o$ = 0.356 M, $[NPDOC]_o$ = 6 mg L$^{-1}$, pH = 7

Based on the above results we need to look into the experimental data reported by this group and try to find out the reason behind $H_2O_2$ behavior. In part 1 of this chapter, the simulation for the experimental data published by the same group [Wang, 2000], the proposed kinetic model was able to describe the system behavior using different initial concentrations of either HA and $H_2O_2$. As can be seen from Table 3.2.2 the initial conditions for the data in Figure 6 [Wang, 2001] are similar to the ones in Table 3.2.1 [Wang, 2000] except that HA is now 5 mg/L. Hence it is supposed that if similar conditions to those ones used in Table 3.2.1 are used again, the simulation should be close. However, by running the simulation for the new set of conditions in Table 3.2.2, the model could predict the experimental behavior of NPDOC while it overestimated that one of hydrogen peroxide.

This behavior raised a question, that is, why the model was able to describe the data by Wang (2000) and not able to describe the data by Wang (2001). In order to answer this question, we looked to the experimental data given by the same author in his two papers and put them in Figure 3.2.6.1.
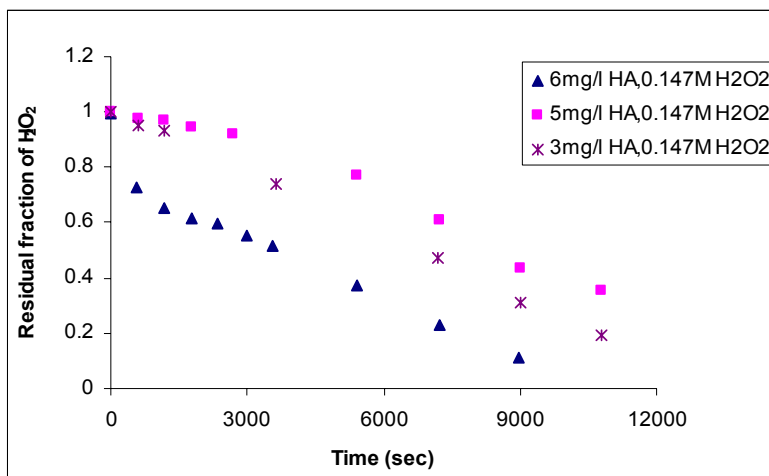


**Fig. 3.2.6.1:** Residual fraction of $H_2O_2$ vs. time at constant initial $H_2O_2$ concentration. Initial conditions; ▲: $[NPDOC]_o = 6$ mg $L^{-1}$ [Wang, 2001], ■: $[NPDOC]_o = 5$ mg $L^{-1}$ [Wang, 2000], ✳: $[NPDOC]_o = 3$ mg $L^{-1}$ [Wang, 2000], $[H_2O_2]_o = 0.147$ M, pH = 7

From Figure 3.2.6.1, it can be seen that increasing initial humic acid concentration at constant initial concentration led to a non systematic behavior. In one case it retarded $H_2O_2$ degradation (increasing from 3 to 5 mg/l) and in the other case it accelerated the degradation (increasing from 5 to 6 mg/l). At least from the kinetic simulation a retarding effect or a negligible effect would be expected by increasing HA from 5 to 6 mg/l as was seen in Figures 3.1.5-A and -B and other simulations in part 1 of this chapter. Earlier, in Part 1 of this chapter, we found that increasing HA from 3, 5 to 8 mg $L^{-1}$ didn't have a major effect on either residual $H_2O_2$ or HA at 0.0882 and 0.147 M $H_2O_2$ (Figures 3.1.4 and 3.1.5, Part 1). This would mean that the experimental data reported in Figure 3.2.6 at 6 mg/L HA and 0.147 M $H_2O_2$ should end up with a residual fraction of $H_2O_2$ that is either the same as or larger the one at 5 mg $L^{-1}$ HA and 0.147 M $H_2O_2$.

Till now the picture is not complete and to get on another clue we had to look to the whole data at 6 mg/l HA and different initial conditions of $H_2O_2$. Figure 3.2.6.2 summarizes the experimental data at these conditions. By looking carefully to Figure 3.2.6.2 it can seen that changes in experimental data with time lies within two regions:

1. 0<t<600 second

2. 600<t.

therefore, it seems that there is a step change between time zero and 600 sec, and this step change becomes less sharp as concentration is increased from 0.178 to 0.356 M of $H_2O_2$. At first, one might suspect a mechanism changes, but why didn't this mechanism change appear with other data of the same group at the other concentrations of HA (3, 5, 8 mg/L, Figure 3.1.5 part 1) at each change of $H_2O_2$ initial concentration.
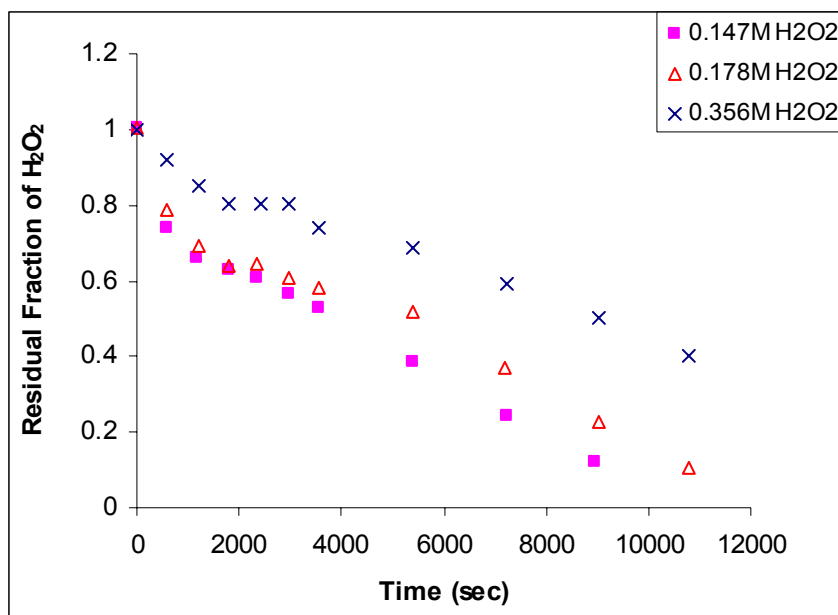
**Fig. 3.2.6.2:** Experimental residual fraction of $H_2O_2$ vs. time at constant initial NPDOC concentration and variable $H_2O_2$ concentration. Initial concentration; ■: $[H_2O_2]_o = 0.147$ M, Δ: $[H_2O_2]_o = 0.178$ M, ×: $[H_2O_2]_o = 0.356$ M, $[NPDOC]_o = 6$ mg L$^{-1}$, pH = 7. Experimental data from Wang (2001)

This leaves us with the other option that it might be something related to the way that $H_2O_2$ was measured in both papers and the concentration of $H_2O_2$ at the start of the experiment. For the data given by Wang (2000) the concentration of the hydrogen peroxide was determined by UV absorbance spectrometry at a wavelength of 260 nm ($UV_{260}$). For correction of the absorbance contributed from humic acid in the water, the $UV_{260}$ from humic acids was deducted from the total absorbance. On the other hand, for the data given by Wang (2001) the concentration of $H_2O_2$ was determined by UV absorbance spectrometry without making correction for the absorbance contributed from HA and it was assumed that this correction is negligible and this was proved by measuring $H_2O_2$ using analytical method and good agreement was obtained. The statement that no correction for HA absorbance might be due to the high initial concentration of $H_2O_2$ compared to HA acid (0.147, 0.178, and 0.356 M $H_2O_2$ compared to 0.0005 M HA initially) therefore the presence of humic acid won't make great

225

influence on absorbance of hydrogen peroxide and this behavior of residual fraction of hydrogen peroxide might not due to this reason. Therefore, if the experimental data in Figure 3.2.6.2 is corrected the model might be able to predict this data in a better way. The procedure for this correction is summarized in the following steps:

1. The experimental data in Figure 3.2..6.2 at 5 mg/l HA and 0.147, 0.178, and 0.356 M $H_2O_2$ will be extrapolated to time zero after excluding the first data point at time zero in order to obtain the actual initial concentration of $H_2O_2$.

2. Two types of fitting; linear and $2^{nd}$ order polynomial were used to extrapolate the data to time 0. No significant difference was seen between the two fittings (Figures 3.2.6.3, and 3.2.6.4). Therefore the residual $H_2O_2$ will be taken from Figure 3.2.6.3.
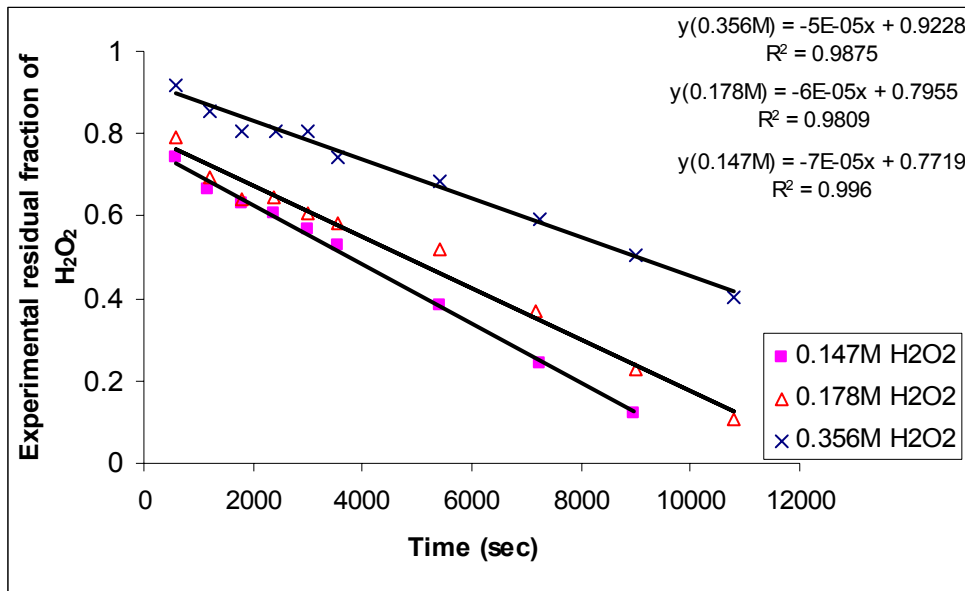


**Fig. 3.2.6.3:** Experimental residual fraction of $H_2O_2$ vs. time [Wang, 2001] at constant initial NPDOC concentration and variable $H_2O_2$ concentration. Initial concentration; ■: $H_2O_2 = 0.147$ M, △: $H_2O_2 = 0.178$ M, ×: $H_2O_2 = 0.356$ M, NPDOC = 6 mg $L^{-1}$, pH = 7. $1^{st}$ order fitting

226

3. The $1^{st}$ order fitting of the experimental data in Figure 3.2.6.3 was extrapolated to time zero and the intersection of the fitting curve with time zero was taken as the initial residual $H_2O_2$

The corrected initial $H_2O_2$ concentration was obtained by multiplying column 1 (reported initial $H_2O_2$) by column 2 (Residual $H_2O_2$ based on extrapolating to zero) in Table 3.2.3.

**Table 3.2. 3:** Corrected initial $H_2O_2$ concentration

| [$H_2O_2$] initial conc. as reported by the author (M) | Residual $H_2O_2$ based on extrapolating to zero | [$H_2O_2$] initial conc. After correction. (M) |
|---|---|---|
| 0.147 | 0.7719 | 0.113469 |
| 0.178 | 0.7955 | 0.141599 |
| 0.356 | 0.9228 | 0.328517 |
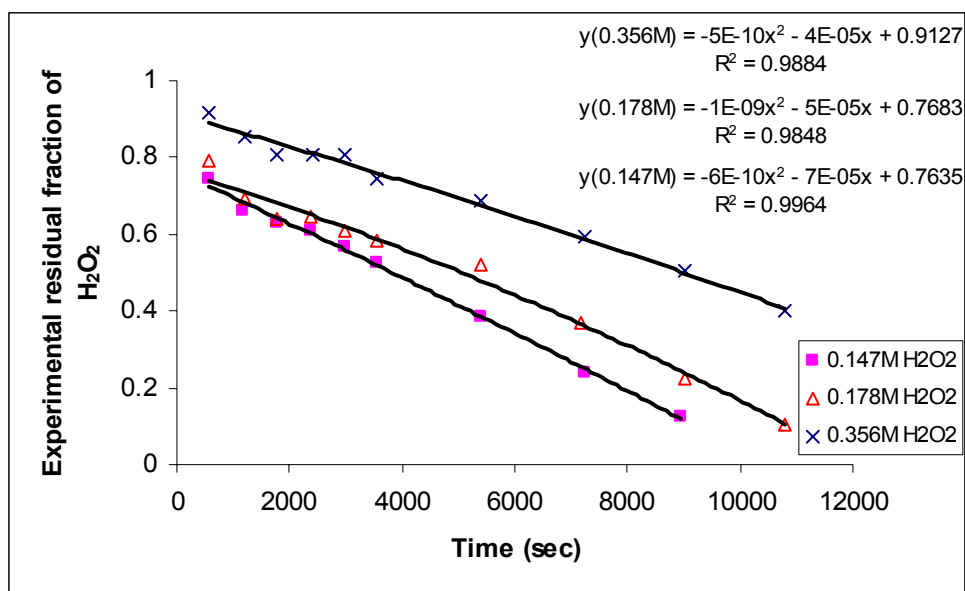


**Fig. 3.2.6.4:** Experimental residual fraction of $H_2O_2$ vs. time [Wang, 2001] at constant initial NPDOC concentration and variable $H_2O_2$ concentration. Initial concentration; ■: $H_2O_2$ = 0.147 M, △: $H_2O_2$ = 0.178 M, ×: $H_2O_2$ = 0.356 M, NPDOC = 6 mg L$^{-1}$, pH= 7. $2^{nd}$ order fitting

4. The new initial concentration of hydrogen peroxide was used for running the simulation.

227

5. After that the experimental data at each concentration were corrected by dividing the reported concentration by the new initial corrected concentration and hence corrected residual $H_2O_2$ was obtained.

Table 3.2.4 summarizes the new initial concentration of hydrogen peroxide with the corresponding rate constants that are used while running the kinetic model to simulate the corrected experimental data.

**Table 3.2.4:** Initial concentrations and fitting parameters values at pH = 7

| $[H_2O_2]$ corrected and used in simulation(M) | $[H_2O_2]$ old (M) | [HA] (mg $l^{-1}$) | $k_1$ $10^{-6}$ (M s$^{-1}$) | $k_2$ $10^{-8}$ (M s$^{-1}$) | $k_{20}$ $10^8$ (M$^{-1}$ s$^{-1}$) |
|---|---|---|---|---|---|
| 0.113469 | 0.147 | 6 | 5.5 | 2.5 | 1.0 |
| 0.141599 | 0.178 | 6 | 5.7 | 2.5 | 1.0 |
| 0.328517 | 0.356 | 6 | 8.3 | 2.5 | 1.0 |

Figures 3.2.7-A, -B, and –C give the residual fraction of hydrogen peroxide from kinetic model and experimental data before and after applying the correction. From these figures it can be seen that now the corrected experimental data matches well with the model simulation. After 6000 seconds, reported experimental data, corrected experimental data, and model simulation are very close.

Figure 3.2.8-A and B gives the residual fraction of NPDOC and hydrogen peroxide, respectively, from the kinetic model simulation using the corrected initial hydrogen peroxide along with the corrected experimental data. No correction was applied to the residual fraction of NPDOC.

228
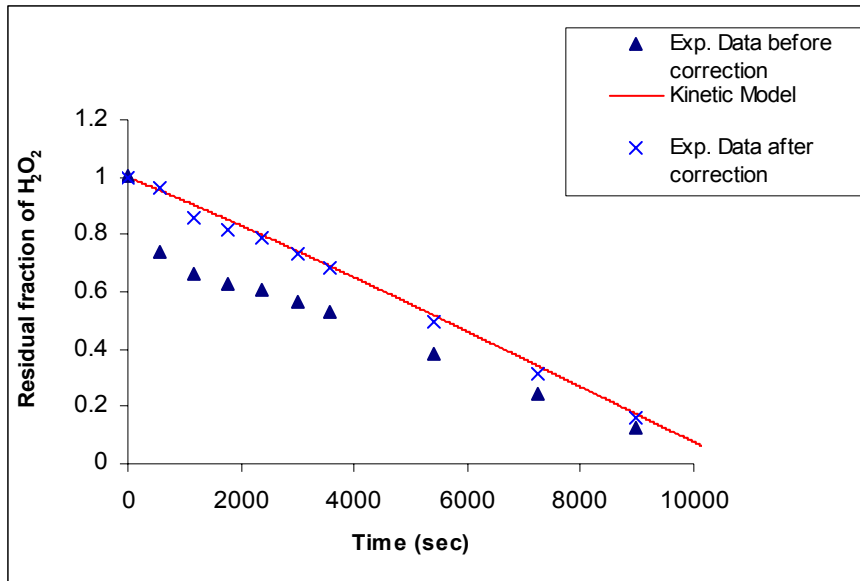
**Fig. 3.2.7-A:** Residual fraction of $H_2O_2$ vs. time. Initial concentration: NPDOC = 6 mg $L^{-1}$; ▲ : $H_2O_2$ = 0.147 M, ×: $H_2O_2$ = 0.113 M, — $H_2O_2$= 0.113 M, pH= 7. Experimental data of Wang [2001]
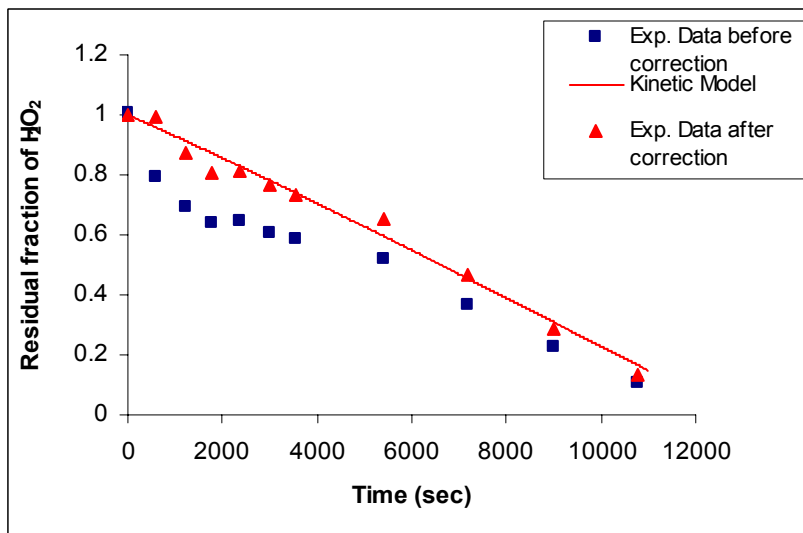


**Fig. 3.2.7-B:** Residual fraction of $H_2O_2$ vs. time. Initial concentration: NPDOC= 6 mg $L^{-1}$; ■: $H_2O_2$= 0.178 M, ▲: $H_2O_2$= 0.142 M, — $H_2O_2$= 0.142 M, pH= 7
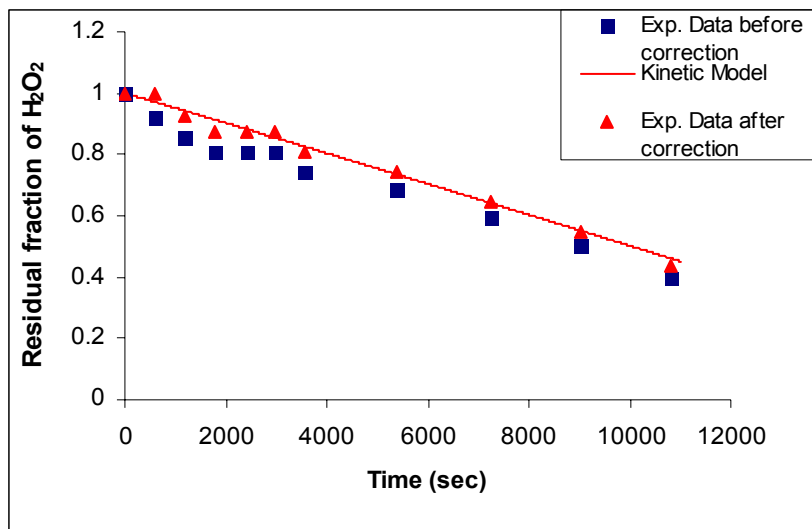
**Fig. 3.2.7-C:** Residual fraction of $H_2O_2$ vs. time. Initial concentration: NPDOC = 6 mg $L^{-1}$; ■: $H_2O_2$ = 0.356 M, ▲: $H_2O_2$ = 0.329 M, — $H_2O_2$ = 0.329 M, pH= 7
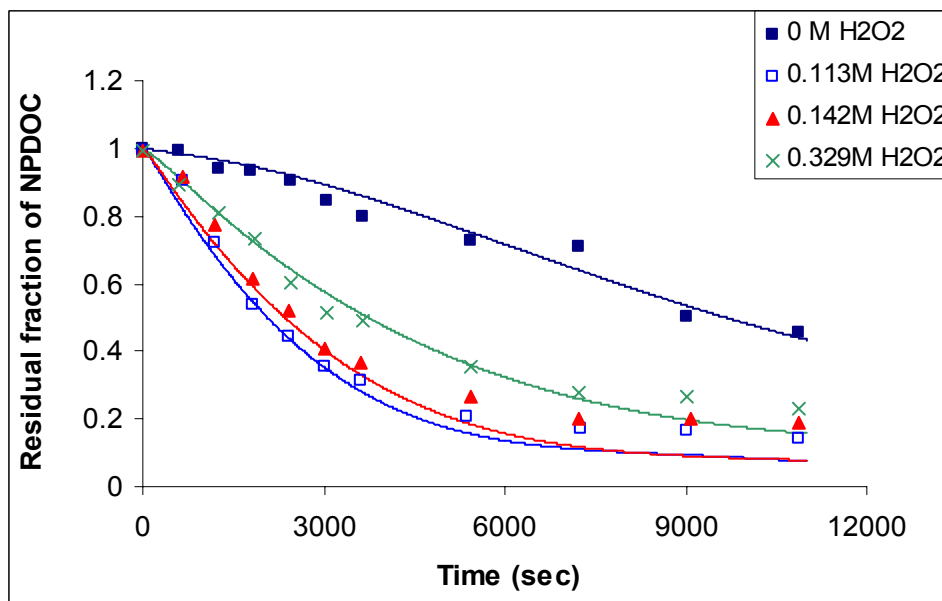


**Fig. 3.2.8-A:** Residual fraction of NPDOC vs. time at constant initial NPDOC concentration and variable $H_2O_2$ concentration. Initial concentration; □, —: $H_2O_2$ = 0.113 M, ▲, —: $H_2O_2$ = 0.142 M, ×, —: $H_2O_2$ = 0.329 M, ■, —: $H_2O_2$ = 0.0 M, NPDOC = 6 mg $L^{-1}$, pH= 7. Solid lines kinetic model simulation with corrected data
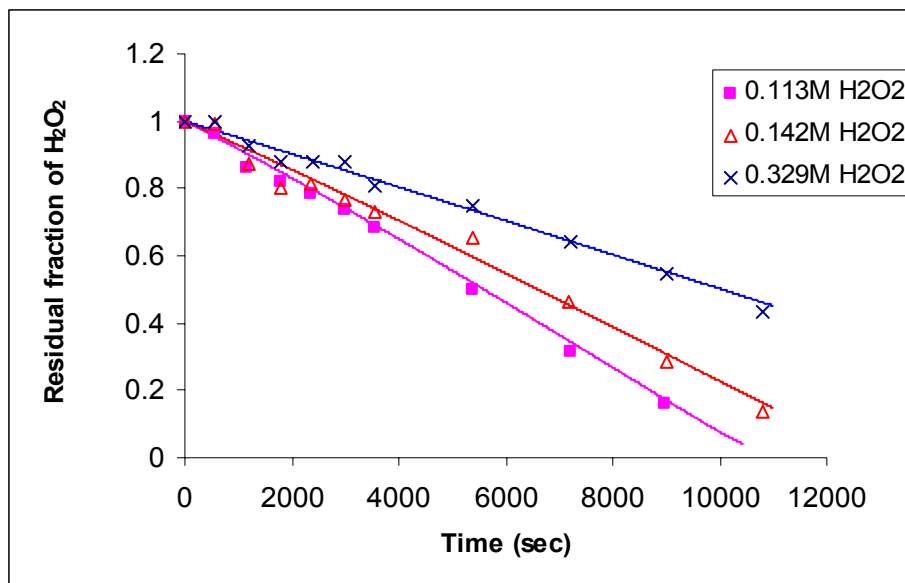
**Fig. 3.2.8-B:** Residual fraction of $H_2O_2$ vs. time at constant initial NPDOC concentration and variable $H_2O_2$ concentration. Initial concentration; ■, —: $H_2O_2$ = 0.113 M, Δ, —: $H_2O_2$ = 0.142 M, ×, —: $H_2O_2$ = 0.329 M, NPDOC = 6 mg $L^{-1}$, pH= 7. Solid lines kinetic model simulation with corrected data

## 4.1. Discussion on Part I Results

From Figure 3.1.1 it can be seen that $H_2O_2$ can be destroyed by direct UV light and this phenomenon was investigated earlier by many workers [Baxendale, 1957; Weeks, 1955; Daniton, 1955; Guittonneau, 1990; Vollman, 1959; Hunt, 1952; Glaze, 1995; Bielski, 1977]. The kinetic model with the rate constants along with the equilibrium constants obtained from literatures, which were given in Table 2.1, and the fitting parameter described in the kinetic model section was applied to the experimental data of Wang (2000). A value of $k_1$ equal to 2.5 x $10^{-6}$ $M^{-1}$ $sec^{-1}$ a long with $k_{20}$= 1.0 x$10^8$ $M^{-1}$ $sec^{-1}$ selected from the range reported in literature [Westerhoff , 1996, 1999; Brezoink, 1998; Zepp, 1987 b; Goldstone, 2002, Liao, 1995] gave the best fitting based on least square error analysis. Based on our simulation, the values of the rate constants for the reaction of $I_3$ and $I_4$ with $^•OH$ radicals ($k_{I3}$ and $k_{I4}$ ) were 3 x $10^8$ and 1 x $10^7$ $M^{-1}$ $s^{-1}$, respectively. The assumed values for the rate constants for the reactions of the

proposed byproducts of HA reactions in this kinetic model with $^\bullet$OH radicals, and obtained from best fitting, were close to the rate constants for the reactions of formic acid, acetic acid, malonic acid, and oxalic acid with $^\bullet$OH radicals ($1.3 \times 10^8$, $1.6 \times 10^7$, $1.6 \times 10^7$, and $1.4 \times 10^6$ $M^{-1}$ $s^{-1}$, respectively) which were obtained from a study of humic matter photolysis by Goldstone (2002). The other fitting parameter $k_{I1}$ and $k_{I5}$ were 5 and 10 $M^{-1}$ $s^{-1}$, respectively.

The kinetic model with same above rate constants, either reported from literature or fitted ones, was applied to the direct photolysis of HA by UV light in the absence of hydrogen peroxide. The results of simulation for pure HA by UV is shown in Figure 3.1.2-A and –B. The fitting parameter was $k_2$. A value of $k_2$ equals to $2.5 \times 10^{-8}$ $M$ $sec^{-1}$ gave the best fit. Assuming that the light intensity was the same in both cases, since it is the same UV source, then the only reason that $k_1$ and $k_2$ are different is the quantum yield value. The estimated value of the light intensity ($I_o$) based on $k_1$ and quantum yield of hydrogen peroxide lies within the range that other workers measured for their UV sources [Daniton, 1953; Baxendale, 1957; Liao, 1995; Glaze, 1995; Hunt, 1952]. Therefore the obtained value of $k_1$ is realistic. On the other hand, estimation of the quantum yield of humic acid based on $k_1$, $k_2$, and $I_o$ is close to the one estimated by Zepp (1987a, 1987b) and Aguer (1999). Therefore, the value of $k_2$ is realistic.

The reason that we have a separate plot for HA in Figure 3.1.2-B from NPDOC in Figure 3.1.2-A is that initially the reaction mixture contained only HA and therefore HA is equal to NPDOC. However, as the reaction takes place HA will be destroyed by direct photolysis and the destruction will lead in part to new organic molecules and carbon dioxide. TOC analysis is measuring the carbon which is present in the mixture and is not

volatile, therefore the reported NPDOC will be the sum of HA and all other reactions intermediates and by products which are not volatile. The model was built in such a way to consider this and to calculate the concentration of these molecules and hence to obtain the overall NPDOC.

Figures 3.1.3-A, 3.1.4-A, and 3.1.5-A show the model predictions for the residual fraction of NPDOC vs. time by increasing $H_2O_2$ concentration from 0.0294 to 0.147 M. The fitting parameter $k_2$ was at the same value which was obtained for pure solution of HA. However, using a value of $k_1$ that is equal to the one obtained from pure solution of $H_2O_2$ described the general behavior of the experimental data but was not able to describe the exact behavior. What is meant by the general behavior is the retarding effect of $H_2O_2$ on the residual fraction of NPDOC and $H_2O_2$ as its initial concentration was increased. In order to fit the data, $k_1$ value was changed and table 4.1.1 summarizes the optimized value (based on least square error analysis) at each condition.

Table 4.1.1: Summary of fitting parameters with different initial $H_2O_2$ concentration.

| [H2O2] M | [NPDOC] mg L$^{-1}$ | $k_1$ M$^{-1}$ s$^{-1}$ | $k_2$ M$^{-1}$ s$^{-1}$ | $k_{20}$ M$^{-1}$ s$^{-1}$ | $k_{l3'}$ (M$^{-1}$ s$^{-1}$) |
|---|---|---|---|---|---|
| 0.0 | 6 | $2.5 \times 10^{-6}$ | $2.5 \times 10^{-8}$ | $1 \times 10^{8}$ | 2 |
| 0.0294 | 3, 5, 8 | $2.5 \times 10^{-6}$ | $2.5 \times 10^{-8}$ | $1 \times 10^{8}$ | 2 |
| 0.0882 | 3, 5, 8 | $3.4 \times 10^{-6}$ | $2.5 \times 10^{-8}$ | $1 \times 10^{8}$ | 0.3 |
| 0.147 | 3, 5, 8 | $4.8 \times 10^{-6}$ | $2.5 \times 10^{-8}$ | $1 \times 10^{8}$ | 0.06 |

$k_1$ in this model is actually equal to $I_o \Phi$ where $I_o$ is the light intensity of the UV source. Since it is the same UV source $I_o$ variation within the experimental study might be negligible. The reason that $I_o$ might vary is that the cooling medium around the UV source as is shown in Figure 4.1.1, which is used to protect the UV lamp from over heating, might not be at a constant rate in all experiment [Blazka, 1983]. If $I_o$ is constant then this leaves us with the other option that $\Phi$ is dependent of initial concentration.

$\Phi$ represents the number of $H_2O_2$ moles destroyed per number of moles of photon (Einstein) absorbed. It has been found that it is not a function of initial $H_2O_2$ concentration within the low concentration range. By referring to the literature we found that the reported value for $\Phi_{H2O_2}$ has been mainly obtained by low pressure mercury lamp and was obtained at low concentration of $H_2O_2$ and high light intensities (0.002-0.035M Volman, 1959; 0.0001-0.001M Baxedndale, 1957; $2x10^{-5}$-$10^{-3}$ M Dainton, 1953). The UV light was filtered to obtain wave length of 253.7. Under these conditions $\Phi_{H2O_2}$ was found to be independent of initial $H_2O_2$ concentrations and light intensities. $\Phi_{H2O_2}$ was found to be 1.0 for the overall process of $H_2O_2$ reactions in pure water [Baxendale, 1957; Volman , 1959]. Using unfiltered UV sources $\Phi_{H2O_2}$ was $1.4 \pm 0.1$ [Lea, 1949] and $1.9 \pm 0.1$ [Dainton, 1953].

Hunt (1952) noticed that $\Phi_{H2O_2}$ changed from 1 to 3.8 when tap water replaced distilled water due to initiation of a chain decomposition of hydrogen peroxide. He attributed this to the involvement of new intermediates ($^{\bullet}OH$ and $HO_2^{\bullet}$) which were formed from some impurity in the tap distilled water. Bielski (1977) found that molar absorptivity of hydrogen peroxide is independent of pH for pH range 6-9 and wave lengths 230-280 nm. In Volman's work (1959) $\Phi_{H2O_2}$ was 0.87-0.92 for 0.00218 M, 0.95 for 0.00433 M, and 1.03 for 0.0356 M $H_2O_2$ and when $H_2O_2$ increased he also increased light intensity. Wang (2000, 2001) used high pressure mercury lamps with unfiltered wave lengths, also higher initial $H_2O_2$ concentrations were used, therefore $\Phi_{H2O_2}$ might be a function of initial $H_2O_2$ concentrations under these conditions.

Another possibility that $\Phi_{H_2O_2}$ has increased is that there might be a reaction which consumes $H_2O_2$ that we didn't include in our model since increment of $\Phi_{H_2O_2}$ means more destruction of $H_2O_2$ [Baxendale, 1957]. Also $\Phi_{H_2O_2}$ decreases as temperature decreases, $\Phi_{H_2O_2}$ was 0.49 and 0.38 at 25 °C and 0 °C respectively for the primary process [Hunt, 1952]. As can be seen from the schematic of the experimental setup in Figure 4.1.1 that cooling water was used to protect UV lamp from over heating, therefore any variation in the temperature by varying the cooling rate will change the value of $\Phi_{H_2O_2}$.

From the above literature review of the quantum yield of hydrogen peroxide measurement it can be seen that most of these studies were performed at low concentration and it is lower than the concentrations of $H_2O_2$ used in our simulation. We can't confirm which variable was actually changed during the experiments since neither $I_o$ nor $\Phi_{H_2O_2}$ was measured at these experimental conditions.
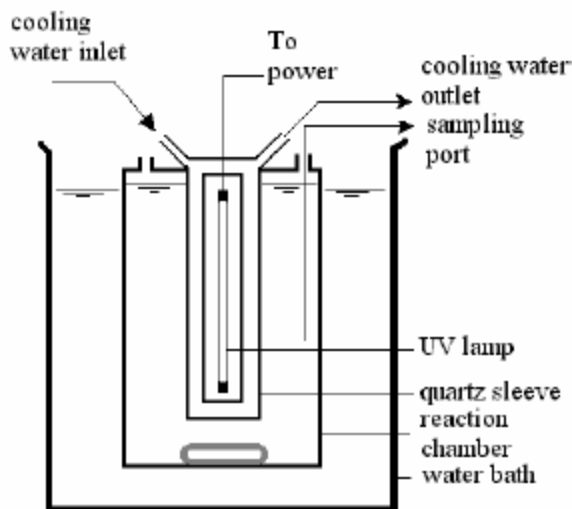


Fig. 4.1.1: Schematic diagram of thermostatic UV reactor, [Wang, 2001]

From the model simulations in Figures 3.1.3-A, 3.1.4-A, 3.1.5-A, it can be seen that the model predicts lower residual fraction of NPDOC than the experimental data when the residual fraction of NPDOC is less than 0.2. We called this period, for which residual fraction of NPDOC is less than 0.2, the tailing period. When we started to simulate these data we have assumed that the reported NPDOC is equal to HA and all destroyed HA is converted to volatile compounds and $CO_2$. Making this assumption made the gap between the model prediction and experimental data in the tailing period larger. Therefore in order to overcome this gap we have modified the mechanism of HA destruction and now not all of the products or intermediates of HA destruction by UV or $^\bullet OH$ radicals are volatile. By this modification we made an assumption for some of the possible reaction intermediates and their fate in the reaction mixture as was shown in section 2.1.2.2. $k_{I3}$, which is the rate constante for the reaction of $H_2O_2$ with one of HA byproducts was also a function of initial $H_2O_2$ concentration. NPDOC was the sum of remaining HA and the nonvolatile organic compounds in the reaction mixture and at the time of TOC measurement the NPDOC is $NPDOC=HA+I_1+I_3+I_4+I_5$

From Figure 3.1.3-A, 3.1.4-A and 3.1.5-A, it can be seen that the model predicts the experimental data pretty well especially in the early time. In the tailing period, the fitting is enhanced as the concentration of $H_2O_2$ is lowered. This is due to that the fitting parameters have to be optimized to fit all of the experimental conditions from zero to 0.147 M $H_2O_2$. Also, although we have proposed a mechanism for HA reactions in the system still we might not have captured the true mechanism and all of the reaction intermediates and by products. In order to have more insight about this mechanism more experimental data and analysis of the HA acids reactions should be available.

236

Also, from these figures it can be seen that residual fraction of NPDOC even for the 0.0294 M $H_2O_2$ becomes similar at the end of the reaction. This is due to that at this period the concentration of HA is very small and its degradation by direct photolysis becomes negligible and mostly it is degraded by $^\bullet OH$ radicals which are produced through direct photolysis of $^\bullet OH$ radicals.

In Figure 3.1.3-B the degradation of $H_2O_2$ is slightly retarded in the presence of humic acid as shown by the model simulation. The retardation of $H_2O_2$ degradation by increasing initial HA concentration is vanishing as initial hydrogen peroxide concentration is increased as can be seen in Figures 3.1.4-B and 3.1.5-B, by experimental data and model predictions. The experimental data at 5 mg $L^{-1}$ HA and 0.0294 M $H_2O_2$ (Figure 3.1.3-B) doesn't match with the model. The experimental residual fraction of $H_2O_2$ at these conditions is even lower than the one for a solution of pure $H_2O_2$. The presence of HA is expected to retard $H_2O_2$ photolysis since it absorbs light [Chu, 2003; Hawari, 1992], but based on Figure 3.1.1-B, $H_2O_2$ degradation is accelerated in the presence of Humic acid. In our kinetic model, we have assumed the production of transients (hydrated electrons), this transient in turn will go through different reactions as was given in the kinetic model and some of these reactions involve direct reaction between this transient and $H_2O_2$, therefore they would compensate for more $H_2O_2$ consumption in the system. Also by looking to the experimental data in Figure 3.1.5-B it can be seen that as initial NPDOC increased from 3 to 5 mg $L^{-1}$ there is a slight retarding effect on residual $H_2O_2$. This conflicts with the experimental data in Figure 3.1.3-B where in going from zero to 5 mg $L^{-1}$ an accelerating effect was observed.

Now we believe that the experimental data for $H_2O_2$ residual fraction at 5 mg $L^{-1}$ NPDOC and 0.0294 M $H_2O_2$ is not accurate.

### 4.1.1. Effect of Initial $H_2O_2$ concentration

### 4.1.1.1. Effect of Initial $H_2O_2$ concentration on residual fraction of NPDOC

It can be see from the experimental data shown in Figures 3.1.6-A, B, and C that, at fixed incident light intensity, pH, and initial NPDOC concentration, as the initial concentration of $H_2O_2$ is increased the residual fraction of NPDOC is increased. This means that NPDOC degradation has been retarded. The results from the simulation are showing the same trend for residual NPDOC and residual HA.  De Laat (1994) observed that there is an optimum hydrogen peroxide dose for the target organic destruction. Similar behavior was observed by Stefan (1996), Glaze (1995), Chu (2003), and Behnajady (2004) when they applied the UV/$H_2O_2$ technology for the contaminant removal. Gallard (1999, 2000) observed a similar behavior when he applied Fenton's technology for contaminant removal. De laat (1994) observed that there is an optimum hydrogen peroxide dose for the oxidation of the target organic.

This phenomena can be explained based on the fact that of $H_2O_2$ has two opposing effect on the process; as a promoter and a scavenger of $^\bullet OH$ radicals. This implies that there should be an optimal dosage of the oxidant $H_2O_2$ to provide the maximum removal of the contaminant per unit of $H_2O_2$.

In the kinetic model $^\bullet OH$ radicals are formed when $H_2O_2$ is exposed to the UV light. If $H_2O_2$ is in excess, the extra $H_2O_2$ moles will deplete the $^\bullet OH$ radical from the solution and form $HO_2^\bullet$ radicals as can be seen from the following reaction (inhibitor effect):

$$H_2O_2 + {}^\bullet OH \rightarrow H_2O + HO_2^\bullet;$$
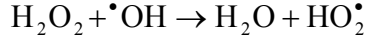
$HO_2^\bullet$ radicals are less reactive than ${}^\bullet OH$ radicals and their reaction with organic dissolved carbon is negligible [Liao, 1995]. Hence the available ${}^\bullet OH$ radicals to react with HA will be decreased.

With the kinetic reaction simulation we can gain more insight into the system and therefore be able to better understand this behavior. The rate of change of ${}^\bullet OH$ radicals is given by the following equation in the kinetic model:

$$
\begin{aligned}
\frac{d{}^\bullet OH}{dt} ={} & 2k_1 f_{H_2O_2}(1 - e^{-A_1}) - k_3[H_2O_2][{}^\bullet OH] - k_5[{}^\bullet OH][HO_2^*] - k_6[{}^\bullet OH][O_2^{\bullet-}] \\
& - 2k_7[{}^\bullet OH][{}^\bullet OH] - k_{11}[{}^\bullet OH][HCO_3^-] - k_{14}[{}^\bullet OH][CO_3^{2-}] - k_{20}[{}^\bullet OH][HA] \\
& - k_{18}[{}^\bullet OH][HO_2^-] - k_{16}[H_2O_2]_T[O_2^{\bullet-}] + k_{17}[H_2O_2]_T[HO_2^\bullet] - \\
& k_{22}[{}^\bullet OH][CO_3^{\bullet-}] - k_{25}[{}^\bullet OH][\bar{e}_{aq}] + k_{27}[H_2O_2][\bar{e}_{aq}] + k_{28}[HO_2^-][\bar{e}_{aq}] - \\
& k_{32}[{}^\bullet OH][H^\bullet] + k_{34}[H_2O_2][H^\bullet] + k_{35}[HO_2^-][H^\bullet] - k_{37}[H_{2aq}][{}^\bullet OH] + \\
& k_{30}[H^\bullet][H_2O] - k_{I3}[I_3][{}^\bullet OH] - k_{I4}[I_4][{}^\bullet OH] - k_{I5}[I_5][{}^\bullet OH]
\end{aligned}
$$

The major route of ${}^\bullet OH$ production is through direct photolysis of $H_2O_2$. Figure 4.1.1.1.1 compares the rate of ${}^\bullet OH$ radical production by direct photolysis of $H_2O_2$ (the first term on the right side of the above equation ($2k_1 f_{H_2O_2}(1-e^{-At})$)) and the sum of all other positive terms in the above equation. From this figure it can be seen that for all times ${}^\bullet OH$ production by direct photolysis of $H_2O_2$ is at least 2 or more orders of magnitude higher than its production by other routes. Therefore, when we will speak about ${}^\bullet OH$ radical production, it will be predominantly through direct photolysis and represented by the term ($2k_1 f_{H_2O_2}(1-e^{-At})$).
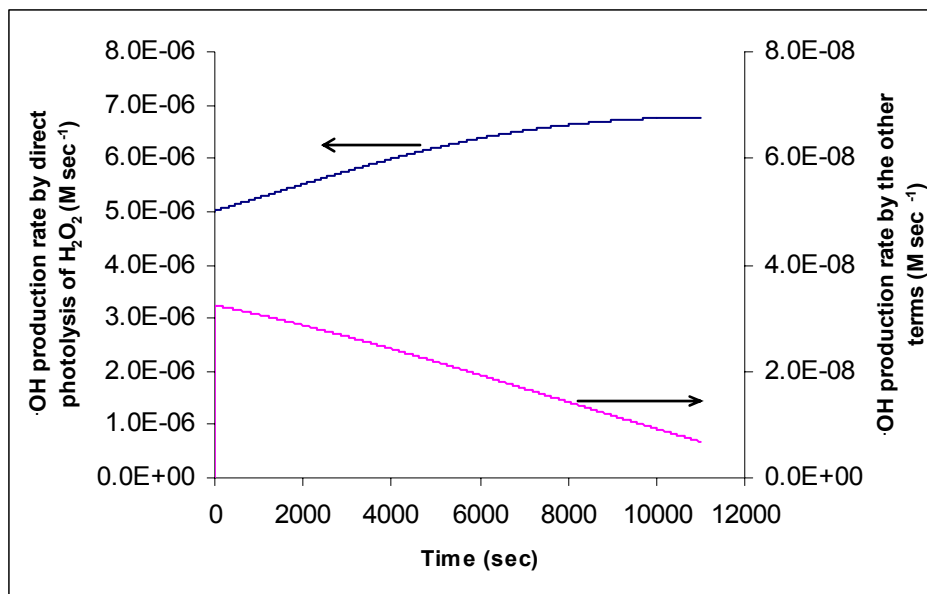
**Fig. 4.1.1.1.1:** Predicted rate of $^\bullet OH$ radical production, comparison between direct photolysis and the sum of the other terms in equation of $\dfrac{d^\bullet OH}{dt}$. Initial conditions: $[H_2O_2]_o = 0.0882$ M. $[HA]_o = 8$ mg $L^{-1}$, pH= 7

It is expected that the more $H_2O_2$ molecules in the reaction system the more $^\bullet OH$ radicals will be produced from the initiation step, Reaction 1 in the kinetic model. From Figure 4.1.1.1.1 it can be seen that rate of $^\bullet OH$ radical production by direct photolysis of hydrogen peroxide is increasing. The reason of this behavior, is due to the reduction of HA concentration with time, due to its degradation, this will lead to increase in the fraction of UV light absorbed by hydrogen peroxide and hence accelerate the rate of its photolysis.

Figure 4.1.1.1.2-A, B, and C give the predicted value of $2k_1 f_{H_2O_2}(1-e^{-At})$, which represents the rate of $^\bullet OH$ radical production through direct photolysis of $H_2O_2$, at 3, 5, and 8 mg $L^{-1}$ NPDOC with $H_2O_2$ concentrations of 0.0294, 0.0882, and 0.147 M $H_2O_2$, respectively. These conditions are similar to the experimental conditions presented in Figure 3.1.3 through 3.1.6 in the results section. From these plots, it can be seen that

$^\bullet OH$ radical production rate increased as the initial concentration of $H_2O_2$ was increased at each initial NPDOC concentration. Also, there is a slight reduction in $^\bullet OH$ radical production rate by $H_2O_2$ at a fixed concentration of $H_2O_2$ as HA concentration is increased from 3, 5, to 8 mg $L^{-1}$ due to UV absorbance by HA. This will be discussed later. The rate of $^\bullet OH$ radical production reaches a maximum value for the case where $H_2O_2$ is initially 0.0294 M and after 6000 sec it starts to decline. This is due to the reduction of $H_2O_2$ concentration to a very low value after 6000 sec as be seen from Figure 3.1.3-B in the results section. The same would happen with the other $H_2O_2$ concentrations if simulation was extended for a longer time. For example the simulation for 8 mg $L^{-1}$ and 0.0882M $H_2O_2$ was extended for a longer time than the one in Figure 4.1.1.1.2-C. As can be seen in Figure 4.1.1.1.2-D after 12000 sec, the rate of $^\bullet OH$ production also declined again since the major route of $^\bullet OH$ production is the direct photolysis of $H_2O_2$ and if $H_2O_2$ is disappearing then this rate will decrease tremendously.
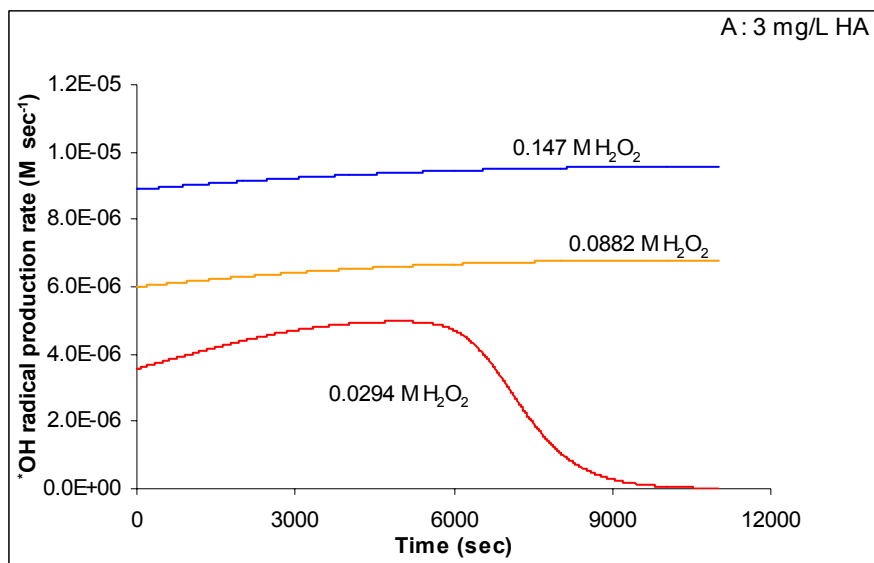


**Fig. 4.1.1.1.2-A:** Predicted rate of $^\bullet OH$ production by direct photolysis of $H_2O_2$ vs. time at constant initial concentration of HA. Initial conditions: ▬: $[H_2O_2]_o = 0.147M$, ▬: $[H_2O_2]_o = 0.0882$ M, ▬: $[H_2O_2]_o = 0.0294$ M. $[HA]_o = 3$ mg $L^{-1}$, pH = 7
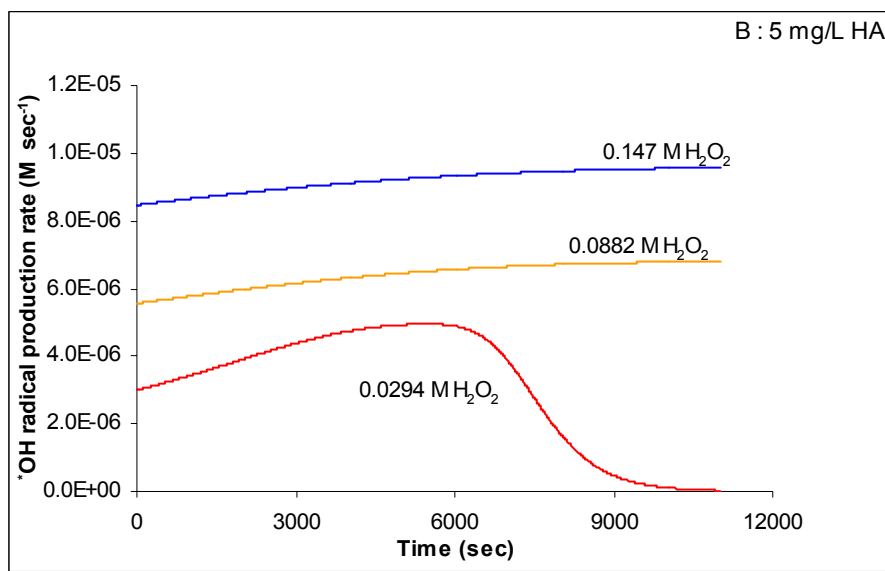
**Fig. 4.1.1.1.2-B:** Predicted rate of $^\bullet OH$ production by direct photolysis of $H_2O_2$ vs. time at constant initial concentration of HA. Initial conditions: —: $[H_2O_2]_o = 0.147M$, —: $[H_2O_2]_o = 0.0882$ M, —: $[H_2O_2]_o = 0.0294$ M. $[HA]_o = 5$ mg L$^{-1}$, pH = 7
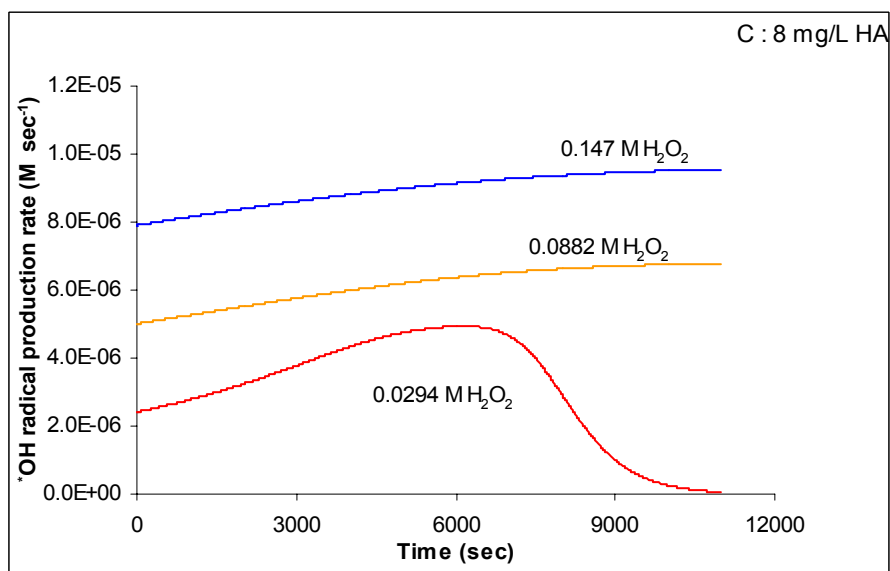


**Fig. 4.1.1.1.2-C:** Predicted rate of $^\bullet OH$ by direct photolysis of $H_2O_2$ vs. time at constant initial concentration of HA. Initial conditions: —: $[H_2O_2]_o = 0.147M$, —: $[H_2O_2]_o = 0.0882$ M, —: $[H_2O_2]_o = 0.0294$ M. $[HA]_o = 8$ mg L$^{-1}$, pH = 7
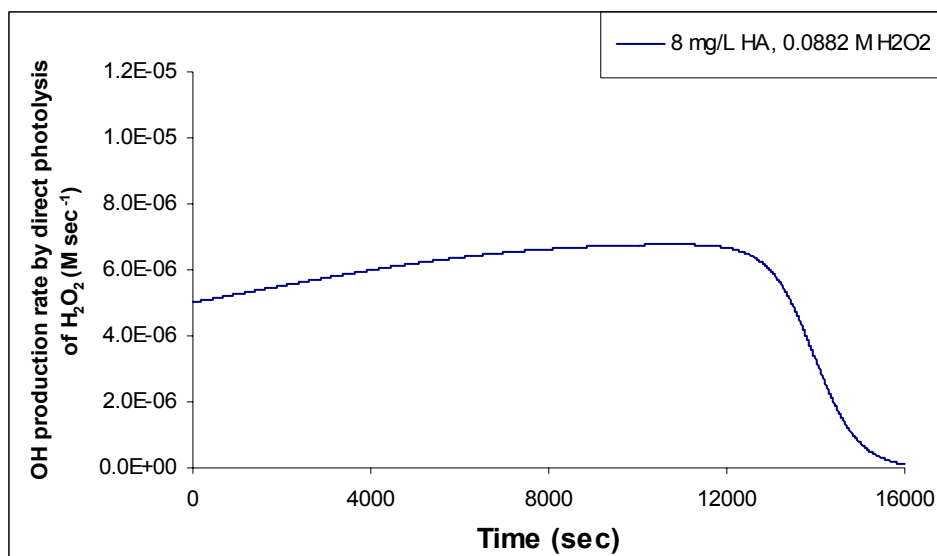
**Fig. 4.1.1.1.2-D:** Predicted rate of $^\bullet OH$ by direct photolysis of $H_2O_2$ vs. time. Initial concentration: $[H_2O_2]_o = 0.0882$ M, $[HA]_o = 8$ mg L$^{-1}$ pH= 7

Until now this is serving an accelerating effect of increasing $H_2O_2$ on HA degradation not a retarding effect as was observed in the experimental data and from the simulation. As said earlier, $H_2O_2$ besides being $^\bullet OH$ radical precursor is also a scavenger of these radicals. The reaction for $^\bullet OH$ radicals with $H_2O_2$ was given by:

$$^\bullet OH + H_2O_2 \rightarrow H_2O + HO_2^\bullet \qquad\qquad k = 2.7\ x10^7\ M^{-1}\ s^{-1}$$

Figures 4.1.1.1.2-E through 4.1.1.1.2-G show the rate of $^\bullet OH$ radical consumption by $H_2O_2$, according to the above reaction, at different initial concentration of $H_2O_2$. It can be seen that regardless of initial NPDOC concentration, more $^\bullet OH$ radicals will be consumed by $H_2O_2$ as its initial concentration is increased. A slight decrease in the reaction of $^\bullet OH$ with $H_2O_2$ reaction is observed as HA is increased from 3, 5, to 8 mg L$^{-1}$ this will be discussed in HA effect section. Consumption of $^\bullet OH$ radical by the conjugate base of $H_2O_2$ was less than 1% of its consumption by $H_2O_2$ at the studied conditions. Therefore, it was neglected in the previously mentioned figures.
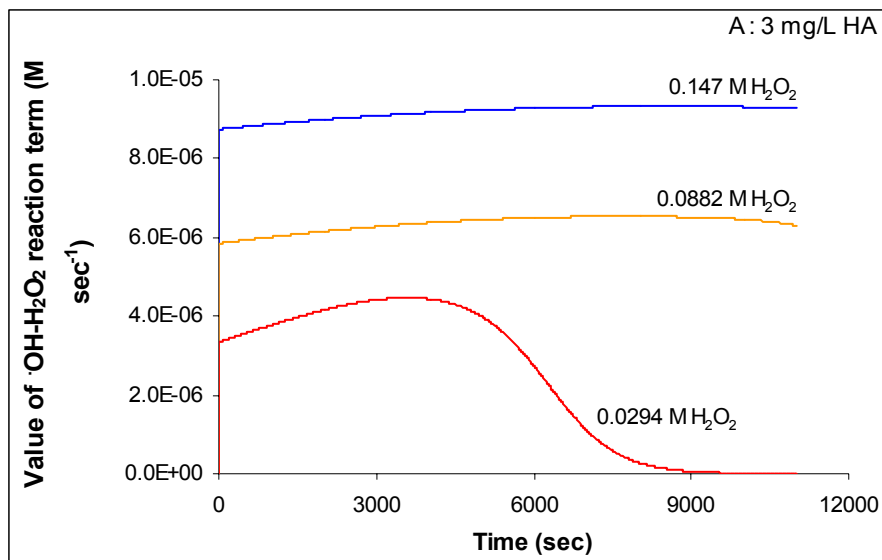
**Fig. 4.1.1.1.2-E:** Predicted rate of $^{\bullet}OH$ and $H_2O_2$ reaction vs. time at constant initial concentration of HA. Initial conditions: ——: $[H_2O_2]_o = 0.147$ M, ——: $[H_2O_2]_o = 0.0882$ M, ——: $[H_2O_2]_o = 0.0294$ M. $[HA]_o = 3$ mg L$^{-1}$, pH = 7
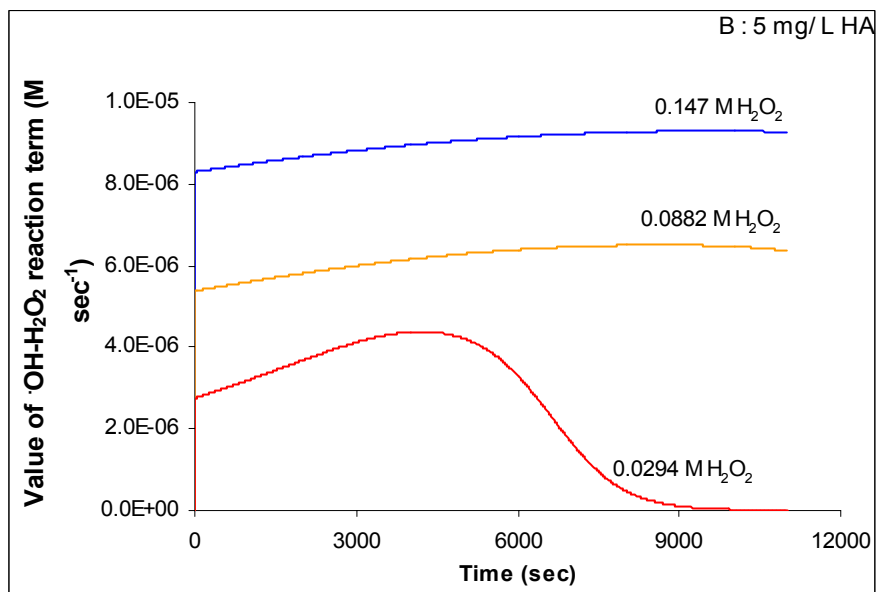


**Fig. 4.1.1.1.2-F:** Predicted rate of $^{\bullet}OH$ and $H_2O_2$ reaction vs. time at constant initial concentration of HA. Initial conditions: ——: $[H_2O_2]_o = 0.147$ M, ——: $[H_2O_2]_o = 0.0882$ M, ——: $[H_2O_2]_o = 0.0294$ M. $[HA]_o = 5$ mg L$^{-1}$, pH = 7

244
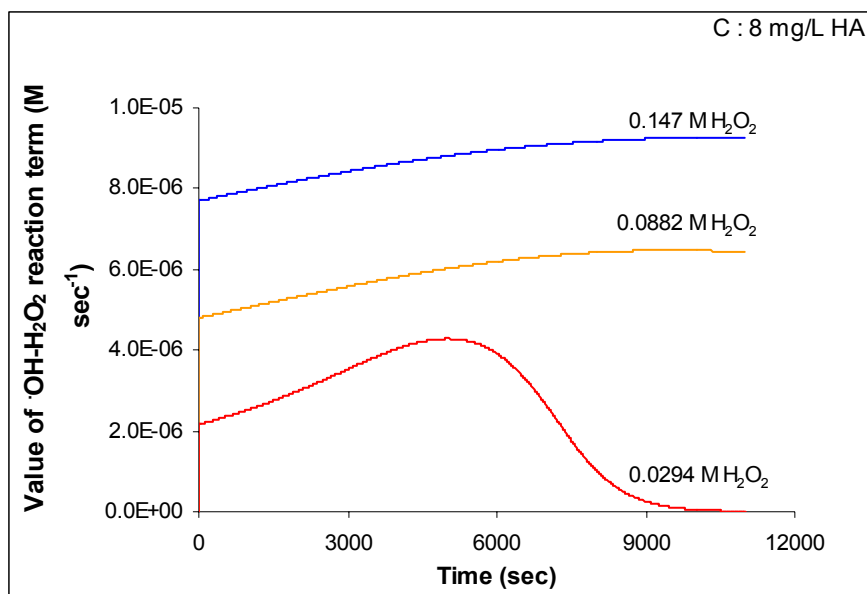
**Fig. 4.1.1.1.2-G:** Predicted rate of $^{\bullet}OH$ and $H_2O_2$ reaction vs. time at constant initial concentration of HA. Initial conditions: ▬: $[H_2O_2]_o = 0.147$ M, ▬: $[H_2O_2]_o = 0.0882$ M, ▬: $[H_2O_2]_o = 0.0294$ M. $[HA]_o = 8$ mg $L^{-1}$, pH = 7

As a result of the increase in $^{\bullet}OH$ radical consumption by $H_2O_2$ as $H_2O_2$ concentration is increased, then the available $^{\bullet}OH$ radicals in the reaction mixture will be reduced at the high concentration of $H_2O_2$. The total effect of increasing initial $H_2O_2$ concentrations can be observed by following the concentration of $^{\bullet}OH$ radicals in the system. For example, at 8 mg $L^{-1}$ and different initial $H_2O_2$ concentrations, as can be seen from Figure 4.1.1.1.2-H, the net $^{\bullet}OH$ radical concentration in the system decreases as more $H_2O_2$ molecules are in the system. In Figure 4.1.1.1.2-H it can be seen that initially the concentration of $^{\bullet}OH$ radicals is zero for all conditions, a very fast production of $^{\bullet}OH$ radicals is obtained directly after photolysis of $H_2O_2$ accompanied at the same time with a rapid consumption by HA which will balance the rate of production. Once the concentration of HA is lowered more $^{\bullet}OH$ radicals will be left in the system since the source of $^{\bullet}OH$ radical (photolysis of $H_2O_2$) is still available and absorbs more UV light as HA concentration is reduced. Therefore, another increase of $^{\bullet}OH$ radicals is observed.

$^{\bullet}$OH radicals will reach a maximum value which depends on the initial concentration of $H_2O_2$. Hydrogen peroxide is also consuming these radicals and after a while its concentration will decrease due to the direct photolysis, consumption of $^{\bullet}$OH radicals, and all the other reactions which consume $H_2O_2$. Once the source of $^{\bullet}$OH radicals starts to deplete ($H_2O_2$) their concentration will decrease also.
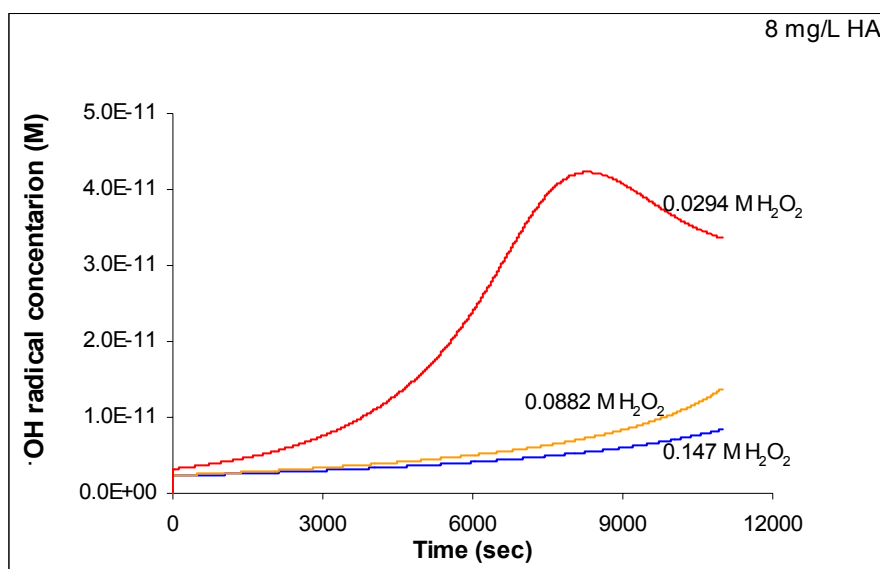


**Fig. 4.1.1.1.2-H:** Predicted $^{\bullet}$OH radicals' concentration vs. time at constant initial concentration of HA. Initial conditions: ▬: $[H_2O_2]_o = 0.147$ M, ▬: $[H_2O_2]_o = 0.0882$ M, ▬: $[H_2O_2]_o = 0.0294$ M. $[HA]_o = 8$ mg L$^{-1}$, pH = 7

HA, according to the kinetic model, is consumed mainly by two routes. The first route is the direct photolysis by UV light and the second one is the oxidation by $^{\bullet}$OH radicals. Therefore, if more $^{\bullet}$OH radicals are consumed by $H_2O_2$ then the available $^{\bullet}$OH radicals to react with HA will decrease, and this will lower the degradation of humic acid. An example is given in Figure 4.1.1.1.2-I where the rate of consumption of $^{\bullet}$OH radicals by HA was based on evaluating the value of the $k_{20}[HA][^{\bullet}OH]$ term vs. time at the indicated conditions. From this figure it can be seen that for time less than

3500 sec the magnitude of $k_{20}[HA][^\bullet OH]$ (M sec$^{-1}$) with 0.0299 M $H_2O_2$ is > 0.0882 M

$H_2O_2$> 0.147 M $H_2O_2$.
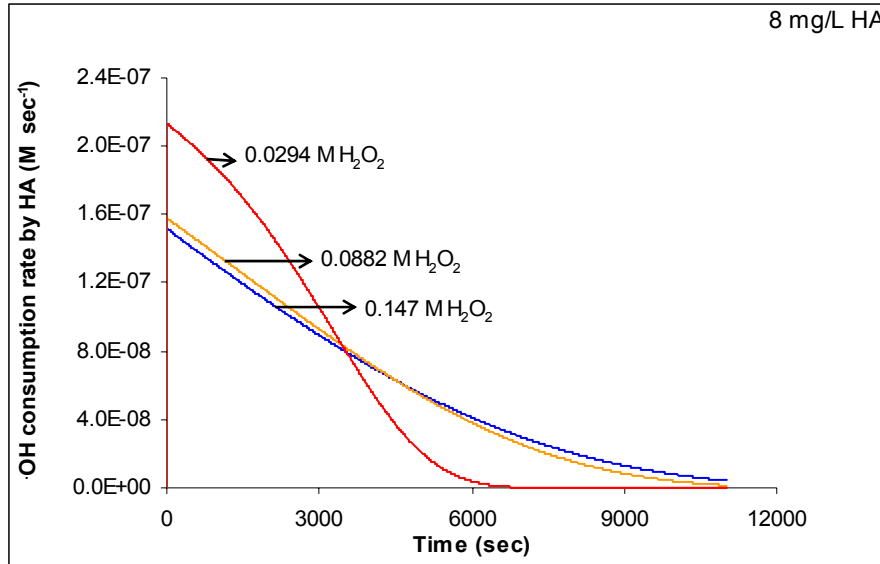


**Fig. 4.1.1.1.2-I:** Predicted magnitude of $k_{20}[HA][^\bullet OH]$ term vs. time at constant initial concentration of HA. Initial conditions: ▬: $[H_2O_2]_o = 0.147$ M, ▬: $[H_2O_2]_o = 0.0882$ M, ▬: $[H_2O_2]_o = 0.0294$ M. $[HA]_o$ = 8 mg L$^{-1}$, pH = 7

Also the change in $k_{20}[HA][^\bullet OH]$ rate is steeper with time for 0.0294 M $H_2O_2$

which will lead to a faster removal of HA and hence will lower its value rapidly. This is

consistent with the more available $^\bullet OH$ at the lower $H_2O_2$ concentration as was shown in

Figure 4.1.1.1.2-H which shows that the concentration of $^\bullet OH$ radicals in the system

increases at lower $H_2O_2$ concentration. After this time, due to the fast HA removal, HA

concentration, as was shown in Figure 3.1.8-C in the results section, will be much lower

at 0.0294 M $H_2O_2$ than the other $H_2O_2$ concentration hence the magnitude of the term

$k_{20}[HA][^\bullet OH]$ will be lower. The same trend was observed at 0.0882 M and 0.147 M

$H_2O_2$ where there is a slight reduction of $k_{20}[HA][^\bullet OH]$ term at the lower $H_2O_2$

concentration.

We need also to explore the effect of increasing $H_2O_2$ concentration on the rate of photolysis of HA and see if that is affecting the removal of humic acid from the system. The rate of HA photolysis was investigated by calculating the value of $k_2 f_{HA}(1-e^{-A_t})$. Figure 4.1.1.1.2-J is showing the magnitude of this term vs. time at different initial concentrations of $H_2O_2$ and constant initial concentration of HA. From Figure 4.1.1.1.2-J it can be seen that not only the rate of HA reaction with $^\bullet OH$ radicals is affected by the increase in $H_2O_2$ concentration, but the rate of HA destruction by direct photolysis is affected. A retarding effect on the direct rate of photolysis is observed as $H_2O_2$ concentration was increased from 0.0294, 0.0882, to 0.147 M. This is due to the fact that $H_2O_2$ is competing with HA for UV light and this competition was given by the fraction of light absorbed by both HA and $H_2O_2$. Fraction of UV light absorbed by HA ($f_{HA}$) was defined as:

$$f_{HA} = \frac{\varepsilon_{HA}[HA]}{\varepsilon_{HA}[HA] + \varepsilon_{H_2O_2}[H_2O_2] + \varepsilon_{HO_2^-}[HO_2^-]}$$

so the higher concentration of $H_2O_2$ will result in a larger denominator and hence lower fraction of light absorbed by HA. Therefore, the magnitude of the $k_2 f_{HA}(1-e^{-A_t})$ term will decrease.

From Figures 4.1.1.1.2-I and 4.1.1.1.2-J, it can be seen that the value of HA photolysis term is always lower than the $^\bullet OH$-HA reaction term at the same conditions. The difference between the two terms at the different initial conditions is at least an order of magnitude. From these figures it can be seen that the main retardation effect comes from the reduction in $^\bullet OH$ radical concentration by the increase in initial $H_2O_2$ concentration since rate of photolysis term is lower than $^\bullet OH$-HA reaction term.
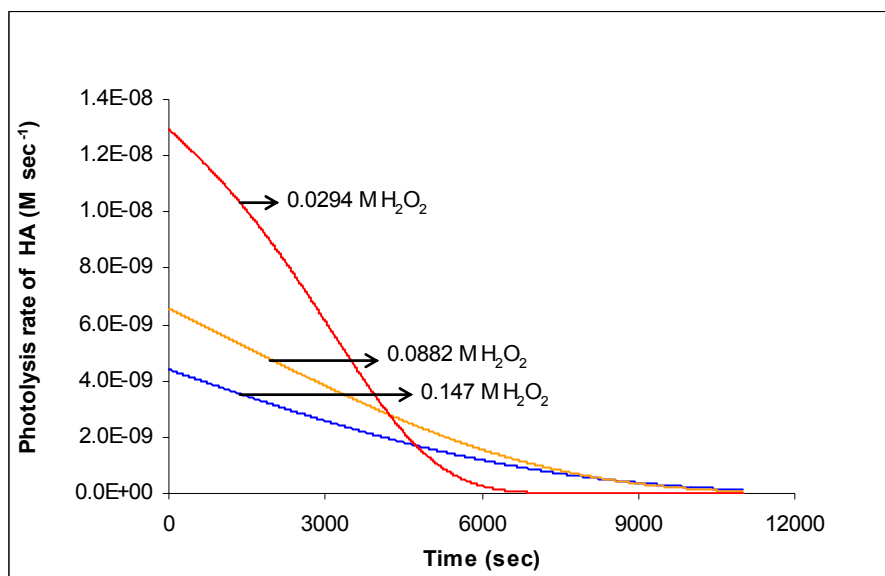
**Fig. 4.1.1.1.2-J:** Predicted magnitude of $k_2 f_{HA}(1-e^{-A_t})$ term vs. time at constant initial concentration of HA. Initial conditions: ▬: $[H_2O_2]_o = 0.147$ M, ▬: $[H_2O_2]_o = 0.0882$ M, ▬: $[H_2O_2]_o = 0.0294$ M. $[HA]_o = 8$ mg L$^{-1}$, pH = 7

An optimum hydrogen peroxide dose for the target organic was observed [Wang, 2000; De Laat, 1994; Stefan, 1996, Chu, 2003; Behnajady, 2004]. This means that the rate of organic oxidation will increase when the concentration of hydrogen peroxide increases after a certain value. However if the hydrogen peroxide concentration such that the term $k[^{\bullet}OH][H_2O_2]$ is high enough compared to $k_{20}[HA][^{\bullet}OH]$ then $H_2O_2$ might inhibit the oxidation of humic acid due to $^{\bullet}OH$ radicals scavenging [De Laat, 1994]. The analysis, in the following paragraphs, was made to test the hypothesis of having optimum hydrogen peroxide concentration and understand the reasons behind having optimum dose of $H_2O_2$.

Figure 4.1.1.1.2-K compares the rate of $^{\bullet}OH$ radicals by hydrogen peroxide and HA. As can be seen in Figure 4.1.1.1.2-K, the magnitude of $k[^{\bullet}OH][H_2O_2]$ is at least one order of magnitude greater than that one of $k_{20}[HA][^{\bullet}OH]$ and hence this might

explain the retardation of the degradation of HA at these conditions. Similar behavior was observed for 0.0294 M and 0.147 M $H_2O_2$.
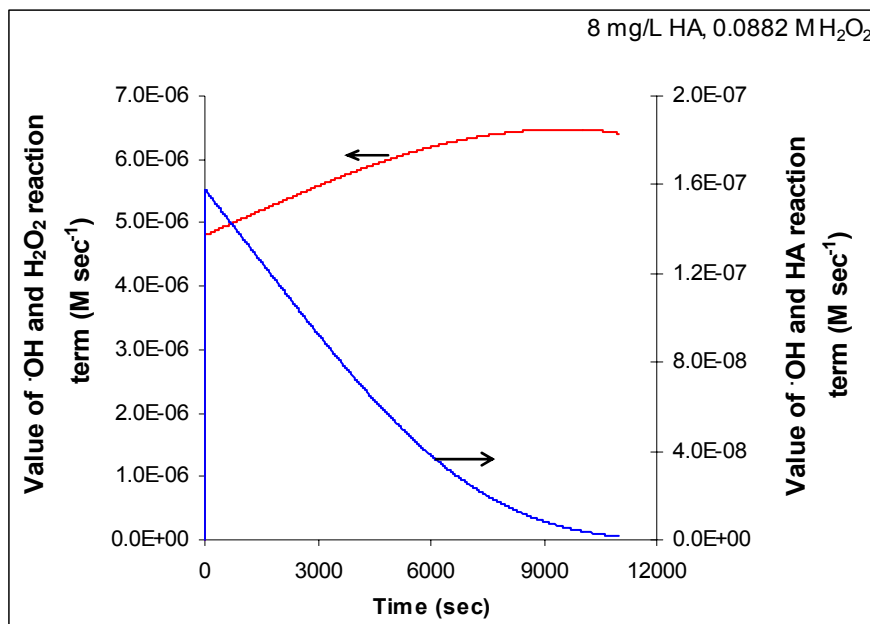


**Fig. 4.1.1.1.2-K:** Comparison between the predicted magnitude of $k[^\bullet OH][H_2O_2]$ and $k_{20}[HA][^\bullet OH]$ terms vs. time at constant. Initial conditions: $[H_2O_2]_o = 0.0882$ M, $[HA]_o = 8$ mg $L^{-1}$, pH= 7

      This means that the optimum value of $H_2O_2$ concentration for these conditions could be lower than 0.0294 M. Figure 4.1.1.1.2-L, taken from Wang (2000), shows a calculated pseudo 1st order rate constant vs. initial $H_2O_2$ concentration and it is clear that there is an optimum in $H_2O_2$ concentration. From this figure it can be seen that adding hydrogen peroxide to the system will improve the degradation of humic acid at all hydrogen peroxide concentrations. Similar behavior was observed by Lopez (2003). He found, from experimental measurement for degradation of pharmaceutical intermediates in aqueous solution using $H_2O_2/UV$ AOP, that substrates degradation by photooxidation was faster than direct photolysis alone.
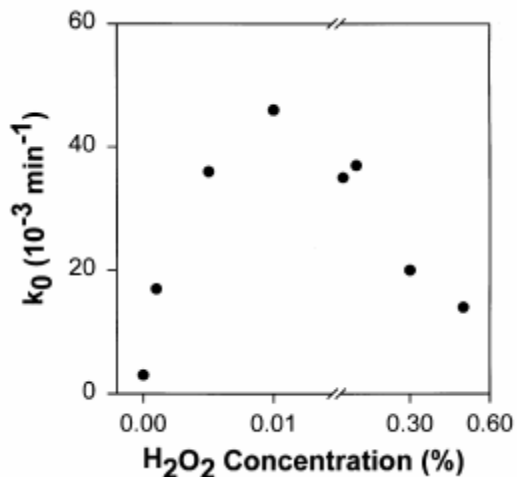
**Fig. 4.1.1.1.2-L:** Apparent first-order rate constant for humic acid degradation with various $H_2O_2$ concentrations. $[HA]_o = 5$ mg/L, pH = 7 [Wang, 2000]

Based on our kinetic model, we assumed that HA is converted to other compounds by direct photolysis and $^\bullet OH$ radicals, and from the simulation results a pseudo first order approximations won't be accurate especially at times longer than 60 min where the experimental residual fraction of NPDOC seems to be at a fixed value, so we can't reproduce Figure 4.1.1.1.2-L. Comparison would be possible if experimental data (residual fraction) of NPDOC were available at the conditions given in Figure 4.1.1.1.2-L. However, we will present an example of a comparison between the predicted magnitude of $^\bullet OH$ consumption by hydrogen peroxide and NPDOC at different initial hydrogen peroxide concentration and we will see if this will help to understand the presence of optimum in $H_2O_2$ concentration. The consumption of $^\bullet OH$ radicals by hydrogen peroxide and its conjugate base was calculated from:

$$-k_3[H_2O_2][^\bullet OH] - k_{18}[^\bullet OH][HO_2^-] \tag{A}$$

On the other hand, the consumption of $^\bullet OH$ radicals by NPDOC was calculated from:

$-k_{20}[^\bullet OH][HA] - k_{13}[I_3][^\bullet OH] - k_{14}[I_4][^\bullet OH] - k_{15}[I_5][^\bullet OH]$  (B)

The ratio of $^\bullet OH$ radicals that were consumed by hydrogen peroxide to the ones consumed by NPDOC is given in Figure 4.1.1.1.2-M for different initial $H_2O_2$ concentrations.
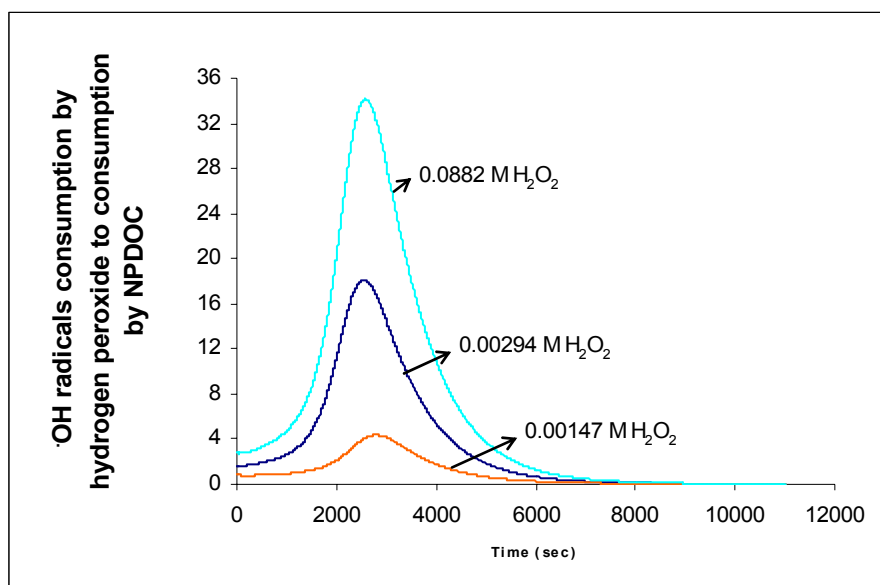


**Fig. 4.1.1.1.2-M:** Predicted ratio of $^\bullet OH$ radical consumption by $H_2O_2$ to consumption by NPDOC (A/B) vs. time at constant initial concentration of NPDOC. Initial conditions: $[NPDOC]_o = 5$ mg $L^{-1}$, pH = 7

The initial hydrogen peroxide concentrations selected in Figure 4.1.1.1.2-M were 0.00147 M, 0.00294 M and 0.0882 M which correspond to 0.005 %, 0.01 % and 0.3 %, respectively, in Figure 4.1.1.1.2-L.  At the conditions shown in Figure 4.1.1.1.2-M, it can be seen that the ratio of $^\bullet OH$ consumption by hydrogen peroxide to the consumption by humic acid and all related by products, i.e. NPDOC, is increasing as the initial $H_2O_2$ concentration is increased. For 0.001147 M $H_2O_2$, this ratio is initially around unity, for 0.00294 M $H_2O_2$ it is initially two, and for 0.0882 M $H_2O_2$ it is initially three. This ratio increases to a maximum value with time; this was noticed earlier in Figure 4.1.1.1.2-H where a maximum was noticed for $^\bullet OH$ concentration. From Figure 4.1.1.1.2-L the ratio

of $^{\bullet}OH$ radicals consumed by $H_2O_2$ to the ones consumed by NPDOC didn't exhibit a maximum value as a function of initial hydrogen peroxide concentration. This might be explained due to that fact that concentration of $^{\bullet}OH$ radicals is incorporated in this ratio and $^{\bullet}OH$ radicals was found from Figure 4.1.1.1.2-H to be a function of initial $H_2O_2$ concentration. To understand the data presented in Figure 4.1.1.1.2-M, $^{\bullet}OH$ concentration vs. time was obtained from model simulation at the conditions in this figure. Figure 4.1.1.1.2-N shows the predicted concentration of $^{\bullet}OH$ using the same initial conditions as the ones in Figure 4.1.1.1.2-M. From this figure it can be seen that for 0.00149 M $H_2O_2$ and 0.0882 M $H_2O_2$, $^{\bullet}OH$ concentration is lower than the one at 0.00294 M $H_2O_2$. Hence the optimum dose of $H_2O_2$ is related to maximum $^{\bullet}OH$ concentration. This maximum of $^{\bullet}OH$ concentration is a function of initial $H_2O_2$ and NPDOC concentration along with the initial pH of the system. Based on this analysis the ratio of $^{\bullet}OH$ radicals consumed by $H_2O_2$ to the ones consumed by NPDOC was not enough to explain the occurrence of an optimum dose of $H_2O_2$.
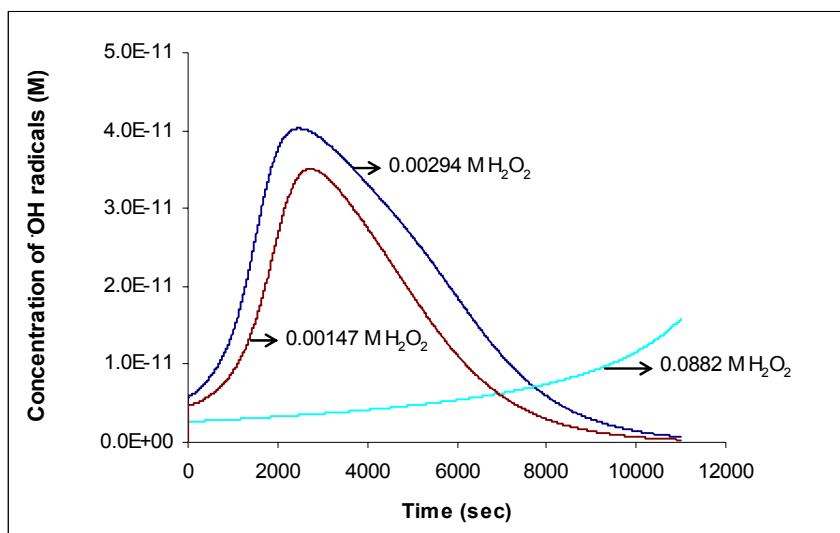


**Fig. 4.1.1.1.2-N: Predicted $^{\bullet}OH$ radicals' concentration vs. time at constant initial concentration of NPDOC and different initial concentrations of $H_2O_2$. Initial conditions: $[NPDOC]_o = 5$ mg $L^{-1}$, pH = 7**

253

**4.1.1.2. Effect of Initial H₂O₂ concentration on residual fraction of H₂O₂**

In the previous section we tried to provide an explanation for the effect of increasing $H_2O_2$ initial concentration on the residual fraction of humic acid. Now we will try to explain the effect of increasing initial $H_2O_2$ concentration on the residual fraction of $H_2O_2$. In Figure 3.1.7-A, B, and C the residual fraction of $H_2O_2$ increased as its initial concentration has been increased at constant HA concentration.

We will start to explain the retarding effect of increasing the initial concentration in general. The main route for $H_2O_2$ destruction is direct photolysis and as can be seen from Figure 4.1.1.2.1, the rate of loss of $H_2O_2$ by direct photolysis, which is calculated from $k_1 f_{H_2O_2} (1 - e^{-At})$, increases as more $H_2O_2$ is available in the system. Also in Figure 4.1.1.1.2-G we have seen that rate of removal of $^\bullet OH$ radical by $H_2O_2$ increased as $H_2O_2$ initial concentrations increased. Irrespective of this, the remaining concentration of $H_2O_2$ when starting with a high concentration remains at a high concentration during the studied time range. This is illustrated by an example in Figure 4.1.1.2.2 which is obtained from running the simulation at constant HA concentration and different $H_2O_2$ concentrations.

In order to have more insight into the system the sum of the positive terms in the differential equation that describes the rate of change of $H_2O_2$ concentration with time was evaluated from simulation. The predicted value of this sum is shown in Figure 4.1.1.2.3. It can be seen that this sum increases in value as the initial concentration of hydrogen peroxide is increased.
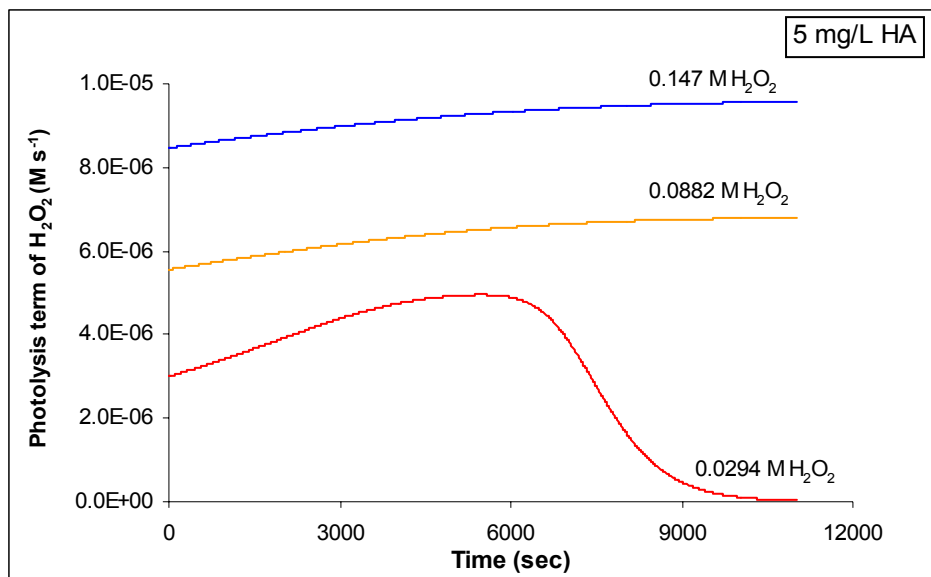
**Fig. 4.1.1.2.1:** Predicted value of $H_2O_2$ photolysis rate ($k_1 f_{H_2O_2}(1 - e^{-A_t})$) vs. time at constant initial concentration of HA. Initial conditions: ▬: $[H_2O_2]_o = 0.147$ M, ▬: $[H_2O_2]_o = 0.0882$ M, ▬: $[H_2O_2]_o = 0.0294$ M. $[HA]_o = 5$ mg L$^{-1}$, pH= 7
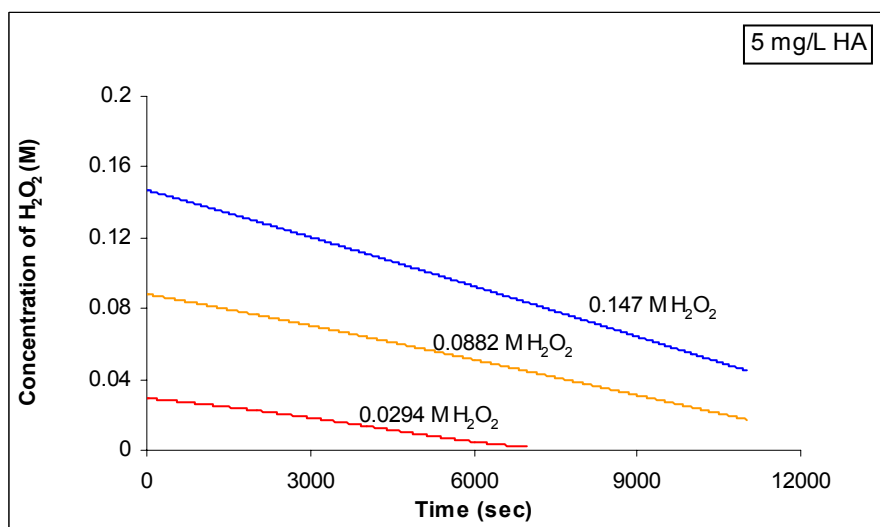


**Fig. 4.1.1.2.2:** Predicted concentration of $H_2O_2$ vs. time at constant initial concentration of HA. Initial conditions: ▬: $[H_2O_2]_o = 0.147$ M, ▬: $[H_2O_2]_o = 0.0882$ M, ▬: $[H_2O_2]_o = 0.0294$ M. $[HA]_o = 5$ mg L$^{-1}$, pH= 7

This increase in the sum of the positive terms will balance the increase in the negative terms and end up with keeping $H_2O_2$ concentration, for example at 0.147 M, from decreasing to a lower value than the concentration at 0.0882 M or 0.0294 M $H_2O_2$. Therefore, the residual fraction of $H_2O_2$ will be higher with high hydrogen peroxide

starting concentrations. The reason that the difference between 0.147 and 0.0294 M is larger than that one between 0.147 and 0.0294 M is that at 0.0294 M hydrogen peroxide the presence of HA will affect the degradation of hydrogen peroxide while at the higher hydrogen peroxide HA only slightly affects degradation of $H_2O_2$.
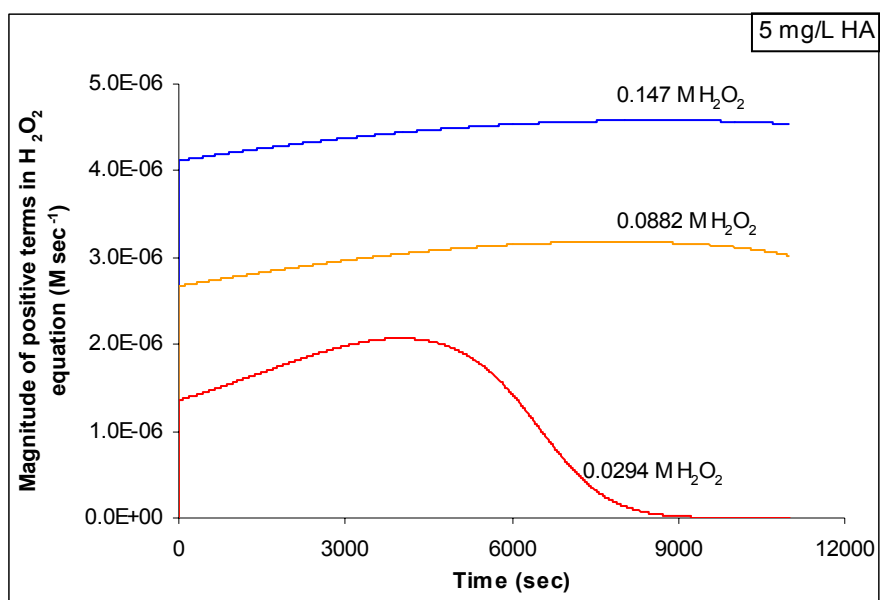


**Fig. 4.1.1.2.3:** Predicted magnitude of the sum of the positive terms in $H_2O_2$ differential equation vs. time at constant initial concentration of HA. Initial conditions: ━: $[H_2O_2]_o = 0.147$ M, ━: $[H_2O_2]_o = 0.0882$ M, ━: $[H_2O_2]_o = 0.0294$ M. $[HA]_o = 5$ mg $L^{-1}$, pH= 7

## 4.1.2. Effect of Initial HA concentration

### 4.1.2.1. Effect of Initial HA concentration on residual fraction of NPDOC

The effect of increasing the initial concentration of HA at constant initial concentration of $H_2O_2$ on the residual fraction of NPDOC was shown in Figures 3.1.3.-A, 3.1.4-A, and 3.1.5-A by increasing initial $H_2O_2$ concentration from 0.0294, 0.0882, to 0.147 M respectively. These figures contain both experimental data and simulation results. From both experimental data and simulation results, it can be seen that initial HA has an effect on residual fraction of NPDOC when $H_2O_2$ is low, e.g., for 0.0294 M. As the concentration of HA is increased the effect decreases and at 0.147 M $H_2O_2$ the

residual fraction is insensitive to HA variation within the reported range. In addition to the light filtering effect, humic material is also known as an effective $^\bullet OH$ scavenger [Liao, 1995; Westerhoff, 1997, 1999; Berzonik, 1998; Nowell, 1992; Mak, 1999]. Since the major source for $^\bullet OH$ radical formation is the photolytic decomposition of $H_2O_2$, the rate of which is controlled by the incident light intensity available for $H_2O_2$, the fraction of the incident light intensity available for $H_2O_2$ is of major concern when the UV-absorbing species HA is present in the solution. This becomes important if $H_2O_2$ concentration is low enough so that the incident light absorbed by $H_2O_2$ will be affected by HA. Therefore, at the low concentration of $H_2O_2$, hydrogen peroxide will be competing for UV light with HA, and, hence, as more HA molecules are in the system light absorbed by hydrogen peroxide will be reduced. As a result the amount of hydroxyl radicals produced is reduced, and, therefore, oxidation of HA will be lowered. Figure 4.1.2.1.1 gives the predicted production of $^\bullet OH$ radical in the system for 0.0294 M $H_2O_2$. From this plot it can be seen that production of $^\bullet OH$ radicals by direct photolysis of hydrogen peroxide increased as less HA is added.

As said earlier the contribution of HA oxidation by $^\bullet OH$ radicals is dominant over the one from direct photolysis (Figures 4.1.1.1.2-I and 4.1.1.1.2-J) hence although more light will be absorbed by HA as its concentration is increased, as shown in Figures 4.1.2.1.2, 4.1.2.1.3, and 4.1.2.1.4, this term won't change the degradation rate of HA tremendously. Also these figures show that the difference in the fraction of UV light absorbed by HA is reduced as initial hydrogen peroxide concentration is increased.
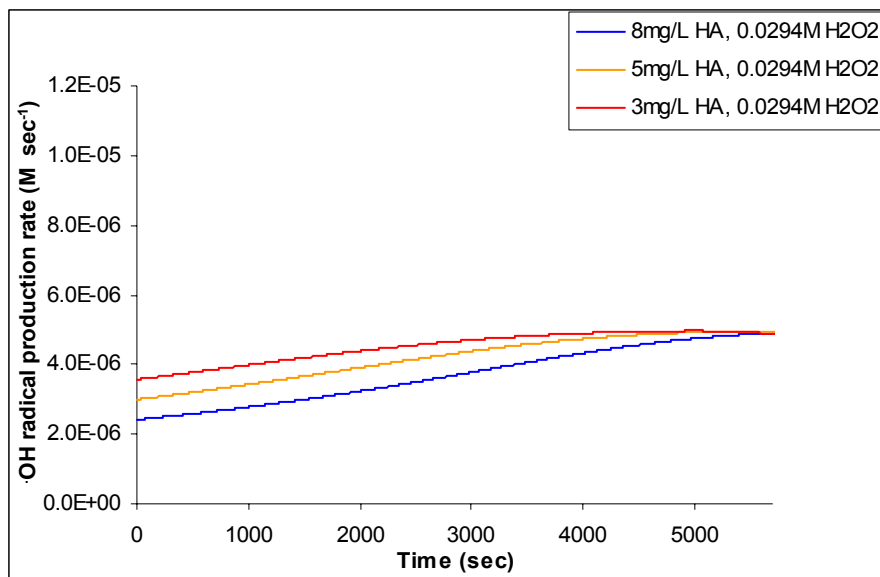
**Fig. 4.1.2.1.1:** Predicted production of $^{\bullet}OH$ radical vs. time at constant initial concentration of $H_2O_2$. Initial conditions: —: $[HA]_o = 3$ mg $L^{-1}$, —: $[HA]_o = 5$ mg $L^{-1}$, —: $[HA]_o = 8$ mg $L^{-1}$. $[H_2O_2]_o = 0.0294$ M, pH = 7

The results from the experimental data and simulation are consistent with the work of Liao (1995). He confirmed the retarding effect of HA on the residual fraction of $H_2O_2$ and chlorobutane (BuCl). Experiments conducted in the presence of humic acid clearly showed that the rate of $H_2O_2$ photolysis and the oxidation rate of BuCl reduced significantly with increasing concentration of HA from 0 to 12 mg $L^{-1}$ starting with 3 x $10^{-5}$ M $H_2O_2$. In our kinetic model the possibility of generating active transients by direct photolysis of humic materials was included in the model.
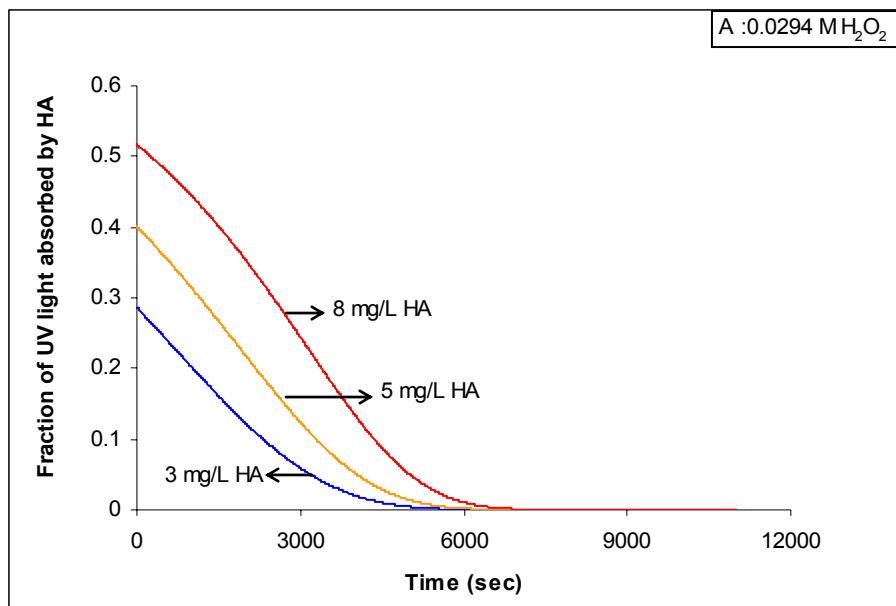
**Fig. 4.1.2.1.2:** Fraction of UV light absorbed by HA vs. time at constant initial concentration of $H_2O_2$. Initial conditions: ▬: $[HA]_o = 3$ mg $L^{-1}$, ▬: $[HA]_o = 5$ mg $L^{-1}$, ▬: $[HA]_o = 8$ mg $L^{-1}$, $[H_2O_2]_o = 0.0294$ M, pH = 7
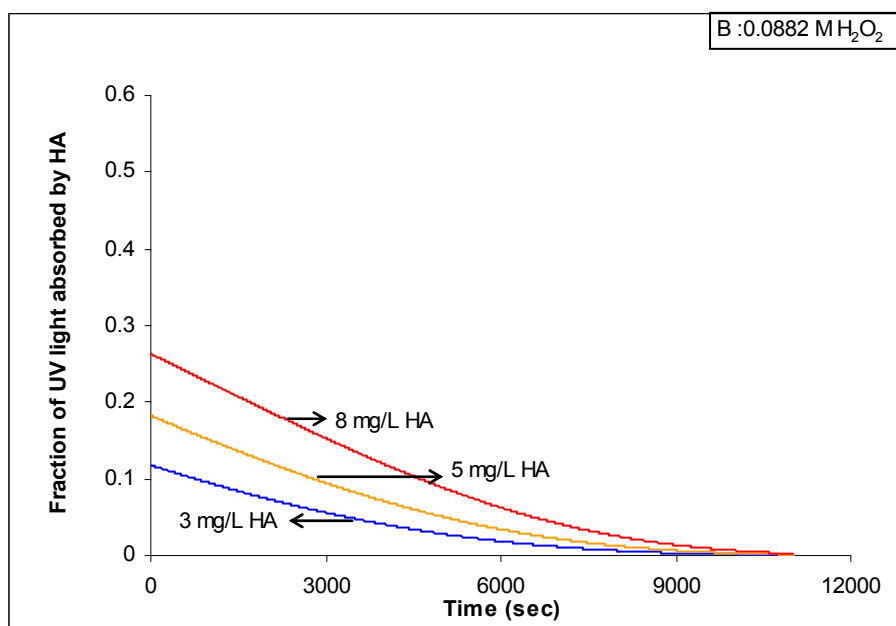


**Fig. 4.1.2.1.3:** Fraction of UV light absorbed by HA vs. time at constant initial concentration of $H_2O_2$. Initial conditions: ▬: $[HA]_o = 3$ mg $L^{-1}$, ▬: $[HA]_o = 5$ mg $L^{-1}$, ▬: $[HA]_o = 8$ mg $L^{-1}$, $[H_2O_2]_o = 0.0882$ M, pH = 7
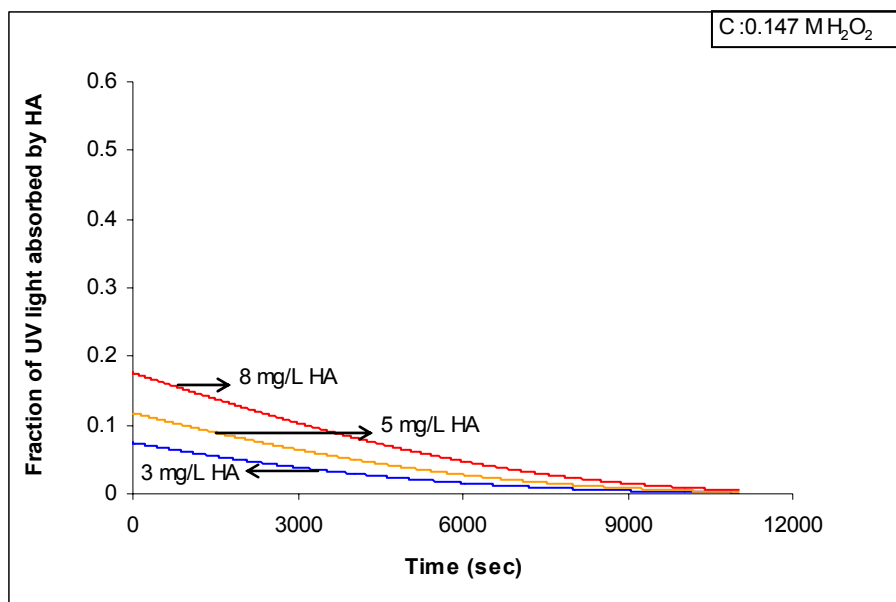
**Fig. 4.1.2.1.4:** Fraction of UV light absorbed by HA vs. time at constant initial concentration of $H_2O_2$. Initial conditions**:** ▬: $[HA]_o = 3$ mg $L^{-1}$, ▬: $[HA]_o = 5$ mg $L^{-1}$, ▬: $[HA]_o = 8$ mg $L^{-1}$, $[H_2O_2]_o = 0.147$ M, pH = 7

The concentration of these transient was also low which is consistent with Liao (1995). In Liao (1995), the possibility of generating active transients by direct photolysis of humic materials was tested experimentally and the results supported this possibility. However, these transients were present at low concentrations implying that the role of humic acid as a promoter of the chain reactions is only minor, and humic material primarily functions as an effective inhibitor in such systems. Lopez (2003) found that a lower initial substrate concentration led to a faster and more efficient degradation. This experimental finding is consistent with our model predictions.

### 4.1.2.2. Effect of Initial HA concentration on residual fraction of $H_2O_2$

The major source for $^\bullet OH$ radical formation and hence $H_2O_2$ degradation is the photolytic decomposition of $H_2O_2$. The rate of $H_2O_2$ degradation is controlled by the incident light intensity available for $H_2O_2$. The fraction of the incident light intensity available for $H_2O_2$ is of major concern when the UV- absorbing species HA is present in

the solution. This becomes important if the $H_2O_2$ concentration is low enough so that the incident light absorbed by $H_2O_2$ will be affected by HA. Therefore, at the low concentrations of $H_2O_2$ the presence of HA will affect the fraction of light absorbed by $H_2O_2$ since as we have defined the photolysis rate as:

$$f_{HA} = \frac{\varepsilon_{HA}[HA]}{\varepsilon_{HA}[HA] + \varepsilon_{H_2O_2}[H_2O_2] + \varepsilon_{HO_2^-}[HO_2^-]}$$

$$f_{H_2O_2} = \frac{\varepsilon_{H_2O_2}[H_2O_2] + \varepsilon_{HO_2^-}[HO_2^-]}{\varepsilon_{HA}[HA] + \varepsilon_{H_2O_2}[H_2O_2] + \varepsilon_{HO_2^-}[HO_2^-]}$$

from these relations it can be seen that the value of the denominator is a function of both $H_2O_2$ ($H_2O_2/HO_2^-$) and HA concentration. At the low limit of $H_2O_2$ concentration the magnitude of ($\varepsilon_{H_2O_2}[H_2O_2] + \varepsilon_{HO_2^-}[HO_2^-]$) decreased and this would allow ($\varepsilon_{HA}[HA]$) term to be more effective while when the initial $H_2O_2$ is high ($\varepsilon_{HA}[HA]$) value becomes too small compared with the ($\varepsilon_{H_2O_2}[H_2O_2] + \varepsilon_{HO_2^-}[HO_2^-]$) term.

From Figures 4.1.2.2.1, 4.1.2.2.2, and 4.1.2.2.3, in which each figure was obtained at a constant $H_2O_2$ concentration and increasing HA, it can be seen that as HA is increased from 3, 5 to 8 mg L$^{-1}$ the fraction of UV light absorbed by $H_2O_2$ is decreased. This behavior is consistent with the relation which was used to predict fraction of UV light absorbed by $H_2O_2$. This would be reflected on the rate of $H_2O_2$ photolysis since as less light is absorbed less degradation will be observed.
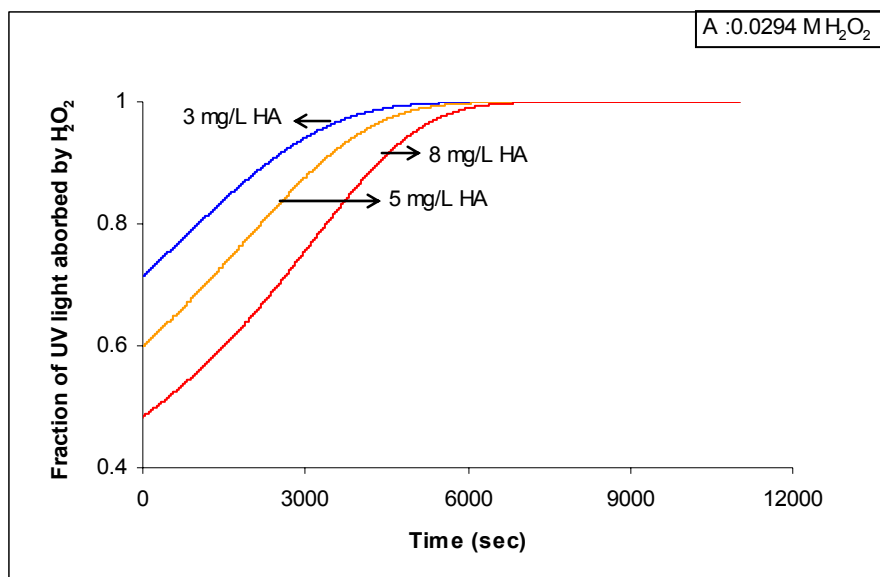
**Fig. 4.1.2.2.1:** Fraction of UV light absorbed by $H_2O_2$ vs. time at constant initial concentration of $H_2O_2$. Initial conditions: ▬: $[HA]_o = 3$ mg $L^{-1}$, ▬: $[HA]_o = 5$ mg $L^{-1}$, ▬: $[HA]_o = 3$ mg $L^{-1}$, $[H_2O_2]_o = 0.0294$ M, pH = 7
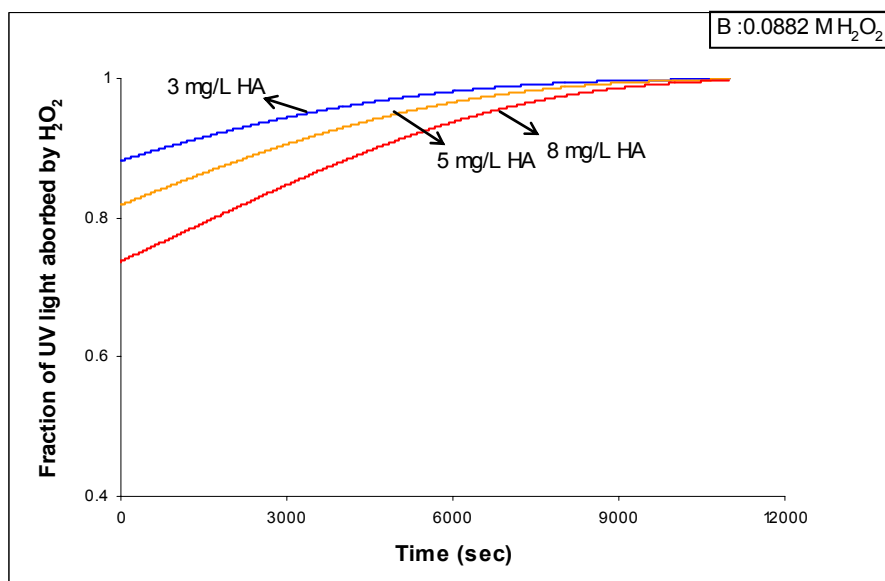


**Fig. 4.1.2.2.2:** Fraction of UV light absorbed by $H_2O_2$ vs. time at constant initial concentration of $H_2O_2$. Initial conditions: ▬: $[HA]_o = 3$ mg $L^{-1}$, ▬: $[HA]_o = 5$ mg $L^{-1}$, ▬: $[HA]_o = 3$ mg $L^{-1}$, $[H_2O_2]_o = 0.0882$ M, pH = 7

The fraction of UV light absorbed by $H_2O_2$ at 0.0882 M and 0.147 M $H_2O_2$ is close which explains the reason that the residual fraction of hydrogen peroxide at 0.147 and 0.0882 M is close.

262
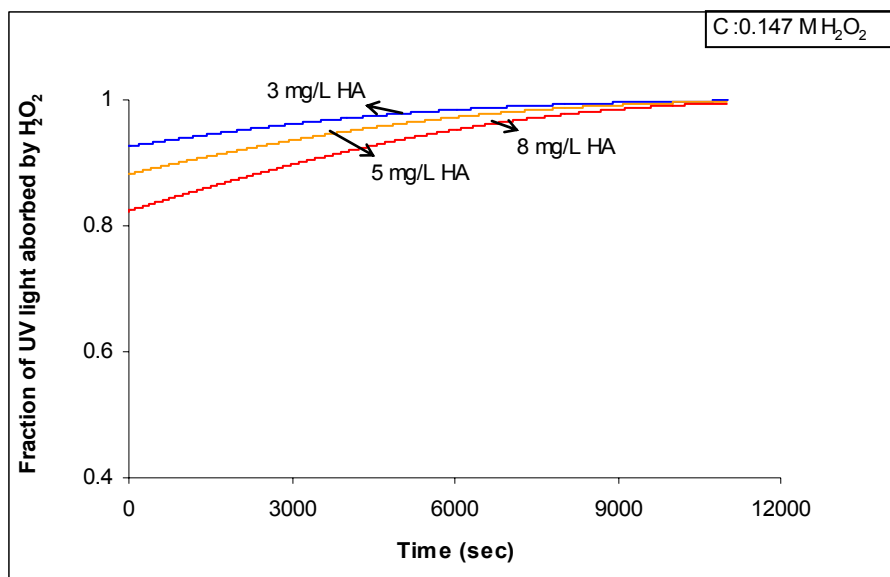
**Fig. 4.1.2.2.3:** Fraction of UV light absorbed by $H_2O_2$ vs. time at constant initial concentration of $H_2O_2$. Initial conditions: ▬: $[HA]_o = 3$ mg $L^{-1}$, ▬: $[HA]_o = 5$ mg $L^{-1}$, ▬: $[HA]_o = 3$ mg $L^{-1}$, $[H_2O_2]_o = 0.147$ M, pH = 7

### 4.1.3. Effect of solvated (hydrated) electrons

In order to investigate the effect of assuming the production of solvated electron the kinetic model developed in this chapter, based on the reaction steps in Table 2.1, was run taken into consideration no production of hydrated electrons. This would mean that reaction intermediates, which were produced due to the production of solvated electron (hydrogen singlet atom and aqueous hydrogen, Table 2.1.1), will disappear from the system. Figures 4.1.3-1 and 4.1.3-2 illustrate examples on simulation results from kinetic model 1 (where solvated electrons are present) and kinetic model 2 where solvated electrons are absent. The same fitting parameters where used in both models along with the rate and equilibrium constants in Table 2.1.1. It can be seen from Figures 4.1.3-1 and 4.1.3-2 that there is no difference in the residual fraction from the two models when hydrogen peroxide is initially 0.0294 M while there is a difference when no hydrogen peroxide was present initially. This is consistent with the results in the previous sections

263

where it was noticed that NPDOC degradation by oxidation with $^\bullet$OH radicals, which are produced from photolysis of $H_2O_2$ is dominant over degradation by direct photolysis at the reported hydrogen peroxide concentrations. Therefore, solvated electron chemistry is expected to be important once the photodegardation of NPDOC is comparable with its oxidation by $^\bullet$OH radicals. This would be satisfied by using low hydrogen peroxide concentration. No experimental data were available at low $H_2O_2$ concentration; therefore a hypothetical case is presented in Figure 4.1.3-3.
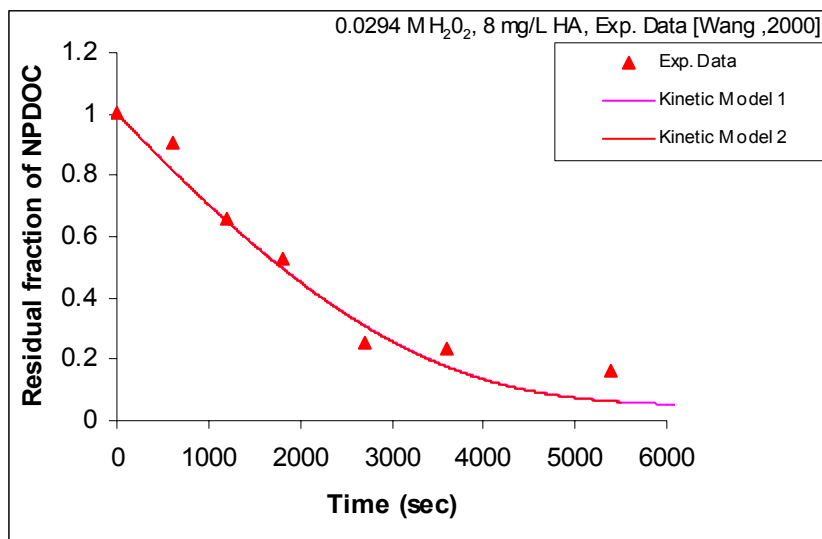


**Fig. 4.1.3-1:** Residual fraction of NPDOC vs. time from experimental data [Wang, 2000], kinetic model 1, and kinetic model 2. Initial conditions: $[H_2O_2]_o = 0.0294$ M, $[HA]_o = 8$ mg $L^{-1}$, pH $= 7$
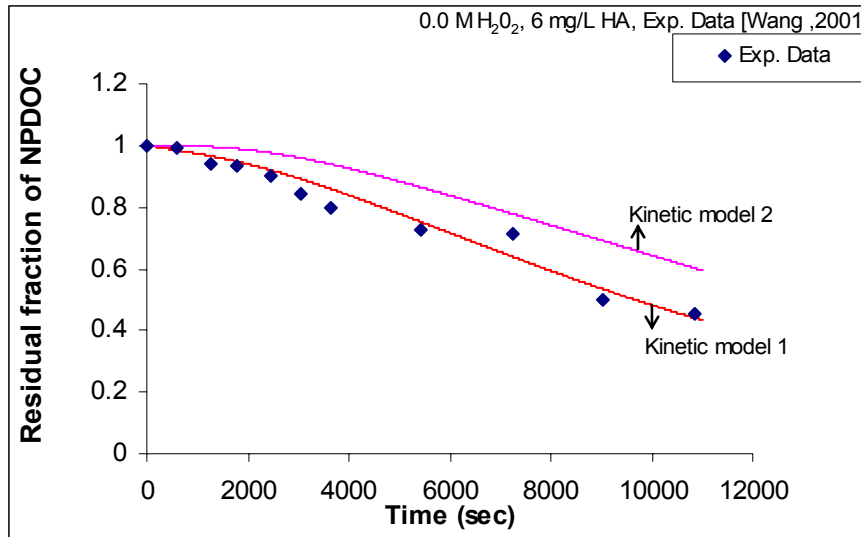
**Fig. 4.1.3-2:** Residual fraction of NPDOC vs. time from experimental data [Wang, 2000], kinetic model 1, and kinetic model 2. Initial conditions: $[H_2O_2]_o = 0.0$ M, $[HA]_o = 8$ mg $L^{-1}$, pH = 7
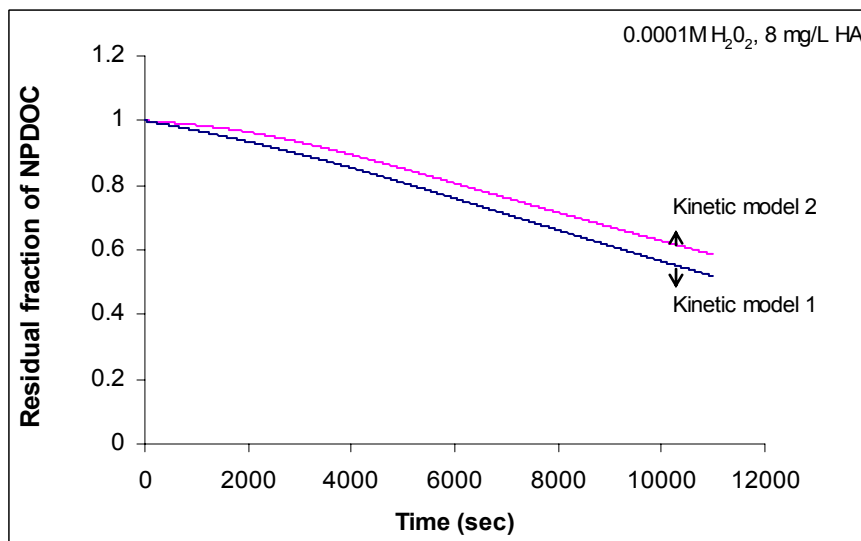


**Fig. 4.1.3-3:** Residual fraction of NPDOC vs. time from kinetic model 1 and kinetic model 2. Initial conditions: $[H_2O_2]_o = 0.0001$ M, $[HA]_o = 8$ mg $L^{-1}$, pH = 7

## 4.2. Discussion on Part II Results

The experimental data of Wang (2001) for which the kinetic model was applied consisted of a study of the effect of initial hydrogen peroxide concentration on the rate of organic matter destruction. This was achieved by keeping the initial concentration of NPDOC at a fixed value (6 mg $L^{-1}$) while increasing hydrogen peroxide concentration from 0.147, 0.178, 0.356 M. When the model was applied using the fitting parameters

265

obtained in the first part of this section, as shown in Figures 3.2.1, 3.2.2 and 3.2.5, the model was able to predict the residual fraction of NPDOC. On the other hand, the residual fraction of hydrogen peroxide from the model was higher than from experimental data. As said earlier in the Part 2 of the result, the shape of the experimental residual fraction data of hydrogen peroxide seemed to follow one pattern if the first experimental data point, at time zero, was excluded from the set. Based on this analysis, the time zero data point was excluded and from extrapolating the linear fitting of the remaining data point, the actual starting initial hydrogen peroxide concentration was obtained. This corrected initial hydrogen peroxide concentration was used in our simulations. Also, the reported residual fraction of hydrogen peroxide was recalculated based on this new corrected value of its initial concentration. Running the kinetic model at these conditions ended up with a good prediction of both residual fraction of hydrogen peroxide and NPDOC as given in Figures 3.2.8-A and –B. As can be seen in Table 3.2.4, the best fitting of model to experimental data, based on least square method, was attained by varying the value of $k_1$, which is the rate constant for direct photolysis of hydrogen peroxide. The value of this rate constant increased as initial concentration of hydrogen peroxide was increased. The same trend was seen in part one of this chapter where $k_1$ value increased by increasing hydrogen peroxide concentration from 0.0294 to 0.147 M. and the reasoning behind this was given in part 1.

### 4.2.1. Effect of Initial $H_2O_2$ concentration

### 4.2.1.1. Effect of Initial $H_2O_2$ concentration on residual fraction of NPDOC

From Figure 3.2.8-A, it can be seen that adding hydrogen peroxide to the reaction mixture enhanced the rate of NPDOC compared to the case where UV alone was applied

to the destruction of NPDOC. However, by increasing the concentration of hydrogen peroxide from 0.113, 0.142, to 0.329 M the rate of NPDOC degradation was retarded. This can be seen easily by following the residual fraction at different initial hydrogen peroxide concentration and fixed time in the above figure. For example, at 1800 sec (30 min) the residual fraction of NPDOC from simulation is 0.494, 0.552, and 0.675 at 0.113, 0.142, to 0.329 M $H_2O_2$, respectively. As we explained in part 1 of this discussion, this effect of hydrogen peroxide is due to that it has a dual rule as a precursor of $^\bullet OH$ radicals and as a scavenger for these radical. Therefore, at the higher concentration of hydrogen peroxide, its scavenging of $^\bullet OH$ radicals will be higher and hence the available $^\bullet OH$ radicals to react with the organic matter will be reduced and hence residual fraction of NPDOC will increase.

### 4.2.1.2. Effect of Initial $H_2O_2$ concentration on residual fraction of $H_2O_2$

The residual fraction of hydrogen peroxide is increased as more hydrogen peroxide is used initially as can be seen from Figure 3.2.8-B. We have seen that by increasing the concentration of hydrogen peroxide, the rate of hydrogen removal by direct photolysis and $^\bullet OH$ radicals has increased. This was also accompanied by an increase in the sum of the rates that lead to hydrogen peroxide production. The simultaneous increase in rate of hydrogen production and consumption make a balance in the differential equation that governs the change of hydrogen peroxide concentration with time. The nest result of these changes that hydrogen peroxide concentration will stay high at the high initial concentration, therefore concentration of hydrogen peroxide at 0.329 > 0.142 > 0.113 M.

## 4.2.1.2. Effect of Initial HA concentration

This set of experiments was performed at a constant initial NPDOC concentration. Therefore, in order to study the effect of initial NPDOC on the system performance we hypothesized two other concentrations for NPDOC which are; 3 and 8 mg L$^{-1}$. The results of model simulation for these new concentrations along with the reported one are shown in Figures 4.2.1.2.1-A, –B ,-C, and –D.
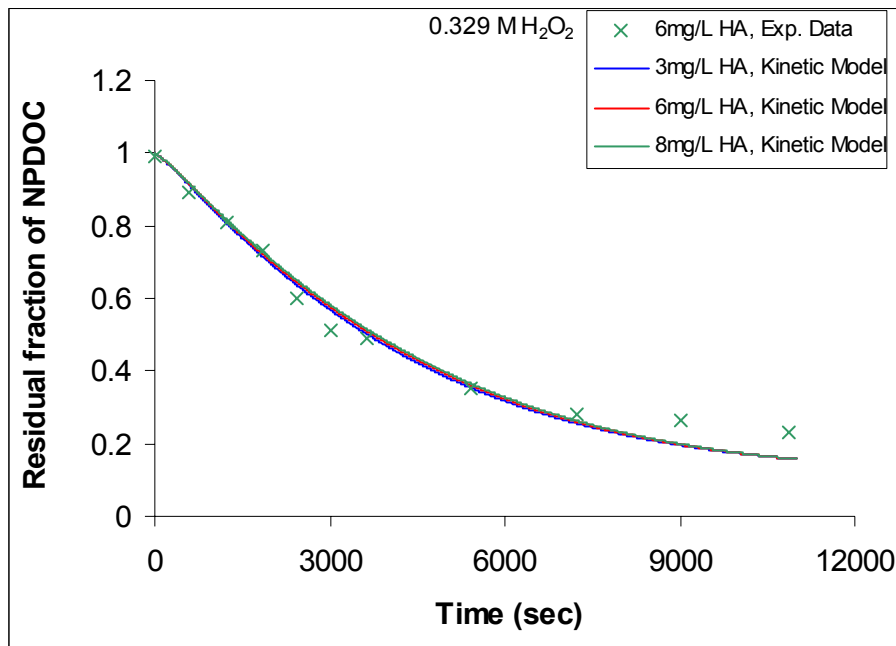


**Fig. 4.2.1.2.1-A:** Residual fraction of NPDOC vs. time at constant initial H$_2$O$_2$ concentration and different initial HA concentrations. Initial concentration; H$_2$O$_2$ = 0.329 M, ×: NPDOC = 6 mg L$^{-1}$ (Experimental data, Wang, 2001).  pH = 7. Solid lines: Model prediction

268
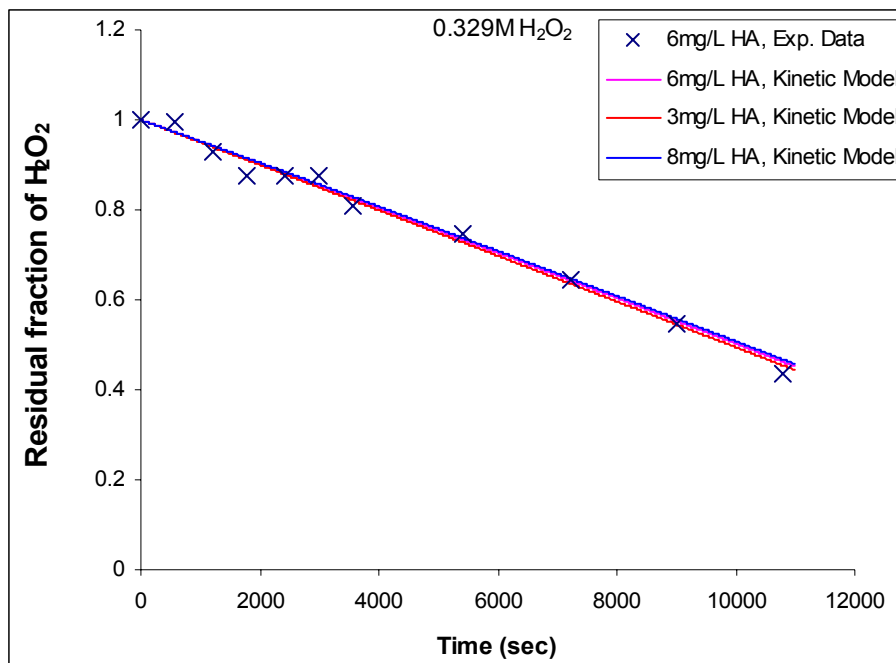
**Fig. 4.2.1.2.1-B:** Residual fraction of $H_2O_2$ vs. time at constant initial $H_2O_2$ concentration and different initial HA concentrations.. Initial concentration; $H_2O_2$ = 0.329 M, ×: NPDOC = 6 mg $L^{-1}$ (Experimental data, Wang, 2001). pH = 7. Solid lines: Model prediction
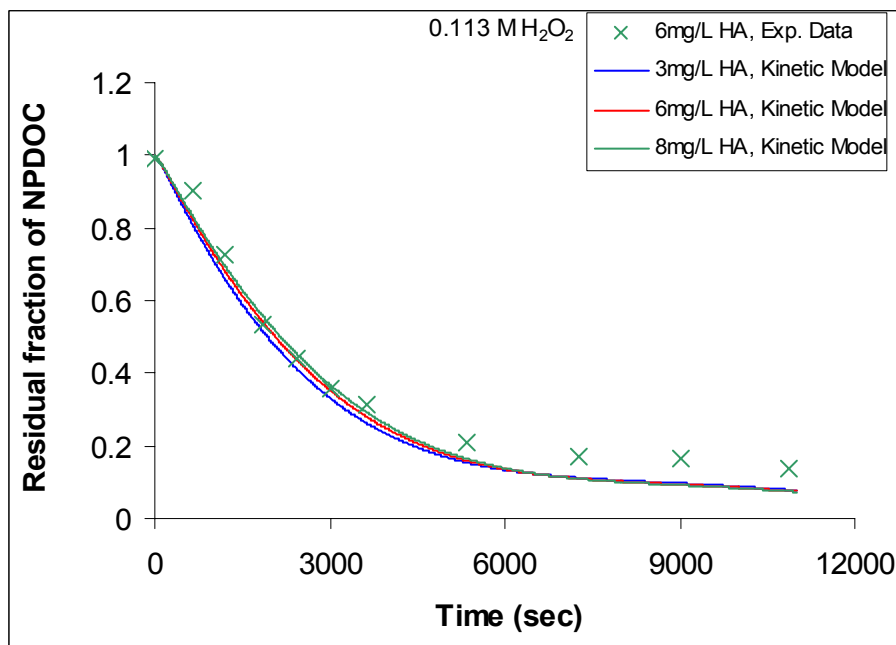


**Fig. 4.2.1.2.1-C:** Residual fraction of NPDOC vs. time at constant initial $H_2O_2$ concentration and different initial HA concentrations.. Initial concentration; $H_2O_2$ = 0.113 M, ×: NPDOC = 6 mg $L^{-1}$ (Experimental data, Wang, 2001). pH = 7. Solid lines: Model prediction
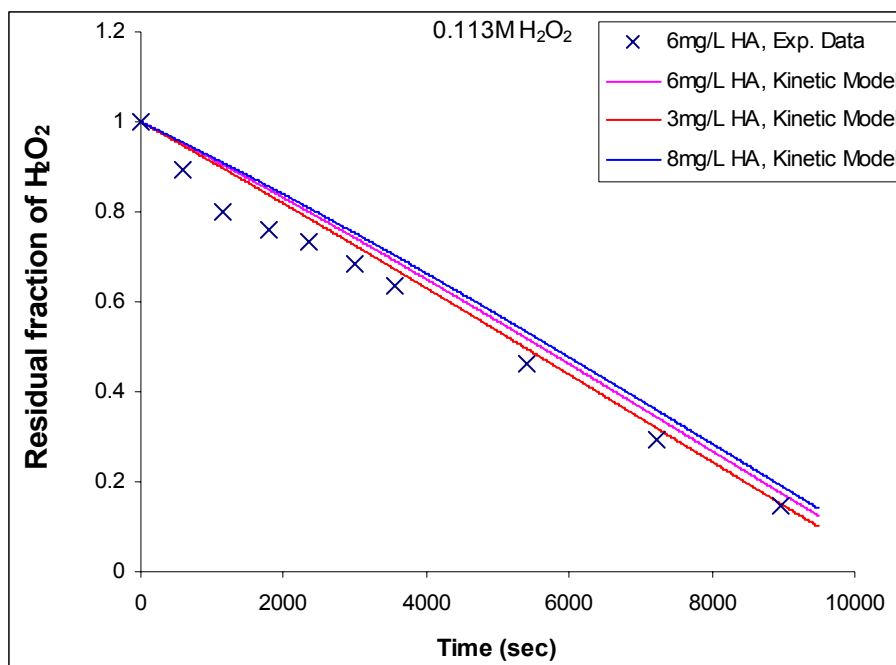
**Fig. 4.2.1.2.1-D:** Residual fraction of $H_2O_2$ vs. time at constant initial $H_2O_2$ concentration and different initial HA concentrations.. Initial concentration; $H_2O_2$ = 0.113 M, ×: NPDOC = 6 mg $L^{-1}$ (Experimental data, Wang, 2001). pH = 7. Solid lines: Model prediction

## 4.2.2.1. Effect of Initial HA concentration on residual fraction of NPDOC

From Figures 4.2.1.2.1-A and 4.2.1.2.1-C it can be seen that when hydrogen peroxide was 0.329 M increasing initial HA concentration from 3, 6, 8 mg $L^{-1}$ didn't affect the rate of NPDOC degradation. When the initial concentration of $H_2O_2$ is 0.113 M, increasing HA concentration from 3, 6, 8 mg $L^{-1}$ didn't affect the rate of NPDOC degradation. This was observed with the simulation in part 1 and the reason that HA affect the system performance is that it is competing with hydrogen peroxide for the UV light, hence when the absorbance of UV light by HA is comparable with that of hydrogen peroxide, the fraction of light absorbed by hydrogen peroxide will be reduced as more HA is in the system. HA is being destroyed by direct photolysis and $^{\bullet}$OH radicals oxidation, with major contribution coming from $^{\bullet}$OH radicals at the studied condition, therefore as less light is absorbed by hydrogen peroxide this means lower production of

270

$^\bullet$OH radicals (Equation 1, Table 2.1.1). The lower the $^\bullet$OH radicals in the reaction mixture the lower is the rate of oxidation of the organic matter. The net effect will end up with higher concentrations of organic matter and hence a higher residual fraction of NPDOC. At 0.329 M $H_2O_2$ the ratio of $H_2O_2$ to NPDOC is too high that the presence of organic matter won't affect the rate of hydrogen peroxide photolysis, and hence rate of $^\bullet$OH radical production. Therefore, residual fraction of NPDOC will be similar for the different initial concentrations of HA.

**4.2.2.2. Effect of Initial HA concentration on residual fraction of $H_2O_2$**

The model prediction of residual fraction of hydrogen peroxide in Figures 4.2.1.2.1-B and 4.2.1.2.1-D shows that the initial concentration of HA has a slight effect on the rate of hydrogen peroxide derogation with this effect vanishing at higher concentrations of hydrogen peroxide concentration. The retarding effect of increasing initial hydrogen peroxide concentration, and its vanishing with higher initial HA concentration, is due to the same reasons which we discussed in section 4.1.2.2.

## 5. Conclusions

This study was conducted to develop a kinetic model for humic acid destruction using $H_2O_2$ and UV light in a well stirred batch reactor under various dosages of $H_2O_2$ and humic acid. The trends of residual fractions of NPDOC and $H_2O_2$ were predicted well by the kinetic model. With the power of modeling we could have a more thorough investigation for the system by predicting the concentration of radicals at the different operating conditions.

Based on the model simulation it was possible to confirm that hydrogen peroxide in the studied system has two main rules a precursor and a scavenger of hydroxyl radicals. The former effect predominates when the initial hydrogen peroxide concentration is low (2.94 mM), the latter at higher concentrations. The variations of initial hydrogen peroxide concentration have more pronounced effect on the system than variations in humic acid concentration within the studied conditions. This is due to that, under the high concentrations of hydrogen peroxide used and relatively low concentration of humic acid, the system is controlled by the direct photolysis of hydrogen peroxide.

Degradation of humic acid by direct photolysis is important at low hydrogen peroxide concentrations. At high hydrogen peroxide concentration, degradation of NPDOC is by $^\bullet OH$ radicals is dominant over its degradation by direct photolysis,

The effect of solvated electrons was evaluated by running the kinetic model considering the presence of solvated electrons, and the related reactions, and by running the model considering no production of solvated electron. Presence and absence of solvated electron from the model was significant at the low initial hydrogen peroxide concentrations, which is consistent with the other results, since degradation of NPDOC by $^\bullet OH$ radicals is dominant over direct photolysis at high hydrogen peroxide concentrations. Further tests of the model with bicarbonate/carbonate are described in next chapters.

## 6. References

Al-Rashhed, R. and Cardin, D.J. "Photocatalytic Degradation of Humic Acid In Saline Waters. Part 1. Artificial Seawater: Influence of $Tio_2$, Temperature, Ph, And Air-Flow." *Chemosphere* **51**, 925-933 (2003)

Acero, J. L. and Urs, V.G. "Influence of Carbonate on the Ozone/Hydrogen Peroxide Based Advanced Oxidation Process for Drinking Water Treatment." *Ozone: Science & Engineering* **22**(3), 305-328 (2000)

Aguer, J. P.;Richard, C.; Andreux, F. "Effect of Light on Humic Substances: Production Of Reactive Species." *Analusis* **27**(5), 387-90 (1999)

Aguer J. P. *et al* " Photoinductive Properties of Soil Humic Acids and Their Fractions by Tanden Size Exclusion Chromatography-Polyacrylamide Gel Electrophoresis." *Chemosphere* **44**, 205-209 (2001)

Aguer, J. P.; Richard, C.;Trubetskaya, O.; Trubetskoj, O.; Leveque, J., Andreux, F. " Photoinductive Efficiency of Soil Extracted Humic and Fulvic Acids." *Chemosphere* **49**, 259-262 (2002)

American Water Works Association (AWWA). Effect of Bicarbonate Alkalinity on Performance of Advanced Oxidation Process. Publisher: (American Water Works Association), USA (1998)

Baxendale, J.H. and Wilson, J. A. "The Photolysis of Hydrogen Peroxide at High Light Intensities." *Trans. Faraday Soc.* **53**, 344-356 (1957)

Beckert, D. and Mehler, K. "Investigation of Hydrogen Atom addition to Vinyl Monomers by time-resolved ESR spectroscopy**."** *Ber. Bunsenges. Phys. Chem* **87**(7), 587-91 (1983)

Behar, D.; Czapski,g.; and Duchovny, I. "Carbonate Radical in Flash Photolysis and Pulse Radiolysis of Aqueous Carbonate Solutions." *The Journal of Physical Chemistry* **74**(10), 2206-2210 (1970)

Behnajady, M. A.; Modirshahla, N.; Shokri, M. "Photodestruction of Acid Orange 7 (AO7) in aqueous solutions by UV/H2O2: influence of operational parameters." *Chemosphere* **55**(1), 129-134 (2004)

Beltran, F.J.; Gnzalez, M.; Gonzalez, J.F "Industrial Waste Water Asdvaned Oxidation. Part 1: UV Radiatiom in the Presence and Absence of Hydrogen Peroxide." *Wat. Res*. **31**(10), 2405-2414 (1997)

Benitez, F. J.; Beltran-Heredia, J.; Acero, J. L.; Rubio, F. J. "Contribution of Free Radicals to Chlorophenols Decomposition by Several Advanced Oxidation Processes." *Chemosphere* **41**(8), 271-7 (2000)

Bielski, Benon H. J.; Allen, Augustine O. "Mechanism of the Disproportionation of Superoxide Radicals." *J. Phys.Chem*. **81**(11), 1048-50 (1977)

Bielski, Benon H. J.; Cabelli, D. E.; Arudi, R. L.; Ross, A. B. "Reactivity of Perhydroxyl/Superoxide Radicals in Aqueous Solution." *J. Phys. Chem. Ref. Data*, **14**(4), 1041-100 (1985)

Blazka, O.; Prochazkova, L. " Mineralization of Organic Matter in Water by U.V. Radiation." *Wat. Res*. **17**(4), 355-364 (1983)

Boyle, J. W.; Ghormley, J. A.; Hochanadel, C. J.; Riley, J. F. "Production of Hydrated Electrons by Flash Photolysis of Liquid Water with Light in the First Vontinuum" *J. Phys. Chem*. **73,** 2886 – 2890 (1969)

Brezonik, P. L., Fulkerson-Brekken, J. " Nitrate-Induced Photolysis in Natural Waters: Control on Concentration of Hydroxyl Radical Photo-Intermediates by Natural Scavenging Agents." *Environ. Sci. Technol*. **32**, 3004-3010 (1998)

Buxton, G. V.; Greenstock, C.L; Helman, W.P.; Ross, A.B. "Critical Rreview of Rate Constants for Reactions of Hydrated Electrons, Hydrogen Atoms and Hydroxyl Radicals ($^{\bullet}OH/O^{\bullet-}$) in Aqueous Solution." *J. Phys. Chem. Ref. Data* **17**, 513-886 (1988)

Calvert, J. G. and Pitts, J. N. Jr. Photochemistry. John Wiley & Sons, Inc. 1966

Cater, S. R.; Stefan, M. I.; Bolton, J. R.; Safarzadeh-Amiri, A. "UV/H2O2 Treatment of Methyl tert-Butyl Ether in Contaminated Waters." *Environ. Sci. Technol*. **34**(4), 659-662 (2002)

Chen, R. and Pignatello, J.J. "Role of Quinone Intermediates as Electron Shuttles in Fenton and Photoassisted Fenton Oxidation of Aromatic compounds." *Environ. Sci. Technol*. **31**, 2399-2406 (1997)

Christensen, H. and Sehested, K.. Pulse Radiolysis at High Temperatures and High Pressures. *Radiation Physics and Chemistry* 16(2), 183-6 (1980)

Christensen, H.; Sehested, K.; Corfitzen, H. "Reactions of Hydroxyl Radicals with Hydrogen Peroxide at Ambient and ElevatedTemperatures." *J. Phys. Chem*. **86**, 1588-1590 (1982)

Christensen, H. and Sehested, K. "The Hydrated Electron and its Reactions at High Temperatures" *J. Phys. Chem*. **90,** 186 – 190 (1986)

Christensen, H.; Sehested, K.; Bjergbakke, E. "Radiolysis of Reactor Water: Reaction of Hydroxyl Radicals with Superoxide ($O_2^-$)." *Water Chemistry of Nuclear Reactor Systems* **5**(1), 141-144 (1989)

Christensen, H.; Sehested, K.; Loegager, T. "Temperature Dependence of the Rate Constant for Reactions of Hydrated Electrons with H, OH and $H_2O_2$." *Radiation Physics and Chemistry* **43**(6), 527-31(1994)

Chu, W. "Modeling the Quantum Yields of Herbicide 2,4-D Decay in UV/$H_2O_2$ Process." *Chemosphere* **44**(5), 935-941 (2001)

Chu, W. and Choy, W.K. "The Mechanism of Rate Enhancing and Quenching of Trichloroethene Photodecay in The presence of Sensitizer and Hydrogen Sources." *Wat. Res.* **36**, 2525-2532 (2002)

Chu, W. and Kwan, C. Y. " Amphoteric Effect of Humic Acids in Surfactant-Aided Photolysis of Polychlorobiphenyls." *Journal of Environmental Engineering* **129**(8), 716-722 (2003)

Cooper, W. J., Zika, R. G., Petasne, R.G., Fischer, A.M. "Sunlight-Induced Photochemistry of Humic Substances in Natural Waters: Major Reactive Species." In: Suffet, I.H., MacCarthy, P.(Eds.), Aquatic Humic Substances: Influence on Fate and Treatment of Pollutants. American Chemical Society, Washington, DC (Chapter22) (1989)

Crittenden, J.C; Hu, S.; Hand, D. W.; Green , A.S. " A kinetic Model For $H_2O_2$/UV process in a completely mixed batch reactor." *Wat. Res*. **33**, 2315-2328 (1999)

Curtis, P.J. " Climatic and Hydrologic Control of DOM Concentration and Quality in the Lakes" Advances in Chemistry Series 133 (1989), (Ecological studies: analysis and synthesis). D. O. Hessen, L. J. Tranvik, editor

Daniton, F. S.; Rowbotton, J. "Primary Radical Yield in Water. Comparison of the Photolysis and Radiolysis of Solutions of Hydrogen Peroxide*." Transactions of The Faraday Society*. **49**, 1160-1173 (1953)

Daniton, F. S. "The primary Quantum Yield in the Photolysis of Hydrogen Peroxide at 3130 $\overset{\circ}{A}$ and the Perimary Radical Yield in the X- and $\gamma$ -Radiolysis of Water*." J. Phys. Chem*. 1278 (1955)

Dean (Ed) J. A., Lange's Handbook of Chemistry, McGraw-Hill, New York, 1979

De Laat, J. and Dore. M. " Degradation of chloroethane in dilute aqueous solution by $H_2O_2$/U.V." *Wat. Res*. **28**(12), 2507-2519 (1994)

De Laat, J.; Berger, P.; Poinot, T.; Leitner, N. K.; Dore. M. "Modeling the Oxidation of Atrazine by $H_2O_2$/UV. Estimation of Kinetic Parameters." *Ozone Science and Engineering* **19**, 395-408 (1997)

Draganic, Z. D.; Negron-Mendoza, A,; Sehested, K.; Vujosevic, S. I. "Radiolysis of Aqueous Solutions of Ammonium Bicarbonate over a Large Dose Range." *Radiat. Phys. Chem.* **38**, 317-321 (1991)

Elliot, Allen John.   "A Pulse Radiolysis Study of the Temperature Dependence of Reactions Involving Atomic Hydrogen, Hydroxyl and Hydrated Electron in Aqueous Solutions."     *Radiation Physics and Chemistry*  **34**(5),  753-8 (1989)

Felix, W. D.; Gall, B. L.; Dorfman, M. D. "Pulse Radiolysis Studies. IX. Reactions of the Ozonide Ion in Aqueous Solution**."** *J. Phys. Chem*. 71,p 384 – 392 (1967)

Fischer, A. M.; Winterle, J. S.; Mill, T. "Direct Observation of Phototransients in Natural Waters." *Chemosphere* **14**(9), 1299-1306 (1985)

Fischer, A. M.; Winterle, J. S.; Mill, T. Primary Photochemical Processes in Photolysis Mediated by Humic Substances.   ACS Symposium Series (1987) 327(*Photochem. Environ. Aquat. Syst.*) 141-56

Fukushima, M.; Tatsumi, K. "Degradation Characterstics of Humic Acid during Photo-Fenton Processes." *Environ. Sci. Technol*. **35**, 3683-3690 (2001)

Fung, P. C.; Poon, C. S.; Chu, C. W.; Tsul, S. M. "Degradation Kinetics of Reactive Dye by UV/$H_2O_2$/US Process under Continuous Mode Operation." *Water Science and Technology*  **44**(6),  67-72 (2001)

Gallard, H.; DeLaat, J.; Legube, B. " Effect of pH on the Oxidation of Organic Compound by Fe(III)/$H_2O_2$. Mechanisms and Simulation." *New J. Chem*. 263-268 (1998)

Gallard, H.; DeLaat, J. " Kinetic Modeling of Fe(III)/$H_2O_2$ Oxidation Reactions in Dilute Aqueous Solution Using Atrazine as a Model Organic Compound." *Wat. Res*. **34**, 3107-3116 (2000)

Glaze, W.H.; Kang, J. W. " Advanced oxidation Processes: Description of a Kinetic model for the Oxidation of Hazardous Materials in Aquoeous Medial with Ozone and Hydrogen Peroxide in a Semibatch Reactor." *Ind. Eng. Chem. Res*. **28**, 1573-1580 (1989a)

Glaze, W. H.; Lay,Y.; Kang, J. " Advanced Oxidation Processes . A Kinetic Model for the Oxidation of 1,2-Dibromo-3-chloropropane in Water by the Combination of Hydrogen Peroxide and UV Radiation." *Ind. Eng. Chem. Res*. **34**, 2314-2323 (1995)

Goldstone, J. V.; Pullin, M. J.; Bertilsson, S.; Voelker, B. M. "Reactions of Hydroxyl Radical with Humic Substances: Bleaching, Mineralization, and Production of Bioavailable Carbon Substrates." *Environ. Sci. Technol.* **36**, 364-372 (2002)

Gordon, S.; Hart, E. J.; Matheson, M. S.; Rabani, J.; Thomas, J. K.  **"**Reaction Constants of the Hydrated Electron**."** J. Am. Chem. Soc. 85, 1375 – 1377 (1963)

Gordon, S.; Hart, E. J.; Thomas, J. K.  "The Ultraviolet Spectra of Transients Produced in the Radiolysis of Aqueous Solutions."   *J. Phys. Chem.*  **68**(5), 1262-4 (1964)

Guittonneau, S.; De Latt, J.; Duguet, J. P., Bonnel, C., Dore, M., " Oxidation of Parachloronitrobenzene in Dilute Aqueous Solution by $O_3$ +UV and $H_2O_2$: A Comparative Study." *Ozone Science and Engineering* **12**, 73-94 (1990)

Hart, E. J.; Gordon, S.; Fielden, E. M.  "Reaction of the Hydrated Electron with Water."   *J. Phys. Chem*. **70**(1), 150-6 (1966)

Hartig, K. J. and Getoff, N**. "**Reactivity of Hydrogen Atoms with Liquid Water**."**  Journal of **18**(1),  29-38 *Photochemistry*  (1982)

Hentz, R. R.; Farhataziz; Hansen, E. M. "Pulse Radiolysis of Liquids at High Pressures. II. Diffusion-controlled Reactions of the Hydrated Electron**."** *Journal of Chemical Physics* **56**(9), 4485-8 (1972)

Hickel, B. and Sehested, K. "Activation Energy for the Reaction $H^{\bullet} + OH^{-} \rightarrow e_{aq}^{-}$. Kinetic Determination of the Enthalpy and Entropy of Solvation of the Hydrated Electron." *J. Phys. Chem*. **89**, 5271 – 5274 (1985)

Hoigne, J. and Bader, H. "Ozonation of Water: Kinetics of Oxidation of Ammonia by Ozone and Hydroxyl Radicals." *Environ. Sci. & Technol*. **12** (1), 79-84 (1978)

Hoigne, J. and Bader, H. "Decomposition of Ozone in Water: Rate of Initiation by Hydroxide Ions and Hydrogen Peroxide." *Environ. Sci. & Technol*. **16**, 676-681 (1982)

Hou, W.; Tsuneda, S.; Hirata, A. " TOC Removal of Raw Industrial Waste Water from LSI Pjoto-resist Processing with $H_2O_2$/UV in a Batch Reactor." *J. Chem. Eng. Japan*. **34**, 444-447 (2001)

Huie, R. E. and Clifton C. L. "Temperature Dependence of the Rate Constants for Reactions of the Sulfate Radical, $SO_4^{-}$, with Anions." *J. Phys. Chem*. **94**, 8561-8567 (1990)

Hunt, J. P. and Taube, H. "The Photochemical Decomposition of Hydrogen Peroxide. Quantum Yields, Tracer and Fractionation Effects." *J. Am. Chem. Soc.* **5**, 5999 (1952)

Hug, S. and Leupin, O., "Iron-Catalyzed Oxidation of Arsenic (III) by Oxygen and by Hydrogen Peroxide: pH-Dependent Formation of Oxidants in the Fenton Reaction." *Environ. Sci. Technol*. **37**, 2734-2742 (2003)

Jonah, C.D.; Miller, J. R.; Matheson, M. S." The Reaction of Hydrated Electron + Oxonium. Concentration Effects of Acid or Salts" *J. Phys. Chem*. **81,**931 – 934 (1977)

Kang J. W and Lee K. H. "A Kinetic Model of the $H_2O_2$/UV Process for the Treatment of Hazardous Water Chemicals." *Environ. Eng. Sci*. **14**(3), 183-192 (1997)

Kim, S.; Kramer, R.W.; Hatcher, P. G. "Graphical Method for Ananlysis of Ultrahigh-Resolution Broadband Mass Spectra of Natural Organic Matter, the Van Krevelen Diagarm." *Anal. Chem*. **75**, 5336-5344, (2003)

Koppenol, W. H.; Bulter, J.; Van Leeuwen, J. W. L. "The Haber-Weiss Cycle." *Photochem. Photobiol*. **28**, 655-660 (1978)

Koubeck, E. "For Oxidation of Refractory Organics in Aqueous Waste Streams by Hydrogen Peroxide and Ultraviolet Light." U.S. Patent, 4,012,321, (1977)

Lea, D.E. *Trans. Farday Soc.,* **45**, 81 (1949)

Liao, C-H.; Gurol, M.D." Chemical Oxidation by Photolytic Decomposition of Hydrogen Peroxide**."** *Environ. Sci. Technol.* **29**, 3007 – 3014 (1995)

Lin, C. F.; Huang, Y. J.; Hao, O. J. "Ultrafiltration Processes for Removing Humic Substances: Effect of Molecular Weight Fractions and PAC Treatment." *Wat. Res*., **33**(5), 1252-1264 (1999)

Lopez, A.; Bozzi, A.; Mascolo, G.; Kiwi, J. "Kinetic Investigation on UV and UV/$H_2O_2$ degradations of Pharmaceutical Intermediates in Aqueous Solutions." *Journal of Photochemistry and Photobiology A: Chemistry* **156**,121-126 (2003)

Lyderson, E., " Humus and Acidification." Advances in Chemistry Series 133 (1989), (<u>Ecological studies: analysis and synthesis</u>). D. O. Hessen, L. J. Tranvik, editor. Springer

Mak, F.T.; Zele, S. R.; Cooper, W. J.; Kurucz, C. N.; Waite, T. D., Nickelsen, M. G. " Kinetic Modeling of Carbon Tetrachloride, Chloroform and Methylene Chloride Removal from Aquoeous Solution Using the Electron Beam Process." *Wat. Res*. **31**(2), 219-228 (1999)

Matheson, M. S. and Rabani, J. "Pulse Radiolysis of Aqueous Hydrogen Solutions. I. Rate Constants for Reaction of $e_{aq}$- with Itself and other Transients. II. The Interconvertibility of $e_{aq}$- and H·." J. Phys. Chem. **69**(4), 1324-35 (1965)

McKnight, D.M. and Aiken, G.R. "Sources and Age of Aquatic humus." Advances in Chemistry Series 133 (1989), (<u>Ecological studies: analysis and synthesis</u>). D. O. Hessen, L. J. Tranvik, editor. Springer

Meisel, D.; Czapski, G.; Matheson, Max S.; Mulac, W. A. "Existence of Dielectrons in Aqueous Solutions." International Journal for Radiation Physics and Chemistry 7(2-3), 233-41 (1975)

Mezyk, S. P. and Bartels, D. M. "Direct EPR Measurement of Arrhenius Parameters for the Reactions of H· atoms with $H_2O_2$ and D· Atoms with $D_2O_2$ in Aqueous Solution*." Journal of the Chemical Society, Faraday Transactions* **91**(18), 3127-32 (1995)

Miller, W.L. " Effect of UV Radiation on Aquatic Humus: Photochemical Principles and Experimental Considerations" Advances in Chemistry Series 133 (1989), (<u>Ecological studies: analysis and synthesis</u>). D. O. Hessen, L. J. Tranvik, editor. Springer

Morgan, M.S.; Trieste, P.V.; Garlick, M. S.; Mahon, M.J; Smith, A. L. " Ultraviolet Molar Absortivity of Aqueous Hydrogen Peroxide and Hydroperoxyl Ion." *Analytical Chimica Acta* **215**, 325-329 (1988)

Nowell, L. H. and Hoigne, I. "Photolysis of Aqueous Chlorine at Sunlight and Ultraviolet Wavelengths— II. Hydroxyl Radical Production" *Wat. Res*. **26**(5), 599-605 (1992)

Pagsberg, P.; Christensen, H.; Rabani, J.; Nilsson, G.; Fenger, J.; Nielsen, S. O. "Far-Ultraviolet Spectra of Hydrogen and Hydroxyl Radicals from Pulse Radiolysis of Aqueous Solutions. Direct measurement of the rate of H + H." *J. Phys. Chem*. **73**(4), 1029-38 (1969)

Power, Joan F.; Sharma, Devendra K.; Langford, Cooper H.; Bonneau, Roland; Joussot-Dubien, Jacques. "Laser Flash Photolytic Studies of a Well-Characterized Soil Humic Substance.**"** ACS Symposium Series (1987), 327(Photochem. Environ. Aquat. Syst.) 157-73

Rodriguez, S.M.; Ritcher, C.; Galvez, J. B.; Vincent, M. " Photocatalytic Degradation of Industrial Residual Waters." *Solar Energy* **56**(5), 401-410 (1996)

Schmidt, K. H. and Bartels, D.M. "Lack of Ionic Strength Effect in the Recombination of Hydrated Electrons: $(e^-)_{aq} + (e^-)_{aq} \longrightarrow 2(OH^-) + H_2$."*Chemical Physics* **190**(1), 145-152 (1995)
Schwarz, H. A. "Reaction of the Hydrated Electron with Eater" *J. Phys. Chem*. **96**, 8937 – 8941 (1992)

Sehested, K.; Rasmussen, O. L.; Fricke, H. "Rate Constants of ·OH with $HO_2$·, $O_2$·-, and $H_2O_2^+$ from Hydrogen Peroxide Formation in Pulse-Irradiated Oxygenated Water." *J. of Phys. Chem.* **72** (2), 626-31(1968)

Sehested, K. and Christensen, H. "The Rate constant of the Bimolecular Reaction of Hydrogen Atoms at Elevated Temperatures." *Radiation Physics and Chemistry* **36**(3), 499-500 (1990)

Sharpless, C. M. and Linden, K. " UV Photolysis of Nitrate: Effects of Natural Matter and Dissolved Inorganic Carbon and Implications for UV Water Disinfection." *Environ. Sci. Technol.* **35**, 2949-2955 (2001)

Selcuk, H.; Sene, J. J.; Anderson, M. A. " Photoelectrocatalytic Humic acid Degradation Kinetics and Effect of pH, Applied Potential and Inorganic Ions." *Journal of chemical Technology and Biotechnology* **78**, 979-987 (2003)

Snoeyink, V. L. and Jenkins, D. Water Chemistry. John Wiley & Sons, 1980, New York USA

Sorensen, M. and Frimmel, F. H. "Photochemical Degradation of Hyfrophilic Xenobiotics in the UV/$H_2O_2$ Process: Influence of Nitrate on the Degradation Rate of EDTA, 2-amino-1-naphthalenesulfonate, Diphenyl-4-Sulfonate and 4,4-Diaminostibelne-2,2-Disulfonate." *Wat. Res*. **31**(11), 2885-2891 (1997)

Stefan, M. I.; Hoy, A. R.; Bolton, J.R.  "Kinetics and Mechanism of the Degradation and Mineralization of Acetone in Dilute Aqueous Solution Sensitized by the UV Photolysis of Hydrogen Peroxide." *Environ. Sci. Technol.* **30**(7), 2382-2390 (1996)

Stepnowski, O.; Siedlecka, E. M.; Behrend, P.; Jastroff, B. "Enhanced Photo-Degradation of Contaminants in Petroleum Refinery Wastewater." *Wat. Res*. **36**, 2167-2172 (2002)

Stumm, W. and Morgan, J.J. Aquatic Chemistry, Prentice-Hall, Englewood NJ, (1996)

Swallow, A. J." Recent Results from Pulse Radiolysis*." Photochemistry and Photobiology* 7(6), 683-94, (1968)

Taylor, H.S. "Quantum Processes in Photochemistry." *Journal of physical chemistry* **4**, 516-528 (1928)

Telser T. and Schindewolf, U. "Reaction of Hydrated Electrons with Alkali Metal Cations in Alkaline Aqueous Solutions" J. Phys. Chem. 90,  5378 – 5382 (1986)

Thomas, J. K.   "Rates of Reaction of the Hydroxyl Radical."     *Transactions of the Faraday Society* **61**(508), 702-7 (1965)

Thomas-Smith, T. E. and Blough, N. V. "Photoproduction of Hydrated Electron from Constituents of Natural Waters." *Environ. Sci. Technol.* **35**, 2721-2726 (2001)

Vollman, D.H.; Chen, J.C., " The Photochemical Decomposition of Hydrogen Peroxide in Aqueous Solutions of Allyl Alcohol at 2537 $\overset{\circ}{A}$ ." *J. Am. Chem. Soc*. **20**, 4141 (1959)

Wang, G.-S.; Hsieh, S.-T.; Hong, C. S.    "Destruction of Humic Acid in Water by UV Light-Catalyzed Oxidation with Hydrogen Peroxide." *Wat. Res*., **34**(15), 3882-3887 (2000)

Wang, Gen-Shuh; Liao, Chih-Hsiang; Wu, Fang-Jui. "Photodegradation of Humic Acids in the Presence of Hhydrogen Peroxide." *Chemosphere* **42**(4), 379-387 (2001)

Weeks, J. L.; Matheson, M. S., "The Primary Qunatum Yield of Hydrogen Peroxide Decomposition*." J. Phys. Chem.* 1273 (1955)

Weeks J. L. and  Rabani, R. "The Pulse Radiolysis of Deaerated Aqueous Carbonate Solutions. I. Transient Optical Spectrum and Mechanism. II. pK for $^{\bullet}OH$  Radicals." *The Journal of Physical Chemistry*  **70**(7), 2100-2106  (1966)

Weinstien, J.; Bielski, H. J. "Kinetics of the interaction of $HO_2$ and $O_2^-$ Radicals with Hydrogen Peroxide. The Haber-Weiss Reaction." *J. Am. Chem. Soc.*  **3**, 58-62 (1979)

Weir, B. A., and Sundstrom,. "Destruction of Trichloroethylene by UV Light-Catalyzed Oxidation with Hhydrogen Peroxide." *Chemosphere* **27**(7), 1279-1291 (1993)

Westerhoff, P.; Song, R.; Minear, R. " Applications of Ozone Models." *Ozone: Sceince and Enginerring* **19**, 55-73 (1997)

Westerhoff, P.; Aiken, G.; Amy, G.; Debroux, J. "Relationships Between the Structure of Natural Organic Matter and its Reactivity Towards Molecular Ozone and Hydroxyl radicals." *Wat. Res*. **33**, 2265-2276 (1999)

Zepp, R. G.; Schiotzhauer, P.F.; Slnk, R. M. "Photosensitized Transformations Involving Electronic Energy Transfer in Natural Waters: Role of Humic Substances." *Environ. Sci. Technol.* **19**, 74-81 (1985)

Zepp, Richard G.; Braun, Andre M.; Hoigne, Juerg; Leenheer, Jerry A. "Photoproduction of Hydrated Electrons from Natural Organic Solutes in Aquatic Environments." *Environ. Sci. Technol.* **21**(5), 485-90 (1987a)

Zepp, R.G.; Hoigne, J.; Bader, H. :Nitrate-Induced Photooxidation of Trace Organic Chemicals in Water." *Environ. Sci. Technol*. **21**, 443-450 (1987b)

# Chapter 3

**A Kinetic Model for Humic Acid Oxidation Using Hydrogen Peroxide and UV Light in the Presence of Carbonate/Bicarbonate**

## Abstract

The kinetic model which was developed in Chapter Two, was used to study the effect of the presence of carbonate/bicarbonate on the rate of degradation of non purgeable dissolved organic carbon (NPDOC) using hydrogen peroxide and UV ($H_2O_2$/UV) advanced oxidation. Experimental data taken from Wang (2000) was used to test the kinetic model in the presence of carbonate/bicarbonate. The kinetic model was able to describe the trend of the experimental data. The kinetic model simulations, along the experimental data [Wang, 2000], for the conditions in this work, showed a retardation effect on the rate of degradation of NPDOC due to the presence of bicarbonate and carbonate. This effect was attributed to the scavenging of the hydroxyl radicals by carbonate and bicarbonate. Also at these conditions, it was hypothesized that carbonate radicals produced from the reaction of carbonate and bicarbonate ions with hydrogen peroxide, were contributing to the rate of NPDOC degradation. The reaction of carbonate radicals was considerable for the degradation of hydrogen peroxide also. Based on the previous analysis it can be seen at the studied conditions of hydrogen peroxide concentration, HA concentration, carbonate/bicarbonate concentration, and pH value that the system was sensitive to the presence of bicarbonate/carbonate in the system.

Based on hypothetical assumptions in the kinetic model it was found that reactions of bicarbonate and carbonate are important and should be included in the kinetic model for the experimental conditions given by Wang (2000). This would also indicate that during treatment processes if UV/$H_2O_2$ treatment would be applied then the

presence of bicarbonate/carbonate will affect the process. Based on this model, their presence will scavenge hydroxyl radicals on one extreme and on the other extreme this scavenging will produce carbonate radicals. These radicals contribute to the degradation of NPDOC.

The kinetic model simulation for the data reported by another work of Wang (2001) showed that carbonate and bicarbonate concentration had a negligible effect at the high concentration of hydrogen peroxide concentration. However, the experimental results showed a significant retardation effect on the degradation of NPDOC. The simulation described well the system behavior for the case where no carbonate/bicarbonate was present.

# 1. Introduction

Some organic compounds are resistant to conventional chemical and biological treatments. For this reason, other methods are being studied as an alternative to biological and classical physical-chemical processes. Of these, Advanced Oxidation Processes (AOPs) may constitute the best option in the near future [Santiago, 2002]. AOPs are those processes which involve the production of reactive free radicals, especially the most important the $^\bullet OH$ radicals, in the reaction mixture. The high reactivity of the $^\bullet OH$ radicals is responsible about the destruction of the organic compounds [Santiago, 2002; Glaze, 1995; Benitz, 2000].

Major growth in the interest and use of AOPs has taken place in the last few years primarily because increasing stringent environmental regulations has made attractive the prospect of organic compound destruction rather than transferring to another phase. Therefore AOPs have become attractive for the control of organic compounds in waste water treatment [Kang, 1997; Stepnowshki, 2002; Hou, 2001].

The hydroxyl radical is an extremely reactive and nonselective oxidant and, thus, when produced in sufficient quantities, can lead to complete oxidation of organic compounds to carbon dioxide, water, and inorganic ions [Acero, 1999; Liao, 1995]. Hydroxyl radicals attack organic compounds with rate constants ranging from $10^7$ to $10^{10}$ $M^{-1} s^{-1}$ oxidizing them by hydrogen atom abstraction or by addition to double bonds [Buxton, 1988]. In AOPs, $^\bullet OH$ radicals can be produced by: ionizing radiation on water, hydrogen peroxide with ozone ($H_2O_2/O_3$) , Fenton's reagent ($H_2O_2$ and Fe(II)), ($H_2O_2$ and Fe(III)), Fenton's like reagent ($H_2O_2$ and $Fe^o$), direct photolysis of $H_2O_2$ by UV light

($H_2O_2$/UV), catalyzed decomposition of ozone ($TiO_2$), ozone with ultraviolet radiation (UV/$O_3$), and UV/$H_2O_2$/$O_3$.

The UV/$H_2O_2$ process is an example of a homogeneous AOP. The effectiveness of this process is associated with very reactive species such as hydroxyl radicals which are generated in the reaction mixture. The chemistry of hydrogen peroxide in aqueous systems has been studied extensively. Therefore, many of the reaction steps with the corresponding rate constants are well documented in the literature to represent the mechanism of hydrogen peroxide photolysis with the corresponding chemical reactions. [Bielski, 1977, 1985; Baxendale, 1988; Hunt, 1952; Behar, 1970; Christensen,1982, 1989; Sehested, 1968; Weeks,1955; Daniton, 1953, 1955; Pagsberg, 1969; Thomas, 1965; Vollman, 1959; Brezonik, 1998; Guittonneau, 1990; Weinstien, 1979 ].

Humic substances are relatively stable organic carbon compounds ubiquitous in the biosphere. This ubiquitous organic is a result of the diverse sources and pathways of formation of humic substances and their slow degradation by geochemical or microbial process. Humic substances vary in molecular weight and contain conjugate olefinic and aromatic functional groups, as well as carboxyl and hydroxyl and sometimes a small percentage of nitrogenous functional groups [Aguer, 2001, 2002; Fischer, 1987; McKnight, 1989; Lyderson, 1989; Kim, 2003; Goldstone, 2002; Chu, 2003]. Humic materials consist mainly of humic acid (HA) and fulvic acids (FA) [Aguer, 2002; Fisher, 1987].

The efficiency of AOPs depends on various parameters, such as oxidant dose, UV light intensity, contact time, structure of the organic pollutant, chemical composition of

the water, absorbance of the solution [Guittonneau, 1990; Hogine, 1978; De Laat, 1997]. The chemical composition of water determines if other species are present in the water matrix, which might consume the $^\bullet$OH radicals or absorb UV light. Bicarbonate and carbonate are constituents of most natural waters and were postulated to have an effect on the performance of AOPs. Their effect is a function of the type of the treatment process and their concentration compared to the concentration of target contaminant and oxidant used.

Carbonate and bicarbonate ions, as scavengers of $^\bullet$OH radicals, are important in surface waters, while it was postulated that scavengers are most important in typical ground waters. This is due to the fact that most ground waters may have relatively high concentrations of scavengers such as bicarbonate or carbonate [Glaze, 1989a]. The reactions of carbonate and bicarbonate with hydroxyl radicals and their effect on the performance of AOPs have been studied by several researchers [Peyton, 1988; Glaze, 1995; Amiri, 2001; Brezonik, 1998; Hug, 2003; King, 2003; AWWA, 1998; Hogine, 1978, 1982; Sharpless, 2001; Beltran 1996a, 1996b; Behar, 1970; Staehelln ,1982; Weeks, 1966].

Bicarbonate ($HCO_3^-$) and carbonate ($CO_3^{2-}$) react with $^\bullet$OH radicals and produce carbonate radicals [Chen, 1975; Buxton, 1988; Hogine, 1978; Dragneic, 1991]. On the other hand, carbonate radicals where found to react with hydrogen peroxide and its conjugate base and produce the hydroperoxyl conjugate base [Dragneic, 1991; Behar, 1970]. Also carbonate radicals were found to react with hydroxyl radicals relatively fast [Buxton, 1988]. Humic substances might react with carbonate radicals with a relatively

low rate constant [AWWA, 1998]. Other reactions for the carbonate/bicarbonate system are given in the kinetic model section and in Table 2.1 of the kinetic model.

Therefore the presence of carbonate/bicarbonate is expected to have an influence on the efficiency of AOPs. This influence is a function of the type of AOP, i.e, oxidant used as a source of the free radicals and the method by which these radicals are produced, concentration of the carbonate/bicarbonate in the reaction mixture, target organic concentration, concentration of the oxidant and hence free radical concentration, and finally the nature of organic contaminant that will be oxidized. The nature of the contaminant becomes a significant factor when this contaminant is degraded by carbonate radicals. Several organic compounds were found to react with carbonate radicals at different second order rate constants depending on the chemical structure of the compound [AWWA, 1998; Alaton, 2002]. The effect of carbonate/bicarbonate on the oxidation rate will be significant when the concentration of the target organic is low. Therefore, carbonate/bicarbonate, besides being a scavenger of $^\bullet$OH radicals, might be a scavenger of the organic compound through the reaction of the produced carbonate radicals with the organic compound. The second effect of carbonate/bicarbonate implies that AOPs performance might be enhanced regarding the increase of organic oxidation.

Alaton (2002) observed that vinylsulphone dyestuffs decomposition by ozonation, was accelerated by the presence of carbonate/bicarbonate in the system. According to his work, carbonate promoted the oxidation process. He said that this might due to the reaction between carbonate radicals ($CO_3^{\bullet-}$), which form from the reaction between carbonate/bicarbonate with $^\bullet$OH radicals, with dye.

Hug (2003) found that high bicarbonate concentration (100 mM) increased the rate of As$^{(III)}$ oxidation when using Fe$^{(II)}$ and hydrogen peroxide AOP. He explained that this might be due to formation of carbonate radicals which will react with As$^{(III)}$, or changes in speciation of Fe$^{(II)}$. In his kinetic model he didn't include the reactions of carbonate ion and carbonate radicals with $^{\bullet}$OH radicals. Also self combination of carbonate radicals was not included in his model.

Hideo (1998) found that the formation of hydroxyl radicals, formed through the Fenton's like reaction employing hydrogen peroxide and Fe$^{3+}$ ions, were stimulated by carbonate ions. Carbonate ions exerted stimulatory effects on the hydroxyl radical formation through the chelation of iron ions, based on his analysis.

Glaze (1989a) used experimental results from the ozone/hydrogen peroxide oxidation to test a kinetic model in bicarbonate-spiked distilled water in a semibatch reactor. Steady state approximation was applied for radical intermediates in the system. The agreement between the model and the experiment was good at the lower hydrogen peroxide/ozone ratios, but significant error was apparent near the stoichiometric optimum. According to Glaze (1989a), this might due either to inaccuracies in some of the assumed rate constants or failure of the model to accurately account for the fate of the carbonate radicals.

Glaze's work (1989b) showed a retardation effect on contaminant destruction in presence of bicarbonate/carbonate in the reaction mixture applying $O_3/H_2O_2$ processes for the oxidation of tetracholoroethylene (PCE). The effect of bicarbonate and carbonate ions was investigated experimentally and compared with model predictions. Steady state was assumed for the free radical concentration in the model and reactions of carbonate

radicals with PCE were neglected. Glaze related the retardation effect of bicarbonate/carbonate to the scavenging of $^\bullet OH$ radicals by the carbonate/bicarbonate. The rate of PCE oxidation increased in going from high to low pH, starting with the same total carbonate concentration, mainly because in the change between bicarbonate/carbonate distribution as a function of pH. Bicarbonate ($HCO_3^-$) ions, which dominate the system at the pH range of 7 to 9, are a less effective scavenger of $^\bullet OH$ radicals than carbonate ($CO_3^{2-}$) [Alaton, 2002]. Therefore, scavenging of $^\bullet OH$ radicals will be reduced at the lower pH values in these experiments. The model didn't predict the non-first order behavior of the system at low pH values.

Glaze (1995) studied the effect of carbonate/bicarbonate on 1,2-Dibromo-3-chloropropane (DBCP) removal by $UV/H_2O_2$ experimentally and developed a kinetic model for DBCP removal by $UV/H_2O_2$ oxidation. Carbonate/bicarbonate retarded the degradation of DBCP in this process. This was attributed to the scavenging of $^\bullet OH$ radicals by the carbonate/bicarbonate. In his model, reactions of carbonate radicals with DBCP and $^\bullet OH$ radicals were not considered and all the radicals were assumed to be at steady-state concentrations. The model was accurate at low levels of carbonate but not at high levels of carbonate. The model underpredicted the rate of organic decomposition at high carbonate levels. Glaze commented that this may indicate that another decomposition mechanism was operating at high levels of carbonate alkalinity perhaps due to carbonate radical ion reactions with DBCP.

Crittenden (1999) used the experimental data of Glaze (1995) to test a kinetic model for the $UV/H_2O_2$ process that incorporated the effects of $HCO_3^-$ and $CO_3^{2-}$ as $^\bullet OH$ radical scavengers. In this model, reactions of carbonate radicals with the organic

compound and $^{\bullet}OH$ radicals were considered. The steady-state assumption for free radicals was not applied in his model. He included dissolved organic carbon (DOC) as a scavenger of $^{\bullet}OH$ radicals, but didn't consider its reaction with carbonate radicals. Agreement between model predictions and experimental data, based on a calculated pseudo- first order constant for the organic degradation, was better than Glaze's model (1995) especially at the high bicarbonate/carbonate concentrations. Increasing $HCO_3^-$ and $CO_3^{2-}$ concentrations decreased the oxidation of the organic compound significantly, while it had little effect on the consumption of $H_2O_2$.

The effect of carbonate/bicarbonate on the degradation of n-chlorobutane (BuCl) applying UV/hydrogen peroxide in a continuous stirred tank reactor (CSTR) was studied by Liao (1995). Carbonate/bicarbonate ions had a negligible effect on the rate of $H_2O_2$ decomposition (0.27-0.45 mM $H_2O_2$) by varying the total carbonate ($C_T$) concentration from 0 M to 90 mM. It had a detrimental effect on the organic compound degradation as the rate of oxidation of BuCl had decreased. This effect on BuCl degradation became more pronounced at the lower concentration of BuCl (0.0012 mM). This effect was explained by the reactions of $HCO_3^-$ and $CO_3^{2-}$ ions with $^{\bullet}OH$ in competition with BuCl. Increasing the pH value above 5 at constant total carbonate concentration retarded the oxidation of BuCl. This effect became more pronounced at the higher pH values. Again, this was explained based on the change of the distribution of bicarbonate and carbonate ions as a function of pH. Hence, at higher pH values, more carbonate ions would be present, which have higher scavenging effect of $^{\bullet}OH$ radicals. In the kinetic model, the reaction between carbonate radicals and BuCl was neglected.

Acero (1999) investigated the influence of carbonate on the ozone/hydrogen peroxide process. Carbonate radicals, which were formed from the reaction of bicarbonate/carbonate with $^{\bullet}OH$ radicals, acted as a chain carrier for ozone decomposition due to their reaction with hydrogen peroxide. It was hypothesized that the reaction between hydrogen peroxide and carbonate radicals resulted in the formation of superoxide radical anions ($O_2^{\bullet-}$), which accelerated ozone decomposition and hence produced more $^{\bullet}OH$ radicals. It was found the consumption of hydrogen peroxide was proportional to the fraction by which bicarbonate and carbonate contributed to the total rate of $^{\bullet}OH$ radical scavenging.

The sonochemical decomposition of 1,4-dioxane by ferrous iron was reduced in the presence of the hydroxyl radical scavenger bicarbonate [Michael, 2002]. The concentration of bicarbonate in this study was relatively high (50 mM) which is much higher than concentrations of bicarbonate typically found in ground and surface waters [Michael, 2002; Stumm & Morgan & Morgan, 1996].

The effect of bicarbonate on the oxidation of atrazine by UV/$H_2O_2$ was studied by De Laat (1997). This study was accomplished experimentally along with a kinetic modeling to predict the system behavior. Reactions of carbonate radicals with hydrogen peroxide, superoxide/hydrperoxyl radicals, atrazine, and carbonate radicals were not included in the kinetic model, because the effects of these reactions on the rate of disappearance of hydrogen peroxide and on the concentration of hydroxyl radicals were assumed negligible. Also, the steady-state approximation was applied for the radical concentrations. From experimental data and model predictions, the bicarbonate and carbonate had a retarding effect on the oxidation of atrazine by this process. The

concentration of sodium bicarbonate initially was in the range of 2-10 mM compared to 0.25 $\mu$M atrazine and 1.25 mM $H_2O_2$. Bicarbonate and carbonate concentrations were relatively high compared to atrazine and $H_2O_2$ and hence it competed with atrazine for $^\bullet OH$ radicals.

De Laat (1994) found that by increasing bicarbonate concentration in the range 0-12 mM at a pH value of 7.5 decreased the efficiency of $H_2O_2$/UV process for the oxidation of 1,1,2-trichloroethane. On the other hand, bicarbonate had no effect on the rate of photodecomposition of hydrogen peroxide. He attributed this to the reaction between carbonate radical anions and hydrogen peroxide that would regenerate hydrogen peroxide via termination reactions.

High bicarbonate ions in solution significantly decreased the efficiency of parachloronitrobenzene removal in $H_2O_2$/UV and $O_3$/UV oxidation processes because bicarbonate/carbonate acted as free radical scavengers and consumed $^\bullet OH$ radicals [Guittonneau, 1990].

Brezonik (1998) found that scavenging of $^\bullet OH$ radicals by carbonate was generally less important than scavenging by dissolved organic matter (DOM) in surface waters. However, these ions can be the major cause of $^\bullet OH$ radical scavenging in low DOC and high alkalinity waters. For example, for $2.2 \times 10^{-3}$ M $HCO_3^-$ ($2.8 \times 10^{-3}$ M $CO_3^{2-}$), 4 mg/L DOC, and pH = 8.4, 28 % of $^\bullet OH$ radicals was scavenged by carbonate and bicarbonate ions [Brezonik, 1998].

Hogine (1978) conducted a study to investigate the kinetics of oxidation of ammonia by ozone and hydroxyl radicals in water. It was found that carbonate and bicarbonate ions, whenever present in a concentration comparable to that of $NH_3$, may

290

protect $NH_3$ from oxidation by reducing the $^\bullet OH$ radicals. This was attributed to the relatively low reaction rate constants ($8.7 \times 10^7$ $M^{-1}$ $s^{-1}$) of $^\bullet OH$ radical reaction with $NH_3$. This reaction is slower than the reaction of carbonate with $^\bullet OH$ radicals. In carbonate-containing systems the yield of ammonia oxidation declined when the pH was raised above 9, due to the increase in $CO_3^{2-}$ ions concentration, based on its equilibrium with $HCO_3^-$ ion. The inhibition effect of carbonate/bicarbonate for pH 10-10.8, on rate of $NH_3$ decomposition, was evident from experimental data for $CO_3^{2-}/NH_3$ ratio in the range 0-5.

Beltran (1996a) found that carbonate/bicarbonate didn't retard the oxidation of fluorine and other polynuclear aromatic hydrocarbons (PAHs) using $UV/H_2O_2$ process, although bicarbonate concentration was increased from $10^{-3}$ M to $10^{-2}$ M starting with $10^{-3}$ M of $H_2O_2$ and $4.7 \times 10^{-6}$ M of fluorine. Using bicarbonate concentrations of $10^{-2}$ M led to a decrease in fluorene oxidation using $O_3/UV$ process and no effect was observed when using $10^{-3}$ M bicarbonate [Beltran, 1995]. The oxidation of other PAHs in the previous study (same PAHs as these ones in Beltran (1996a)) wasn't affected by bicarbonate. Also, in another study by Beltran (1996b) carbonate/bicarbonate caused a significant inhibition of the $UV/H_2O_2$ oxidation of while it had no effect on the direct photolysis of deethylatrazine and deisopropylatrazine. This inhibition was explained based on the hydroxyl radical scavenging character of bicarbonate and carbonate.

Bicarbonate and carbonate decreased the yield of nitrite production during UV photolysis of nitrate at pH 8 but not at pH 6 [Sharpless, 2001]. Amiri (2001) studied the oxidation of methyl tert-butyl ether (MTBE) applying $O_3/H_2O_2$ oxidation process. He found that, for the same initial MTBE concentration, the ozone demand for the treatment

of spiked-tap water (16 mg L$^{-1}$ bicarbonate alkalinity) is at least two times smaller than in contaminated ground water which has high bicarbonate (550-700 mg L$^{-1}$ bicarbonate alkalinity).

## 1.1. Objectives and hypothesis

The kinetic model which was developed in Chapter Two, to describe the degradation of humic acid using UV/H$_2$O$_2$ technology, will be used in this chapter to describe the effect of the presence of bicarbonate and carbonate on the performance of the process and compared with experimental data taken from the literature. What is meant by the performance is the effect of adding bicarbonate and carbonate on the rate of degradation of humic acid, and hence the residual fraction of it. Also, the effect of carbonate and bicarbonate on the rate of oxidation of hydrogen peroxide will be studied. These effects are expected since bicarbonate and carbonate are considered as effective $^\bullet$OH radical scavenger [Weeks, 1966; Glaze, 1995; Brezonik, 1998; Hogine, 1978; Buxton, 1988].

Also, ($CO_3^{\bullet-}$), the product of bicarbonate/carbonate reaction with $^\bullet$OH, reacts with H$_2$O$_2$ and its conjugate base [Behar, 1970; Dragnice, 1991; Glaze, 1995]. The effect of this reaction on the system will be analyzed. The reaction of carbonate radicals with humic acid will be considered and analysis will be made to reveal the effect of this reaction on the system. The interactions of bicarbonate and carbonate with other radicals in the system are given in Table 2.1.

# 2. Kinetic model

## 2.1. Reaction mechanism

### 2.1.1. Reaction Mechanism in Pure Water

The chemistry of hydrogen peroxide in aqueous systems has been studied extensively by many [Bielski,1977,1985; Baxendale, 1988; Hunt, 1952; Behar, 1970; Christensen, 1882, 1989; Sehested, 1968; Weeks, 1955; Daniton, 1955, 1953; Pagsberg, 1969; Thomas, 1965; Vollman, 1959; Guittonneau, 1990; Weinstein, 1979; Hogine, 1982]. Degradation of $H_2O_2$ by UV light arises essentially from the absorption of incident radiation at 254 nm and leads to the production of two hydroxyl free radicals per molecule of $H_2O_2$ decomposed (Reaction 1 Table 2.1). Then these radicals initiate chain reactions as shown in Table 2.1.

**Table 2.1**: Reactions and rate constants in the kinetic model for the degradation of humic acid using hydrogen peroxide and UV light

| # | Reaction | Rate Constant | Reference(s) |
|---|----------|---------------|--------------|
| 1 | $H_2O_2 + h\nu \rightarrow 2\,^{\bullet}OH$ | $k_1 = \Phi_{H_2O_2} f_{H_2O_2} I_o$ | Glaze (1995) Crittenden (1999) |
| 2 | $HA + h\nu \rightarrow$ | $k_2 = \Phi_{HA} f_{HA} I_o$ | Glaze (1995) |
| 3 | $^{\bullet}OH + H_2O_2 \rightarrow H_2O + HO_2^{\bullet}$ | $k_3 = 2.7 \times 10^7$ $M^{-1}$ $s^{-1}$ <br> $k_3 = 2.7 \times 10^7$ $M^{-1}$ $s^{-1}$ (used) | Glaze (1995) Buxton (1988) <br> Gallard (2000) Crittenden (1999) Christensen (1982) |
| 4 | $HO_2^{\bullet} + O_2^{\bullet -} + H_2O \rightarrow H_2O_2 + O_2 + OH^-$ | $k_4 = 9.7 \times 10^7$ $M^{-1}$ $s^{-1}$ (used) <br> $k_4 = 1.02 \times 10^8$ $M^{-1}$ $s^{-1}$ <br> $k_4 = 9.7 \times 10^7$ $M^{-1}$ $s^{-1}$ <br> $k_4 = 9.7 \times 10^7$ $M^{-1}$ $s^{-1}$ <br> $k_4 = 9.7 \times 10^7$ $M^{-1}$ $s^{-1}$ | Gallard (2000) <br> Weinstein (1979) <br> Glaze (1995) <br> Gallard (1998) <br> Chen (1997) |
| 5 | $HO_2^{\bullet} + \,^{\bullet}OH \rightarrow H_2O + O_2$ | $k_5 = 0.71 \times 10^{10}$ $M^{-1}$ $s^{-1}$ (used) <br> $k_5 = 6.6 \times 10^9$ $M^{-1}$ $s^{-1}$ | Buxton (1988) <br> Sehested (1968) |
| 6 | $^{\bullet}OH + O_2^{\bullet -} \rightarrow O_2 + OH^-$ | $k_6 = 1.01 \times 10^{10}$ $M^{-1}$ $s^{-1}$ (used) <br> $k_6 = 1.0 \times 10^{10}$ $M^{-1}$ $s^{-1}$ <br> $k_6 = 9.4 \times 10^9$ $M^{-1}$ $s^{-1}$ | Gallard, 1999, Buxton, 1988 <br> Christensen (1989) <br> Sehested (1968) |

| 7 | $^\bullet OH + ^\bullet OH \rightarrow H_2O_2$ | $k_7 = 5.2\text{x}\,10^9\ M^{-1}\,s^{-1}$ (used) | Pasberg (1969) |
| | | $k_7 = 5.2\text{x}\,10^9\ M^{-1}\,s^{-1}$ | Thomas (1965) |
| | | $k_7 = 4.2\text{x}\,10^9\ M^{-1}\,s^{-1}$ | Buxton (1988) |
| 8 | $HO_2^\bullet + HO_2^\bullet \rightarrow H_2O_2 + O_2$ | $k_8 = 8.3 \times 10^5\ M^{-1}\,s^{-1}$ | Bielski (1985) |
| 9 | $O_2^{\bullet -} + H^+ \rightarrow HO_2^\bullet$ | $k_9 = 1 \times 10^{10}\ M^{-1}\,s^{-1}$ (used) | De Laat (1999) |
| | | $k_9 = 5 \times 10^{10}\ M^{-1}\,s^{-1}$ | Bielski (1985) |
| 10 | $HO_2^\bullet \rightarrow O_2^{\bullet -} + H^+$ | $k_{10} = 1.58 \times 10^5\ s^{-1}$ | De Laat (1999), |
| | | $k_{10} = k_9\,K$ | Chen (1997), |
| | | $pK_a = 4.8$ | Sehested (1968), |
| | | | Bielski (1977) |
| 11 | $^\bullet OH + HCO_3^- \rightarrow H_2O + ^\bullet CO_3^-$ | $k_{11} = 8.5\text{ x}10^6 M^{-1}\,s^{-1}$ | Glaze (1995), Buxton (1988) |
| | | $k_{11} = 8.5\text{ x}10^6 M^{-1}\,s^{-1}$ | Crittenden (1999) |
| | | $k_{11} = 1.5\text{ x}10^7 M^{-1}\,s^{-1}$ (used) | Brezonik (1998), Hogine (1982), Weeks (1966) |
| 12 | $O_2^{\bullet -} + ^\bullet CO_3^- \rightarrow CO_3^{2-} + O_2$ | $k_{12} = 6.5 \times 10^8\ M^{-1}\,s^{-1}$ (used) | Glaze (1995) |
| | | $k_{12} = 6.0 \times 10^8\ M^{-1}\,s^{-1}$ | Crittenden (1999) |
| | | $k_{12} = 4.0 \times 10^8\ M^{-1}\,s^{-1}$ | Behar (1970) |
| 13 | $^\bullet CO_3^- + H_2O_2 \rightarrow HCO_3^- + O_2^{\bullet -} + H^+$ | $k_{13} = 8.0\text{x}\,10^5\ M^{-1}\,s^{-1}$ (used) | Glaze (1995) |
| | | $k_{13} = 8.0\text{x}\,10^5\ M^{-1}\,s^{-1}$ | Behar (1970) |
| | | $k_{13} = 4.3\text{x}\,10^5\ M^{-1}\,s^{-1}$ | Crittenden (1999), Dragnice (1991) |
| | | $k_{13} = 4.3 \times 10^5\ M^{-1}\,s^{-1}$ | Amiri (2001) |
| 14 | $^\bullet OH + CO_3^{2-} \rightarrow OH^- + ^\bullet CO_3^-$ | $k_{14} = 3.9 \times 10^8\ M^{-1}\,s^{-1}$ (used) | Glaze (1995), Buxton (1988) |
| | | $k_{14} = 4.2 \times 10^8\ M^{-1}\,s^{-1}$ | Brezonik (1998), Weeks (1966) |
| 15 | $^\bullet CO_3^- + ^\bullet CO_3^- \rightarrow ?$ | $k_{15} = 3.0 \times 10^7\ M^{-1}\,s^{-1}$ (used) | Glaze (1995), Crittenden (1999) |
| | | $k_{15} = 2.2 \times 10^6\ M^{-1}\,s^{-1}$ | Huie (1990) |
| | | $2k_{15} = 2.2 \times 10^6\ M^{-1}\,s^{-1}$ | Weeks (1966) |
| | | $k_{15} = 3.0 \times 10^7\ M^{-1}\,s^{-1}$ | Dragnice (1991) |
| 16 | $CO_{2(g)} \leftrightarrow CO_{2(aq)}$ | $K_5 = 10^{-1.468}$ | Stumm & Morgan (1996) Snoeyink (1980) |
| 17 | $CO_{2(aq)} + H_2O \leftrightarrow HCO_3^- + H^+$ | $K_6 = 10^{-6.352}\ (k_{f1}/k_{b1})$ | Stumm & Morgan (1996), Huie (1990) |
| | | $K_6 = 10^{-6.3}$ | Snoeyink (1980) |
| | | $(4.46\text{x}10^5/3\text{x}10^{12})\ pK_a = 6.352$ | Hug (2003) |
| 18 | $HCO_3^- \leftrightarrow CO_3^{2-} + H^+$ | $K_7 = 10^{-10.33}\ (k_{f2}/k_{b2})$ | Stumm & Morgan (1996), Huie (1990) |
| | | $K_7 = 10^{-10.3}$ | Snoeyink (1980) |
| | | $(4.67\text{x}10^1/1\text{x}10^{12})\ pK_a = 10.33$ | Hug (2003) |

| # | Reaction | Rate Constant | Ref. |
|---|---|---|---|
| 19 | $O_2^{\bullet -} + H_2O_2 \rightarrow {}^{\bullet}OH + OH^- + O_2$ | $k_{16}=0.13$ M$^{-1}$ s$^{-1}$ | Crittenden (1999), Weinstein (1979) |
| 20 | $H_2O_2 + HO_2^{\bullet} \rightarrow HO^{\bullet} + O_2 + H_2O$ | $k_{17}=3$ M$^{-1}$ s$^{-1}$ | Weinstein (1979), Koppenel (1978) |
| 21 | $HO^{\bullet} + HO_2^- \rightarrow HO_2^{\bullet} + OH^-$ | $k_{18}=7.5$x $10^9$ M$^{-1}$ s$^{-1}$ | Glaze (1995), Crittenden (1999), Christensen (1982) |
| 22 | $H_2O_2 \leftrightarrow H^+ + HO_2^-$ | $pK_a=11.6$, $K_8$<br>$pK_a=11.65$ (used)<br>$pK_a=11.65$ | Crittenden (1999) Buxton (1988) Dean (1979) |
| 23 | ${}^{\bullet}CO_3^- + HO_2^- \rightarrow HCO_3^- + O_2^{\bullet -}$ | $k_{19}=3$ x $10^7$ M$^{-1}$ s$^{-1}$ | Crittenden (1999) Glaze (1995), Dragnice (1991) Behar (1970) |
| 24 | $HO^{\bullet} + NOM \rightarrow$ | $k_{20}= 2$x $10^8$ M$^{-1}$ s$^{-1}$( fitted from a rage of $10^8$ -$10^9$) | Westerhoff (1997), (1999) |
| | | $k_{20}= 2.3$x $10^4$ (mg of C/L)$^{-1}$ s$^{-1}$ $(2.3*10^4$l/mg*(1000mg/g*12g/ mole))=2.8x$10^8$ M$^{-1}$ s$^{-1}$ | Brezonik (1998) |
| | | $0.1$-$1$ x $10^4$ (mg of C/L)$^{-1}$ s$^{-1}$<br>$1.7$x $10^4$ (mg of C/L)$^{-1}$ s$^{-1}$<br>$1$ x$10^8$ M$^{-1}$ s$^{-1}$<br>($8.3$ x1 x$10^3$ (mg of C/L)$^{-1}$ s$^{-1}$ | Liao (1995) Nowell (1992) Mak (1997) |
| | $HO^{\bullet} + HA \rightarrow$ | $1$ x$10^8$ M$^{-1}$ s$^{-1}$ ( used at pH =7)<br>$7$ x$10^8$ M$^{-1}$ s$^{-1}$ ( used at pH =10) | |
| 25 | $CO_3^{\bullet -} + NOM \rightarrow$ | $k_{21}=$ 50 (mg of C/L)$^{-1}$ s$^{-1}$ $(50*10^4$ l/mg*(1000 mg/g*12g/ mole))=4.2 x$10^3$ M$^{-1}$ s$^{-1}$<br>$k_{21}=$ 5 x$10^5$ M$^{-1}$ s$^{-1}$ (used value) | AWWA (1989) |
| 27 | ${}^{\bullet}CO_3^- + {}^{\bullet}OH \rightarrow$ ? | $k_{22}=3.0$x $10^9$ M$^{-1}$ s$^{-1}$ | Buxton (1988) |

Solvated (hydrated) electron chemistry,  from here

| # | Reaction | Rate Constant | Ref. |
|---|---|---|---|
| 28 | $\bar{e}_{aq} + H_2O \rightarrow H^{\bullet} + OH^-$ | $k=19.0$ M$^{-1}$ s$^{-1}$ | Buxton (1988) |
| 29 | $\bar{e}_{aq} + \bar{e}_{aq} \rightarrow H_2 + OH^-$ | $2k_{23}=1.1$x $10^{10}$ M$^{-1}$ s$^{-1}$ | Buxton (1988) |
| 30 | $\bar{e}_{aq} + H^{\bullet} \rightarrow H_2 + OH^-$ | $k_{24}=2.5$ x $10^{10}$ M$^{-1}$ s$^{-1}$ | Buxton (1988) |
| 31 | $\bar{e}_{aq} + {}^{\bullet}OH \rightarrow OH^- + H_2O$ | $k_{25}=3.0$ x $10^{10}$ M$^{-1}$ s$^{-1}$ | Buxton (1988) |
| 32 | $\bar{e}_{aq} + H^+ \rightarrow H^{\bullet}$ | $k_{26}=2.3$ x $10^{10}$ M$^{-1}$ s$^{-1}$ | Buxton (1988) |
| 33 | $\bar{e}_{aq} + H_2O_2 \rightarrow {}^{\bullet}OH + OH^-$ | $k_{27}=1.1$ x $10^{10}$ M$^{-1}$ s$^{-1}$ | Buxton (1988) |

| 34 | $\bar{e}_{aq} + HO_2^- \rightarrow {}^{\bullet}OH + 2OH^-$ | $k_{28}=0.35 \times 10^{10}$ M$^{-1}$ s$^{-1}$ | Buxton (1988) |
|---|---|---|---|
| 35 | $\bar{e}_{aq} + O_2^{\bullet-} \rightarrow O_2^{2-}$ | $k_{29} = 1.3 \times 10^{10}$ M$^{-1}$ s$^{-1}$ | Buxton (1988) |
| 36 | $H^{\bullet} + H_2O \rightarrow H_2 + OH^-$ | $k_{30} = 10$ M$^{-1}$ s$^{-1}$ | Buxton (1988) |
| 37 | $H^{\bullet} + H^{\bullet} \rightarrow H_2$ | $2k_{31} = 1.55 \times 10^{10}$ M$^{-1}$ s$^{-1}$ | Buxton (1988) |
| 38 | $H^{\bullet} + {}^{\bullet}OH \rightarrow H_2O$ | $k_{32} = 0.7 \times 10^{10}$ M$^{-1}$ s$^{-1}$ | Buxton (1988) |
| 39 | $H^{\bullet} + OH^- \xrightarrow{H_2O} \bar{e}_{aq}$ | $k_{33} = 2.2 \times 10^7$ M$^{-1}$ s$^{-1}$ | Buxton (1988) |
| 40 | $H^{\bullet} + H_2O_2 \rightarrow {}^{\bullet}OH + H_2O$ | $k_{34} = 9 \times 10^7$ M$^{-1}$ s$^{-1}$ | Buxton (1988) |
| 41 | $H^{\bullet} + HO_2^- \rightarrow {}^{\bullet}OH + H_2O$ | $k_{35} = 1.2 \times 10^9$ M$^{-1}$ s$^{-1}$ | http://allen.rad.nd.edu Mezyk, S. P. |
| 42 | $H^{\bullet} + HO_2^{\bullet} \rightarrow H_2O_2$ | $k_{36} = 1 \times 10^{10}$ M$^{-1}$ s$^{-1}$ | Buxton (1988) |
| 43 | $H_2 + {}^{\bullet}OH \xrightarrow{H_2O} H^{\bullet}$ | $k_{37} = 4.2 \times 10^7$ M$^{-1}$ s$^{-1}$ | Buxton (1988) |

The overall decomposition rate of H$_2$O$_2$ in pure water by direct photolysis can be described as follows:

$$r_{H_2O_2} = -\frac{dH_2O_2}{dt} = \Phi_{H_2O_2} I_{ab} \quad \text{[Liao, 1995; Glaze, 1995]}$$

where $\Phi_{H_2O_2}$ is the primary quantum yield of H$_2$O$_2$ photolysis, $I_{ab}$ is the light intensity absorbed by H$_2$O$_2$ (Einstein L$^{-1}$ s$^{-1}$) and is defined as

$$I_{ab} = I_0 (1 - e^{-A_t}) \quad \text{[Liao, 1995; Glaze, 1995]}$$

where $I_o$ is the incident light intensity (Einstein L$^{-1}$ s$^{-1}$), and $A_t$ is the total absorbance of UV light by species that absorb light. For an aqueous solution containing hydrogen peroxide this will be H$_2$O$_2$. $\Phi$ for A reacted or B produced is defined as molecules of A reacted/moles of B produced per unit volume per unit time divided by the quanta of light absorbed by A per unit volume per unit time.

## 2.1.2. Reaction Mechanism in the presence of Humic Acid

The presence of humic acids (HA) may affect $UV/H_2O_2$ oxidation process through two mechanisms. The process might be inhibited due to absorption of UV light by HA (reaction 2 Table 2.1). HA is also known as an effective $^\bullet OH$ scavenger (reaction 24, Table 2.1) [Liao, 1995; Westerhoff, 1997, 1999; Brezonik, 1998; Hogine, 1978; Mak, 1997; Cooper, 1982]. The reactions of HA with ($HO_2^\bullet/O_2^{\bullet-}$) were found to be negligible from model simulation of Liao's data (1995). Hence in this model reactions between ($HO_2^\bullet/O_2^{\bullet-}$) and HA were neglected. Also, it was assumed that there is no interaction between oxidation byproducts with UV light. The rate of hydrogen peroxide destruction by UV light in the presence of HA will be given by [Glaze, 1995]:

$$-\frac{dH_2O_2}{dt} = \Phi_{H_2O_2} f_{H_2O_2} I_{ab}$$

$$I_{ab} = I_o(1 - e^{-A_t})$$

For HA the rate of disappearance of HA will be given by

$$\frac{dHA}{dt} = -k_{20}[HA][^\bullet OH] - \Phi_{HA} f_{HA} I_o(1 - e^{-A_t})$$

where $I_{ab}$ is the light intensity in the reaction mixture (Einstein $L^{-1} s^{-1}$), $I_o$ is the incident light intensity (Einstein $L^{-1} s^{-1}$), $A_t$ is the total absorbance of the solution ($cm^{-1}$), $f_{H_2O_2}$, and $f_{HA}$ is the fraction of radiation absorbed by species $H_2O_2$ and HA, respectively, and $\Phi_i$ is the quantum yield and is the number of moles of species i decomposed per mole of light photon absorbed [Baxendale, 1988; Hunt, 1952; Liao,1995].

The total absorbance of the solution is given by:

$$A_t = 2.303b(\varepsilon_{H_2O_2}[H_2O_2] + \varepsilon_{HA}[HA]) \quad \text{[Glaze, 1995; Crittenden, 1999]}$$

where $\varepsilon_i$ is the molar absorbance of specie i $(M^{-1} cm^{-1})$, and b is effective optical path length of the reactor [Baxendale, 1988; Glaze, 1995], and is equal to the radius of the reactor [Glaze, 1995; Crittenden, 1999; Liao, 1995]

The fraction of absorbed radiation absorbed by species i in a mixture is given by:

$$f_i = \frac{2.303b\varepsilon_i[M_i]}{A_t} = \frac{2.303b\varepsilon_i[M_i]}{2.303b\sum_i \varepsilon_i[M_i]}$$

$H_2O_2$ is a weak acid with $pk_a$ value of 11.65 [Buxton, 1988; Dean, 1979] and its dissociation is given by:

$$H_2O_2 \leftrightarrow H^+ + HO_2^-$$

The total hydrogen peroxide concentration is:

$$[H_2O_2]_T = [H_2O_2] + [HO_2^-] = [H_2O_2] + \frac{K_8}{[H^+]}[H_2O_2] = [H_2O_2](1 + \frac{K_8}{[H^+]})$$

$$HO_2^- = \frac{K_8[H_2O_2]}{[H^+]}$$

where $K_8$ is the equilibrium constant for $H_2O_2$ dissociation.

If $H_2O_2$ and HA are the only UV light absorbers the fraction of UV light absorbed by $H_2O_2$ and HA is given by:

$$f_{H2O2} = \frac{\varepsilon_{H2O2}[H_2O_2] + \varepsilon_{HO_2^-}[HO_2^-]}{\varepsilon_{HA}[HA] + \varepsilon_{H2O2}[H_2O_2] + \varepsilon_{HO_2^-}[HO_2^-]}$$

$$f_{HA} = \frac{\varepsilon_{HA}[HA]}{\varepsilon_{HA}[HA] + \varepsilon_{H_2O_2}[H_2O_2] + \varepsilon_{HO_2^-}[HO_2^-]}$$

### 2.1.2.1. Solvated (hydrated) electrons

The photolysis of humic material was found to produce active transients. The solvated electron was firmly identified by literature [Power, 1987; Fisher, 1985, 1987; Zepp, 1987a, 1987b, 1985; Aguer; 1999, 2001, 2002; Cooper, 1989, Thomas-Smith, 2001]. The production of solvated electron by direct photolysis of humic acids was included in the kinetic model. The presence of this intermediate led to a series of other reactions, as shown in Table 2.1, that were incorporated in the kinetic model. The corresponding chemical reactions with the rate constants of hydrated electrons were taken from the literature as shown in Table 2.1.

### 2.1.2.2. Proposed mechanism for HA acid byproducts

The degradation of humic acid (HA) by direct photolysis and $^{\bullet}OH$ radicals is based on the work done in Chapter 2. The products of UV photolysis of HA were assumed to be the solvated electron and an intermediate, $I_1$ which was defined earlier as $HS^{\bullet+}$. $I_1$ was assumed to disappear through self recombination. The end product of this, $I_2$, has been assumed to be volatile compound so it doesn't interfere with the measurement of non purgeable dissolved organic carbon (NPDOC) [Miller, 1987]. These reactions were given as:

$$HA \xrightarrow{\hspace{0.3cm}h\upsilon\hspace{0.3cm}} I_1 + \overline{e}$$

$$I_1 + I_1 \rightarrow I_2 + xCO_2 + yH_2O \hspace{3cm} k_{I1}$$
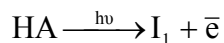
The mechanism for the reaction of HA with $^{\bullet}OH$ radicals and the mechanism for the reactions of the byproducts (from HA with $^{\bullet}OH$ reaction) were given by [Chapter 2]:

$$HA + ^{\bullet}OH \rightarrow I_3 \hspace{3cm} 0.5k_{20}$$

$HA + {}^\bullet OH \rightarrow I$                                                 $0.5k_{20}$

$I_3 + H_2O_2 \rightarrow xCO_2 + yH_2O$                             $k_{I3'}$

$I_3 + {}^* OH \rightarrow I_4 + xCO_2 + yH_2O$          $k_{I3}$

$2I_4 + {}^\bullet OH \rightarrow I_5 + xCO_2 + yH_2O$         $k_{I4}$

$I_5 + {}^\bullet OH \rightarrow I_6 + xCO_2 + yH_2O$           $k_{I5}$
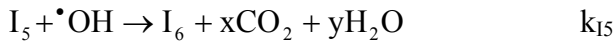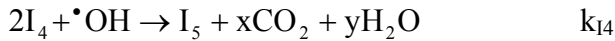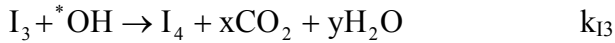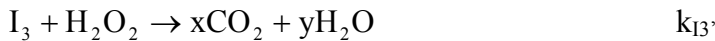
therefore, at the time of TOC measurement the NPDOC is:

NPDOC=HA+$I_1$+$I_3$+$I_4$+$I_5$

The rate constants for some of the proposed reaction intermediates $k_{I3}$, $k_{I4}$, $k_{I5}$, were $3 \times 10^8 \, M^{-1} \, s^{-1}$, $1 \times 10^7 \, M^{-1} \, s^{-1}$, and $10 \, M^{-1} \, s^{-1}$ respectively based on Chapter 2.

## 2.1.3. Reactions of Carbonate and Bicarbonate

Reactions of ${}^\bullet OH$ radicals with bicarbonate $HCO_3^-$ and carbonate $CO_3^{2-}$ produce carbonate radicals as given by the following reactions [Chen, 1975; Buxton, 1988].

$${}^\bullet OH + HCO_3^- \rightarrow H_2O + {}^\bullet CO_3^-$$          $k = 8.5 \times 10^6 \, M^{-1} \, s^{-1}$

$${}^\bullet OH + CO_3^{2-} \rightarrow OH^- + {}^\bullet CO_3^-$$         $k = 3.9 \times 10^8 \, M^{-1} \, s^{-1}$

Carbonate radicals was found to react with hydrogen peroxide and its conjugate base to produce hydroperoxyl conjugate base [Dragneic, 1991; Behar, 1970] based on the following reactions:

$${}^\bullet CO_3^- + H_2O_2 \rightarrow HCO_3^- + O_2^{\bullet -} + H^+$$     $k = 8.0 \times 10^5 \, M^{-1} \, s^{-1}$

$${}^\bullet CO_3^- + HO_2^- \rightarrow HCO_3^- + O_2^{\bullet -}$$          $k = 3 \times 10^7 \, M^{-1} \, s^{-1}$
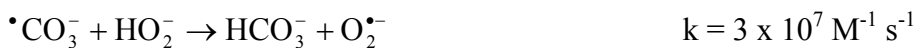
Also carbonate radical was found to react with hydroxyl radical relatively quickly [Buxton, 1988] according to the following reaction:

$$^\bullet CO_3^- + {}^\bullet OH \rightarrow ? \qquad\qquad\qquad k = 3.9 \times 10^8 \ M^{-1} \ s^{-1}$$

Carbonate radicals could also go through self combination reaction according to the following reaction [Huie, 1990; Weeks, 1966; Glaze, 1995; Crittenden, 1999] :

$$^\bullet CO_3^- + {}^\bullet CO_3^- \rightarrow ? \qquad\qquad\qquad k = 3 \times 10^7 \ M^{-1} \ s^{-1}$$

Humic substance might react with carbonate radicals with a relatively low rate constant [AWWA, 1998]. According to some data given in American Water Work Association (AWWA) (1998) carbonate radicals were found to react with natural organic matter (NOM) according to the following reaction:

$$CO_3^{\bullet -} + NOM \rightarrow products, \quad k = 50 \ (\text{mg of C/L})^{-1} \ s^{-1} \ (4.2 \times 10^3 \ M^{-1} \ s^{-1})$$
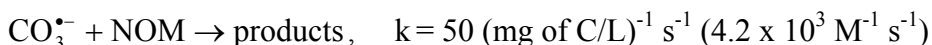
The above value of the rate constant gave higher predicted residual fraction of NPDOC than experimental data. Therefore, a value of $5.0 \times 10^5 \ M^{-1} \ s^{-1}$ was used in the simulation and gave better prediction of the experimental data. The difference of this value than the reported one for NOM is expected since in this system we had HA with a different origin then the NOM in AWWA (1998). Also, in AWWA the rate constant for aromatic compounds with carbonate radicals was in the order of $10^5$-$10^6 \ M^{-1} \ s^{-1}$ and the one for some olefin compounds was in the order of $10^4 \ M^{-1} \ s^{-1}$. Therefore, a value of $5.0 \times 10^5 \ M^{-1} \ s^{-1}$ seems to be reasonable considering that humic substances contain conjugate olefinic and aromatic functional groups, as well as carboxyl and hydroxyl and sometimes a small percentage of nitrogenous functional groups [Aguer, 2001, 2002; Fischer, 1987; McKnight, 1989; Lyderson, 1989; Kim, 2003; Goldstone, 2002; Chu, 2003].

Also carbonate radicals may react with the conjugate base of hydroperoxyl radical according to the following reaction [Glaze, 1995; Crittenden, 1999; Eriksen, 1985]

$$O_2^{\bullet -} + {}^\bullet CO_3^- \rightarrow CO_3^{-2} + O_2 , \ k = 6.5 \times 10^8 \ M^{-1} \ s^{-1}$$

The various components of carbonate system are interrelated by the following equilibrium in aqueous systems [Stumm & Morgan, 1996; Snoeyink, 1980; Hug, 2003]

$$CO_{2(aq)} + H_2O \leftrightarrow HCO_3^- + H^+$$

$K_6 = 10^{-6.352}$ ($k_{f1}/k_{b1}$)
($4.46 \times 10^5 / 1 \times 10^{12}$)
pKa=6.352

$$HCO_3^- \leftrightarrow CO_3^{2-} + H^+$$

$K_7 = 10^{-10.33}$ ($k_{f2}/k_{b2}$)
($4.67 \times 10^1 / 1 \times 10^{12}$)
pKa=10.33
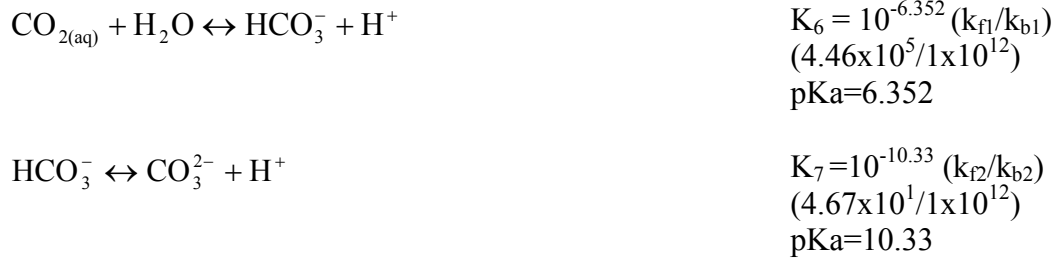
At high pH values (pH > 7) the concentration of aqueous carbon dioxide ($CO_{2(aq)}$) will be very small compared to the carbonate ($CO_3^{2-}$) and bicarbonate ($HCO_3^-$) [Stumm & Morgan, 1996; Snoeyink, 1980]. Therefore, reactions of $CO_{2(aq)}$ with other species, mainly its reaction with $^\bullet OH$, will be neglected [Glaze, 1989a]. Even at lower pH values, for example pH = 5.3 where $CO_{2(aq)}$ concentration is considerable, Glaze (1989a) neglected $CO_{2(aq)}$ reaction with $^\bullet OH$ radicals and others did the same.

If the concentration of either $CO_3^{2-}$ or $HCO_3^-$ is known initially, then the initial concentration of the other forms of carbonate system can be calculated based on the following relations for a closed system [Stumm & Morgan, 1996]:

$$[HCO_3^-] = \frac{C_T}{\left(1 + \frac{[H^+]}{K_6} + \frac{K_7}{[H^+]}\right)}$$

$$[CO_3^{2-}] = \frac{C_T}{\left(1 + \frac{[H^+]}{K_7} + \frac{[H^+]^2}{K_7 K_6}\right)}$$

$$[CO_{2(aq)}] = \frac{C_T}{\left(1 + \dfrac{K_6}{[H^+]} + \dfrac{K_6 K_7}{[H^+]^2}\right)}$$

where $C_T = [HCO_3^-] + [CO_3^{2-}] + [CO_{2(aq)}]$

## 2.1.3. Model parameters

The quantum yield for the photolysis of hydrogen peroxide ($\Phi_{H_2O_2}$) in pure water has been estimated as 1 for the overall reactions of $H_2O_2$ including the initiation, propagation and termination step [Glaze, 1995; Baxendale, 1957; Guittonneau, 1990; Crittenden, 1999]. The primary quantum yield was estimated as 0.5 (reaction 1 in Table 2.1), i.e, for the initiation reaction, for relatively high light intensity, and low peroxide concentrations [Baxendale, 1957; Volman, 1959; Liao, 1995]. Molar absorptivity of hydrogen peroxide ($\varepsilon_{H_2O_2}$) is available in the literature within the range 17.8-19.7 $M^{-1}$ $cm^{-1}$ at 254 nm [Baxendale, 1956; Bielski, 1977; Guittonneau, 1990; Morgan, 1988]. The value for $\varepsilon_{H_2O_2}$ used in this kinetic model is 17.8 $M^{-1}cm^{-1}$. The molar absorptivity of the conjugate base of hydrogen peroxide ($HO_2^-$) ($\varepsilon_{HO_2^-}$) is 228 $M^{-1}cm^{-1}$ at 254 nm [Baxendale, 1957; Morgan, 1988].

$I_o$ which is the light intensity (Einstein $L^{-1}$ $s^{-1}$) was not measured for this system. Therefore it was lumped in the fitting parameters $k_1$ and $k_2$ where:

$$k_1 = \Phi_{H_2O_2} I_o$$

$$k_2 = \Phi_{HA} I_o$$

where $\Phi_{H_2O_2}$ and $\Phi_{HA}$ are the quantum yield for $H_2O_2$ and HA photolysis, respectively.

The parameter b represents the effective path length of the UV light inside the reactor (cm). The value of this parameter has been taken as the radius of the reactor which contains the reaction solution. The reactor used by Wang (2001) has a diameter of 20 cm, with a hollow UV quartz tube of 5.5 cm outside diameter placed in the center of this reactor, therefore the effective radius for this set up was 7.25 cm. The radius of the reactor was used as the effective path length by Glaze (1995) and Crittenden (1999). Liao (1995) used the diameter as the effective path length since his reactor was surrounded by the equally spaced UV sources.

The molar absorptivity of humic acid $\varepsilon_{HA}$ is 0.066 (mg/L of DOC)$^{-1}$ cm$^{-1}$ at 254 nm [Wang, 2001]. This value is consistent with the value reported by Liao (1995) which is $\varepsilon_{HA}$ = 0.0867 cm$^{-1}$ (mg/L of DOC)$^{-1}$. Also, Westerhoff (1999) found an average value of $\varepsilon_{HA}$ is 0.037 cm$^{-1}$ (mg/L of DOC)$^{-1}$ at 254 nm for different isolates of natural organic matter (NOM). Since all of the measurement are based on dissolved carbon (which has 12 gm per mole), then $\varepsilon_{HA} = 840$ M$^{-1}$cm$^{-1}$ after converting from mass to mole unit.

### 2.1.4. Model equations

Some or all of the proposed elementary reactions in Table 2.1 have been included by others to describe the destruction of organic compounds by $H_2O_2$/UV process or other AOPs [Glaze, 1995; Crittenden , 1999; Chen, 1997; Gallard, 1999; Mak, 1997]. However, in previous work although humic acid was present its rate of destruction by photolysis was neglected [Crittenden, 1999; Glaze, 1995]. This could be applicable when $H_2O_2$ is relatively high compared to HA. When the concentration of $H_2O_2$ is comparable to humic acid, then this term may not be neglected. To our knowledge, this is the first

time any one has tried to describe the kinetics of humic acid destruction by $H_2O_2/UV$ process for the available experimental data in the literature.

A completely mixed batch reactor was used in the experimental work of Wang (2000, 2001). The mass balance of species i at any time is given by the following ordinary differential equation:

$$\frac{dC_i}{dt} = r_i$$

which describes the change of species i concentration as a function of time starting with initial concentration $C_{io}$ in a completely mixed batch reactor in a liquid solution.

Substituting each species in Table 2.1 into this equation, we get a set of ordinary nonlinear differential equation that describes the rate of changes in the concentration of each species with respect to time.

Humic acid:

$$\frac{dHA}{dt} = -k_{20}[HA][^\bullet OH] - \Phi_{HA} f_{HA} I_o (1 - e^{-A_t}) - k_{21}[CO_3^{\bullet -}][HA]$$

$$= -k_{20}[HA][^\bullet OH] - k_2 f_{HA} (1 - e^{-A_t}) - k_{21}[CO_3^{\bullet -}][HA]$$

where $k_2 = \Phi_{HA} I_o$

Hydrogen peroxide:

$$\frac{dH_2O_{2T}}{dt} = -\Phi_{H2O2} f_{H2O2} I_o (1 - e^{-A_t}) - k_3[H_2O_2][^\bullet OH] - k_{13}[H_2O_2][^\bullet CO_3^-] + k_8[HO_2^\bullet][HO_2^\bullet]$$
$$+ k_4[HO_2^\bullet][O_2^{\bullet -}] + k_7[^\bullet OH][^\bullet OH] - k_{16}[H_2O_2]_T[O_2^{\bullet -}] - k_{17}[H_2O_2]_T[HO_2^\bullet] -$$
$$k_{18}[HO_2^-][^\bullet OH] - k_{19}[HO_2^-][CO_3^{\bullet -}] - k_{27}[\bar{e}_{aq}][H_2O_2] - k_{28}[\bar{e}_{aq}][HO_2^-] -$$
$$k_{34}[H_2O_2][H^\bullet] - k_{35}[HO_2^-][H^\bullet] - k_{13'}[H_2O_2]_T[I_3] + k_{36}[H^\bullet][HO_2^\bullet]$$

with $k_1 = \Phi_{H2O2} I_o$, taking $\Phi_{H2O2} = \Phi_{HO_2^-}$

The total hydrogen peroxide concentration is:

$$[H_2O_2]_T = [H_2O_2] + [HO_2^-] = [H_2O_2] + \frac{K_8}{[H^+]}[H_2O_2] = [H_2O_2](1 + \frac{K_8}{[H^+]})$$

$$HO_2^- = \frac{K_8[H_2O_2]}{[H^+]}$$

Hydroxyl radical:

$$\frac{d^\bullet OH}{dt} = 2\Phi_{H_2O_2} f_{H_2O_2} I_o (1 - e^{-A_t}) - k_3[H_2O_2][^\bullet OH] - k_5[^\bullet OH][HO_2^*] - k_6[^\bullet OH][O_2^{\bullet -}]$$
$$- 2k_7[^\bullet OH][^\bullet OH] - k_{11}[^\bullet OH][HCO_3^-] - k_{14}[^\bullet OH][CO_3^{2-}] - k_{20}[^\bullet OH][HA]$$
$$- k_{18}[^\bullet OH][HO_2^-] - k_{16}[H_2O_2]_T[O_2^{\bullet -}] + k_{17}[H_2O_2]_T[HO_2^\bullet] - k_{22}[^\bullet OH][CO_3^{\bullet -}]$$
$$- k_{25}[^\bullet OH][\overline{e}_{aq}] + k_{27}[H_2O_2][\overline{e}_{aq}] + k_{28}[HO_2^-][\overline{e}_{aq}] - k_{32}[^\bullet OH][H^\bullet]$$
$$+ k_{34}[H_2O_2][H^\bullet] + k_{35}[HO_2^-][H^\bullet] - k_{37}[H_{2aq}][^\bullet OH] + k_{30}[H^\bullet][H_2O]$$
$$- k_{I3}[I_3][^\bullet OH] - k_{I4}[I_4][^\bullet OH] - k_{I5}[I_5][^\bullet OH]$$

$$\frac{d^\bullet OH}{dt} = 2k_1 f_{H_2O_2}(1 - e^{-A_t}) - k_3[H_2O_2][^\bullet OH] - k_5[^\bullet OH][HO_2^*] - k_6[^\bullet OH][O_2^{\bullet -}]$$
$$- 2k_7[^\bullet OH][^\bullet OH] - k_{11}[^\bullet OH][HCO_3^-] - k_{14}[^\bullet OH][CO_3^{2-}] - k_{20}[^\bullet OH][HA]$$
$$- k_{18}[^\bullet OH][HO_2^-] - k_{16}[H_2O_2]_T[O_2^{\bullet -}] + k_{17}[H_2O_2]_T[HO_2^\bullet] - k_{22}[^\bullet OH][CO_3^{\bullet -}]$$
$$- k_{25}[^\bullet OH][\overline{e}_{aq}] + k_{27}[H_2O_2][\overline{e}_{aq}] + k_{28}[HO_2^-][\overline{e}_{aq}] - k_{32}[^\bullet OH][H^\bullet]$$
$$+ k_{34}[H_2O_2][H^\bullet] + k_{35}[HO_2^-][H^\bullet] - k_{37}[H_{2aq}][^\bullet OH] + k_{30}[H^\bullet][H_2O]$$
$$- k_{I3}[I_3][^\bullet OH] - k_{I4}[I_4][^\bullet OH] - k_{I5}[I_5][^\bullet OH]$$

Hydrperoxyl radical:

$$\frac{dHO_2^\bullet}{dt} = k_3[H_2O_2][^\bullet OH] - k_4[HO_2^\bullet][O_2^{\bullet -}] - k_5[^\bullet OH][HO_2^\bullet] - 2k_8[HO_2^\bullet][HO_2^\bullet]$$
$$- k_{10}[HO_2^\bullet] + k_9[O_2^{\bullet -}][H^+] - k_{17}[H_2O_2]_T[HO_2^\bullet] + k_{18}[^\bullet OH][HO_2^-] - k_{36}[H^\bullet][HO_2^\bullet]$$

Superoxide radical anion:

$$\frac{dO_2^{\bullet -}}{dt} = k_{10}[HO_2^\bullet] + k_{13}[CO_3^{\bullet -}][H_2O_2]_T - k_9[O_2^{\bullet -}][H^+] - k_4[HO_2^\bullet][O_2^{\bullet -}]$$
$$- k_6[^\bullet OH][O_2^{\bullet -}] - k_{12}[O_2^{\bullet -}][CO_3^{\bullet -}] - k_{16}[H_2O_2]_T[O_2^{\bullet -}] + k_{19}[CO_3^{\bullet -}][HO_2^-] - k_{29}[O_2^{\bullet -}][\overline{e}_{aq}]$$

Carbonate radical ion:

$$\frac{dCO_3^{\bullet-}}{dt} = k_{11}[HCO_3^-][{}^\bullet OH] - k_{12}[O_2^{\bullet-}][CO_3^{\bullet-}] - k_{13}[CO_3^{\bullet-}][H_2O_2]$$

$$- 2k_{15}[CO_3^{\bullet-}][CO_3^{\bullet-}] + k_{14}[CO_3^{2-}][{}^\bullet OH] - k_{19}[CO_3^{\bullet-}][HO_2^-]$$

$$- k_{22}[{}^\bullet OH][CO_3^{\bullet-}] - k_{21}[CO_3^{\bullet-}][HA]$$

Bicarbonate ion:

$$\frac{dHCO_3^-}{dt} = -k_{11}[HCO_3^-][{}^\bullet OH] + k_{13}[H_2O_2][CO_3^{\bullet-}] + k_{19}[HO_2^-][CO_3^{\bullet-}]$$

$$- k_{b1}[HCO_3^-][H^+] + k_{f1}[CO_{2(aq)}] - k_{f2}[HCO_3^-] + k_{b2}[CO_3^{2-}][H^+]$$

Carbonate ion:

$$\frac{dCO_3^{2-}}{dt} = k_{12}[CO_3^{\bullet-}][O_2^{\bullet-}] - k_{14}[{}^\bullet OH][CO_3^{2-}] + k_{f2}[HCO_3^-] - k_{b2}[CO_3^{2-}][H^+]$$

Aqueous carbon dioxide:

$$\frac{dCO_{2(aq)}}{dt} = -k_{b1}[HCO_3^-][H^+] + k_{f1}[CO_{2(aq)}]$$

Solvated or hydrated electron:

$$\frac{d\bar{e}_{aq}}{dt} = k_2 f_{HA}(1 - e^{-At}) - k\ [\bar{e}_{aq}][H_2O] - 2k_{23}[\bar{e}_{aq}][\bar{e}_{aq}] - k_{24}[\bar{e}_{aq}][H^\bullet] - k_{25}[\bar{e}_{aq}][{}^\bullet OH]$$

$$- k_{26}[\bar{e}_{aq}][H^+] - k_{27}[\bar{e}_{aq}][H_2O_2] - k_{28}[\bar{e}_{aq}][HO_2^-] - k_{29}[\bar{e}_{aq}][O_2^{\bullet-}] + k_{33}[H^\bullet][OH^-]$$

Singlet hydrogen atom:

$$\frac{dH^\bullet}{dt} = k\ [\bar{e}_{aq}][H_2O] - k_{24}[\bar{e}_{aq}][H^\bullet] + k_{26}[\bar{e}_{aq}][H^+] - k_{30}[H^\bullet][H_2O] - 2k_{31}[H^\bullet][H^\bullet] - k_{32}[H^\bullet][{}^\bullet OH]$$

$$- k_{33}[H^\bullet][OH^-] - k_{34}[H^\bullet][H_2O_2] - k_{35}[H^\bullet][HO_2^-] - k_{36}[H^\bullet][HO_2^\bullet] + k_{37}[H_2][{}^\bullet OH]$$

Aqueous Hydrogen:

$$\frac{dH_{2aq}}{dt} = k_{23}[\bar{e}_{aq}][\bar{e}_{aq}] + k_{24}[\bar{e}_{aq}][H^\bullet] + k_{30}[H^\bullet][H_2O] + k_{31}[H^\bullet][H^\bullet] - k_{37}[H_2][{}^\bullet OH]$$

Intermediates from humic acid destruction:

$$\frac{dI_3}{dt} = 0.5k_{20}[HA][^\bullet OH] - k_{I3}[I_3][^\bullet OH] - k_{I3'}[I_2][H_2O_2]_T$$

$$\frac{dI_4}{dt} = k_{I3}[I_3][^\bullet OH] - k_{I4}[I_4][^\bullet OH]$$

$$\frac{dI_5}{dt} = k_{I4}[I_4][^\bullet OH] - k_{I5}[I_5][^\bullet OH]$$

The above system of stiff nonlinear ordinary differential equations was solved numerically using the Matlab (R13) program developed by Math Works Inc. For this, the process parameters t, pH, initial concentration of $H_2O_2$ ($[H_2O_2]_0$) and HA ($[HA]_0$), b, and molar absorptivity of $H_2O_2$ ($H_2O_2^{'}/HO_2^{-}$) and HA were specified as inputs to the program. The nitial concentration of all radicals was taken as zero. The reaction rate constants along with the equilibrium constants presented in Table 2.1 were also used as input to the program. The rate constant for the reaction between humic acid and $^\bullet OH$ radicals is reported in the literature in terms of dissolved organic carbon. Westerhoff (1996) used a value of 2 x $10^8$ $M^{-1}$ $s^{-1}$ which was fitted from a rage of $10^8$-$10^9$ $M^{-1}$ $s^{-1}$. Westerhoff (1999) reported a measured value, from experimental data, of the rate constant for the reaction of $^\bullet OH$ with dissolved organic carbon of 3.8 x $10^8$ $M^{-1}$ $s^{-1}$. He converted from M to mg $L^{-1}$ unit by dividing 3.8 x $10^8$ $M^{-1}$ $s^{-1}$ by 12 (molecular weight of carbon) and 1000 to go from mg to g. Brezoink (1998) found that the rate constant for $^\bullet OH$ radicals scavenging by dissolved organic matter (DOM) is 2.3 x $10^4$ (mg of C/L)$^{-1}$ $s^{-1}$ and if it is divided by the molecular weight of carbon (12) this will give a value of 2.8 x $10^8$ $M^{-1}$ $s^{-1}$. Also, he found that rate constants for $^\bullet OH$ radicals scavenging by the five different DOM sources were in a narrow range suggesting that the importance of DOM as $^\bullet OH$

sink can be estimated simply from the dissolved organic carbon (DOC) concentration in water. This value lies within the range of Westerhoff's range ($10^8$-$10^9$ $M^{-1}$ $s^{-1}$)(1996, 1999). A value of 2.6 x $10^4$ (mg of C/L)$^{-1}$ $s^{-1}$ was reported by Zepp (1987b). Goldstone, (2002) measured a value of 1.9 x $10^4$ (mg of C/L)$^{-1}$ $s^{-1}$ for the reaction of $^{\bullet}$OH radicals with humic acid. Cooper (1999) based on experimental data fitting to a kinetic model found a value of 1.0 x $10^8$ $M^{-1}$ $s^{-1}$. Liao (1995), from model fitting, obtained a value of 0.12-1.2 x $10^8$ $M^{-1}$ $s^{-1}$ (0.1-1 x $10^4$ (mg of C/L)$^{-1}$ $s^{-1}$) with the best fitting at a value of 1.9 x $10^8$ $M^{-1}$ $s^{-1}$ (1.6 x $10^4$ (mg of C/L)$^{-1}$ $s^{-1}$). Another value for this rate constant was reported by Hogine (1992) and it was 2.0 x $10^8$ $M^{-1}$ $s^{-1}$ (1.7 x $10^4$ (mg of C/L)$^{-1}$ $s^{-1}$). For our model a value of 7.0 x $10^8$ $M^{-1}$ $s^{-1}$ gave the best fit to the experimental data used in this chapter. The other fitted parameters were $k_1$ and $k_2$. Also the rate constants for the by products of HA photolysis and $^{\bullet}$OH reactions were found from fitting to the data. The best fit was found using least square error analysis.

Based on our simulation, the value of the rate constant for the reaction of $I_3$ with $^{\bullet}$OH radicals is 3 x $10^8$ $M^{-1}$ $s^{-1}$. This value is close to the rate constant of formic acid (one of the identified products of Goldstone's work (2002)) reaction with $^{\bullet}$OH radical which is 1.3 x $10^8$ $M^{-1}$ $s^{-1}$ [Buxton, 1988].

We assumed that contributions of wave lengths other than 254 nm were negligible and therefore molar absorptivity was taken at a wave length of 254 nm. Also, we considered pH to remain constant. This is based on the experimental observation of Wang (2001, 2000) who didn't notice a significant change in pH during the experiment. Also, in Crittenden model (1999) he made a comparison in his model prediction between assuming a constant and a variable pH and he didn't find a significant difference. Also,

we assumed that the only absorbers for UV light in this system are hydrogen peroxide with its conjugate base and humic acid.

## 3. Results

### 3.1. Part 1: Simulation of the experimental data of Wang (2000)

This part gives the simulation results for the developed kinetic model in this chapter. The model was tested on experimental data published by Wang (2000). In this set of data bicarbonate/carbonate was added to the reaction mixture of humic acid (HA) using hydrogen peroxide ($H_2O_2$) and ultraviolet (UV) light as a removal process. This effect was examined with an initial carbonate concentration of 100-400 mg/L as $CaCO_3$. The results for the effect of carbonate/bicarbonate, which were reported by Wang (2000), were given in terms of different initial carbonate ($CO_3^{2-}$) and bicarbonate ($HCO_3^-$) concentrations at constant initial concentration of HA, constant initial concentration of $H_2O_2$, and constant pH. In the model simulation, the carbonate and bicarbonate were converted to $CaCO_3$ alkalinity. Therefore, the different species in the carbonate system, which were carbonate ($CO_3^{2-}$), bicarbonate ($HCO_3^-$), and aqueous carbon dioxide ($CO_{2(aq)}$), will be present in the reaction mixture due to the equilibrium between these different forms. The initial concentration of each carbonate form was calculated based on the equilibrium relations as was given in section 2.1.5.

The fitting parameters were the same as the ones introduced in Chapter 2 ($k_1$, $k_2$, $k_{I3}$, $k_{I4}$, and $k_{I5}$). The rate constants for the direct photolysis of HA and hydrogen peroxide were used as fitting parameters instead of being measured quantities. The definition of $k_1$ was given by the following equation in the kinetic model:

$$k_1 = \Phi_{H_2O_2} I_o \quad (1)$$

The quantum yield of $H_2O_2$ ($\Phi_{H_2O_2}$) is available in the literature (either 0.5 or 1) [Baxendale, 1988; Guittonneau, 1990; Glaze, 1995; Crittenden, 1999; Hunt, 1952]. Therefore, light intensity ($I_o$) (Einstein $L^{-1}$ $s^{-1}$) is needed to calculate $k_1$. This value was not measured (personal communication with the author). $I_o$ needs to be measured for the UV source used for each set of experimental data. Its value depends on the UV source and life time of the source. Therefore, since $I_o$ was not available, $k_1$ was a fitting parameter instead of being a calculated quantity. In this work, the value of $k_1$ used was $2.5 \times 10^{-6}$ M $s^{-1}$, which is the same value which was obtained at the low hydrogen peroxide concentration in Chapter 2. If $k_1$ is divided by $\Phi_{H_2O_2}$, then the value of $I_o$ from relation 1 above will be in the range $5 \times 10^{-6}$ Einstein $L^{-1}$ $s^{-1}$. This value of $I_o$ lies within the range that other workers measured for their UV sources [Daniton, 1953; Baxendale, 1957; Liao, 1995; Glaze, 1995; Hunt, 1952]. Therefore the obtained value of $k_1$ is realistic.

On the other hand, the rate of HA photolysis in solutions containing only HA was given by:

$$-\frac{dHA}{dt} = \Phi_{HA} I_o (1 - e^{-A_t}) = k_2 (1 - e^{-A_t}) \text{ with } k_2 = \Phi_{HA} I_o$$

In Chapter 2, $k_2$ was found to be $2.5 \times 10^{-8}$ M $sec^{-1}$ from best fitting of the model to the experimental data. In this chapter, $k_2$ was found to be $2.5 \times 10^{-9}$ M $sec^{-1}$ from best fitting of the model to the experimental data. The only reason that $k_2$ values are different, under the same light intensity ($I_o$), is the quantum yield value. The light intensity ($I_o$) was $5.0 \times 10^{-6}$ Einstein $L^{-1}$ $s^{-1}$ from the previous paragraph. Dividing $k_2$ by this value of $I_o$

gives $\Phi_{HA}$ = 0.0005 which is the quantum yield for HA destruction by UV or products formation from HA destruction by UV photolysis. The calculated $\Phi_{HA}$ is within the reported range by Thomas-smith (2001). In one set of data reported by Wang (2000), the effect of changing ($HCO_3^-/CO_3^{2-}$) concentration was studied in a system that had initially 5 mg L$^{-1}$ HA and 0.00147 M $H_2O_2$. The results of simulation for this set of data are given in Figures 3.1.1-A and 3.1.1-B. Figure 3.1.1-A gives model predictions and experimental data for residual fraction of NPDOC. Figure 3.1.1.B gives the predicted residual fraction of hydrogen peroxide vs. time.

Another set of experimental data was published by Wang [2000] at different initial total carbonate concentrations ($HCO_3^-/CO_3^{2-}$). The results of simulation for these data are given in Figures 3.1.2.A and 3.1.2.B for the residual fraction of NPDOC and hydrogen peroxide, respectively. Predicted concentrations of $^\bullet$OH radicals at the conditions presented in Figures 3.1.1 and 3.1.2 are given in Figures 3.1.I and 3.1.II respectively.
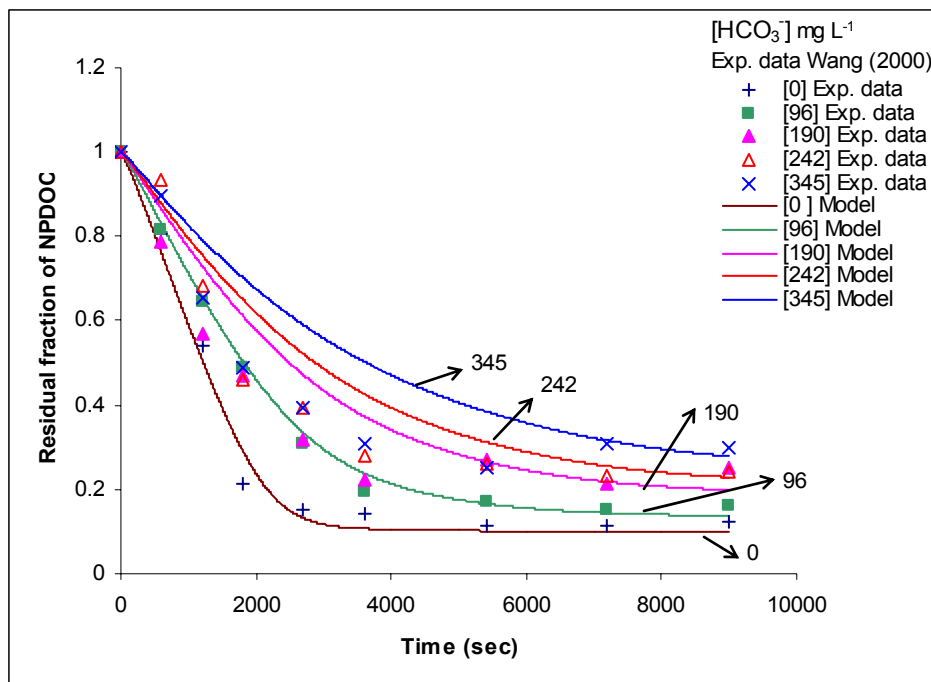
**Fig. 3.1.1.A:** Residual fraction of NPDOC vs. time from experimental data [Wang, 2000] and model predictions at different initial $HCO_3^-$ concentrations. Initial conditions: $[NPDOC]_o = 5$ mg $L^{-1}$, $[H_2O_2] = 0.00147$ M, pH = 10.
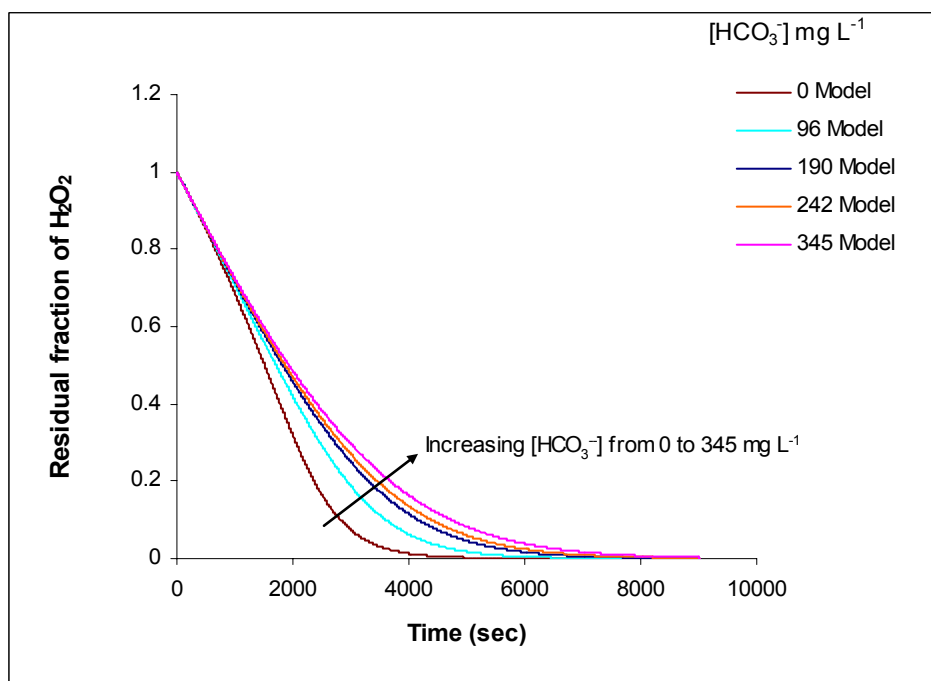


**Fig. 3.1.1.B:** Predicted residual fraction of hydrogen peroxide vs. time at different initial $HCO_3^-$ concentrations. Initial conditions: $[NPDOC]_o = 5$ mg $L^{-1}$, $[H_2O_2] = 0.00147$ M, pH = 10

The ratios of $^\bullet OH$ radicals consumed by hydrogen peroxide and its conjugate base to the $^\bullet OH$ radicals consumed by bicarbonate ($HCO_3^-$) and carbonate ($CO_3^{2-}$) at the conditions presented in Figure 3.1.1 are shown in Figure 3.1.III. Figure 3.1.IV shows the ratios of $^\bullet OH$ radicals consumed by hydrogen peroxide and its conjugate base to the $^\bullet OH$ radicals consumed by bicarbonate ($HCO_3^-$) and carbonate ($CO_3^{2-}$) for the conditions presented in Figure 3.1.2. From these figures it can be seen that consumption of hydroxyl radicals by hydrogen peroxide and by carbonate/bicarbonate are comparable.
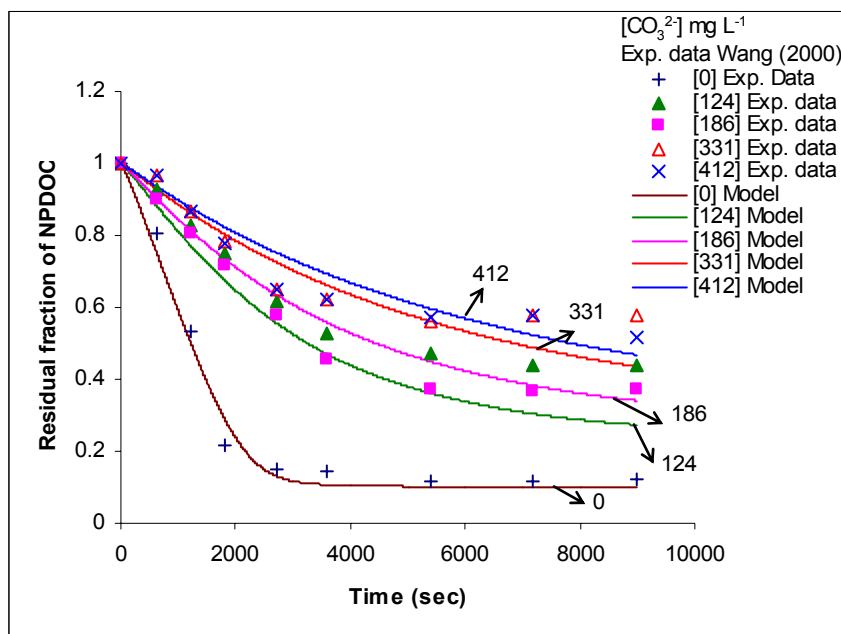


**Fig. 3.1.2.A:** Residual fraction of NPDOC vs. time from experimental data [Wang, 2000] and model predictions at different initial $CO_3^{2-}$ concentrations. Initial conditions: $[NPDOC]_o = 5$ mg L$^{-1}$, $[H_2O_2] = 0.00147$ M, pH = 10
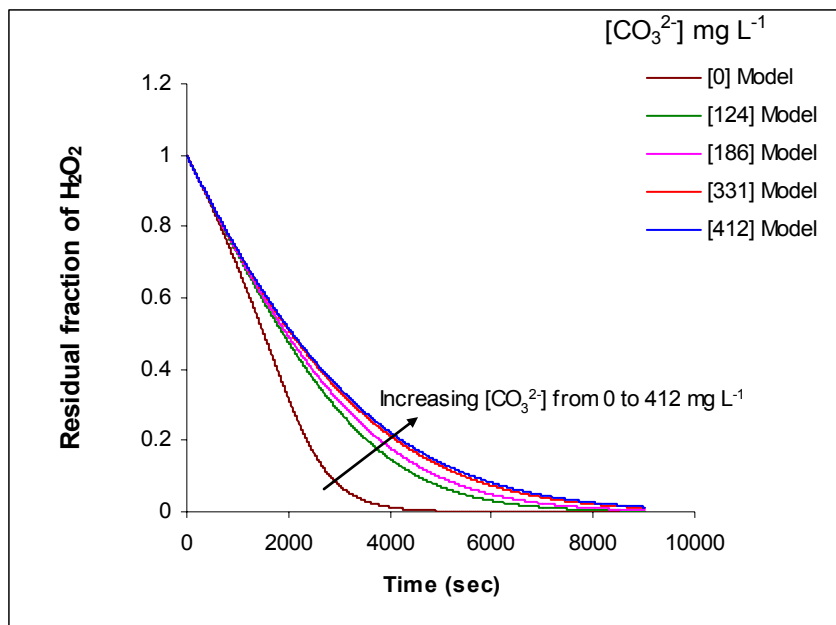
**Fig. 3.1.2.B:** Predicted residual fraction of hydrogen peroxide vs. time at different initial $CO_3^{2-}$ concentrations. Initial conditions: $[NPDOC]_o = 5$ mg L$^{-1}$, $[H_2O_2] = 0.00147$ M, pH = 10
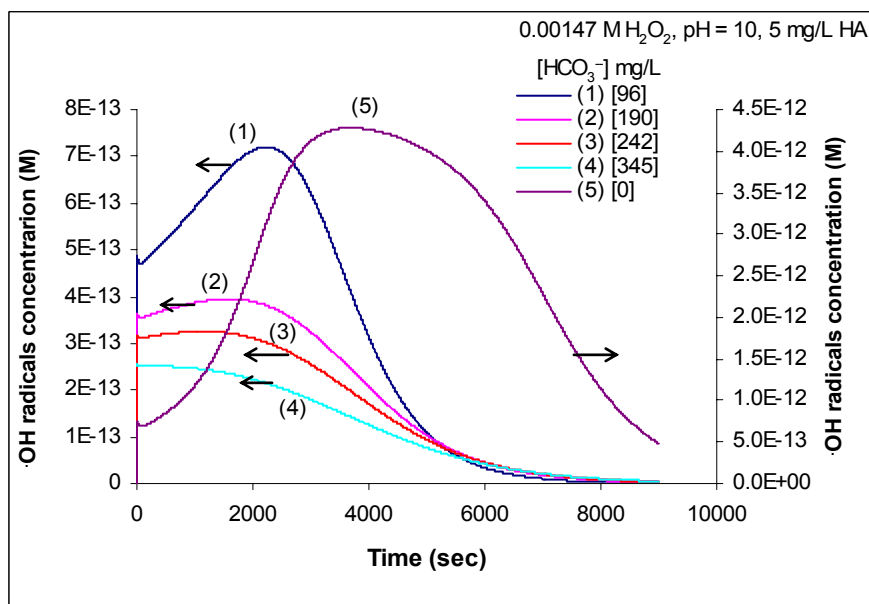


**Fig. 3.1-I:** Predicted concentration of $^{\bullet}OH$ radicals vs. different initial $HCO_3^-$ concentrations. Initial conditions: $[NPDOC]_o = 5$ mg L$^{-1}$, $[H_2O_2] = 0.00147$ M, pH = 10
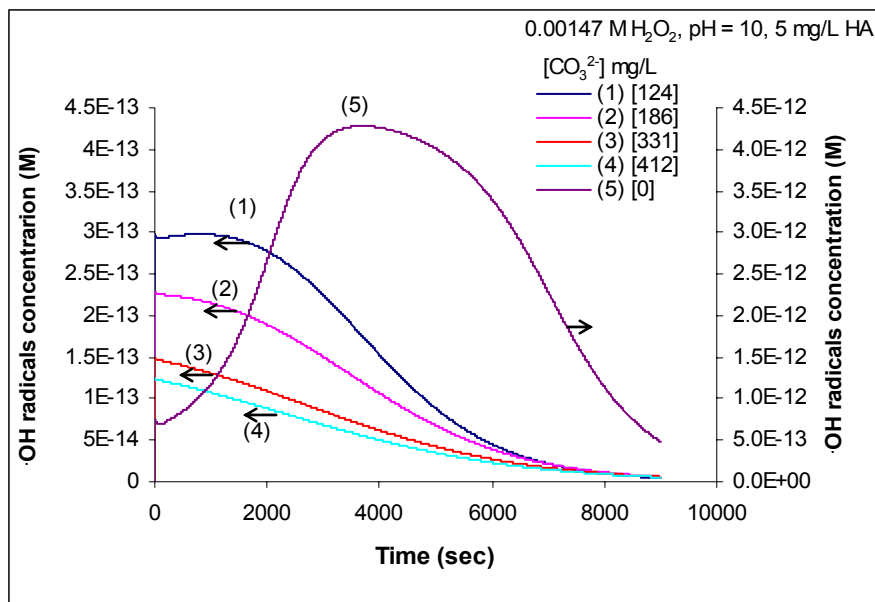
**Fig. 3.1-II:** Predicted concentration of $^{\bullet}OH$ radicals vs. different initial $CO_3^{2-}$ concentrations. Initial conditions: $[NPDOC]_o = 5$ mg $L^{-1}$, $[H_2O_2] = 0.00147$ M, pH = 10
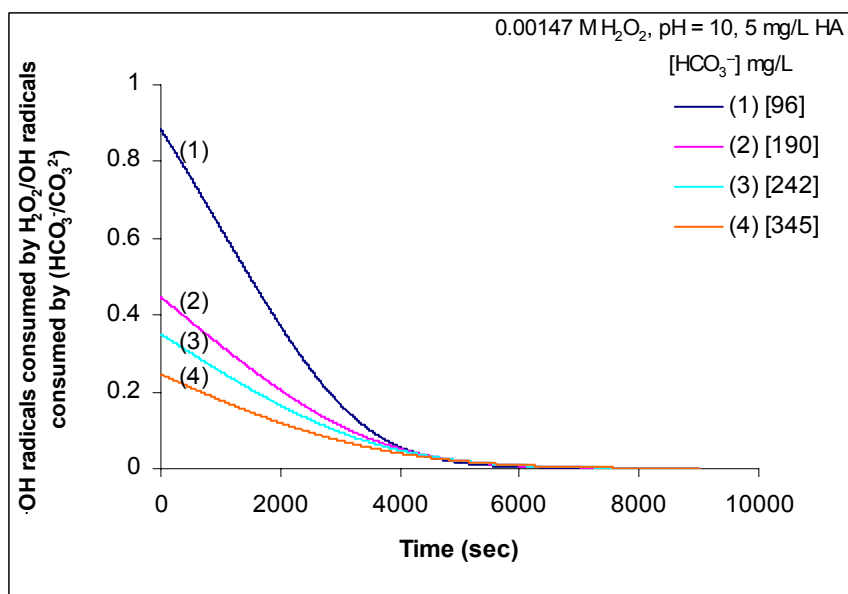


**Fig. 3.1-III:** Predicted ratio of $^{\bullet}OH$ radicals consumption by ($H_2O_2/$ $HO_2^-$) to their consumption by ($HCO_3^-/CO_3^{2-}$) vs. different initial $HCO_3^-$ concentrations. Initial conditions; $[NPDOC]_o = 5$ mg $L^{-1}$, $[H_2O_2] = 0.00147$ M, pH = 10
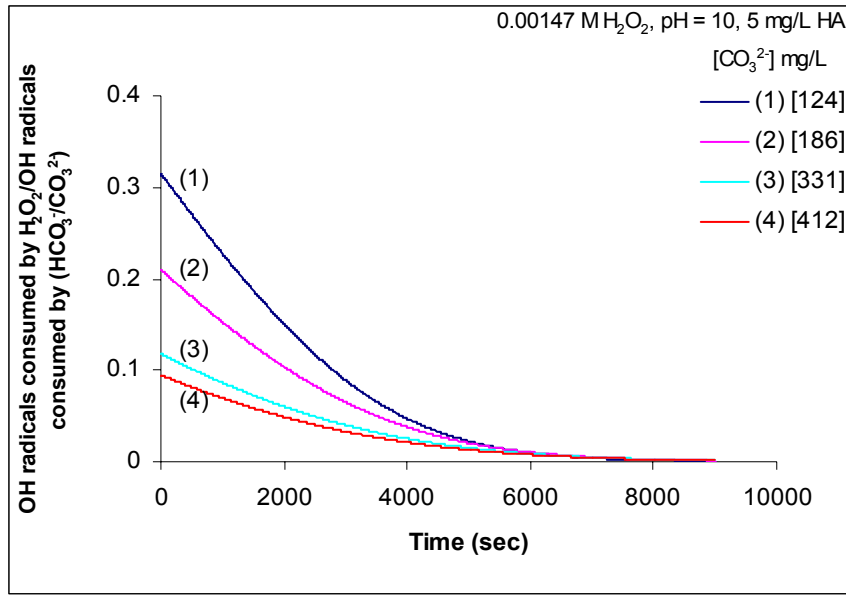
**Fig. 3.1-IV:** Predicted ratio of $^\bullet OH$ radicals consumption by ($H_2O_2/ HO_2^-$) to their consumption by ($HCO_3^-/CO_3^{2-}$) vs. different initial $CO_3^{2-}$ concentrations. Initial conditions; $[NPDOC]_o = 5$ mg L$^{-1}$, $[H_2O_2] = 0.00147$ M, pH = 10

### 3.2. Part 2: Simulation of the experimental data of Wang (2001)

The kinetic model which was used in the simulation of the data in Section 3.1 was used to simulate a new set of experimental data published by Wang (2001). The same rate constants and fitting parameters which were used in section 3.1, except for $k_1$ and $k_2$, were used in this section. The value of $k_1$ was 2.5 x 10$^{-6}$ M s$^{-1}$ (Section 3.1), $k_1$ was increased to 2.7 x 10$^{-6}$ M s$^{-1}$ in this section. This increase in $k_1$ might be related to changes in light intensity ($I_o$). In order to be consistent, $k_2$ has to be increased from 2.5 x 10$^{-9}$ M s$^{-1}$ (section 3.1) to 2.7 x 10$^{-9}$ M s-$^1$. Therefore, the ratio of $k_1$ value in Section 3.1 to its value in this section will be the same as the ratio of $k_2$ value of Section 3.1 to $k_2$ value in this section. Hence changes in both $k_1$ and $k_2$ can be attributed to changes in $I_o$. Figure 3.2.A and 3.2.B compare the residual fraction of NPDOC and $H_2O_2$ by using $k_1$ and $k_2$ the same as in section 3.1 and by increasing them. It can be seen that the residual fraction of NPDOC is the same in both cases. On the other hand simulation seems to be

317

closer to the experimental data regarding residual fraction of hydrogen peroxide. Based on the analysis of the sum of the squared error increasing $k_1$ and $k_2$ is better for the data of $H_2O_2$. On the other hand, this sum has increased from 2.1% to 2.3% for NPDOC by increasing $k_1$ and $k_2$. The average of the sum of the error for the data of NPDOC and $H_2O_2$ was lower by increasing $k_1$ and $k_2$ hence $k_1$ and $k_2$ values will be 2.7 x $10^{-5}$M s$^{-1}$, 7 x $10^{-9}$ M s-$^{1}$, respectively, in the next simulations.
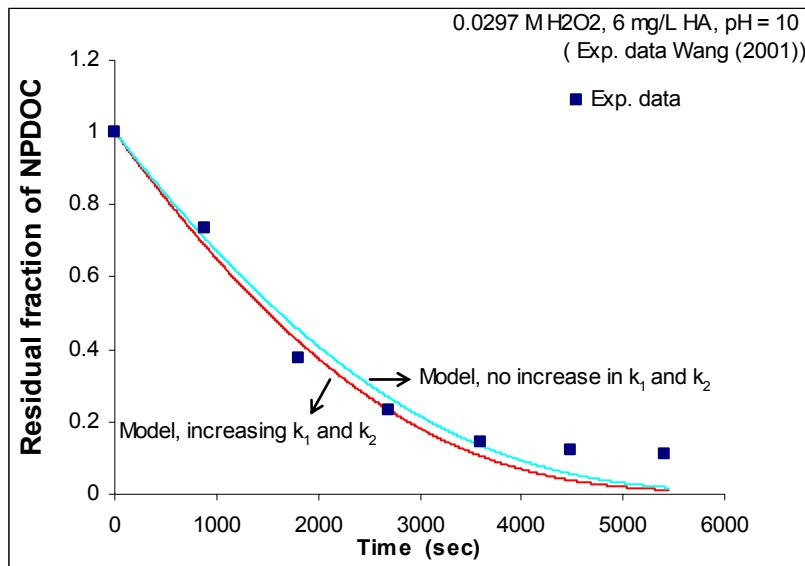


**Fig. 3.2.A:** Residual fraction of NPDOC vs. time from experimental data [Wang, 2001] and model prediction. Initial conditions: [NPDOC]$_o$ = 6 mg L$^{-1}$, [$H_2O_2$] = 0.0297 M, pH = 10, total carbonate ([$HCO_3^- / CO_3^{2-}$])= 0 M
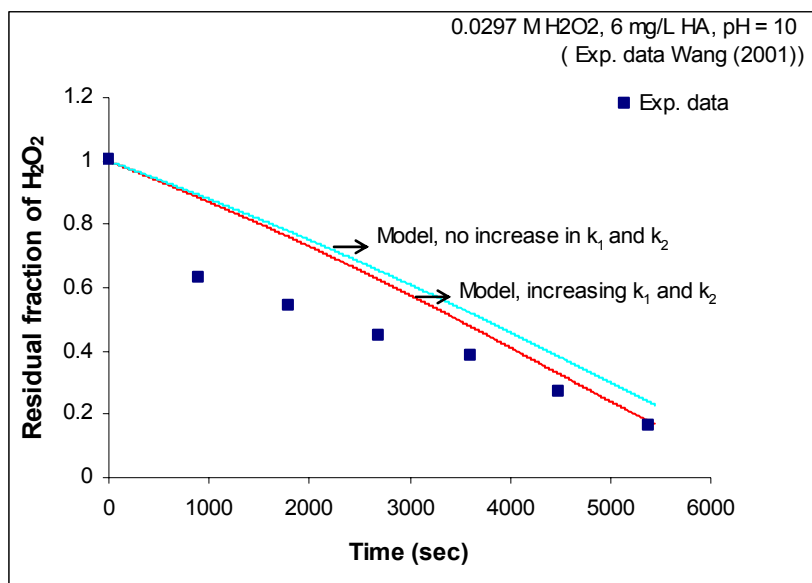
**Fig. 3.2.B:** Residual fraction of $H_2O_2$ vs. time from experimental data [Wang, 2001] and model predictions. Initial conditions: $[NPDOC]_o$ = 6 mg $L^{-1}$, $[H_2O_2]$ = 0.0297 M, pH = 10, total carbonate ($[HCO_3^-/CO_3^{2-}]$ )= 0 M

In this set of experimental data [Wang, 2001], higher initial hydrogen peroxide concentration was used (0.0297 M) than the data in Section 3.1 (0.00147 M). The concentration of NPDOC was 6 mg $L^{-1}$ in this section compared to 5 mg $L^{-1}$ in Section 3.1. Also, in this section, the concentration of total carbonate ($HCO_3^-/CO_3^{2-}$) was increased from 1.25 x $10^{-3}$ M to 2.5 x $10^{-3}$ M at pH = 10. The results of simulation are presented in Figures 3.2.2.A and 3.2.2.B for the residual fraction of NPDOC and hydrogen peroxide, respectively.
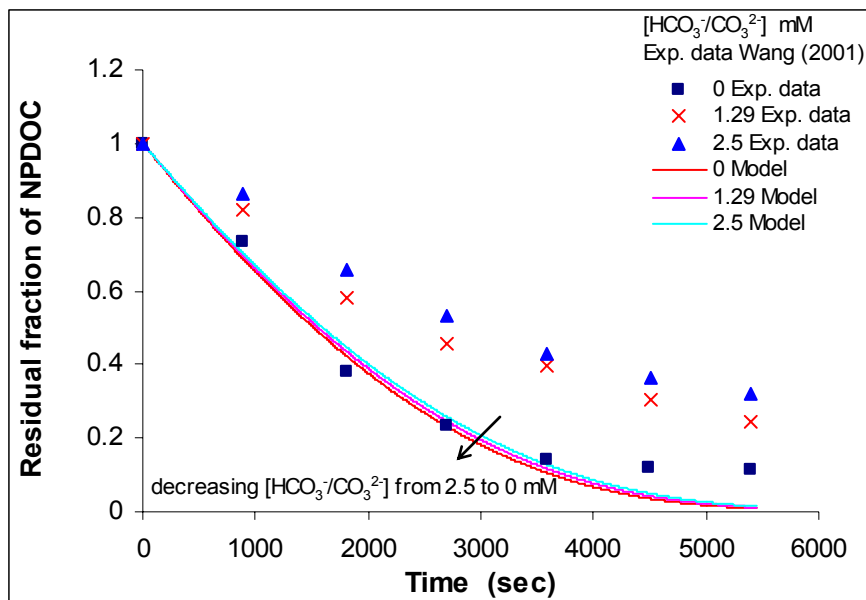
**Fig. 3.2.2.A:** Residual fraction of NPDOC vs. time from experimental data [Wang, 2001] and model predictions at different initial total carbonate ($HCO_3^-/CO_3^{2-}$) concentrations. Initial conditions: $[NPDOC]_o = 6$ mg L$^{-1}$, $[H_2O_2] = 0.0297$ M, pH = 10
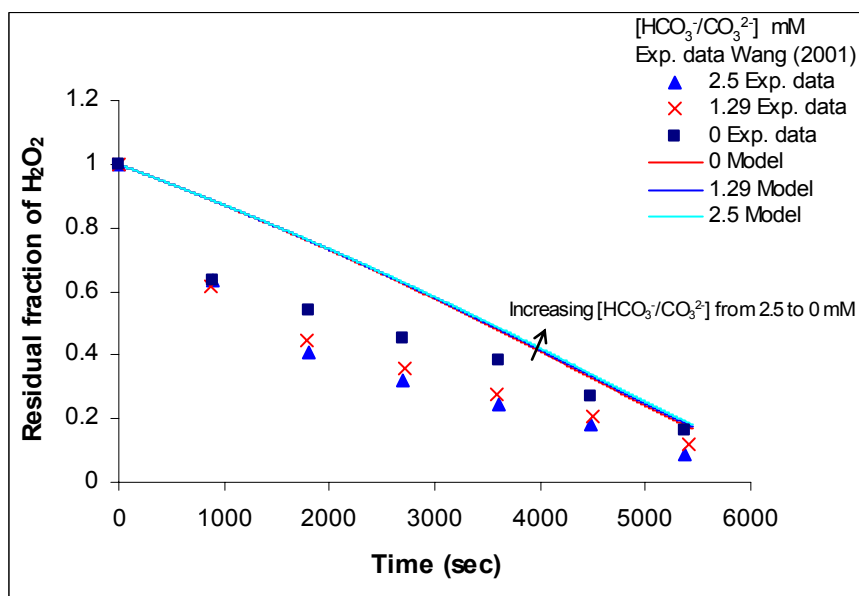


**Fig. 3.2.2.B:** Residual fraction of $H_2O_2$ vs. time from experimental data [Wang, 2001] and model predictions at different initial total carbonate ($HCO_3^-/CO_3^{2-}$) concentrations. Initial conditions: $[NPDOC]_o = 6$ mg L$^{-1}$, $[H_2O_2] = 0.0297$ M, pH = 10

# 4. Discussion

**4.1. Discussion on Part 1 (simulation of experimental data of Wang (2000))**

The results in Figures 3.1.1 and 3.1.2 give the model simulation for the data published by Wang (2000). It can be seen that the model was able to describe the trend of the system by going from zero carbonate/bicarbonate content to the case were carbonate/ bicarbonate was present. Although the results in Figure 3.1.1 were given in term of different initial $CO_3^{2-}$ concentrations, the concentration of the other forms of carbonate system ($HCO_3^-$ and $CO_{2(aq)}$) were calculated from the initial $CO_3^{2-}$ concentration based on the relations from equilibrium that were presented in section 2.1.2. The same was done when the data were given in terms of initial $HCO_3^-$ concentrations. Figures 3.1.1 and 3.1.2 were kept in the term of $CO_3^{2-}$ and $HCO_3^-$, respectively, in order to be consistent with notation of the experimental data from Wang (2000).

It can be seen from Figure 3.1.1.A that the model described the experimental data well when the concentrations of $HCO_3^-$ were zero and 96 mg $L^{-1}$. For the other concentrations of $HCO_3^-$, the model describes the experimental data well for times greater than 4000 seconds. It is expected that carbonate will lead to retardation in the degradation of NPDOC; therefore, if this retardation is apparent for times greater than 4000 sec, it should also be present for times less than 4000 seconds. Hence, the experimental data for times less than 4000 might have some error during measurement of residual concentration of NPDOC. Usually, in order to prevent carbonate from

interference with total organic carbon measurements (TOC), the solution will be acidified to get rid of carbonate.

It can be seen from the simulation results in Figure 3.1.2.A, that the model prediction for the residual fraction of NPDOC at 124 mg L$^{-1}$ of $CO_3^{2-}$ matches with the experimental data of 186 mg L$^{-1}$ $CO_3^{2-}$ and the model simulation of 186 mg L$^{-1}$ of $CO_3^{2-}$ matches with the experimental data of 124 mg L$^{-1}$ $CO_3^{2-}$ for time greater than 3500 seconds. The experimental data at 124 mg L$^{-1}$ $CO_3^{2-}$ and 186 mg L$^{-1}$ $CO_3^{2-}$ are very close up to 3500 seconds. After this time, the residual fraction of NPDOC at 124 mg L$^{-1}$ $CO_3^{2-}$ became higher than at 186 mg L$^{-1}$ $CO_3^{2-}$. We believe that the model prediction is correct and there might be an error in the measurement of NPDOC or initial carbonate alkalinity in the system (based on direct contact with author) since the other experimental data in this figure and Figure 3.1.1.A show a retardation effect as initial carbonate and bicarbonate concentrations were increased. Therefore, residual fraction of NPDOC at 186 mg L$^{-1}$ $CO_3^{2-}$ is expected to be higher than the residual fraction of NPDOC at 124 mg L$^{-1}$ $CO_3^{2-}$ at all reaction times.

During the simulation, the value of the rate constant of direct photolysis of HA ($k_2$) was found to be 2.5 x 10$^{-9}$ M sec$^{-1}$ from best fitting to the experimental data in section 3.1. In Chapter 2, $k_2$ was found to be 2.5 x 10$^{-8}$ M sec$^{-1}$. In Chapter 2, the simulation was applied for experimental data for the degradation of humic acid by UV/H$_2$O$_2$ process with no carbonate at a pH value of 7. In this chapter, the simulation was performed on experimental data for the degradation of humic acid by UV/H$_2$O$_2$ process with the absence and presence of carbonate at a pH value of 10. The reduction of

$k_2$ as the pH value was increased from 7 to 10 could be due mainly to two reasons; changes in light intensity ($I_o$) between the two sets of data, or changes in the quantum yield of HA photolysis. The value of $k_1$ ( rate constant of direct photolysis of hydrogen peroxide) was found to be $2.5 \times 10^{-6}$ M s$^{-1}$ at 0.0294 M $H_2O_2$ using 0 and 5 mg L$^{-1}$ HA at pH = 7 (Chapter 2) and at 0.00147 M $H_2O_2$ using 6 mg L$^{-1}$ HA in this chapter. Therefore, since $k_1$ was the same, it can be assumed that the light intensity ($I_o$) is the same in both set of data. If this assumption is valid, then the reason behind the change in $k_2$ is due to change of quantum yield of HA photolysis ($\Phi_{HA}$) since $k_2 = \Phi_{HA} I_o$. The quantum yield of HA photolysis is a measure to the degree of HA mineralization for the amount of UV light absorbed by HA. Therefore, if $k_2$ had decreased as pH value increased from 7 to 10, this would mean that the rate of photolysis of HA had decreased. A change in the degree of HA photolysis, as a function of the degree of the acidity might be expected, since humic substances are heterogeneous molecules that have been characterized to contain conjugate olefinic and aromatic functional groups, as well as carboxyl and hydroxyl and sometimes a small percentage of nitrogenous functional groups [Aguer, 2001, 2002; Fischer, 1987; McKnight, 1989; Lyderson, 1989; Kim, 2003; Goldstone, 2002; Chu, 2003]. Therefore there might be a dependence of their rate of photolysis on degree of acidity of the solution due to their heterogeneity. Another possibility is that $I_o$ has decreased at the same time that the quantum yield of $H_2O_2$ has increased and the net results was that $k_1$ remained at the same value as the one in Chapter 2. If this is valid, then the quantum yield of HA could have been constant and the reduction in $k_2$ might be due to reduction in $I_o$. Light intensity was not measured, so it can't be confirmed what is the actual reason behind the change in $k_2$.

The rate constant for the reaction between $^{\bullet}OH$ radicals and HA ($k_{20}$) was 7.0 x $10^8$ $M^{-1}$ $s^{-1}$ in this chapter at pH = 10. In Chapter 2, this rate constant was 1.0 x $10^8$ $M^{-1}$ $s^{-1}$ at pH = 7. The change in $k_{20}$ might also be related to the heterogeneity of HA. Therefore, if HA would dissociate to different forms as a function of pH, then it might be expected that the rate constant of HA oxidation by $^{\bullet}OH$ radicals will vary as pH value changes. For example, the rate constant for the reaction of hydrogen peroxide with $^{\bullet}OH$ radicals exhibits different values at different pH values [Christensen, 1982, Buxton, 1988]. This was explained based on the dissociation reaction of hydrogen peroxide where:

$H_2O_2 \leftrightarrow H^+ + HO_2^-$ $\qquad\qquad\qquad$ $pK_a = 11.65$

$H_2O_2 + {}^{\bullet}OH \rightarrow H_2O + HO_2^{\bullet}$ $\qquad\qquad$ $k_3 = 2.7 \times 10^7$ $M^{-1}$ $s^{-1}$

$HO_2^- + {}^{\bullet}OH \rightarrow HO_2^{\bullet} + OH^-$ $\qquad\qquad$ $k_{18} = 7.5 \times 10^9$ $M^{-1}$ $s^{-1}$

hence, the rate constant for the reaction of hydrogen peroxide with $^{\bullet}OH$ radical will depend on which form(s) of hydrogen peroxide is(are) in the system which is related to the acidity of the solution.

The other fitting parameters, in this chapter at pH = 10, $k_{I3}$, $k_{I4}$, $k_{I1}$, and $k_{I5}$ were the same as those ones at pH = 7 (Chapter 2) and their values were 3 x $10^8$ $M^{-1}$ $s^{-1}$, 1 x $10^7$ $M^{-1}$ $s^{-1}$, 5 $M^{-1}$ $s^{-1}$, and 10 $M^{-1}$ $s^{-1}$, respectively. The obtained values of $k_{I3}$ and $k_{I4}$ were close to the rate constants for the reactions of formic acid, acetic acid, malonic acid, and oxalic acid with $^{\bullet}OH$ radicals (1.3 x$10^8$, 1.6 x$10^7$, 1.6 x$10^7$, and 1.4 x$10^6$ $M^{-1}$ $s^{-1}$, respectively) which were obtained from a study of humic matter photolysis by Goldstone (2002). The value of $k_{I3'}$ was 4 $M^{-1}$ $s^{-1}$ while in Chapter 2 (pH = 7) it was 2 $M^{-1}$ $s^{-1}$. The change in $k_{I3'}$ as pH was changed might be explained in the same way that $k_{20}$ has changed.

**4.1.1. Residual Fraction of NPDOC**

The experimental data and the model predictions, presented in Figures 3.1.1.A and 3.1.2.A, show a retarding effect on the rate of degradation of NPDOC as initial carbonate and bicarbonate concentrations were increased. The retardation increased as initial concentrations of carbonate and bicarbonate were increased.

The hydroxyl radical scavenging character of bicarbonate and carbonate can explain these inhibition effects. Although bicarbonate and carbonate do not adsorb UV light, they react readily with hydroxyl radicals which are the primary oxidizing species in the UV/$H_2O_2$ process [Beltran, 1996; Hogine, 1978; Buxton, 1988; Glaze, 1995]. Although the generated carbonate radical anion has been shown to be an oxidant itself, its oxidation potential is less than that of the $^•OH$ radicals [Beltran, 1996]. The rate constant for the reaction of carbonate radicals with HA is 5.0 x$10^5$ $M^{-1}$ $s^{-1}$ compared to 7.0 x $10^8$ $M^{-1}$ $s^{-1}$ for the reaction between $^•OH$ radicals and HA. Therefore reaction of HA with $^•OH$ radicals is at least three orders of magnitude geater than its reaction with carbonate radicals.

From the model predictions for the concentration of $^•OH$ radicals in Figures 3.1-I and 3.1-II it can be seen that the available concentration of $^•OH$ radicals were decreasing as the initial concentrations of carbonate and bicarbonate had increased. This decrease was due to more scavenging of $^•OH$ radicals by carbonate and bicarbonate at higher carbonate/bicarbonate concentrations resulting in less degradation of NPDOC. As a consequence, the concentration of NPDOC will be higher for a given reaction time. This will reduce the fraction of UV light absorbed by hydrogen peroxide and will produce fewer $^•OH$ radicals at the higher bicarbonate and carbonate concentrations.

From the model simulation in Figures 3.1-I and 3.1-II, it can be seen that in all cases, the concentration of $^\bullet OH$ radicals rises rapidly from zero in a very short time once the photolysis of $H_2O_2$ has started. After that, a slower increase in $^\bullet OH$ radicals is observed. The slowing of the rate of these radicals production is due to its consumption from the system. This consumption is mainly due to HA, hydrogen peroxide and its conjugate base, and $HCO_3^-/CO_3^{2-}$. This increment in the concentration of $^\bullet OH$ radicals will reach a maximum value which is function of the initial $HCO_3^-$ and $CO_3^{2-}$ concentration in the system.

Also, it can be seen from Figures 3.1-I and 3.1-II that, when there was no $HCO_3^-$ or $CO_3^{2-}$, the concentration of $^\bullet OH$ radicals reached a maximum value of 4.3 x 10 $^{-12}$ M. This maximum appears at the same time in which the concentration of NPDOC has been reduced to a low value as can be seen from Figure 3.1.1.A when the carbonate and bicarbonate were absent. At the same time, in which NPDOC concentration was decreased, there is still production of $^\bullet OH$ radicals by direct photolysis of hydrogen peroxide therefore, these radicals will accumulate in the system since they are in excess of the system capacity. After this maximum, there is a decline in the concentration of $^\bullet OH$ radicals which is due to its continuing consumption by all the scavengers and mainly to the depletion of hydrogen peroxide, as can be seen from Figure 3.1.1.A, from the system which is the source of these radicals through direct photolysis.

The predicted concentration of $^\bullet OH$ radicals exhibited the highest maximum value when the carbonate was absent, and this maximum value decreased or disappeared as more $HCO_3^-$ and $CO_3^{2-}$ concentrations was added as can be seen from Figures 3.1-I

and 3.1-II. This would mean that the concentration of $^{\bullet}$OH radicals is no longer in excess. Also, this maximum was reached faster as more carbonate was in the system due to greater scavenging of $^{\bullet}$OH radicals.

Also, it can be seen from Figures 3.1-I and 3.1-II that the concentration of $^{\bullet}$OH radicals at an initial $CO_3^{2-}$ concentration of 186 mg L$^{-1}$ was lower than the one at an initial concentration of 190 mg L$^{-1}$ of $HCO_3^-$. This is due to that $CO_3^{2-}$ has a higher rate constant for the reaction with $^{\bullet}$OH radical than the corresponding one of $HCO_3^-$, based on the rate constants in Table 2.1. Therefore, scavenging of $^{\bullet}$OH radicals will be higher and the net result is lower concentration of these radicals.

In order to analyze the system in more detail, the rate of $^{\bullet}$OH radical reaction with NPDOC at the different initial concentrations of $HCO_3^-$ and $CO_3^{2-}$, is obtained from the model simulations and is presented in Figures 4.1.1 and 4.1.2. The data in Figure 4.1.1 are consistent with the results in Figures 3.1.1-A since it shows that fewer $^{\bullet}$OH radicals are being consumed by NPDOC as more $HCO_3^-$ concentration (lower concentration of $^{\bullet}$OH radicals, Figure 3.1-I) was used which will lead to lower degradation of NPDOC and hence higher residual fraction of NPDOC. The same is true for the results in Figure 4.1.2 where less consumption of $^{\bullet}$OH radicals by NPDOC was obtained as more $CO_3^{2-}$ concentration was initially present in the system. It should be remembered that once carbonate or bicarbonate were introduced to the system then the other forms of total carbonate ($HCO_3^-$, $CO_3^{2-}$, and $CO_{2(aq)}$) would be present through equilibrium reactions. Therefore, the effect of increasing initial carbonate or bicarbonate

concentration is a combined effect of increasing total carbonate in the system and the scavenging of the $^\bullet OH$ radicals will be by $CO_3^{2-}$ and $HCO_3^-$ as was shown in the kinetic model.

In this kinetic model HA was assumed to be degraded by direct photolysis, oxidation with $^\bullet OH$ radicals and by reaction with carbonate radicals according to the following equation:

$$\frac{dHA}{dt} = -k_{20}[HA][^\bullet OH] - k_2 f_{HA}(1-e^{-At}) - k_{21}[CO_3^{\bullet -}][HA]$$
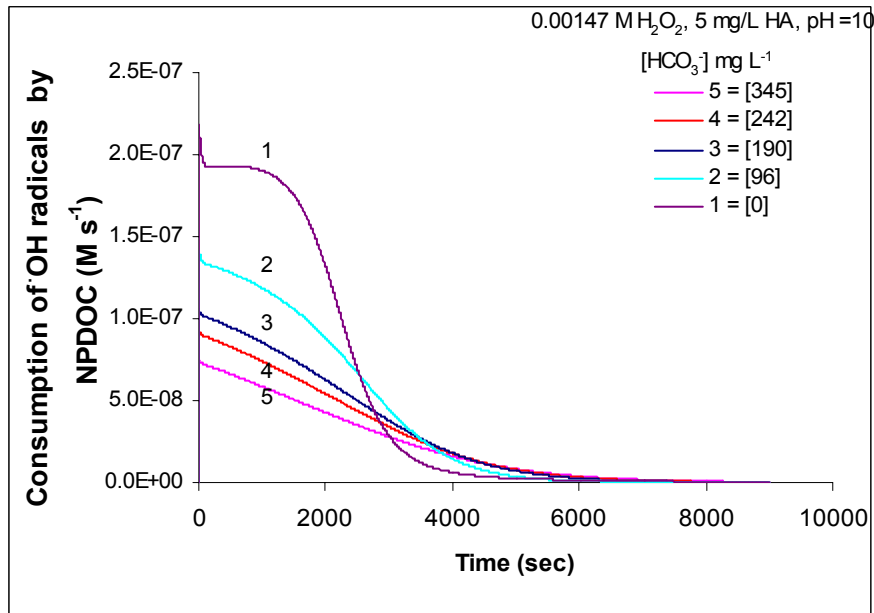


**Fig. 4.1.1:** Predicted rate of consumption of $^\bullet OH$ radicals by NPDOC vs. time at different initial $HCO_3^-$ concentrations. Initial conditions: $[NPDOC]_o = 5$ mg $L^{-1}$, $[H_2O_2] = 0.00147$ M, pH = 10
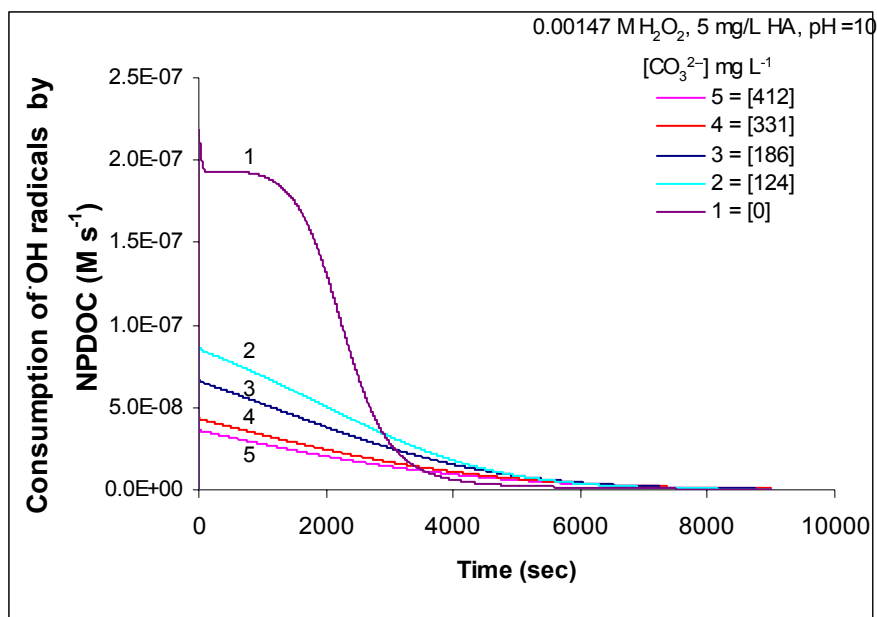
**Fig. 4.1.2:** Predicted rate of consumption of $^{\bullet}OH$ radicals by NPDOC vs. time at different initial $CO_3^{2-}$ concentrations. Initial conditions: $[NPDOC]_o = 5$ mg L$^{-1}$, $[H_2O_2] = 0.00147$ M, pH = 10

The byproducts of HA reactions were assumed to be consumed by $^{\bullet}OH$ radicals and were not absorbing UV light. Hence, consumption of $^{\bullet}OH$ radicals by NPDOC is due to reactions of $^{\bullet}OH$ radicals with HA and the other byproducts of HA reactions in the system.

Figure 4.1.3 shows the predicted magnitude of the degradation of NPDOC by the different routes. It can be seen that consumption of NPDOC by $^{\bullet}OH$ radicals and carbonate radicals ($CO_3^{\bullet-}$) is within the same order of magnitude. On the other hand, degradation of NPDOC by direct photolysis is lower than the other routes. A slight increment in the consumption by carbonate radicals can be observed. This is due to increase in carbonate radical concentration from the reaction between $^{\bullet}OH$ radicals and carbonate/bicarbonate species as can be seen in Figure 4.1.4.

329
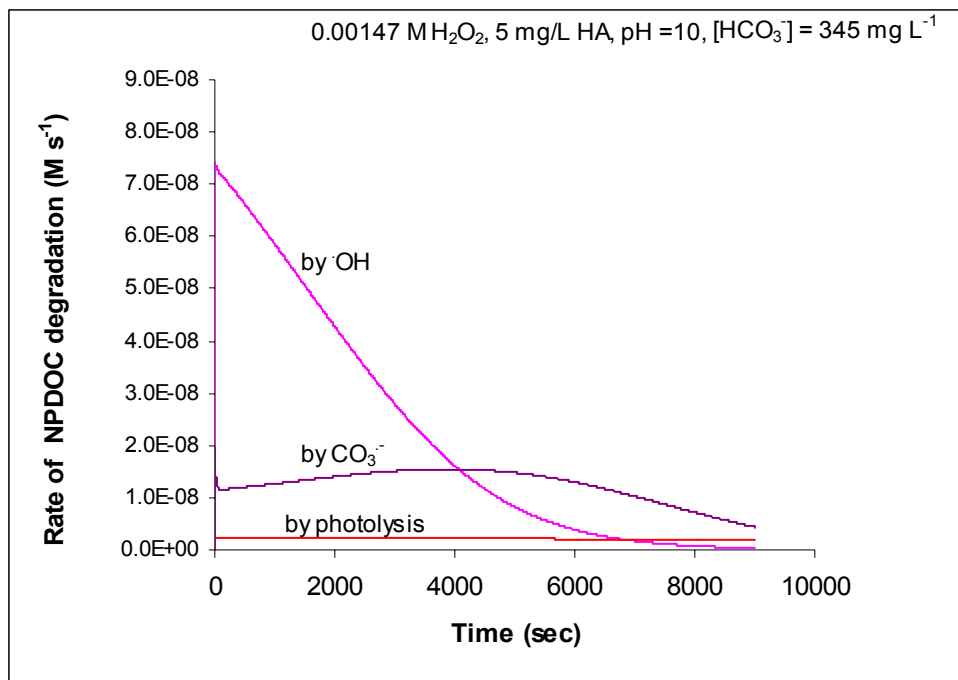
**Fig. 4.1.3:** Predicted rate of consumption of NPDOC by $^\bullet OH$ radicals, direct photolysis and $CO_3^{\bullet-}$ radicals vs. time. Initial conditions: $[NPDOC]_o = 6$ mg $L^{-1}$, $[H_2O_2] = 0.00147$ M, pH = 10, $[HCO_3^-]_o = 345$ mg $L^{-1}$
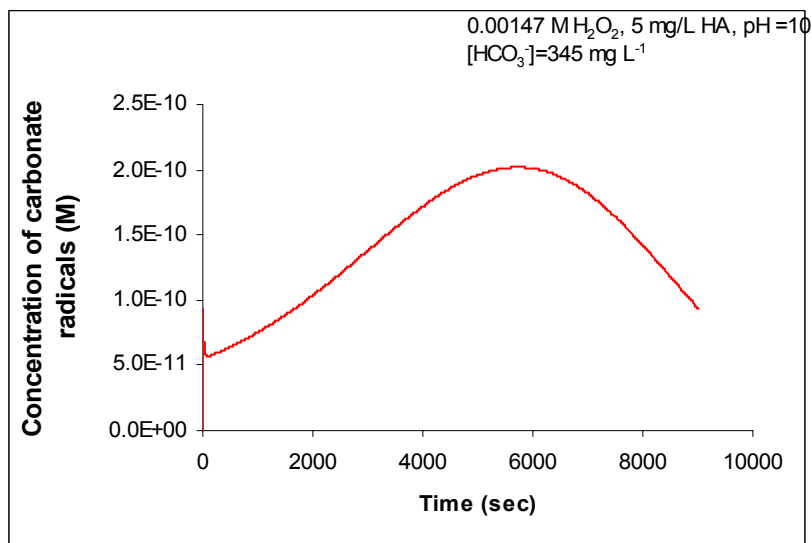


**Fig. 4.1.4:** Predicted concentration of $CO_3^{\bullet-}$ radicals vs. time. Initial conditions: $[NPDOC]_o = 6$ mg $L^{-1}$, $[H_2O_2] = 0.00147$ M, pH = 10, $[HCO_3^-]_o = 345$ mg $L^{-1}$

The residual fraction of NPDOC by neglecting and considering its reaction with $CO_3^{\bullet-}$ radicals is shown in Figures 4.1.5, for the conditions presented in Figure 4.1.3.

330

From this figure, it can be seen that at these conditions neglecting the reaction between HA with $CO_3^{\bullet-}$ radicals will give a higher residual fraction of NPDOC at the given conditions. The difference increased with time since, as can be seen from Figure 4.1.3 above, the rate of NPDOC degradation by $^{\bullet}OH$ radicals decreased with time and for time greater than 4000 seconds it will be lower than scavenging by $CO_3^{\bullet-}$ radicals. Therefore, if the carbonate reaction with HA is absent then the degradation of HA will be slower and end up with higher residual fraction of NPDOC.
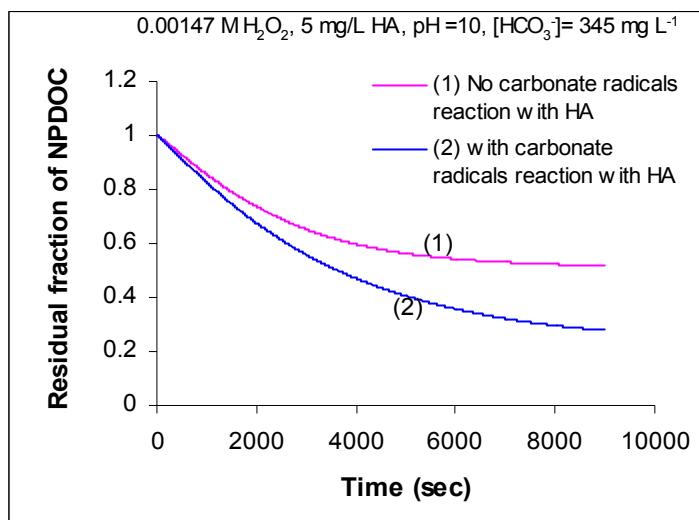


**Fig. 4.1.5:** Predicted residual fraction of NPDOC vs. time assuming there is a reaction between HA and $CO_3^{\bullet-}$ radicals and neglecting the reaction between HA and $CO_3^{\bullet-}$ radicals. Initial conditions: [NPDOC]$_o$ = 5 mg L$^{-1}$, [H$_2$O$_2$] = 0.00147 M, pH = 10, [ $HCO_3^-$ ]$_o$ = 345 mg L$^{-1}$

The difference in the residual fraction of NPDOC between the two cases, considering and neglecting the reaction of HA with $CO_3^{\bullet-}$ radicals, decreased as the initial bicarbonate concentration decreased since scavenging of $^{\bullet}OH$ radicals by carbonate and bicarbonate decreases as initial concentration of bicarbonate increases (Figure 4.1.1). An example at a lower bicarbonate concentration is shown in Figure 4.1.6.
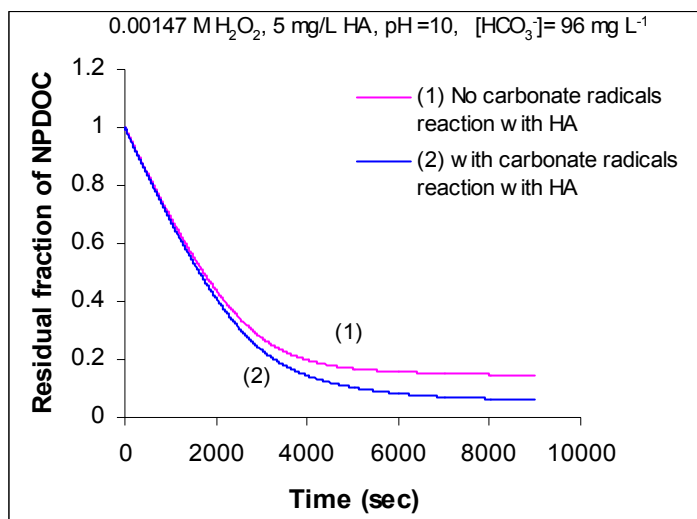
**Fig. 4.1.6:** Predicted residual fraction of NPDOC vs. time assuming there is a reaction between HA and $CO_3^{\bullet-}$ radicals and neglecting the reaction between HA and $CO_3^{\bullet-}$ radicals. Initial conditions: $[\text{NPDOC}]_o$ = 5 mg L$^{-1}$, $[\text{H}_2\text{O}_2]$ = 0.00147 M, pH = 10, $[HCO_3^-]_o$ = 96 mg L$^{-1}$

The predicted rates of HA photolysis, at the same conditions as these ones in Figures 3.1.1.A and 4.1.1, are given in Figure 4.1.7. It can be seen that the absolute magnitude of the rate of photolysis increased as concentration of $HCO_3^-$ increased. This is due to the higher remaining concentration of HA and hence the higher fraction of UV light absorbed by HA since rate of photolysis of HA was defined as:

Rate of HA photolysis = $- k_2 f_{HA} (1 - e^{-At})$

therefore, increasing bicarbonate/carbonate concentration seems to increase the fraction of UV light absorbed by HA ($f_{HA}$) by accumulating more HA in the system. This also explained the faster decline in the rate of photolysis when the carbonate was decreased, since at these conditions the concentration of NPDOC dropped to a lower value as was seen in Figure 3.1.1.A. Although, the model simulation in Figure 4.1.7 will imply a higher removal of NPDOC as bicarbonate concentration was increased, this is not

happening since the rate of photolysis of NPDOC is much lower than its degradation by
$^\bullet$OH radicals, by comparing the results in Figures 4.1.1 and 4.1.7. Hence, the
degradation of NPDOC will be driven mainly by oxidation with $^\bullet$OH radicals, which
showed retardation in oxidation of NPDOC with $^\bullet$OH radicals as more
carbonate/bicarbonate was present.
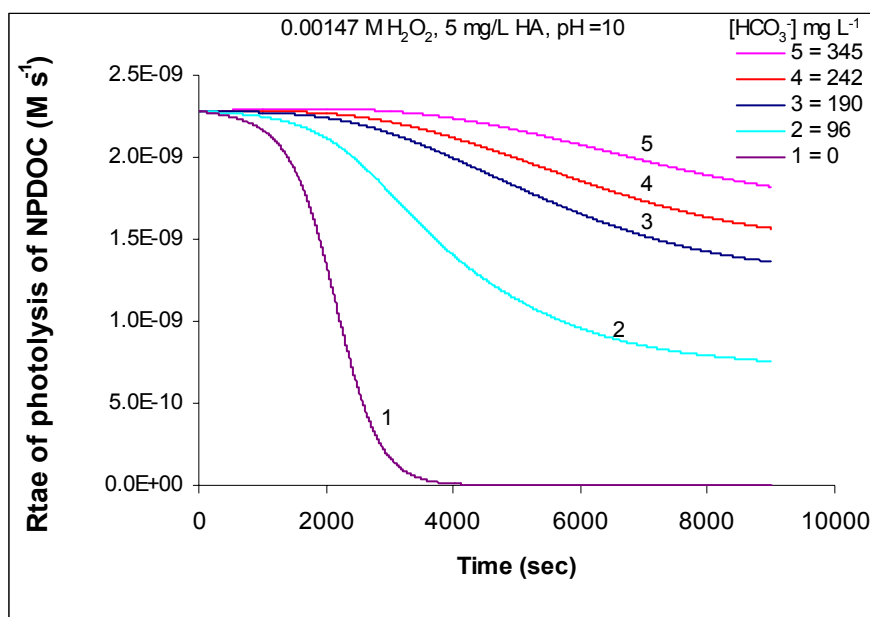


**Fig. 4.1.7:** Predicted rate of photolysis of HA vs. time at different initial $HCO_3^-$ concentrations. Initial
conditions: $[NPDOC]_o = 6$ mg $L^{-1}$, $[H_2O_2] = 0.00147$ M, pH = 10

The products from the reaction of carbonate radicals with hydrogen peroxide and
its conjugate base were bicarbonate and hydroperoxyl radicals and its conjugate base
($HO_2^{\bullet-}/O_2^{\bullet-}$). Hydroperoxyl and its conjugate base radicals are less effective oxidants
than hydroxyl radicals based on the value of their rate constants. Liao (1995) found that
the reactions of $HO_2^{\bullet-}/O_2^{\bullet-}$ with humic substances were negligible. Therefore, it was
assumed that no reaction took place between these radicals and humic acid. Hence the
increase of $HO_2^{\bullet-}/O_2^{\bullet-}$ won't accelerate the degradation of humic acid. The analysis that

333

has been presented above at one concentration of bicarbonate concentrations applies to other concentrations of bicarbonate or carbonate for this system.

**4.1.2. Residual fraction of hydrogen peroxide**

The predicted residual fractions of hydrogen peroxide at the same conditions as the ones in Figures 3.1.1-A and 3.1.2-A were shown in Figures 3.1.1-B and 3.1.2-B, respectively. It can be seen from Figures 3.1.1-B and 3.1.2-B, that the residual fraction of hydrogen peroxide is initially similar at different total carbonate concentrations. When the concentration of $H_2O_2$ dropped to greater than 30 % of its initial concentration, a retarding effect by total carbonate was observed. However, this retarding effect is smaller than the retarding effect on the residual fraction of NPDOC (Figures 3.1.1.A and 3.1.2.A). The retarding effect in Figure 3.1.2.B is higher than the one in Figure 3.1.1.B, since the total carbonate concentration for the conditions in Figure 3.1.2.B is higher than Figure 3.1.1.B.

Hydrogen peroxide ($H_2O_2/HO_2^-$) is mainly degraded by direct photolysis and any effect on this rate will be reflected in all of the reactions in this kinetic model since this reaction is the initiator of the radicals reaction in this system. Therefore, it is expected that the retardation of hydrogen peroxide degradation will be due to lower rates of hydrogen peroxide reactions.

In Section 4.1.1 it was found that increasing total carbonate concentration led to lower degradation of NPDOC for a given time. This will leave higher concentrations of HA in the system. Photolysis of hydrogen peroxide is proportional to the fraction of UV light absorbed, as was defined in the following relation:

$$f_{H_2O_2} = \frac{\varepsilon_{H_2O_2}[H_2O_2] + \varepsilon_{HO_2^-}[HO_2^-]}{\varepsilon_{HA}[HA] + \varepsilon_{H_2O_2}[H_2O_2] + \varepsilon_{HO_2^-}[HO_2^-]}$$

As more HA is present in the system, the rate of hydrogen peroxide photolysis will be lower. Figures 4.1.8 and 4.1.9 show the predicted rate of photolysis of hydrogen peroxide at the conditions of Figures 3.1.1-B and 3.1.1.A, respectively. It can be seen from Figures 4.1.8 and 4.1.9 that the rate of hydrogen peroxide photolysis decreased as carbonate and bicarbonate were introduced into the system.

In Figure 4.1.8, for time less than 3500 seconds the rate of photolysis decreased as more bicarbonate was used. After 3500 seconds this behavior was reversed. This is due to the fact that the concentration of hydrogen peroxide became higher at the higher bicarbonate concentration which will lead to higher absorption of UV light. The results in Figure 4.1.9 are similar except that the rate of hydrogen peroxide is lower due to higher carbonate concentration.
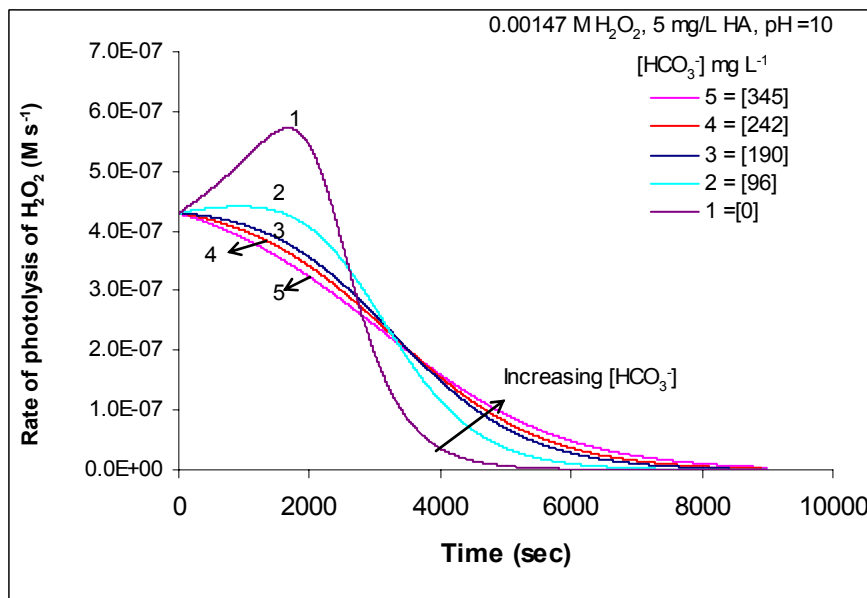


**Fig. 4.1.8:** Predicted rate of photolysis of hydrogen peroxide vs. time at different initial $HCO_3^-$ concentrations. Initial conditions: $[NPDOC]_o$ = 5 mg L$^{-1}$, $[H_2O_2]$ = 0.00147 M, pH = 10 (Same conditions as Figure 3.1.1-B)
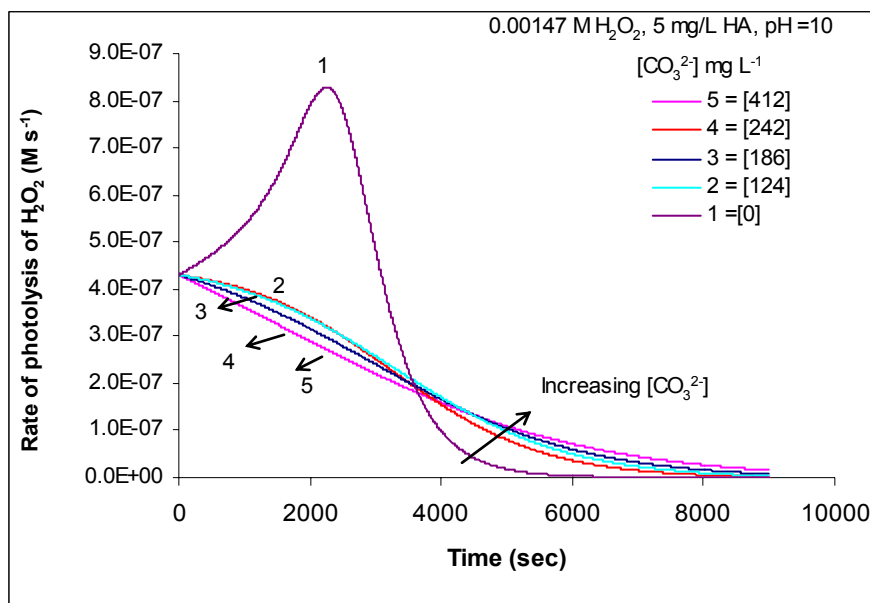
**Fig. 4.1.9:** Predicted rate of photolysis of hydrogen peroxide vs. time at different initial $CO_3^{2-}$ concentrations. Initial conditions: $[NPDOC]_o$ = 5 mg L$^{-1}$, $[H_2O_2]$ = 0.00147 M, pH = 10 (Same conditions as Figure 3.1.2-B)

It is also expected that the rate of degradation of hydrogen peroxide by reaction with $^{\bullet}OH$ radicals will be affected by the presence of bicarbonate and carbonate. Figures 4.1.10 and 4.1.11 show the rate of reaction between $^{\bullet}OH$ radicals and hydrogen peroxide for the conditions presented in Figures 3.1.1.B and 3.1.2.B. It can be seen that the consumption of $^{\bullet}OH$ radicals decreases as more bicarbonate/carbonate was used. This effect is due to the competition of reactions with these radicals from bicarbonate and carbonate as was explained earlier in section 4.1.1. Comparing the results in Figures 4.1.10 and 4.1.11 to the results in Figures 4.1.1 and 4.1.2, it can be seen that the rate of degradation of NPDOC by $^{\bullet}OH$ radicals, although lower, is comparable to the rate of degradation of hydrogen peroxide by these radicals at the studied initial conditions.

336

In the kinetic model, carbonate radicals were reacting with hydrogen peroxide and its conjugate base. Therefore, it is expected that the rate of hydrogen peroxide might be accelerated due to this reaction.
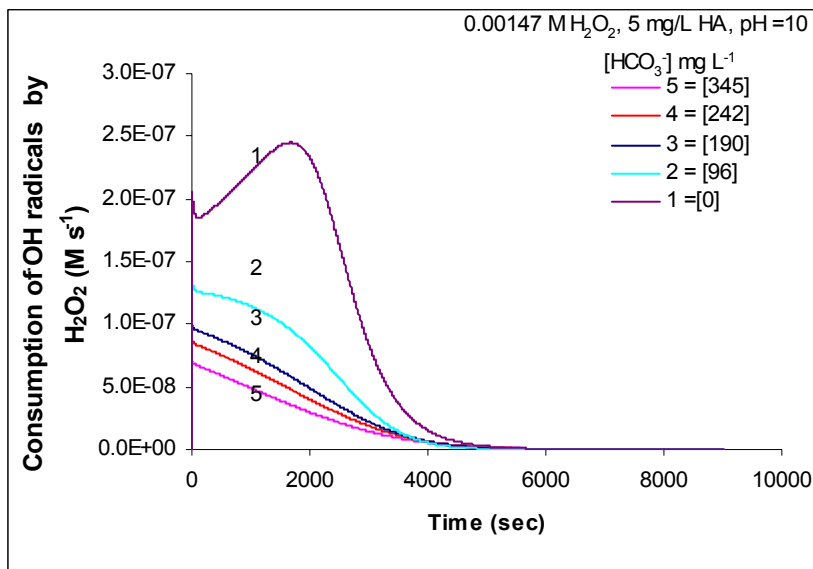


**Fig. 4.1.10**: Predicted rate of consumption of $^\bullet OH$ radicals by hydrogen peroxide vs. time at different initial $HCO_3^-$ concentrations. Initial conditions: $[NPDOC]_o = 5$ mg L$^{-1}$, $[H_2O_2] = 0.00147$ M, pH = 10
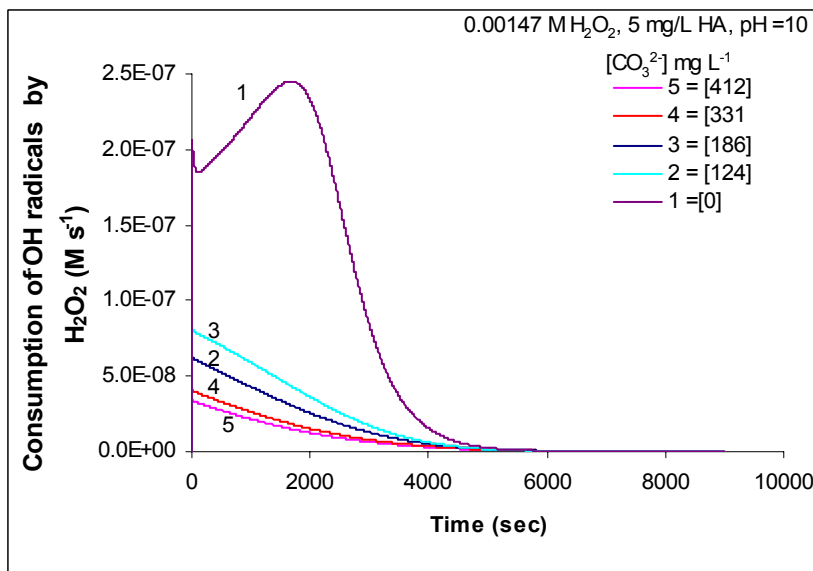


**Fig. 4.1.11:** Predicted rate of consumption of $^\bullet OH$ radicals by hydrogen peroxide vs. time at different initial $CO_3^{2-}$ concentrations. Initial conditions: $[NPDOC]_o = 5$ mg L$^{-1}$, $[H_2O_2] = 0.00147$ M, pH = 10
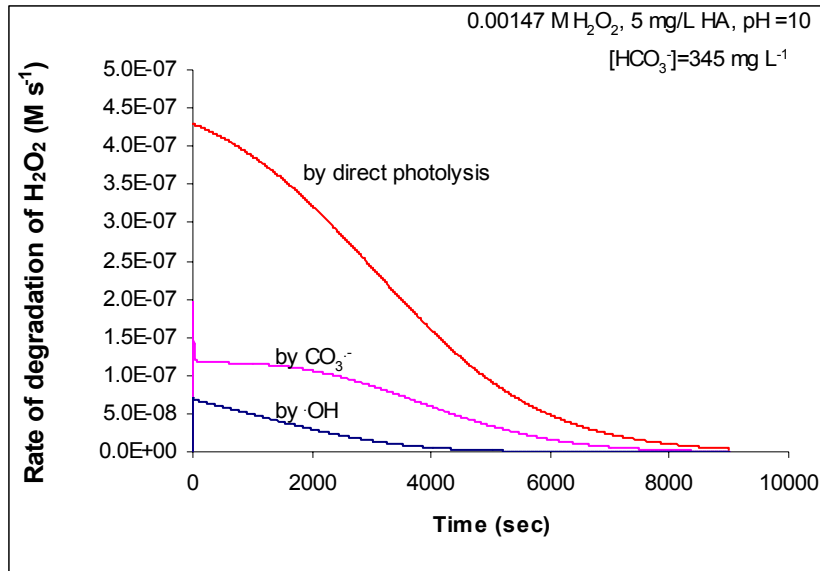
**Fig. 4.1.12:** Predicted rate of degradation of hydrogen peroxide by direct photolysis, $^\bullet OH$ radicals, and $CO_3^{\bullet-}$ vs. time. Initial conditions: $[NPDOC]_o = 5$ mg L$^{-1}$, $[H_2O_2] = 0.00147$ M, pH = 10, $[HCO_3^-]_o = 345$ mg L$^{-1}$

Figure 4.1.12 shows the rate of hydrogen peroxide degradation by direct photolysis, hydroxyl radicals, and carbonate radicals at 345 mg L$^{-1}$ of bicarbonate. From this figure it can be seen that the contribution of carbonate radicals to the consumption of hydrogen peroxide is considerable at such high level of bicarbonate. Therefore, it might be expected that enhancement of the overall degradation of hydrogen peroxide might appear. This effect will be investigated more in the following section through making some modifications in the kinetic model.

**4.1.3. Modifications in the kinetic model**

Figures 4.1.13 and 4.1.14 were obtained by running the simulation at the same conditions as these ones in Figure 4.1.12 and with some modification in the kinetic model, keeping the values of the rate constants at the same values as the ones where carbonate radicals were reacting with hydrogen peroxide and humic acid.

**Case 1: Carbonate radical does not react with HA**

From the simulation results in Figure 4.1.13 it can be seen that when carbonate radicals were assumed not to react with HA, the residual fraction of $H_2O_2$ is almost unaffected compared to the case where it is reacting with $H_2O_2$ (the original model). On the other hand, for the same case, it can be seen, from Figure 4.1.14 that the residual fraction of NPDOC has increased compared to the case where carbonate radicals react with $H_2O_2$ and HA. It seems that making this modification was not affecting the kinetics of hydrogen peroxide. From Figures 4.1.15, 4.1.16 and 4.1.17 it can be seen that the concentrations of hydroxyl radicals and carbonate radicals and the rate of photolysis of hydrogen peroxide were not affected also. This explains the why the residual fraction hydrogen peroxide was not affected.
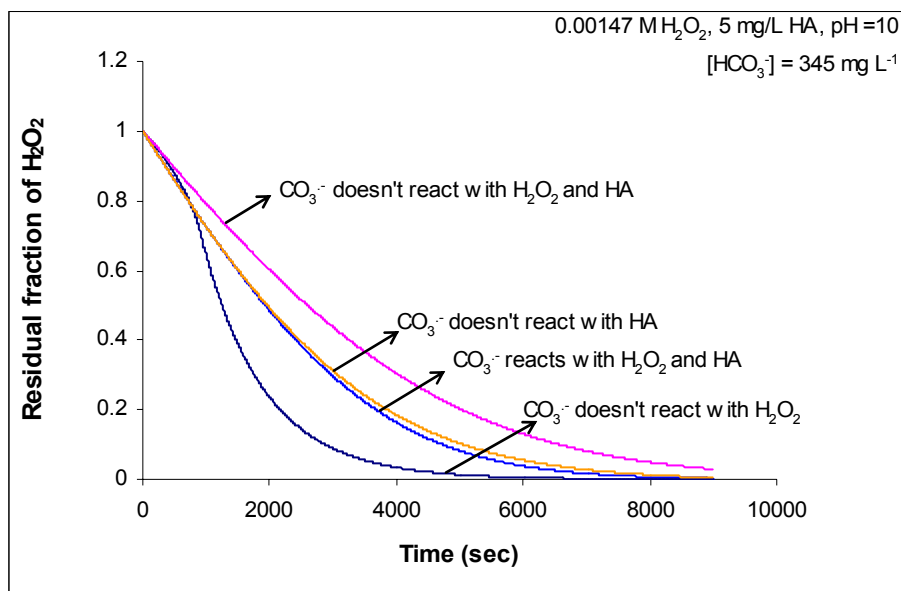


**Fig. 4.1.13:** Residual fraction of hydrogen peroxide vs. time. Initial conditions: $[NPDOC]_o = 5$ mg $L^{-1}$, $[H_2O_2] = 0.00147$ M, pH = 10, $[HCO_3^-]_o = 345$ mg $L^{-1}$

When reaction between HA and carbonate radicals was neglected this led to a slower degradation of HA, but at the same time left more carbonate radicals to react with

hydrogen peroxide . Therefore, more degradation of hydrogen peroxide was taking place and the net result was that hydrogen peroxide is slightly affected by this change.
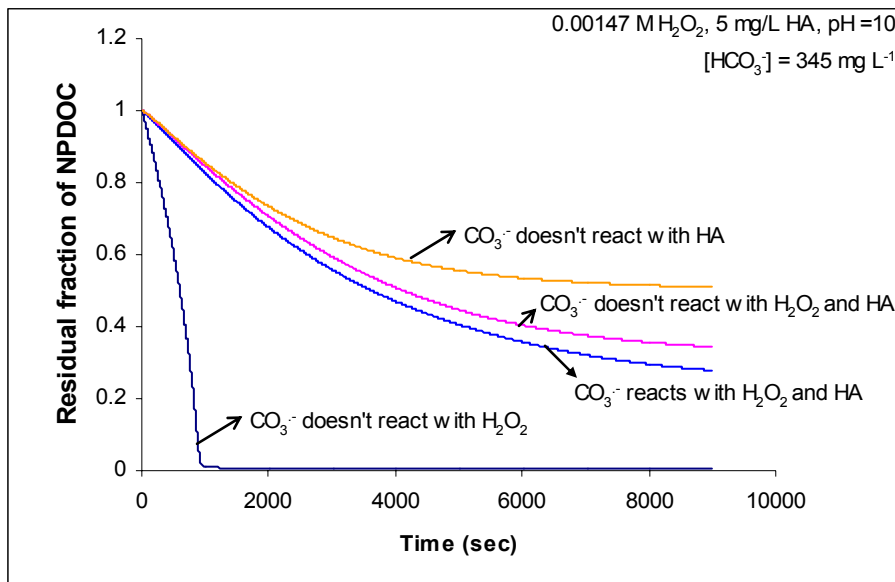


**Fig. 4.1.14:** Residual fraction of NPDOC vs. time. Initial conditions: $[NPDOC]_o$ = 5 mg L$^{-1}$, $[H_2O_2]$ = 0.00147 M, pH = 10, $[HCO_3^-]_o$ = 345 mg L$^{-1}$
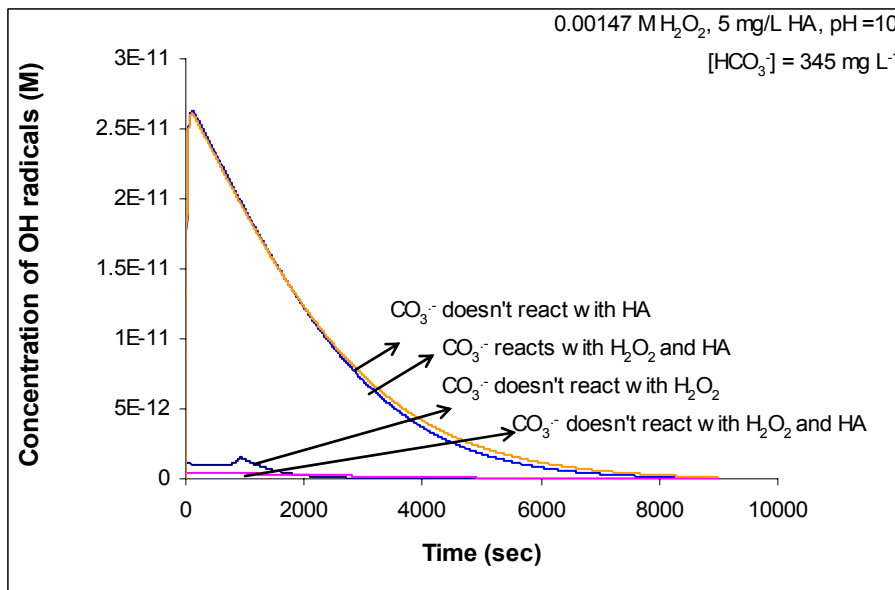


**Fig. 4.1.15:** Concentration of $^\bullet OH$ radicals vs. time. Initial conditions: $[NPDOC]_o$ = 5 mg L$^{-1}$, $[H_2O_2]$ = 0.00147 M, pH = 10, $[HCO_3^-]_o$ = 345 mg L$^{-1}$

**Case 2: Carbonate radicals do not react with HA or H$_2$O$_2$**

340

When carbonate radicals were assumed to not react with either $H_2O_2$ or HA, the rate of degradation of HA and $H_2O_2$ have decreased compared to the case where they were reacting with HA and $H_2O_2$ as can be seen in Figures 4.1.13 and 4.1.14. Assuming no reactions between the carbonate radicals with HA and $H_2O_2$, a higher level of carbonate radicals will remain in the system, as shown in Figure 4.1.16. This will consume more hydroxyl radicals, and hence reduce their concentration as can be seen from Figure 4.1.15. For this case, photolysis of hydrogen peroxide has increased compared to the case where reactions of carbonate radicals with HA and $H_2O_2$ were taking place. This increment is due to the higher concentration of hydrogen peroxide left in the system and hence more absorption of UV light. Although the rate of hydrogen peroxide photolysis has increased, the output of this (more production of $^\bullet OH$ radicals) is going for the benefit of bicarbonate, carbonate and carbonate radicals in the system and the rate of NPDOC degradation by hydroxyl radicals will be lower (Figure 4.1.18).
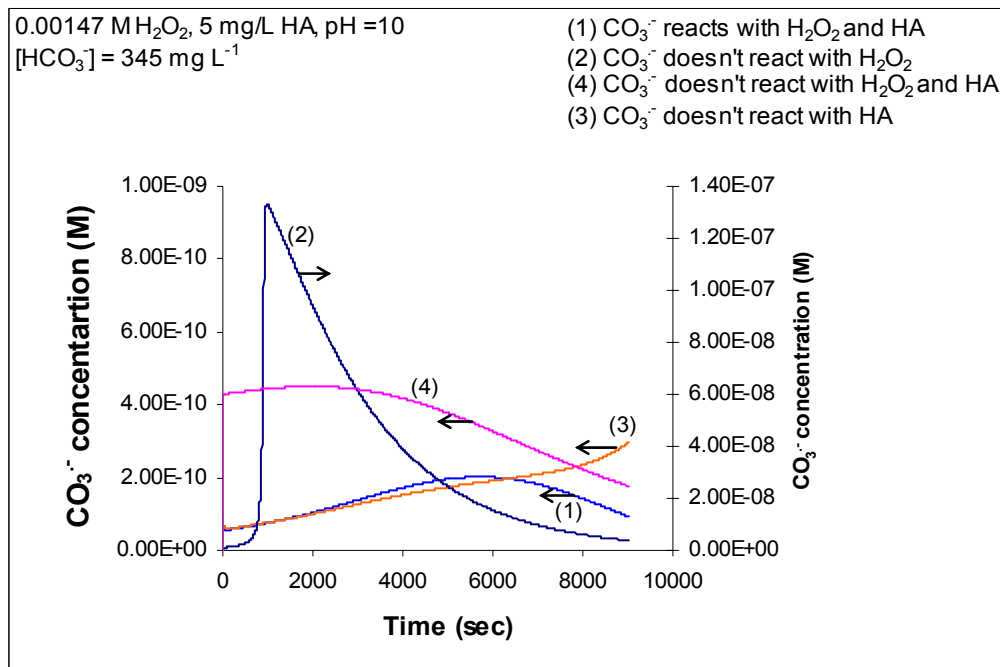


**Fig. 4.1.16:** Concentration of carbonate radicals vs. time. Initial conditions: $[NPDOC]_o = 5$ mg $L^{-1}$, $[H_2O_2]$ = 0.00147 M, pH = 10, $[HCO_3^-]_o$ = 345 mg $L^{-1}$

341

**Case 3: Carbonate radical does not react with H$_2$O$_2$**

A new hypothetical case was assumed. In this case it was assumed that carbonate radicals do not react with hydrogen peroxide or its conjugate base. This assumption is just only theoretical, since literature showed that carbonate radicals react with hydrogen peroxide and its conjugate base [Behar, 1970; Dragenic, 1991]. Interestingly, the degradation of NPDOC was very fast and was removed quickly from the system (Figure 4.1.14). This will make the fraction of UV light absorbed by H$_2$O$_2$ much higher since now the system mainly contain hydrogen peroxide. Therefore, the rate of photolysis of hydrogen peroxide will be higher compared to the case where reactions were taking place between carbonate radicals, HA, and H$_2$O$_2$, as can be seen in Figure 4.1.17. This will also accelerate the removal of hydrogen peroxide and will lead to lower residual fraction of H$_2$O$_2$ as can be seen in Figure 4.1.16. Higher concentration of carbonate radical was left in the system when they didn't react with hydrogen peroxide as can be seen in Figure 4.1.16. This will lead to faster predicted degradation of HA by these radicals as can be seen in Figure 4.1.19. Since, as shown earlier, hydrogen peroxide was mainly degraded by photolysis, then faster degradation of HA will end in lower concentration of HA which will allow the fraction of UV light absorbed by H$_2$O$_2$ to increase. More absorbance of UV light will lead to greater degradation of H$_2$O$_2$.
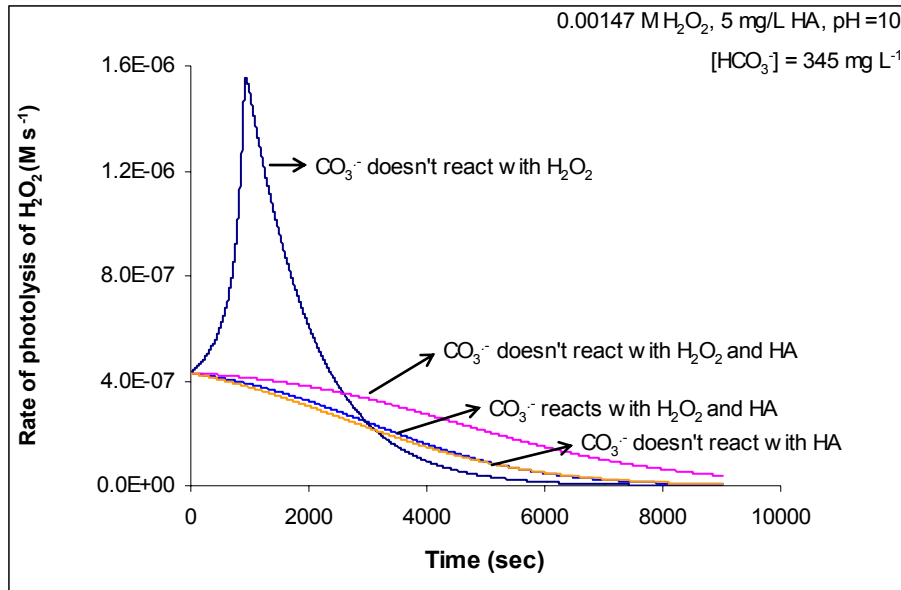
**Fig. 4.1.17:** Rate of photolysis of hydrogen peroxide vs. time. Initial conditions: $[NPDOC]_o = 5$ mg L$^{-1}$, $[H_2O_2] = 0.00147$ M, pH = 10, $[HCO_3^-]_o = 345$ mg L$^{-1}$

Based on the previous analysis it can be seen at the conditions studied, the system is sensitive to the presence of bicarbonate/carbonate. Their presence is important they scavenge hydroxyl radicals which will lead to the production of carbonate radicals. The carbonate radicals go through different reactions in the system, as was shown by the kinetic model. These reactions will affect the rate of degradation of NPDOC and hydrogen peroxide. This would indicate that during a treatment processes if UV/H$_2$O$_2$ is to be applied then the presence of total carbonate should be taken into consideration.
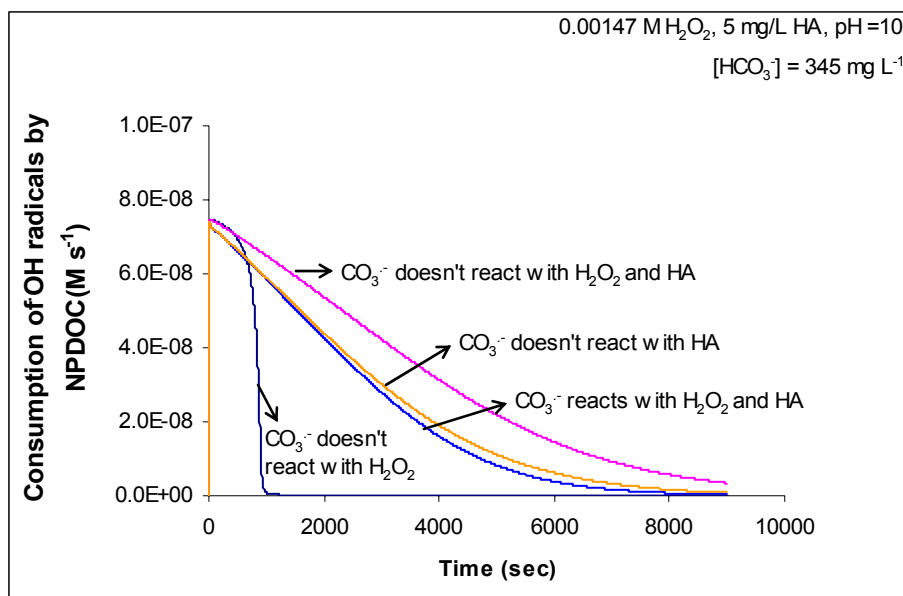
**Fig. 4.1.18:** Rate of consumption of $^\bullet OH$ radicals by NPDOC vs. time. Initial conditions: $[NPDOC]_o = 5$ mg L$^{-1}$, $[H_2O_2] = 0.00147$ M, pH = 10, $[HCO_3^-]_o = 345$ mg L$^{-1}$
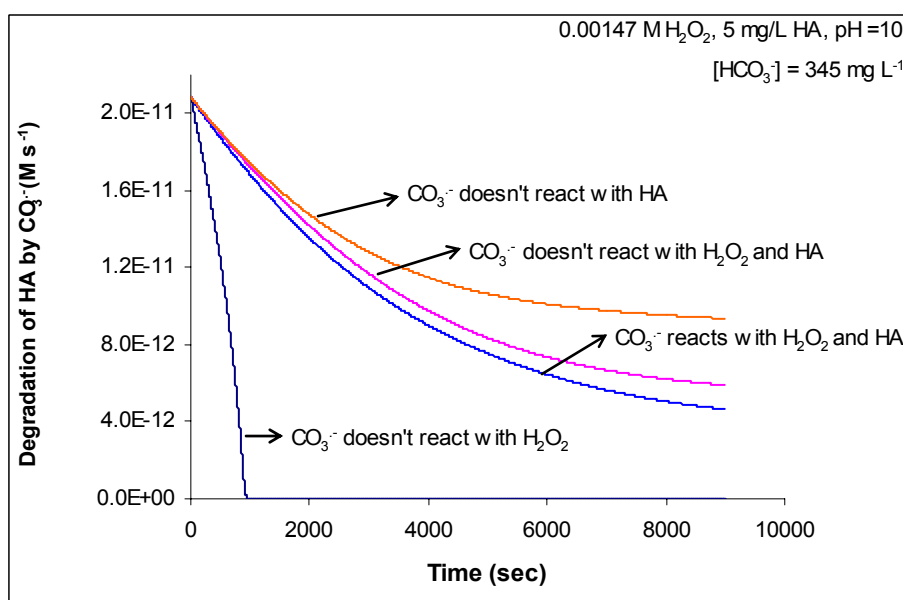


**Fig. 4.1.19:** Degradation of HA by carbonate radicals vs. time. Initial conditions; $[NPDOC]_o = 5$ mg L$^{-1}$, $[H_2O_2] = 0.00147$ M, pH = 10, $[HCO_3^-]_o = 345$ mg L$^{-1}$

## 4.1.4. Reactions of bicarbonate and carbonate

In the previous sections the retardation in the degradation of NPDOC and hydrogen peroxide was attributed to the scavenging of $^\bullet OH$ radicals. The predicted rates

344

of consumption of $^\bullet$OH radicals by carbonate and bicarbonate for the conditions presented in Section 4.1.1 and 4.1.2 are shown in Figures 4.1.20 and 4.1.21. It is clear from these figures, that as more carbonate/bicarbonate was initially present in the system the more is the scavenging of $^\bullet$OH radicals. Also, it can be seen that the rate of scavenging is higher at the conditions presented in Figure 4.1.21. This explains the higher retardation in the residual fraction in NPDOC for the results shown in Figure 3.1.1.A. The higher scavenging is due to the higher total carbonate content in the system.
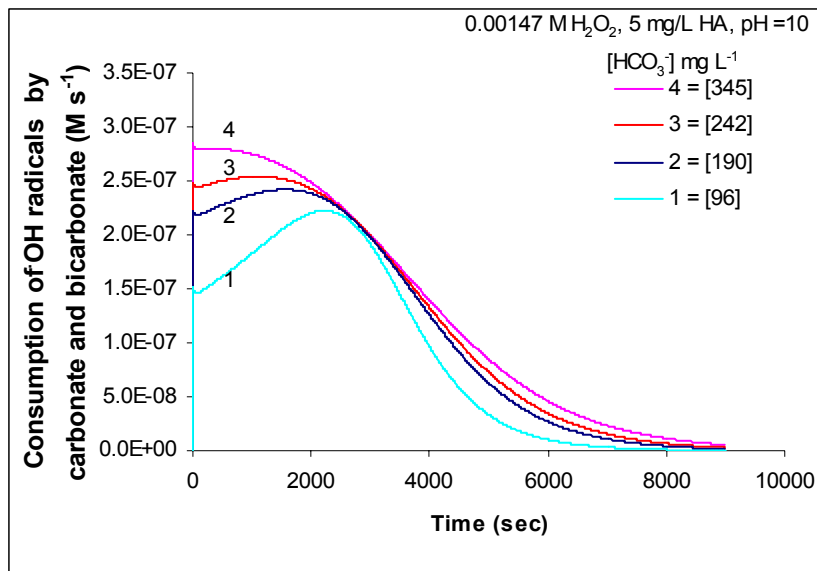


**Fig. 4.1.20:** Predicted rate of consumption of $^\bullet$OH radicals by carbonate and bicarbonate vs. time at different initial $HCO_3^-$ concentrations. Initial conditions: $[NPDOC]_o = 5$ mg $L^{-1}$, $[H_2O_2] = 0.00147$ M, pH = 10
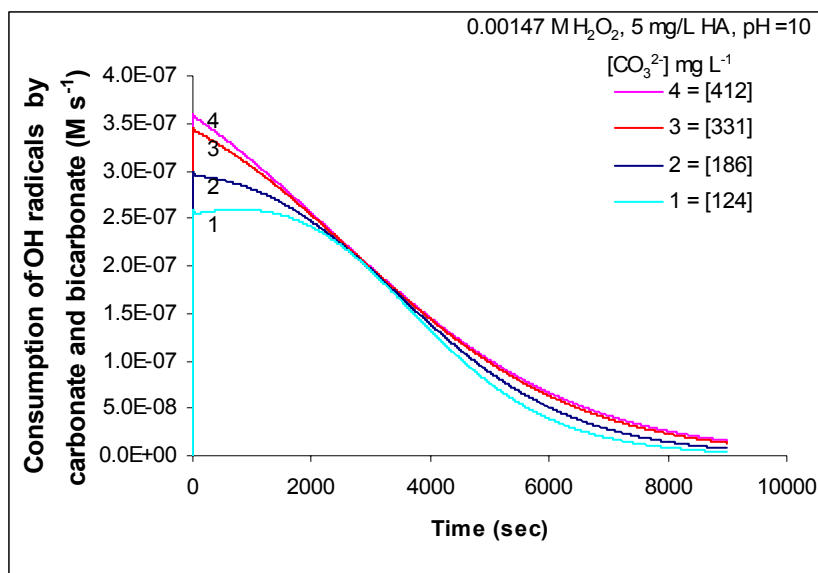
**Fig. 4.1.21:** Predicted rate of consumption of $^{\bullet}OH$ radicals by carbonate and bicarbonate vs. time at different initial $CO_3^{2-}$ concentrations. Initial conditions: $[NPDOC]_o$ = 5 mg $L^{-1}$, $[H_2O_2]$ = 0.00147 M, pH = 10

## 4.2. Discussion on part 2

The results of the simulation for the data taken from Wang (2001) were presented in Figures 3.2.2-A and 3.2.2-B. Figure 3.2.2-A shows the residual fraction of NPDOC at the conditions examined while Figure 3.2.2-B shows the residual fraction of hydrogen peroxide. It can be seen that, for the case where no bicarbonate/carbonate was present, the model describes the residual fraction of NPDOC well. On the other hand, the model approaches the experimental data for the residual fraction of hydrogen peroxide for time greater than 3000 seconds. This might be related to some error in the measurement of hydrogen peroxide concentration. It should be noted that in Chapter 2 the model simulations for other experimental data from the same work [Wang, 2001] showed a difference between model simulations and experimental data for hydrogen peroxide concentration vs. time.

The model simulations in Figures 3.2.2.A and 3.2.2.B show a slight retardation of the residual fraction of NPDOC effect of increasing bicarbonate and carbonate concentration from 1.25 mM to 2.5 mM. The same behavior was observed for the residual fraction of hydrogen peroxide. On the other hand, the experimental data show a retardation effect on the degradation of NPDOC and an acceleration effect on the degradation of hydrogen peroxide. The difference between kinetic model and experimental data might due to some errors in the experimental measurement of either NPDOC, $H_2O_2$, or in the initial carbonate alkalinity in the system as discussed in Section 4.1 of this chapter.

In Section 3.1 the initial concentration of hydrogen peroxide was 0.00147 M and the initial concentration of humic acid was 5 mg $L^{-1}$. In this section, the concentration of hydrogen peroxide was 0.0297 M and the concentration of HA was 6 mg $L^{-1}$. Hence, the hydrogen peroxide concentration in this section to the one in section 20 times that in Section 3.1 while concentration of HA is comparable. Also, the concentrations of used bicarbonate and bicarbonate in this section (1.25 and 2.5 mM) were close to the low concentrations of bicarbonate and carbonate that were used in section 3.1. Therefore, it is expected with such low level of carbonate and high hydrogen peroxide concentration that the system will be insensitive to the presence of carbonate and bicarbonate.

The model results were consistent with this expectation; however, the experimental data were not. Crittenden (1999) found that increasing the total carbonate concentration decreased the oxidation of the organic compound significantly, while it had little effect on the consumption of $H_2O_2$. His findings were observed at $1 \times 10^{-3}$ M of $H_2O_2$ with the organic compound that has a lower absorbance of UV light than hydrogen

peroxide. Therefore, the contribution of the organic compound to the total absorbance will be negligible taking into consideration also its lower concentration than hydrogen peroxide (in the order of $10^{-6}$ M). Therefore, even if the organic compound degradation was retarded the fraction of UV light absorbed by $H_2O_2$ might not be significantly affected. Also, the carbonate concentration was within the same order of magnitude as hydrogen peroxide (0.1, 1, 2, and 4 M). This is similar to the work done in section 3.1 where concentrations of hydrogen peroxide and carbonate/bicarbonate were comparable and therefore the oxidation process was sensitive to the presence of carbonate/bicarbonate.

Beltran (1996a) found that carbonate/bicarbonate didn't retard the oxidation of fluorine and other polynuclear aromatic hydrocarbons (PAHs) using $UV/H_2O_2$ process, although the bicarbonate concentration was increased from $10^{-3}$ M to $10^{-2}$ M starting with $10^{-3}$ M of $H_2O_2$ and 4.7 x $10^{-6}$ M of fluorine. Beltran gave explanations for this but the expectation is that this is due to the high rate constants for the reaction between PAHs and hydroxyl radicals (8.8-13.4 x $10^9$ M s$^{-1}$) compared to the ones for the reactions between carbonate and bicarbonate (Table 2.1). Therefore, most of the time hydroxyl radicals will be consumed by PAHs.

In order to analyze the results in this section in more detail, the following figures were obtained from the model simulation. Figure 4.2.1 shows that the rate of degradation of hydrogen peroxide by reaction with carbonate radicals is much lower than its rate of degradation by either direct photolysis or reaction with hydroxyl radicals. In Section 3.1 the degradation of hydrogen peroxide by carbonate radicals was within the same order of magnitude as that by direct photolysis and reaction with hydroxyl radicals.

348
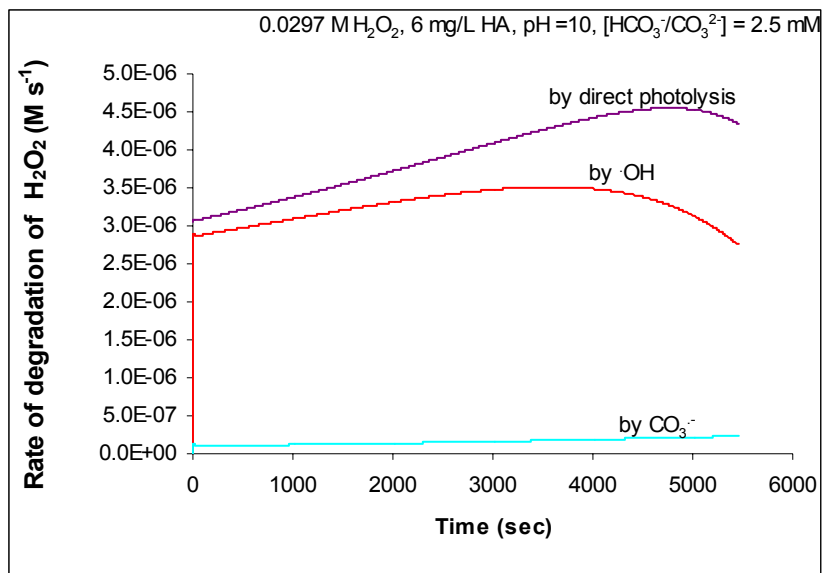
**Fig. 4.2.1:** Predicted rate of degradation of hydrogen peroxide by direct photolysis, $^\bullet OH$ radicals, and $CO_3^{\bullet -}$ vs. time. Initial conditions: $[NPDOC]_o = 5$ mg $L^{-1}$, $[H_2O_2]_o = 0.0297$ M, pH = 10, total carbonate $([HCO_3^-/CO_3^{2-}]_o) = 2.5$ mM
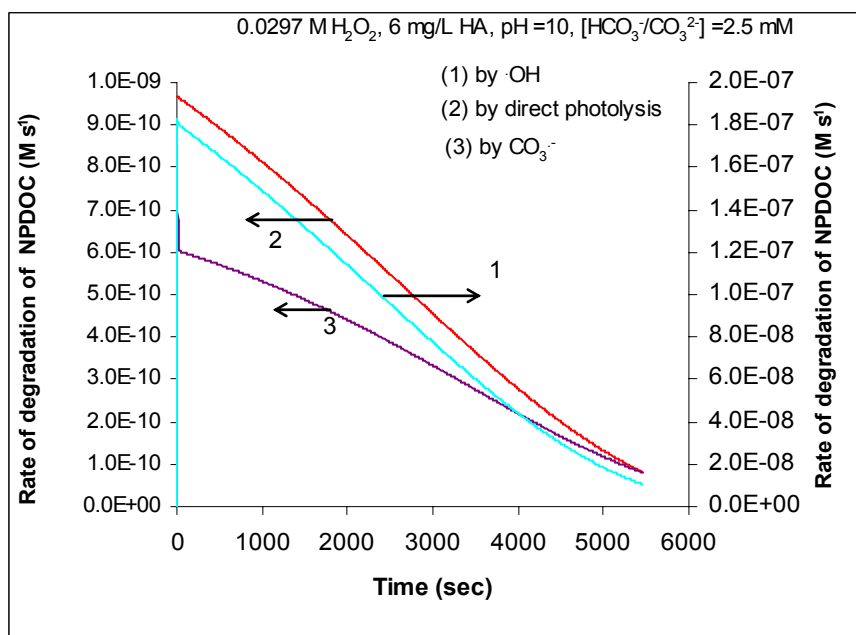


**Fig. 4.2.2:** Predicted rate of degradation of NPDOC by direct photolysis, $^\bullet OH$ radicals, and $CO_3^{\bullet -}$ vs. time. Initial conditions: $[NPDOC]_o = 5$ mg $L^{-1}$, $[H_2O_2] = 0.0297$ M, pH = 10 total carbonate $([HCO_3^-/CO_3^{2-}]_o) = 2.5$ mM

On the other hand, the rate of degradation of NPDOC by reaction with hydroxyl radicals is the dominant route for the degradation (by over two orders of magnitude) compared to its degradation by direct photolysis and reaction with carbonate radicals as can be seen from Figure 4.2.2. The simulations results in Figures 4.2.1 and 4.2.2 explain the reason that the rate of degradation of NPDOC is not affected by the presence of carbonate/bicarbonate for the conditions, for the conditions presented in these figures, since it's mainly degraded by hydroxyl radicals. The reason that the rate of photolysis at these conditions is low is due to the high initial hydrogen peroxide concentration that was used. Therefore, most of the UV light will be absorbed by hydrogen peroxide.

The ratios of $^{\bullet}OH$ radicals consumed by hydrogen peroxide and its conjugate base to the $^{\bullet}OH$ radicals consumed by bicarbonate ($HCO_3^-$) and carbonate ($CO_3^{2-}$) ions at the conditions presented in Figure 3.2.2 are shown in Figure 4.2.3. Comparing the ratios to the ratios in Figures 3.1.5 and 3.1.6, it can be seen that a much higher consumption of $^{\bullet}OH$ radicals by $H_2O_2$ compared to carbonate/bicarbonate was taking place for 0.0294 M $H_2O_2$ while the data in Figures 3.1.III and 3.2.IV showed a comparable levels of the consumptions by both carbonate and hydrogen peroxide. This gives evidence that the carbonate/bicarbonate presence is not affecting the oxidation process at this high hydrogen peroxide concentration.

The concentration of hydroxyl radicals is shown in Figure 4.3.4. From this figure it can be seen that the system has excess concentration of these radicals. The reason that these radicals concentration increases with time is that with high initial hydrogen peroxide concentration, the produced hydroxyl radicals will be sufficient to lead to fast removal of NPDOC , as was seen in Figure 3.2.2.A. Once NPDOC is removed more of

these radicals will be accumulated in the system. The part of the chemistry which is important is the part where NPDOC is present in the system. After the removal of NPDOC, he concentration of hydroxyl radicals will increase up to a maximum value after which their concentration will decrease with time because of all of the series reactions that consume these radicals from the system at the same time where concentration of the source (hydrogen peroxide has decreased). Also, there is a slight decrease in hydroxyl radicals' concentration as bicarbonate/carbonate initial concentration was increased.
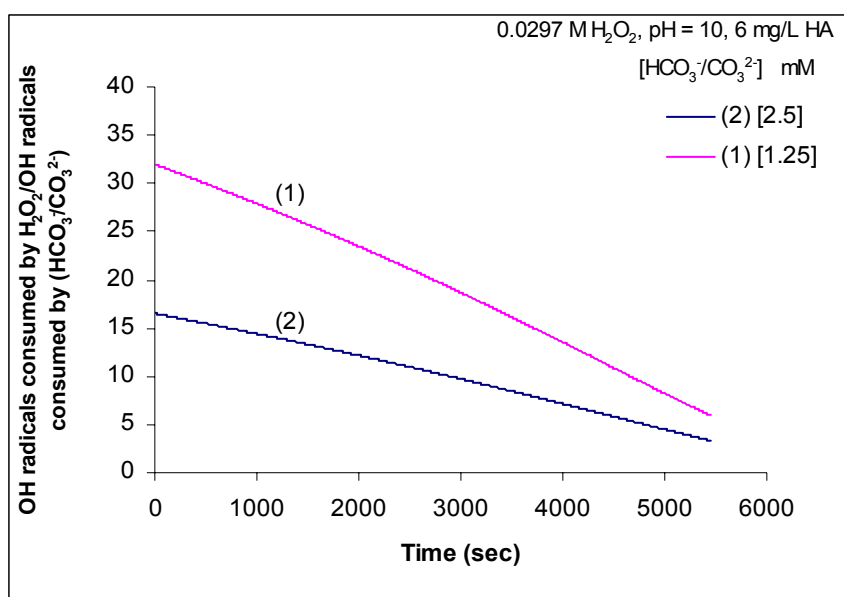


**Fig. 4.2.3:** Predicted ratio of $^{\bullet}OH$ radical consumption by hydrogen peroxide to its consumption by ($HCO_3^- / CO_3^{2-}$) vs. different initial total carbonate ([$HCO_3^- / CO_3^{2-}$]) concentrations. Initial conditions: [NPDOC]$_o$ = 6 mg L$^{-1}$, [H$_2$O$_2$]$_o$ = 0.0294 M, pH = 10
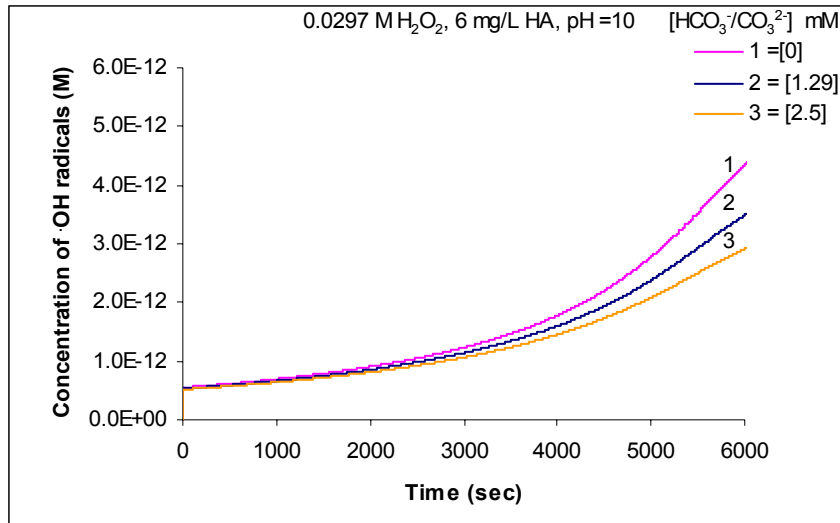
**Fig. 4.2.4:** Predicted concentration of $^\bullet OH$ radical vs. different initial total carbonate ($[HCO_3^-/CO_3^{2-}]$) concentrations. Initial conditions: $[NPDOC]_o = 6$ mg L$^{-1}$, $[H_2O_2]_o = 0.0294$ M, pH = 10

In the introduction of this chapter it was noted that researchers found different effects of bicarbonate/carbonate on the oxidation process using AOPs. It seems that the effect of bicarbonate/carbonate is a function of the concentration of $H_2O_2$, the concentration of the target organic compound, the absorbance of the target compound, the speed of the reaction between the target compound and hydroxyl radicals, and if there is a possible reaction between the organic compound and carbonate radicals. This is the reason the researchers found different effects of carbonate/bicarbonate. Therefore, if an organic compound is reacting with hydroxyl radicals with a comparable rate constant to that for the reaction of carbonate/bicarbonate with these radicals then the carbonate/bicarbonate will compete with the organic compound for these radicals. This will slow down its degradation, especially if its degradation by direct photolysis is negligible. If this compound has high UV absorbance compared to hydrogen peroxide and its conjugate base, then the higher concentration of the organic compound will lead to lower fraction of UV light absorbed by hydrogen peroxide. This will show a retardation effect on degradation of hydrogen peroxide. On the other hand, if absorbance

352

of UV light by the organic compound is negligible then fraction of UV light absorbed by hydrogen peroxide will not be affected.

For the system studied NPDOC is an effective UV absorber, therefore if retardation of its degradation is taking place, then the fraction of UV light absorbed by hydrogen peroxide will be reduced and this would also lead to retardation in the degradation of hydrogen peroxide.

The common factor between all of the studies on systems that contain bicarbonate/carbonate is that scavenging of hydroxyl radicals by carbonate/bicarbonate takes place and carbonate radicals are produced which will in turn react with hydrogen peroxide. Whether the organic compound degradation will be retarded, unaffected, or accelerated is then dependent on each system's components and initial conditions.

## 5. Conclusions

The kinetic model was able to describe the trend of the experimental data taken from Wang's work (2000). The model simulations, along with the experimental data [Wang, 2000] showed a retardation effect due to the presence of bicarbonate and carbonate on the rate of degradation of nonpurgeable dissolved organic carbon (NPDOC). This effect was mainly attributed to the scavenging of the hydroxyl radicals by carbonate and bicarbonate. Also at these conditions, carbonate radicals that were produced from reaction of carbonate and bicarbonate ions with hydrogen peroxide, were contributing to the rate of NPDOC degradation by reacting with humic acid. The reactions of carbonate radicals were considerable for the degradation of hydrogen peroxide also. Based on the previous analysis it can be seen at the studied system conditions (hydrogen peroxide

concentration, HA concentration, carbonate/bicarbonate concentration, and pH) that the system is sensitive to the presence of total carbonate in the system.

Based on theoretical analysis of the kinetic model it was found that reactions of bicarbonate and carbonate, which were included in this model, are important and should be included in the kinetic model since it is not obvious before analysis of experimental data which ones are important and which can be neglected. Therefore, people working with such kind of systems where carbonate/bicarbonate is present should include all of the available reactions. This would also indicate that during treatment processes if $UV/H_2O_2$ would be applied then the presence of bicarbonate/carbonate will affect the process. Based on this model, their presence will scavenge hydroxyl radicals and produce carbonate radicals. These radicals will also contribute to the degradation of NPDOC.

The kinetic simulation for the data reported in another Wang's work (2001) showed a negligible effect due to carbonate and bicarbonate presence at the high concentration of hydrogen peroxide concentration. The experimental results were showing a retardation effect on the degradation of NPDOC which was explained well by this model.

# 6. References

Acero, J. L.; and Urs, V. G. "Influence of Carbonate on The Ozone/Hydrogen Peroxide Based Advanced Oxidation Process for Drinking Water Treatment." *Ozone: Science & Engineering* **22**(3), 305-328 (2000)

Aguer, J. P.;Richard, C.; Andreux, F. "Effect of light on humic substances: Production of reactive species." *Analusis*, 27(5) 387-90 (1999)

Aguer J.P. *et al*. " Photoinductive Properties of Soil Humic Acids and their Fractions by Tandem Size Exclusion Chromatography-polyacrylamide Gel Electrophoresis." *Chemosphere* **44,** 205-209 (2001)

Aguer, J. P.; Richard, C.;Trubetskaya, O.; Trubetskoj, O.; Leveque, J., Andreux, F. " Photoinductive efficiency of Soil Extracted Humic and Fulvic Acids." *Chemosphere* **49,** 259-262 (2002)

Alaton, I. A; Anja, A. K.; and Jekel, M. R. "Ozonation of Spent Reactive Dye-Baths: Effect of $HCO_3^-/CO_3^{2-}$ Alkalinity" *Journal of Environmental Engineering* 689-696 (2002)

Amiri, A.S. "$O_3$/UV Treatment of Methyl-tert-Butyl Ether (MTBE) in contaminated Waters." *Wat. Res*. **33** (15), 3706-3714 (2001)

AWWA (American Water Works Association). Effect of Bicarbonate Alkalinity on Performance of Advanced Oxidation Process. Publisher: (American Water Works Association), USA (1998)

Baxendale, J.H. and Wilson, J. A., "The Photolysis of Hydrogen Peroxide at High Light Intensities." *Trans. Faraday Soc*. 53, 344-356 (1957)

Behar, D.; Czapski, G.; Duchovny, I. "Carbonate Radical in Flash Photolysis and Pulse Radiolysis of Aqueous Carbonate Solutions." *The Journal of Physical Chemistry* **74** (10), 2206-2210 (1970)

Beltran, F.J; Ovejero, G.; Rivas, J. "Oxidation of Polynuclear Aromatic Hydrocarbons in Water. 3 UV Radiation Combined with Hydrogen Peroxide." *Ind. Eng. Chem. Res*. **35**, 883-890 (1996a)

Beltran, F. J., Gonzalez, M., Rivas, F.J. and Alvarez, P. "Aqueous UV radiation and UV/$TiO_2$ oxidation of atrazine first degradation products: Deethylatrazine and deisopropylatrazine." *Environ. Toxicol. Chem.* **15**, 868–872 (1996b)

Bielski, Benon H. J.; and Allen, Augustine O. Mechanism of the Disproportionation of Superoxide Radicals. *Journal of Physical Chemistry* **81**(11), 1048-50 (1977)

Bielski, Benon H. J.; Cabelli, D. E.; Arudi, R. L.; Ross, A. B. "Reactivity of perhydroxyl/superoxide radicals in aqueous solution." *J. Phys. Chem. Ref. Data* **14** (4), 1041-100 (1985)

Benitez, F. J.; Beltran-Heredia, J.; Acero, J. L.; Rubio, F. J. "Contribution of Free Radicals to Chlorophenols Decomposition by Several Advanced Oxidation Processes." *Chemosphere* 41(8), 1271-7, (2000)

Brezonik, P. L. and Fulkerson-Brekken, J. " Nitrate-Induced Photolysis in Natural Waters: Control on Concentration of Hydroxyl Radical Photo-Intermediates by Natural Scavenging Agents." *Env. Sci. Technol*. **32**, 3004-3010 (1998)

Buxton, G. V.; Greenstock, C.L; Helman, W.P.; Ross, A.B. "Critical Rreview of Rate Constants for Reactions of Hydrated Electrons, Hydrogen Atoms and Hydroxyl Radicals ($^\bullet OH / O^{\bullet -}$) in Aqueous Solution." *J. Phys. Chem. Ref. Data* **17**, 513-886 (1988)

Chen, S. N.; and Holfman, M. Z. "Effect of pH on the reactivity of the carbonate radicals in aqueous solutions." *Radiat. Res*. **62**, 18-27 (1975)


Christensen, H.; Sehested, K.; Corfitzen, H. "Reactions of Hydroxyl Radicals with Hydrogen Peroxide at Ambient and ElevatedTemperatures." *J. Phys. Chem. 86*, 1588-1590 (1982)

Christensen, H.; Sehested, K.; Bjergbakke, E. "Radiolysis of reactor water: reaction of hydroxyl radicals with superoxide ($O^{2-}$)." *Water Chemistry of Nuclear Reactor Systems,* **5**(1), 141-144 (1989)

Cooper,W. J., Zika, R. G., Petasne, R.G., Fischer, A.M., 1989. "Sunlight-induced photochemistry of humic substances in natural waters: major reactive species." In: Suffet, I.H., MacCarthy, P.(Eds.), Aquatic Humic Substances: Influence on Fate and Treatment of Pollutants. American Chemical Society, Washington, DC (Chapter22)

Chu, W. and Kwan, C. Y. " Amphoteric Effect of Humic Acids in Surfactant-Aided Photolysis of Polychlorobiphenyls." *Journal of Environmental Engineering* **129** (8), 716-722 (2003)

Crittenden, J.C; Hu, S.; Hand, D. W.; Green , A.S. " A kinetic Model For $H_2O_2$/UV process in a completely mixed batch reactor." *Wat. Res*. **33**, 2315-2328 (1999)

Daniton, F. S.; Rowbotton, J. "Primary Radical Yield in Water. Comparison of the Photolysis and Radiolysis of Solutions of Hydrogen Peroxide*." Transactions of The Faraday Society*. **49**, 1160-1173 (1953)

Daniton, F. S. "The primary Quantum Yield in the Photolysis of Hydrogen Peroxide at 3130 $\overset{\circ}{A}$ and the Primary Radical Yield in the X- and $\gamma$-Radiolysis of Water." *J. Phys. Chem.* 1278 (1955)

Dean (Ed) J. A., Lange's Handbook of Chemistry, McGraw-Hill, New York, 1979

De Laat, J. and Dore. M. "Degradation of Chloroethanes in Dilute Aqueous Solutions by $H_2O_2$/UV." *Wat. Res*. **28**(12), 2507-2519 (1994)

De Laat, J.; Berger, P.; Poinot, T.; Leitner, N. K.; Dore. M. "Modeling the Oxidation of Atrazine by $H_2O_2$/UV. Estimation of Kinetic Parameters." *Ozone Science and Engineering* **19**, 395-408 (1997)

Draganic, Z. D.; Negron-Mendoza, A,; Sehested, K.; Vujosevic, S. I. "Radiolysis of Aqueous Solutions of Ammonium Bicarbonate over a Large Dose Range." *Radiat. Phys. Chem.* **38**, 317-321 (1991)

Eriksen, T. E.; Lind, J.; Merenyi, G. "On the Acid-Base Equilibrium of the Carbonate Radical." *Radiat. Phys. Chem*. **26**, 197-199 (1985)

Fischer, A. M.; Winterle, J. S.; Mill, T. Primary Photochemical Processes in Photolysis Mediated by Humic Substances. ACS Symposium Series (1987), 327 (Photochem. Environ. Aquat. Syst.) 141-56

Gallard, H.; DeLaat, J.; Legube, B. " Effect of pH on the Oxidation of Organic Compound by Fe(III)/$H_2O_2$. Mechanisms and simulation." *New J. Chem*. 263-268 (1998)

Gallard, H.; DeLaat, J. " Kinetic Modeling of Fe(III)/$H_2O_2$ Oxidation Reactions in Dilute Aqueous Solution Using Atrazine as a Model Organic Compound." *Wat. Res*. **34**, 3107-3116 (2000)

Glaze, W.H.; Kang, J. W. " Advanced oxidation Processes: Description of a Kinetic Model for the Oxidation of Hazardous Materials in Aqueous Medial with Ozone and Hydrogen Peroxide in a Semibatch Reactor." *Ind. Eng. Chem. Res*. **28**, 1573-1580 (1989a)

Glaze, W.H.; Kang, J. W. "Advanced oxidation Processes: Test of a Kinetic Model for the Oxidation of Organic Compounds with Ozone and Hydrogen Peroxide in a Semibatch Reactor." Ind. Eng. Chem. Res. 28 (11), 1580-1587 (1989b)

Glaze, W. H.; Lay,Y.; Kang, J. " Advanced Oxidation Processes . A Kinetic Model for the oxidation of 1,2-Dibromo-3-chloropropane in Water by the Combination of Hydrogen Peroxide and UV Radiation." *Ind. Eng. Chem. Res*. **34**, 2314-2323 (1995)

Goldstone, J. V.; Pullin, M. J.; Bertilsson, S.; Voelker, B. M. "Reactions of hydroxyl radical with humic substances: Bleaching, Mineralization, and Production of Bioavailable Carbon Substrates." *Environ. Sci. Technol*. **36**, 364-372 (2002)

Guittonneau, S.; De Latt, J.; Duguet, J. P., Bonnel, C., Dore, M., " Oxidation of Parachloronitrobenzene in   Dilute  Aqueous  Solution  by  $O_3$+UV  and  $H_2O_2$:  A comparative Study." *Ozone Science and Engineering* **12**, 73-94 (1990)

Hideo, I. "Effects of several endogenous and exogenous compounds on the free radical formation." *Geka to Taisha, Eiyo*  **32**(6), 327-334, (1998)

Hoigne, J. and Bader, H. "Ozonation of Water: Kinetics of Oxidation of Ammonia by Ozone and Hydroxyl Radicals." *Environ. Sci. & Technol*.  **12** (1), 79-84 (1978)

Hoigne, J. and Bader, H. "Decomposition of Ozone in Water: Rate of Initiation by Hydroxide Ions and Hydrogen Peroxide." *Environ. Sci. & Technol*.  **16**, 676-681 (1982)

Hou, W.; Tsuneda, S.; Hirata, A. "TOC Removal of Raw Industrial Waste Water from LSI Pjoto-resist Processing with $H_2O_2$/UV in a batch reactor." *J. Chem. Eng. Japan* **34**, 444-447 (2001)

Hug, S. and Leupin, O., "Iron-Catalyzed Oxidation of Arsenic (III) by Oxygen and by Hydrogen Peroxide: pH-Dependent Formation of Oxidants in the Fenton Reaction." *Environ. Sci. Technol*. **37**, 2734-2742 (2003)

Huie, R. E.  and Clifton C. L. "Temperature Dependence of the Rate Constants for Reactions of the Sulfate Radical, $SO_4^-$, with Anions." *J. Phys. Chem*. **94**, 8561-8567 (1990)

Hunt, J. P. and Taube, H. "The Photochemical Decomposition of Hydrogen Peroxide. Quantum Yields, Tracer and Fractionation Effects." *J. Am. Chem. Soc*. **5**, 5999 (1952)

Kang, J. W and Lee, K. H. "A Kinetic Model Of  The $H_2O_2$/UV Process for The Treatment of Hazardous Waster Chemicals." *Environ. Eng. Sci*. **14**(3), 183-192 (1997)

Kim, S.; Kramer, R.W.; Hatcher, P. G. "Graphical Method for Ananlysis of Ultrahigh-Resolution Broadband Mass Spectra of Natural Organic Matter, the Van Krevelen Diagarm." *Anal. Chem*. **75**, 5336-5344, (2003)

King, D. W.; Farlow, R. "Role of carbonate speciation on the oxidation of Fe(II) by $H_2O_2$." *Marine Chemistry* **70**,201–209 (2000)

Koppenol, W. H.; Bulter, J.; Van Leeuwen, J. W. L. "The Haber-Weiss Cycle." *Photochem. Photobiol*. **28**, 655-660 (1978)

Liao, C-H.; Gurol, M.D." Chemical Oxidation by Photolytic Decomposition of Hydrogen Peroxide**.**" *Environ. Sci. Technol.* **29,** 3007 – 3014 (1995)

Lyderson, E. " Humus and acidification." Advances in Chemistry Series 133 (1989), (Ecological Studies: Analysis and Synthesis) Hessen, D.O and Tranvik, L.J editors, Springer

Mak, F.T.; Zele, S. R.; Cooper, W. J.; Kurucz, C. N.; Waite, T. D., Nickelsen, M. G. " Kinetic Modeling of Carbon Tetrachloride, Chloroform and Methylene Chloride Removal from Aquoeous Solution Using the Electron Beam Process." *Wat. Res.* **31**(2), 219-228 (1997)

McKnight, D.M. and Aiken, G.R. "Sources and Age of Aquatic humus." Advances in Chemistry Series 133 (1989), (Ecological studies: Analysis and Synthesis) Hessen, D.O and Tranvik, L.J editors, Springer

Michael, A. B. and Inez, H.. "Enhanced sonochemical decomposition of 1,4-dioxane by ferrous iron.**"** *Wat. Res.* **37** (10), 2372-2376 (2003)

Morgan, M.S.; Trieste, P.V.; Garlick, M. S.; Mahon, M.J; Smith, A. L. " Ultraviolet Molar Absortivity of Aqueous Hydrogen Peroxide and Hydroperoxyl Ion." *Analytical Chimica Acta*, **215**, 325-329 (1988)

Nowell, L. H. and Hoigne, I. "Photolysis of Aqueous Chlorine at Sunlight and Ultraviolet Wavelengths—II. Hydroxyl Radical Production" *WaT. Res.* **26**(5), 599-605 (1992)

Pagsberg, P.; Christensen, H.; Rabani, J.; Nilsson, G.; Fenger, J.; Nielsen, S. O. "Far-Ultraviolet Spectra of Hydrogen and Hydroxyl Radicals from Pulse Radiolysis of Aqueous Solutions. Direct measurement of the rate of H + H." *J. Phys. Chem.* (**73**(4), 1029-38 (1969)

Peyton, G. R. and Glaze, W., H. "Destruction of Pollutants in Water with Ozone in Combination with Ultraviolet Radiation. 3. Photolysis of Aqueous Ozone." *Environ. Sci. Technol.* **22**, 761-767 (1988)

Power, Joan F.; Sharma, Devendra K.; Langford, Cooper H.; Bonneau, Roland; Joussot-Dubien, Jacques. "Laser flash photolytic studies of a well-characterized soil humic substance.**"** ACS Symposium Series (1987), 327(Photochem. Environ. Aquat. Syst.), 157-73

Santiago, E; Jaime, G.; Sandra, C.; Esther, P.; Miguel, R. "Comparison of Different Advanced Oxidation Processes for Phenol Degradation.**"** *Wat. Res.* 36 (4), 1034-1042 (2002)

Sehested, K.; Rasmussen, O. L.; Fricke, H. "Rate Constants of $^\bullet OH$ with $HO_2$, $O_2^-$, and $H_2O_2^+$ from Hydrogen Peroxide Formation in Pulse-Irradiated Oxygenated Water." *J. of Phys. Chem.* **72**(2), 626-31(1968)

Sharpless, C. M. and Linden, K. " UV Photolysis of Nitrate: Effects of Natural Matter and Dissolved Inorganic Carbon and Implications for UV Water Disinfection." *Environ. Sci. Technol.* **35**, 2949-2955 (2001)

Snoeyink, V. L. and Jenkins, D. Water Chemistry. John Wiley & Sons, 1980, New York USA

Staehelln, J. and Hoigne, J. "Decomposition of Ozone in Water: Rate of Initiation by Hydroxide Ions and Hydrogen Peroxide." *Environ. Scl. Technol.* **16**, 676-681 (1982)

Stepnowski, O.; Siedlecka, E. M.; Behrend, P.; Jastroff, B. "Enhanced Photo-degradation of Contaminants in Petroleum Refinery Wastewater." *Wat. Res.* **36**, 2167-2172 (2002)

Stumm, W. and Morgan, J.J. Aquatic Chemistry, Prentice-Hall, Englewood NJ, (1996)

Thomas, J. K. "Rates of Reaction of the Hydroxyl Radical." *Transactions of the Faraday Society* **61** (508), 702-7 (1965)

Thomas-Smith, T.E.; Blough, N.V. "Photoproduction of Solvated Electron From Constituents of Natural Waters. " *Environ. Sci. Technol.* **35**, 2721-2726 (2001)

Vollman, D.H.; Chen, J.C., "The Photochemical Decomposition of Hydrogen Peroxide in Aqueous Solutions of Allyl Alcohol at 2537 $\overset{\circ}{A}$ ." *J. Am. Chem. Soc.* **20**, 4141 (1959)

Wang, G.-S.; Hsieh, S.-T.; Hong, C.-S. "Destruction of Humic Acid in Water by UV Light-catalyzed Oxidation with Hydrogen Peroxide." *Wat. Res.* **34**(15), 3882-3887 (2000)

Wang, Gen-Shuh; Liao, Chih-Hsiang; Wu, Fang-Jui. "Photodegradation of Humic Acids in the Presence of Hydrogen Peroxide." *Chemosphere* **42**(4), 379-387 (2001)

Weeks, J. L.; Matheson, M. S., "The Primary Quantum Yield of Hydrogen Peroxide Decomposition." *J. Phys. Chem.* 1273 (1955)

Weeks J. L. and Rabani, R. "The Pulse Radiolysis of Deaerated Aqueous Carbonate Solutions. I. Transient Optical Spectrum and Mechanism. II. pK for $^\bullet OH$ Radicals." *The Journal of Physical Chemistry* **70** (7), 2100-2106 (1966)

Weinstein, J. and Bielski, H. J. "Kinetics of the Interaction of $HO_2$ and $O_2^-$ Radicals with Hydrogen Peroxide. The Haber-Weiss Reaction." *J. Am. Chem. Soc.* **3**, 58-62 (1979)

Westerhoff, P.; Aiken, G.; Amy, G.; Debroux, J. " Relationships Between the Structure of Natural Organic Matter and its Reactivity Towards Molecular Ozone and Hydroxyl Radicals." *Wat. Res*. **33**, 2265-2276(1999)

Westerhoff, P.; Song, R.; Minear, R. " Applications of Ozone Models." Ozone: *Science and Engineering* **19**, 55-73 (1997)

Zepp, R. G.; Schiotzhauer, P.F.; Slnk, R. M. "Photosensitized Transformations Involving Electronic Energy Transfer in Natural Waters: Role of Humic Substances." Environ. Sci. Technol. 19, 74-81 (1985)

Zepp, Richard G.; Braun, Andre M.; Hoigne, Juerg; Leenheer, Jerry A. "Photoproduction of hydrated electrons from natural organic solutes in aquatic environments." *Environmental Science and Technology* , **21**(5), 485-90 (1987a),

Zepp, R.G.; Hoigne, J.; Bader, H. :Nitrate-Induced Photooxidation of Trace Organic Chemicals in Water." Environ. Sci. Technol. **21**, 443-450 (1987b)

# Chapter 4

## A Kinetic Model for the Degradation of Methyl tert-Butyl Ether (MTBE) in Aqueous Solution by Fenton's Reagent  (Fe$^{II}$/ H$_2$O$_2$) and Fenton-Like Reagent (Fe$^{o}$/ H$_2$O$_2$)

## Abstract

A kinetic model for the degradation of methyl tert-butyl ether (MTBE) in batch reactors applying Fenton's reagent (Fe$^{II}$/ H$_2$O$_2$) and Fenton-like reagent (Fe$^{o}$/ H$_2$O$_2$) in aqueous solutions was proposed. This kinetic model consisted of three major parts: hydrogen peroxide chemistry in aqueous solution, iron speciation, and MTBE oxidation. Hydrogen peroxide chemistry in aqueous solution is well documented and therefore all of the rate and equilibrium constants for this chemistry were taken from the literature. The iron chemistry consisted of many of the reactions of ferrous and ferric iron in aqueous systems containing hydrogen peroxide. Rate and equilibrium constants for ferric and ferrous iron reactions in this model were taken from the reported values in the literature except for the rate constant for the reaction of ferric iron with hydrogen peroxide where it was fitted within the range that was reported in the literature. The rate constant for iron dissolution was also a fitted parameter and it was a function of the solution acidity. The mechanism of MTBE degradation by the hydroxyl radicals, which were formed from ferrous iron and hydrogen peroxide reactions, the pathways for the formation of the byproducts that follow MTBE oxidation, and the degradation of these byproducts was proposed based on  studies performed by Stefan (2000), Wu (2002), and Cooper (2004). Most of the rate constants regarding the MTBE degradation mechanism were taken from the literature.  Proportions of reactions that proceeded in different routes, other than

hydrogen abstraction from MTBE which was taken from the literature, were optimized based on the best fit of the model parameters to the experimental data.

The proposed model was tested on available experimental data from the literature which involved the use of Fenton's reagent [Xu, 2004] and Fenton-like reagent [Bergendahl, 2004] for MTBE degradation. The set of ordinary nonlinear stiff differential equations that described rate of reaction of each species in this system was solved using Matlab (R13) software.

The degradation of MTBE in Xu's work was characterized to proceed by two stages, a fast one which involved the reaction of ferrous iron with hydrogen peroxide ($Fe^{II}/H_2O_2$ stage) and another, relatively, slower stage which involved the reaction of ferric iron with hydrogen peroxide ($Fe^{III}/H_2O_2$ stage). The experimental data of MTBE degradation in the $Fe^{II}/H_2O_2$ stage were not enough to validate the model; however the model predictions of MTBE degradation in the $Fe^{III}/H_2O_2$ stage were good. Also, the model was able to well predict the byproducts formation and degradation especially methyl acetate (MA), and tert-butyl alcohol (TBA).

A sensitivity analysis, which was based on calculating the sum of the squares of the residual (SSR) after making a perturbation in one rate constant at a time, was applied for MTBE degradation by Fenton's reagent at one set of conditions. The effect of each proposed reaction on MTBE degradation and the byproducts formation and degradation was elucidated based on this analysis.

The kinetic model was able to predict the experimental degradation of MTBE for the case where Fenton-like reagent was applied. However, for the only reported

byproduct in this study [Bergendahl, 2004], the model predictions were different from the experimental results.

## 1. Introduction

Methyl tert-butyl ether (MTBE) was used as a gasoline additive to enhance the octane number, as a replacement for alkyl lead compounds, and as a fuel oxygenate to improve air quality by reducing the level of carbon monoxide in vehicle exhausts [Squillace, 1996; Stephan, 2000, Wu, 2002, Mezyk, 2001]. The initial concern for MTBE was its occurrence in the air from vehicle exhausts [Cooper, 2002]. Growing concern took place due to its occurrence in ground water. Recently MTBE was found in ground waters and surface waters at many locations [Chang, 2000]. The source of MTBE in ground water might be from leaking underground fuel tanks and leaking pipes, tank overfilling and faulty construction at gas stations, spillage from vehicle accidents and homeowner releases [Johnson, 2000; Wagler, 1994] and transport from the gas phase [Pankow, 1997]. In the United States alone releases of gasoline containing MTBE may have occured at more than 250,000 sites, potentially threatening over 9000 municipal water supply wells [O'Shea, 2002a].

Despite some benefits of using MTBE as a fuel additive, several concerns have been raised about its impact on human health [Stefan, 2000, Cooper, 2003]. EPA tentatively classified MTBE as a possible human carcinogen and issued a draft lifetime health advisory limit of 20-40 $\mu g/L$ for drinking water [Stefan, 2000; Squilace; 1996 Hardisaon 2002]. MTBE has high solubility in water (51 g/L) [Cooper, 2002; Wagler, 1994; Squillace, 1996; Pankow, 1997]. Therefore, it will be very mobile in water and may persist in groundwater. Therefore, the current MTBE contamination problems will

exist for many years if not treated [O'Shea, 2002a]. MTBE presence in ground water poses a potential health problem [Cooper, 2002; Stephan, 2000].

The remediation of MTBE and other oxygenate-contaminated drinking water still remains a pressing environmental problem. Potential remediation technologies for ground water have been reviewed. These reviews have shown that MTBE has a low Henry's law constant and therefore is not amenable for air stripping as most volatile contaminants [Mezyk, 2001; Robbins, 1993]. Bioremediation of MTBE is difficult to apply at large volumes of waters that have $\mu g/L$-mg/L of MTBE since its biodegradation is very slow [Cooper, 2002; Sulfita, 1993; Mezyk, 2001]. Adsorption of MTBE to granular activated carbon (GAC) is effective for the low concentration range (1-100 $\mu g/L$) [Stephan, 2000; Cater, 2000; Mezyk, 2001]. However, by using GAC MTBE is just only being transferred from one phase to another [Arenzo, 1999, Speth, 1990].

Therefore, in order to mineralize MTBE and especially over a wide range of concentrations, alternative methods need to be applied. Among these advanced oxidation processes (AOPs) seem to be promising [Stephan, 2000; Bolton, 1998; Cater, 2000; Barreto, 1995, Kang, 1999]. These processes depend on the production of active species especially hydroxyl radicals to degrade the contaminant of interest. The AOPs include $H_2O_2/UV$, Fenton's process ($H_2O_2/Fe(II)$), Fenton-like process ($H_2O_2/Fe(III)$) and $H_2O_2/Fe^o$), $H_2O_2/O_3$, $O_3$, $TiO_2/UV$, sonolysis, and electron beam. In the latter process solvated electron is present as an active intermediate in addition to the well known hydroxyl radicals.

MTBE degradation by AOPs in aqueous solution has been the focous of several studies. For example the application of ozone, ozone/$H_2O_2$, UV/$H_2O_2$ for the treatment of

dilute MTBE solutions was investigated [Kang, 1998, 1999; Stephan, 2000; Cater, 2000; Wagler, 1994; Chang, 2000; Acero, 2001]. The major identified byproducts were tert-butyl formate (TBF), tert-butyl alcohol (TBA), acetone, methyl acetate, and formaldehyde [Barreto, 1995; Yeh, 1995, Kang, 1998; Stefan, 2000]. The objectives of the previous studies were to investigate the feasibility of the degradation process, identify the byproducts formed, understand the mechanisms and in some cases to evaluate the system kinetic parameters. A pseudo first order rate expression was used to analyze the experimental results.

Barreto (1994) degraded MTBE photocatalytically and found that the degradation rate of MTBE was faster than the direct reaction between MTBE and ozone ($O_3$). Barreto (1994) used pseudo-first order kinetics to analyze MTBE degradation.

Wagler (1994) explored the removal of MTBE from ground water using UV/$H_2O_2$ oxidation. This was the first study that reported the possibility of MTBE degradation using UV/$H_2O_2$ process in aqueous solutions. Removal of MTBE by UV or $H_2O_2$ as single oxidants was not significant. The kinetics of MTBE degradation was fitted to pseudo-first order kinetics. The UV/$H_2O_2$ process produced over 95 % removal of MTBE.

Neppolian (2002) investigated the sonolytic degradation of methyl tert-butyl ether. He found that the rate of degradation of MTBE increased with the increase of the power density of ultrasonicator and also with the rise in reactor system temperature. Also, he found that tert-butyl formate (TBF) and acetone were the major intermediates of the degradation of MTBE. He also found that the ultrasound/$Fe^{2+}$/$H_2O_2$ method was a promising process for the degradation of MTBE and he could achieve good removal of

MTBE along with its intermediate products by applying the coupled ultrasound/Fe$^{2+}$/H$_2$O$_2$ method under the studied conditions. This was due to the high amounts of $^\bullet$OH radical that were produced from Fenton's reaction and from the thermolytic cleavage of water and MTBE as a result of applying ultrasound waves. Formic and acetic acid were considered as the final compounds from MTBE degradation.

Chang (2000) investigated the degradation of methyl tert-butyl ether and byproducts formation applying UV/hydrogen peroxide treatment in a batch flow through reactor. TBF was the major quantified byproduct in this study. He mentioned that other byproducts such as acetone and formaldehyde were probably formed but went undetected because they were not purgable or were too volatile to appear in the analysis results. Tert-butyl alcohol (TBA) was detectable, but was not quantified.

Stefan (2000) studied the degradation of pathways of MTBE by the application of the UV/H$_2$O$_2$ in dilute aqueous solution. In this study all the possible byproducts from MTBE degradation were quantified. The primary byproducts were TBF, TBA, acetone, formaldehyde, and 2-methoxy-2-methyl propioaldehyde (MMP). Other intermediates were also detected and quantified. A good organic carbon balance was obtained indicating that almost all of the byproducts and intermediates were detected. Stefan (2000) proposed a detailed reaction mechanism for the degradation of MTBE by $^\bullet$OH radicals in aerated solutions which accounts for all the observed byproducts and intermediates in his study. Stefan's study provided the first detailed mechanism for MTBE degradation in $^\bullet$OH-driven oxidation processes in aqueous solutions that was validated with total organic carbon balance.

Kang (1998) studied the kinetics and mechanism of the sonolytic destruction of MTBE by ultrasonic irradiation in the presence of ozone. TBF, TBA, methyl acetate (MA), and acetone were the primary products in Kang (1998) study. A reaction mechanism was suggested for this system which involved three parallel pathways that included the direct pyrolytic decomposition of MTBE, the direct reaction of MTBE with ozone, and the reaction of MTBE with hydroxyl radicals. Pseudo-first order kinetic was used by Kang (1998) to analyze the experimental results for MTBE degradation.

The oxidation of MTBE by potassium permanganate was studied by Damm (2002). The rate of MTBE oxidation was 2-3 orders of magnitude lower than of other advanced oxidation processes. Pseudo-first order kinetic was used to simulate the experimental degradation of MTBE.

Wu (2002) used gamma radiolysis for aqueous solutions of MTBE (100 ppm) to study hydroxyl radical mediated reaction pathways. This was the first reported detailed study of Gamma radiolysis of MTBE in aqueous solutions. The major volatile organic compounds produced were TBA, TBF, acetone and methyl acetate. TBF didn't yield TBA under the reaction conditions, but rather acetone as the major product. He couldn't confirm the existence of 2-methyl-2methoxy-propionaldehyde (MMP), which was detected in Stefan's study (2000) and he proposed a reaction pathway, which didn't include MMP, as the predominant path leading to the formation of methyl acetate. Acetone and methyl acetate were formed at significantly lower yield than TBF. TBA was observed during the initial stages of the reaction but TBF was the major product initially, at longer times TBA was the major product.

Cooper (2002a, 2000b) found that the use of the electron beam process was effective for the treatment of water containing MTBE over a wide range of concentrations. TBF and TBA were the major identified byproducts from MTBE degradation in Cooper's study (2000b). MTBE degradation was adversely affected by increasing the carbonate concentration since it was a scavenger of the hydroxyl radicals [Cooper, 2002b]. Cooper (2000a) used a kinetic model to interpret the experimental data. In this model, the byproducts of MTBE $^\bullet$OH -oxidation mediated reactions were TBA, formaldehyde, and formic acid. The comparison of the model prediction to the experimental data was presented in terms of remaining concentration of MTBE at each dose of electron beam process. This model didn't account for TBF and acetone formation and degradation pathways. This model was not used for high concentration of MTBE (22-31 mg L$^{-1}$) since a detailed mechanism was not used (2002a). Model at pH = 8.41 significantly over predicted MTBE removal at all doses and this was attributed to the presence of $^\bullet$OH radicals scavengers that were not considered in the model.

Cooper (2003) studied the destruction of MTBE applying electron beam process using a kinetic model. This model was based on the work of Wu (2002), Hardison (2002), Mak (1997), and other works in which Cooper was involved. A kinetic interpretation was formulated based on the proposed mechanism of MTBE degradation in the previous studies. The formulation was not complete since many of the rate constants and some of the details of the mechanism have not been fully elucidated. This formulation was not provided in this work. In the reported results of this work, results of kinetic model were shown alone without experimental data.

O'Shea (2002a) studied the degradation of MTBE/BTEX mixtures using gamma radiolysis at neutral pH and the results were compared to the kinetic model predictions. The kinetic model contained the full set of water radiolysis reactions and rate constants of the reactions of the generated hydroxyl radicals, hydrated electrons, and hydrogen atoms with MTBE, benzene, toluene, ethyl benzene and para-xylene. The model agreed well with the data but deviation at longer irradiation times was observed. The byproducts formation and degradation pathways were not included in the model. They corrected for this deviation by grouping the degradation products of MTBE/BTEX into a single class of N identical species and using a rate constant for the hydroxyl radical with this species of $5 \times 10\ \text{M}^{-1}\ \text{s}^{-1}$.

TiO$_2$ photocatalysis of MTBE, as one type of AOPs, was evaluated by O'Shea (2002b). Kinetic parameters, and effects of catalyst types and loading on the degradation of MTBE was studied and optimal catalyst loading was suggested for the studied reaction conditions. TBF, TBA, acetone and isobutylene were identified as stable products during the TiO$_2$ photocatalysis of MTBE. In addition to the previous products, O'Shea (2002b) identified methyl acetate, formaldehyde, and methane as reaction products from the TiO$_2$ photocatalysis of MTBE. Also, it was found that MTBE degradation was more complex than simple first order kinetics.

Hardison (2002) investigated the kinetics of degradation of TBF, using radiation chemical techniques to evaluate the rate constants relevant to all AOPs. Based on the obtained rate constants the impact of TBF formation in the electron beam treatment of MTBE contaminated water was estimated. This was performed by a kinetic model for this process. the kinetic model used accounted only for TBF formation and degradation

370

by the hydroxyl radicals, hydrated electrons, and hydrogen atom without considering the other possible byproducts from MTBE degradation.

Cater (2000) investigated the removal of MTBE from contaminated water applying UV/$H_2O_2$ to determine its effectiveness in the treatment of MTBE. The degradation of MTBE was studied applying the pseudo-first order approximation.

The efficiency and the kinetics of the oxidation of MTBE in contaminated water employing $O_3$/$H_2O_2$ was evaluated by Safarzadeh-Amiri (2001). The degradation of MTBE was described by pseudo-first order kinetics in two phases. The first phase covered MTBE concentration greater than 10 mg $L^{-1}$ and the second phase covered MTBE concentration below 10 mg $L^{-1}$. It was found that the $O_3$/$H_2O_2$ process was more efficient than the UV/$H_2O_2$ for the degradation of MTBE.

Although a number of reports have appeared on the degradation of MTBE by AOPs, there is still uncertainty with respect to the hydroxyl mediated degradation pathways and many of the necessary rate constants have not been reported [Stefan, 2000, Barreto, 1995, Kang, 1998, O'Shea, 2002b, Wu, 2002, Copper, 2003]. The differences in the reaction conditions that were used to generate the hydroxyl radicals might be the reason behind the significant uncertainties and/or differences regarding the degradation mechanisms of MTBE by $^\bullet OH$ radicals in the literature, although similar byproducts were observed [Wu, 2002].

Fenton's reagent was discovered about 100 years ago, but its application as an oxidizing process for destroying organic compounds was not applied until the late 1960s [Neyens, 2003]. Fenton's reagent (Fe(II)/$H_2O_2$) and Fenton-like reagent (Fe(III)/$H_2O_2$) have been investigated by several groups in order to study the mechanism and kinetics of

reaction [Harber, 1934; Bary, 1934; Walling, 1973, 1975, 1998; Knight, 1974; Rush, 1985; Evans, 1948a, 1948b; De Laat, 1999, 1998; Gallard, 1999; Ensing, 2002]. In the classic Fenton reaction, a ferrous salt, typically ferrous sulfate is mixed with hydrogen peroxide to produce the hydroxyl radical. Iron in its zero-valent state ($Fe^o$), dissolved ferrous form ($Fe^{II}$), or as ferric ion ($Fe^{III}$) has proven effective in the degradation of contaminants in ground waters, landfill leachate, soil, sediment, and slurries [Arenzo, 2001]. Other studies were conducted to evaluate the effectiveness of Fenton's reagent and Fenton-like reagent for organic destruction [Pignatello, 1992; Gallrad, 2001; Arenzo, 2001; Lindesy, 2000; Safarzadeh-Amiri, 1996; Rivas, 2001; Bergendahl, 2004].

King (2000) investigated the oxidation of $Fe^{II}$ by $H_2O_2$ in the pH range (5-8) in presence and absence of carbonate. They reported that $Fe(CO_3)$ was the most kinetically active iron(II) species for the decomposition of $H_2O_2$ in organic-free water.

De Laat (2004) investigated the effects of chloride, sulfate and nitrate ions on the rates of decomposition of $H_2O_2$ and organic compounds by $Fe^{II}/H_2O_2$ and $Fe^{III}/H_2O_2$ processes. For $Fe^{II}/H_2O_2$ process, it was found that the rates of reaction between $Fe^{II}$ and $H_2O_2$ were in the order sulfate > perchlorate = nitrate= chloride. For $Fe^{III}/H_2O_2$, identical rates were obtained in the presence of nitrate and perchlorate, whereas the presence of sulfate or chloride markedly decreased the rates of decomposition of $H_2O_2$ by $Fe^{III}$. The kinetic model which he used was a more simplified model than the one which he used earlier [De Laat, 1999; Gallard, 2000].

Hug (2003) looked at the oxidation of arsenic (As(III)) applying Fenton's reagent in the pH range 3.5-7.5. He used ferric and ferrous iron with hydrogen peroxide in aqueous solutions. Hug (2003) found that As(III) was not measurably oxidized by $O_2$, 20-

$100 \mu M$ $H_2O_2$, dissolved Fe(III), or iron(III) hydroxides as single oxidants and that As(III) was completely oxidized in solutions of Fenton's reagent (Fe(II)/$H_2O_2$) at the studied conditions. Also, he found that high bicarbonate concentration led to increased concentration of As(III). Hug (2003) applied a kinetic model to describe the destruction of As(III) in this system. His model was based on the known chemistry of ferric and ferrous iron for hydrogen peroxide systems. He suggested that the reaction of $Fe^{II}$ and $H_2O_2$ forms hydroxyl radicals at low pH but a different oxidant at higher pH in order that the model be able to explain the pH dependence.

Esplagus (2002) found that Fenton's reagent was the fastest one of the evaluated advanced oxidation processes for phenol degradation. He used pseudo-first order kinetics for the analysis of the experimental data.

Chen (1997) used dark Fenton's reagent and photoassisted Fenton's reagent to study the degradation of phenol in aqueous systems. The photoassisted Fenton's degradation was faster than the dark one in this study.

Other studies have used the classic Fenton or Fenton-like reaction for removing explosives from water [Arienzo, 1999; Hunda, 1997; Li, 1997, 1998]. Arienzo (1999) studied the possibility for the removal of trinitrotoluene (TNT) applying classical reaction ($H_2O_2$/$Fe^{II}$) and a modified Fenton's reaction in which he used solid pyrite ($FeS_2$). He found that at acidic conditions complete oxidation of TNT with modified Fenton reagent was slower with respect to classic Fenton's reagent (48 h vs. 24 h). However mineralization of TNT with 1.8 mM Fe(II) from pyrite using 0.029 M $H_2O_2$ under dark/light conditions was of the same order of magnitude as with classical Fenton's reagent using a 10 times higher concentration of hydrogen peroxide (0.29 M $H_2O_2$).

Yeh (1995) evaluated the use of Fenton's reagent for the degradation of MTBE in soils. Acetone and TBA were produced as a result of this treatment which indicated that MTBE was chemical oxidized by $Fe^{II}/H_2O_2$ process. This oxidation was influenced by $H_2O_2$ concentration, presence of ferrous iron and the pH.

## 1.2. Objectives and hypothesis

Mathematical modeling can assest in the selection of the most appropriate and cost-effective remediation treatment. Mathematical modeling gives much information and provides a good test of the model against actual engineering data. These kinetics models are dependent on degradation mechanism and availability of rate constant data. Mathematical modeling can be performed at several levels, depending on the known chemistry, available computational resources, and the overall modeling objective [Mezyk, 2001; Crittenden, 1999]

The only group that did considerable modeling of MTBE degradation mediated by hydroxyl radicals was Cooper and his coworker in which electron beam was mainly used for the destruction of MTBE [Cooper, 2002a; Hardison, 2002; Cooper, 2003]. Cooper (2003) was the only work that showed model prediction of TBF, TBA, acetone, and methyl acetate. However in this work no experimental data were shown. The formulation of MTBE degradation was not provided in Cooper's work (2003).

A kinetic model for the degradation of methyl tert-butyl ether (MTBE) in a batch reactor applying Fenton's reagent ($Fe^{II}/ H_2O_2$) and Fenton-like reagent ($Fe^o/ H_2O_2$) in aqueous solutions was proposed in this work. In this model, hydrogen peroxide chemistry, iron chemistry, and MTBE chemistry were included. Hydrogen peroxide chemistry in aqueous solutions is well documented and therefore all of the rate and

equilibrium constants for this chemistry were taken from the literature. The iron chemistry consisted of many of the possible reactions of ferrous and ferric iron in aqueous systems containing hydrogen peroxide. Rate and equilibrium constants for ferric and ferrous iron reactions in this model were taken from the reported values in the literature except for the rate constant for the reaction of ferric iron with hydrogen peroxide where it was fitted within the range that was reported in the literature. Rate constant for iron dissolution was also a fitted parameter and it was a function of the solution acidity. The mechanism of MTBE degradation by hydroxyl radicals, which were formed from ferrous iron and hydrogen peroxide reaction, the path ways for the formation of the byproducts that follow MTBE by these radicals, and the degradation of these byproducts were proposed.

The proposed model was tested on available experimental data from the literature which involved the use of Fenton's reagent [Xu, 2004] and Fenton's like reagent [Bergendahl, 2004] for MTBE degradation. The degradation of MTBE in Xu's work is a recent experimental work and has not been modeled by anyone else. Destruction of MTBE applying Fenton-like reagent has been studied previously by Bergendahl (2004). In Bergendahl's work a simplified model was suggested for MTBE degradation in which ferrous iron were produced from zero valent iron dissolution by hydrogen peroxide. Then ferrous iron reacted with hydrogen peroxide to produce hydroxyl radicals and ferric iron. Ferric iron was suggested to react with hydrogen peroxide to reproduce ferrous iron and hydroperoxyl radicals. The fate of hydroxyl radicals was to react with MTBE and hydrogen peroxide. Degradation pathways of MTBE and the byproducts formation and degradations were not included in Bergendahl model.

A sensitivity analysis, which was based on calculating the sum of the squares of the residual (SSR) after making a perturbation in one rate constant at a time, was applied for MTBE degradation by Fenton's reagent at one set of conditions. The effect of each reaction on MTBE degradation and the byproducts formation and degradation was elucidated based on this analysis.

The proposed kinetic model is a comprehensive model that can be used for MTBE degradation by $Fe^{II}/H_2O_2$, $Fe^o/H_2O_2$, and $Fe^{III}/H_2O_2$ and describes not only MTBE degradations, but also possible pathways for byproducts formation and degradation. This mechanism was derived from a general mechanism of MTBE degradation by hydroxyl radicals in aerated aqueous solutions that was suggested by Stefan (2000), Wu (2002), Cooper (2002), and Cooper (2004). This mechanism was simplified since it did not include all the suggested reaction byproducts and intermediates for the oxidation of MTBE by hydroxyl radicals. Most of the rate constants regarding MTBE mechanism were taken from the literature and when a rate constant for a certain reaction was not available, analogy between this reaction and another reaction that proceeded in a similar way was made. Proportions of one reaction that proceeded in different routes, other than hydrogen abstraction from MTBE which was taken from the literature was optimized based on the best fitting of the model parameters to the experimental data.

## 2. Kinetic Model

**Table 4.1:** The reactions steps involved in the kinetic model for MTBE degradation in aqueous solutions applying Hydrogen peroxide chemistry Fenton's Reagent $(H_2O_2/Fe^{II})$ and Fenton-Like Reagent $(H_2O_2/Fe^o)^*$

$H_2O_2$ Chemistry:

| # | Reaction | Rate Constant | Reference(s) |
|---|----------|---------------|--------------|
| 1 | $^\bullet OH + H_2O_2 \rightarrow H_2O + O_2^{\bullet -} + H^+$ | $k_1 = 2.7 \times 10^7$ M$^{-1}$ s$^{-1}$ | Glaze (1995), Buxton (1988) |
|   | $^\bullet OH + H_2O_2 \rightarrow H_2O + HO_2^\bullet$ | $k_1 = 2.7 \times 10^7$ M$^{-1}$ s$^{-1}$ (used value) | Gallard (2000), Crittenden (1999), Christensen (1982) |
| 2 | $HO_2^\bullet + O_2^{\bullet -} + H_2O \rightarrow H_2O_2 + O_2 + OH^-$ | $k_2 = 9.7 \times 10^7$ M$^{-1}$ s$^{-1}$ (used value) | Gallard (2000) |
|   | $HO_2^\bullet + O_2^{\bullet -} + H_2O \rightarrow H_2O_2 + O_2 + ^\bullet OH$ | $k_2 = 1.02 \times 10^8$ M$^{-1}$ s$^{-1}$ | Weinstein (1979) |
|   | $HO_2^\bullet + O_2^{\bullet -} \rightarrow HO_2^- + O_2$ | $k_2 = 9.7 \times 10^7$ M$^{-1}$ s$^{-1}$ | Glaze (1995) |
|   |  | $k_4 = 9.7 \times 10^7$ M$^{-1}$ s$^{-1}$ | Gallard (1998) |
|   | $HO_2^\bullet + O_2^{\bullet -} \xrightarrow{H^+} H_2O_2 + O_2$ | $k_2 = 9.7 \times 10^7$ M$^{-1}$ s$^{-1}$ | Chen (1997) |
| 3 | $HO_2^\bullet + ^\bullet OH \rightarrow H_2O + O_2$ | $k_3 = 0.71 \times 10^{10}$ M$^{-1}$ s$^{-1}$ (used value) | Buxton (1988) |
|   |  | $k_3 = 6.6 \times 10^9$ M$^{-1}$ s$^{-1}$ | Sehested (1968) |
| 4 | $^\bullet OH + O_2^{\bullet -} \rightarrow O_2 + OH^-$ | $k_4 = 1.01 \times 10^{10}$ M$^{-1}$ s$^{-1}$ (used value) | Gallard (1999) Buxton, 1988 |
|   |  | $k_4 = 1.0 \times 10^{10}$ M$^{-1}$ s$^{-1}$ | Christensen (1989) |
|   |  | $k_4 = 9.4 \times 10^9$ M$^{-1}$ s$^{-1}$ | Sehested (1968) |
| 5 | $^\bullet OH + ^\bullet OH \rightarrow H_2O_2$ | $k_5 = 5.2 \times 10^9$ M$^{-1}$ s$^{-1}$ (used value) | Gallard (1999) |
|   |  | $k_5 = 5.2 \times 10^9$ M$^{-1}$ s$^{-1}$ | Pasberg (1969) |
|   |  | $k_5 = 5.2 \times 10^9$ M$^{-1}$ s$^{-1}$ | Thomas (1965) |
|   |  | $k_5 = 4.2 \times 10^9$ M$^{-1}$ s$^{-1}$ | Buxton (1988) |
| 6 | $HO_2^\bullet + HO_2^\bullet \rightarrow H_2O_2 + O_2$ | $k_6 = 8.3 \times 10^5$ M$^{-1}$ s$^{-1}$ | De Laat (1999) |
|   |  | $k_6 = 8.3 \times 10^5$ M$^{-1}$ s$^{-1}$ | Belski (1985) |
| 7 | $O_2^{\bullet -} + H^+ \rightarrow HO_2^\bullet$ | $k_7 = 1 \times 10^{10}$ M$^{-1}$ s$^{-1}$ (used value) | De Laat (1999) |
|   |  | $k_7 = 5 \times 10^{10}$ M$^{-1}$ s$^{-1}$ | Bielski (1985) |

377

| 8 | $HO_2^{\bullet} \rightarrow O_2^{\bullet -} + H^+$ | $k_8 = 1.58 \times 10^5\ s^{-1}$ (used value) | De Laat (1999) |
|---|---|---|---|
| | | $k_8 = k_7\ K_a$ $pK_a = 4.8$ | Chen (1997) Sehested (1968) Bielski (1977) |
| 9 | $O_2^{\bullet -} + H_2O_2 \rightarrow {}^{\bullet}OH + OH^- + O_2$ | $k_9 = 0.13\ M^{-1}\ s^{-1}$ | Crittenden (1999) Bielski (1979) |
| 10 | $H_2O_2 + HO_2^{\bullet} \rightarrow HO^{\bullet} + O_2 + H_2O$ | $k_{10} = 3\ M^{-1}\ s^{-1}$ | Weinstein (1979) Koppenel (1978) |
| 11 | $HO^{\bullet} + HO_2^- \rightarrow HO_2^{\bullet} + OH^-$ | $k_{11} = 7.5 \times 10^9\ M^{-1}\ s^{-1}$ | Glaze (1995), Crittenden (1999), Christensen (1982) |
| 12 | $H_2O_2 \leftrightarrow H^+ + HO_2^-$ | $pK_a = 11.6, K_{12}$ $pK_a = 11.65$ (used value) $pK_a = 11.65$ | Crittenden (Perry) Buxton (1988) Dean (1979) |

Iron Chemistry

| # | Reaction | Rate Constant | Reference(s) |
|---|---|---|---|
| 13 | $Fe^o + H_2O_2 \rightarrow Fe^{2+} + 2OH^-$ | $k_{13} = 6.0 \times 10^{-5}\ M^{-1}\ s^1$ (at pH = 4) | This work |
| | | $k_{13} = 4.0 \times 10^{-5}\ M^{-1}\ s^1$ (pH=7) | This work |
| 14 | $Fe^{2+} + H_2O_2 \rightarrow Fe^{3+} + {}^{\bullet}OH + OH^-$ | $k_{14} = 63\ M^{-1}\ s^{-1}$ $k_{14} = 63\ M^{-1}\ s^{-1}$ $k_{14} = 76\ M^{-1}\ s^{-1}$ $k_{14} = 76\ M^{-1}\ s^{-1}$ (used value) | De Laat (1999) Gallard (1998) Chen (1997) Walling (1975) |
| 15 | $Fe^{2+} + H_2O \Leftrightarrow FeOH^+ + H^+$ | $K_{16} = 10^{-9}$ (used value) | Snoeyink (1980) |
| | | $K_{16} = 10^{-9.5}$ $K_{16} = 10^{-9.87}$ | Turner (1981) De Laat (1998) |
| 16 | $Fe^{II}OH^+ + H_2O_2 \rightarrow Fe^{3+} + OH^{\bullet} + 2OH^-$ | $k_{16} = 5.9 \times 10^6\ M^{-1}\ s^{-1}$ (used value) | Gallard (1998) |
| | | $k_{16} = 1.9 \times 10^6\ M^{-1}\ s^{-1}$ | Moffet (1987) |

| 17 | $Fe^{II} + {}^{\bullet}OH \rightarrow Fe^{3+} + OH^{-}$ | $k_{17} = 4.3 \times 10^8$ M$^{-1}$ s$^{-1}$ | Chen (1997), Buxton (1988) |
| | | $k_{17} = 3.2 \times 10^8$ M$^{-1}$ s$^{-1}$ (used value) | De Laat (1999) Gallard (1998) |
| 18 | $Fe^{II} + HO_2^{\bullet} \rightarrow Fe^{III}(HO_2)^{2+}$ | $k_{18} = 1.2 \times 10^6$ M$^{-1}$ s$^{-1}$ | De Laat (1999) |
| | $Fe^{II} + HO_2^{\bullet} + H^+ \rightarrow Fe^{3+} + H_2O_2$ | $k_{18} = 1.2 \times 10^6$ M$^{-1}$ s$^{-1}$ | Gallard (1998) |
| | | $k_{18} = 1.2 \times 10^6$ M$^{-1}$ s$^{-1}$ | Pignatello (1997) Rush (1985) |
| 19 | $Fe^{II} + O_2^{\bullet-} + H^+ \rightarrow Fe^{III}(HO_2)^{2+}$ | $k_{19} = 1.0 \times 10^7$ M$^{-1}$ s$^{-1}$ | De Laat (1999) |
| | $Fe^{II} + O_2^{\bullet-} \xrightarrow{2H^+} Fe^{3+} + H_2O_2$ | $k_{19} = 1.0 \times 10^7$ M$^{-1}$ s$^{-1}$ | Chen (1997) Rush (1985) |
| 20 | $Fe^{III} + HO_2^{\bullet} \rightarrow Fe^{2+} + O_2 + H^+$ | $k_{20} < 2 \times 10^3$ M$^{-1}$ s$^{-1}$ | De Laat (1999) |
| | $Fe^{III} + HO_2^{\bullet} + H^+ \rightarrow Fe^{2+} + O_2 + H_2O$ | $k_{20} = 1 \times 10^3$ M$^{-1}$ s$^{-1}$ | Gallard (1998) |
| | $Fe^{III} + HO_2^{\bullet} \rightarrow Fe^{2+} + O_2 + H^+$ | $k_{20} = 1 \times 10^4$ M$^{-1}$ s$^{-1}$ | Chen (1997), |
| | | $k_{20} = 1 \times 10^3$ M$^{-1}$ s$^{-1}$ (used value) | Rush (1985) |
| 21 | $Fe^{III} + O_2^{\bullet-} \rightarrow Fe^{2+} + O_2$ | $k_{21} = 5 \times 10^7$ M$^{-1}$ s$^{-1}$ | De Laat (1999) |
| | $Fe^{III} + O_2^{\bullet-} + H^+ \rightarrow Fe^{2+} + O_2 + OH^-$ | $k_{21} = 1.5 \times 10^8$ M$^{-1}$ s$^{-1}$ | Gallard (1998) |
| | $Fe^{III} + O_2^{\bullet-} \rightarrow Fe^{2+} + O_2$ | $k_{21} = 1.5 \times 10^8$ M$^{-1}$ s$^{-1}$ (used value) | Chen (1997) |
| 22 | $Fe^{3+} + H_2O \Leftrightarrow Fe^{III}OH^{2+} + H^+$ | $K_{23} = 10^{-2.16}$ | Snoeyink (1980) |
| | | $K_{23} = 10^{-2.17}$ | De Laat (1999) |
| | | $K_{23} = 10^{-2.17}$ | Millborn (1955) |
| | | $K_{23} = 10^{-2.3}$ (used value) | Hug (2003) |
| 23 | $Fe^{3+} + 2H_2O \Leftrightarrow Fe^{III}(HO)_2^+ + 2H^+$ | $K_{23} = 10^{-6.74}$ | Snoeyink (1980) |
| | | $K_{23} = 7.62 \times 10^{-7}$ | De Laat (1999) |
| | | $K_{23} = 10^{-5.9}$ (used value) | Stumm (1996), (calculated) |
| 24 | $2Fe^{3+} + 2H_2O \Leftrightarrow Fe_2^{III}(HO)_2^{4+} + H^+$ | $K_{24} = 10^{-2.85}$ | Snoeyink (1980) |
| 25 | $Fe^{III} + H_2O_2 \rightarrow Fe^{2+} + HO_2^{\bullet} + H^+$ | $k_{25} = 0.02\text{-}0.001$ M$^{-1}$ s$^{-1}$ 0.0032 M$^{-1}$ s$^{-1}$ (used value) | Walling (1971, 1975), Chen (1997) |
| | $Fe^{3+} + H_2O_2 \Leftrightarrow Fe^{III}(HO_2)^{2+} + H^+$ | $K_{25} = 3.65 \times 10^{-3}$ $K_{25} = 4.8 \times 10^{-3}$ (used value) | De Laat (1999) Stumm (1996) (calculated) |
| 26 | $Fe^{III}OH^{2+} + H_2O_2 \Leftrightarrow Fe^{III}(HO)(HO_2)^{2+} + H^+$ | $K_{26} = 2.0 \times 10^{-4}$ | De Laat (1999) |
| | | $K_{26} = 2.65 \times 10^{-4}$ | Stumm (1996), |

|  | (used value) | (calculated) |
|---|---|---|

27    $Fe^{III}(HO_2)^{2+} \rightarrow Fe^{2+} + HO_2^{\bullet}$      $k_{27} = 2.7 \times 10^{-3} \text{ s}^{-1}$      De Laat (1999)

28    $Fe^{III}(HO)(HO_2)^{2+} \rightarrow Fe^{2+} + HO_2^{\bullet} + OH^{-}$      $k_{28} = 2.7 \times 10^{-3} \text{ s}^{-1}$      De Laat (1999)

29    $Fe^{III}(OH)_2^{+} + H_2O \leftrightarrow Fe^{III}(OH)_3 + H^{+}$      $K_{29} = 1 \times 10^{-7.9}$      Hug (2003)

                                                                   Turner (1981)

30    $Fe^{3+} + 3H_2O \leftrightarrow Fe^{III}(OH)_3 + 3H^{+}$      $K_{30} = 1 \times 10^{-13.8}$      Stumm (1996),

31    $Fe^{III}(OH)_3 + Fe^{III}(OH)_3 \rightarrow Fe_{III}(OH)_{3(S)}$      $K_{31} = 1 \times 10^{8.29} \text{ M}^{-1}\text{s}^{-1}$      Hug (2003)


MTBE Chemistry

| # | Reaction | Rate Constant | Reference(s) |
|---|---|---|---|
| 32 | $(CH_3)_3COCH_3 + {}^{\bullet}OH \xrightarrow{\alpha-abstraction \quad (71\%)} (CH_3)_3COCH_2^{\bullet} + H_2O$ <br> $(MTBE + {}^{\bullet}OH \xrightarrow{\alpha-abstraction \quad (71\%)} MTBE_1^{\bullet} + H_2O)$ | $1.6 \times 10^9 \text{ M}^{-1}\text{s}^{-1}$ <br> $2 \times 10^9 \text{ M}^{-1}\text{s}^{-1}$ <br> $3.9 \times 10^9 \text{ M}^{-1}\text{s}^{-1}$ <br> $1.9 \times 10^9 \text{ M}^{-1}\text{s}^{-1}$ <br> $1.6 \times 10^9 \text{ M}^{-1}\text{s}^{-1}$ <br> (used value) | Buxton (1988) <br> Hardison <br> (2002) <br> Chang (2000) <br> Acero (2001) |
| 33 | $(CH_3)_3COCH_3 + {}^{\bullet}OH \xrightarrow{\beta-abstraction \quad (29\%)} {}^{\bullet}CH_2(CH_3)_2COCH_3 + H_2O$ <br> $(MTBE + {}^{\bullet}OH \xrightarrow{\beta-abstraction \quad (29\%)} MTBE_2^{\bullet} + H_2O)$ | $1.6 \times 10^9 \text{ M}^{-1}\text{s}^{-1}$ <br> $2 \times 10^9 \text{ M}^{-1}\text{s}^{-1}$ <br> $3.9 \times 10^9 \text{ M}^{-1}\text{s}^{-1}$ <br> $1.9 \times 10^9 \text{ M}^{-1}\text{s}^{-1}$ <br> $1.6 \times 10^9 \text{ M}^{-1}\text{s}^{-1}$ <br> (used value) | Buxton (1988) <br> Hardison <br> (2002) <br> Chang (2000) <br> Acero (2001) |
| 34 | $(CH_3)_3COCH_2^{\bullet} + O_2 \rightarrow (CH_3)_3COCH_2O_2^{\bullet}$ <br> $(MTBE_1^{\bullet} + O_2 \rightarrow MTBE_1O_2^{\bullet})$ | $10^9\text{-}10^{10} \text{ M}^{-1}\text{s}^{-1}$ <br> $1.24 \times 10^9 \text{ M}^{-1}\text{s}^{-1}$ <br> $1.24 \times 10^9 \text{ M}^{-1}\text{s}^{-1}$ <br> $1.0 \times 10^9 \text{ M}^{-1}\text{s}^{-1}$ <br> (used value) | Stefan (2000) <br> Cooper (2002) <br> Hardison <br> (2002) |
| 35 | ${}^{\bullet}CH_2(CH_3)_2COCH_3 + O_2 \rightarrow {}^{\bullet}O_2CH_2(CH_3)_2COCH_3$ <br> $(MTBE_2^{\bullet} + O_2 \rightarrow {}^{\bullet}O_2MTBE_2)$ | $10^9\text{-}10^{10} \text{ M}^{-1}\text{s}^{-1}$ <br> $1.24 \times 10^9 \text{ M}^{-1}\text{s}^{-1}$ <br> $1.24 \times 10^9 \text{ M}^{-1}\text{s}^{-1}$ <br> $1.0 \times 10^9 \text{ M}^{-1}\text{s}^{-1}$ <br> (used value) | Stefan (2000) <br> Cooper (2002) <br> Hardison <br> (2002) |
| 36 | $2(CH_3)_3COCH_2O_2^{\bullet} \rightarrow (CH_3)_3COCH_2 - O_4 - CH_2OC(CH_3)_3$ <br> $(2MTBE_1O_2^{\bullet} \rightarrow R_1)$ | $1.0 \times 10^9 \text{ M}^{-1}\text{s}^{-1}$ <br> (used value) | Hardison <br> (2002) |

         ==${}^{\bullet}O_2CH_2(CH_3)_2COCH_3 \rightarrow TBA + F$==      $1 \times 10^5 \text{ M}^{-1}\text{s}^{-1}$

Cooper (2002)

37  $2^\bullet O_2CH_2(CH_3)_2COCH_3 \rightarrow CH_3O(CH_3)_2CCH_2 - O_4 - CH_2C(CH_3)_2OCH_3$     $1.0 \times 10^9\,M^{-1}s^{-1}$    Hardison

$(2MTBE_2O_2^\bullet \rightarrow R_2)$     (used value)    (2002)

<mark>$^\bullet O_2CH_2(CH_3)_2COCH_3 \rightarrow TBA + F$</mark>     $1 \times 10^5\,M^{-1}s^{-1}$

Cooper (2002)

38  $(CH_3)_3COCH_2 - O_4 - CH_2OC(CH_3)_3 \rightarrow 2^\bullet OCH_2 - O - C(CH_3)_3 + O_2$     $1.0 \times 10^6\,s^{-1}$    Hardison

$(R_1 \rightarrow 2R_3 + O_2)$     (used value)    (2002)

$(CH_3)_3COCH_2 - O_4 - CH_2OC(CH_3)_3 \rightarrow 2(CH_3)_3COCHO + H_2O_2$     $1.0 \times 10^6\,s^{-1}$

$(R_{11})$                 $(2TBF)$     (used value)

39  $2^\bullet OCH_2 - O - C(CH_3)_3 \rightarrow (CH_3)_3COCHO + HOCH_2 - O - C(CH_3)_3$     $1.0 \times 10^9\,M^{-1}s^{-1}$    Hardison

                   TBF     (used value)    (2002)

$(2R_3 \rightarrow TBF + R_4)$

40  $HOCH_2 - O - C(CH_3)_3 + H_2O \rightarrow HOC(CH_3)_3 + CH_2O$     $1 \times 10^{10}\,M^{-1}s^{-1}$    Cooper (2002)

                  TBA        F     (used value)    Wu (2002)

$(2R_4 \rightarrow TBA + F)$

41  $TBF + {}^\bullet OH \rightarrow (CH_3)_3CO\dot{C}O + H_2O$     $5.23 \times 10^8\,M^{-1}s^{-1}$    Hardison

$(TBF + {}^\bullet OH \rightarrow R_5 + H_2O)$     $4.1 \times 10^8\,M^{-1}s^{-1}$    (2002)

                  $7 \times 10^8\,M^{-1}s^{-1}$    Onstein(1999)

                  $3.1 \times 10^8\,M^{-1}s^{-1}$    Acero(2001)

                  (used value)

42  $(CH_3)_3CO\dot{C}O + 0.5O_2 \rightarrow {}^\bullet OC(CH_3)_3 + CO_2$     $10^9\text{-}10^{10}\,M^{-1}s^{-1}$    Stefan (2000)

$(R_5 + O_2 \rightarrow R_6 + CO_2)$     $1.24 \times 10^9\,M^{-1}s^{-1}$    Cooper (2002)

                  $1.24 \times 10^9\,M^{-1}s^{-1}$    Hardison

                  $1.0 \times 10^9\,M^{-1}s^{-1}$    (2002)

                  (used value)

43  ${}^\bullet OC(CH_3)_3 \rightarrow OC(CH_3)_2 + CH_3^\bullet;$     $10^6 - 10^7\,s^{-1}$    Cooper (2004)

            Acetone

$(R_6 \rightarrow Acetone + R_7)$     $1 \times 10^6\,s^{-1}$

                  (used value)

${}^\bullet OC(CH_3)_3 \xrightarrow{H2O} CH_2O + product$     $1 \times 10^6\,s^{-1}$

44  $CH_3^\bullet + O_2 \rightarrow CH_2O$     $10^9\text{-}10^{10}\,M^{-1}s^{-1}$    Stefan (2000)

$(R_7 + O_2 \rightarrow F)$     $1.24 \times 10^9\,M^{-1}s^{-1}$    Cooper (2002)

                  $1.24 \times 10^9\,M^{-1}s^{-1}$    Hardison

|  |  | $1.0 \times 10^9 \, M^{-1} s^{-1}$ <br> (used value) | (2002) |
|---|---|---|---|

45    $CH_2O + {}^{\bullet}OH \rightarrow HCO_2H$

           Formic Acid

    $(F + {}^{\bullet}OH \rightarrow FA)$

| $1 \times 10^9 \, M^{-1} s^{-1}$ | Buxton(1988) |
|---|---|
| $1 \times 10^9 \, M^{-1} s^{-1}$ | Cooper (2002) |
| (used value) | |

46    $HCO_2H + {}^{\bullet}OH \rightarrow CO_2$

    $(FA + {}^{\bullet}OH \rightarrow CO_2)$

| $1.3 \times 10^8 \, M^{-1} s^{-1}$ | Buxton(1988) |
|---|---|
| $1.3 \times 10^8 \, M^{-1} s^{-1}$ | Cooper (2002) |
| (used value) | |

47    $Acetone + {}^{\bullet}OH \rightarrow CO_2 + produtcs$

| $1.1 \times 10^8 \, M^{-1} s^{-1}$ | Buxton(1988) |
|---|---|
| (used value) | |

| $1.1 \times 10^8 \, M^{-1} s^{-1}$ | Cooper (2002) |
|---|---|
| $0.77 \times 10^8 \, M^{-1} s^{-1}$ | Thomas(1965) |

48    $TBA + {}^{\bullet}OH \rightarrow CO_2 + produtcs$

| $6.0 \times 10^8 \, M^{-1} s^{-1}$ | Buxton(1988) |
|---|---|
| $2.0 \times 10^8 \, M^{-1} s^{-1}$ | |
| (used value) | |

49    $(CH_3)_3COCH_2 - O_4 - CH_2OC(CH_3)_3 \rightarrow 2CH_3O(CH_3)_2CCH_2O^{\bullet} + O_2$

    $(R_2 \rightarrow 2R_8 + O_2)$

| $1.0 \times 10^6 \, M^{-1} s^{-1}$ | Hardison |
|---|---|
| (used value) | (2002) |

50    $CH_3O(CH_3)_2CCH_2O^{\bullet} \rightarrow {}^{\bullet}C - (CH_3)_2OCH_3 + CH_2O$

    $(R_8 \rightarrow R_9 + F)$

| $1.0 \times 10^6 \, s^{-1}$ |
|---|
| (used value) |

51    ${}^{\bullet}C - O(CH_3)_3 + \dfrac{1}{2}O_2 \rightarrow {}^{\bullet}OC - O(CH_3)_3$

    $(R_9 + O_2 \rightarrow R_{10})$

| $10^9\text{-}10^{10} \, M^{-1} s^{-1}$ | Stefan (2000) |
|---|---|
| $1.24 \times 10^9 \, M^{-1} s^{-1}$ | Cooper (2002) |
| $1.24 \times 10^9 \, M^{-1} s^{-1}$ | Hardison |
| $1 \times 10^9 \, M^{-1} s^{-1}$ | (2002) |
| (used value) | |

52    ${}^{\bullet}OC - O(CH_3)_3 \rightarrow OC(CH_3)_2 + CH_3O^{\bullet}$

           *Acetone*

    $(R_{10} \rightarrow Acetone + R_{11})$

| $10^6 \, s^{-1}$ |
|---|
| (used value) |

53    ${}^{\bullet}OC - O(CH_3)_3 \rightarrow OC - O(CH_3)_2 + CH_3{}^{\bullet}$

           Methyl   Acetate

    $(R_{10} \rightarrow Methyl \;\; Acetate + R_7)$

| $10^6 \, s^{-1}$ |
|---|
| (used value) |

| 54 | Methyl Acetate $+ \,^\bullet OH \rightarrow CO_2 +$ produtcs | $1.2 \times 10^8\,M^{-1}\,s^{-1}$ | Buxton(1988) |
| | | $2.2 \times 10^8\,M^{-1}\,s^{-1}$ | Ebert(1965) |
| | | $2.5 \times 10^8\,M^{-1}\,s^{-1}$ (used value) | |

55 $(CH_3)_3COCH_2 - O_4 - CH_2OC(CH_3)_3 \rightarrow 2(CH_3)_3COCHO + H_2O_2$
$(TBF)$
 $1.0 \times 10^6\,M^{-1}\,s^{-1}$ (used value)   Hardison (2002)

56 $HCO_2H \xleftrightarrow{\;pKa=3.75\;} HCO_2^- + H^+$   Neta, 1996; Cooper, 2004

57 $HCO_2^- + \,^\bullet OH \rightarrow \,^\bullet CO_2^- + H_2O$

| | | $3.2 \times 10^9\,M^{-1}\,s^{-1}$ | Buxton (1988) |
| | | $2.2 \times 10^9\,M^{-1}\,s^{-1}$ | Baxendale (1969) |
| | | $3.8 \times 10^9\,M^{-1}\,s^{-1}$ | Elliot (1984) |
| | | $3.5 \times 10^9\,M^{-1}\,s^{-1}$ | Willson |
| | | $2.45 \times 10^9\,M^{-1}\,s^{-1}$ | (1971) |
| | | $2.7 \times 10^7\,M^{-1}\,s^{-1}$ | Thomas, 1965 |
| | | $4.1 \times 10^9\,M^{-1}\,s^{-1}$ | Rabani (1962) |
| | | (used value) | Buxton, 1969 |

58 $^\bullet OC(CH_3)_3 \xrightarrow{\;H2O\;} HCOH +$ product   $10^6\,s^{-1}$ (used value)

59 $CH_3O^\bullet \xrightarrow{\;H2O\;} R \rightarrow\rightarrow$ Methyl Acetate   $10^6\,s^{-1}$ (used value)

[*] Shaded equations were not used in this model

## 2.1. Hydrogen peroxide chemistry

The chemistry of hydrogen peroxide in aqueous systems (reactions 1 to 13 in Table 2.1) has been studied extensively by many [Belski, 1977,1985; Baxendale, 1988; Behar, 1970; Christensen, 1989; Sehested, 1968; Weeks, 1955; Daniton,1953; Pagsberg, 1969, Thomas, 1965; Vollman, 1959; Weinstein, 1979; Walling, 1973, 1975; Harber, 1943; Rush, 1985; Evans, 1948]. Many of the $H_2O_2$ reactions are presented in Table 4.1. The initial reaction for this system is the production of $^\bullet OH$ radicals. These radicals are

mainly produced from the reaction of ferrous iron with hydrogen peroxide in Fenton's reagent ($Fe^{II}/H_2O_2$) systems. Dissolution of zero-valent iron ($Fe^o$) by hydrogen peroxide ($H_2O_2$) was proposed to produce the ferrous iron ($Fe^{2+}$) (reactions 13 Table 4.1) [Pourbaix, 1966, Bergendahl, 2004]. Then ferrous iron reacts with $H_2O_2$ through the well known Fenton's reaction (reactions 14 and 17 Table 2.1) to produce hydroxyl radicals ($^{\bullet}OH$) and the ferric ion ($Fe^{3+}$) [Walling, 1973, 1975; Harber, 1943; Rush, 1985; Evans, 1948]. Then ferrous and ferric iron along with these radicals initiate chain reactions as shown in Table 4.1. The propagation reaction includes the reaction of $H_2O_2$ and its conjugate with hydroxyl radicals and hydroperoxyl radicals and its conjugate. Also, the reaction of ferrous ion with hydrogen peroxide and the reactions of the ferric and ferrous iron with the other radicals in the system are considered as propagation reaction [De Laat, 1999]. The termination reactions include radical-radical reactions.

## 2.2. Iron chemistry

### 2.2.1. Iron dissolution

A rate law applicable to many of the recent studies on mineral-water or mineral-melt surface growth and dissolution reactions can be written as [Lasaga, 1998]:

$$Rate = k_o A e^{-E_a/RT} \prod_i a_i^{ni} f(\Delta G) \qquad\qquad 2.2.1.1$$

where A is the reactive surface area of the mineral and $E_a$ is the apparent activation energy of the overall reaction. The temperature dependence will enter largely in the Arrhenius equation for the rate constant k:

$$k = k_o^{'} e^{-E_a/RT} \qquad\qquad 2.2.1.2$$

where $k_o^{'} = k_0 A$.

The term involving the activities of other species in solution, $a_i$, incorporates other possible catalytic or inhibitory effects on the overall growth or dissolution rate. This also includes the effect of pH ($a_H^+$) where the effect of pH can be modeled with a power law. The final term $f(\Delta G)$ introduces the dependences of the overall growth rate on the supersaturation or undersaturation state of the system, expressed as a function ($f$) of the free energy change for the growth or dissolution reaction ($\Delta G$). At equilibrium, $\Delta G = 0$ [Lasaga, 1998]. All of the thermodynamics is embedded in the requirement that $f(0) = 0$. This relation guaranties that the kinetics will be fully compatible with thermodynamics. The behavior of $f$ away from the zero point is completely dependent on the kinetic mechanism.

For aqueous solutions, $\Delta G$ can be written as:

$$\Delta G = RT \ln\left(\frac{\prod_j a_j^{\upsilon_j}}{K_{eq}}\right) \qquad\qquad 2.2.1.3$$

where $a_j$ is the activity of the each species in the solution and $K_{eq}$ is the solubility product. Various forms of $f(\Delta G)$ where obtained such as:

1. $f(\Delta G) = -(1 - \exp(\frac{\Delta G}{RT}))$ \qquad [ Lasaga, 1984] \qquad\qquad 2.2.1.4

The above relation near equilibrium, (using the expansion $e^x \sim 1 + x$ for small x) is reduced to :

$$f(\Delta G) = \frac{\Delta G}{RT} \qquad\qquad 2.2.1.5$$

Relation 2.2.1.4 can be generalized to the following form [Lasaga, 1984, 1998].

$$f(\Delta G) = -(1 - \exp(\frac{n\Delta G}{RT})) \qquad\qquad 2.2.1.6$$

where n is not necessarily equal to 1. Equation 2.1.6 is valid for:

1.  the case in which a complex reaction sequence has all elementary reactions very near equilibrium except for a single slow determining step; in this case, equation 2.1.6 holds with n = 1

2.  The more common case, in which a steady state is established among the entire sequence of elementary steps. In this case equation 2. 2.1.6 is correct for small $\dfrac{\Delta G}{RT}$ and approximately correct for bigger deviations from equilibrium and in this case n $\neq$ 1 [Nagy, 1991].

From the work done by Cama (2000, 1999), Ganor (1995, 1999) a similar rate law has been defined for heterogeneous mineral surface reactions where:

$$Rate = k_o A_{\min} e^{-E_{app}/RT} a_{H^+}^{nH^+} \prod_i a_i^{ni} g(I) f(\Delta G_r) \qquad 2.2.1.7$$

where $k_o$ is a constant, $A_{\min}$ is the reactive surface area of the mineral, $E_{app}$ is the apparent activation energy of the overall reaction, R is the gas constant, T is the absolute temperature, $a_i$ and $a_{H+}$ are the activities in solution of species i and $H^+$, respectively, $n_i$ and $n_H^+$ are the orders of the reaction with respect to these species, g(I) is a function of the ionic strength (I), and $f(\Delta G_r)$ is a function of the Gibbs free energy and accounts for important variation of the rate with deviation from equilibrium. A more general expression for $f(\Delta G_r)$ can be written as:

$$f(\Delta G_r) = 1 - \exp(m.(\frac{\Delta G_r}{RT})^n) \qquad 2.2.1.8$$

where m and n are constants with the free energy being defined as before by:

$$\Delta G_r = RT \ln \left( \frac{\prod_j a_j^{\upsilon_j}}{K_{eq}} \right) = RT \ln \left( \frac{IAP}{K_{eq}} \right) \qquad 2.2.1.9$$

Under constant temperature, pH, ionic strength, and in the absence of catalysts and inhibitors, the dissolution rate normalized to the surface area, based on relation 2.2.1.7 at these conditions, is given by:

$$\frac{Rate}{A_{min}} = kf(\Delta G_r) = \left( 1 - \exp\left( m \left( \frac{\Delta G_r}{RT} \right)^n \right) \right) \qquad 2.2.1.10$$

In Lasaga (2000), k, m, n were calculated from a non linear regression of equation (2.2.1.10 using least squares. The resulting coefficients were: $k=-8.1 \times 10^{-12}$ mol m$^{-2}$ s$^{-1}$, m $= -6 \times 10^{-10}$, and n = 6. It is important that different combinations of the three coefficients yield other values that adequately describe the experimental data. According to their work they said that the value of the coefficients should be refined using additional experimental data that were not available at that time and far from equilibrium $f(\Delta G) = 1$ [Lasaga, 1984, 1998].

For one of the systems that will be studied in this chapter, zero valent iron (Fe$^o$) was being dissolved by hydrogen peroxide, therefore an analogy between iron dissolution by hydrogen peroxide and the previous derived relations will be made. For this work the reaction of Fe$^o$ and H$_2$O$_2$ is given by [Bergendahl, 2004; Pourbaix, 1966; Arenzo, 1999]

$$Fe^0 + H_2O_2 \rightarrow Fe^{II} + 2OH^- \qquad 2.2.1.11$$

the rate of Fe$^o$ dissolution will be given by:

$$Rate = \frac{dFe^0}{dt} = \frac{dH_2O_2}{dt} = k_o A_{min} e^{-E_{app}/RT} a_{H^+}^{nH^+} \prod_i a_i^{ni} g(I) f(\Delta G_r) \ (\text{mol L}^{-1} \text{ s}^{-1}) \qquad 2.2.1.12$$

At fixed temperature, ionic strength, pH, and at a certain initial concentration of $Fe^o$ in the system ($A_{min}$) then the above equation can be reduced to:

$$Rate = k[Fe^o]_o \prod_i a_i^{ni} f(\Delta G_r)$$

2.2.1.13

with

$$f(\Delta G_r) = (1 - \exp(m(\frac{|\Delta G_r|}{RT})^n))$$

2.2.1.8

The free energy term for this system, assuming activity coefficients is unity for the aqueous species and the activity of the solid iron is one, can be written as [Stumm, 1996]:

$$\Delta G = RT \ln\left(\frac{\prod_j a_j^{\upsilon j}}{K_{eq}}\right) \approx RT \ln\left(\frac{[Fe^{2+}][OH^-]^2}{K_{eq}[H_2O_2]}\right)$$

2.2.1.14

$K_{eq}$ for reaction 2.1.11 can be calculated from [Snoeyink, 1980; Stumm, 1996; Pourbaix, 1966]:

$$\Delta G^o = -RT \ln K_{eq}$$

2.2.1.15

and:

$$\Delta G^o = \sum_i \nu_i \mu_i^o$$

2.2.1.16

where $\nu_i$ is the stoichiometric coefficient of species i in the reaction, and $\mu_i$ is the chemical potential (or heat of formation) of species i.

The above calculations embedded an assumption that the activity of pure solid or liquids is equal to 1, where:

$$\overline{G_i} = \Delta\overline{G}^o_{f,i} + RT \ln\{i\} = \Delta\overline{G}^o_{f,i} + RT \ln(1) = \Delta\overline{G}^o_{f,i} = \mu_i^o$$

2.2.1.17

where:

$\overline{G}_i$ = the free energy per mole of substance i in state other than standard measured relative to an established reference [Snoeyink, 1980].

{i} = the active concentration or activity of specie i.

R = ideal gas constant, 1.987 cal/($^o$K mol)

T = temperature in $^o$K( 25$^o$C=298.15 k).

The heats of formation for the species in reaction 2.2.1.11 are given in Table 4.2 [Stumm, 1996; Snoeyink, 1980].

Table 2.2.1.1: Heat of formation for iron species and hydrogen peroxide

| Specie | $\mu_i$ ($\Delta\overline{G}^o_{f,i}$) cal/mole |
|---|---|
| Fe$^o$ (solid) | 0.0 |
| Fe$^{2+}$ (dissolved) | -20300 |
| Fe$^{3+}$ (dissolved) | -2530 |
| H$_2$O$_2$ (liquid) | -31470 |

Now substituting the values in Table 2.2.1.1 into equations 2.2.1.16 and using 25$^o$C and R= 1.987 cal/( $^o$K mol) then $\Delta G^o = \sum_i v_i \mu^o_i$ = -64020 cal/mol, hence K$_{eq}$ for reaction 2.2.1.7, calculated from equation 2.1.15 is $10^{46..9}$. Therefore equation 2.2.1.14, at room temperature, becomes:

$$\Delta G = RT \ln\left(\frac{[Fe^{2+}][OH^-]^2}{K_{eq}[H_2O_2]}\right) = RT \ln\left(\frac{[Fe^{2+}][OH^-]^2}{[H_2O_2]}\right) - RT \ln K_{eq}$$

$$\Delta G = RT \ln\left(\frac{[Fe^{2+}][OH^-]^2}{[H_2O_2]}\right) + 64020 \qquad\qquad 2.2.1.18$$

However, under conditions far from equilibrium as was said above $f(\Delta G) = 1$ ( Q << K$_{eq}$) therefore equation, 2.2.1.18 reduces to:

$$Rate = k[Fe^o]_o \prod_i a_i^{ni} \qquad\qquad 2.2.1.19$$

The promoter for $Fe^o$ dissolution in this work was $H_2O_2$ since the rate of MTBE degradation was a function of $H_2O_2$ concentration initially present in the system [Bergendahl, 2004]. This would mean that the more $H_2O_2$ is present the more $Fe^o$ will be converted to Fe(II) and hence more $^\bullet OH$ radicals will be present as will be shown later. $H^+$ was not considered as a promoter or an inhibitor since during each run the pH was assumed to be constant based on experimental observations. Therefore equation 2.2.1.19 becomes:

$$Rate = k'[H_2O_2]^n \qquad\qquad 2.2.1.20$$

For the promoting effect, it was found that the rate constant is proportional to the concentration of the promoter to a power ranging from 0.44 to 1 at most  [Plummer, 1982; Chou, 1989, Gautelier, 1999; Luttge, 2003]. Hence a value of 1 was assigned to n and equation 2.2.1.20 becomes:

$$Rate = k'[H_2O_2] \qquad\qquad 2.2.1.21$$

Another possible dissolution promotor of iron is water [Steven yabusaki, 2001, Pourbaix, 1978]. The rate of $Fe^o$ dissolution in aerobic conditions was found to be slow [Steven yabusaki, 2001] and hence under the studied time range $Fe^o$ dissolution will be due only to $H_2O_2$.

## 2.2.2. Ferrous ($Fe^{II}$) and Ferric ($Fe^{III}$) iron:

Iron dissolution will lead to the production of ferrous iron as was shown in equation 2.1.11 in the previous section.

$$Fe^o + H_2O_2 \rightarrow Fe^{2+} + 2OH^- \qquad\qquad 2.2.1.11$$

Fenton's reagent ($Fe(II)/H_2O_2$) and the Fenton-like reagent ($Fe(III)/H_2O_2$) have been investigated by several studies in order to study the mechanism and kinetics of reaction [Harber, 1934, Walling, 1973, 1975, Rush, 1985; Evans, 1948]. Therefore reactions of ferric iron and ferrous iron with hydrogen peroxide are well documented.

Ferrous iron hydrolyzes in water according to the following reaction with the corresponding equilibrium constant given in Table 4.1 [Snoeyink, 1980, Gallard, 1998]:

$$Fe^{2+} + H_2O \xleftrightarrow{K_{eq}} Fe^{II}OH^+ + H^+$$  2.2.2.1

Therefore, at any time the total ferrous iron concentration ($Fe^{II}$) will be given by [Stumm, 1996; Snoeyink, 1980; Pankow, 1991]:

$$[Fe^{II}] = [Fe^{2+}] + [Fe^{II}OH^+]$$  2.2.2.1

The reaction of ferrous ion with hydrogen peroxide (Fenton's reaction) is the initiator for the degradation of MTBE since it produces $^\bullet OH$ radicals in the system according to the following reaction [De Laat, 1999, Chen, 1997, Walling, 1973, 1975, Harber, 1934, Gallard, 1998, King, 2000]:

$$Fe^{2+} + H_2O_2 \rightarrow Fe^{3+} + {}^\bullet OH + OH^-$$  2.2.2.2

The other form of ferrous iron ($FeOH^+$) was found to react with hydrogen peroxide to produce $^\bullet OH$ radicals and ferric iron according to the following reaction [De Laat, 1998; Mofet, 1987; King, 2000]:

$$Fe^{III}OH^+ + H_2O_2 \rightarrow Fe^{3+} + OH^\bullet + OH^-$$  2.2.2.3

Another important $Fe^{II}$ reaction is its reaction with $^\bullet OH$ radicals according to the following reaction [Chen, 1997, Buxton, 1988, De Latt, 1999]:

$$Fe^{II} + {}^\bullet OH \rightarrow Fe^{III} + OH^-$$  2.2.2.4

In reaction 2.2.2.3, $Fe^{II}$ is the total ferrous ion. No individual values were available for $FeOH^+$ reaction with $^\bullet OH$ radical and hence the given rate constant for reaction 2.2.2.4 in Table 4.1 would be the apparent rate constant [King, 2000, De Laat, 1999]. Also, for other reactions involving ferrous iron with the radicals in this system, total ferrous ion ($Fe^{II}$) was used to represent both forms of ferrous ion [De Laat, 1999]. Equilibrium constants were obtained and if necessary corrected to the zero ionic strength value [Stumm, 1996].

Ferric iron also reacts with hydrogen peroxide to produce hydroxyl radicals. However this reaction is much slower than the reaction between ferrous iron and hydrogen peroxide. The value of the rate constant for reaction of ferric iron with hydrogen peroxide was found to be in the range 0.02-0.001 $M^{-1}$ $s^{-1}$[Walling, 1973, 1975; Chen, 1997, De Laat, 1999]. Although this rate constant is low, it has a major contribution to the kinetic model as will be shown later.

De Laat (1999) suggested that the interaction of ferric iron with hydrogen peroxide will take place according to the following reactions with the corresponding equilibrium constants:

$$Fe^{3+} + H_2O_2 \Leftrightarrow Fe^{III}(HO_2)^{2+} + H^+ \qquad \text{,} (K_{25} = 3.65 \text{ x } 10^{-3}) \qquad 2.2.2.5$$

$$Fe^{III}OH^{2+} + H_2O_2 \Leftrightarrow Fe^{III}(HO)(HO_2)^{2+} + H^+ \qquad (K_{26} = 2.0 \text{ x } 10^{-4}) \qquad 2.2.2.6$$

The products of the above reactions will then decompose to give ferrous iron and hydroperoxyl radicals according to the following reactions:

$$Fe^{III}(HO_2)^{2+} \rightarrow Fe^{2+} + HO_2^\bullet \qquad\qquad 2.2.2.7$$

$$Fe^{III}(HO)(HO_2)^{2+} \rightarrow Fe^{2+} + HO_2^\bullet + OH^- \qquad\qquad 2.2.2.8$$

De Laat (1999) obtained the rate constants for the above reactions by fitting to the data and found a value of $2.7 \times 10^{-3}$ $M^{-1}$ $s^{-1}$ for both reactions.

The reactions suggested by De Laat (1999) are similar to the following reaction between ferric iron that is usually used to describe Fenton's reactions [Walling, 1973, 1975, Chen; 1997; Hug, 2003, Harber, 1943]

$$Fe^{III} + H_2O_2 \xrightarrow{k} Fe^{2+} + 2HO_2^{\bullet} \qquad\qquad 2.2.2.9$$

with a rate constant of 0.01-0.001 $M^{-1}$ $s^{-1}$.

Both methods for $Fe^{III}$ interaction with hydrogen peroxide were tested with this model and the difference was not significant. Therefore, in the simulation the traditional form of Fenton's reaction was used (Reaction 2.2.2.9) in order not to add extra fitting parameters to this model, since this reaction was mainly reported by De Laat (1999).

Once ferrous and ferric iron are produced in the system, then they will go through the different reactions that are shown in Table 4.1. Most of these reactions of ferrous and ferric iron in aqueous solutions of hydrogen peroxide were described by De Laat (1999). The work of Chen (1997) didn't include all the proposed reactions by De Laat (1999). As can be seen from reaction 2.2.2.2 ferric iron Fe(III) is also produced.

The total concentration of ferric iron ($Fe(III)_T$) at any time will be the sum of all the soluble forms of $Fe^{3+}$ (Free and complexed $Fe^{3+}$ species) [Stumm, 1996]:

$$[Fe(III)_T] = [Fe^{3+}] + [FeOH^{2+}] + Fe(OH)_2^+] + 2[Fe_2(OH)_2^{4+}] \qquad 2.2.2.10$$

The last three terms in the above relation result from $Fe^{3+}$ hydrolysis. The complexes, which results from $Fe^{3+}$ and $H_2O_2$ equilibrium, were not include in relation 2.2.2.10 since relation 2.2.2.9 was used in this model.

Each soluble form of ferric ion is presented through the corresponding equilibrium reactions in Table 4.1 where [Stumm, 1996]:

$$[Fe^{III}OH^{2+}] = \frac{K_{22}[Fe^{3+}]}{[H^+]}$$ 2.2.2.11

$$[Fe^{III}(OH)_2^+] = \frac{K_{23}[Fe^{3+}]}{[H^+]^2}$$ 2.2.2.12

$$[Fe_2^{III}(OH)_2]^{4+} = \frac{K_{24}[Fe^{3+}]^2}{[H^+]^2}$$ 2.2.2.13
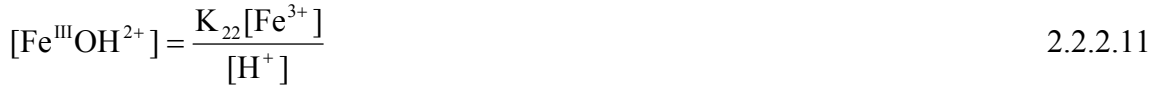
The equilibrium constants for the different reactions in Table 4.1 were used at zero ionic strength. Therefore, whenever equilibrium constant is not available at zero strength it was corrected to zero ionic strength based on correlations from Stumm (1996) and Snoeyink (1980) and the corrected value was used in simulation.

Based on concentration-pH diagrams (pC-pH) available for Fe(III) equilibrium in water [Stumm, 1996; Snoeyink, 1980], there is a possibility for Fe(III) to precipitate to form $Fe(OH)_{3(S)}$ at a certain combination of concentration and pH values. The formation of $Fe^{III}(OH)_3$ complex starting with $Fe^{3+}$ according to the following reaction with $pK_a$ = (12-13.8) [Stumm, 1996; Turner, 1981, Martell. 1976]:

$$Fe^{3+} + 3H_2O \leftrightarrow Fe^{III}(OH)_3 + 3H^+$$ 2.2.2.14

Between pH 5-7 $Fe(OH)_2^+$ is the predominant species and likewise it forms the solution boundary for $Fe(OH)_{3(S)}$. Hug (2003) accounted for this form by considering another soluble complex form of Fe(III), beside the other ones described earlier, which is formed from the hydrolysis of $Fe(OH)_2^+$ , with $pK_a$ = 7.9, according to the following reaction:

$$Fe^{III}(OH)_2^+ + H_2O \leftrightarrow Fe^{III}(OH)_3 + H^+$$ 2.2.2.15

Using either equation 2.2.2.14 or 2.2.2.15 would compensate for $Fe^{III}(OH)_3$ complex since equation 2.2.2.15 is basically derived from equation 2.2.2.14 and 2.2.2.16 below. Therefore equation 2.2.2.13 was used [Stumm, 1996; Turner, 1981].

$$Fe^{3+} + 2H_2O \leftrightarrow Fe^{III}(OH)_2^+ + H^+ \qquad 2.2.2.16$$

In Hug (2003) $Fe(OH)_3$ was assumed to precipitate to $Fe(OH)_{3(S)}$ according to the following reaction:

$$Fe^{III}(OH)_3 + Fe^{III}(OH)_3 \rightarrow Fe_{III}(OH)_{3(S)} \qquad 2.2.2.17$$
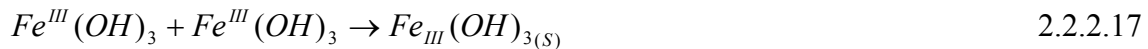
The rate constant for reaction 2.2.17 was a fitted parameter in Hug's work in the range $10^{8.29}$ $M^{-1}$ $s^{-1}$ to $10^{9.12}$ $M^{-1}$ $s^{-1}$.

For $Fe^{II}$ ($Fe^{2+}$ and $FeOH^+$) precipitation does not take place in the pH range 2-7 according to (pC-pH) [Snoeyink, 1980] unless the concentration of $Fe^{II}$ is high (greater than 0.2 M) which is not the case for this work and most Fenton's systems. Hence, precipitation reactions of $Fe^{II}$ will be neglected.

With the additional complex form of $Fe(OH)_3$ equation 2.22.10 becomes:

$$[Fe(III)_T] = Fe(III) + [Fe(OH)_3] \qquad 2.2.2.18$$

where $[(Fe^{III}(OH)_3]$ was obtained from 2.2.2.15 and hence the following relation will describe its concentration:

$$[Fe^{III}(OH)_3] = \frac{K_{29}[Fe^{III}(OH)_2^+]}{[H^+]} \qquad 2.2.2.19$$

Substituting equations 2.2.2.11, 2.2.2.12, 2.2.13, and 2.2.2.19 into equation 2.2.2.18 the following relation was obtained which relates the total concentration of ferric iron to the concentrations of the individual forms:

$$\text{Fe(III)}_T = [\text{Fe}^{3+}]\left[1 + \frac{K_{22}}{[H^+]} + \frac{K_{23}}{[H^+]^2} + \frac{2K_{24}[\text{Fe}^{3+}]}{[H^+]^2} + \frac{K_{23}K_{29}}{[H^+]^3}\right] \qquad 2.2.2.20$$

In the above relation other possible forms of $Fe^{3+}$ are possible [Stumm, 1996]. ($Fe_3(OH)_5^{5+}$) is possible, however its concentration will be at least three orders of magnitude less than $Fe^{3+}$ at pH 3 or less [Stumm, 1996]. Therefore, it was not used in the simulations for Xu's data where pH was 2.8. Also, for the simulation of these data, the concentration of $Fe(OH)_3$ was always less than $10^{-9}$ M and hence it formation and its disappearance reactions were not included in this part of the simulations. Also, when the rate constant that was suggested by Hug (2003) for $Fe(OH)_3$ was included in the model, loss of Fe(III) due to precipitation was not significant since $Fe(OH)_3$ was always less than $10^{-9}$ M. Therefore, for the simulation of Xu's data (2004) formation and precipitation of $Fe(OH)_3$ was neglected.

At any time the amount of the different forms of iron present in the system should be equal to the initial amount of iron that was used:

$$\text{Fe}^{II}\big|_{t=t} + \text{Fe(III)}_T\big|_{t=t} + \text{Fe}^o\big|_{t=t} + \text{Fe(OH)}_{3(S)}\big|_{t=t} = \text{Fe}^o\big|_{t=0}$$

## 2.3. Mechanism of MTBE degradation

MTBE degradation in this work was due to its oxidation by hydroxyl radicals. Reactions of MTBE with $H_2O_2$ alone, or with $Fe^o$ were not observed based on the control experiments Bergendahl (2004). Wagler (1994) and Chang (2000) also found that there was no removal of MTBE by aqueous $H_2O_2$. This suggests that in this system degradation of MTBE is due to oxidation by hydroxyl radicals. Also, no reaction between MTBE and ferrous iron was observed [Xu, 2004].

Hydroxyl radical production is initiated by the reaction of $Fe^{II}$ with hydrogen peroxide [Walling, 1973, 1975, Chen, 1997]. Ferrous iron can be introduced into the aqueous solution directly or they can be produced from the dissolution of $Fe^o$ by $H_2O_2$ as was described earlier. In either method, hydroxyl radicals were produced according to Reaction 14 (Table 2.1). In the coming paragraphs we will suggest a mechanism that will describe the experimental data that were used in the kinetic model. The suggested mechanism will be a simplified one since it did not include all the reaction pathways that were suggested by Stefan (2000).

Recent investigations have proposed that MTBE oxidative degradation by $^\bullet OH$ radicals follows two major pathways. Both pathways are initiated with hydrogen atom abstraction at either the methoxy group or any of the three equivalent methyl groups in the MTBE molecule leading to carbon centered radicals [Stefan, 2000; Wu, 2002, Neppolian, 2002; Chang, 2000]. These reactions are summarized in reactions 2.3.1 and 2.3.2. The different routes for the reaction of $^\bullet OH$ radical with MTBE were suggested based on fundamental studies of MTBE reactions with $^\bullet OH$ radicals [Eibenberger, 1980, Wu, 2002].

$$(CH_3)_3COCH_3 + {^\bullet OH} \xrightarrow{\alpha-abstraction \quad (71\%)} (CH_3)_3COCH_2^\bullet + H_2O \qquad 2.3.1$$

$$(CH_3)_3COCH_3 + {^\bullet OH} \xrightarrow{\beta-abstraction \quad (29\%)} {^\bullet CH_2}(CH_3)_2COCH_3 + H_2O \qquad 2.3.2$$

The branching ratio of reactions 2.3.1 and 2.3.2 was found to be 71:29 [Cooper, 2002; Eibenberger, 1980]. The higher ratio for reaction 2.3.1 due to that attack at the formyl group is more likely because of the charge distribution and electrophilic character of $^\bullet OH$ radicals [Stephan, 2000]. The rate constant for the reaction of $^\bullet OH$ radical with MTBE (k) has been reported in the literature at relatively close values. Hardison (2000)

reported a value of 2 x $10^9$ $M^{-1}$ $s^{-1}$. Another value of 1.6 x $10^9$ $M^{-1}$ $s^{-1}$ was given by Buxton (1988) in his review. Chang (2000) found a value 3.9 x $10^9$ $M^{-1}$ $s^{-1}$ based on calculations for experimental data from MTBE degradation using UV/$H_2O_2$.

The carbon centered radicals produced from reactions 2.3.1 and 2.3.2 were suggested to react with oxygen to form peroxyl radicals according to reactions 2.3.3 and 2.3.4, respectively [Stefan, 2000; Wu, 2002]:

$$(CH_3)_3COCH_2^\bullet + O_2 \rightarrow (CH_3)_3COCH_2O_2^\bullet \qquad 2.3.3$$

$$^\bullet CH_2(CH_3)_2COCH_3 + O_2 \rightarrow {}^\bullet O_2CH_2(CH_3)_2COCH_3 \qquad 2.3.4$$
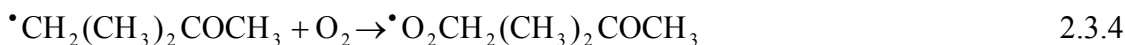
The carbon centered radicals generated in reactions 2.3.1 and 2.3.3 usually react with oxygen at diffusion-controlled rate constants (~$10^9$-$10^{10}$ $M^{-1}$ $s^{-1}$) generating peroxyl radicals [Stephan, 2000]. A value of 1.24 x $10^9$ $M^{-1}$ $s^{-1}$ was used by Cooper (2002) in simulating the kinetics of MTBE using the electron beam process for the destruction of MTBE for the rate constant in reaction 2.3.4. Hardison (2002) suggested a value of 1.24 x $10^9$ $M^{-1}$ $s^{-1}$ for the rate constant in reaction 2.3.3.

The peroxyl radicals, from reaction 2.3.3 and 2.3.4, undergo self recombination to produce a tetroxide intermediate, according to reactions 2.3.5 and 2.3.6, respectively [Wu, 2002, Stephan, 2000];

$$2(CH_3)_3COCH_2O_2^\bullet \rightarrow (CH_3)_3COCH_2 - O_4 - CH_2OC(CH_3)_3 \qquad 2.3.5$$

$$2^\bullet O_2CH_2(CH_3)_2COCH_3 \rightarrow CH_3O(CH_3)_2CCH_2 - O_4 - CH_2C(CH_3)_2OCH_3 \qquad 2.3.6$$
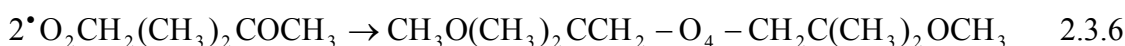
The value of the rate constants for reactions 2.3.5 and 2.3.6 was chosen as 1.0 x $10^9$ $M^{-1}$ $s^{-1}$ by Hardison [2002]. When the rate constant was reduced to $10^6$ $M^{-1}$ $s^{-1}$ it didn't affect the results significantly. The value used for this rate constant was $10^9$ $M^{-1}$ $s^{-1}$.

The tetroxide intermediate produced in reactions 2.3.5 and 2.3.6 can decompose by different routes to give a variety of products [Wu, 2002, Stephan, 2000, Hardison, 2002, Cooper, 2002].

One possible route for tetroxide (produced in reaction 2.3.5) decay is given by the following reaction [Wu, 2002; Stephan, 2000; Hardison, 2002]

$$(CH_3)_3COCH_2 - O_4 - CH_2OC(CH_3)_3 \rightarrow 2^{\bullet}OCH_2 - O - C(CH_3)_3 + O_2$$
$$(R_{11}) \qquad\qquad\qquad\qquad (2R_{12})$$
<div align="right">2.3.7</div>
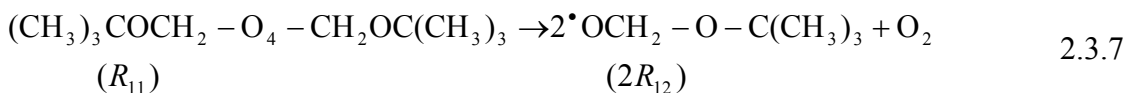
Another possible route for tetroxide decompositions is [Stephan, 2000; Hardison, 2002]:

$$(CH_3)_3COCH_2 - O_4 - CH_2OC(CH_3)_3 \rightarrow 2(CH_3)_3COCHO + H_2O_2$$
$$(R_{11}) \qquad\qquad\qquad\qquad (TBF)$$
<div align="right">2.3.8</div>
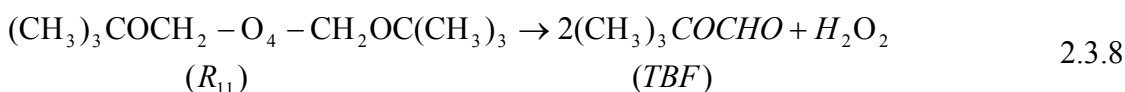
Hardison (2002) used a value of 6 x $10^6$ s$^{-1}$ for the rate constant in reactions 2.3.7.and 2.3.8. Varying both tetroxide formation and decay rate constants by several orders of magnitude had no impact on the removal of MTBE predicted by the kinetic model [Hardison, 2002]. The branching ratio of reactions 2.3.7 and 2.3.8 had been optimized in this model and it was found that almost 38 % of the tetroxide goes through reaction 2.3.7. Cooper (2004) suggested a value of 42-50 % based on the product distribution of experimental data.

The radical produced from reaction 2.3.7 goes through disproportionation according to the following reaction producing tert-butyl formate (TBF) and hemi-acetal [Wu, 2002, Stephan, 2000]

$$2^{\bullet}OCH_2 - O - C(CH_3)_3 \rightarrow (CH_3)_3COCHO + HOCH_2 - O - C(CH_3)_3$$
$$TBF$$
<div align="right">2.3.9</div>
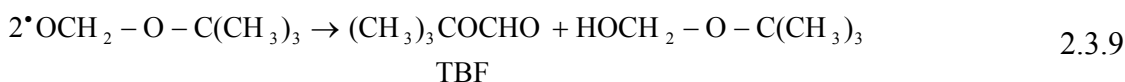
Hardsion [2002] found that a value of 1.0 x $10^9$ M$^{-1}$ s$^{-1}$ for the rate constant in reaction 2.3.9 gives a good fit of the model to the experimental data. Then the hemi-acetal will hydrolyze to formaldehyde (F) and tert-butyl alcohol (TBA) [Wu, 2002, Stephan, 2000]:

$$HOCH_2 - O - C(CH_3)_3 + H_2O \rightarrow HOC(CH_3)_3 + CH_2O$$
$$\qquad\qquad\qquad\qquad\qquad TBA \qquad\quad F$$

2.3.10
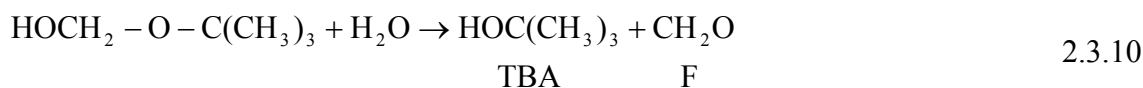
Rate constant for the above reaction was not available directly, however Cooper (2002) suggested a rate constant of 1.0 x $10^{10}$ M$^{-1}$ s$^{-1}$ for hydrolysis of TBA-oxygen radical.

The formation of acetone from MTBE degradation might occur through different routes. The first route was derived from a mechanism suggested by Wu (2002). In this route TBF will first react with an $^\bullet OH$ radical to form a relatively inert 2-methyl-2-propanol radical and water according to the following reaction [Hardison, 2002, Buxton, 1988].

$$TBF + ^\bullet OH \rightarrow (CH_3)_3 CO\overset{\bullet}{C}O + H_2O$$

2.3.11

The rate constant for the reaction of TBF with $^\bullet OH$ radical has been reported in several studies. Hardison (2002) investigated the kinetics of degradation of TBF using radiation chemical techniques and found a value of 5.23 x $10^8$ M$^{-1}$ s$^{-1}$. Another value of 4.1 x $10^8$ M$^{-1}$ s$^{-1}$ was reported by Onstein (1999). The value used in the simulation was 3.1 x $10^8$ M$^{-1}$ s$^{-1}$ based on best fitting of model to experimental data.

The radical produced in reaction 2.3.11 can further react with O$_2$ according to the following reaction [Wu, 2002]:

$$(CH_3)_3 CO\overset{\bullet}{C}O + 0.5O_2 \rightarrow ^\bullet OC(CH_3)_3 + CO_2$$

2.3.12

Similar to the reactions of the other radicals with oxygen in this system a value of $1.0 \times 10^9$ M$^{-1}$ s$^{-1}$ was assigned to reaction 2.3.12. The *tert*-butoxy radical produced in reaction 2.3.12 can decompose to produce acetone and another radical [Wu, 2002, Cooper, 2004]:

$$^{\bullet}OC(CH_3)_3 \rightarrow OC(CH_3)_2 + CH_3^{\bullet}$$
$$\text{Acetone}$$

2.3.13

The *tert*-butoxy radicals decompose to give acetone and a methyl radical with a first order rate constant of between $10^6 - 10^7$ s$^{-1}$ [Cooper, 2004]. The used value in this model was $10^6$ s$^{-1}$.

Another possible reaction for tert-butoxy radical can produce formaldehyde and another product according to the following reaction:

$$^{\bullet}OC(CH_3)_3 \xrightarrow{\ H2O\ } HCOH + product$$

2.3.14

It was assumed that the branching ratio between reactions 2.3.13 and 2.3.14 was 0.55 to 0.45 considering that both reactions proceed at the same speed based on best fitting of model.

The methyl radical produced in reaction 2.3.13 can be oxidized further by oxygen to form formaldehyde according to the following reaction [Hardison, 2002]:

$$CH_3^{\bullet} + 0.5O_2 \rightarrow CH_2O$$

2.3.15

Reaction 2.3.15 was given a rate constant value of $1.0 \times 10^9$ M$^{-1}$ s$^{-1}$ in analogy to the reactions of the other carbon radicals with oxygen in this system.

Another possible route for acetone in this system is based on reaction 2.3.6. One possible route for tetroxide (produced in reaction 2.3.6) decay is given by the following reaction [Wu, 2002; Stephan, 2000; Hardison, 2002]:

$$(CH_3)_3COCH_2 - O_4 - CH_2OC(CH_3)_3 \rightarrow 2CH_3O(CH_3)_2CCH_2O^\bullet + O_2 \qquad \text{2.3.16}$$

The rate constant for this reaction was not provided but it can be assumed as 1 x $10^6\,s^{-1}$ analogous to reaction 2.3.7. The radical produced from reaction 2.3.16 could lose a formaldehyde molecule producing a new radical according to the following reaction [Stephan, 2000, Hardison, 2002]:

$$CH_3O(CH_3)_2CCH_2O^\bullet \rightarrow {}^\bullet C - (CH_3)_2OCH_3 + CH_2O \qquad \text{2.3.17}$$
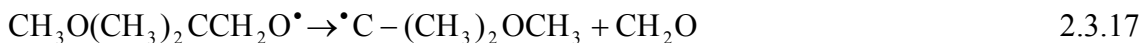
The radical produced in reaction 2.3.17 will react with oxygen according to equation 2.3.18. Then the produced radicals go through two different reactions to produce acetone and methyl acetate according to reactions 2.3.18 and 2.3.19 [Stephan, 2000, Wu, 2002]. The rate constant of reaction 2.3.17 was assigned a value of 1.0 x $10^9\,M^{-1}\,s^{-1}$ analogous to reaction 2.3.9. Also the rate constants for reactions 2.3.19 and 2.3.20 were taken as 1.0 x $10^6\,M^{-1}\,s^{-1}$ similar to reaction 2.3.13.

$${}^\bullet C - O(CH_3)_3 + 0.5O_2 \rightarrow {}^\bullet OC - O(CH_3)_3 \qquad \text{2.3.18}$$

$${}^\bullet OC - O(CH_3)_3 \rightarrow OC(CH_3)_2 + CH_3O^\bullet \qquad \text{2.3.19}$$
$$\textit{Acetone}$$

$${}^\bullet OC - O(CH_3)_3 \rightarrow OC - O(CH_3)_2 + CH_3^\bullet \qquad \text{2.3.20}$$
$$\text{Methyl \quad Acetate}$$
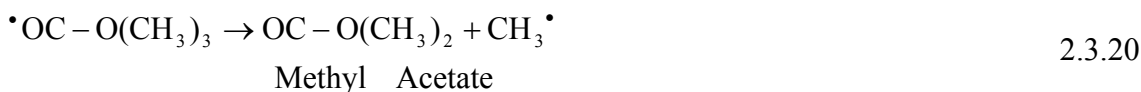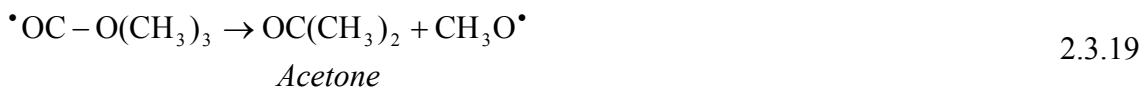
The produced radical in reaction 2.3.19 was assumed to go through reaction 2.3.21 and then the product of this reaction will go through another reaction that will give methyl acetate as one possible product.

$$CH_3O^\bullet \xrightarrow{H2O} R \qquad \text{2.3.21}$$

$$R \rightarrow \text{Methyl \quad Acetate} \qquad \text{2.3.22}$$

TBA, acetone, methyl acetate and F react with $^{\bullet}OH$ radicals according to the following reactions [Buxton, 1988; Cooper, 2002]:

$$CH_2O + {}^{\bullet}OH \rightarrow HCO_2H$$
$$(FA)$$
2.3.23

$$HCO_2H + {}^{\bullet}OH \rightarrow CO_2$$
2.3.24

$$Acetone + {}^{\bullet}OH \rightarrow CO_2 + produtcs$$
2.3.25

$$Methyl\,Acetate + {}^{\bullet}OH \rightarrow CO_2 + produtcs$$
2.3.26

The values of the rate constants for reactions 2.3.23, 2.3.24, 2.3.25, and 2.3.26 are $1 \times 10^9\ M^{-1}s^{-1}$, $1.3 \times 10^8\ M^{-1}s^{-1}$, $1.1 \times 10^8\ M^{-1}s^{-1}$, and $1.2 \times 10^8\ M^{-1}s^{-1}$, respectively [Buxton, 1988; Cooper, 2002, Cooper, 2004].

Formic acid ($HCO_2H$) and formate ions ($HCO_2^-$) are related through the following equilibrium [Neta, 1996; Cooper, 2004]:

$$HCO_2H \xleftarrow{\ pKa=3.75\ } HCO_2^- + H^+$$
2.3.27

Formate ion will also react with hydroxyl radical according to the following reaction [Buxton, 1988; Thomas, 1965; Wilson, 1971]:

$$HCO_2^- + {}^{\bullet}OH \rightarrow {}^{\bullet}CO_2^- + H_2O$$
2.3.28

Rate constant for the formate ion reaction with the hydroxyl radical was taken as $4.1 \times 10^9\ M^{-1}s^{-1}$ [Buxton, 1988].

## 2.4. Kinetic model equations

The proposed elementary reactions for MTBE degradation in Table 4.1 have been derived based on different investigations that studied MTBE degradation by hydroxyl

radicals [De Laat, 1999; Cooper, 2002, Wu, 2002, Hardison, 2002, Cooper, 2004, Stefan, 2000, Chang, 2000, Crittenden , 1999; Chen, 1997; Gallard, 2000].

A completely mixed constant volume batch reactor was used in running the experiments. Therefore, a mass balance was applied for a batch reactor model. The mass balance of species i at any time will be given by the following ordinary differential equation:

$$\frac{dC_i}{dt} = r_i$$

which describes the change of species i concentration as a function of time starting with initial concentration $C_{io}$ in a completely mixed batch reactor in a liquid solution.

Substituting each species in Table 4.1 into this equation, with the proposed reactions proportions that were suggested in section 2.3, a set of ordinary nonlinear differential equations that describe the rates of changes in the concentration of each species with respect to time was obtained.

$H_2O_2$ is a weak acid with a dissociation constant ($pK_a$) of 11.65 [Buxton, Dean, 1979] and its dissociation is given by:

$$H_2O_2 \leftrightarrow H^+ + HO_2^-$$
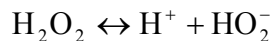
then the total hydrogen peroxide concentration is given by:

$$[H_2O_2]_T = [H_2O_2] + [HO_2^-] = [H_2O_2] + \frac{K_{12}}{[H^+]}[H_2O_2] = [H_2O_2](1 + \frac{K_{12}}{[H^+]})$$

and the concentration of the conjugate base of hydrogen peroxide is given by:

$$HO_2^- = \frac{K_{12}[H_2O_2]}{[H^+]}$$

404

where $K_{12}$ is the equilibrium constant for $H_2O_2$ dissociation. The following differential equations describe the change of the concentration of the different species in this system.

Hydrogen peroxide ($H_2O_{2T}$):

$$\frac{d[H_2O_{2T}]}{dt} = -k_1[H_2O_2][^\bullet OH] + k_2[HO_2^\bullet][O_2^{\bullet -}] + k_5[^\bullet OH][^\bullet OH] + k_6[HO_2^\bullet][HO_2^\bullet]$$
$$- k_9[H_2O_2]_T[O_2^{\bullet -}] - k_{10}[H_2O_2]_T[HO_2^\bullet] - k_{11}[HO_2^-][^\bullet OH] - k_{13}[H_2O_2]_T$$
$$- k_{14}[H_2O_2]_T[Fe^{2+}] - k_{16}[[H_2O_2]_T[Fe^{II}OH^+] - k_{25}[Fe^{III}][H_2O_2] + 0.65k_{38}[R_{11}]$$

Hydroxyl radical ($^\bullet OH$):

$$\frac{d[^\bullet OH]}{dt} = -k_1[H_2O_2][^\bullet OH] - k_3[^\bullet OH][HO_2^\bullet] - k_4[^\bullet OH][O_2^{\bullet -}] - 2k_5[^\bullet OH][^\bullet OH]$$
$$+ k_9[H_2O_2]_T[O_2^{\bullet -}] + k_{10}[H_2O_2]_T[HO_2^\bullet] - k_{11}[^\bullet OH][HO_2^-] + k_{14}[H_2O_2]_T[Fe^{2+}]$$
$$+ k_{16}[[H_2O_2]_T[Fe^{II}OH^+] - k_{17}[[^\bullet OH][Fe^{II}] - (0.71k_{32} + 0.29k_{33})[MTBE][^\bullet OH]$$
$$- k_{41}[TBF][^\bullet OH] - k_{45}[F][^\bullet OH] - k_{46}[FA][^\bullet OH] - k_{47}[Acetone][^\bullet OH]$$
$$- k_{48}[TBA][^\bullet OH] - k_{54}[MA][^\bullet OH] - k_{58}[HCO_2^-][^\bullet OH]$$

Hydroperoxyl radical ($HO_2^\bullet$):

$$\frac{d[HO_2^\bullet]}{dt} = k_1[H_2O_2][^\bullet OH] - k_2[HO_2^\bullet][O_2^{\bullet -}] - k_3[^\bullet OH][HO_2^\bullet] - 2k_6[HO_2^\bullet][HO_2^\bullet]$$
$$+ k_7[O_2^{\bullet -}][H^+] - k_8[HO_2^\bullet] - k_{10}[H_2O_2]_T[HO_2^\bullet] + k_{11}[^\bullet OH][HO_2^-]$$
$$- k_{18}[Fe^{II}][HO_2^\bullet] - k_{20}[Fe^{III}][HO_2^\bullet] + k_{25}[Fe^{III}][H_2O_2]_T$$

Superoxide radical anion ($O_2^{\bullet -}$):

$$\frac{d[O_2^{\bullet -}]}{dt} = -k_2[HO_2^\bullet][O_2^{\bullet -}] - k_4[^\bullet OH][O_2^{\bullet -}] - k_7[O_2^{\bullet -}][H^+] + k_8[HO_2^\bullet] - k_9[H_2O_2]_T[O_2^{\bullet -}]$$
$$- k_{19}[Fe^{II}][O_2^{\bullet -}] - k_{21}[Fe^{III}][O_2^{\bullet -}]$$

Zero-valent Iron ($Fe^0$) dissolution:

$$\frac{dFe^0}{dt} = -k_{13}[H_2O_2]_T$$

Aqueous ferrous ion ($Fe^{II}$):

$$\frac{d[Fe^{II}]}{dt} = k_{13}[H_2O_2]_T - k_{14}[H_2O_2]_T[Fe^{2+}] - k_{16}[[H_2O_2]_T[Fe^{II}OH^+]$$

$$- k_{17}[[^\bullet OH][Fe^{II}] - k_{18}[[HO_2^\bullet][Fe^{II}] - k_{19}[O_2^{\bullet-}][Fe^{II}] + k_{20}[[HO_2^\bullet][Fe^{III}]$$

$$+ k_{21}[O_2^{\bullet-}][Fe^{III}] + k_{25}[Fe^{III}][H_2O_2]_T$$

with $[Fe^{II}] = [Fe^{2+}] + [Fe^{II}OH^+] = [Fe^{2+}](1 + \frac{K_{15}}{[H^+]})$

Total aqueous ferric ion ($Fe(III)_T$):

$$\frac{d[Fe(III)_T]}{dt} = k_{14}[H_2O_2]_T[Fe^{2+}] + k_{16}[[H_2O_2]_T[Fe^{II}OH^+] + k_{17}[[^\bullet OH][Fe^{II}]$$

$$+ k_{18}[[HO_2^\bullet][Fe^{II}] + k_{19}[O_2^{\bullet-}][Fe^{II}] - k_{20}[[HO_2^\bullet][Fe^{III}] - k_{21}[O_2^{\bullet-}][Fe^{III}]$$

$$- k_{25}[Fe^{III}][H_2O_2]_T - 2k_{31}[Fe^{III}(HO)_3][Fe^{III}(HO)_3]$$

Methyl tert-butyl ether (MTBE):

$$\frac{dMTBE}{dt} = -(0.71k_{32} + 0.29k_{33})[MTBE][^\bullet OH]$$

Table 4.2 gives the differential equations that describe the reaction that follow MTBE oxidation by $^\bullet OH$ radical. The nomenclatures that were used in Table 4.2 for the name of the molecule and in the differential equations were given in Table 4.1.

**Table 4.2:** The differential equations for the change of concentration of the different products from MTBE and $^\bullet$OH radicals reaction with respect to time

| Molecule | Differential equation |
|---|---|
| $MTBE_1^\bullet$ | $\dfrac{d[MTBE_1^\bullet]}{dt} = 0.71k_{32}[MTBE][^\bullet OH] - k_{34}[MTBE_1^\bullet][O_2]$ |
| $MTBE_1O_2^\bullet$ | $\dfrac{d[MTBE_1O_2^\bullet]}{dt} = k_{34}[MTBE_1^\bullet][O_2] - 2k_{36}[MTBE_1O_2^\bullet][MTBE_1O_2^\bullet]$ |
| $R_1$ | $\dfrac{d[R_1]}{dt} = k_{36}[MTBE_1O_2^\bullet][MTBE_1O_2^\bullet] - k_{38}[R_1]$ |
| $R_3$ | $\dfrac{d[R_3]}{dt} = 2 * 0.38k_{38}[R_1] - 2k_{39}[R_3][R_3]$ |
| $R_4$ | $\dfrac{d[R_4]}{dt} = k_{39}[R_3][R_3] - k_{40}[R_4]$ |
| $R_5$ | $\dfrac{d[R_5]}{dt} = k_{41}[TBF][^\bullet OH] - k_{42}[R_5][O_2]$ |
| $R_6$ | $\dfrac{d[R_6]}{dt} = k_{42}[R_5][O_2] - k_{43}[R_6]$ |
| $R_7$ | $\dfrac{d[R_7]}{dt} = 0.55k_{43}[R_6] - k_{44}[R_7][O_2] + k_{53}[R_{10}]$ |
| TBF | $\dfrac{d[TBF]}{dt} = k_{39}[R_3][R_3] + 2 * 0.62k_{38}[R_1] - k_{41}[TBF][^\bullet OH]$ |
| TBA | $\dfrac{d[TBA]}{dt} = k_{40}[R_4] - k_{48}[TBA][^\bullet OH]$ |
| Acetone | $\dfrac{d[Acetone]}{dt} = 0.55k_{43}[R_6] - k_{47}[Acetone][^\bullet OH] + k_{52}[R_{10}]$ |
| F | $\dfrac{d[F]}{dt} = k_{40}[R_4] + k_{44}[R_7][O_2] - k_{45}[F][^\bullet OH] + 0.45k_{43}[R_6] + k_{50}[R_8]$ |
| FA | $\dfrac{d[FA]}{dt} = k_{45}[F][^\bullet OH] - k_{46}[FA][^\bullet OH]$ |

| | |
|---|---|
| $MTBE_2^{\bullet}$ | $\dfrac{d[MTBE_2^{\bullet}]}{dt} = 0.29k_{33}[MTBE][^{\bullet}OH] - k_{35}[MTBE_2^{\bullet}][O_2]$ |
| $MTBE_2O_2^{\bullet}$ | $\dfrac{d[MTBE_2O_2^{\bullet}]}{dt} = k_{35}[MTBE_2^{\bullet}][O_2] - 2k_{37}[MTBE_2O_2^{\bullet}][MTBE_2O_2^{\bullet}]$ |
| $R_2$ | $\dfrac{d[R_2]}{dt} = k_{37}[MTBE_2O_2^{\bullet}][MTBE_2O_2^{\bullet}] - k_{49}[R_2]$ |
| $R_8$ | $\dfrac{d[R_8]}{dt} = 2k_{49}[R_2] - k_{50}[R_8]$ |
| $R_9$ | $\dfrac{d[R_9]}{dt} = k_{50}[R_8] - k_{51}[R_9][O_2]$ |
| $R_{10}$ | $\dfrac{d[R_{10}]}{dt} = k_{51}[R_9][O_2] - k_{52}[R_{10}] - k_{53}[R_{10}]$ |
| Methyl Acetate (MA) | $\dfrac{d[MA]}{dt} = k_{53}[R_{10}] - k_{54}[MA][^{\bullet}OH] + k_{60}[R]$ |

The initial $O_2$ level in water was 8.5 mg/L ( $2.64 \times 10^{-4}$ M) from direct equilibrium with the atmosphere at 1 atm and 25 °C, ($pO_2$= 0.21 atm, $k_H$= $10^{-2.9}$ M atm$^{-1}$) [Pankow, 1991; Gallard, 2001]. This would explain the source of $O_2$ required for performing the oxidation reactions that were outlined in Table 4.1. Stephan (2000) measured comparable levels of $O_2$ in his reaction mixture. In Xu's work (2004) the initial level of oxygen was about 9.8 mg/L.

Aqueous Oxygen ($O_{2(aq)}$):

$$\frac{\mathrm{d}[O_{2(aq)}]}{\mathrm{dt}} = k_2[HO_2^\bullet][O_2^{\bullet-}] + k_3[HO_2^\bullet][^\bullet OH] + k_4[O_2^{\bullet-}][^\bullet OH] + k_6[HO_2^\bullet][HO_2^\bullet] +$$

$$k_9[O_2^{\bullet-}][H_2O_2]_T + k_{20}[Fe^{III}][HO_2^\bullet] + k_{21}[Fe^{III}][O_2^{\bullet-}] - k_{34}[MTBE_1^\bullet][O_2] -$$

$$k_{35}[MTBE_2^\bullet][O_2] + 0.38k_{38}[R_1] - 0.5k_{42}[R_5][O_2] - 0.5k_{44}[R_7][O_2]$$

$$+ k_{49}[R_2] - 0.5k_{51}[R_9][O_2]$$

The above system of the stiff nonlinear ordinary differential equations was solved numerically using Matlab (R13) program developed by Math Works Inc. For this, the process parameters time (t), pH, initial concentration of $H_2O_2$ ($[H_2O_2]_0$) and MTBE ($[MTBE]_0$), and ferrous ion $[Fe^{II}]$ were specified as inputs to the program. Initial concentration of all radicals was taken as zero. The reaction rate constants along with the equilibrium constants presented in Table 2.1 were also used as input to the program.

The rate constant for the reaction between methyl acetate and $^\bullet OH$ radicals was $2.5 \times 10^8$ $M^{-1}$ $s^{-1}$ compared to the reported value which was $2.2 \times 10^8$ $M^{-1}$ $s^{-1}$. It can be seen from Table 4.2, for example, for Reaction 58 that for the same compound there are several reported values (with in the same order of magnitude) for the rate constant for the reaction with hydroxyl radical. Therefore it is expected that there might be a difference in these rate constants since in measuring any rate constant certain conditions should be applied and these conditions might not be exactly the same between one study and another. For the same reasoning the value of the rate constant for the reaction of $^\bullet OH$ with tert-butyl alcohol (TBA) was $2 \times 10^8$ $M^{-1}$ $s^{-1}$ compared to reported one value of value $6 \times 10^8$ $M^{-1}$ $s^{-1}$.

## 2.5. Sensitivity analysis

In order to examine the sensitivity of the model to variations in a particular rate constant, the square of the residual between the original (control) model output and the

perturbed model output was calculated. The sum of the squares of the residual (SSR) was calculated from the following relation [Waite, 1998]:

$$SSR = \sum \frac{(m_i - p_i)^2}{m_i}$$

2.5.1

where $m_i$ is the predicted concentration of species i from the control model and $p_i$ is the concentration of species i in the perturbed model. This analysis was performed over a certain time and for the data of Xu (2004) this time was 420 min which is the time by which MTBE is completely degraded at the conditions of the control model.

## 3. Results

### 3.1. Simulation of experimental data of Xu (2004)

The kinetic model was used to simulate a set of experimental data reported by Xu et al (2004). In these data the remediation of methyl tert-butyl ether (MTBE) was studied using hydrogen peroxide ($H_2O_2$) and ferrous iron at acidic aqueous solution (pH = 2.8) using a batch reactor. In this study byproducts concentrations were observed and quantified. The main byproducts which were detected in this work were acetone, tert-butyl alcohol (TBA), tert-butyl formate (TBF) and methyl acetate (MA). The starting concentration of MTBE was 1 mM oxidized using aqueous solution of $H_2O_2$ at 15 mM and in presence of 2 mM ferrous iron ($Fe^{2+}$).

Figure 4.1 shows the results of model predictions and experimental data for MTBE concentration with time. Model simulations and experimental data shows that MTBE degradation reduced very fast and then a relatively slower degradation of MTBE took place, as can be seen from Figure 4.1, which will be discussed later. The results of the simulations and experimental data for the byproducts formation from MTBE degradations are shown in Figures 4.2 through 4.6. Figure 4.2 shows TBF from experimental data and model simulations. The predicted concentrations of TBA along with the experimental data are shown in Figure 4.3. Figure 4.3 shows the predicted and experimental concentrations of MA. The predicted and experimental concentrations of acetone are shown in Figure 4.4. Predicted concentration of formaldehyde and hydrogen peroxide are shown in Figures 4.5 and 4.6, respectively.

411
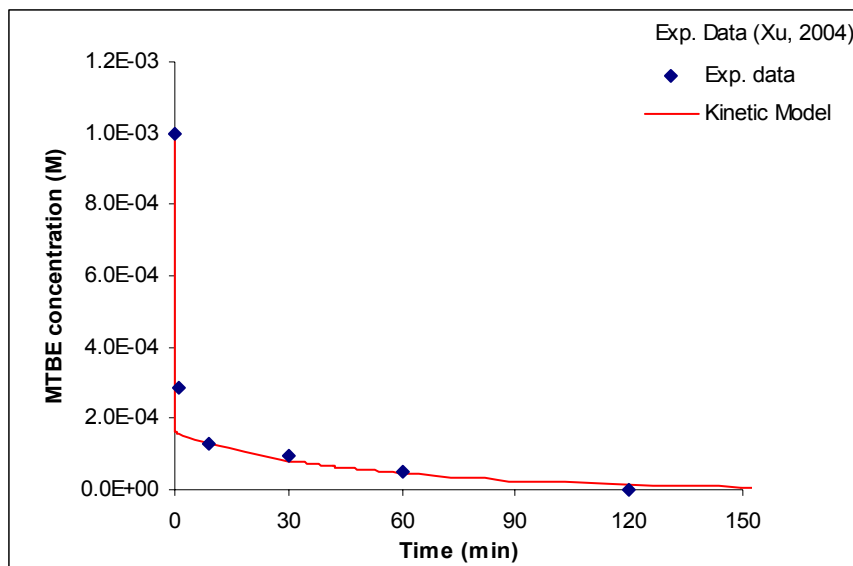
**Fig. 4.1**: Predicted concentration of MTBE from kinetic model and MTBE concentration from experimental data vs. time applying Fenton's treatment. Initial conditions: $[MTBE]_o = 1$ mM, $[Fe^{II}]_o = 2$ mM, $[H_2O_2]_o = 0.015$ mM, pH = 2.8
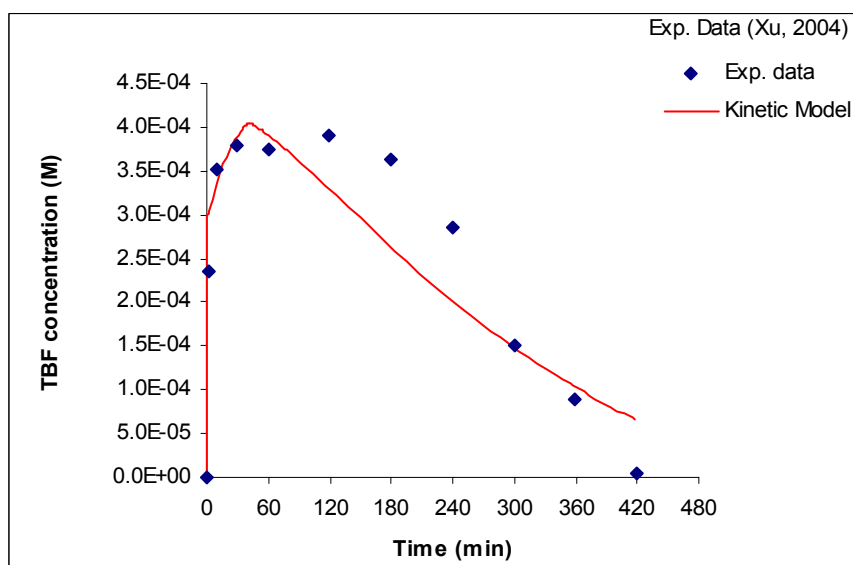


**Fig. 4.2:** Predicted concentration of tert-butyl formate (TBF) from kinetic model and TBF concentration from experimental data vs. time applying Fenton's treatment. Initial conditions: $[MTBE]_o = 1$ mM, $[Fe^{II}]_o = 2$ mM, $[H_2O_2]_o = 0.015$ mM, pH = 2.8
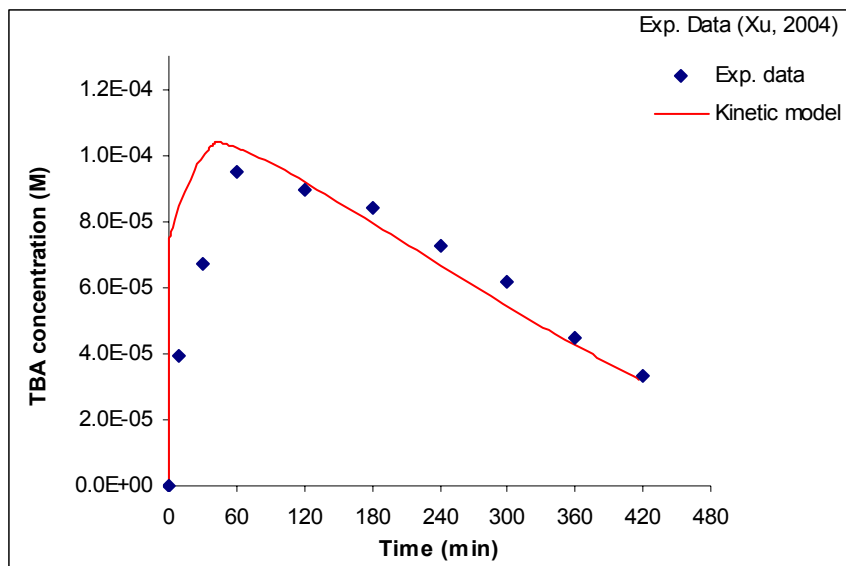
**Fig. 4.3:** Predicted concentration of tert-butyl alcohol (TBA) from kinetic model and TBA concentration from experimental data vs. time applying Fenton's treatment. Initial conditions: $[MTBE]_o = 1$ mM, $[Fe^{II}]_o = 2$ mM, $[H_2O_2]_o = 0.015$ mM, pH = 2.8
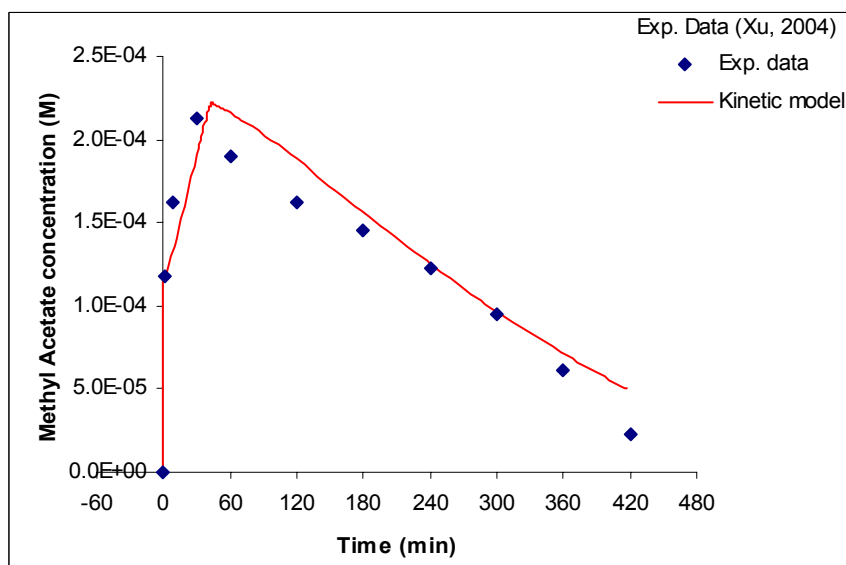


**Fig. 4.4:** Predicted concentration of methyl acetate (MA) from kinetic model and MA concentration from experimental data vs. time applying Fenton's treatment. Initial conditions: $[MTBE]_o = 1$ mM, $[Fe^{II}]_o = 2$ mM, $[H_2O_2]_o = 0.015$ mM, pH = 2.8
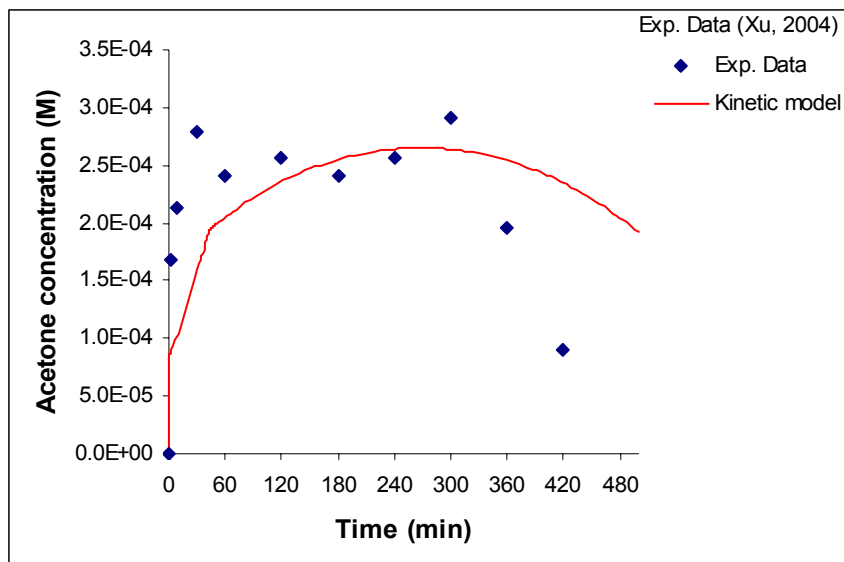
**Fig. 4.5:** Predicted concentration of acetone from kinetic model and acetone concentration from experimental data vs. time applying Fenton's treatment. Initial conditions: $[MTBE]_o = 1$ mM, $[Fe^{II}]_o = 2$ mM, $[H_2O_2]_o = 0.015$ mM, pH = 2.8
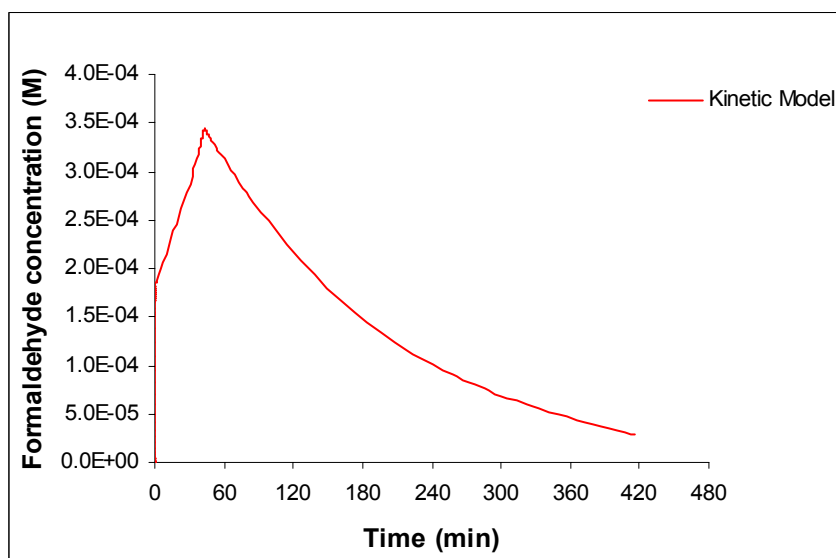


**Fig. 4.6:** Predicted concentration of formaldehyde (F) from simulations vs. time applying Fenton's treatment. Initial conditions: $[MTBE]_o = 1$ mM, $[Fe^{II}]_o = 2$ mM, $[H_2O_2]_o = 0.015$ mM, pH = 2.8

414
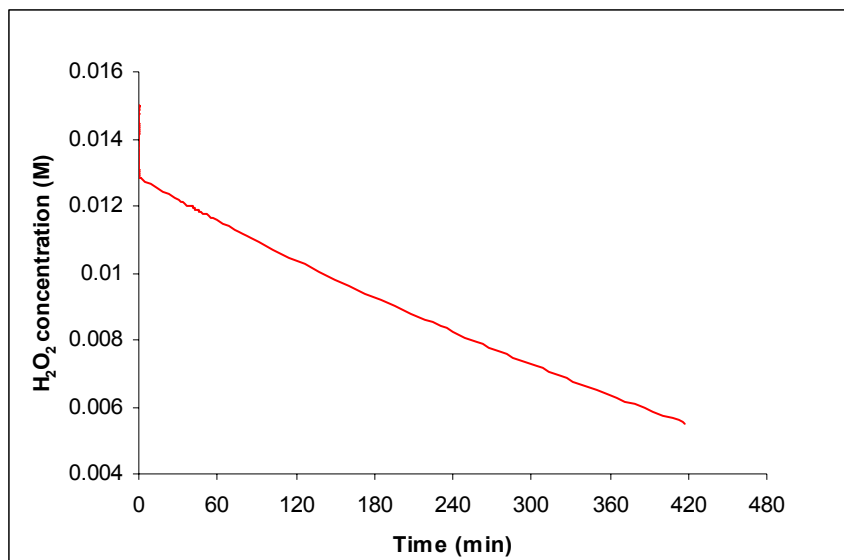
**Fig. 4.7:** Predicted concentration of $H_2O_2$ from simulations vs. time applying Fenton's treatment. Initial conditions: $[MTBE]_o = 1$ mM, $[Fe^{II}]_o = 2$ mM, $[H_2O_2]_o = 0.015$ mM, pH = 2.8

### 3.1.1. Sensitivity analysis

The results of the sensitivity analysis, which was performed by perturbing the value of the rate constant (by one order of magnitude increase or decease) for the reaction of interest in Table 4.1 and keeping the values for the other rate constants constant, are shown in Figures 4.8 through 4.11 for MTBE and its by products. Sensitivity analysis of MTBE show a dominance of certain reaction steps on MTBE degradation as can be seen from Figure 4.8. The sensitivity analysis for the byproducts, as can be seen from Figure 4.9 through 4.11, shows a similar trend. These results will be discussed in more detail in the discussion section.
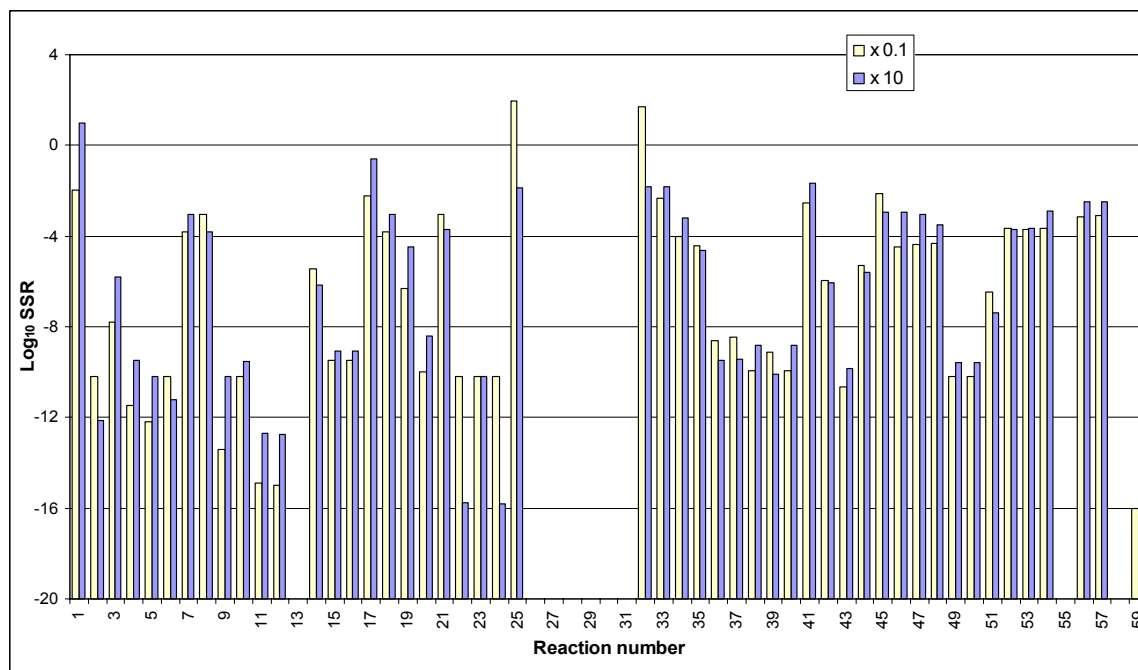
**Fig. 4.8:** Log sum of squares of the residuals ($Log_{10}$ SSR) for order of magnitude (increase and decrease) perturbation of each rate constant for the MTBE concentration. Initial conditions: $[MTBE]_o = 1$ mM, $[H_2O_2]_o = 15$ mM, $[Fe^{II}]_o = 2$ mM, pH = 2.8
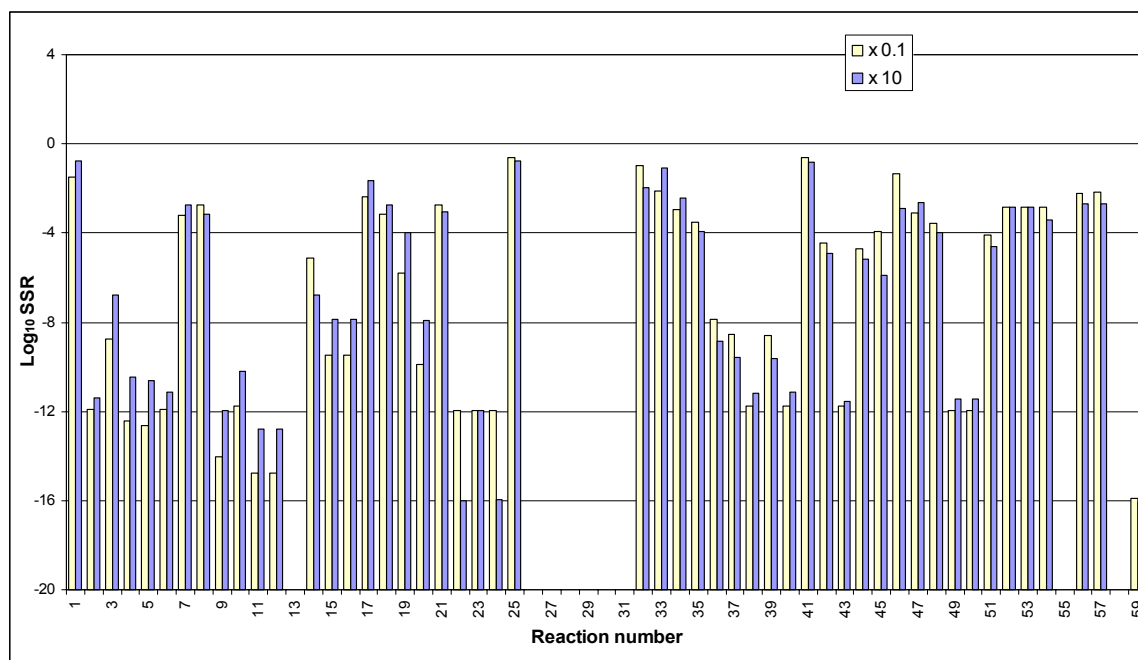


**Fig. 4.9:** Log sum of squares of the residuals ($Log_{10}$ SSR) for order of magnitude (increase and decrease) perturbation of each rate constant for the TBF concentration. Initial conditions: $[MTBE]_o = 1$ mM, $[H_2O_2]_o = 15$ mM, $[Fe^{II}]_o = 2$ mM, pH = 2.8

416
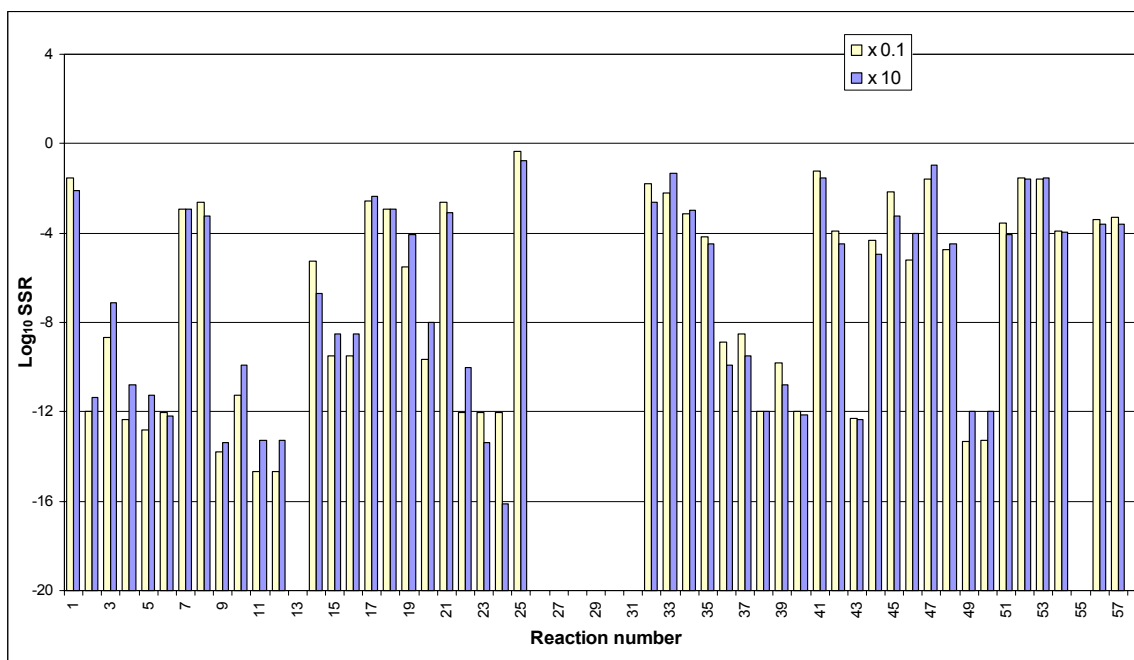
**Fig. 4.10:** Log sum of squares of the residuals ($\text{Log}_{10}$ SSR) for order of magnitude (increase and decrease) perturbation of each rate constant for the acetone concentration. Initial conditions: $[\text{MTBE}]_o = 1$ mM, $[\text{H}_2\text{O}_2]_o = 15$ mM, $[\text{Fe}^{\text{II}}]_o = 2$ mM, pH = 2.8
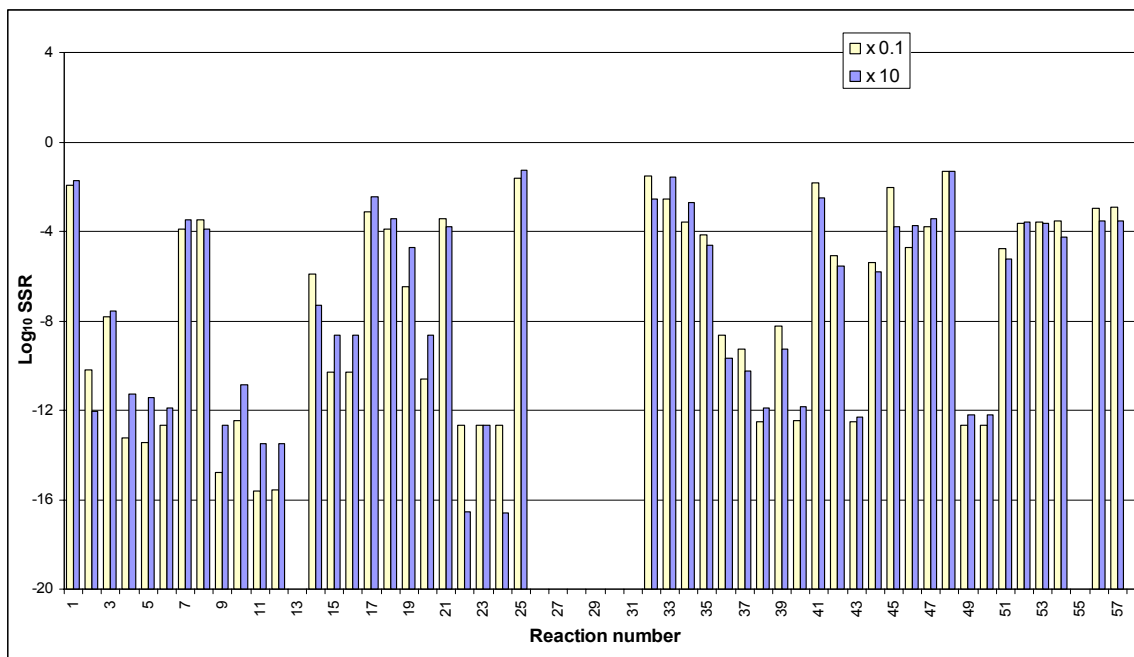


**Fig. 4.11:** Log sum of squares of the residuals ($\text{Log}_{10}$ SSR) for order of magnitude (increase and decrease) perturbation of each rate constant for the TBA concentration. Initial conditions: $[\text{MTBE}]_o = 1$ mM, $[\text{H}_2\text{O}_2]_o = 15$ mM, $[\text{Fe}^{\text{II}}]_o = 2$ mM, pH = 2.8
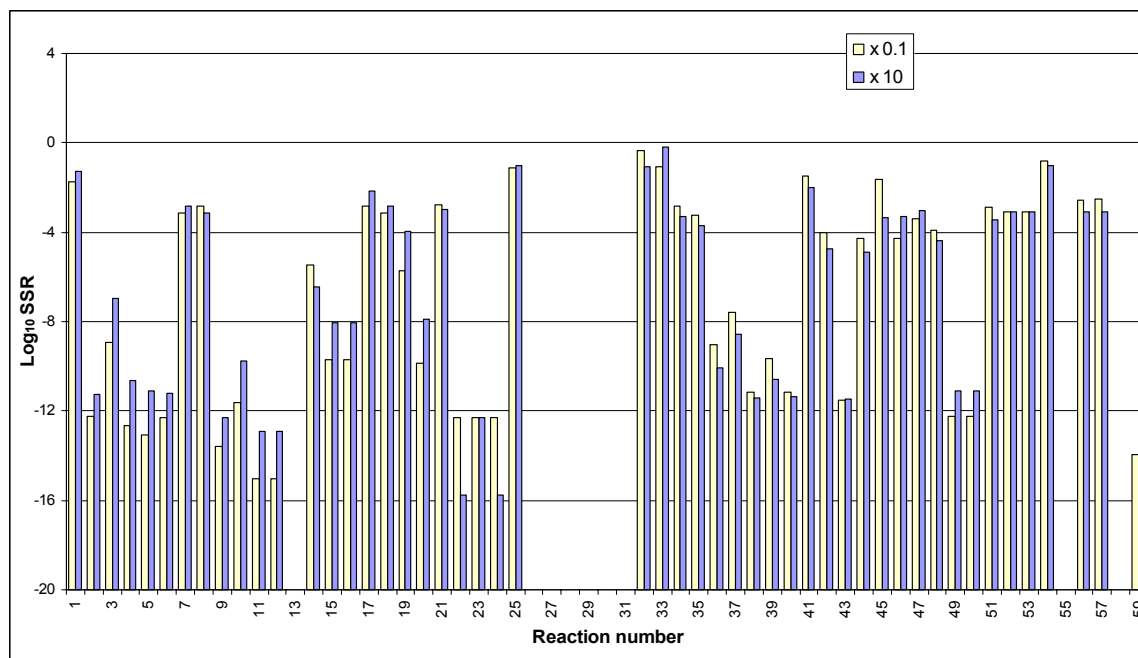
**Fig. 4.12:** Log sum of squares of the residuals (Log$_{10}$ SSR) for order of magnitude (increase and decrease) perturbation of each rate constant for the MA concentration. Initial conditions: $[MTBE]_o = 1$ mM, $[H_2O_2]_o = 15$ mM, $[Fe^{II}]_o = 2$ mM, pH = 2.8

### 3.1.2. Effect of Ferrous iron (Fe$^{II}$) on MTBE removal

Experimental and simulations results for the effect of initial ferrous iron concentration on MTBE removal is shown in Figure 4.13 for the experimental conditions of 1mM MTBE, 10 mM H$_2$O$_2$, and pH = 2.8 at the various initial concentrations of the ferrous iron. In one runs of the model simulations the rate constants for the reaction between ferric iron and H$_2$O$_2$ (k$_{25}$) was 0.0032 M$^{-1}$ s$^{-1}$, which was similar to the value that was used in all other simulations of this chapter. The agreement between the model and the experimental data improved as the initial concentration of Fe$^{II}$ was increased. Increasing k$_{25}$ to 0.007 M$^{-1}$ s$^{-1}$, slightly affected the model predictions. These findings will be discussed further later.

418
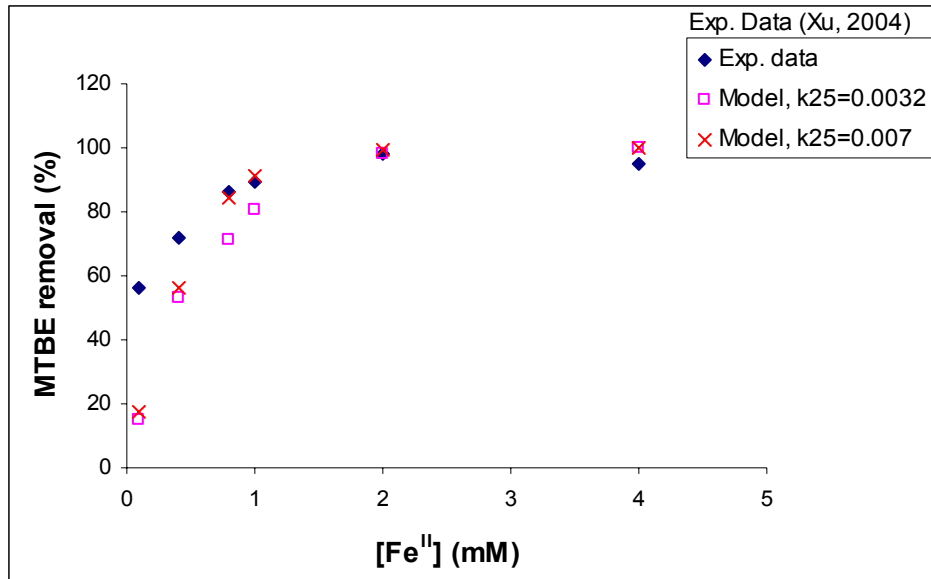
**Fig. 4.13:** Experimental and predicted percentage of MTBE removal vs. $Fe^{II}$ concentration applying Fenton's treatment. Initial conditions: $[MTBE]_o = 1$ mM, $[H_2O_2]_o = 0.01$ mM, pH = 2.8

### 3.2. Simulations of the experimental data of Bergendahl (2004)

The proposed kinetic model was tested by applying it to another set of experimental data provided by Bergendahl (2004). In these data MTBE was degraded applying $Fe^o/H_2O_2$ for the aqueous solutions in a batch reactor. For the studied conditions, fast removal of MTBE by $Fe^o$ was observed. Since acetone was produced this confirms the participation of Fenton's reaction in MTBE removal. The reaction rate constants that were used in simulating the data of Xu (2004) in Section 3.1 were used in this section too. It was assumed that the branching ratio between reactions 2.3.13 and 2.3.14 (Reactions are in Section 2.3) was 0.68 to 0.32 considering that both reactions proceed at the same speed based on best fitting of model. Another fitting parameter was used. This fitting parameter was the rate constant for the dissolution of $Fe^{o+}$ by $H_2O_2$ (Reaction 13, Table 1.2). At pH = 4, the value of this rate constant was $6.0 \times 10^{-5}$ $M^{-1}$ $s^{-1}$ and decreased to $3.7 \times 10^{-5}$ $M^{-1}$ $s^{-1}$ at pH = 7. The experimental and predicted concentrations of MTBE and acetone, at pH = 4, are shown in Figures 4.14 and 4.15,

419

respectively. The model prediction of MTBE data was good. However, model predictions of acetone data were different from experimental data. These results will be discussed later.
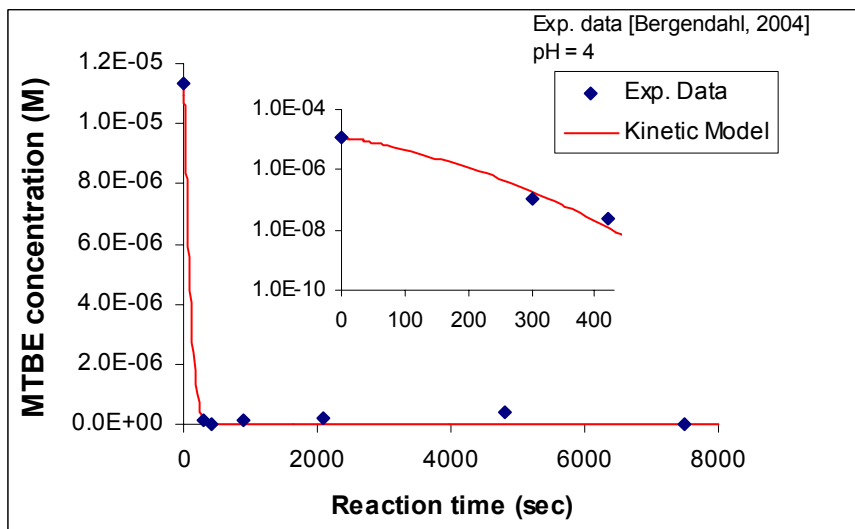


**Fig. 4.14:** Predicted and experimental concentrations of MTBE vs. time applying $Fe^o/H_2O_2$ treatment. Initial conditions: $[MTBE]_o = 11.3$ $\mu M$ (1 ppm), $[H_2O_2]_o = 2.5$ mM; $[Fe^o]_o = 250$ ppm, pH = 4.0. Insets are plots of the first three data points on a log-linear scale
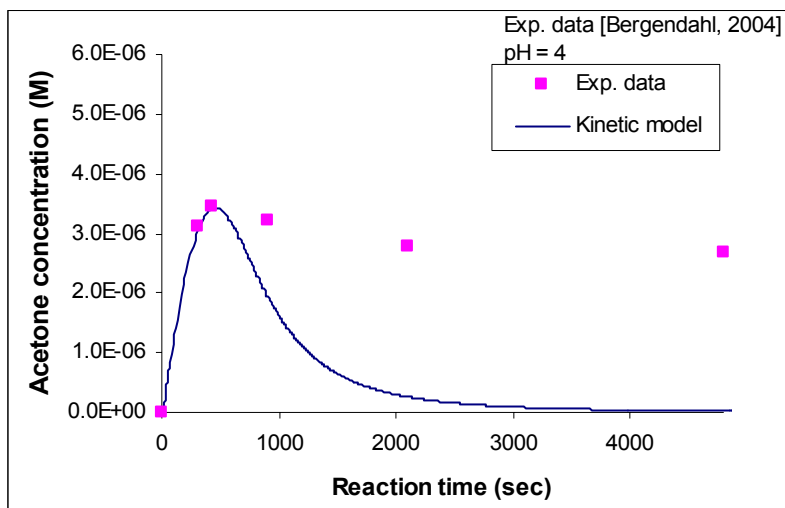


**Fig. 4.15:** Predicted and experimental concentrations of acetone vs. time applying $Fe^o/H_2O_2$ treatment. Initial conditions: $[MTBE]_o = 11.3$ $\mu M$ (1 ppm), $[H_2O_2]_o = 2.5$ mM; $[Fe^o]_o = 250$ ppm, pH = 4.0

The experimental and predicted concentrations of MTBE and acetone, at pH = 7, are shown in Figures 4.16 and 4.17, respectively. The same behavior of the model, which

420

was observed earlier at pH = 4 is observed at pH = 7. It can be seen good predictions of

MTBE data were observed while predictions of acetone data were different from
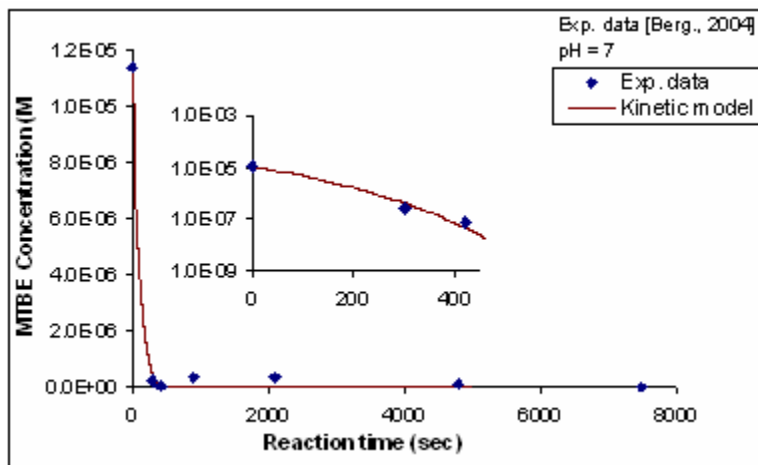
experiment.



**Fig. 4.16:** Predicted and experimental concentrations of MTBE vs. time applying $Fe^o/H_2O_2$ treatment. Initial conditions: $[MTBE]o = 11.3$ $\mu$ M (1 ppm), $[H_2O_2]_o = 2.5$ Mm; $[Fe^o]_o = 250$ ppm, pH = 7.0. Insets are plots of the first three data points on a log-linear scale
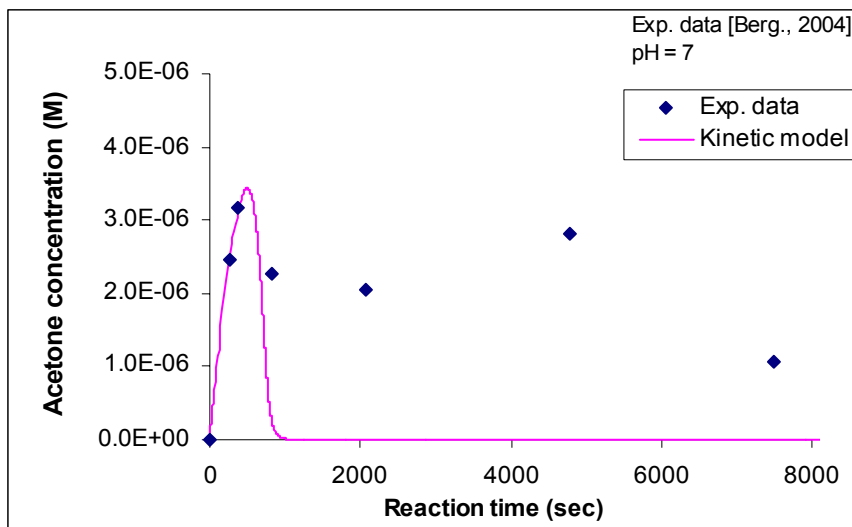


**Fig. 4.17:** Predicted and experimental concentrations of acetone vs. time applying $Fe^o/H_2O_2$ treatment. Initial conditions: $[MTBE]o = 11.3$ $\mu$ M (1 ppm), $[H_2O_2]_o = 2.5$ Mm; $[Fe^o]_o = 250$ ppm, pH = 7.0

The model was applied to other data reported by Bergendahl (2004) where no MTBE was present. The simulation results for pH = 4 and pH = 7 are shown in Figures 4.18 and 4.19, respectively.
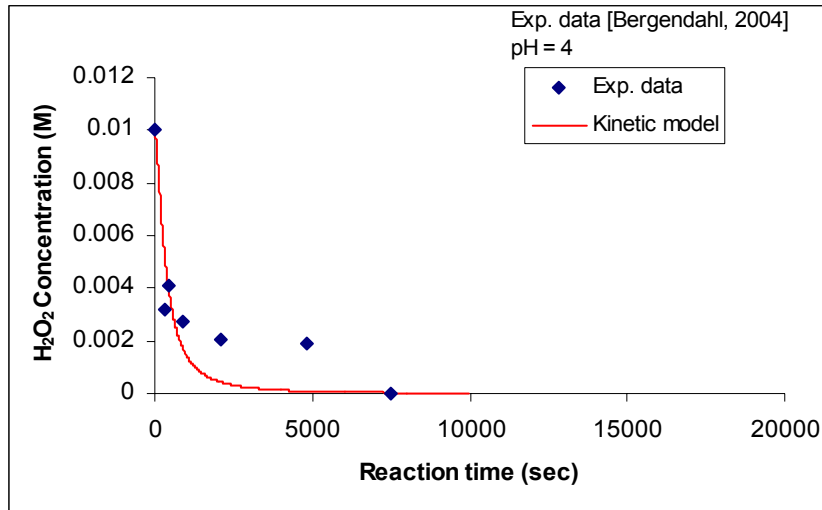


**Fig. 4.18:** Predicted and experimental concentrations of $H_2O_2$ vs. time applying $Fe^o/H_2O_2$ treatment. Initial conditions: $[MTBE]o = 0 \ \mu M$, $[H_2O_2]_o = 10 \ Mm$; $[Fe^o]_o = 250 \ ppm$, pH = 4.0
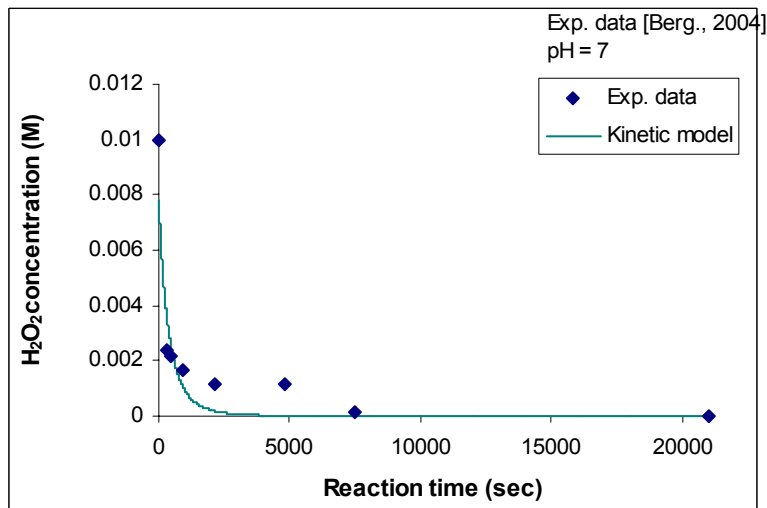


**Fig. 4.19:** Predicted and experimental concentrations of $H_2O_2$ vs. time applying $Fe^o/H_2O_2$ treatment. Initial conditions: $[MTBE]o = 0 \ \mu M$, $[H_2O_2]_o = 10 \ Mm$; $[Fe^o]_o = 250 \ ppm$, pH = 7.0

## 4. Discussion

### 4.1. Simulation of experimental data of Xu (2004)

The kinetic model was used to simulate a set of experimental data reported by Xu et al (2004). In these data the removal of methyl tert-butyl ether (MTBE) was studied using hydrogen peroxide ($H_2O_2$) and ferrous iron at acidic aqueous solution (pH = 2.8) using a batch reactor. In this study byproduct concentrations were observed and quantified. The main byproducts which were detected in this work were acetone, tert-butyl alcohol (TBA), tert-butyl formate (TBF) and methyl acetate (MA). The rate constant for Reaction 25 in Table 4.1 (reaction between ferric iron and hydrogen peroxide) was optimized within the reported range (0.02-0.001 $M^{-1}$ $s^{-1}$) [Walling, 1973, 1975; Chen, 1997, De Laat, 1999] and a value of $k_{25}$ = 0.0032 $M^{-1}$ $s^{-1}$ was found to give the best fitting of the model to the experimental data of MTBE and its byproducts based on lease square error analysis. The reaction between ferric iron and hydrogen peroxide is pH dependent [Walling, 1973], and this explains, the reason that it is reported within a range in the literature.

From the results shown in Figure 4.1 through 4.5 it can be seen that the proposed model along with the reported and optimized rate constants was able to describe the experimental behaviors for MTBE degradation and the byproducts formation. The predicted concentration of TBF and acetone was at a lesser accuracy than the predicted concentration of MTBE, TBA, and MA. This is expected since we just only proposed a mechanism based on the analysis of MTBE degradation by hydroxyl radicals [Cooper, 2004; Cooper, 2002, Wu, 2002, Stephan, 2000], and some of the proposed steps are still not experimentally validated. Also, in the proposed mechanism we have not accounted

for all the possible pathways for MTBE and byproducts formation and degradation. In order to account for other possible pathways more experimental data should be available. Stefan (2000) detected all the possible primary and secondary byproducts from MTBE degradation. His study was performed in batch flow through reactor using UV/H$_2$O$_2$ treatment. However, Stefan (2000), the primary intermediates were TBF, acetone, MA, and TBA and the developed model accounts for these major byproducts. Most of the other byproducts from Stephan (2000) mostly appear from the degradation of the major byproducts which was not taken into account in this model. Taking to account the formation and degradation of the byproducts which were detected in Stefan (2000) requires that the proposed mechanism be refined to include the secondary byproducts and this opens the door for new work in this field. Also, there is a possibility for the experimental errors and this might explain the deviation between the model and experimental data. Regardless of the above, we believe that the model was adequate to represent the work of Xu *et al* (2004).

Formaldehyde was not reported in the experimental data, however based on model simulations it was formed at comparable concentrations of TBF concentrations. Stephan (2000) quantified the production of formaldehyde and it was present at comparable concentrations of TBF. Cooper (2003) reported the formation of formaldehyde at considerable levels from MTBE degradation. The reason that formaldehyde might not have been detected by Xu's work (2000) might be that the method by which MTBE and its byproducts was analyzed was not adequate to sense formaldehyde formation. This is expected considering that formaldehyde has a very low boiling point (-21 $^\circ$C) compared to the boiling points of MTBE and the other quantified

424

byproducts (for example boiling point of acetone is 56 $^\circ$C) [CRC, 1975]. Hence, formaldehyde is highly volatile and would be present as gas. Chang (2000), from a study for MTBE degradation using UV/H$_2$O$_2$, found that TBF was the major quantified byproduct in this study. He mentioned that other byproducts, such as acetone and formaldehyde, were probably formed but went undetected, because they were not purgable or were too volatile to appear in the analysis results.

The predicted and experimental concentration of MTBE shows that MTBE degradation passes through two stages. In the first stage a rapid removal of MTBE is observed while in the second stage a slower degradation of MTBE takes place. This is due to the fact that once Fe$^{II}$ is added to the system it reacts very fast with hydrogen peroxide (Reaction 14, Table 4.1) producing large amount of $^\bullet$OH as can be seen from Figure 4.20 from the concentration of $^\bullet$OH radicals in the system. These radicals, at such a high concentration, will react also in a fast way with MTBE according to Reaction 32 and 33 (Table 4.1) leading to a fast degradation of MTBE in the first stage. The fast reaction of ferrous iron (Fe$^{II}$) and hydrogen peroxide will produce also ferric iron (Fe(III)). The disappearance of ferrous iron and production of ferric iron is shown in Figure 4.21.

From Figure 4.21 it can be seen that ferrous iron converts rapidly to ferric iron. This is consistent with the experimental observation of Xu (2004) where ferrous iron became undetectable within 1-2 minutes of reaction time. Ferric iron reacts to a much slower extent with hydrogen peroxide than the reaction of ferrous iron with hydrogen peroxide. The rate constant of hydrogen peroxide with ferrous iron is 76 M$^{-1}$ s$^{-1}$ compared

to 0.0032 $M^{-1}$ $s^{-1}$ for rate constant for the reaction of ferric iron and hydrogen peroxide [Walling, 1973, 1975; Chen, 1997].
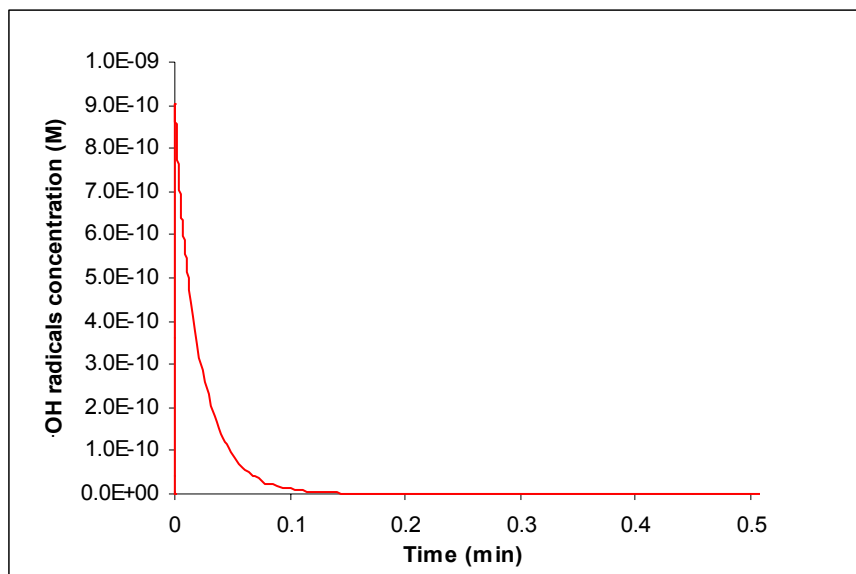


**Fig. 4.20:** Predicted concentration of hydroxyl radicals from simulations vs. time applying Fenton's treatment. Initial conditions: $[MTBE]_o = 1$ mM, $[Fe^{II}]_o = 2$ mM, $[H_2O_2]_o = 0.015$ mM, pH = 2.8
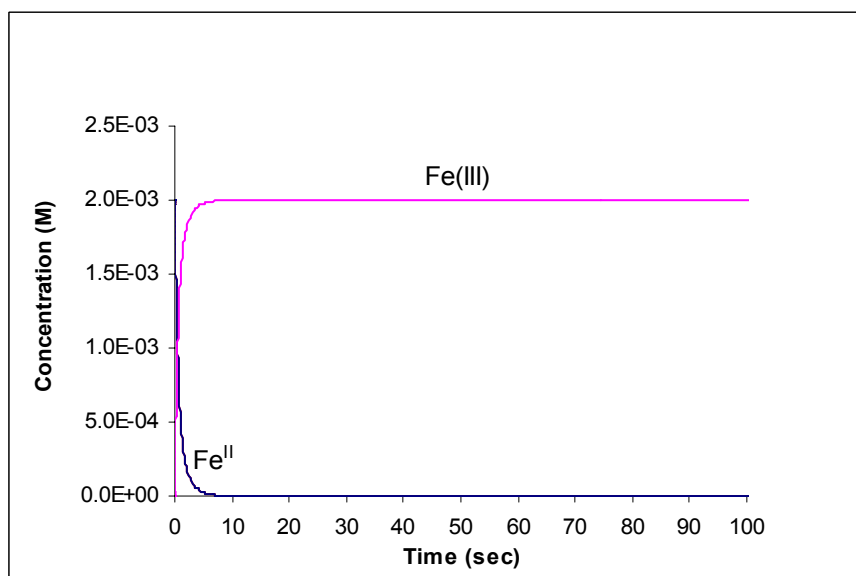


**Fig. 4.21:** Predicted concentration of ferric iron (Fe(III)) and ferrous iron Fe(II) from simulations vs. time applying Fenton's treatment. Initial conditions: $[MTBE]_o = 1$ mM, $[Fe^{II}]_o = 2$ mM, $[H_2O_2]_o = 0.015$ mM, pH = 2.8

Hence the rate of $^\bullet OH$ radicals production from Fe(III)/$H_2O_2$ reaction will be slower than its production from $Fe^{II}$/$H_2O_2$ reaction. This slower production of $^\bullet OH$

radicals explains the lower degradation of MTBE in the second stage of Figure 4.1. Also, in this stage byproducts of MTBE degradation (TBF, TBA, MA, acetone, formaldehyde, formic acid, and formate ions) compete with MTBE for the hydroxyl radicals which will lower its degradation rate.

The two stage reaction is noticed on the predicted concentration of hydrogen peroxide as can be seen from Figure 4.7. It can be seen from Figure 4.7 that hydrogen peroxide is consumed very fast in the first stage by $Fe^{II}$ ions ($Fe^{II}/H_2O_2$ stage) followed by a slower removal due to the dominance of ferric iron in the system ($Fe(III)/H_2O_2$ stage).

The fast reaction of MTBE in the first stage is reflected in the byproduct concentrations. It can be seen from Figure 4.2 through 4.6 that a fast production of all the detected products took place at the same time where a fast degradation of MTBE has happened. It can be seen from the previous figures that TBF, TBA, MA and formaldehyde concentration increases from zero to a certain value and then once these compounds are formed they start to react with hydroxyl radicals and this explains the slowdown in their concentration vs. reactions time. Although, there is a reaction of these compounds with hydroxyl radicals the rates of production of these compounds are happening at higher extent than their rates of consumption and hence their concentrations will continue to rise. After that, the concentrations of these compounds reach a maximum value at approximately 60 minutes of reaction time. After this maximum concentration, the byproduct concentrations start to decrease. This is expected since the rate of their productions are no longer greater than their rates of consumptions, since the concentration of the source (MTBE), Figure 4.1, has declined to a very small value after

60 minutes. Once the source is exhausted, these byproducts will continue to degrade as long there are hydroxyl radicals in the system. An example is shown in Figure 4.22. Figure 4.22 shows the predicted rate of TBF production and consumption. The rate of TBF production was found by summing the positive terms in equation 4.1.1 while the rate of TBF consumption is its rate of reaction with the hydroxyl radicals.

$$\frac{d[TBF]}{dt} = k_{39}[R_3][R_3] + 2*0.62k_{38}[R_1] - k_{41}[TBF][^{\bullet}OH] \qquad\qquad 4.1.1$$

Figure 4.22 supports the above argument where it can be seen that there is a fast production of TBF once the reactants are mixed. Then at the same time where TBF is produced it is consumed by the hydroxyl radical. However up to 50 minutes the rate of TBF production; although decreasing is still higher than its consumption. A sharp drop in TBF production takes place at 50 min due to the reduction in MTBE concentration to less than 5 % of its initial concentration. After that the rate of TBF consumption is higher than its production which results in reduction of TFB concentration as seen in Figure 4.2. This analysis applies also to TBA, MA, and formaldehyde.
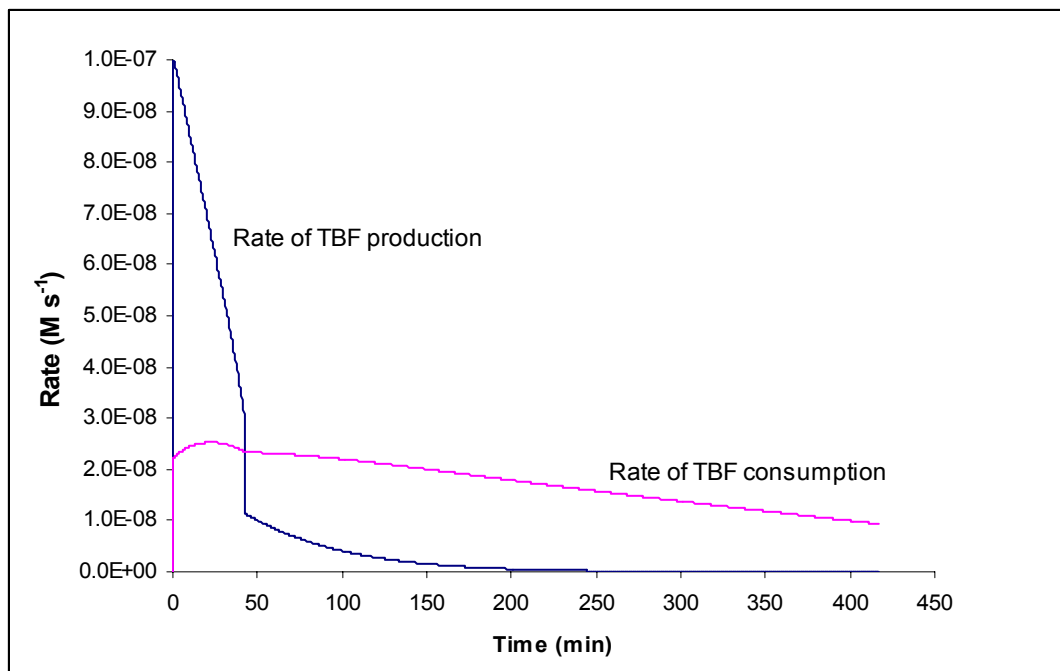
**Fig. 4.22:** Predicted rate of TBF production and consumption vs. time applying Fenton's treatment. Initial conditions: $[MTBE]_o = 1$ mM, $[Fe^{II}]_o = 2$ mM, $[H_2O_2]_o = 0.015$ mM, pH = 2.8

For acetone concentration, it can be seen from Figure 4.6 that its concentration increased from zero to approximately 0.16 mM in the fast stage ($Fe^{II}/H_2O_2$ stage) and continued to increase in the reaction mixture up to 240 min. This is due to the fact that acetone, as was proposed in this mechanism, was produced through different routes. In the first route acetone was a product of series of reaction that follows $\beta$ - abstraction of hydrogen atoms from MTBE by hydroxyl radicals and in the second route it was a byproduct of TBF reaction with hydroxyl radicals as explained earlier in Section 2.3. Therefore, although MTBE will be consumed from the system, acetone will still accumulate due to the degradation of TBF. Also, acetone reacts to a lesser extent with hydroxyl radicals than the other byproducts based on the values of the rate constant that were given in Table 4.1. Hence, the hydroxyl radicals will be consumed by

429

formaldehyde, MA, and TBA faster than their consumption by acetone allowing acetone to accumulate in the reaction mixture.

The increment in acetone concentration is followed with a short period of constant concentration during which the rates of production and consumption are similar. This also, explains why once the concentration of the other byproducts become low then acetone concentration starts to decrease more rapidly. At this time the degradation of acetone is faster than its production as can be seen from Figure 4.5 after 300 minutes of reaction time which is due to the reduction in the concentration of TBF, which will reduce the rate of acetone production, and the reduction in the concentrations of the other byproducts, which will increase the rate of acetone oxidation by the hydroxyl radicals.

TBA was produced in a lower yield than the other products as can be seen from Figures 4.2 through 4.5. This suggests that the rate of TBA formation and consumption are comparable [O'Shea, 2002b].

### 4.1.1. Sensitivity analysis

Sensitivity analysis was undertaken by varying the rate constant for a particular reaction whilst the other rate constants were unchanged. This approach assumes that the rate constants in the original model are close to the correct value, since a change in one of the rate constants may affect the sensitivity of the model to a change on another rate constant by an order of magnitude (both increase and decrease) [Waite, 2002].

The results of applying perturbation analysis to the degradation of MTBE using $Fe^{II}/H_2O_2$ treatment are shown in Figure 4.8 for MTBE concentration. As can be seen from Figure 4.8, the rate of MTBE degradations is strongly influenced by Reactions number 1, 17, 25, 32. Reactions, 7, 8, 18, 21, 33-35, 41, 45-48, 52-54, 56, and 57 seem to

have a similar effect on MTBE degradation but to a lesser extent than Reactions 1, 25, and 32 and we will call this Category 2. In Category 3 are the reactions with $\log_{10}$ SSR between approximately -6 and -8 which are Reactions 3, 14, 42, 44, 51. The remaining reactions have a small effect since most of them have a $\log_{10}$ SSR less than -8 which is called Category 4.

Reactions 1, 17, 25, and 32 were given by the following equations in Table 2.1:

1. $^\bullet OH + H_2O_2 \rightarrow H_2O + HO_2^\bullet$ $\qquad$ $k_1 = 2.7 \times 10^7 \ M^{-1} \ s^{-1}$

17. $Fe^{II} + {}^\bullet OH \rightarrow Fe^{3+} + OH^-$ $\qquad$ $k_{17} = 3.2 \times 10^8 \ M^{-1} \ s^{-1}$

25. $Fe^{III} + H_2O_2 \rightarrow Fe^{2+} + HO_2^\bullet + H^+$ $\qquad$ $k_{25} = 0.0032 \ M^{-1} \ s^{-1}$

32. $(CH_3)_3COCH_3 + {}^\bullet OH \xrightarrow{\ \alpha-abstraction \quad (71\%)\ } (CH_3)_3COCH_2^\bullet + H_2O$ $\quad$ $k_{32} = 1.6 \times 10^9 \ M^{-1} \ s^{-1}$
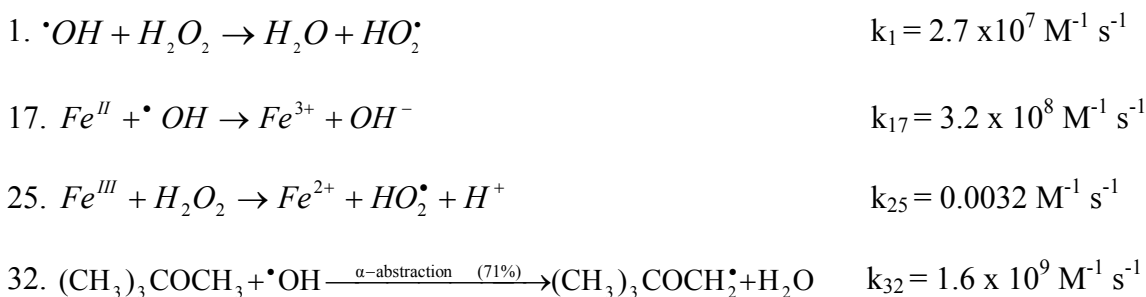
It can be seen from Reactions 32, 1, and 17 that they all represent consumption of the hydroxyl ($^\bullet OH$) radicals. Since MTBE degradation is due to oxidation by the $^\bullet OH$ radicals, any reactant that would scavenge these radical will greatly affect the rate of MTBE degradation. Reaction 32 has a more significant rule than its parallel reaction 33 since 71 % of MTBE was degraded by Reaction 32 compared to 29 % of MTBE degraded by Reaction 33. The rate constants for Reactions 1, 17, and 25 were taken directly from the literature.

Reaction 25, although it has a relatively low rate constant, plays a significant role in MTBE degradation since it regenerates ferrous iron from the reaction of hydroxyl radicals and ferric iron. Once ferrous iron is produced it will react with hydrogen peroxide according to Reaction 14 in Table 4.1 to reproduce the strong oxidants ($^\bullet OH$ radicals). Hydroperoxyl radicals ($HO_2^\bullet$) are also generated from Reactions 1 and

25, however no reported interaction for these radicals with MTBE or its byproducts was found. Therefore, their effect on MTBE degradation will be to a lesser extent.

Hydroxyl radicals are also scavenged by hydroxyl radicals (Reaction 5), hydroperoxyl radicals (Reaction 3), the conjugate base of hydrogen peroxide (Reaction 11), TBF, TBA, MA, acetone, formaldehyde. From Figure 4.8 Reactions 5 and 11 lie in Category 4, although the rate constant for these reactions are high ($10^9$ $M^{-1}$ $s^{-1}$). This is due to the fact that the concentrations of hydroxyl radicals and conjugate base of $H_2O_2$ are much lower than the concentration of MTBE, $H_2O_2$ and ferrous iron in this system. Therefore, the rate of the hydroxyl radical reactions by the latter species will be a much higher value than the previous ones. Reaction 3 lies within Category 3 which has a less important effect compared to the reactions in Category 2, but a higher effect of Reaction 5 (Category 4). This due to the fact that hydroperoxyl radicals were present at higher concentrations during the reaction time as can be seen by comparing Figure 4.23 in this section and Figure 4.20 in the previous section. The reason that the hydroperoxyl radicals concentration is higher is that they were not involved in the degradation of MTBE and its byproducts, unlike the hydroxyl radicals, which will leave higher concentrations of these radicals in the system.
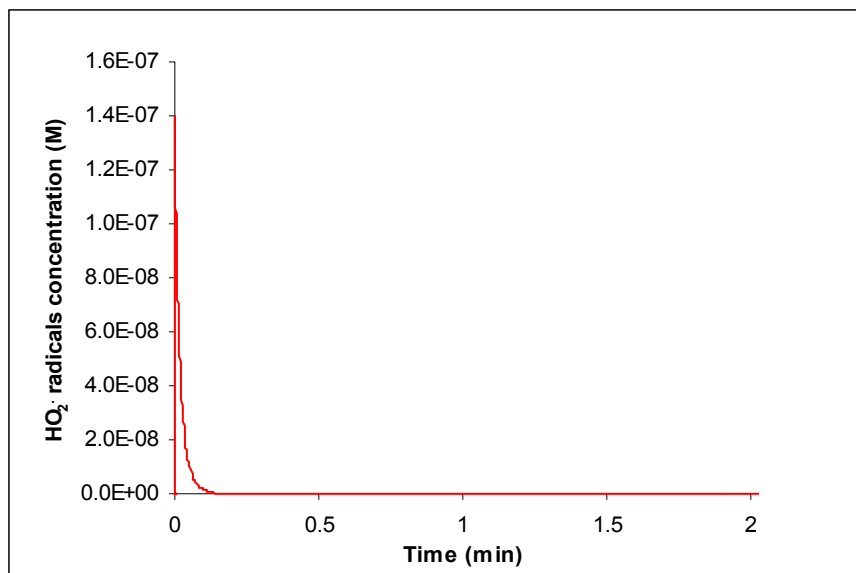
**Fig. 4.23:** Predicted concentration of hydroperoxyl radicals from simulations vs. time applying Fenton's treatment. Initial conditions: $[MTBE]_o = 1$ mM, $[Fe^{II}]_o = 2$ mM, $[H_2O_2]_o = 0.015$ mM, pH = 2.8

Scavenging of $^\bullet OH$ radicals by TBF, TBA, MA, acetone, formic acid and formaldehyde was given by Reactions, 41, 48, 54, 47, 46, and 45, respectively. All of the previous products are byproducts of MTBE degradation by the $^\bullet OH$ radicals, therefore their scavenging effect will be in Category 2, since most of MTBE is removed in the first stage ($Fe^{II}/H_2O_2$) and competition between MTBE and these byproducts will start to be more significant in the second stage ($Fe(III)/H_2O_2$). TBF scavenging of the $^\bullet OH$ radicals seems to be to a higher extent than the other ones (Figure 4.8), since it was initially produced in the largest amounts.

The other reactions that were classified to be in Category 2 were Reactions, 7, 8, 14, 18, 21, 34, 35, 52, 53, 54, 56, and 57. Reactions 7 and 8 involve the production and consumption of hydroperoxyl radicals and its conjugate base which both react with hydroxyl radicals with a high rate constant. Therefore, these reactions will compete with MTBE for $^\bullet OH$ radicals. Reaction 18 represents the reaction of hydroperoxyl radicals

433

with ferrous iron and this reaction consumes the ferrous iron and reduces the chance of $^\bullet$OH radical production. Reaction 21 represents scavenging of ferric iron at a relatively high rate constant $(1.5 \times 10^8$ $M^{-1}$ $s^{-1})$ to reproduce ferrous iron which is the most important source of the hydroxyl radicals. Reactions 34 and 35 are the initiations steps for the production of all the previously mentioned byproducts which will compete with MTBE for the $^\bullet$OH radicals. Reactions 52 and 53 are a pair of the suggested routes that will produce acetone and methyl acetate along with the methyl radicals (that will be oxidized by oxygen to form formaldehyde). As said earlier these byproducts compete with MTBE for the $^\bullet$OH radicals. The direct consumption of the $^\bullet$OH radicals by methyl acetate is given by Reaction 54 and hence this reaction competes with MTBE reaction with the $^\bullet$OH radicals. Reaction 56 represents the equilibrium reaction between formic acid and formate ions which both reacts with the hydroxyl radicals. However, formate ions react with a high rate constant with the hydroxyl radicals $(4.1 \times 10^9$ $M^{-1}$ $s^{-1})$, therefore this equilibrium will determine which form prevails and consequently Reaction 57 (reactions of formate ions with hydroxyl radicals) will compete for the $^\bullet$OH radicals. It can be seen that the reactions which were classified to be in Category 2 were mainly, excluding reactions 7, 8, 18, 21, the formation and consumptions reactions of MTBE byproducts.

The reactions that were classified to be in Category 3 were Reactions 3, 14, 42, 44, and 51. Reaction 3 has been discussed previously. Reaction 14 is the initiator of all the reactions in the system, since it involves the reaction of ferrous iron with hydrogen peroxide to produce the hydroxyl radicals. This reaction is proceeding at a relatively high speed with high concentrations of the reactants. Therefore, even with the change in the

rate constant the produced $^\bullet OH$ radicals were high enough so that MTBE degradation was not affected by the perturbation with the rate constant greatly. Reactions 42, 51, and 44 involve the reactions of the radical species with oxygen with the end products being other radicals and formaldehyde. The produced radicals don't compete with MTBE for $^\bullet OH$ radicals, and formaldehyde was produced earlier in time through other routes. Therefore, the effect of theses reactions on MTBE degradation will not be major.

The remaining reactions, which were classified to be in Category 4, have a lower effect on MTBE degradation since they either proceed with a relatively lower speed or involve the reactions of reactants with low concentrations or the combinations of low concentration and low rate constants making their absolute rate (either production or consumption) relatively low.

For TBF, acetone, TBA, and MA the sensitivity results, which were presented in Figures 4.9, 4.10, 4.11, and 4.12, respectively, show that there is no dominance of certain reactions on the degradation of these by products. This is expected since these compounds were produced from MTBE degradation and not initially present in the system. However the different reactions can be classified, roughly, to lie within two major categories; Category 1 for which $\log_{10}$ SSR is greater than -8 and Category 2 with $\log_{10}$ SSR less than -8.

For the sensitivity analysis of TBF, as can be seen in Figure 4.9, Reactions 1, 3, 7, 8, 14, 17, 18, 19, 21, 25, 32, 33, 34, 35, 41, 42, , 44-48, 51-54, 56, and 57 lie in Category 1. Reactions 1, 17, 32, 33, 41, 45-48, 54, and 57 represent scavenging of the $^\bullet OH$ radicals by $Fe^{II}$, MTBE, and all the byproducts from MTBE degradation (including TBF). Therefore, it is expected that these reactions should be in the same category, since

435

TBF formation and consumption is related to the concentration of the $^\bullet$OH radicals in the system and any reaction that competes with TBF on these radicals will affect its degradation. Reactions 7 and 8 represent the production and consumption of hydroperoxyl radicals and its conjugate base which scavenge the $^\bullet$OH radicals and ferrous iron, as shown in the kinetic model in Table 4.2. Reactions 44, 51, 52, 53, and 56 lead to the formation of formaldehyde, methyl acetate, acetone, and formate ions which compete with TBF for the hydroxyl radicals. Reactions 34 and 35 are the steps which follow MTBE oxidation by the $^\bullet$OH radicals and the speed of these reactions determine how fast or slow and how much of all the byproducts will be produced in the system.

The results of the sensitivity analysis for acetone in Figure 4.10, TBA in Figure 4.11, and MA in Figure 4.12 show that the same reactions which were classified to be in Category 1 for TBF are also in Category 1 for acetone, TBA, and MA. Having the same reactions in Category 1 for TBF, acetone, TBA, and MA, is expected since all of these compounds are byproducts of MTBE degradations and their productions and consumptions were related to the presence of the $^\bullet$OH radicals. Therefore, any reaction that will affect the concentration of the $^\bullet$OH radicals, either in a direct way by scavenging these radicals or indirectly by producing or consuming the ferrous iron, will affect the rate of these byproducts formation and rate of their degradation by the $^\bullet$OH radicals in the reaction mixture.

From the sensitivity analysis for MTBE and byproducts degradation it can be seen that each proposed reaction step plays a rule on MTBE degradation. However, the extent of the effect of these reactions varies from one reaction to another. This effect is a function of the rate constant of each reaction, the concentration of the reactants that were

involved in the reaction, the production and consumption pathways of the involved reactants. Therefore, in a kinetic model all of these reactions should be included since it is not possible to predict in advance which reaction can be excluded, and especially given the available technology of highly efficient computers. Excluding any reaction will give a rough estimate of the actual kinetics.

## 4.1.2. Effect of the initial concentration of ferrous iron (Fe$^{II}$) on MTBE removal

The effect of initial ferrous iron concentrations on the degradation of MTBE was shown in Figure 4.13. In this figure the initial concentration of MTBE was 1 mM, the initial concentration of $H_2O_2$ was 10 mM and the results were obtained by varying the initial concentration of ferrous iron. The model predictions, using the same rate constants as the ones which were used earlier for which $k_{25}$ was 0.0032 M$^{-1}$ s$^{-1}$, were showing that increasing Fe$^{II}$ concentration will increase the degree of MTBE removal until a plateau value of MTBE removal is reached between 2 and 4 mM Fe$^{II}$. This was similar to the experimental results. The agreement between the model and the experimental data improved as the concentration of Fe$^{II}$ increased with the best prediction at 2 mM Fe$^{II}$ since the model was originally optimized at this concentration for MTBE and the other byproducts for the results shown in Figures 4.1 through 4.7. We didn't want evaluate optimization of the model at each Fe$^{II}$ concentration, since concentration of the byproducts were not available, and the model even with this deviation was able to predict the effect of ferrous iron reasonably. However, one change in $k_{25}$ (the rate constant for the reaction between ferric iron and $H_2O_2$) was made. It can be seen from Figure 4.13 that increasing $k_{25}$ resulted in better prediction at 0.8 and 1 mM Fe$^{II}$. For the plateau region,

which represents almost complete MTBE degradation, no difference was observed between the two values of $k_{25}$.

The reason behind the enhancement of MTBE removal by the increase in $Fe^{II}$ is the increased production of $^{\bullet}OH$ radicals according to reaction 14 in Table 4.2. Figures 4.24 and 4.25 show the concentration of $^{\bullet}OH$ radicals at different initial $Fe^{II}$ concentrations. The time scale used in these figures was short compared to the total reaction time in order to show the difference of $^{\bullet}OH$ radical production as a function of $Fe^{II}$ concentration. It can be seen from Figures 4.24 and 4.25 that the concentration of $^{\bullet}OH$ radicals increased as more $Fe^{II}$ was used. Higher concentration of $^{\bullet}OH$ radicals will result in more degradation of MTBE and hence higher percentage of MTBE removal.
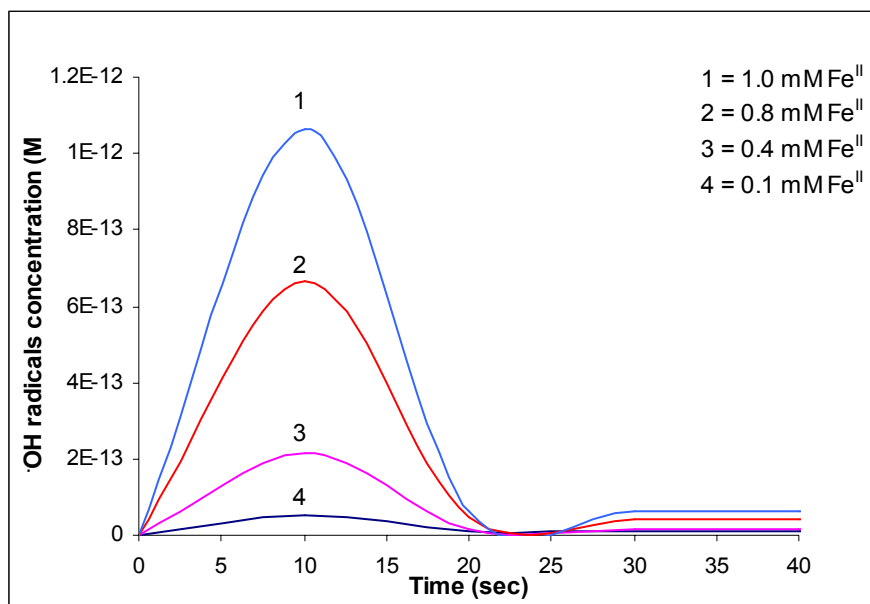


**Fig. 4.24:** Predicted concentration of the $^{\bullet}OH$ radicals vs. $Fe^{II}$ concentration applying Fenton's treatment. Initial conditions: $[MTBE]_o = 1$ mM, $[H_2O_2]_o = 0.01$ mM, pH = 2.8
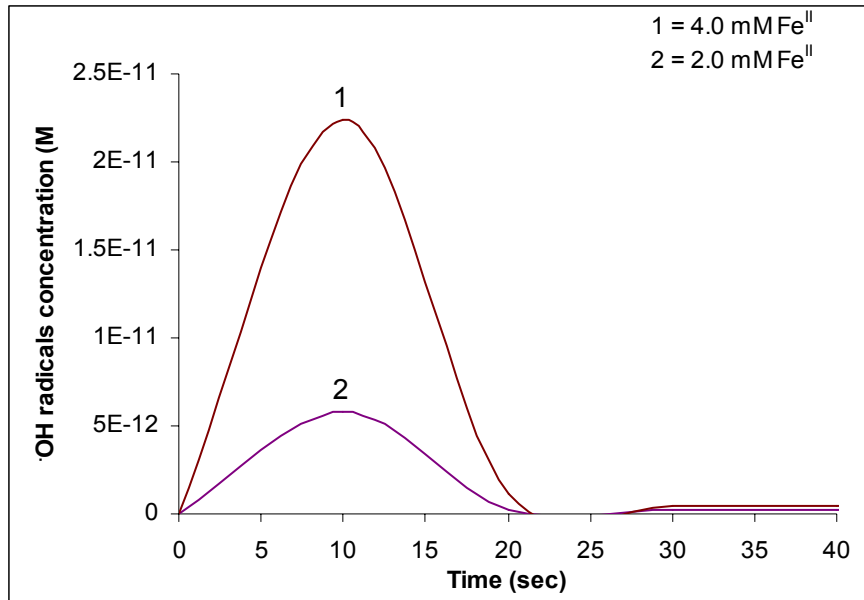
**Fig. 4.25:** Predicted concentration of the $^\bullet OH$ radicals vs. $Fe^{II}$ concentration applying Fenton's treatment. Initial conditions: $[MTBE]_o = 1$ mM, $[H_2O_2]_o = 0.01$ mM, pH = 2.8

MTBE removal was not significantly affected as initial concentration of $H_2O_2$ was increased and decreased by 0.005 molar, where the initial concentration of MTBE was 1 mM, the initial concentration of $Fe^{II}$ was 2 mM and the pH value was 2.8. At the previous conditions the concentration of $^\bullet OH$ radicals was similar and hence the degradation of MTBE was similar.

## 4.2. Simulation of the experimental data of Bergendahl (2004)

The results of the simulations after applying the kinetic model to another set of experimental data reported by Bergendahl (2004) were shown in Figures 4.14 through 4.19. In these data MTBE was degraded applying $Fe^o/H_2O_2$ for the aqueous solutions in a batch reactor. The reaction rate constants that were used in simulating the data of Xu (2004) in Section 3.1 were used in this section too. Another fitting parameter however was used. This fitting parameter was the rate constant for the dissolution of $Fe^o$ by $H_2O_2$ (Reaction 13, Table 4.1). At pH = 4, the value of this rate constant was $6.0 \times 10^{-5}$ $M^{-1}$ $s^{-1}$

and at pH = 7 it was 3.7 x $10^{-5}$ $M^{-1}$ $s^{-1}$. Such a dependency on pH is expected since as discussed earlier in section 2.2.1 the rate of iron dissolution was a function of solution pH and since each set of experimental data was performed at a certain pH this dependency was lumped within the rate constant for iron dissolution. Therefore, it is expected that the degree of the acidity of the solution will affect the rate of iron dissolution. Similar finding where iron dissolution was enhanced by pH reduction was reported by Arenzo (2001) and Teel (2001).

The kinetic model, as can be seen from Figures 4.14 and 4.16, was able to describe the experiential degradation of MTBE in this system at the studied conditions and at the two different pH values. However, the predicted concentration of acetone was different than the experimental data at reaction times greater than 15 minutes (900 sec) as can be seen from Figures 4.15 and 4.17 at pH = 4 and pH =7, respectively. Based on the fast degradation of MTBE it is expected that the system has a high concentration of the hydroxyl radical, therefore since acetone is also degraded by these radicals it should also be degraded in a faster way than what the experimental data suggest. Other data for MTBE degradation by the hydroxyl radicals also showed that acetone will not remain in the system for such a long time [Stefan, 2000; Cooper, 2002a], and after the acetone concentration reached a maximum value it started to degrade relatively fast which is similar to the kinetic model predictions. Also, in Bergendahl (2004) data, only acetone was quantified while the literature, as said in the introduction, showed the formation of other byproducts from MTBE degradation. Therefore, the persistence of acetone for such a long time in the system as the experimental data showed might be due to inaccuracy in byproducts quantification and measurement. If we accepted that the experimental data are

440

correct then this would mean that after the 15 minutes of reaction time the production of hydroxyl radicals has stopped. This would be related to the active sites on the surface of iron that were responsible for iron dissolution. Such deactivation of the active sites might be due to the blocking of these active sites which might due to different reasons. One of them is the precipitation of reactions byproducts and intermediates on these active sites or the formation of iron complexes on the surface. Once these sites are blocked then iron dissolution is ceased. Any of these assumptions needs experiment to be justified.

In systems where only hydrogen peroxide and iron were presents, kinetic model along with the experimental data showed a decline in hydrogen peroxide concentration as was shown in Figures 4.18 and 4.19 at the different pH values. Comparing the degradation of $H_2O_2$ by the different reactions steps is shown in Figure 4.26. In this figure the nomenclature is as follows:

$$
\begin{aligned}
&-k_1[H_2O_2][{}^{\bullet}OH] - k_9[H_2O_2]_T[O_2^{\bullet-}] - k_{10}[H_2O_2]_T[HO_2^{\bullet}] - k_{11}[HO_2^-][{}^{\bullet}OH] \\
&-k_{13}[H_2O_2]_T - k_{14}[H_2O_2]_T[Fe^{2+}] - k_{16}[[H_2O_2]_T[Fe^{II}OH^+] - k_{25}[Fe^{III}][H_2O_2]_T
\end{aligned} = 1
$$

$$\left| -k_1[H_2O_2][{}^{\bullet}OH] - k_{11}[HO_2^-][{}^{\bullet}OH] \right| = 2$$

$$\left| -k_{16}[[H_2O_2]_T[Fe^{II}OH^+] \right| = 3$$

$$\left| -k_{14}[H_2O_2]_T[Fe^{2+}] \right| = 4$$

$$\left| -k_{13}[H_2O_2]_T \right| = 5$$

where 1 represents the terms that represents total consumption of hydrogen peroxide, 2 the term that represents the consumption of $H_2O_2$ and its conjugate base by the hydroxyl radicals, 3 is the consumption by of $H_2O_2$ by $FeOH^+$, 4 is the consumption by of $H_2O_2$ by $Fe^{2+}$, and 5 is the consumption of hydrogen peroxide in iron dissolution. Other terms in

the above differential equation of hydrogen peroxide were not considered since the absolute value of each was at the most in the order of $10^{-9}$.

It can be seen from the simulations results in Figure 4.26 that of $^{\bullet}OH$ radicals make the biggest contribution to the degradation of hydrogen peroxide degradation. This is due to the high concentration of the hydroxyl radicals that were produced following the degradation by routes 3 and 4 in Figure 4.26, which were also significantly contributing to the degradation of hydrogen peroxide. Although the concentration of $FeOH^{+}$ was low( $10^{-10}$ M), it has a high rate constant for its reaction with hydrogen peroxide, as can be seen in Table 4.1, and this is the reason that it contributes greatly to hydrogen peroxide degradation.
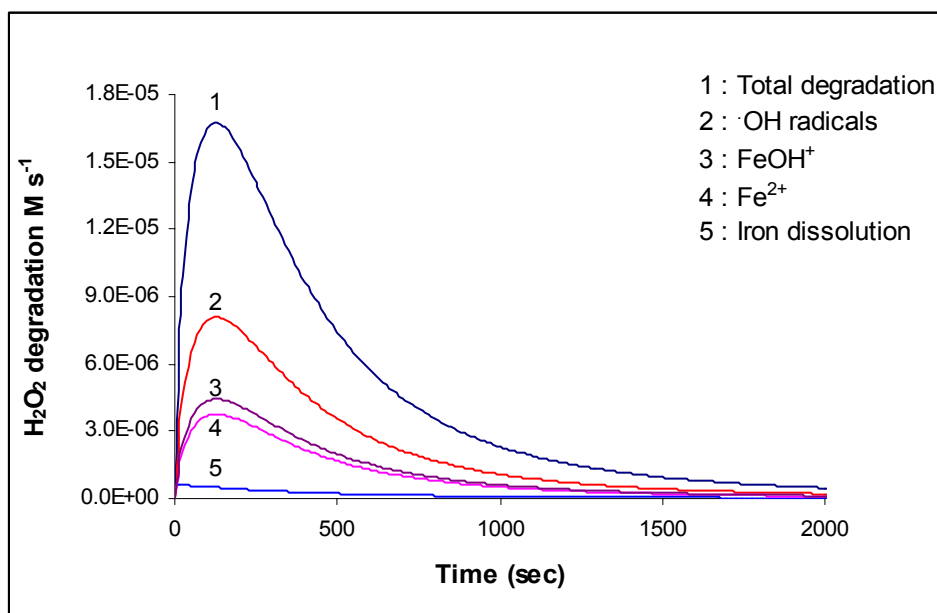


**Fig. 4.26:** Predicted contribution of some of the reactions in $H_2O_2$ degradation vs. time. Initial conditions: $[MTBE]o = 0 \ \mu M$ , $[H_2O_2]_o = 10 \ Mm$; $[Fe^o]_o = 250 \ ppm$, $pH = 4.0$

## 5. Conclusions

A kinetic model for the degradation of methyl tert-butyl ether (MTBE) in a batch reactor applying Fenton's reagent ($Fe^{II}$/ $H_2O_2$) and Fenton-like reagent ($Fe^o$/ $H_2O_2$) aqueous solutions was proposed. This kinetic model consisted of three major parts, hydrogen peroxide chemistry in aqueous solutions, iron chemistry, and MTBE chemistry. Hydrogen peroxide chemistry in aqueous solutions is well documented, and, therefore all of the rate and equilibrium constants for this chemistry were taken from the literature. The iron chemistry consisted of all the possible reactions of ferrous and ferric iron in aqueous systems containing hydrogen peroxide beside iron dissolution by hydrogen peroxide. Rate and equilibrium constants for ferric and ferrous iron reactions in this model were taken from the reported values in the literature except for the rate constant for the reaction of ferric iron with hydrogen peroxide where it was fitted within the range that was reported in the literature. The rate constant for iron dissolution also was a fitted parameter, and it was a function of the solution acidity. The mechanism of MTBE degradation by the hydroxyl radicals, which were formed from ferrous iron and hydrogen peroxide reaction, the pathways for the formation of the byproducts that follow MTBE by these radicals, and the degradation of these byproducts was proposed based on studies performed by Stefan (2000), Wu (2002), and Cooper (2004). Most of the rate constants for this MTBE oxidation mechanism were taken from the literature and when a rate constant for a certain reaction was not available, analogy between this reaction and another reaction that proceed in a similar way was made. Proportions of one reaction that proceed in different routes, other than hydrogen abstraction from MTBE which was

taken from the literature, was optimized based on the best fitting of the model to the experimental data.

The proposed model was tested on available experimental data from the literature which involved the use of Fenton's reagent [Xu, 2004] and Fenton-like reagent [Bergendahl, 2004] for MTBE degradation. The degradation of MTBE in Xu's work was characterized to proceed by two stages, a fast one which involves the reaction of ferrous iron with hydrogen peroxide ($Fe^{II}/H_2O_2$ stage) and another, relatively, slower stage which involves the reaction of ferric iron with hydrogen peroxide ($Fe^{III}/H_2O_2$ stage). The experimental data of MTBE degradation in the $Fe^{II}/H_2O_2$ stage were not enough to validate the model, however the model predictions of MTBE degradation in the $Fe^{III}/H_2O_2$ stage was good. Also, the model was able to predict the byproducts formation from MTBE degradation and their degradation especially methyl acetate (MA), and tert-butyl alcohol (TBA). Within the studied conditions increasing ferrous ion concentration ($Fe^{II}$) increased MTBE removal since this led to higher production of the $^\bullet OH$ radicals, which were responsible for MTBE degradation. Model predictions of the $Fe^{II}$ effect on MTBE removal enhanced at higher concentrations of $Fe^{II}$.

From the sensitivity analysis for MTBE degradation it can be seen all the proposed reaction steps played a role in MTBE degradation. However, the extent of the effect of these reactions varies from one reaction to another. This effect is a function of the rate constant of each reaction, the concentration of the reactants that were involved in the reaction, and the production and consumption pathways of the involved reactants. Therefore, in a kinetic model all of these reactions should be included to cover a wide range of experimental conditions.

The dominant reactions for MTBE degradation, from the results of the sensitivity analysis at the studied conditions, were the reaction between ferric iron and hydrogen peroxide, reaction between ferric iron and the hydroxyl radicals, reaction between the hydroxyl radicals and hydrogen peroxide, and the reaction between MTBE and the hydroxyl radicals. These reactions represent the major consumers of the $^\bullet OH$ radicals and will compete with MTBE for the consumption of these radicals.

The sensitivity results for tert-butyl format (TBF), tert-butyl alcohol (TBA), methyl acetate (MA), and acetone were similar and didn't show the dominance of any particular reaction(s). This is due to the fact that these compounds were byproducts of MTBE degradation. The major reactions which affected these compounds consisted of reactions that consume the $^\bullet OH$ radicals or were related to $^\bullet OH$ radical production. These effects were expected, since all of the previous byproducts were consumed by the $^\bullet OH$ radicals and also were products of MTBE reactions with these radicals after a series of reactions.

There is uncertainty in the mechanism of MTBE degradation and more work needs to be performed to validate the different reaction pathways for MTBE degradation and to obtain those rate constants which were not available. This can be performed by performing more experimental work in this direction and applying the kinetic modeling for the experimental data.

The kinetic model was able to predict the experimental degradation of MTBE for the case where Fenton-like reagent was applied. However, for the only reported byproduct in this study [Bergendahl, 2004], the model predictions were different from the experimental results.

445

# 6. References

Acero, J.L.; Haderlein, S.B.; Schmidt, T.C.; Suter, M.J.-F.; von Gunten, U. MTBE oxidation by conventional ozonation and the combination ozone/hydrogen peroxide: efficiency of the processes and bromate formation. *Environ. Sci. Technol.* **35**, 4252-4259 (2001)

Arienzo, M., "Oxidizing 2,4,6-Trinitrotoluene with Pyrite-$H_2O_2$, Suspensions." *Chemosphere* **39** (10), 1629-1638 (1999)

Arenzo, M.; Chairenzelli, J.; Scrudato, R., Pagano, J.; Falanag, L.; Connor, B., " Iron-Mediated Reactions of Polychlorinated biphenyls in Electrochemical peroxidation process (ECP)." *Chemosphere* **44**, 1339-1346 (2001)

Barreto, D.R.; Gray, K. A.; Anders, K., " Photocatalytic degradation of methyl tert-butyl ether in $TiO_2$ slurries: a proposed reaction scheme." *Wat. res.* **29**(5), 1243-8 (1995)

Baxendale, J.H. and Wilson, J. A., "The photolysis of hydrogen heroxide at high light intensities." *Trans. Faraday Soc*. 53, 344-356 (1957)

Baxendale, J.H. and Khan, A.A. "The Pulse Radiolysis of P-Nitrosodimethylaniline in Aqueous Solution." *Int. J. Radiat. Phys. Chem*. **1**, 11-24 (1969)

Behar, D.; Czapski,g.; and Duchovny, I. "Carbonate radical in flash photolysis and pulse radiolysis of aqueous carbonate solutions." *The Journal of Physical Chemistry* **74** (10), 2206-2210, (1970)

Bergendahl, J. A., Thies, T. P.; "Fenton's oxidation of MTBE with zero-valent iron" *Wat. Res*. 38, 327-334 (2004)

Bielski, Benon H. J.; Cabelli, D. E.; Arudi, R. L.; Ross, A. B. "Reactivity of hydroperoxyl/superoxide radicals in aqueous solution." *J. Phys. Chem. Ref. Data* **14** (4), 1041-100 (1985)

Bolton, J. R., *et al*, "Figures-of-Merit for Advanced Oxidation Technologies: A Comparison of Homogeneous $UV/H_2O_2$, Heterogeneous $UV/TiO_2$ and Electron Beam Processes" J. Adv. Oxid. Technol. 3(2) 174-181 (1998)

Bray, E. and Hershey, A., " The Hydrolysis of Ferric ion. The Standard Potentoal of the Ferric-Ferrous Electrode at 25°. The Equilibrium $Fe^{III}+Cl^- = FeCl^{2+}$." J. Am. Che. Soc. , 1889-1893 (1934)

Buxton, G. V.; Greenstock, C. L.; Helman, W. P.; Ross; A. B., "Critical review of rate constants for reactions of hydrated electrons, hydrogen atoms and hydroxyl radicals ($^\bullet OH/O^{\bullet-}$) in aqueous solution." *J. Phys. Chem. Ref. Data* 17(2), 513-886 (1988)

Cama, J.; Ayora, C.; Lasaga, C. A., "The Deviation from Equilibrium Effect on Dissolution Rate and on Apparent Variations In Activation Energy." *Geochimica et Cosmochimica Acta* 63(17) 2481–2486 (1999)

Cama, J.; Ganor, J.; Ayora, C.; Lasaga, C. A., "Smectite dissolution kinetics at 80 °C and pH 8.8." *Geochimica et Cosmochimica Acta* 64 (15), 2701–2717 (2000)

Cater, S.; Stefan, M.; Bolton, J. R.; Safarzadeh-Amiri, A., UV/$H_2O_2$ Treatment of Methyl tert-Butyl Ether in Contaminated Waters." *Environ. Sci. Technol*. **34**, 659-662 (2000)

Chang, P. L. and YOUNG, T., "Kinetics of Methyl Tert-Butyl Ether Degradation and Byproduct Formation during UV/Hydrogen Peroxide Water Treatment." *Wat. Res*. 34(8), 2233-2240 (2000)

Chen, P. and Pignatello, J.J., "Role of Quinone Intermediates as Electron Shuttles in Fenton and Photoassisted Fenton Oxidations of Aromatic Compounds." *Envrion. Sci. Technol*. 31, 2399-2406 (1997)

Christensen, H.; Sehested, K.; Corfitzen, H. "Reactions of Hydroxyl Radicals with Hydrogen Peroxide at Ambient and ElevatedTemperatures." *J. Phys. Chem. 86*, 1588-1590 (1982)

Christensen, H.; Sehested, K.; Bjergbakke, E. "Radiolysis of reactor water: reaction of hydroxyl radicals with superoxide ($O^{2-}$)." *Water Chemistry of Nuclear Reactor Systems,* **5**(1), 141-144 (1989)

Cooper, W. J.; Tobien, T.; Mezyk, S. P.; Adams, J. W.; Nickelsen, M. G.; O'Shea, K. E.; Inclan, G.; Tornatore, P. M.; Hajali, P.; Weidman, D. J., "The electron-beam process for the destruction of methyl tert-butyl ether." ACS Symposium Series (2002a), 799 (Oxygenates in Gasoline), 153-164

Cooper, W. J.; Nickelsen, M. G.; Mezyk, S. P.; Lesli, G.; Tornatore, P. M.; Hardison, W.; Hajali, P. A., " MTBE and priority contaminant treatment with high energy electron beam injection." *Radiation Physics and Chemistry* **65**, 451-460 (2002b)

Cooper, W.J.; Mezyk, S. P.; Lesli, G.; O'Shea, K. E..; Kim, D. K.; Hardison, W., " Kinetic modeling of the destruction of methyl tert-butyl ether (MTBE) Radiation Physics and Chemistry 67 523-526 (2003)

Cooper, W. J.; Christopher Cramer, C;Ned H. Martin, N. H.; Mezyk, S. P.; O'Shea., K. E.; Von Sonntag, C.,"A Free Radical-Mechanism for the Destruction of Methyl- *tert*-Butyl Ether (MTBE) *via* Advanced Oxidation Processes." (2004) In press

CRC, Handbook of Chemistry and Physics, 55th edition, CRC Press, 1974-1975

Crittenden, J.C; Hu, S.; Hand, D. W.; Green , A.S. " A kinetic Model For $H_2O_2$/UV process in a completely mixed batch reactor." *Wat. Res*. **33**, 2315-2328 (1999)

Damm, J. H.; Hardacre, C.; Kalin, R. M.; Walsh, K. P., " Kinetics of the Oxidation of Methyl tert-butyl ether (MTBE) by potassium permanganate." *Wat. Res*. **36**, 3638-3624 (2002)

Daniton, F. S.; Rowbotton, J.  "Primary Radical Yield in Water. Comparison of the Photolysis and Radiolysis of Solutions   of Hydrogen Peroxide*." Transactions of The Faraday Society.* **49**, 1160-1173 (1953)

Dean (Ed) J. A., Lange's Handbook of Chemistry, McGraw-Hill, New York, 1979, p5

De Laat, J. and Gallard, H., "Catalytic Decomposition of Hydrogen Peroxide by $Fe^{III}$ in Homogeneous Aqueous Solution: Mechanism and kinetic Modeling." *Envrion. Sci. Technol*. 33, 2726-2732 (1999)

De Laat, J.; Le, G. T.; Legube, B., "A comparative study of the effects of chloride, sulfate and nitrate ions on the rates of decomposition of $H_2O_2$ and organic compounds by Fe(II)/$H_2O_2$ and Fe(III)/$H_2O_2$." *Chemosphere* 55, 715-723 (2004)

Ebert, M.; Keene, J. P.; Swallow, A. J.; Baxendale, J. H. (eds.), Pulse Radiolysis, Acdemic Press, New York, 1965.

Eibenberger, J.; Schulte, D.; Steenken, S. " One-Electron Oxidation of $\alpha$-Monoalkoxyalkyl Radicals by Tetranitromethane via an Intermediate Adduct. Influence of Radical Structure on Rate of Decomposition of the Adduct." *J. Phys. Chem*. 84, 704-710 (1980)

Elliot, A.J. and Simson, A.S. "Rate Constants for Reactions Of Hydroxyl Radicals as a Function of Temperature." *Rad. Phys. Chem*. **24**, 229-231(1984)

Ensing, B. and Baerends, E. J., " Reaction Path Sampling of the Reaction between Iron(II) and Hydrogen Peroxide in Aqueous Solutions." *J. Phys. Chem*. *A* **106**, 7902-7910 (2002)

Esplugas, S. *et al*., "Comparison of different advanced oxidation processes for phenol degradation." *Wat. Res*. **36**, 1034-1042 (2002)

Evans, M. G.; Baxendale, J. H.; Uri, N., "The Heat of the Reaction Between Ferrous Ions and Hydrogen Peroxide in Aqueous Solution." *Proc. Roy. Soc. A* **147**, 334 (1948a)

Evans, M. G.; George, P.; Uri, N., "The $[Fe(OH)]^{2+}$ and $[Fe(O_2H)]^{2+}$ complexes." *Proc. Roy. Soc. A* **147**, 230 (1948b)

Gallard, H.; De Laat, J.; Legybe, B., " Spectrophotometric Study of the Formation of Iron(III)-Hydroperoxy complexes in Homogeneous Aqueous Solutions." *Wat. Res*. **33**, 2929-2936 (1999).

Gallard, H.; De Laat, J.; Legube, B.," Effect of pH on the Oxidation of organic compounds by $Fe^{II}/H_2O_2$. Mechanism and simulation." New J, Chem. 263-268 (1998)

Gallard, H.; De Laat, J.,," Kinetic Modeling of $Fe^{II}/H_2O_2$ Oxidation reactions in Dilute Aqueous Solution Using Atrazine as a Model Organic Compound." *Wat. Res*. 34(12), 3107-3116 (2000)

Gallard, H.; De Laat, J.,," Kinetic oxidation of chlorobenzene and phenyl-ureas by $Fe(II)/H_2O_2$ and $Fe(III)/H_2O_2$. Evidence of reduction and oxidation reactions of intermediates by Fe(II) or Fe(III)." *Chemosphere* 42(12), 405-413 (2001)

Ganor, J.; Mogollon, J. L.; Lasaga, A. C.," The effect of ph on Kalonite Dissolution rates and on Activation Energy." Geochimica et Cosmochimica Acta 59(11/12) 1037–1052 (1995)

Ganor, J.; Mogollon, J. L.; Lasaga, A. C., "Kinetics Of Gibbsite Dissolution Under Low Ionic Strength Conditions." Geochimica et Cosmochimica Acta 63(11/12) 1635–1651 (1999)

Gautelier, M.; Oelkers, E.; Schott, J., "An experimental study of dolomite dissolution rates as a function of pH from -0.5 to 5 and temperature from 25 to 80 $^{o}$C." Chemical Geology 157, 13–26 (1999)

Glaze, W. H.; Lay,Y.; Kang, J. " Advanced Oxidation Processes . A kinetic model dor the oxidation of 1,2-Dibromo-3-chloropropane in Water by the Combination of Hydrogen Peroxide and UV Radiation." *Ind. Eng. Chem. Res*. **34**, 2314-2323 (1995)

Harber, F. and Weiss, J., " The catalytic decomposition of hydrogen peroxide by iron salts." Proc. Roy. Soc. A 134, 332-351 (1934)

Hardison, D. R.; Cooper, W. J.; Mezyl, S.P.; Bartels, D. M., "The free radical chemistry of tert-butyl formate: rate constants for hydroxyl radical, hydrated electron and hydrogen atom reaction in aqueous media." *Rad. Phys. Chem*. **65**, 309-315 (2002)

Hug, S. and Leupin, O., "Iron-Catalyzed Oxidation of Arsenic (III) by Oxygen and by Hydrogen Peroxide: pH-Dependent Formation of Oxidants in the Fenton Reaction." *Environ. Sci. Technol*. **37**, 2734-2742 (2003)

Hundal, L. S, Singh, J.; Bier, E. L.; Shea, P. J.; Comfort; S. D.; Powers. W. L., "Removal of TNT and RDX from water and soil using iron metal." *Environ. Pollu*. **97**, 55-64 (1997)

Johnson, R.; Pankow, J., Bender, D, Price, C, Zogoroski, J. "MTBE: to What Extent Will Past Releases Contaminant Community Water Supply Wells." *Envirn. Sci. Technol.* **34**, 210-217A (2000)

Kang, J. W. and Hofmann, M. R.," Kinetics and Mechansim of the Sonolytic Destruction of methyl tert-butyl ether by ultrasonic irradiation in the presence of Ozone." *Envirn. Sci. Technol.* **32**, 3194-3199 (1998)

Kang, J. W.; Hung, H. M., Lin, A.; Hofmann, M. R.," Sonolytic destruction of methyl tert-butyl ether by ultrasonic irradiation: the role of $O_3$, $H_2O_2$, frequency, and power supply." *Envirn. Sci. Technol.* **33**, 199-205 (1999)

King, D. W. and Farlow, R., "Role of Carbonate Speciation on the Oxidation of Fe(II) by $H_2O_2$." *Marine Chemistry* **70**, 201–209 (2000)

Koppenol, W. H.; Butler J.; Van Leeuwen J. W. L. "The Haber-Weiss Cycle." *Photochem. Photobiol* **28**, 655-660 (1978)

Kwan, W. P.; Velker, B. M., " Decompostion of Hydrogen Peroxide and Organic compounds in the presence of Dissolved Iron and Ferrihydrate." *Envirn. Sci. Technol.* **33**, 199-205 (1999)

Lasaga, A. C., "Chemical Kinetics of Water-Rock Interactions." *J. Geophys. Res.* B6:4009-4025 (1984)

Lasaga, Antonio, C. Kinetic Theory in the Earth Sciences, 1998, Princeton Press.

Li, Z. M.,Peterson, M. M.; Comfort, S. D.; Horst, G. L.; Shea, P. J.; B. T. Oh. B. T., "Remediating TNT-contaminated soil by soil washing and Fenton oxidation." *Sci. Total Environ.* **204**, 107-115 (1997)

Li, Z. M., Shea, P. J; Comfort, S. D., "Nitrotoluene destruction by UV-catalyzed Fenton oxidation." *Chemosphere* **36**, 1849-1865 (1998)

Lindesy, M. E. and Tarr, M. A." Quantitation of Hydroxyl Radical during Fenton Oxidation following a Single addition of Iron and Peroxide." *Chemsphere* **41**, 409-417 (2000)

Luttge, A; U. Winkler, U.; Lasaga, A. C., "Interferometric study of the dolomite dissolution: A new conceptual model for mineral." *Geochimica et Cosmochimica Acta* **67**(6), 1099–1116 (2003)

Martell, A. and Smith, R. M., Critical Stability Constants, vol. 3 Other Organic Ligands, Plenum Press, 1976.

Mezyk, S. P.; Copper, W. J.;  Bartels, D. M.; O'Shea, K. E.; Wu, Taixing, " Radiation Chemistry of Alternative Fuel Oxygenates: Substituted Ethers" J. Phys. Chem. A **105**, 3521-3526 (2001)

Millborn, R. M. and Vosburgh, W. C., " A Spectrophotometric Study of the Hydrolysis of Iron(III) Ion. II. Polynuclear Species." *J. Am. Chem. Soc*. **77**, 1352 (1955)

Moffettt J.W., and Rod G. Zika, R. G., "Reaction Kinetics of Hydrogen Peroxide with Copper and Iron in Seawater" *Environ. Sci. Technol*. *21,* 804-810 (1987**)**

Nagy, K. L., Blum, A. E., Lasaga, A. C., "Dissolution and Precipitation Kinetics of Kaolinite at 80$^o$ C and ph 3: The Dependence on Solution Saturation State." *Amer. J. Sci.* 291 649-686 (1991)

Neppolian, B.; Jung, H.; Choi, H.; Lee, J. H.; Kang, J-W., "Sonolytic Degradation of Methyl Tert-Butyl Ether: The Role of Coupled Fenton Process and Persulphate Ion." *Wat. Res*. **36,** 4699–4708 (2002)

Neta, P.; Simic, M.; Hayon, E. Pulse radiolysis of aliphatic acids in aqueous solutions. I. Simple monocarboxylic acids. *J. Phys. Chem*., **73**, 4207-4213 (1969)

Neyens, E. and Baeyens, J. " A Reniew of Classical Fenton's peroxidation as an advanced oxidation technique." *J. Hazrad. Mat*. **B98**, 33-50 (2003)

Night, R, J. and Sylva, R. N., " Spectrophotometric Investigation of Iron(III) Hydrolysis in Light and Heavy Water at 25 $^o$C." *J. Inorg. Nucl. Chem*. **37**, 779-783 (1975)

Onstein, P.; Stefan, M. I.; Bolton, J. R. "Competition Kinetic Method for the Determination of rate constants for the Reaction of Hydroxyl Radicals with Organic Pollutants using the UV/$H_2O_2$ advanced Oxidation Technology: the Rate Constants for tert-butyl formate ester and 2,4-dinitrophenol." *J. Adv. Oxid. Technol.* **4**, 231-236  (1999)

O'Shea, K. E; Kim, D. K.; Wu, T.; Cooper, W.J.; Mezyk, S. P., " The degradation of MTBE-BTEX mixtures by gamma radiolysis. A kinetic modeling study" *Radiation Physics and Chemistry* **65**, 343-347 (2002a)

O'Shea, K. E; Wu, Taixing; Copper, W. J., $TiO_2$ Phtocatalysis of Gasoline Oxygenates. Kinetic Parameters, and effects of Catalyst types and Loading on the degradation of Methyl tert-Butyl Ether" ACS Symposium Series (2002b), 799 (Oxygenates in Gasoline), 165-176

Pankow, J. F., Aquatic Chemistry Concepts. Lewis Publisher, 1991

Pankow, J. F.; Thomson, N. R.; Johnson, R. L.; Baehr, A. L.; Zogorski J. S., "The Urban Atmosphere as a Non-Point Source for the Transport of MTBE and Other Volatile

Organic Compounds (VOCs) to Shallow Groundwater.*" Environ. Sci. Technol.* **31**, 2821 – 2828 (1997)

Pagsberg, P.; Christensen, H.; Rabani, J.; Nilsson, G.; Fenger, J.; Nielsen, S. O. "Far-ultraviolet spectra of hydrogen and hydroxyl radicals from pulse radiolysis of aqueous solutions. Direct measurement of the rate of H + H." *J. Phys. Chem.* (1969) **73**(4), 1029-38 (1969)

Pignatello, J.J. " Dark and Photoasstsed $Fe^{3+}$ Catalyzed Degradation of Chlorophenoxy Herbicides by hydrogen Peroxide." *Environ. Sci. Technol.* **26**, 944-951 (1992)

Pourbaix, M., Atlas of Electrochemical equilibria in aqueous solutions. Oxford, Pergamon Press (1966)

Rabani, J. and Stein, G. "The reactivity of $^{\bullet}OH$ radicals with ferro-ferricyanide, formate, ethanol and amino acids in irradiated solutions." *Trans. Faraday Soc.* **58**, 2150-2159 (1962)

Rivas, F., Beltran, F.; Frdaes, J.; Buxeda, P., " Oxidation of p-Hydroxybenzene Acid by Fenton's Reagent." *Wat. Res.* **35**, 387-396 (2001)

Robbins, G.A.; Wang, S.; Stuart, J. D., " Using the static headspace method to determine Henry's law constants" *Analy. Chem.* **65,** 175 (1993)

Rush, J. D. and Bielski, H. J., " Pulse Radiolysis of the Reactions of $HO_2/O_2^-$ with Fe(II)/Fe(III) Ions. The Reactivity of $HO_2/O_2^-$ with Ferric Ions and Its Implication on the Occurrence of the Haber-Weiss Reaction." *J. Phys. Chem.* **89**, 5062-5066 (1985)

Safarzadeh-Amiri, A.; Bolton, J. R.; Cater, S. R., " The Use of iron in Advanced Oxidation Processes." *J. Adv. Oxid. Technol.* **1**, 18-26 (1996)

Safarzadeh-Amiri, A., " $O_3/H_2O_2$ Treatment of Methyl tert-Butyl Ether (MTBE) in Contaminated Waters." *Wat. Res.* **35**, 3706-3714 (2001)

Sehested, K.; Rasmussen, O. L.; Fricke, H. "Rate constants of $^{\bullet}OH$ with $HO_2,O_2^-$, and H2O2+ from hydrogen peroxide formation in pulse-irradiated oxygenated water." *J. of Phys. Chem.* **72**(2), 626-31(1968)

Snoeyink, V. L. and Jenkins, D. Water Chemistry. John Wiley & Sons,New York USA, (1980)

Speth, T. F. and Millter, J. R. " Technical Note: adsorption capacity of GAC for synthetic organic" *J. Am. Water Works Assoc.* **82,** 72-75 (1990)

Squillace, P. J.; Zogorski, J. S.; Wilber, W. G.; Price C. V., "Preliminary Assessment of the Occurrence and Possible Sources of MTBE in Groundwater in the United States." *Environ. Sci. Technol*. **30**, 1721-1730 (1996)

Stefan, M.; Mack, J.; Bolton, J. R., "Degradation Pathways during the Treatment of Methyl *tert*-Butyl Ether by the UV/$H_2O_2$ Process." *Environ. Sci. Technol*. **34**, 650-658 (2000)

Stumm, W. and Morgan, J.J. Aquatic Chemistry, Prentice-Hall, Engelwood, NJ, (1996)

Sulfita, J. M. and Mormole, M. R., "Anaerobic biodegradation of known and potential gasoline oxygenates in the terrestrial subsurfaces." *Environ. Sci. Technol*. **27**(5), 976 (1993)

Teel. A. L.; Warberg, C. R.; Atkison, D. A.; Watts, R., " Comparison of mineral and soluble iron Fenton's catalysts for the Treatment of Trichloroethylene." *Wat. Res*. **35**, 977-984 (2001)

Thomas, J. K.  "Rates of Reaction of the Hydroxyl Radical."    *Transactions of the Faraday Society*  **61** (508),  702-7 (1965)

Turner, D. R.; Whitfield, M.; Dickson, A. G., " The Equilibrium Speciation of Dissolved Components in Fresh Water and Seawater at 25 $^o$C and 1 atm Pressure." *Geochimica et Cosmochimica Acta* **45**, 855–881 (1981)

Vollman, D.H.; Chen, J.C., "The Photochemical Decomposition of Hydrogen Peroxide in Aqueous Solutions of Allyl Alcohol at 2537 $\overset{\circ}{A}$ ." *J. Am. Chem. Soc*. **20**, 4141 (1959)

Wagler, J.L. and Malley Jr., J.P., "The Removal of Methyl Tert-Butyl Ether from a Model Ground Water Using UV/Peroxide Oxidation." *J. New Engl. Water Works Assoc*. September, 236-260 (1994)

Waite, T. D.; Feitz, A. J.; Aplin, R. " Application of Kinetic Modeling to Optimization of Advanced Oxidation Processes in Wastewater Treatment." *Chemical Water and Wastewater Treatment*, 2, 93-108 (2002)

Walling, C. and Goosen A., " Mechanism of the Ferric Ion Catalyzed Decomposition of Hydrogen Peroxide. Effect of Organic Substrates." *J. Am. Chem. Soc*. **95**(5), 2987-2991 (1973)

Walling, C., "Fenton's Reagent Revisted." *Acc. Chem. Res*. **8**, 125-131 (1975)

Walling, C., "Commentary." *Acc. Chem. Res*. **31**, 155 (1998)

Weeks, J. L.; Matheson, M. S., "The Primary Quantum Yield of Hydrogen Peroxide Decomposition*." J. Phys. Chem*. 1273 (1955)

Weinstein, J.; Bielski, H. J. "Kinetics of the interaction of $HO_2$ and $O_2^-$ Radicals with Hydrogen Peroxide. The Haber-Weiss Reaction." *J. Am. Chem. Soc*. **3**, 58-62 (1979)


Willson, R.L.; Greenstock, C.L.; Adams, G.E.; Wageman, R.; Dorfman, L.M. "The standardization of hydroxyl radical rate data from radiation chemistry." *Int. J. Radiat. Phys. Chem*. **3**, 211-220 (1971)

Wu, T.; Cruz, V.; Mezyk, S.; Cooper, W. J.; O'Shea, K. E. "Gamma radiolysis of methyl tert-butyl ether: a study of hydroxyl radical mediated reaction pathways" *Radiat. Phys. Chem.* 65(4-5), 335-341 (2002)

Xu, X-R.; Zhao, Z-Y.; Gu Li, X-Y; J-D., "Chemical oxidative degradation of methyl tert-butyl ether in aqueous solution by Fenton's reagent." *Chemosphere* **55**, 73–79 (2004)

Yeh, C.K.; Novak, J. T., " The effect of $H_2O_2$ on the degradation of methyl and ethyl-tert butyl ethers in soils." *Wat. Environ. Res.* **76**, 828-834 (1995)

# Chapter 5

## Conclusions and Recommendations

In the experimental part of this work, Chapter 1, benzene was partially oxidized to phenol. Results at low conversion of benzene to phenol were obtained with a different selectivity from the reported work. High conversion to phenol was not obtained using the same arrangement as the reported one. High conversion to phenol was obtained using a scheme different from Niwa *et al* (2002). From the present work, it was found that producing phenol from benzene was not a Pd-membrane technology since phenol was produced using either Pd in the form of a supported catalyst or pure metal. Within the studied experimental conditioned, formation of phenol was related to Pd catalyst since Pt catalyst wasn't capable of activating benzene to produce phenol. Another evident was the result of a blank experiment, where no catalyst was used. From this experiment no phenol was produced. The produced amount of water (secondary product) was at least 23 times greater than the produced amount of phenol (primary product). The reaction between hydrogen and oxygen at the studied conditions produced water in the primary reaction and active intermediates especially $^\bullet OH$ radical based on analysis from literature. It is established that the reaction of $^\bullet OH$ radical with benzene proceeds by addition to the aromatic ring and after subsequent reactions phenol is produced. Formation of other detected products was proposed based on the available literature. Observed chain products were proposed to be produced as a consequence of aromatic ring opening. In order to elucidate the true mechanism behind the observed partial oxidation of benzene to phenol other desings schemes need to be tested. Short contact time reactor might provide

a good tool for such kind of tests. Also, in order to clarify the role of the support on the Pd membrane reactivity, other support materials need to be tested.

Both kinetic models (for humic acids degradation and MTBE mineralization) were similar in that $^{\bullet}OH$ radical was responsible for the destruction of the contaminant of interest. The difference between the two models lies in the way by which these radicals were produced. In UV/$H_2O_2$ process, $^{\bullet}OH$ radical was produced by direct photolysis of $H_2O_2$. In Fenton's reagent and Fenton-like process $^{\bullet}OH$ radical was produced by the reaction of ferrous iron and $H_2O_2$. Also, $H_2O_2$ chemistry in aqueous systems was the same in both models. Another difference between the two models comes from the studied contaminant since each compound will have its own mechanism.

A kinetic model for humic acid destruction using $H_2O_2$ and UV light in a well stirred batch reactor under various dosages of $H_2O_2$ and humic acid was developed and tested on experimental data (Chapter 2). The kinetic model predicted the trends in residual fractions of NPDOC and $H_2O_2$ well. The variations of initial hydrogen peroxide concentration have more pronounced effect on the system than variations in humic acid concentration within the studied conditions. Degradation of humic acid by direct photolysis is important at low hydrogen peroxide concentrations. At high hydrogen peroxide concentration, degradation of NPDOC is by $^{\bullet}OH$ radicals is dominant over its degradation by direct photolysis. Further testing of the previous kinetic model for the effect of total carbonate was studied in Chapter 3. The kinetic model simulations were able to predict the effect of bicarbonate/carbonate on the degradation of humic acids. A retardation effect on humic acids was observed due to the scavenging of the hydroxyl radicals by carbonate and bicarbonate. Carbonate radicals, which were produced from

reactions of carbonate and bicarbonate ions with hydrogen peroxide, were contributing to the rate of NPDOC degradation by reacting with humic acid. The system was sensitive to the presence of total carbonate in the system. Therefore, people working with such kind of systems where carbonate/bicarbonate is present should include all of the available reactions in their simulations. This would also indicate that during treatment processes if UV/$H_2O_2$ would be applied then the effect of bicarbonate/carbonate on the oxidation process should be taken into account. The kinetic model, for HA destruction using UV/$H_2O_2$ oxidation, needs to be verified further. This could be achieved by applying it to more experimental data. Such data are not available for the time being.

A kinetic model for the degradation of methyl tert-butyl ether (MTBE) in a batch reactor applying Fenton's reagent ($Fe^{II}$/ $H_2O_2$) and Fenton-like reagent ($Fe^{o}$/ $H_2O_2$) aqueous solutions was proposed (Chapter 4). The kinetic model consisted of three major parts, hydrogen peroxide chemistry in aqueous solutions, iron chemistry, and MTBE chemistry. Rate and equilibrium constants were taken from literature. The rate constant for the reaction of ferric iron with hydrogen peroxide was fitted within the range that was reported in the literature. The rate constant for iron dissolution also was a fitted parameter, and it was a function of the solution acidity. A mechanism for MTBE degradation by the hydroxyl radicals, which were formed from ferrous iron and hydrogen peroxide reaction, was proposed based on literature. Most of the rate constants for this MTBE oxidation mechanism were taken from the literature and when a rate constant for a certain reaction was not available, analogy between this reaction and another reaction that proceed in a similar  way was made.  Proportions of one reaction that proceed in different routes, other than hydrogen abstraction from MTBE which was taken from the literature,

was optimized based on the best fitting of the model to the experimental data. The kinetic model showed good predictions of the reported experimental data which involved the use of Fenton's reagent. The degradation of MTBE in Fenton's reagent work was characterized to proceed by two stages, a fast one which involve the reaction of ferrous iron with hydrogen peroxide ($Fe^{II}/H_2O_2$ stage) and another, relatively, slower stage which involves the reaction of ferric iron with hydrogen peroxide ($Fe^{III}/H_2O_2$ stage). Within the studied conditions increasing ferrous ion concentration ($Fe^{II}$) increased MTBE removal since this led to higher production of the $^\bullet OH$ radicals, which were responsible for MTBE degradation. Model predictions of the $Fe^{II}$ effect on MTBE removal enhanced at higher concentrations of $Fe^{II}$. A sensitivity analysis for MTBE degradation elucidated that all the proposed reaction steps played a role in MTBE degradation. However, the extent of the effect of these reactions varies from one reaction to another. This effect was a function of the rate constant of each reaction, the concentration of the reactants that were involved in the reaction, and the production and consumption pathways of the involved reactants. Therefore, in a kinetic model all of these reactions should be included to cover a wide range of experimental conditions. The sensitivity results for tert-butyl format (TBF), tert-butyl alcohol (TBA), methyl acetate (MA), and acetone were similar and didn't show the dominance of any particular reaction(s). The kinetic model was able to predict the experimental degradation of MTBE for the case where Fenton-like reagent was applied. However, for the only reported byproduct acetone, the model predictions were different from the experimental results. This issue remained unresolved and requires experimental data to solve it.

There is uncertainty in the mechanism of MTBE degradation and more work needs to be performed to validate the different reaction pathways for MTBE degradation and to obtain those rate constants which were not available. This can be performed by performing more experimental work in this direction and applying the kinetic modeling for the experimental data.